1974

A Study Of General Analytical Approaches Applied To Plates And Thin-walled Structures

Samir Fouad Bassily

A STUDY OF GENERAL ANALYTICAL APPROACHES APPLIED TO PLATES AND THIN-WALLED STRUCTURES

by

Samir Fouad Bassily

Faculty of Engineering Science

Submitted in partial fulfillment

of the requirements for the degree of

Doctor of Philosophy

Faculty of Graduate Studies

The University of Western Ontario

London, Ontario

July, 1974

I	area moment of inertia for a beam cross-section
I_{js}	definite integral defined by equation *(3.8)*
$i, j, k, l, m, n, p, q, r, s, t,$	integers
J_{js}	definite integral defined by equation *(3.8)*
$[K]$	stiffness matrix
$K, L, M, N,$	positive integers
K^o_{ir}, K^k_{ir}	definite integrals defined by equations *(5.5a)* and *(5.5b)*
L, L_1, L_2	linear differential operators
M, M_B	bending moments per unit length of a plate
$[M]$	mass matrix
N_x, N_y, N_{xy}	arbitrary time-independent inplane loads per unit length of a plate element
n	unit vector normal to a plate edge
P, Q	normal and tangential components of the external loads
p, q	normal and tangential components of the external loads per unit area
Q, Q_K	Kirchhoff shear force per unit length of a plate edge
Q^o_{js}, Q^l_{js}	definite integrals defined by equations *(5.5a)* and *(5.5b)*
q_i	an assumed function of time
R_{js}	definite integral defined by equations *(3.8)*
S_{js}	definite integral defined by equation *(3.8)*
s	unit vector tangential to a plate edge
T^o_{js}, T^l_{js}	definite integrals defined by equations *(5.5a)* and *(5.5b)*

employing continuous coordinates - such as the Ritz method - are most suited. For very complicated structures, on the other hand, discrete coordinate methods, and more specifically Finite Elements, seem to be a natural choice. Neither of the two types of coordinates, however, can be considered optimal for all classes of problems; thus a combined approach - the *Large Element Method* - is postulated.

The proposed Large Element approach is a tool for solving a wide class of problems in continuum mechanics. The method is basically a blend of the Finite Element and Ritz methods into a unified formulation which is continuously optimal for problems having any degree of complexity. In this blend, the character of each of the constituent methods is preserved and the approach allows a pure Ritz or a pure Finite Element solution to be obtained for a problem. The technique therefore features all the advantages of both methods and eliminates most of their shortcomings.

To demonstrate the accuracy and application of the proposed method, it is used to solve a large variety of test problems. Whenever possible, the solutions obtained are compared with those obtained using conventional approaches. In all cases investigated, the results are quite accurate and, whenever comparison is made with Finite Element or Finite Difference solutions, better accuracy is obtained by the use of the same, or smaller number of equations in the proposed method.

ACKNOWLEDGEMENTS

It is the pleasure of the author to acknowledge the aid he received from several individuals and organizations without which the completion of this work would have been impossible.

The author sincerely acknowledges the help of Professor S.M.Dickinson and his constant guidance throughout the course of this work. The material presented in this thesis has been appreciably refined through hundreds of useful discussions with him.

The author wishes also to thank Professor S.H.Abu-Sitta, Professor M. Novak, and Professor M.G.Hashish for their encouragement and many useful discussions. Acknowledgements are also due to Dr. A. Harris for revising the manuscript, to Mr. D. Barrit who helped in preparing the illustrations, and to Mrs. B. Pollard whose meticulous typing of the manuscript has been a great help. The financial assistance of the Canadian National Research Council is greatfully acknowledged.

Last, but not least, the author is greatly indebted to his wife, Nazek, who has borne the brunt of the compilation of the tables and whose continuing encouragement, help and patience throughout the years have enabled this work to be completed.

TABLE OF CONTENTS

NOMENCLATURE

The following is a list of the main symbols used. Other symbols are defined as they appear in the text:

a, a_i	length of a plate or a plate element
A_i, A_m, A_{ij}	coefficients in assumed displacement series (generalized coordinates)
b, b_i	width of a plate or a plate element
B_{ij}	coefficient in assumed displacement series (generalized coordinate)
C_1, C_2, ...	constants of integration
D	the domain of interest
$D=Eh^3/12(1-\nu^2)$	isotropic plate flexural rigidity
D_x, D_y, D_{xy}, D_k	orthotropic plate stiffness coefficients defined in equation *(7.12)*
E	Young's modulus for an isotropic plate
E_{ir}	definite integral defined by equation *(3.8)*
E_x, E_y	constants of elasticity for an orthotropic plate
F_{ir}	definite integral defined by equation *(3.8)*
F_x, F_y	components of the inplane body force
g	the gravitational acceleration
G	modulus of rigidity
G_{ir}	definite integral defined by equation *(3.8)*
h, h_{ij}	thickness of plate or plate element
H_{ir}	definite integral defined by equation *(3.8)*

I	area moment of inertia for a beam cross-section
I_{js}	definite integral defined by equation *(3.8)*
$i, j, k, l, m, n, p, q, r, s, t,$	integers
J_{js}	definite integral defined by equation *(3.8)*
$[K]$	stiffness matrix
$K, L, M, N,$	positive integers
K^o_{ir}, K^k_{ir}	definite integrals defined by equations *(5.5a)* and *(5.5b)*
L, L_1, L_2	linear differential operators
M, M_B	bending moments per unit length of a plate
$[M]$	mass matrix
N_x, N_y, N_{xy}	arbitrary time-independent inplane loads per unit length of a plate element
n	unit vector normal to a plate edge
P, Q	normal and tangential components of the external loads
p, q	normal and tangential components of the external loads per unit area
Q, Q_K	Kirchhoff shear force per unit length of a plate edge
Q^o_{js}, Q^l_{js}	definite integrals defined by equations *(5.5a)* and *(5.5b)*
q_i	an assumed function of time
R_{js}	definite integral defined by equations *(3.8)*
S_{js}	definite integral defined by equation *(3.8)*
s	unit vector tangential to a plate edge
T^o_{js}, T^l_{js}	definite integrals defined by equations *(5.5a)* and *(5.5b)*

TDF	Total Degrees of Freedom
t	time
U	strain energy
U^o_{ir}, U^k_{ir}	definite integrals defined by equations *(5.5a)* and *(5.5b)*
u, v, w	displacement components
V	body force potential function
V^o_{js}, V^l_{js}	definite integrals defined by equations *(5.5a)* and *(5.5b)*
W_i	displacement at node *(i)* of a beam element
W^o_{ir}, W^k_{ir}	definite integrals defined by equations *(5.5a)* and *(5.5b)*
X, Y, Z	non-dimensional Cartesian coordinates
x, y, z	Cartesian coordinates
Y	the width of a slab
Y_e	effective width of a slab, i.e. the width of a beam having the same depth and length which provides the same stiffness as the slab
Γ	the boundary of a domain
Δ	the Laplacian operator
$\Delta\Delta$	the biharmonic operator
Δ_1, Δ_2	relative displacements
δ	variation sign
$\{\delta\}$	vector of degrees of freedom
ε_d	the descritization error, in a Finite Difference solution
ε_s	the relative error in a solution due to the misrepresentation of the support conditions
$\varepsilon_s, \varepsilon_n, \varepsilon_x, \varepsilon_y, \varepsilon_{xy}$	inplane normal and shear strain components

ν, ξ, λ	normalized spacial coordinates
θ_i	the rotational degree of freedom at node (i)
Θ	angle defining the direction of the principle axes
λ, μ	eigenvalues (nondimensional frequency parameter)
λ_i, ε_i	eigenfunction parameters and eigenvalues associated with the beam functions
ν	a material property (e.g. Poisson's ratio in the case of plate bending)
ν_x, ν_y	Poisson's ratios of an orthotropic plate
ρ, ρ_{ij}	mass density of a plate or a plate element
$\{\sigma\}$	stress vector
$\sigma_x, \sigma_y, \sigma_z, \sigma_n$	normal stress components
$\sigma_{max}, \sigma_{min}$	inplane principle stresses
τ_{xy}, τ_{ns}	inplane shear stress components
τ_{max}	maximum inplane shear stress
Φ_i, Ψ_i	families of assumed functions
ϕ_i, ψ_i	admissible ordinary or degenerated beam functions
$\bar{\phi}, \bar{\bar{\phi}}_i, \tilde{\phi}_i, \tilde{\tilde{\phi}}_i$	families of degenerated beam functions
χ	the curvature of a plate
Ψ	stress or force potential function in a two dimensional elasticity problem
ψ	an eigenfunction
ω	circular frequency of vibration

CHAPTER I

SCOPE AND A STATE-OF-THE-ART REPORT

1.1 Introduction

Unlike most research projects, the purpose of this project is *not* to study a specific pre-defined problem. Instead, its object is to critically examine and further develop some of the fundamental techniques for solving problems of Applied Mechanics. For the greater part of this work, attention is focused upon problems concerning the static and dynamic behaviour of plates and plate systems. Further, the scope of this investigation has been limited to the study of linear steady state applications.

This work has resulted in at least three basic achievements: a new family of functions suitable for use with plates under natural boundary conditions has been developed; a complete analogy between the flexure and the inplane problems of thin-walled structures has been drawn, which prompted a unified treatment for the two classes of problems; and finally an optimum approach combining the advantages of the continuum methods (such as the Ritz approach) and the discrete methods (such as Finite Elements) has been proposed.

The thesis is divided into two main parts: part I

deals with the application of the classical Ritz method to rectangular plate problems; and part II deals with the development and application of a new versatile approach to problems of more complicated nature. In each of the two parts, three basic classes of problems are dealt with: 1) the flexure problem, including both static and dynamic loads (natural vibrations); 2) the inplane elasticity problem; and 3) the stability problem representing the interaction between the inplane loads and the out-of-plane vibrations and stability of a system.

Due to the nature of the subject of this research project, and the wide class of problems considered, a literature survey for the field is an exhaustive and extremely difficult task. In addition, since it is not problem oriented research, a historical review for the subject becomes almost irrelevant. Instead, a state-of-the-art review will be outlined in the following few pages.

In a previous publication by the author [1]*, a summary of the major classical methods which can be used for the treatment of plate problems has been presented. It included a brief description for the methods of Rayleigh, Ritz, Galerkin, Lagrangian multipliers, Finite Elements and Finite Differences. A useful perturbation power series approach originally suggested by Trubert and Nash [2] was described

---

* Numbers in brackets designate References listed at the end of the thesis.

and extended in [1,3]. The method was further extended into a multi-parameter perturbation approach and applied to problems of plates under combined inplane loading in references [1,4]. In addition, references [1,5] describe an extension for the Galerkin method which permits its application to problems under natural boundary conditions using functions that do not necessarily pre-satisfy those boundary conditions.

In his famous monograph [6], Kantorovich suggested his well known method of reduction to a one dimensional problem. In its original development, the method did not permit improvement of the approximate solution in one of its two spacial dimensions. This was overcome in 1966 in an extension suggested by Kerr [7] which treats the Kantorovich method as a first step in an iterative technique. The method however, requires the successive solution of a series of ordinary differential equations and a set of transcendental equations, which makes the algebra involved rather tedious. In addition, it assumes separation of variables which means, in a vibration problem, that the nodal lines are parallel to the plate edges. This is known to be an unacceptable approximation for some modes for which the nodal lines may be approximately diagonal.

In addition to the above-mentioned techniques, a large number of extensions and developments of these basic fundamental approaches have been developed. While some of

those extensions are quite general and have a range of application which is - sometimes - beyond the realm of the fundamental method upon which the development is based, the majority of such extensions have limited application due to the use of simplifying assumptions regarding the boundary conditions. Examples of such assumptions are the existence of two or more simply-supported edges, two edges being very long compared to the other two, the existence of no free edges or no free corners ... etc. Since the existence of such assumptions usually precludes the use of the method as a general analysis tool applicable to a more general class of problems, methods of this nature will be excluded from the following discussion.

In the following five sections, a brief description of a number of the important recent developments in the field of interest of this research project will be presented. Also, an account of the assets and liabilities of these methods is given in each case.

1.2 The Finite Strip Method

This method was first introduced in a paper by Cheung, Y.K. [8] in 1968. It was also described by Zienkieviez in the latest edition of his well known book [9] as a "semi-analytical Finite Element" approach. The method is a variation of the Finite Element technique applicable to thin walled structures in which no structural or boundary

discontinuities occur in the direction of one of the basic coordinates. The method is particularly useful for problems of continuous plates, box-type bridges, and plates with properties (or thickness) varying in one direction. It has also been used for skewed slabs and sectorial plates satisfying the condition of continuity stated above.

In this method, orthogonal function series which satisfy the fundamental boundary conditions are selected in the direction where no discontinuities occur. In the other direction, however, the plate is divided into narrow strips and a suitable polynomial expression assumed within each element (strip). Two examples for such strips are shown in Figure (1.1). The first is a rectangular strip with the coordinates $\eta = x$, and $\xi = y/a$, while the second is a curved strip with $\eta = (r-r_i)$, and $\xi = \frac{\theta}{\alpha}$. The degrees of freedom in each case are defined as w_i, w_j, $\frac{\partial w_i}{\partial \eta}$, and $\frac{\partial w_j}{\partial \eta}$. The displacement w at any point within the strip is then assumed to take the form:

$$w = \sum_{m=1}^{M} \left[f_1(\eta)\, w_i + f_2(\eta)\frac{\partial w_i}{\partial \eta} + f_3(\eta) w_j + f_4(\eta)\frac{\partial w_j}{\partial \eta} \right]_m \cdot Y_m(\xi) \qquad (1.1)$$

in which the functions f_1 through f_4 are suitable cubic polynomials (Hermitian functions of the first order), and Y_m are beam vibration modes (beam functions) for a beam having the same "type" of edge fixity as the actual plate (simply supported, clamped, or free) at the edges in the η

direction. In matrix form, this can be written as:

$$\omega = [N]\{\delta\} = \sum_{m=1}^{M} [N]_m \{\delta\}_m ,$$

in which $\{\delta\}_m = \{\omega_i, \frac{\partial \omega_i}{\partial \eta}, \omega_j, \frac{\partial \omega_j}{\partial \eta}\}_m^T$.

The curvatures of the plate strip can then be obtained as:

$$\{\chi\} = \{-\frac{\partial^2}{\partial \eta^2}, -\frac{1}{l_i^2}\cdot\frac{\partial^2}{\partial \xi^2}, \frac{2}{l_i}\frac{\partial^2 \omega}{\partial \eta \partial \xi}\}^T = [B]\{\delta\}$$

$$= \sum_{m=1}^{M} [B]_m \{\delta\}_m ,$$

where $l_i = a$ for the rectangular strip and $l_i = r_i \alpha$ for the sectorial strip. The bending and twisting moments are thus:

$$\{MB\} = \{M_x, M_y, M_{xy}\}^T = [D][B]\{\delta\}$$

$$= \sum_{m=1}^{M} [D][B]_m \{\delta\}_m ,$$

in which $[D]$ is a property matrix that may be a function of the spatial coordinates η and ξ. The stiffness matrix of the plate strip can now be obtained from the well-known relationship [9]

$$[K]^e = \int_0^1 \int_0^{d_i} [B]^T [D][B]\, d\eta\, d\xi$$

$$= \sum_{m=1}^{M}\sum_{n=1}^{M} \int_0^1 \int_0^{d_i} [B]_m^T [D][B]_n \, d\eta\, d\xi . \qquad (1.2)$$

For a rectangular strip simply-supported at both ends, the above series uncouples considerably reducing the storage and computations required for the solution.

The consistent mass matrix for the strip can also be obtained using the relationship [9]:

$$[M]^e = \int_0^1 \int_0^{d_i} \rho h\, [N]^T [N]\, d\eta . d\xi$$

$$= \sum_{m=1}^{M} \sum_{n=1}^{M} \int_0^1 \int_0^{d_i} \rho h\, [N]_m^T [N]_m\, d\eta . d\xi \qquad (1.3)$$

Finally, the eigenvalue matrix

$$([K] - \omega^2 [M])\{\delta\} = 0, \qquad (1.4)$$

in which $[K]$ and $[M]$ are the assembled stiffness and mass matrices for the whole structure, can be constructed and solved for the eigenvalues and eigenvectors of the problem.

The method has the advantage of using only relatively small matrices (compared to those required for a Finite Element solution) thus requiring small core storage and little time for execution of problems. It is especially advantageous for plates with two opposite edges simply-supported, since in such a case the series uncouples and the matrices are reduced even further. The major short-coming of the method is that it is limited to structures having simple continuous properties and boundary conditions in at least one direction. In addition, in its present form the method yields relatively poor results if the strips have free ends,

and stresses obtainable in that case are incorrect.

1.3 The Finite Layer Method

The finite strip method is an extension of the well-known finite element method and the newly developed finite strip method, and was first used by Cheung and Chakrabarti [10] in 1971. Essentially, the approach incorporates the reduction of a three-dimensional problem to a one-dimensional problem. This is achieved by requiring the three dimensional solid to be divided into a number of layers one on top of the other. Orthogonal function series which satisfy the fundamental boundary conditions are selected in the plane of the layers (the x-y plane), while in the z-direction, a polynomial with undetermined coefficients is used - figure (1.2).

Thus the displacements u, v and w of a layer are assumed to be of the form:

$$u = \sum_{m=1}^{r} \sum_{n=1}^{s} [(1-\frac{z}{c})\ u^1_{mn} + (\frac{z}{c})\ u^2_{mn}] X'_m(x)\ Y_n(y),$$

$$v = \sum_{m=1}^{r} \sum_{n=1}^{s} [(1-\frac{z}{c})\ v^1_{mn} + (\frac{z}{c})\ v^2_{mn}] X_m(x)\ Y'_n(y), \qquad (1.5)$$

$$w = \sum_{m=1}^{r} \sum_{n=1}^{s} [(1-\frac{z}{c})\ w^1_{mn} + (\frac{z}{c})\ w^2_{mn}] X_m(x)\ Y_n(y),$$

in which u^1_{mn}, u^2_{mn}, v^1_{mn}, ... etc. refer to the displacement parameters and $X_m(x)$, $Y_n(y)$, $X'_m(x)$, $Y'_n(y)$ are beam functions.

and their first derivatives. Notice that $X'_m(x)$, $Y'_n(y)$ are incorporated in the expressions for u and v respectively because of the relationships $u=A\ \partial w/\partial x$ and $v=B\ \partial w/\partial y$ in thin plate theory, and they are used as an approximation for each individual layer.

The displacement matrix can then be written as

$$\{u\ v\ w\}^T = \sum_{m=1}^{r} \sum_{n=1}^{s} N_{mn}\ \delta^e_{mn} = N\ \delta^e,$$

in which

$$\delta^e_{mn} = \{u^1_{mn}\ v^1_{mn}\ w^1_{mn}\ u^2_{mn}\ v^2_{mn}\ w^2_{mn}\}^T$$

The strain matrix of a three dimensional solid is

$$\{\varepsilon\} = \sum_{m=1}^{r} \sum_{n=1}^{s} B_{mn}\ \delta^e_{mn} = B.\ \delta^e$$

The stress-strain relationships are

$$\sigma = D\varepsilon = \sum_{m=1}^{r} \sum_{n=1}^{s} D\ B_{mn}\ \delta^e_{mn} = D\ B\ \delta^e$$

in which the stress matrix σ is

$$\sigma = \{\ \sigma_x\ \sigma_y\ \sigma_z\ \tau_{xy}\ \tau_{yz}\ \tau_{zx}\ \}^T,$$

and D is the elasticity matrix for the material of the layer.

The stiffness matrix of the layer can then be easily obtained from the well known relationship:

$$K^e = \int_{vol} B^T\ D\ B\ d(vol)$$

The formula for deriving the mass matrix is also standard

$$M^e = \int_{vol} \rho N^T N \, d(vol),$$

where ρ is the material density of the layer which, generally, does not need to be uniform over the area of the layer.

The final eigenvalue matrix is

$$(K - \omega^2 M)\, \delta = 0,$$

in which K and M are the assembled stiffness and mass matrices of the layered plate, and ω is the circular frequency.

The Finite Layer method has the advantage of being applicable to thick, multilayered plates with varying material properties such as composites and sandwiches. It has the disadvantage, however, of being limited to plates of simple shape and boundary conditions for which the standard Ritz method can be applied. The method has also been used for the analyses of thick cylinders.

1.4 The Super (Large) Finite Elements - Matrix Partitioning

On attempting to solve large Finite Element (and Finite difference) problems on small size computers, many matrix partitioning techniques have been devised. While some of those techniques have been based upon purely mathematical considerations, the majority are related, in one way or another, to some physical operations. One of the widely applied techniques of this category is "substructuring" [11]. In this technique, the structure is first divided into Finite Elements in the usual manner using a

large number of nodes and elements. The Finite Element model is then subdivided into a number of "sub-structures" inter-connected through a relatively small number of nodes lying on the separation surfaces as shown in figure (1.3).

The total degrees of freedom of the structure $\{u_f\}$ are partitioned into two sets; $\{u_a\}$ or the "analysis" set of coordinates which must include *all* the degrees of freedom at the separation surfaces, and $\{u_o\}$ or the "omitted" degrees of freedom which includes the rest of the coordinates. Thus:

$$\{u_f\} = \left\{\begin{matrix} u_a \\ \hline u_o \end{matrix}\right\} .$$

Consequently, the equilibrium equations - in the case of a static problem - can be written as:

$$\left[\begin{array}{c|c} K_{aa} & K_{ao} \\ \hline K_{ao}^T & K_{oo} \end{array}\right] \left\{\begin{matrix} u_a \\ \hline u_o \end{matrix}\right\} = \left\{\begin{matrix} P_a \\ \hline P_o \end{matrix}\right\} \qquad (1.6)$$

After rearranging, the bottom half of this equation becomes:

$$[K_{oo}]\{u_o\} = \{P_o\} - [K_{ao}]^T \{u_a\}.$$

Solving for $\{u_o\}$ and substituting into the top half of *(1.6)* it finally yields:

$$[\bar{K}_{aa}]\{u_a\} = \{\bar{P}_a\} \qquad (1.7)$$

where:

$$[\bar{K}_{aa}] = [K_{aa}] + [K_{ao}]\,[G_o],$$

$$\{\bar{P}_a\} = \{P_a\} + [G_o]^T \{P_o\},$$

in which $[G_o] = -[K_{oo}]^{-1}[K_{ao}]^T$, and, since the inversion of the stiffness matrix $[K_{oo}]$ is an inefficient operation, it is practically obtained by solving the equation:

$$[K_{oo}]\,[G_o] = -[K_{ao}]^T,$$

where the matrix $[K_{oo}]$ is decomposed into upper and lower triangular factors, and $[K_{ao}]^T$ is then treated as a set of load vectors in order to generate $[G_o]$ column by column.

Equation (1.7) is then solved for $\{u_a\}$, after which $\{u_o\}$ is obtained from

$$\{u_o\} = \{u_o^o\} + [G_o]\,\{u_a\} \qquad (1.8)$$

where $\{u_o^o\}$ is the solution of

$$[K_{oo}]\,\{u_o^o\} = \{P_o\}.$$

Due to the particular choice of $\{u_a\}$ to be lying on the inter-connecting boundaries, the matrix $[K_{oo}]$ uncouples into several sub-matrices representing the different regions (or sub-structures) such that:

$$[K_{oo}] = \begin{bmatrix} K_{oo}^{(1)} & 0 & 0 & 0 \\ 0 & K_{oo}^{(2)} & 0 & 0 \\ 0 & 0 & K_{oo}^{(3)} & 0 \\ 0 & 0 & 0 & etc. \end{bmatrix}$$

Consequently, the reduced stiffness matrix $[\bar{K}_{aa}]$ and load vector $[\bar{P}_a]$ can be generated separately for each individual sub-structure and then summed for the overall structure such that:

$$[\bar{K}_{aa}] = \sum_i [\bar{K}_{aa}^{(i)}] ,$$

$$\{\bar{P}_a\} = \sum_i \{\bar{P}_a^{(i)}\}$$

where $[\bar{K}_{aa}^{(i)}] = [\bar{K}_{ao}^{(i)}]\ [G_o^{(i)}] + [K_{aa}^{(i)}]$,

and $\{\bar{P}_a^{(i)}\} = \{P_a^{(i)}\} + [G_o^{(i)}]\ \{P_o^{(i)}\}$.

It can be seen from the above equations that in no instance will it be necessary to deal with a matrix larger in order, or in band width, than the largest of $[K_{oo}^{(i)}]$ or $[\bar{K}_{aa}]$. This can result in a considerable reduction in the computing time and the required storage capacity. In addition, the sub-structuring procedure may prove advantageous for purely logistic reasons in problem operation. The task of preparing the mathematical model of the structure may be assigned to separate groups which work at different places, times, or rates with a minimal amount of interaction between the groups.

While the above-mentioned technique is applicable only for static problems, similar techniques (such as the Guyan reduction) can be used for dynamic problems [11]. When used in dynamics, however, certain approximations are involved restricting the freedom in the choice of the member of the a-set degrees of freedom and resulting in some loss of accuracy.

The concept of the "super" Finite Element is basically a form of sub-structuring which permits the formation of one large element which internally includes a number of

ordinary Finite Elements with the internal degrees of freedom condensed in terms of those of the boundary nodes as described above. As before, these elements can only be used for static analysis. However, with some approximation and restriction as to the size of the elements, they may also be used for dynamic problems through the use of the Guyan reduction technique.

In a recently developed Large Finite Element technique [12,13], a combined Finite Element and Finite Difference approach is used. The method is similar in concept to the sub-structuring technique described above inasmuch as the stiffness matrix for each sub-structure (large element) is constructed separately and then condensed in terms of the boundary degrees of freedom. The condensed stiffness matrices for the different large elements are then assembled and the resulting global matrix solved for the loading condition (only static loading can be handled). In the method of references [12,13], however, central Finite Difference equations are used for the derivation of the non-condensed stiffness matrix for the Large Finite Element. The Finite Element type-boundary degrees of freedom are then related to the Finite Difference mesh displacements using forward (or backward) Finite Differences and condensation performed in the regular manner. Several approximations have to be made during the construction of the element stiffness matrix to improve its accuracy and avoid the non-symmetry which ordinarily results from Finite Difference derived stiffness

matrices.

While the method of references [12,13] may be considered as an improvement over the conventional Finite Difference approach permitting the convenient accommodation of discontinuities and natural boundary conditions in static plate bending problems, it is not obvious, however, if the method bears any advantages over the conventional Finite Element approach with sub-structuring. Compared to sub-structuring, this approach has the disadvantage of restricting the geometry of the element to simple rectangular and right-angle plates with equally spaced edge nodes. It is also felt that poorer accuracy would result from this approach since it is the experience of the writer that Finite Element analyses usually yield better results than the equivalent conventional Finite Difference solutions. No estimate was given in [12,13] for the relative accuracy of the results obtained compared to conventional approximate approaches.

1.5 A Recent Extension for the Ritz Method

It has been said that there is no method having the simplicity, flexibility, and generality equal to the Ritz method, at least for one-dimensional problems [14]. However, when the Ritz method is applied to two or three dimensional problems it is not so straightforward, especially when a complicated boundary configuration is involved. Since many engineering problems are of this type, which are virtually

beyond the realm of applicability of the classical Ritz method, discrete coordinate methods (such as Finite Elements and Finite Differences) are usually recommended for the solution of these problems. Undoubtedly, this may be necessary for those structures which are immensely complicated. However, an examination of many common structures may reveal that they are basically simple structures except for slight complications which are more or less local in nature. It is for this class of problems that the extended Ritz method presented in reference [14] may prove most useful.

In this method, a given structure is divided into two main parts; (1) a simple basic structure, and (2) any modifications which contribute to its complexity. The former, (1), is regarded as a "reference structure", and the latter (2), are taken into account through Lagrangian generalized forces acting on the reference structure.

A region R_A whose boundary Γ_A is simple - i.e. natural to some standard coordinate systems, such as a rectangle in the case of a two dimensional cartesian coordinate system - is assumed to represent the reference structure. The eigenvalue problem:

$$L\psi_i = \lambda_i \psi_i \text{ in } R_A, \qquad \psi_i = 0 \text{ on } \Gamma_A \tag{1.9}$$

is assumed to be easily soluble with λ_i and ψ_i as its i^{th} eigenvalue and eigenfunction respectively. In equation (1.9) L is assumed to be a real self-adjoint positive definite elliptic operator, and the boundary conditions are taken to be of the Dirichlet type for simplicity. Considering u to

be a virtual displacement imposed upon the structure, it can be verified that the total energy in the structure (E) may be given by

$$E = {}^1/_2\ (Lu,u) + {}^1/_2\ (\rho\ddot{u},u) - (P,u), \qquad (1.10)$$

where $(,)$ denotes an inner product, P and ρ represent the external transverse forces and mass density respectively, and the dots denote the time derivatives. It is also assumed that u has the following representation:

$$u = \sum_{i=1}^{\infty} \psi_i \cdot q_i(t) \qquad (1.11)$$

where $q_i(t)$ is usually a complex exponential function allowing a closed form integration in the time domain.

Many physical problems having regions R_B which are irregular may be considered as generated by cutting one or more subregions R_C off the region R_A described above such that $R_B \subset R_A$. To solve the corresponding problem for the region R_B, the same representation in *(1.11)* can be used provided that the functional in *(1.10)* is modified to subtract the energy in the regions R_C such that:

$$\bar{E} = {}^1/_2\ (Lu,u) + {}^1/_2\ (\rho\ \ddot{u},\ \dot{u}) - (P,u)_B - \sum_k W_k \qquad (1.12)$$

where W_k represents the virtual work contributed by the k^{th} region of R_C and $(\ ,\ )_B$ denotes the inner product for region R_B. The formulation of W_k depends upon the nature of the problem and has to be derived separately for each individual problem. The following two special cases have been formulated in [14]:

1) In the case of holes or cavities in the interior, the virtual work W_k can be given by

$$W_k = {}^1/_2 (Lu,u)_{C_k} + {}^1/_2 (\rho\ddot{u},u)_{C_k} \qquad (1.13)$$

where $(\ ,\ )_{C_k}$ denotes the inner product in the k^{th} sub-region C_k of R_c. Clearly, any partial reduction can be accounted for by the difference in energy contributions. On the other hand, any local *thickening* can be treated as a "negative" reduction of thickness and accounted for by an energy of the opposite sign.

2) In the case of an irregular boundary, the homogeneous boundary condition $u(\Gamma_A) = 0$ must be constrained into the homogeneous boundary condition $u(\Gamma_B) = 0$. This can be achieved by imposing distributed forces of unknown intensity throughout the region R_c such that the displacements there vanish at all times. These unknown forces are represented by an infinite set of Lagrangian multipliers θ_k, and the vanishing displacements in R_c by an infinite power series such that in the two dimensional case:

$$u_k = \sum_m x^{k-1} \cdot y^{k-1} \cdot \psi_m \, q_m(t) \qquad (1.14)$$

hence

$$W_k = \theta_k \sum_m q_m \cdot C_k^m , \qquad (1.15)$$

where

$$C_k^m = \int_{R_c} x^{k-1} \cdot y^{k-1} \cdot \psi_m \cdot dR_c .$$

Despite the usefulness of the method and the simplicity of the approach, it may be subject to the following criticism:

- The expression for W_k has to be formulated independently for each problem. This precludes the possibility of having a unified treatment for a wide class of problems as it is the case with the Finite Element method, for example, which allows the preparation of a general purpose program that can be used for almost any kind of structural configuration.
- The reference structure has to be one for which the associated eigenvalue problem can be easily solved. As a result, the method has exclusively been applied to simply supported structures (plates, cylinders, and membranes). It is therefore questionable whether the method could be conveniently used for structures having other boundary conditions, e.g. a cantilevered plate with a hole.
- No consideration for the boundary conditions at the edges of an internal cavity is taken into account. While there may be grounds to believe that this is unnecessary if those edges were under natural boundary conditions, this will obviously lead to errors if those boundaries were clamped, for example.
- Judging by the only comparative results presented in [14], comparing the natural frequencies obtained for a simply-supported stiffened cylindrical shell with those obtained by eight other approaches, the accuracy of the method is questionable. In some instances the solutions were more than 30% higher than those obtained

by the other approaches. In addition, no improvement (within the full number of significant figures published) was achieved when the determinant size used for the solution was doubled. This indicates that either the solution obtained is exact to the full number of significant figures published (which is doubtful), or that no appreciable improvement can be achieved by increasing the number of terms in the solution series.

1.6 Modified Finite Differences with Mixed Formulations

In an attempt to develop an "ideal" numerical process, A. Noor and others [15] recently proposed a modified finite difference approach utilizing both stress and displacement parameters as its fundamental unknowns. These unknowns are chosen to simplify both the form of the governing equations and the treatment of boundary, discontinuity, and interface conditions. In the case of a linear three-dimensional anisotropic solid, the fundamental unknowns are chosen to be the three components of the displacement field $\{u\}$ and the six independent components of the stress field $\{\sigma\}$.

The governing equations for the static behaviour of the solid include:

i) the three equations of equilibrium

$$[L_1]\ \{\sigma\} = \{P\}, \qquad (1.16)$$

and ii) the six constitutive relations expressed in terms

of displacement gradients and stresses

$$[L_2]\{u\} = [F]\{\sigma\} \quad \{\varepsilon_o\} \qquad (1.17)$$

where $[L_1]$ and $[L_2]$ are linear first order differential operators, $[F]$ is the matrix of elastic compliances, $\{P\}$ is the vector of body forces, and $\{\varepsilon_o\}$ is the vector of initial and thermal strains.

For Cartesian coordinates $[L_1] = [L_2]^T$, and the governing equations can be arranged in a symmetric matrix as follows:

$$\begin{bmatrix} -F & L \\ L^T & O \end{bmatrix} \begin{Bmatrix} \sigma \\ u \end{Bmatrix} = \begin{Bmatrix} \varepsilon_o \\ P \end{Bmatrix} \qquad (1.18)$$

Unlike the governing equations for the displacement formulation, the above equations are free of the derivatives of the elastic characteristics of the solid and contain no derivatives of the fundamental unknowns higher than the first.

Due to the simplicity of the form of the above equations, the derivation of this formulation is simplified. This is particularly true for systems with complicated configurations where non-orthogonal coordinates have to be used; or in the presence of spatial or time variations of the system properties due to, for example, non homogeneities or temperature dependent elastic properties.

In this process, a modified finite difference scheme is used for the discretization of the above mixed first-order differential equations. The basic characteristic of the modified finite difference scheme is that the first

derivatives of the fundamental unknowns are defined at points lying midway between the points of definition of the same functions. This is accomplished by using sets of interlacing grids for the different fundamental unknowns. Consequently, subsets of the governing differential equations are satisfied at different sets of points consistent with the control points for the fundamental unknowns.

It can be shown that with a proper selection of nodes, elements, and interpolation functions, hybrid-type finite elements can lead to formulations identical to those obtained by the above approach.

The modified finite difference equations representing the above system of equations *(1.18)* are obtained by replacing the first derivatives in these equations by their appropriate difference-quotients depending upon the order of approximation desired. Central differences are used at interior points, and backward (or forward) unsymmetric differences are used at points lying on or near the boundaries. The number of such specialized unsymmetric difference formulae is dependent upon the order of approximation of the central differences used in the interior.

The following advantages may be claimed for the above mentioned procedure:

- Simplicity of formulation and ease of treatment of boundary, discontinuity, and interface conditions. The simplicity of the governing equations also provides flexibility for easily improving or modifying

the discretization techniques. Consequently, the use of any or all of the following improved techniques becomes feasible:

i) Use of the modified finite differences.

ii) Use of variable and non-orthogonal networks.

iii) Use of higher-order difference-quotients for the discretization.

- Accuracy of stress predictions even in the presence of steep gradients or singularities. The absence of the derivatives of the elastic characteristics of the medium in the governing equations, and the derivatives of the fundamental variables in the boundary conditions, contributes considerably to the increased accuracy of the method compared to the standard finite difference techniques, since no approximation for the gradients of these quantities is involved.
- The method is versatile and expandable to other problem areas such as incompressible materials and viscoelastic analysis.

Despite the above-mentioned advantages, the method suffers from the following major difficulties:

- The increase in the number of degrees of freedom used in the mixed formulation results in a substantial increase in the number of simultaneous equations and their corresponding band-width for the same mesh size. This is particularly true in the case of branched structures where the discontinuity of the stress com-

ponents requires the introduction of additional unknowns (as compared to stiffness finite elements). This latter difficulty, however, is also encountered with ordinary finite differences.

- The governing equations *(1.18)* and the resulting matrix are not positive definite. This complicates the numerical solution and precludes the use of many of the efficient solution algorithms.
- As compared to conforming finite elements, the method has the disadvantage of not bounding the exact solutions. Again, this applys to all finite difference solutions.

FIG. (1-1)

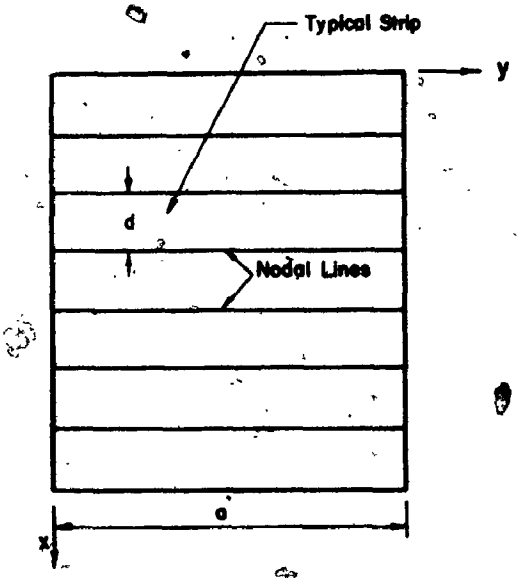

(a) TOP VIEW OF IDEALIZED STRUCTURE WITH ANY BOUNDARY CONDITIONS

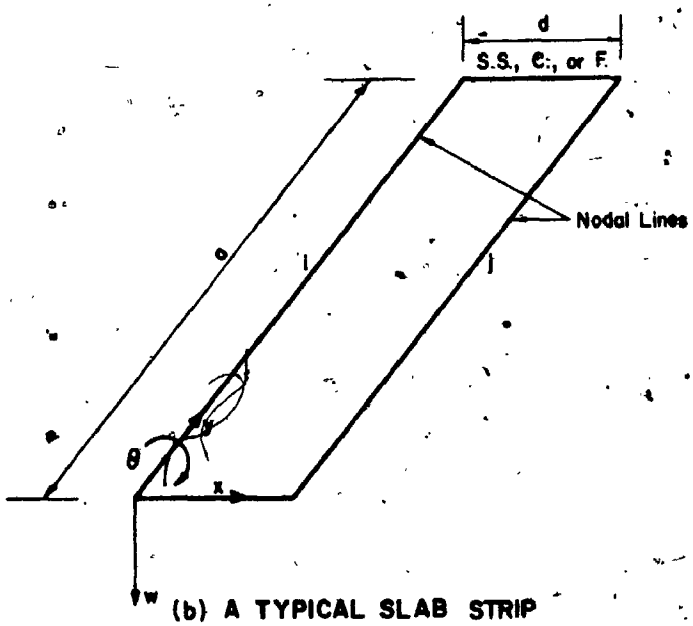

(b) A TYPICAL SLAB STRIP

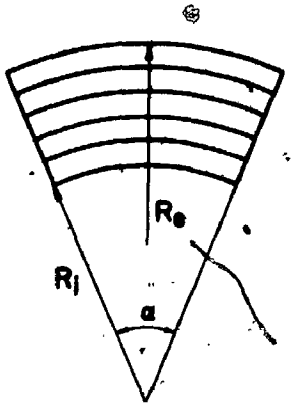

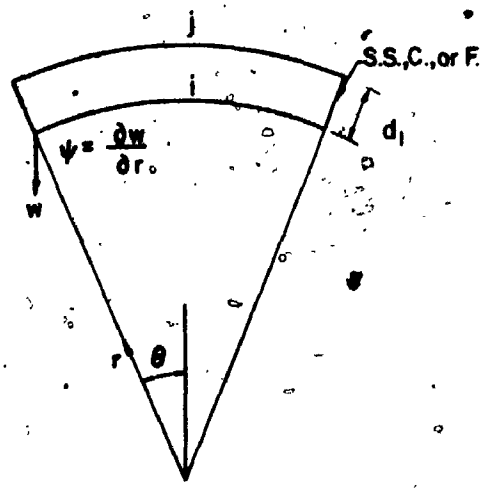

(C) SECTOR PLATE WITH ANY BOUNDARY CONDITIONS

(d.) A CURVED STRIP

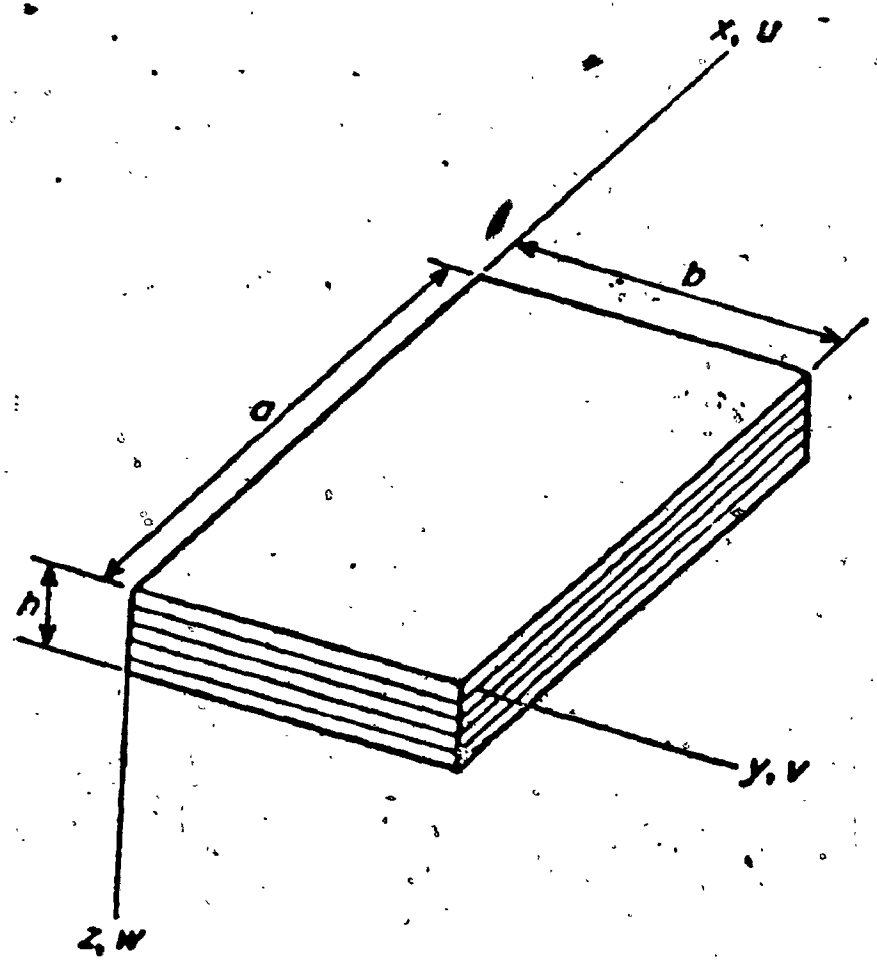

(a)

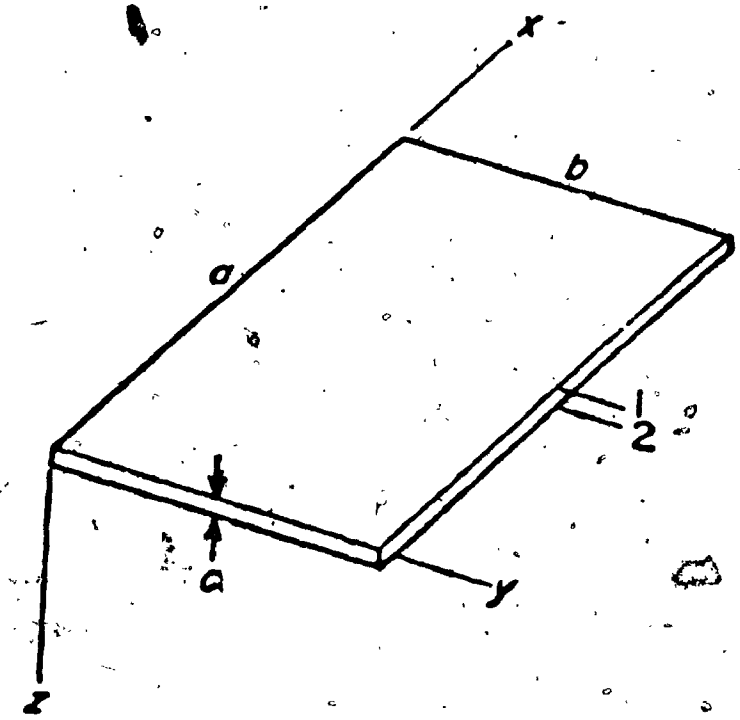

(b)

Figure 1.2(a) Assemblage of elements. (b) An element.

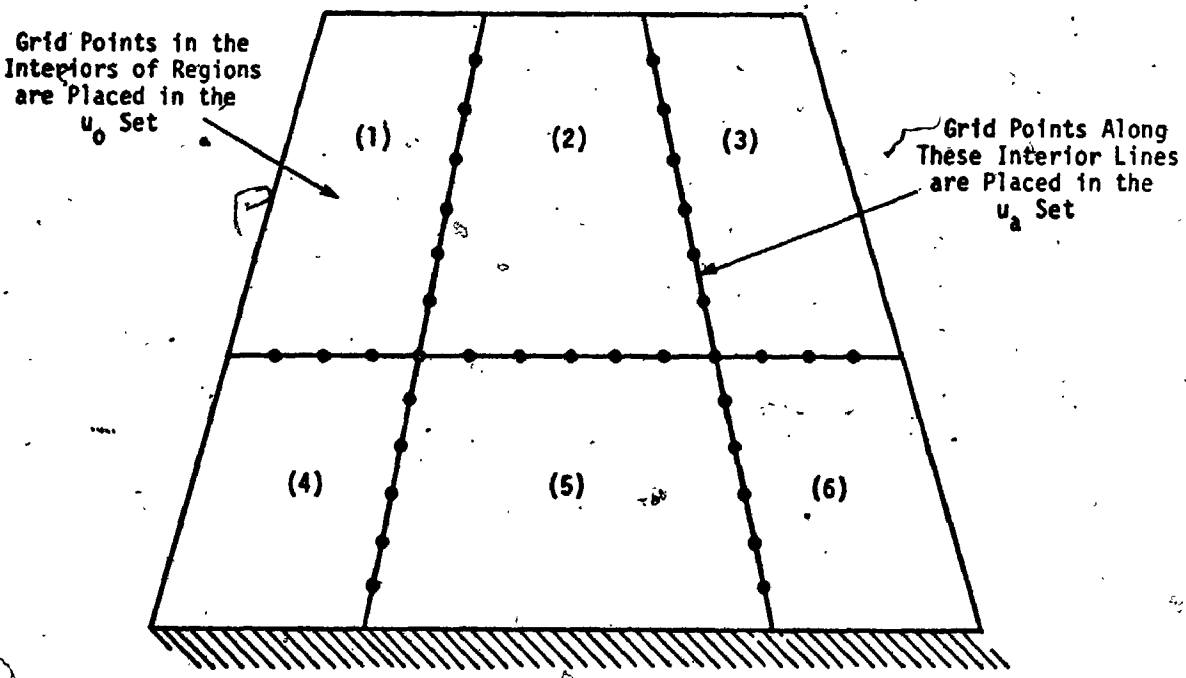

Figure(1.3)Use of partitioning to decouple regions of the structure.

CHAPTER II

ON THE COMPLETENESS REQUIREMENTS FOR THE RITZ METHOD

2.1 Ritz's Variational Procedure

Solutions for a wide class of differential equations resulting from physical problems can be obtained through the variation of certain associated integral expressions. Often the variational process bears a definite physical meaning, such as the minimization of the energy of the system; however, in general they can be derived through purely mathematical considerations.

Let it be considered for illustration purposes, without loss of generality, the two-dimensional variational equation

$$\delta\left[\iint_D L\,(u,x,y)\,dx\,dy\right] = 0, \qquad (2.1)$$

where u is the main (dependent) variable, x and y are the spatial (independent) variables, D is the domain under consideration, and L is a differential operator. This equation indicates that the exact solution for the problem $u^*(x,y)$ must render the bracketed integral stationary, i.e. give it its absolute minimum or maximum value (m). It is clear that if a function $\bar{u}(x,y)$ could be constructed,

which satisfies certain continuity conditions as well as the essential boundary conditions for the problem, and for which the value of the integral is very close to its minimum (stationary) value (m), it could be expected that $\bar{u}(x,y)$ would be a good approximation to the true solution of the problem. If, moreover, it was possible to find a minimizing sequence $\bar{u}_n$, i.e. a sequence of n functions satisfying the essential boundary and continuity conditions (which will be defined in the following section), and for which the value of the integral tends to (m) as $n \to \infty$, there would be grounds for expecting such a sequence to converge, in one sense or another, to the solution.

For the actual determination of the function $\bar{u}(x,y)$ giving the integral mentioned above a value close to the minimal one, W. Ritz in 1908 proposed this device:

Let a family of functions depending on several independent parameters be considered

$$u_n = \Phi\ (x, y, a_1, a_2, \ldots, a_n) \qquad (2.2)$$

such that for all values of the parameters the essential continuity and boundary conditions are satisfied. Now, limiting the class of admissible functions to the functions of the family (2.2), substituting it into the variational expression (2.1), and performing the necessary differentiations and integrations, the result is a function of the n variables $a_1, a_2, \ldots, a_n$:

$$\delta[F\ (a_1, a_2, \ldots, a_n)] = 0,$$

which, due to the fundamental lemma of variational calculus, makes it necessary to have

$$\frac{\partial F}{\partial a_i} = 0, \qquad i = 1, 2, \ldots, n \qquad (2.3)$$

This is a system of n algebraic equations which is, generally speaking, sufficient to obtain definite values of the parameters $\bar{a}_1, \bar{a}_2, \ldots, \bar{a}_n$ giving the function $F(a_1, a_2, \ldots, a_n)$ its absolute minimum (or maximum). On choosing the function in family (2.2) corresponding to these values of the parameters, the required approximate solution would thus be obtained such that:

$$\bar{u}(x,y) = \phi(x,y,\bar{a}_1,\bar{a}_2,\ldots,\bar{a}_n)$$

It should be remarked that in most practical cases, the actual process of determining this approximate solution turns out, as will be seen in later sections, to be very simple. The fact is that in the most important cases the integral in (2.1) is quadratic in u, and family (2.2) is taken to depend *linearly* on the parameters $a_1, a_2, \ldots, a_n$. As a consequence of this, the conditions (2.3) prove to be a set of linear equations in $a_1, a_2, \ldots a_n$.

2.2 Variational Problems Connected with the Biharmonic Equations

A number of problems in the theory of elasticity lead to different boundary-value problems for the biharmonic equation*

*Note that only the homogeneous equation $\Delta\Delta u = 0$ is ordinarily called biharmonic.

$$\Delta\Delta(u) \equiv \frac{\partial^4 u}{\partial x^4} + 2\,\frac{\partial^4 u}{\partial x^2 \partial y^2} + \frac{\partial^4 u}{\partial y^4} = P(x,y) \qquad (2.4)$$

in which u may represent the flexure of a plate laterally loaded by the load P or the Airy stress function in a plane stress or plane strain problem, and Δ is the Laplacian operator. The equation may also represent the flexural vibration of a plate, in which case the load P will be proportional to the displacement u.

With this equation is connected the problem of the minimum of the integral

$$U = \iint_D \left[(\Delta u)^2 - 2(1-\nu)\left[\frac{\partial^2 u}{\partial x^2}\,\frac{\partial^2 u}{\partial y^2} - \left(\frac{\partial^2 u}{\partial x \partial y}\right)^2 \right] - 2Pu \right] dx\,dy -$$

$$-2\int_\Gamma q(s)u\,ds + 2\int_\Gamma m(s)\frac{\partial u}{\partial n}\,ds, \qquad (2.5)$$

where D is the domain under consideration surrounded by the contour Γ; s and n are unit vectors along and normal to the boundary Γ and ν, q and m are quantities related to the natural boundary conditions of the problem.

Following the idea of Ritz, a solution is sought in the form $u_m = \sum_{k=1}^{m} a_k \phi_k(x,y)$.

For the determination of the constants a_k, substituting the expression for u_m in place of u in (2.5) and equating to zero the derivative with respect to a_r, the following set of equations is obtained:

$$\iint_D \left[\Delta u_m \Delta \phi_r - (1-\nu)\left(\frac{\partial^2 u_m}{\partial x^2}\,\frac{\partial^2 \phi_r}{\partial y^2} + \frac{\partial^2 u_m}{\partial y^2}\,\frac{\partial^2 \phi_r}{\partial x^2} - 2\,\frac{\partial^2 u_m}{\partial x \partial y} \right.\right.$$

$$\Delta\Delta(u) \equiv \frac{\partial^4 u}{\partial x^4} + 2\,\frac{\partial^4 u}{\partial x^2 \partial y^2} + \frac{\partial^4 u}{\partial y^4} = P(x,y) \qquad (2.4)$$

in which u may represent the flexure of a plate laterally loaded by the load P or the Airy stress function in a plane stress or plane strain problem, and Δ is the Laplacian operator. The equation may also represent the flexural vibration of a plate, in which case the load P will be proportional to the displacement u.

With this equation is connected the problem of the minimum of the integral

$$U = \iint_D \left[(\Delta u)^2 - 2(1-\nu)\left[\frac{\partial^2 u}{\partial x^2}\,\frac{\partial^2 u}{\partial y^2} - \left(\frac{\partial^2 u}{\partial x \partial y}\right)^2 \right] - 2Pu \right] dx\,dy -$$

$$-2\int_\Gamma q(s)u\,ds + 2\int_\Gamma m(s)\frac{\partial u}{\partial n}\,ds, \qquad (2.5)$$

where D is the domain under consideration surrounded by the contour Γ; s and n are unit vectors along and normal to the boundary Γ and ν, q and m are quantities related to the natural boundary conditions of the problem.

Following the idea of Ritz, a solution is sought in the form $u_m = \sum_{k=1}^{m} a_k \Phi_k(x,y)$.

For the determination of the constants a_k; substituting the expression for u_m in place of u in (2.5) and equating to zero the derivative with respect to a_r, the following set of equations is obtained:

$$\iint_D \left[\Delta u_m \Delta\Phi_r - (1-\nu)\left(\frac{\partial^2 u_m}{\partial x^2}\,\frac{\partial^2 \Phi_r}{\partial y^2} + \frac{\partial^2 u_m}{\partial y^2}\,\frac{\partial^2 \Phi_r}{\partial x^2} - 2\,\frac{\partial^2 u_m}{\partial x \partial y}\right.\right.$$

$$\frac{\partial^2 \Phi_r}{\partial x \partial y}\Big) - P\Phi_r\Big] dxdy - \int_\Gamma q(s)\Phi_r\, ds + \int_\Gamma m(s)\,\frac{\partial \Phi_r}{\partial n}\, ds = 0$$

$$(r = 1, 2, \ldots . m) \qquad (2.6)$$

On transforming this expression by integrating twice by parts - assuming that no free corners exist - it can be brought into the form:

$$\iint_D [\Delta\Delta(u_m) - P]\Phi_r\, dxdy + \int_\Gamma [M(u_m) + m(s)]\,\frac{\partial \Phi_r}{\partial n}\, ds -$$

$$- \int_\Gamma [Q(u_m) + q(s)]\Phi_r\, ds = 0$$

$$(r = 1, 2, \ldots, m) \qquad (2.7)$$

where

$$M(u_m) = \nu\Delta u_m + (1-\nu)\Big(\frac{\partial^2 u_m}{\partial x^2} x_n^2 + 2\frac{\partial^2 u_m}{\partial x \partial y} x_m y_m + \frac{\partial u_m}{\partial y^2} y^2 n$$

$$Q(u_m) = \frac{\partial}{\partial_n}\Delta u_m + (1-\nu)\frac{\partial}{\partial_s}\Big[\frac{\partial^2 u_m}{\partial x^2} x_n x_s + \frac{\partial^2 u_m}{\partial x \partial y}(x_n y_s + \qquad (2.8)$$

$$+ x_s y_n) + \frac{\partial^2 u_m}{\partial y^2} y_n y_s\Big]$$

in which $x_n y_n$ and $x_s y_s$ denote the direction cosines of the normal and the tangent.

For generality, consider the solution for the case of mixed boundary conditions. Consider the boundary Γ to be divided into two parts; Γ_c along which the boundary conditions are: $u = 0,\ \frac{\partial u}{\partial n} = 0$ on Γ_c, (2.9)

which represents a "clamped" portion in the case of plate

and

$$M(u_m) + m(s) = 0, \quad Q(u_m) + q(s) = 0 \text{ on } \Gamma_f.$$

Consequently, the Ritz solution will converge towards satisfying both the differential equation *(2.5)* and the natural boundary conditions along the free boundary Γ_f by *(2.10')*. Hence, the important result is that pre-satisfaction of the natural boundary conditions is not necessary. The solution will automatically converge towards satisfying the conditions along the free portions of the boundary; i.e. those portions which are not subjected to other forced boundary conditions regarding the main variable and/or its first derivatives. In other words, solving the variational equation for a problem is equivalent to satisfying both the corresponding differential equation and the natural boundary conditions.

2.3 Sufficient Conditions for the Convergence of the Ritz Solution

In this section, conditions which are sufficient to ensure convergence of the solution obtained by the Ritz method towards the exact solution of the problem will be stated. No proofs will be quoted, however, the reader may find such in standard variational calculus texts (for example see Kantorovitch's monograph [6]).*

Firstly: Each member of the assumed family of functions must satisfy the *fundamental* boundary conditions imposed upon the system. The fundamental boundary conditions are those which

* These conditions are paraphrased from [6].

are not *natural* with respect to the problem on hand. For example, in the case of a biharmonic equation, the fundamental boundary conditions are those associated with the fundamental variable itself or its derivatives of the first order. Boundary conditions concerning higher order derivatives are considered natural w.r.t. the problem as was shown in section (2.2).

Secondly: The assumed functions must be continuous, together with their *fundamental* derivatives, within the assumed domain. They should possess only a finite number of discontinuities in their higher derivatives. Again, the fundamental derivatives here are those of the first order in the case of a biharmonic equation; i.e. those for which the boundary conditions must be satisfied.

Thirdly: The assumed set of trial functions must be *complete* both within the domain and at those portions of the boundary which are subject to natural (free) boundary conditions:

a) By the condition of completeness within the domain "D", in the case of a biharmonic equation, it is meant that whatever be an admissible function $u(x,y)$ which satisfies conditions 1 and 2 above, and whatever be the positive number $\epsilon > 0$, it is possible to indicate an n, and a function of the nth family u^*_n such that the following inequalities will be valid everywhere in the region D:

$$|u^*_m - u| < \varepsilon, \quad \left|\frac{\partial u^*_n}{\partial x} - \frac{\partial u}{\partial x}\right| < \varepsilon, \quad \left|\frac{\partial u^*_n}{\partial y} - \frac{\partial u}{\partial y}\right| < \varepsilon, \tag{2.12}$$

$$\left|\frac{\partial^2 u^*_n}{\partial x^2} - \frac{\partial^2 u}{\partial x^2}\right| < \varepsilon, \quad \left|\frac{\partial^2 u^*_n}{\partial y^2} - \frac{\partial^2 y}{\partial y^2}\right| < \varepsilon, \quad \left|\frac{\partial^2 u^*_n}{\partial x \partial y} - \frac{\partial^2 u}{\partial x \partial y}\right| < \varepsilon$$

Note that only the first three inequalities need be satisfied in the case of a second order differential equation such as the Laplacian equation. In physical terms, there must exist the possibility of approximating - to any required accuracy - any admissible function, together with its derivatives which appear in the variational expression, with a linear combination of the assumed set of trial functions.

b) By completeness on the boundary, it is meant that the imposed natural boundary conditions at the "free" portions of the boundary can be approximated, to the desired degree of accuracy, by a linear combination of the assumed set of trial functions.

It is worth noting, however, that a limited degree of convergence may still be achieved if some of the above mentioned completeness conditions were not met. The solutions obtainable in such a case may converge towards the correct answers. Nevertheless, their derivatives of certain orders will not converge to the correct solutions. Since in most practical problems the derivatives of the solutions are of importance, indeed sometimes even more important than the fundamental variables themselves (e.g. stresses rather than displacements are often the quantities of prime importanee in a plate flexure problem), attention

will be focused only upon functions which converge to the correct answers for both the fundamental quantities and their derivatives of practical importance. Moreover, convergence of the solutions obtained with functions which do not satisfy *all* the completeness conditions mentioned above is usually considerably slower than that of functions which satisfy these conditions. For the above reasons, this type of limited convergence is considered of pure academic interest and satisfaction of all the completeness conditions mentioned previously is essential for a practically useful family of functions.

2.4 On the Non-Completeness of Beam Functions Used to Approximate Plates with Free Edges

Soon after the appearance of his fundamental memoir, Ritz published an example of the application of his method to the solution of a difficult problem concerning the vibration of a homogeneous plate with free boundaries [16]. For the trial sequence, he used a series of multiplications of the vibration modes of free beams. After Ritz, a large number of researchers - including the writer - followed the same route and used beam functions to obtain approximate solutions for a wide class of problems (e.g. free vibrations, plate stability, and recently in the finite strip and finite layer methods) covering almost all types of simple boundary conditions and, of course, including free edges [1, 8 , 10, 17 thru. 27]. Despite this vast literature and the remarkable numerical success achieved upon

the use of beam series in the case of fully supported plates, and despite the strong physical resemblance and mathematical similarity to the exact solution (whenever available), it is the author's belief that their use, in cases where free edges are involved, is not mathematically justifiable and leads to erroneous or inaccurate results. Although many articles have been written discussing the accuracy of the Ritz method and the conditions to be satisfied by the assumed series, as yet nobody - to the author's knowledge - has questioned the validity or the accuracy of a series of multiplications of beam modes when used to approximate a plate involving one or more free edges, despite the clear lack of accuracy in such solutions when contrasted with those obtained for fully supported plates. Apparently, this lack of accuracy was attributed to the nature of the problem and the fact that the solution obtained not only has to approximate the differential equations of equilibrium, but it also has to approximate the natural boundary conditions at the free edges. Lack of knowledge of the exact solutions for most such problems has left this fact unquestioned. It is the object of this section to show that with a finite series of multiplications of beam functions - no matter how long - convergence to the exact solution cannot be assured if free edges are involved.

It has been the common notion that since the free beam functions satisfy the free beam boundary conditions, which

in turn are somewhat similar to the plate free edge boundary conditions, this should make the choice of the beam functions even more justifiable (since functions which satisfy the actual plate boundary conditions are not available) and should expedite convergence towards satisfying the boundary conditions. However, this does not seem to be true. Indeed, the very fact that free beam functions satisfy the free beam boundary conditions makes it impossible for a series of such functions to satisfy the boundary conditions at the free edge, and hence destroys the completeness of such a sequence at the free boundary. This is obvious since any linear combination of beam functions will always possess zero curvature and third derivative at the edge instead of a certain finite value resulting from the effect of anticlastic curvature. This is most easily illustrated by an example. Suppose the fundamental mode shape for a rectangular plate (see Fig. [2.1]) simply supported at the edges $x = \pm a/2$ and free at $y = \pm b/2$ is approximated by

$$u = [\sum_{i=1}^{n} A_i \phi_i(y)] \cos(\pi x/a) \qquad (2.13)$$

where $\phi_i(y)$ is the i^{th} vibration mode for a free-free beam.

The free edge boundary conditions are known to be

$$M_B\Big|_{y=\pm b/2} = -D\left(\frac{\partial^2 u}{\partial y^2} + \nu\frac{\partial^2 u}{\partial x^2}\right)\Big|_{y=\pm b/2} = 0 \qquad (2.14)$$

and

$$Q_K\Big|_{y=\pm b/2} = -D\left(\frac{\partial^3 u}{\partial y^3} + (2-\nu)\frac{\partial^3 u}{\partial x^2 \partial y}\right)\Big|_{y=\pm b/2} = 0$$

where M_B and Q_K are the bending moment and Kirchhoff shear force respectively, while D is the plate flexural rigidity.

Substituting the assumed expression *(2.13)* into the expressions for M_B and Q_K, and remembering that $\phi_i'' = \phi_i''' = 0$ at $y = \pm b/2$ (which are the free beam boundary conditions); the following results

$$M_B\Big|_{y=\pm b/2} = D\nu\frac{\pi^2}{a^2} \cdot u\Big|_{y=\pm b/2}, \qquad (2.15)$$

and $$Q_K\Big|_{y=\pm b/2} = D(2-\nu)\frac{\pi^2}{a^2} \cdot \frac{\partial u}{\partial y}\Big|_{y=\pm b/2}$$

Thus, the free edge boundary conditions *(2.14)* are obviously impossible to satisfy with the series *(2.13)*. Consequently, the set of free beam functions is imcomplete; and hence does not compose a minimal sequence. Clearly, this is due to the fact that the beam functions are over-restrained with unnecessary end conditions (i.e. $\phi_i'' = \phi_i''' = 0$ at $y = \pm b/2$). As a result, the eigenvalues obtained from any finite series will be somewhat higher than the exact solutions, and stresses computed will converge to incorrect values (how incorrect will be illustrated later!).

2.5 The Degenerated (or Relaxed) Beam Function

As has been argued in the preceding discussion and will be shown numerically in the next chapter, the fact that a series of beam functions satisfy the boundary conditions of the free edged beam prevents it from being able to converge towards the satisfaction of the plate free edge boundary conditions.

In order to remedy this situation, and still retain the obvious advantages of the beam functions (e.g. their physical significance, mathematical similarity to the exact solution whenever available, approximation for all possible vibration modes, and demonstrated success when used with supported plate problems) a means for handling cases of free-edged plates will now be suggested which involves the introduction of the concept of the degenerated beam functions.

2.5.1 Free-Free and Simply Supported-Free Beam Functions

The vibration modes for a free-free beam are represented by

$$\phi_o = 1, \quad \phi_1 = \xi,$$

$$\phi_i = \cosh \varepsilon_i \xi + \lambda_i \cos \varepsilon_i \xi \quad ; \text{ for } i = 2,4,\ldots$$

(symmetric modes)

and

$$\phi_i = \sinh \varepsilon_i \xi + \lambda_i \sin \varepsilon_i \xi \quad ; \text{ for } i = 3,5,\ldots$$

(anti-symmetric modes),

where ξ is the non-dimensional spatial variable varying between ± 1.

The two coefficients ε_i and λ_i are determined such that the second and third derivatives of Φ_i with respect to ξ vanish at $\xi = \pm 1$; hence

$$\lambda_i = (-1)^{i+1} \frac{\sin \varepsilon_i}{\sinh \varepsilon_i}, \tan \varepsilon_i + (-1)^i \tanh \varepsilon_i = 0; \quad i = 2, 3, \ldots \tag{2.16}$$

Numerical values for λ_i and ε_i are tabulated in many references (e.g. see [17]).

The idea is to relax the unnecessary beam end conditions imposed through the particular choice of λ_i and ε_i in accordance with equation *(2.16)*, simply by *floating* the values of either - or both - of them. By floating the λ_i's for example, it is meant that their constant numerical values are replaced by certain arbitrary coefficients to be determined subsequently during the regular variational minimization procedure. Since the beam functions depend linearly upon the λ's, floating their values will result in degenerating each of the beam functions into their two constituent functions (except for those corresponding to solid body motions, i.e. ϕ_0, ϕ_1). Consequently, the series of beam functions degenerates into two series; one composed of hyperbolic and the other of circular functions. Hence, for example, the series given by equation *(2.13)* becomes:

$$u = [A_0 + A_2 \cosh (\varepsilon_2 \cdot \frac{2y}{b}) + \bar{A}_2 \cos (\varepsilon_2 \cdot \frac{2y}{b}) +$$

$$+ A_4 \cosh (\varepsilon_4 \cdot \frac{2y}{b}) + \bar{A}_4 \cos (\varepsilon_4 \cdot \frac{2y}{b}) + \ldots] \cos (\frac{\pi x}{a}).$$

The determination of the $A's$ and $\bar{A}'s$ follows henceforth the standard Ritz procedure leading to an eigenvalue problem of the form

$$[B] - \mu [C] = 0,$$

where $[B]$ and $[C]$ are symmetric real matrices and μ is the eigenvalue sought. Note that $[C]$ is not a unit matrix as would be the case if the ordinary beam functions were used since the degenerated beam functions are no longer orthogonal.

On the other hand, floating the $\varepsilon_i's$ is not so straightforward. Since the beam functions do not depend linearly upon the $\varepsilon's$, application of the direct variational minimization procedure for their determination would result in a set of transcendental equations. However, in the case of small numbers of terms, optimization with respect to the $\varepsilon's$ can be done by simply plotting the variation of the natural frequencies with each of the $\varepsilon's$ varying independently. Fortunately - as will be shown in the numerical examples of the following chapter - it was found that the solutions are not sensitive to the choice of the values of the $\varepsilon's$, and that those actually used in the beam functions are very close to the optimum values. Thence, it is considered sufficient to float the values of the $\lambda's$ only while treating the $\varepsilon's$ as constants equal to those obtained from equation *(2.16)*.

The vibration modes for a beam simply supported at $\xi = 0$ and free at $\xi = 1$ are the same as the anti-symmetric

modes for a free-free beam given earlier (except that ξ varies from *0* to *1* rather than between *±1*), and the degeneration process follows exactly the procedure outlined above.

2.5.2 Clamped-Free and Elastically Restrained-free Beam Functions

The vibration modes for a clamped-free beam can be represented as:

$$\phi_i = (\cosh \varepsilon_i \xi - \cos \varepsilon_i \xi) + \lambda_i (\sinh \varepsilon_i \xi - \sin \varepsilon_i \xi); i=1,2,\ldots$$

where ξ varies from *0* to *1*, and the coefficients ε_i and λ_i are defined such that the second and third derivatives at the free end ($\xi = 1$) vanish. Hence we have:

$$\lambda_i = - \frac{\cosh \varepsilon_i + \cos \varepsilon_i}{\sinh \varepsilon_i + \sin \varepsilon_i}, \quad \cosh \varepsilon_i \cdot \cos \varepsilon_i = -1. \qquad (2.17)$$

Again here, in order to relax the free end conditions, one has to float at least one of these two coefficients. Upon floating the λ's, as previously, the beam functions degenerate into the two partial functions:

$$\bar{\phi}_i = \cosh \varepsilon_i \xi - \cos \varepsilon_i \xi, \quad \bar{\bar{\phi}}_i = \sinh \varepsilon_i \xi - \sin \varepsilon_i \xi, \qquad (2.18)$$

each of them satisfying *only* the clamped end boundary conditions, at $\xi = 0$. However, as ε_i becomes large for higher modes, the two functions $\bar{\phi}_i$ and $\bar{\bar{\phi}}_i$ become very close and numerical loss of accuracy can arise. Therefore, it is preferable to replace the two functions *(2.10)* by the two equivalent ones

$$\tilde{\phi}_i = \bar{\phi}_i + \bar{\bar{\phi}}_i = e^{\varepsilon_i \xi} - \cos \varepsilon_i \xi - \sin \varepsilon_i \xi \equiv \tilde{\phi}(\varepsilon_i)$$

$$\tilde{\tilde{\phi}}_i = \bar{\phi}_i - \bar{\bar{\phi}}_i = e^{-\varepsilon_i \xi} - \cos \varepsilon_i \xi + \sin \varepsilon_i \xi \equiv \tilde{\phi}(-\varepsilon_i) \qquad (2.19)$$

This representation has the additional advantage of reducing the two degenerated beam functions into the same form with ε_i taking both positive and negative values; a feature which simplifies considerably the mathematics involved in evaluating the integrals required for the Ritz solution. The two functions $\tilde{\phi}_i$ and $\tilde{\tilde{\phi}}_i$ are related to the beam functions ϕ_i by the equation

$$\phi_i = \frac{\lambda_i - 1}{2} \tilde{\phi}_i + \frac{\lambda_i + 1}{2} \tilde{\tilde{\phi}}_i \qquad (2.20)$$

It is interesting to note that for higher modes λ_i tends to unity; and hence ϕ_i becomes practically identical to $\tilde{\tilde{\phi}}_i$ (except at ξ very close to 1) as indicated by equation (2.20). As a result, only the first two or three terms of the series $\tilde{\phi}_i$ need be taken into consideration, while for higher modes it is sufficient to retain the functions $\tilde{\tilde{\phi}}_i$ only. The purpose of this cut-off of the $\tilde{\phi}_i$ functions is two-fold: firstly; to reduce the total number of terms that need be carried in the solution in order to represent a certain number of vibration modes, and secondly; to avoid rapid loss of numerical accuracy which could arise due to the very high power exponentials associated with higher order $\tilde{\phi}_i$'s.

In a similar manner, the vibration modes for a beam

elastically restrained against rotation at $\xi = 0$ and free at $\xi = 1$ can be written as:

$$\phi_i = [e^{\varepsilon_i \xi} - \cos \varepsilon_i \xi - (1 - \frac{2\varepsilon_i}{K}) \sin \varepsilon_i \xi] +$$

$$+ \lambda_i [e^{-\varepsilon_i \xi} - \cos \varepsilon_i \xi + (1 + \frac{2\varepsilon_i}{K}) \sin \varepsilon_i \xi]$$

$$\text{or} \quad \phi_i = \overset{\sim}{\phi}(\varepsilon_i) + \lambda_i \overset{\sim}{\phi}(-\varepsilon_i), \qquad (2.21)$$

where K is the coefficient of the elastic restraint, and ε_i, λ_i are being adjusted such that the free end conditions ($\phi_i'' = \phi_i''' = 0$) are satisfied at $\xi = 1$. These functions can be separated into two groups $\overset{\sim}{\phi}(\varepsilon_i)$ and $\overset{\sim}{\phi}(-\varepsilon_i)$ as was shown in the case of the clamped-free beams. Note again that the two sub-functions $\overset{\sim}{\phi}(\varepsilon_i)$ and $\overset{\sim}{\phi}(-\varepsilon_i)$ each satisfy the boundary conditions at the supported end ($\xi = 0$). Note also that as the elastic restraint coefficient K tends to infinity, the Elastically restrained-Free beam functions tend towards those of the Clamped-Free beam.

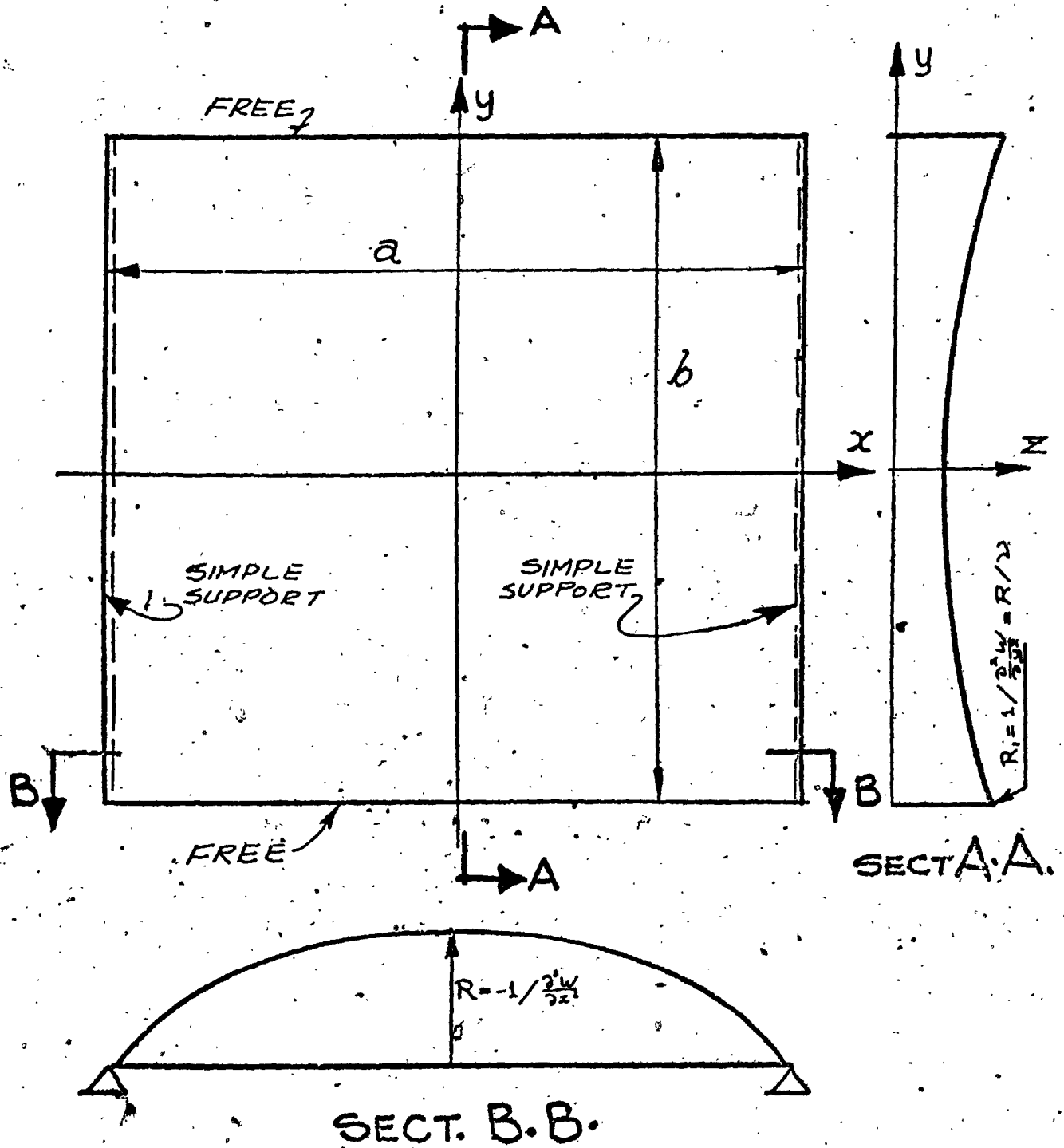

Fig. (2.1)
Vibration of a SS-F-SS-F Plate

CHAPTER III

THE USE OF DEGENERATED BEAM FUNCTIONS IN PLATE FLEXURE PROBLEMS

3.1 General Formulation

A series of multiplications of ordinary and/or degenerated beam functions is used in this chapter to solve several problems concerning either the flexural free vibrations or the static deformations of plates under transverse loads. In all problems, the plates are assumed to be thin, flat, uniform, of elastic, homogeneous, and isotropic material, undergoing small lateral displacements, such that the assumptions of the linear thin plate theory are all valid.

The plate is considered lying in the x - y plane with its edges parallel to the coordinate axes. The location of the origin will be chosen separately for each problem to suit the particular set of boundary conditions used. In general, the coordinate axes are placed along two of the plate edges but, if symmetry exists, the appropriate coordinate axis is placed along the axis of symmetry.

The differential equation governing the plate deflection under lateral loads is the biharmonic equation

(2.4), where u represents the lateral displacement at any point, and P is the applied load per unit area of the plate middle surface divided by the plate flexural rigidity D. Three types of end conditions are considered: for a clamped edge,

$$u = \frac{\partial u}{\partial n} = 0; \qquad (3.1)$$

for a simply supported edge,

$$u = \frac{\partial^2 u}{\partial n^2} = 0; \qquad (3.2)$$

and for a free edge,

$$M_B \equiv - D \cdot M(u) = 0, \quad Q_K \equiv - D \cdot Q(u) = 0, \qquad (3.3)$$

where M_B and Q_K are the bending moment and Kirchhoff shear force at the free edge. Both M and Q are as defined by equation (2.8) in which ν would then represent Poisson's ratio. Note that these natural boundary conditions are considerably simplified for a straight edge parallel to one of the coordinate axes; thus on a line $x = a$ they take the form:

$$M \equiv \frac{\partial^2 u}{\partial x^2} + \nu \frac{\partial^2 u}{\partial y^2} = 0, \quad Q \equiv \frac{\partial^3 u}{\partial x^2} + (2 - \nu) \frac{\partial^3 u}{\partial x \partial y^2} = 0. \qquad (3.4)$$

Using the Ritz procedure, as outlined in the previous chapter, the solution is sought in the form of a series of admissible functions such that

$$u_{mn} = \sum_{i=1}^{m} \sum_{j=1}^{n} A_{ij} \cdot \phi_i(x) \psi_j(y), \qquad (3.5)$$

where ϕ_i and ψ_j are ordinary or degenerated beam functions satisfying the boundary conditions of the type *(3.1)* or *(3.2)*, wherever imposed, however they do not necessarily satisfy the natural boundary conditions *(3.3)* at the free edges. It is also assumed that the load on the plate can be expressed in terms of a series similar to *(3.5)* such that

$$P(x,y) = \sum_{i=1}^{m} \sum_{j=1}^{n} B_{ij}\, \phi_i(x)\, \psi_j(y), \qquad (3.5a)$$

where B_{ij} are certain known coefficients depending upon the loading pattern.

Replacing ϕ_r in *(2.6)* by $\phi_r(x)\,\psi_s(y)$, u_m by u_{mn}, and setting $q(s)$ and $m(s)$ to zero from a comparison of the natural boundary conditions *(3.3)* and *(2.10)*, the following results:

$$\int_0^b \int_0^a \Big\{ \sum_{i=1}^{m} \sum_{j=1}^{n} A_{ij} \big[(\phi_i''\psi_j + \phi_i\psi_j'')(\phi_r''\psi_s + \phi_r\psi_s'') - (1-\nu)\cdot$$

$$\cdot (\phi_i''\psi_j \cdot \phi_r\psi_s'' + \phi_i\psi_j'' \cdot \phi_r''\psi_s - 2\cdot \phi_i'\psi_j' \cdot \phi_r'\psi_s') \big]$$

$$- B_{ij}[\phi_i\psi_j \cdot \phi_r\psi_s] \Big\} dx\,dy = 0, \quad (r=1,2,\ldots,m;\ s=1,2,\ldots,n). \qquad (3.6)$$

Interchanging the summations and integrations and rearranging, it finally yields the set of equations

$$\sum_{i=1}^{m} \sum_{j=1}^{n} C_{ij}^{(rs)} \cdot A_{ij} = \bar{P}^{(rs)}, \quad (r=1,2,\ldots,m;\ s=1,2,\ldots,n), \qquad (3.7)$$

where

$$C_{ij}^{(rs)} = H_{ir} I_{js} + \alpha^4 E_{ir} S_{js} + \nu\alpha^2 (G_{ir} R_{sj} + G_{ri} R_{js}) + 2(1-\nu)\alpha^2 \cdot F_{ir} J_{js},$$

and

$$\bar{P}^{(rs)} = \sum_{i=1}^{m} \sum_{j=1}^{n} a^4 B_{ij} \cdot E_{ir} I_{js},$$

in which

$$E_{ir} = \frac{1}{a} \int_0^a \phi_i \phi_r \, dx, \qquad I_{js} = \frac{1}{b} \int_0^b \psi_j \psi_s \, dy,$$

$$F_{ir} = a \int_0^a \phi_i' \phi_r' \, dx, \qquad J_{js} = b \int_0^b \psi_j' \psi_s' \, dy,$$

$$G_{ir} = a \int_0^a \phi_i \, \phi_r'' \, dx, \qquad R_{js} = b \int_0^b \psi_j \, \psi_s'' \, dy, \qquad (3.8)$$

$$H_{ir} = a^3 \int_0^a \phi_i'' \phi_r'' \, dx, \qquad S_{js} = b^3 \int_0^b \psi_j'' \psi_s'' \, dy,$$

and $\alpha = a/b$.

Equations *(3.7)* are a set of $m \times n$ linear equations sufficient for the determination of the coefficients A_{ij} in the Ritz solution.

In the case of a free vibration problem, the load P will be replaced by the inertia force. After eliminating the time variable by assuming a harmonic time history in the usual manner, considering u as the time-independent displacement, and replacing P by the inertia force parameter $\rho h w^2 u/D$, an equation analogus to *(3.7)* may now be

written as

$$\sum_{i=1}^{m}\sum_{j=1}^{n}[C_{ij}^{(rs)} - \lambda(E_{ir} \cdot I_{js})]A_{ij} = 0, (r=1,2,..,m; s=1,2,..,n), \tag{3.9}$$

where $\lambda = \rho h\omega^2 a^4/D$ is the frequency parameter; $C_{ij}^{(rs)}$, E_{ir} and I_{js} are as defined above. Equation (3.9) is of the standard eigenvalue form and is readily soluble on a computer yielding the frequency parameters λ and the coefficients A_{ij} from which the mode shapes may be determined.

3.2 Test Problems

In this section, relatively simple test problems concerning plates having two parallel edges simply supported - for which separation of variables may be feasible and used to obtain exact solutions - are considered. The object is to assess the accuracy of the solutions obtained using the degenerated beam functions, and to demonstrate quantitatively the lack of accuracy resulting from the use of the ordinary beam functions in cases where free edges are involved.

Two sets of test problems are presented; the first is that of determining the natural frequencies, mode shapes and dynamic stresses of the plates, while the second concerns the static deflections and stresses under a load sinusoidally varying in the direction perpendicular

to the pair of simply supported edges and uniform in the other direction. In each case, two types of plates are analysed: a plate with two parallel edges simply supported, the other two free; and another having two parallel simply supported edges, the third clamped, and the fourth free.

3.2.1 Dynamic Problems

Figures (3.1) and (3.2) show the coordinate systems and boundary conditions for the two types of plates considered. Due to the existence of two parallel simply-supported edges, separation of variables is feasible by assuming a sine or a cosine wave in the y-direction. In this example, only modes symmetric about the x-axis having one half wave in the y-direction are considered.

The exact solutions for these two problems are available in the literature for a variety of side ratios (for example see Liessa's monograph p.p.51-58[28]).. However, for a more reliable comparison; and in order to ensure sufficient accuracy, the exact solutions were re-computed by the author using different numbers of significant figures (six, eight, and thirteen significant figures) for each case. No appreciable rounding off errors were detected, and the results obtained are guaranteed to be accurate at least to eight significant figures.

The Ritz solutions were obtained using a cosine wave in the y-direction and a series of ordinary, or degenerated

beam functions in the x-directions. These beam functions have been defined in section (2.5).

The integrals involved in the Ritz procedure - equation (3.8) - were first computed for both the ordinary and degenerated beam functions up to the maximum number of terms expected to be needed. The procedure and the expressions used for evaluating these integrals are described in Appendix I. The idea is to express each ordinary beam function, or its derivative, as the sum of four complex exponentials, and each of the degenerated beam functions, or derivatives thereof, as two (in the case of Free-Free beams) or three (in the case of Clamped-Free beams) exponentials; such that:

$$F_n(\xi) = \sum_{i=1}^{K} \alpha_{in} \, Exp. [\beta_{in} \xi],$$

where the α's and β's are complex coefficients dependent upon the end conditions and upon whether $F(\xi)$ represents the beam function itself or one of its derivatives. Any of the integrals (3.8) can then be represented in the general form:

$$I_{mn} = \int_0^1 F_m(\xi) \, F_n(\xi) \, d\xi$$

$$= \sum_{i=1}^{K} \sum_{j=1}^{L} \alpha_{im} \alpha_{jn} \, [Exp \, (\beta_{im}+\beta_{jn}) - 1]/(\beta_{im}+\beta_{jn}) \quad (3.10)$$

Complex arithmetic on the CDC 6400 computer was then used to evaluate this integral for all the cases of interest, and the resulting matrices were obtained on punched cards

for subsequent usage with the different Ritz solutions. This procedure was found most satisfactory because of its high reliability, since the algebra and programming effort required are minimized. The procedure is of particular value in more complicated cases, such as the vibration of plates with in-plane loads and some large deflection problems, where integrals involving the multiplication of three beam functions by the direct methods would involve $4 \times 4 \times 4 = 64$ different terms to be integrated separately. The algebra involved would then be prohibitive and the results obtained unreliable. With the use of equations similar to *(3.10)* the procedure is systemized and the possibility of errors minimized.

With the integrals *(3.8)* at disposal, the set of equations *(3.9)* is easily constructed and the resulting eigenvalue problem readily solved using standard routines. For small size problems, including the test problems, the roots of the determinant (the eigenvalues) were found by direct iteration using a modified false-positions technique with the value of the determinant computed at each iteration step. The corresponding eigenfunctions were subsequently found by arbitrarily setting one of the unknown coefficients to any specified value then solving the resulting set of linear equations for each of the eigenvectors separately. For moderate size problems (10 to 30 equations) a more efficient eigenvalue solving routine based upon the Jacobi algorithm was used to extract all the eigenvalues and

eigenvectors simultaneously.

The first procedure, although inefficient, yields extremely accurate eigenvalues and offers the advantage of providing direct estimates for the accuracy of the roots through knowledge of the value of the step used in the final iteration as well as the residual value of the determinant. In view of this advantage, the determinant procedure was used for the test problems in order to ensure a high degree of accuracy throughout. This method was also used for relatively large problems (30 to 70 equations) since the degree of accuracy obtainable from the Jacobi procedure is not predictable for new problems of such a size. In addition, for these large problems, since only the first one or two eigenvalues, in a given group of symmetry, is usually of interest, the determinant evaluation procedure might prove to be of an efficiency comparable to - and sometimes better than - the Jacobi's method which produces a large number of eigenvalues and eigenvectors that may not be of interest.

Table (3.1) shows the results obtained using 3, 5 and 7 terms in the series employing both the ordinary and degenerated beam functions as compared to the exact solutions. The results are for the fundamental mode of vibration - normalized to a unit maximum displacement - for the plate of figure (3.1). In general, the percentage errors reported are defined as:

$$Error\ \% = \frac{Approximate\ value - Exact\ value}{Reference\ Exact\ value} \times 100\%$$

Table (3.1)

Vibration of a SS-F-SS-F Square Plate

Percentage deviation from exact solution. Maximum displacement normalized to unity in all cases (exact solutions given in brackets). Poisson's Ratio = 0.3.

Determinant	Size	3 x 3	5 x 5	7 x 7
eigenvalue	O†	1.6%	1.0%	0.7%
[92.762755]	D†	0.003%	0.0001%	0.0000%
edge rise ($W_{edge} - W_{centre}$)	O	-6.7%	-3.1%	-2.0%
[0.13559]	D	0.2%	-0.003%	0.0001%
max. M_B (at centre)	O	27.2%	17.0%	12.3%
[-1.76208]	D	-2.1%	0.03%	-0.003%
edge M_B^* (at free edge centre) [zero]	O	168.0%	168.0%	168.0%
	D	-7.3%	0.3%	-0.005%
max. shear (at free edge centre)	O	-198.0%	-216.1%	-223.8%
[4.90208]	D	50.0%	-8.1%	0.4%
edge Q_x^{**} (at free edge centre) [zero]	O	-166.6%	-179.4%	-210.6%
	D	50.0%	-8.08%	0.4%

* % error related to exact maximum M_B

** % error related to exact maximum shear

† O = ordinary beams, D = degenerated beams

where the reference value is taken as the exact local value unless otherwise specified by the footnotes on the table. The results reveal the extremely rapid convergence achieved by the use of small numbers of terms in the series when the degenerated beam functions are employed. In contrast, the very poor convergence rate and large relative errors resulting from the use of ordinary beam functions for the determination of the frequency and the mode shape may be seen. The stress results obtained by the ordinary beam functions are, obviously, grossly in error. The stresses at the free edge either do not converge at all or converge towards incorrect results.

It is worth noticing that the comparison shown is based upon the total number of terms in the series, which is rather unfair with respect to the degenerated beam functions since each two terms - except for the first term - represent only one beam function. Hence, for example, the five-term degenerated beam function series corresponds to three beam functions with each of the second and third beams degenerated into its two constituent functions.

Figure (3.3) is a graphical display of the 5-term solutions of table (3.1). The non-dimensional displacements, bending moments and shear forces along the plane of symmetry parallel to the simply-supported edges are plotted. The degenerated beam series solutions coincide - within the thickness of the lines - with the exact solutions almost throughout the graphs. While the errors in displacements

obtained by the ordinary beam functions might be acceptable, the stresses are certainly not. Note that the errors in the stresses tend to be higher towards the free edge reflecting the fact that they are mainly introduced due to the non-completeness of the beam functions at the boundaries which, in turn, is caused by the unnecessary beam end conditions. As soon as these extra conditions are relaxed, the resulting degenerated beam functions become complete and able to converge, very rapidly, to the exact solution.

The behaviour of the degenerated and ordinary beam function solutions for higher modes is shown in table (3.2) and Figure (3.4). Only five-term solutions are shown and compared with the exact solutions. For the antisymmetric mode, since the displacement W is always zero at the centre and unity at the centre of the edge, the slopes - rather than the displacements - were used as the basis of comparison. Comparing the results obtained using the degenerated beam functions for the first three modes - as shown in the table - reveals that the lower modes are generally more accurate. This is the expected behaviour of an approximate numerical solution and is also desirable since they are usually of more practical interest and induce more significant stresses. The ordinary beam solutions, however, behave differently; higher modes tend to show less errors. This is explainable since the effect of the boundary conditions becomes less significant for higher modes. Hence, the nonsatisfaction of the boundary conditions has less adverse effect on the

Table (3.2)

Vibration of a SS-F-SS-F Square Plate

- Higher Modes

Percentage deviations of 5-term solutions from exact Maximum displacements normalized to unity in all cases (exact solutions given in brackets). Poisson's ratio = 0.3

Eigenvalue	Exact	[92.7628]	[260.3299]	[1348.7687]
$[\lambda=\omega^2 a^4 \rho h/D]$	O†	1.0%	0.6%	0.1%
	D†	0.0001%	0.0002%	0.0002%
Displacements	Exact	[0.13559]	{0.20462 }	[1.67030]
$[W_{max}-W_{min}]$ or	O	-3.1%	5.6%	0.7%
$\{a(W'_{max}-W'_{min})\}$	D	-0.003%	0.2%	0.005%
Maximum	Exact	[-1.76208]	[-2.45605]	[21.9486]
Bending Moment	O	17.0%	20.6%	0.01%
$[M_B.a/D]_{max}$	D	0.08%	0.08%	0.02%
Free Edge	Exact	[zero]	[zero]	[zero]
Bending Moment	O	168.0%	120.6%	13.5%
$[M_B.a/D]^*_{edge}$	D	0.3%	2.3%	0.8%
Maximum	Exact	[4.90208]	[26.6772]	[109.8225]
Shear Force	O	-216.1%	20.0%	0.9%
$[Q.a^2/D]_{max}$	D	-8.1%	1.0%	-0.8%
Kirchhoff	Exact	[zero]	[zero]	[zero]
Shear force	O	-179.4%	-72.8%	-72.3%
$[Q_k a^2/D]^{**}_{edge}$	D	-8.1%	18.0%	11.4%

* % error related to exact maximum Bending Moment

** % error related to exact maximum Shear Force

† O = Ordinary beam functions, D = Degenerated Beam functions

higher modes than it does with the fundamental. The same conclusion can also be reached by comparing figure (3.4) with figure (3.3). While the two figures show the same general trends explained in association with the first mode, the magnitudes of the errors in the second mode are marginally reduced.

In order to assess the effect of optimizing the values of the ε's in a degenerated beam series, the same example mentioned above is examined. A three term series (a straight line plus one beam mode degenerated into two terms) is used for simplicity. Hence, there is only one parameter ε (i.e.ε_2) to optimize. Figure (3.5) shows the effect of varying ε_2 on the first two eigenvalues (for fully symmetric modes). Referring to this figure, the following conclusions can be drawn immediately:

First: The eigenvalues obtained are not sensitive to variations in ε_2 for a wide range of values.

Second: The value of ε_2 corresponding to the minimum of λ_1 is different from, but close to, that corresponding to the minimum of λ_2.

Third: The value of ε_2 corresponding to the ordinary beam function as obtained from Eq. *(2.16)* - i.e. $\varepsilon_2 = 4.730$ - represents an intermediate value between the two minima points. Hence, it can be considered as "a good guess" for an optimum value with respect to both eigenvalues.

In order to examine the behaviour and accuracy of a series of degenerated Clamped-Free beam functions, the funda-

mental mode of vibration for the plate of figure (3.2) is examined. Five, seven and nine terms were used in the series employing both ordinary and degenerated beam functions alternatively. The results are compared with the exact solutions in table (3.3). Here, as the displacements take fixed values at both ends (zero at the clamped edge and unity at the centre of the free edge), the slope at the free edge centre is used as the basis of comparison instead of the displacements themselves.

The table shows the same orders of errors and same trends as were found with the previous problem as far as the frequencies, slopes and free edge stresses are concerned. Since the maxima for the bending moments and shear forces occur at the clamped edge, the respective results obtained using both the ordinary and degenerated beam functions are of comparable order . This is due to the fact that the degenerated beam function $\tilde{\phi}_i$ is very close to the ordinary beam function ϕ_i near the clamped edge (as was shown in section [2.5.2]. Also, for this example, only the first two members of the family $\tilde{\phi}_i$ are included in the degenerated beam series. Consequently, the solutions obtained, using ordinary and degenerated beam functions, were very close near the clamped edge.

The same trends are also evident in the graphical comparison shown in Fig.(3.6). The figure is a plot of the displacements, bending moments, and shear forces along the line of symmetry as obtained using nine-term approximate

Table (3.3)

Vibration of a SS-C-SS-F Square Plate

rcentage deviation from exact solution.
aximum displacement normalized to unity in all cases
(exact solutions given in brackets). Poisson's Ratio = 0.3.

Determinant eigenvalue [160.96804]	Size	5 x 5	7 x 7	9 x 9
	O†	.9%	0.8%	0.7
	D†	.3%	.006%	.002%
max. slope (at free edge centre) [1.37219]	O	-12.6%	-10.0%	-8.4%
	D	.02%	.004%	.001%
max. M_B (at clamped edge centre) [6.80511]	O	-.2%	-4.0%	-3.3%
	D	-7.1%	-3.8%	-2.2%
free edge M_B* [ZERO]	O	-43.5%	-43.5%	-43.5%
	D	2.8%	1.0%	0.4%
max.shear (at clamped edge centre [-31.8499]	O	-35.8%	-33.2%	-30.5%
	D	-37.6%	-28.3%	-21.5%
Kirchhoff shear** (at free edge centre [ZERO]	O	63.2%	64.7%	66.6%
	D	34.8%	-9.8%	-5.8%

* % error related to exact maximum M_B

** % error related to exact maximum shear

† O = ordinary beams, D = degenerated beams

Table (3.3)

Vibration of a SS-C*SS-F Square Plate

Percentage deviation from exact solution.

Maximum displacement normalized to unity in all cases

(exact solutions given in brackets). Poisson's Ratio = 0.3.

Determinant	Size	5 x 5	7 x 7	9 x 9
eigenvalue	O†	.9%	0.8%	0.7
[160.96804]	D†	.3%	.006%	.002%
max. slope (at free edge centre)	O	-12.6%	-10.0%	-8.4%
[1.37219]	D	.02%	.004%	.001%
max. M_B (at clamped edge centre)	O	-.2%	-4.0%	-3.3%
[6.80511]	D	-7.1%	-3.8%	-2.2%
free edge M_B*	O	-43.5%	-43.5%	-43.5%
[ZERO]	D	2.8%	1.0%	0.4%
max. shear (at clamped edge centre	O	-35.8%	-33.2%	-30.5%
[-31.8499]	D	-37.6%	-28.3%	-21.5%
Kirchhoff shear** (at free edge centre	O	63.2%	64.7%	66.6%
[ZERO]	D	34.8%	-9.8%	-5.8%

* % error related to exact maximum M_B

** % error related to exact maximum shear

† O = ordinary beams, D = degenerated beams

solutions as well as the exact analysis. All three solutions coincide - within the thickness of the lines - for the displacements. As before, the degenerated beam results remain very close to the exact solution almost throughout the graphs. The stresses obtained using ordinary beam functions, however, deviate considerably, especially near the free edge.

It is worth noticing that the highest errors in the degenerated beam solutions occur in the shear forces near the clamped edge. This can be explained by observing that these forces do negligible work, and hence contribute a minimal quantity to the energy of the plate. The result is that the strain energy of the plate is extremely insensitive to variations in these forces. Hence, they are given the least priority during optimizing the coefficients in the assumed series for minimizing the frequencies.*

3.2.2 Static Problems

The two plates analysed in the previous section are re-examined here. This time, however, the deflections and stresses under a transverse static load are considered. Fourier series solutions for many static loading conditions

---

* The same behaviour was also noticed in a set of solutions obtained for a plate having two parallel clamped edges and two simply supported ones using a series of ordinary beam functions. Errors of the same order of magnitude as those found in the above-mentioned case were observed near the clamped edges.

are available in the literature. However, closed-form exact solutions were found only for plates having two parallel simply-supported (or sliding) edges under a load sinusoidally varying in the direction perpendicular to the simple supports. Therefore, in the present examples, the load is considered to take the form of a half sine wave in the y-direction [see fig. (3.1)] and to be uniform in the x-direction.

Again, the numerical exact solutions are available for this problem. However, they were re-computed by the author in order to establish confidence in the number of significant figures required for the comparison. As before, six, eight and thirteen significant figures were used in the computations, and a minimum accuracy of eight significant figures is assured.

The Ritz solutions were obtained as described in section (3.2). Here, the load series *(3.6)* is reduced to a single term (i.e. $m = n = 1$) and B_{11} is taken to be unity. With the integrals *(3.8)* on hand (evaluated as described in relation to the dynamic problems), the matrix relation *(3.7)* is readily constructed using any desired number of terms in the displacement series *(3.5)*. In view of the orthogonality of the trigonometric functions, only terms corresponding to $j = 1$ in *(3.5)* will have non-zero coefficients under the single half-wave loading pattern; hence the double series *(3.5)* is reduced to a single series. The resulting set of $(m \times 1)$ simultaneous linear equations is then solved using

the well known Gaussian Elimination procedure and thirteen significant figures on the CDC 6400 computer. Both ordinary and degenerated beam functions were used and the results were compared to the exact solutions.

Table (3.4) shows the convergence and comparison of the maximum displacements, bending moments, and shear forces, as well as the edge bending moment and Kirshhoff shear force, for the plate having two parallel simply supported edges and two free ones. Three, five, and seven terms were used with both the ordinary and degenerated beam functions. The results of the same problem are also displayed in figure (3.7) for the 5-term solutions. It is worth noticing that the general character of these graphs and the order of magnitude of the different errors is very similar to the results of the dynamic problem shown in figure (3.3) and table (3.1). This is expected since the static load distribution is close to the distribution of the inertia forces when the plate vibrates in its fundamental mode. Note also that the errors in the displacements in the static solutions are more representative for the accuracy of the solutions than those of the dynamic problem. This is because the latter solutions are biased by the fact that the mode shapes are always normalized to a unit maximum displacements.

While for some dynamic applications where the approximate frequencies and mode shapes might be the only quantities of interest, the inaccuracies associated with these quantities in an ordinary beam series solution may be acceptable; for static problems - where stresses are usually

Table (3.4)

Statically Loaded SS-F-SS-F Square Plate

Percentage deviation form exact solutions (given in brackets). Poisson's ratio = 0.3

Determinant	Size	3 x 3	5 x 5	6 x 6	7 x 7
maximum Displacement	O†	1.6%	0.9%	0.7%	0.6%
[0.01618013]	D†	0.02%	0.0001%	0.0000%	0.0000%
maximum Bending Moment	O	47.6%	48.7%	49.0%	49.1%
[-0.0266102]	D	1.8%	0.06%	0.009%	0.002%
Free Edge Bending Moment*	O	147.6%	148.7%	149.0%	149.1%
[Zero]	D	-6.7%	0.3%	-0.04%	-0.009%
Maximum Shear Force	O	195.1%	532.7%	612.7%	813.3%
[0.067768]	D	50.5%	7.3%	1.8%	0.6%
Kirchhoff shear at free edge**	O	88.6%	106.7%	111.2%	114.4%
[Zero]	D	52.8%	7.3%	1.8%	0.6%

* % error related to exact maximum M_B

** % error related to exact maximum shear

† O = ordinary beams, D = degenerated beams

Table (3.5)

Statically Loaded SS-C-SS-F Square Plate

Percentage deviation from exact solutions (given in brackets). Poisson's ratio = 0.3

Determinant	Size	5 x 5	6 x 6	8 x 8	9 x 9
Maximum Displacement	O†	1.0%	0.9%	0.7%	0.6%
[0.01203413]	D†	0.84%	0.003%	0.0005%	0.0001%
Maximum Bending Moment	O	-5.2%	-6.4%	-4.2%	-6.2%
[0.135533]	D	-11.2%	-6.7%	-3.6%	-3.4%
Free Edge Bending Moment*	O	21.7%	21.7%	21.8%	23.5%
[zero]	D	-4.4%	3.1%	1.7%	0.7%
Maximum Shear Force	O	-60.8%	-32.9%	-27.0%	-14.7%
[-0.86443]	D	-43.2%	-33.8%	-25.3%	-24.0%
Kirchhoff Shear at free edge**	O	-21.1%	-23.7%	-24.1%	-24.3%
[zero]	D	40.6%	12.4%	-10.0%	-6.7%

* % error related to exact maximum I_B

** % error related to exact maximum shear

† O = ordinary beams, D = degenerated beams

of primary importance - the erroneous stresses obtainable with beam functions cannot be tolerated.

The results for the plate having two simply supported, one clamped, and one free edges are shown in table (3.5). The 9-term results are also plotted in figure (3.8). Again, the similarity to the results of the dynamic problem should be noticed. The errors at the clamped edge, obtained using either the ordinary or the degenerated beam functions, are of the same order. At the free edge, however, the inadequacy of the ordinary beam series becomes obvious. While the errors associated with the degenerated beam solutions decrease as the number of terms increase, those of the ordinary beam series diverge, at least near the free edge.

3.3 Degenerated Beam Functions Applied to Non-Separable Dynamic Problems

In this section, a double series composed of multiplications of ordinary and/or degenerated beam functions is applied to dynamic problems involving three plates having combinations of free and clamped edges; namely a fully free plate, a cantilevered plate, and a plate having two parallel free edges and the other two clamped. For this class of problems, separation of variables is not possible, and hence exact closed form solutions do not exist. No stress results were found in the literature for comparison, and only experimentally determined mode shapes for the free plates were available with sufficient details to allow

meaningful comparison. On the other hand, however, an abundance of frequency results have been reported in the literature. Since it is the object of the present investigation to demonstrate the applicability and accuracy of the series of degenerated beam functions for solving this class of problems rather than adding another complete set of results to those already available; only sample results are presented and compared (whenever found of interest) to those already published in the literature.

Table (3.6) shows some frequency results for doubly-antisymmetric modes of fully free plates of side ratios 1:1 and 1:4 obtained using a series of multiplications of degenerated free-free beam functions. The comparison results are due to Bazely et.al.[20] who used fifty selected multiplications of ordinary beam functions in the Ritz method. The fact that the results obtained using 25 and 49 degenerated beam functions are very close indicates highly accurate results. Since both sets of results represent higher bounds for the actual frequency parameters, the ordinary beam function results of reference [20] - except for the fundamental of the square plate - are at least one percent too high. The relatively small error in the fundamental frequency is due to the nature of this mode being an almost purely twisting mode where the edges remain approximately straight minimizing the anti-clastic curvature effects.

Experimental results for several rectangular free plates were recently reported in reference [29] and compared

Table (3.6)

Eigenvalues of Fully Free Rectangular Plates

Convergence of the eigenvalues for the doubly antisymmetric modes and comparison with ordinary beam results.

Poisson's Ratio = 0.3

side ratio	Mode Number	Degenerated beam functions		Ordinary beams [20]
		25-term series	49-term series	50-term series
1/1	1	181.395	181.392	181.55
	2	4797.704	4797.703	4840.8
	3	5955.606	5955.470	5995.4
1/4	1	---	10.6256	10.6302
	2	---	114.7136	115.090

with degenerated beam series results especially furnished by the present author. The results are reproduced in table (3.7) showing the normalized displacements along the longer axis of symmetry (the x-axis) for the lowest mode of the group symmetric about the x-axis and antisymmetric about the y-axis. The experimental results are for 0.2" thick steel plates (Poisson's ratio was evaluated as 0.26) of a length equal to 20", and various widths. The theoretical results were obtained using 35 terms in the series and Poisson's ratio equal to 0.26. From a study of the bulk of the experimental results, the scatter of the results and their mutual inconsistancies seems to suggest experimental errors of the order of two to three percent. Hence, agreement between the theoretical and experimental results is considered satisfactory and most of the differences may be attributed to experimental inaccuracies. A more extensive comparison is shown in figure (3.9) for the case of the 8 1/2" wide plate. Good agreement throughout the plate is shown. The frequency parameters corresponding to these modes, as well as the fundamental modes of four other rectangular plates, are displayed in table (3.8).

Convergence and comparison of the fundamental and second symmetric frequencies for cantilever plates of side ratios 1:1 and 1:4 are given in table (3.9). Once more, good convergence is achieved when degenerated beam functions are used. Also, the comparison results by Bazely et.al.

Table (3.7)

Mode Shapes of Fully Free Rectangular Plates

Comparison with experimentally measured displacements [29] for the second symmetric/antisymmetric mode. Poisson's ratio = 0.26.

$\frac{b}{a}$	x/a =	0.0	0.1	0.2	0.3	0.4	0.5
$8\frac{1}{2}$" / 20"	Theory:	0.0	-0.429	-0.582	-0.328	0.261	1.0
	Experiment*	0.0	-0.438	-0.572	-0.333	0.260	1.0
7" / 20"	Theory:	0.0	-0.445	-0.607	-0.351	0.248	1.0
	Experiment*	0.0	-0.416	-0.584	-0.348	0.250	1.0
$5\frac{1}{2}$" / 20"	Theory:	0.0	-0.458	-0.625	-0.368	0.239	1.0
	Experiment*	0.0	-0.448	-0.606	- .365	0.231	1.0

* The scatter and lack of symmetry in the experimental results shows errors up to 2 to 3% of the maximum displacement

Table (3.8)

Variation of eigenvalues of beam-like modes of free plates

Poisson's ratio = 0.26

b/a:	4/8	3/8	2/8	1/8	zero
first free beam mode:	470.756	470.276	468.975	467.453	466.726

b/a:	$8\frac{1}{2}$ /20	7/20	$5\frac{1}{2}$/20	4/20	$2\frac{1}{2}$/20	zero
second free beam mode:	3621.60	3615.13	3602.45	3584.99	3565.38	3546.42

[21] obtained using 30 multiplications of ordinary beam functions are shown to be considerably less accurate.

The fundamental frequency of a square plate having two parallel clamped edges and two free ones is shown in table (3.10). The comparison results have been previously published by the author [1,19] and were obtained using a sixteen-term series composed of multiplications of *ordinary beam* functions. The present results are obtained by using two, nine, and fifteen terms in a series composed of multiplications of ordinary clamped-clamped beam functions and degenerated free-free beam functions. Note that with the use of degenerated beams in the free-free direction, even a two term series yields better results than that obtained using a sixteen term ordinary beam series.

3.4 Concluding Remarks

The careful study of the numerical examples presented in this chapter prompts several interesting remarks. Of particular importance are the following two results:

1. Highly accurate solutions and very good convergence characteristics are obtained through the use of the degenerated beam functions. Although these degenerated beam functions are intentionally chosen so that the individual members do not satisfy any end conditions at the free edges, the series composed of these functions converges rapidly towards satisfying the natural

Table (3.9)

Eigenvalues of Cantilevered Rectangular Plates

Convergence of the eigenvalues for the symmetric modes and comparison with ordinary beam results. Poisson's ratio = .3

side ratio	Mode Number	Degenerated beam functions			Ordinary beams [21] 30 term series
		25-terms	30-terms	45-terms	
1/1	1	12.086	12.079	12.060	12.157
	2	453.86	453.76	453.43	457.54
4/1	1	3147.0	3146.6	3145.9	3152.8
	2	7771.2	7770.3	7769.0	7792.3

Table (3.10)

Fundamental Eigenvalue of a C-F-C-F Square Plate

Convergence and comparison with ordinary beam results.
Poisson's ratio = 0.3

Degenerated beam functions			Ordinary beams [1] 16-term series
2-terms	9-terms	15-terms	
493.94	493.10	492.79	495.23

boundary conditions at the free edges. Extremely accurate eigenvalues and eigenvectors, as well as reasonably accurate bending moments and shear forces, are obtainable with the use of a relatively small numbers of terms (five to nine terms in each direction depending upon the end conditions and the accuracy required). It is striking that the largest errors generally occur at the clamped edges, where the boundary conditions are pre-satisfied, rather than at the free edges. This is explainable since a virtual force or moment near the clamped edge will contribute a negligible work to the energy of the plate, while at the free edge - where the displacements and slopes usually reach their maximum values - any slight stress perturbation will significantly affect the total energy of the plate. Hence, a minimum energy criterion will tend to focus more attention upon stresses near the free edges on the account of those at the clamped edges. It is hence conceivable that, contrary to that which is commonly believed, problems with natural boundary conditions (a free plate for example) are easier to solve approximately than those involving forced boundary conditions where inaccuracies in the stresses might be introduced near the clamped edges.

2. Ordinary beam functions, in view of their non-completeness at the free boundaries (in the sense of completeness defined in this work), yield considerably less

accurate eigenvalues and eigenvectors, when used for problems involving free boundaries, even if a large number of terms is used in the solution. Moreover, while inaccuracies in the displacements and frequencies might sometimes be tolerable and decrease with increasing the number of terms in the series, errors in the stresses are certainly not acceptable. The errors in the stresses near the free edges generally increase as more terms are taken in the series - or at least remain constant. Near the clamped edges - if they exist - both the ordinary and degenerated beam functions yield the same order of errors. This is expected since it has been shown that the two types of functions are very similar near the clamped end - see equation *(2.20)*.

Finally, since the *necessary* conditions which must be satisfied by a family of functions in order to compose a minimal sequence are not yet known, and only *sufficient* conditions are normally conceived through the techniques of functional analysis, it becomes virtually impossible to present an analytical proof for the inadequacy of the ordinary beam functions. It is therefore considered that the fact that beam functions are not complete in the sense of Kantorovich [6] as was conceived in section (2.4), in addition to the foregoing numerical exercise, is sufficiently strong evidence that, at least for the class of problems investigated, ordinary beam functions yield inaccurate eigenvalues and displacements as well as incorrect stresses.

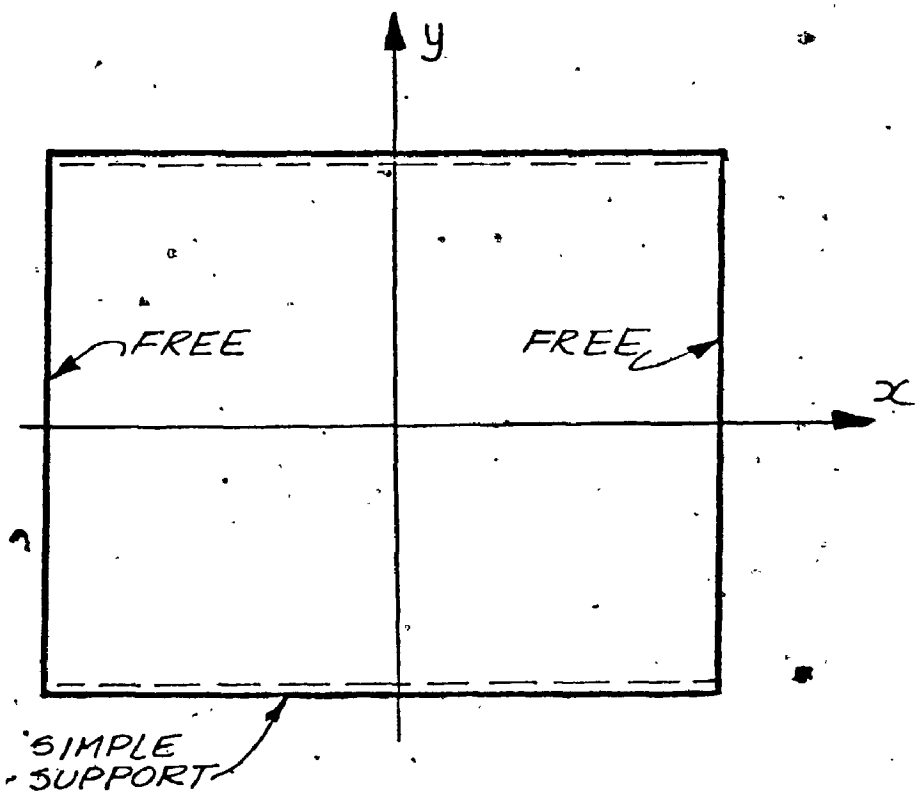

Fig. (3.1)

SS-F-SS-F Plate

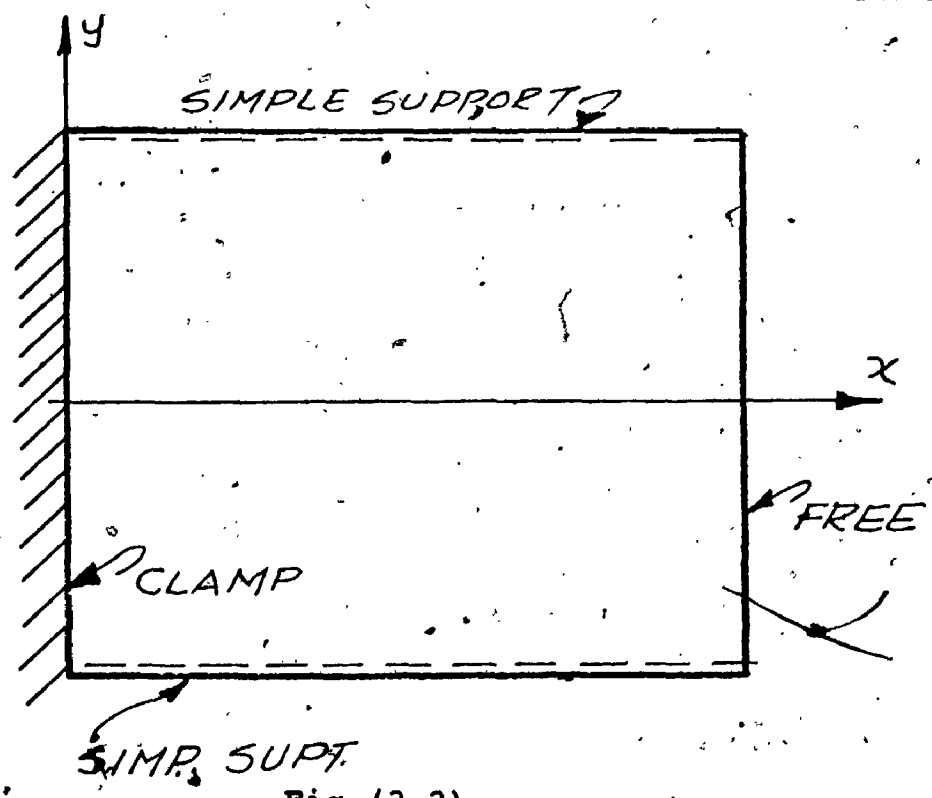

Fig. (3.2)

SS-C-SS-F Plate

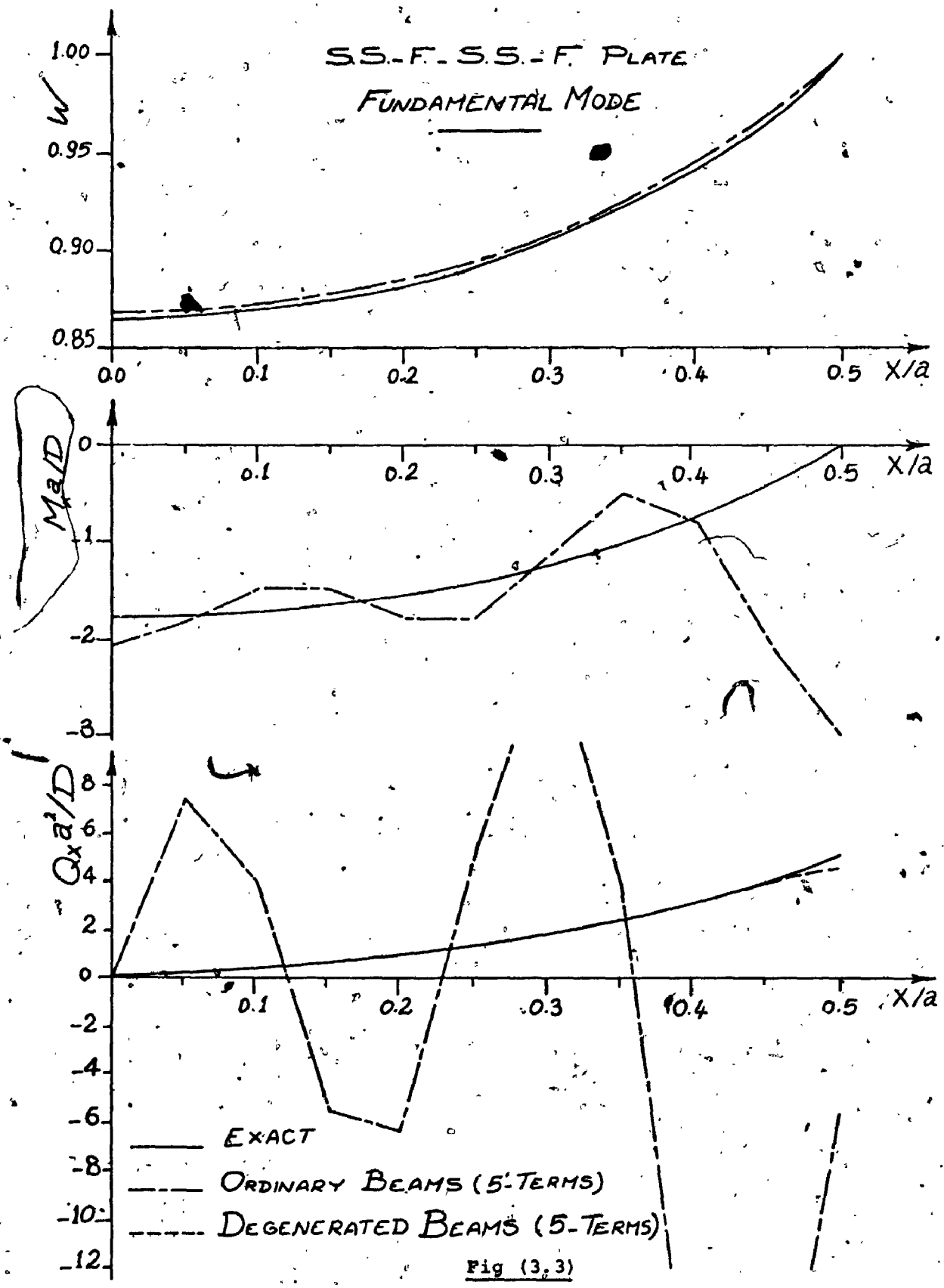
S.S.-F.-S.S.-F. PLATE
FUNDAMENTAL MODE
W
1.00
0.95
0.90
0.85
0.0
0.1
0.2
0.3
0.4
0.5
X/a
Ma²/D
0
-1
-2
-3
Qx a²/D
8
6
4
2
-2
-4
-6
-8
-10
-12
EXACT
ORDINARY BEAMS (5-TERMS)
DEGENERATED BEAMS (5-TERMS)

Fig (3.3)

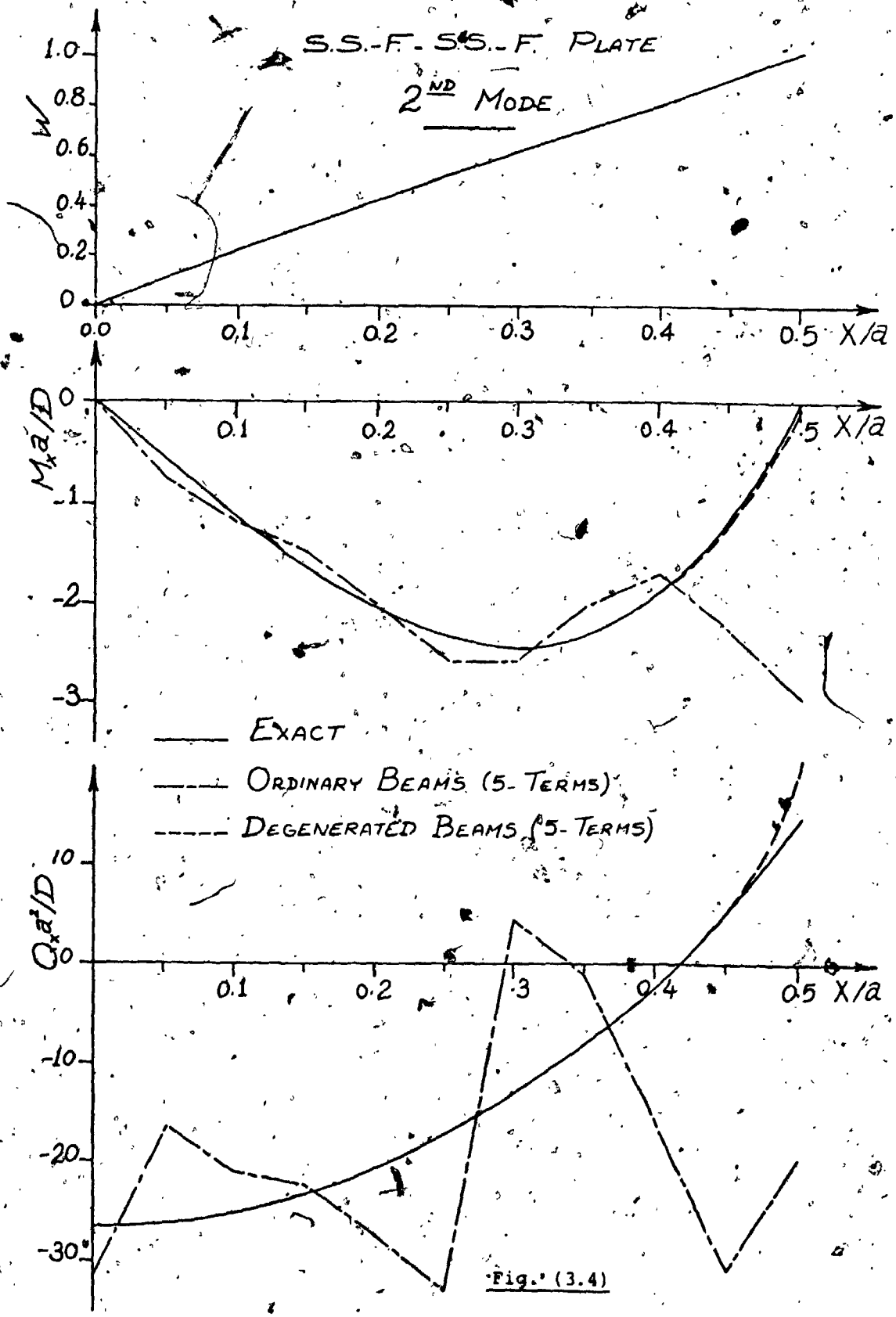
S.S.-F.-S.S.-F. PLATE
2ND MODE
W
1.0
0.8
0.6
0.4
0.2
0
0.0
0.1
0.2
0.3
0.4
0.5 X/a
Mx a²/D
0
-1
-2
-3
0.1
0.2
0.3
0.4
.5 X/a
EXACT
ORDINARY BEAMS (5-TERMS)
DEGENERATED BEAMS (5-TERMS)
Qx a²/D
10
0
-10
-20
-30
0.1
0.2
.3
0.4
0.5 X/a

Fig. (3.4)

2 6

OF/DE

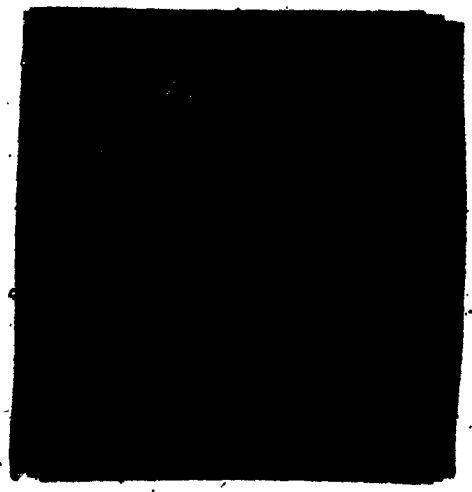

Fig. (3.5)

EFFECT OF ϵ ON THE FREQUENCY-PARAMETER λ FOR A S.S.-F.-S.S.-F. PLATE

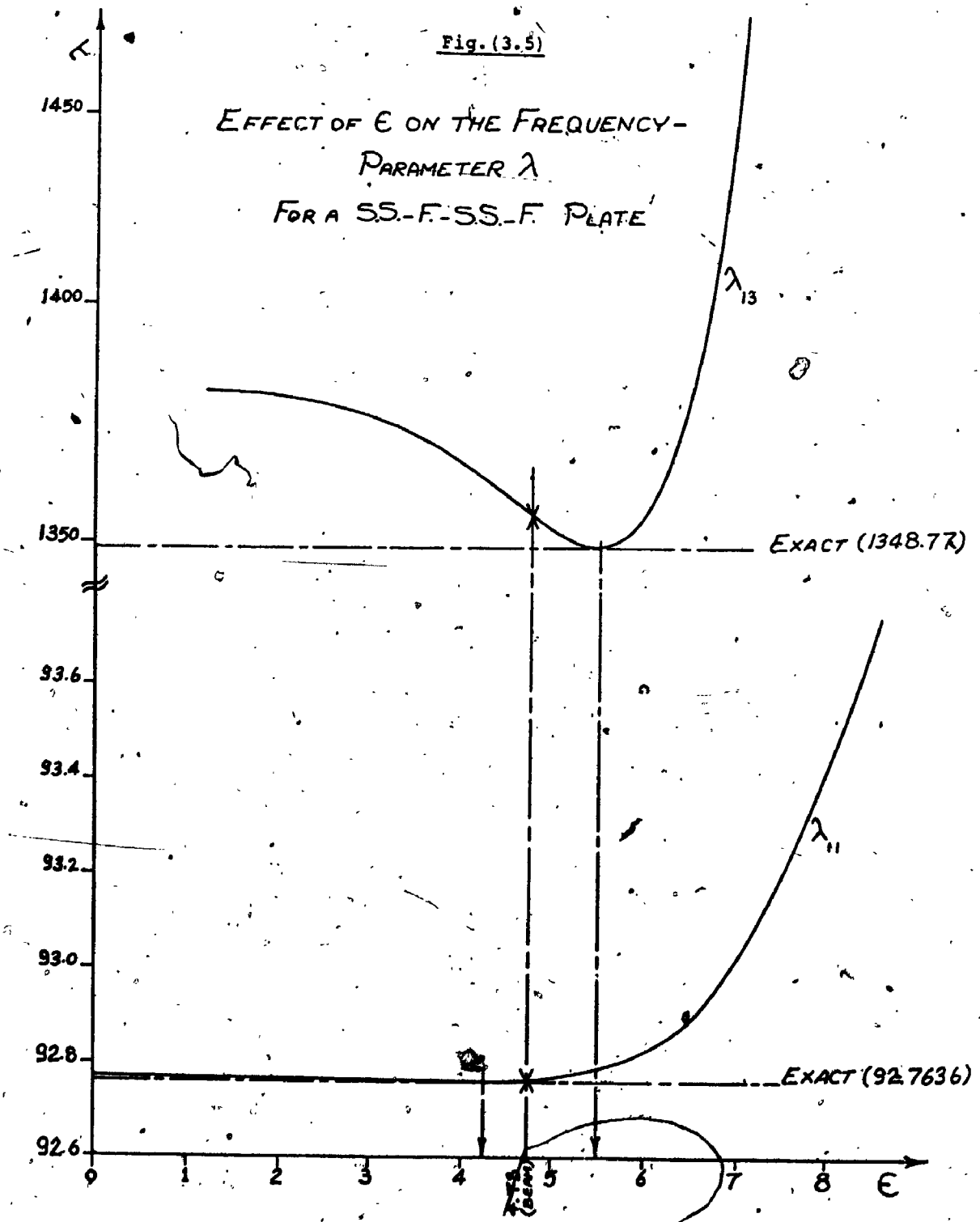

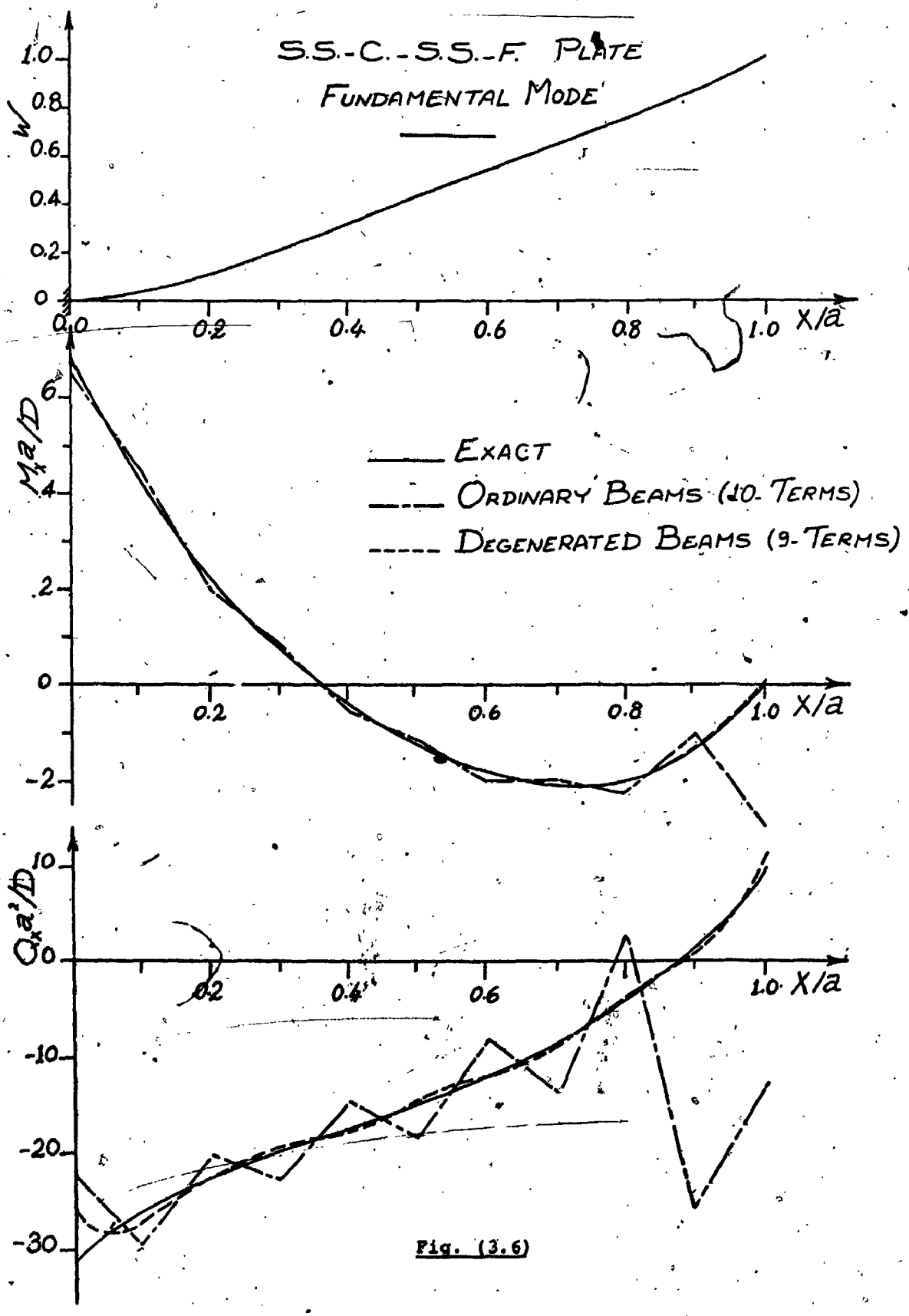
S.S.-C.-S.S.-F. PLATE
FUNDAMENTAL MODE
w
1.0
0.8
0.6
0.4
0.2
0
0.0
0.2
0.4
0.6
0.8
1.0 X/a
Mx a²/D
6
4
2
0
-2
0.2
0.6
0.8
1.0 X/a
EXACT
ORDINARY BEAMS (10 TERMS)
DEGENERATED BEAMS (9-TERMS)
Qx a²/D
10
0
-10
-20
-30
0.2
0.4
0.6
1.0 X/a

Fig. (3.6)

Fig. (3.7)
SS-F-SS-F Plate
Static Loading

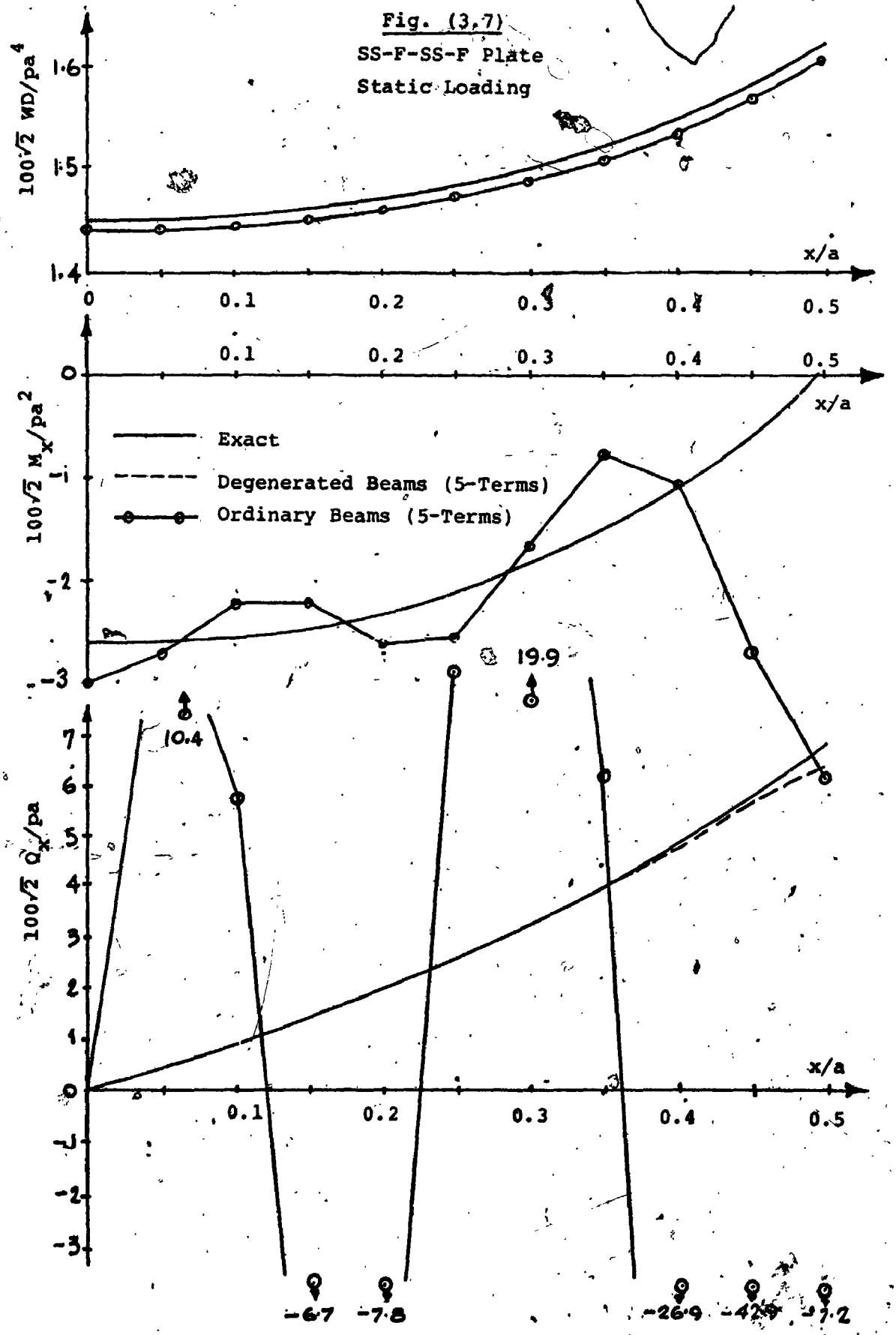

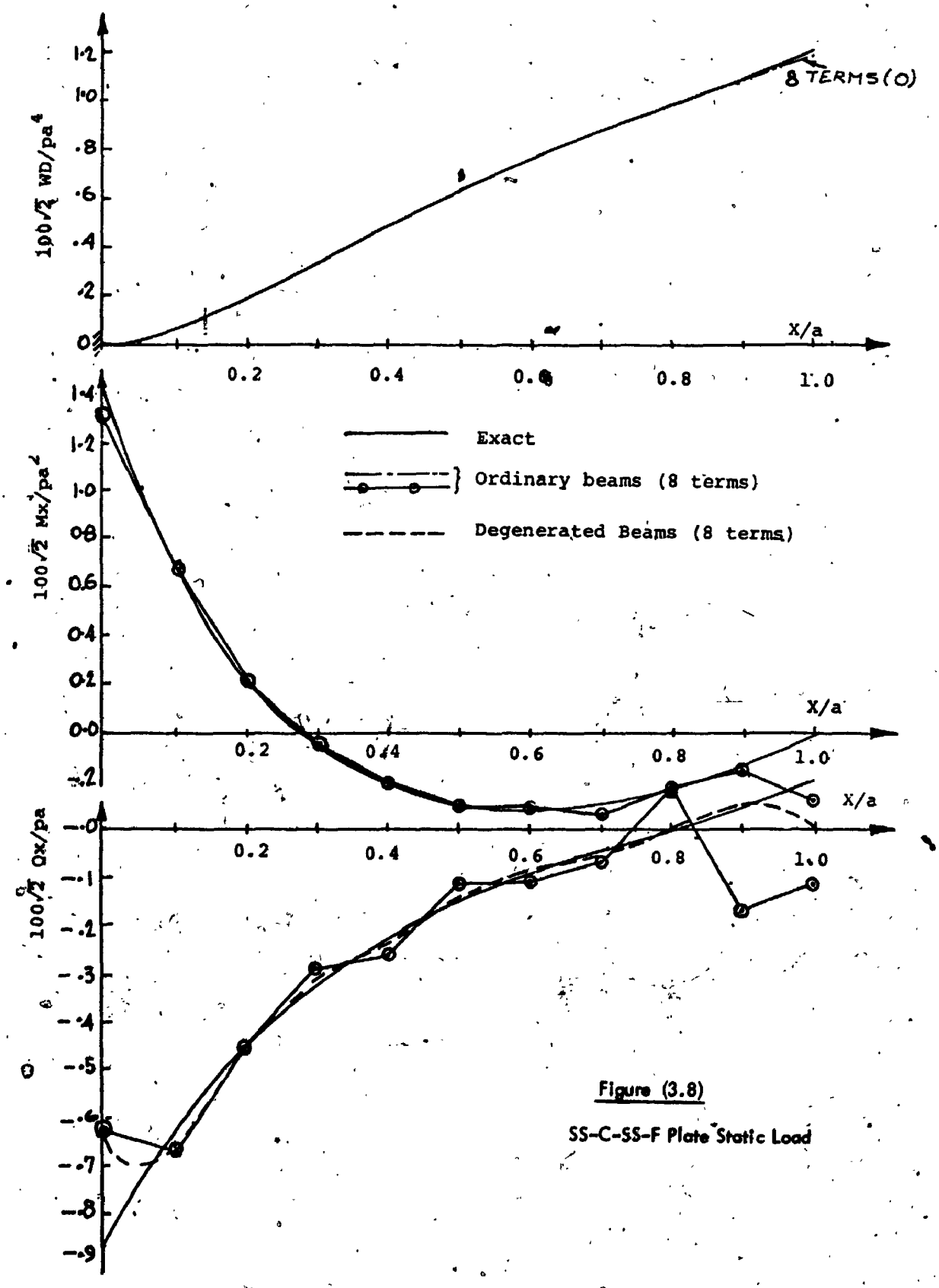

Figure (3.8)

SS-C-SS-F Plate Static Load

Comparison of Second Beam-like Mode Shapes of Fully Free 8 1/2" x 20" x 0.2" Rectangular Plates (Max. Disp. Normalized to -1.0).

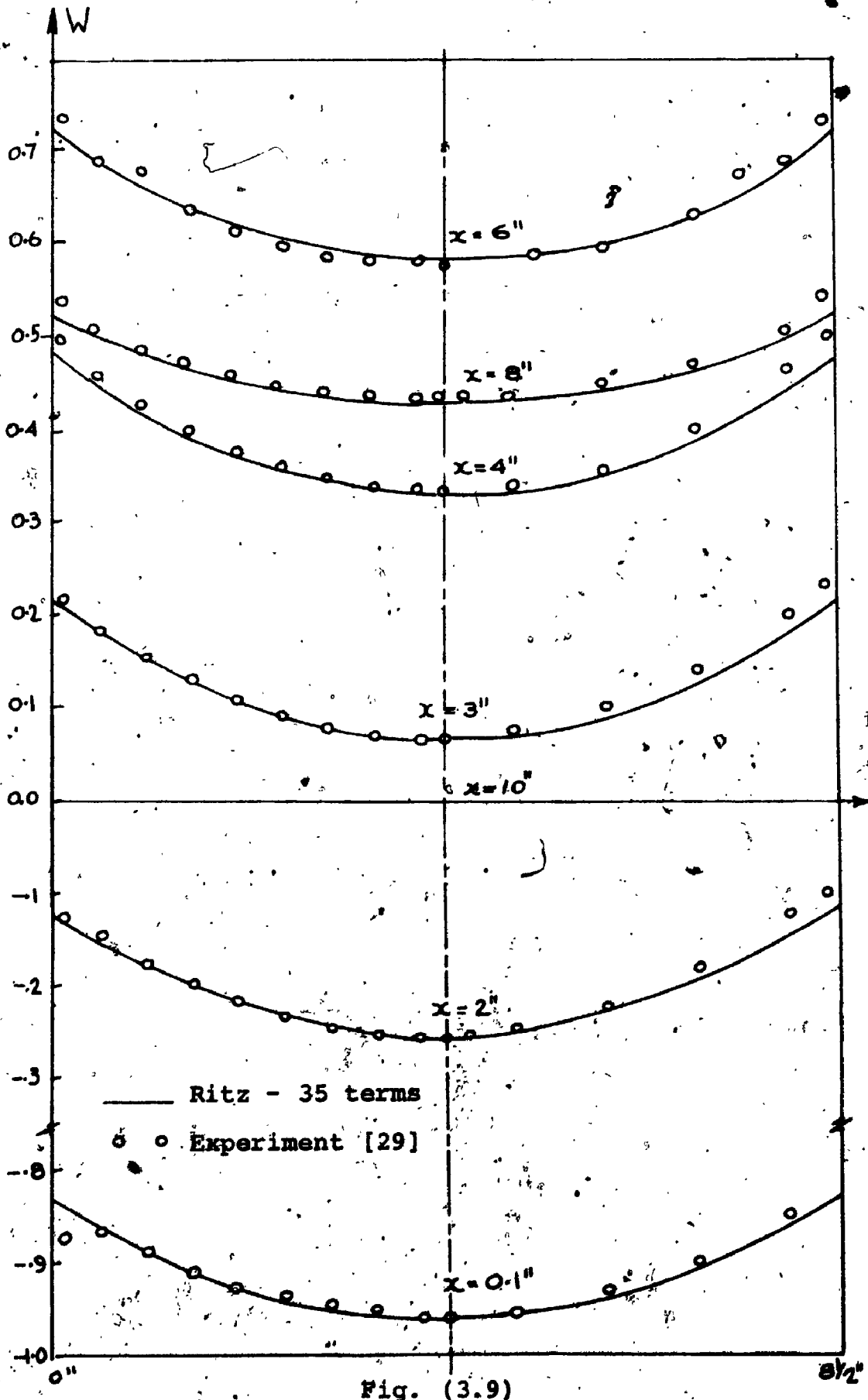

Fig. (3.9)

CHAPTER IV

THE INPLANE PROBLEM

4.1 Introduction

Another important class of plate problems is that of finding the stress components resulting in a plate subject to a given set of boundary and/or body forces acting in the plane of the plate middle surface. This is identified in the field of elasticity as the *plane stress* problem. The importance of this problem is twofold:

- In many practical problems concerning plates or plate systems, the resulting inplane stresses may represent the failure criterion of the structure.
- In the case of a thin plate under de-stabilizing inplane loads, the buckling strength of the plate might limit its load carrying capacity. Determination of the inplane stress resultants acting in the plate mid-surface is an essential step in solving the stability problem.

The two dimensional elasticity problem - including the plane stress problem - has been extensively treated in the standard books on Elasticity. However, analytical solutions for this problem are only obtainable under homogeneous boundary conditions. Problems involving mixed boundary

conditions have been solved using numerical methods (in particular the Finite Difference and Finite Element methods) or experimental techniques (such as Photoelasticity). In addition, a single example was presented in a paper by Timoshenko in 1924 in which he used a four-term polynomial in an energy approach to solve the problem of a billet in a compression test. Relatively poor results were obtained as will be shown in section (4.4.1). In all solutions found, body forces were neglected.

In general, three approaches can be used for the solution of a two-dimensional elasticity problem: the stress function approach; the displacement approach; and a hybrid - or mixed formulation approach. The first of these involves only one independent variable and thus the number of equations to be simultaneously solved in the course of the numerical solution is reduced. Therefore the stress function formulation is used in the following sections for the solution of a variety of plane elasticity problems. The variational formulation presented in chapter II is shown to be applicable, and a direct analogy with the plate bending problem is drawn.

4.2 Statement of the Problem

Again, the plate is assumed to be thin, flat, rectangular, of isotropic material and uniform thickness. The stresses and body forces are assumed to be time independent

and to remain constant across the thickness of the plate. Consequently, the general equations of two-dimensional plane elasticity apply.

The normal stresses in the x and y directions and the shear stress in the xy-plane will be denoted by σ_x, σ_y and τ_{xy} respectively. The equilibrium equations of plane elasticity are

$$\frac{\partial \sigma_x}{\partial x} + \frac{\partial \tau_{xy}}{\partial y} = - F_x,$$

$$\frac{\partial \tau_{xy}}{\partial x} + \frac{\partial \sigma_y}{\partial y} = - F_y, \tag{4.1}$$

where F_x and F_y are the body force components in the x- and y-directions. Furthermore, assuming that the body forces are derivable from a potential function $V(x,y)$ such that

$$\frac{\partial V}{\partial x} = - F_x,$$

$$\frac{\partial V}{\partial y} = - F_y, \tag{4.2}$$

an Airy stress function $\Psi(x,y)$ can be defined by

$$\sigma_x = \frac{\partial^2 \Psi}{\partial y^2} + V,$$

$$\sigma_y = \frac{\partial^2 \Psi}{\partial x^2} + V, \tag{4.3}$$

$$\tau_{xy} = - \frac{\partial^2 \Psi}{\partial x \, \partial y},$$

which guarantees that equations *(4.1)* are identically satisfied. The compatability condition among the inplane stresses then becomes:

$$\Delta\Delta\Psi = -(1-\nu)\Delta V. \qquad (4.4)$$

The problem considered thus turns out to be the solution of equation *(4.4)* under a given set of boundary conditions. Four types of simple boundary conditions may be sought:

1. Free edge; for which the boundary conditions are

$$\sigma_n\big|_\Gamma = p, \qquad \tau_{ns}\big|_\Gamma = q, \qquad (4.5)$$

where σ_n is the component of the stress normal to the free edge; τ_{ns} is the shear stress along the edge; p and q are the normal and tangential components of the external load.

2. Clamped edge; for which the displacements are restricted to those of a rigid body motion; i.e.

$$u_s\big|_\Gamma = C_1, \qquad u_n\big|_\Gamma = C_2 + C_3 s, \qquad (4.6)$$

where u_n and u_s are the normal and tangential components of the displacement, s is the spatial coordinate along the edge, and C_1, C_2, C_3 are constants determined by the externally applied displacements.

3. Normally restrained edge; such as the case of an edge resting against a rigid, frictionless, flat platform [figure (4.1.a)] for which the boundary conditions are

$$u_n\big|_\Gamma = C_2 + C_3 s, \qquad \tau_{ns}\big|_\Gamma = q. \qquad (4.7)$$

4. Laterally restrained edge; in which lateral displacements are restrained, however warping is permitted [see

figure (4.1.b). The boundary conditions in this case are

$$u_s\Big|_\Gamma = C_1, \quad \sigma_n\Big|_\Gamma = p. \qquad (4.8)$$

The plate will be considered to have any combination of these four types of boundary conditions.

4.3 Natural Boundary Conditions and the Variational Formulation

Since the differential equation on hand *(4.4)* is biharmonic in the Airy stress function Ψ, in order to obtain a solution it is necessary to be able to express the boundary conditions given by equations *(4.5)* through *(4.8)* in terms of the same dependent variable (Ψ). The stress boundary conditions given by *(4.5)* may be written directly in terms of Ψ as follows:

$$\sigma_n\Big|_\Gamma = \left(\frac{\partial^2\Psi}{\partial s^2} + V\right)\Big|_\Gamma = p,$$

Hence, $\Psi\Big|_\Gamma = \int \left[\int (p - V\Big|_\Gamma)\, ds\right] ds + [illegible] + B.$

Since only derivatives of the second order of Ψ bear a physical meaning, the constants of integration can be arbitrarily set to zero, yielding

$$\Psi\Big|_\Gamma = \int \left[\int (p - V\Big|_\Gamma)\, ds\right] ds \qquad (4.9)$$

Similarly:

$$\tau_{ns}\Big|_\Gamma = -\frac{\partial^2\Psi}{\partial n\, \partial s}\Big|_\Gamma = q_s$$

Hence, $\frac{\partial \Psi}{\partial n}\Big|_{\Gamma} = -\int q \, ds.$ (4.10)

The clamped edge boundary conditions (4.6) can also be transformed as follows:

$$u_s\Big|_{\Gamma} = \int \varepsilon_s\Big|_{\Gamma} ds + A = C_1,$$

where ε_s is the tangential strain,

hence; $\varepsilon_s\Big|_{\Gamma} = \frac{1}{E}(\sigma_s - \nu \sigma_n)\Big|_{\Gamma} = 0,$

or; $\left(\frac{\partial^2 \Psi}{\partial n^2} - \nu \frac{\partial^2 \Psi}{\partial s^2}\right)\Big|_{\Gamma} + (1 - \nu)V\Big|_{\Gamma} = 0.$ (4.11)

Also,

$$u_n\Big|_{\Gamma} = \int \frac{\partial u_n}{\partial s}\Big|_{\Gamma} ds + B = C_2 + C_3 s,$$

hence; $\frac{\partial u_n}{\partial s}\Big|_{\Gamma} = \left(2\gamma - \frac{\partial u_s}{\partial n}\right)\Big|_{\Gamma} = C_3,$

where γ is the shear strain,

or; $\left(2\frac{\partial \gamma}{\partial s} - \frac{\partial \varepsilon_s}{\partial n}\right)\Big|_{\Gamma} = 0,$

finally it yields;

$$\frac{1}{E}\left[2(1+\nu)\frac{\partial \tau_{ns}}{\partial s} - \frac{\partial}{\partial n}(\sigma_s - \nu\sigma_n)\right]\Big|_{\Gamma} = 0,$$

leading to;

$$\left[-2(1+\nu)\frac{\partial^3 \Psi}{\partial s^2 \partial n} - \frac{\partial}{\partial n}\left(\frac{\partial^2 \Psi}{\partial n^2} - \nu \frac{\partial^2 \Psi}{\partial s^2} + (1-\nu)V\right)\right]\Big|_{\Gamma} = 0$$

or; $\left[\frac{\partial^3 \Psi}{\partial n^3} + (2+\nu)\frac{\partial^3 \Psi}{\partial n \partial s^2}\right]\Big|_{\Gamma} + (1-\nu)\frac{\partial V}{\partial n}\Big|_{\Gamma} = 0.$ (4.12)

The boundary conditions defined by cases (3) and (4) can be expressed as combinations of equations *(4.9)* through *(4.12)*.

Since the boundary conditions *(4.9)* and *(4.10)* include only the fundamental variable Ψ and its first order derivatives, they represent the essential, or forced, boundary conditions of the problem. On the other hand, conditions *(4.11)* and *(4.12)* are the *natural* boundary conditions. In order to arrive at the appropriate variational expression for the plane stress problem, these natural boundary conditions are compared with those given by equation *(2.10)* in the general formulation of Chapter II for the case of an edge parallel to one of the coordinate axes. Also, the differential equation of compatibility *(4.4)* is compared with the general biharmonic equation given by *(2.4)*. From these comparisons, the general variational expression *(2.5)* can be used for the present problem provided the following substitutions are made:

$$P(x,y) = -(1-\nu)\,\Delta V,$$

$$m(s) = (1-\nu)\,V\Big|_{\Gamma},$$

$$q(s) = (1-\nu)\frac{\partial V}{\partial n}\Big|_{\Gamma},$$

also, ν in equation *(2.5)* is to be replaced by $(-\nu)$ and u by Ψ in order to satisfy the expressions for the natural boundary conditions. Equation *(2.5)* now becomes:

$$U = \iint_D \{(\Delta\Psi)^2 - 2(1+\nu)\left[\frac{\partial^2\Psi}{\partial x^2}\frac{\partial^2\Psi}{\partial y^2} - \left(\frac{\partial^2\Psi}{\partial x \partial y}\right)^2\right] + 2(1-\nu)\Delta V \cdot \Psi\}\, dx dy + 2(1-\nu)\int_{\Gamma_1} \frac{\partial}{\partial n}(V\Psi)\, ds. \qquad (4.13)$$

Following the Ritz procedure, the solution is assumed to take the form of a series of trial functions with unknown coefficients. In view of the non-homogeneous forced boundary conditions *(4.9)* and *(4.10)*, the series is assumed to take the form:

$$\Psi_m = \Phi_o + \sum_{k=1}^{m} a_k \Phi_k, \qquad (4.14)$$

such that Φ_o is chosen to satisfy the non-homogeneous boundary conditions *(4.9)* and *(4.10)* whenever they are applied. The functions Φ_k, hence, need only satisfy the homogeneous parts of the forced boundary conditions such that

$$\Phi_k\Big|_\Gamma = \frac{\partial \Phi_k}{\partial n}\Big|_\Gamma = 0, \qquad (4.15)$$

at the free portions of the boundary. At a clamped boundary, however, Φ_o is only required to satisfy the *overall* equilibrium conditions for such portions of the boundary. For example, for a clamped edge of length "l" adjacent to two free edges, it will be required that;

$$\int_0^l \left(\frac{\partial^2 \Phi_o}{\partial s^2} + V\right) ds = P,$$

$$\int_0^l \left(-\frac{\partial^2 \Phi_o}{\partial s \partial n}\right) ds = Q,$$

$$\int_0^l \left(\frac{\partial^2 \Phi_o}{\partial s^2} + V\right) . s\,ds = M,$$

where M, P, and Q are the resultant inplane bending moments, normal and tangential forces per unit thickness acting at the clamped edge. This requirement is due to the fact that the resultant forces and moments due to each of the terms Φ is nil. This may be shown as follows:

$$\int_0^l \left(\frac{\partial^2 \Phi_k}{\partial s^2}\right) ds = \left[\frac{\partial \Phi_k}{\partial s}\right]_0^l = 0$$

in view of the boundary conditions (4.15) applicable at the free edges adjacent to the clamped edge under consideration, and consequently applicable at $s = o, l$. Similarly;

$$\int_0^l \left(-\frac{\partial^2 \Phi_k}{\partial s \partial n}\right) ds = \left[\frac{\partial \Phi_k}{\partial n}\right]_0^l = 0$$

since Φ_k is identically equal to zero along the adjacent free edges. Finally;

$$\int_0^l \left(\frac{\partial^2 \Phi_k}{\partial s^2}\right) s\,.\,ds = \left[s\frac{\partial \Phi_k}{\partial s}\right]_0^l - \int_0^l \left(\frac{\partial \Phi_k}{\partial s}\right) ds$$

$$= l \left.\frac{\partial \Phi_k}{\partial s}\right|_l - \left[\Phi_k\right]_0^l = 0.$$

The set of functions Φ_k is also required to satisfy the continuity and completeness conditions mentioned in section (2.3) both in the domain and at the portions of the

boundary subject to natural boundary conditions (e.g. at the clamped edges). The obvious combinations of these conditions can be easily stated for the boundary conditions of types (3) and (4) mentioned earlier.

Looking back at the homogeneous parts of the boundary conditions *(4.9)* through *(4.12)*, and comparing them to those of the plate in bending given in section (3.1) by equations *(3.1)* through *(3.4)*, a complete analogy between the two types of problems can be immediately established:

1. The inplane free edge corresponds to the out-of-plane clamped edge. The non-homogeneous parts of the inplane boundary conditions - corresponding to the applied inplane loads - are analogous to prescribed displacements and rotations being applied at the clamped edge in the case of the plate in bending.
2. The inplane clamped edge corresponds to an out-of-plane free edge provided that ν-Poisson's ratio - is given the opposite sense. The non-homogeneous parts of the inplane edge conditions may be looked upon as bending moments and shear forces applied at the out-of-plane free edge.
3. Similarly, a laterally restrained edge corresponds to an out-of-plane simply supported edge and a normally restrained edge corresponds to an out-of-plane sliding edge.
4. Comparing the inplane compatability equation and the out-of-plane equilibrium equation indicates that the

quantity $-(1-\nu)\,\Delta V$ corresponds to a transverse load $P(x,y)$ which may be acting on the plate in the case of the plate bending problem.

With this analogy in mind, the set of assumed functions Φ_k of equation (4.14) may be conveniently replaced by a set of multiplications of appropriately chosen ordinary and/or degenerated beam functions. Hence equation (4.14) becomes:

$$\Psi_{mn} = \Phi_o + \sum_{i=1}^{m}\sum_{j=1}^{n} A_{ij}\,\phi_i(x)\,\psi_j(y), \qquad (4.16)$$

where ϕ_i and ψ_j are beam functions chosen in light of the above-mentioned analogy. Following the same analogy, the right hand side of equation (4.4) is expanded in a series similar to (3.6) such that:

$$-(1-\nu)\,\Delta V = \sum_{i=1}^{m}\sum_{j=1}^{n} B_{ij}\,\phi_i(x)\,\psi_j(y). \qquad (4.17)$$

substituting (4.16) and (4.17) into (4.13) and following the Ritz procedure outlined in Chapter II, one obtains

$$\int_0^b\int_0^a \Big\{ \sum_{i=1}^{m}\sum_{j=1}^{n} A_{ij}\,[(\phi_i''\psi_j + \phi_i\psi_j'')(\phi_r''\phi_s + \phi_r\phi_s'') - (1+\nu)\cdot$$

$$\cdot(\phi_i''\psi_j\cdot\phi_r\psi_s'' + \phi_i\psi_j''\cdot\phi_r''\psi_s - 2\cdot\phi_i'\psi_j'\cdot\phi_r'\psi_s')\,] -$$

$$- B_{ij}[\phi_i\psi_j\phi_r\psi_s]\Big\}\,dx\,dy + (1-\nu)\int_\Gamma \frac{\partial}{\partial n}(V\phi_r\psi_s)\,ds +$$

$$+ \int_0^b\int_0^a [(\Phi_{o,xx} + \Phi_{o,yy})(\phi_r''\psi_s + \phi_r\psi_s'') - (1-\nu)\cdot(\Phi_{o,xx}\cdot$$

$$\cdot\,\phi_r\psi_s'' + \Phi_{o,yy}\cdot\phi_r''\psi_s - 2\cdot\Phi_{o,xy}\cdot\phi_r'\psi_s')]\,dx\,dy = 0,$$

$$(r = 1,2,\ldots,m;\ s = 1,2,\ldots,n).$$

This can be rearranged in a form analogous to equation (3.7) such that:

$$\sum_{i=1}^{m}\sum_{j=1}^{n} C_{ij}^{(rs)} \cdot A_{ij} = \bar{P}^{(rs)} + \bar{Q}^{(rs)}, \quad (r=1,2,\ldots,n;\ s=1,2,\ldots,m), \tag{4.18}$$

where

$$\bar{Q}^{(rs)} = -(1-\nu)\int_{\Gamma} \frac{\partial}{\partial n}(\nabla\phi_r\psi_s)\,ds - \int_{o}^{b}\int_{o}^{a} [(\Phi_{o,xx} + \Phi_{o,yy})$$

$$(\phi_r''\psi_s + \phi_r\psi_s'') - (1+\nu)(\Phi_{o,xx} \cdot \phi_r\psi_s'' + \Phi_{o,yy} \cdot \phi_r''\psi_s - 2\Phi_{o,xy}$$

$$\cdot \phi_r'\psi_s')]\,dx\,dy \,. \tag{4.18a}$$

The coefficients $C_{ij}^{(rs)}$ and $\bar{P}^{(rs)}$ are the same as were defined in equation (3.7) with ν replaced by $(-\nu)$. Consequently, the same integrals defined in (3.8) may be used in the in-plane problem. Moreover, the same computer program used for the bending problem - with the exception of an additional loading vector - may be used for the plane stress problem with Poisson's ratio being defined as a negative value. The only additional task is the evaluation of the $\bar{Q}$ vector involving integrals of multiplications of Φ_o and the beam functions and/or their derivatives. Since in most practical cases Φ_o is found to be a low order polynomial, this usually proves to be a simple task as will be shown in the numerical examples presented in the following section.

4.4 Numerical Examples

In this section, a number of numerical examples are presented in which the above-mentioned procedure is applied to specific problems and the results realized are compared to those obtained by alternate methods of solution. The purpose of this numerical study is threefold: Firstly; to prove the applicability of the preceding analysis for solving different types of problems, and to establish levels of confidence in these solutions as opposed to those arrived at through other means. Secondly; to obtain solutions for problems for which satisfactory solutions have not been published before. And thirdly; to obtain reliable series representations for the stress fields resulting in certain plate problems of particular importance in order to be used as the basis for the stability analysis of such plates as will be presented in the following chapter.

Three classes of problems will be analysed:

Example (1); A plate having two parallel clamped edges and the other two free undergoing direct compression.

Example (2); Cantilever plates, and plates having two parallel edges clamped and the other two free under an end shearing load.

Example (3); A cantilever plate under a general inplane acceleration load.

For each case it is only necessary to choose the value of Φ_o, to identify the type of symmetry which may be avail-

able, and then to obtain the expression for $\bar{Q}^{(rs)}$ and evaluate the integrals involved therein. Once this has been accomplished, the matrix relation *(4.18)* can be set up and solved as mentioned previously in the case of plate bending. The resulting coefficients A_{ij} are then used to evaluate the inplane stresses σ_x, σ_y and τ_{xy} through substituting *(4.16)* into *(4.3)* and performing the necessary differentiations. The principle stresses σ_{max}, σ_{min}, and τ_{max}, as well as the direction of principle stress θ at any point, can then be evaluated using the well known relations:

$$\tau_{max} = \sqrt{\left(\frac{\sigma x - \sigma y}{2}\right)^2 + \tau_{xy}^2}$$

$$\sigma_{max} = \frac{\sigma x + \sigma y}{2} + \tau_{max}, \qquad (4.19)$$

$$\sigma_{min} = \frac{\sigma x + \sigma y}{2} - \tau_{max}, \text{ and}$$

$$\theta = \frac{1}{2} \tan^{-1} \left[2 \tau_{xy} / (\sigma n - \sigma y)\right].$$

4.4.1 Plates Under Direct Compression

A look at the barrelled shape of an initially cylindrical specimen after a compression test reveals the important role of Poisson's expansion in a nominally "pure" compression test. If the coefficient of friction between the crossheads and the test specimen is of order comparable to Poisson's ratio, it becomes unrealistic to assume the loaded edges to be free and the assumption of a uniform

state of stress becomes a matter of pure academic interest. In fact, if the coefficient of friction is equal to, or greater than, Poisson's ratio, the test specimen will behave as if it were perfectly clamped - provided that the crossheads may be assumed to remain rigid. The same argument applies for a plate under compression (or tension) since it is virtually impossible to apply mechanical loads to a completely free edge. Consequently, the assumption of a uniform uniaxial state of stress frequently used to investigate the stability of plates is not realistic, and the actual stress pattern set up in practice may deviate considerably from this assumption.

Timoshenko in 1924 was first to study this problem using essentially the same technique as presented in this Chapter. Timoshenko, however, used a four-term polynomial series in his solution. His results, although representing the general trend of the solution, will be shown to be of insufficient accuracy.

The ordinary narrow-plate solution for a problem often offers a suggestion for the choice of the function ϕ_o. For this problem - for instance - this solution is represented by a uniform uniaxial compression; $\sigma_y = p$, $\sigma_x = \tau_{xy} = 0$. This is achieved by assuming - in the coordinate system shown in Figure (4.2) - that

$$\phi_o = px^2/2 \qquad (4.20)$$

This function satisfies the boundary conditions of zero normal and shear forces at the free edges $x = \pm\, a/2$.

It also satisfies the overall equilibrium conditions at the clamped edges $y = \pm b/2$.

It is obvious from the symmetry of the geometry and loading that the stress function Ψ will be symmetric about both the x- and the y- axes. ϕ_r and ψ_s will be chosen as the first m and n *symmetric* members of the families of clamped-clamped beam functions and free-free *degenerated* beam functions respectively. Since there are no body forces acting on the plate, $\bar{P}^{(rs)}$ is equal to zero. The vector $\bar{Q}^{(rs)}$ is calculated as follows:

Starting with its definition given by equation *(4.18a)*, substituting from *(4.20)*, and remembering that the body force potential function V is zero, it may be written that

$$\bar{Q}^{(rs)} = p \int_{-b/2}^{b/2} \int_{-a/2}^{a/2} [-(\phi_r'' \psi_s + \phi_r \psi_s'') + (1+\nu)\phi_r'' \psi_s''] \, dx\,dy .$$

Since, due to the boundary conditions *(4.15)*, $\int_{-a/2}^{a/2} \phi_r'' \, dx$ is zero, the above equation becomes:

$$\bar{Q}^{(rs)} = \nu p \cdot \left(\int_{-a/2}^{a/2} \phi_r \, dx \right) \cdot \left(\int_{-b/2}^{b/2} \psi_s'' \, dy \right) . \qquad (4.21)$$

Remembering that for the beam functions

$$\phi_r'''' = \varepsilon_r^4 \, \phi_r / a^4 , \qquad (4.22)$$

where ε_r is the eigen value of the beam function, equation *(4.21)* now becomes:

$$\bar{Q}^{(rs)} = \frac{4\nu p a^4}{\varepsilon^4} \cdot \phi_r''' (a/2) \cdot \psi_s' (b/2) .$$

which can easily be computed for all the values of r and s of interest.

Table (4.1) shows the results obtained using 3, 10, 20, 35 and 49 terms in the Ritz series for a square plate with ν equal to 0.25 at different characteristic positions within the plate. The corresponding results obtained by Timoshenko [30] using a four-term polynomial are also shown in the table. It can be seen that everywhere, except at the clamped edges themselves, the 20 and 49 term solutions differ by less than 0.2% indicating a high rate of convergence. However, at the plate corners the stress does not seem to be converging to a particular value but, instead, keeps on increasing as more terms are taken in the series. This is due to the fact that singularity occurs at the corner points because of the stress concentration resulting from the sudden change of geometry encountered as the stresses flow from the plate into the infinitely stiff support. In mathematical terms, this singularity can be shown as follows: At the free edge, due to the boundary conditions, the following applies at any point - including the corner point

$$\sigma_x = 0, \quad \frac{\partial \sigma x}{\partial x} \equiv \frac{\partial \tau xy}{\partial y} = 0. \qquad (4.23)$$

Also on the clamped edge, at a small distance δx from the corner, equation (4.11) gives

$$\frac{\partial^2 \Psi}{\partial y^2} - \nu \frac{\partial^2 \Psi}{\partial x^2} = 0,$$

or $\sigma x = \nu . \sigma y \neq 0,$

Table(4.1)

Convergence and comparison of stresses in a C-F-C-F square plate under direct Compression, Poisson's ratio = .25. P/(at) = 1

Position	Stress	Degenerated beam series -(m x n) terms					4 term polynomial [30]
		1 x 3	2 x 5	4 x 5	5 x 7	7 x 7	
y = 0 x = 0	σ_x σ_y	.017 1.042	.024 1.035	.025 1.037	.025 1.037	.025 1.036	.013 1.041
y = 0 x = .25	σ_x σ_y	0.009 1.007	0.010 1.014	.011 1.014	0.010 1.013	.010 1.013	--- 1.009
y = 0 x = .4	σ_x σ_y	.002 .963	.001 .962	0.001 .963	0.001 0.964	.001 0.964	--- .963
y = .3 x = 0	σ_x σ_y	.110 1.017	.103 1.002	.107 1.005	.107 1.007	.107 1.006	.113 1.013
y = .3 x = .3	σ_x σ_y τ_{xy}	.043 .997 .043	.057 1.010 .047	.062 1.012 0.052	.061 1.009 0.052	.062 1.010 .052	--- --- ---
y = .5* x = 0	σ_x σ_y	.309 .912	.189 .978	.213 .969	.260 .932	.254 .935	.292 .959
y = .5* x = .25	σ_x σ_y τ_{xy}	.168 .986 .163	.294 .920 .121	.213 .977 .067	.246 .943 .066	.249 .944 .062	--- .949 .148
y = .5 x = .5	σ_y	1.144	1.261	1.425	1.495	1.590	1.302

* Exact solution requires that $\sigma_x = 0.25\sigma_y$

which contradicts (4.23) except if

$$\left(\frac{\partial^2 \sigma x}{\partial x^2} = \frac{\partial^4 \Psi}{\partial x^2 \partial y^2} = \frac{\partial^2 \sigma y}{\partial y^2}\right)\Bigg|_{x = y = a/2} \to \infty$$

Since the rate of change of σy - $\partial \sigma y / \partial y$ - at a small distance from the clamped edge is finite; hence $\partial \sigma y / \partial y \to (-\infty)$ at the corner point and σ_y itself grows indefinitely.

Despite this singularity, which introduces an inevitable error at the corner points, only small errors are experienced at a small distance from the corner, as can be seen from the table. These errors, however, are much higher than those at a large distance from the corners. A comparison with the results of Timoshenko, shows that they are close to those obtained using the three term series, indicating an error of the order of 5 to 10% at a distance of $(a/4)$ from the corner.

Although no exact solutions are known in order to be used as a basis for assessing the accuracy of the solution, the known boundary conditions of zero displacements at the clamped edge can be used for this purpose. This measure, however, seems to be too severe - due to the existence of the singular points on the clamped edges - leading to a very conservative estimate for the expected errors. The actual errors at a small distance from the clamped edge are much smaller, as indicated by the rate of convergence of the solutions. Figure (4.3) shows a plot of the edge displacements obtained using 25 and 49 terms in the series as compared

to the maximum plate displacements. It can be seen that the edge displacements diminish as the solution is refined and converge towards the exact value of a zero edge displacement. Except for a very small distance near the singular point, the displacements obtained using the 49 term series are less than 2% of the maximum displacement of the plate. However, at the points of maximum displacements, the very small difference between the 25 and 49 term solutions indicates much better accuracy. Note that the normal displacement results plotted represent the difference between the displacements at any point on a cross section and that at the centre line $(x = 0)$ of this section in order to eliminate the rigid body motions of the edge. Poisson's ratio is taken as 0.3.

In Figure (4.4), contour lines representing the principle stresses σ_1 and σ_2, the principle shear τ and the angle θ defining the direction of the principle stresses, are plotted. These four quantities were computed at the corners of a 15 x 15 square mesh, on one quarter of the plate, using equation *(4.19)*. A contour plotting routine (UCON2) was then modified and used to plot the contour lines shown in the figure based upon this mesh. The different points on the contour lines are obtained using linear interpolation between the nearest mesh points. A smoothing function was then applied to the resulting broken contour lines to obtain the continuous smooth contours shown in the figure.

Finally, these lines were plotted on the CALCOMP plotter using the PDP11 computing system, and the resulting plots photographically reduced to the desired size. The results shown are for a square plate under compression with Poisson's ratio taken as 0.3 as well as a plate of a side ratio 2:1.

4.4.2 Plates Under End Shearing Loads

Two plates under end shearing loads are considered in this section. The first plate has two parallel edges clamped and the other two free, while the second is a cantilever. In both cases, an end shearing load is applied in a direction perpendicular to the two parallel free edges. The coordinate system and the loading condition in each case are shown in figure (4.5). Approximate stress patterns for these two problems have been assumed by the author in 1971 [19] and used as the basis for a stability analysis. These approximate solutions satisfy only the free edge boundary conditions, the equilibrium and compatability conditions, and the overall equilibrium conditions at the clamped edges. It is therefore found desirable to re-examine these assumed loading patterns in the light of the present more rigorous approach in order to be able to establish the effect of similar approximations upon the accuracy of the stability analysis discussed in the next chapter.

The approximate solutions suggested in reference [19], which are composed of parabolically varying shear stresses

and linearly varying bending stresses, will be used as the starting solution - i.e. Φ_o - for the present analysis. As mentioned above, these solutions satisfy the free edge boundary conditions as well as overall equilibrium conditions for the clamped edges; which are the conditions required for the choice of Φ_o stated in section (4.3). Moreover, these solutions are expected to be good approximations away from the clamped edges since they only violate those boundary conditions. The function Φ_o is thus chosen to be:

$$\Phi_o = \frac{6P}{a^3}\left(\frac{x^3}{3} - \frac{a^2x}{4}\right) \cdot y, \qquad (4.24)$$

which is valid for both cases. "P" represents the shearing force per unit width of the plate.

It can be seen that the plate geometries are symmetric about the y-axes and so are the applied shearing loads. Since the shear stresses include the first derivative with respect to x (*i.e.* $\partial^2\Psi/\partial x.\partial y$), the stress functions $\Psi(x,y)$ must be anti-symmetric about the y-axes. Since Φ_o is also anti-symmetric, only the anti-symmetric members of the clamped-clamped beam functions need be considered for the family $\phi_r(x)$ in equation *(4.14)*. Similarly, for the case of the plate having two parallel clamped edges, anti-symmetry conditions about the x axis also exist, and only anti-symmetric members of the *degenerated* free-free beam functions need be considered for the family $\psi_s(y)$. Obviously, clamped - free *degenerated* beam functions are to be used in the y-direction for the case of the cantilever plate.

As soon as the choice of ϕ_o, ϕ_r and ψ_s has been made for the problem, the evaluation of $\bar{Q}^{(rs)}$ becomes a matter of performing the necessary differentiations and integrations. For the plate with two parallel clamped edges:

$$\bar{Q}^{(rs)} = \frac{-12P}{a^3} \int_{-b/2}^{b/2} \int_{-a/2}^{a/2} \{ x \cdot y \, (\phi_r'' \psi_s + \phi_r \psi_s'') - (1+\nu) \cdot$$

$$\cdot [x \cdot y \cdot \phi_r \psi_s'' - (x^2 - \frac{a^2}{4}) \cdot \phi_r' \psi_s'] \} \, dx dy$$

$$= \frac{-12P}{a^3} [I_r^{12} J_s^{10} - \nu I_r^{10} J_s^{12} + (1+\nu)(I_r^{21} - \frac{a^2}{4} I_r^{01}) J_s^{01}],$$

where $I_r^{ij} = \int_{-a/2}^{a/2} x^i \frac{d^j \phi_r}{dx^j} \, dx,$

and $J_s^{ij} = \int_{-b/2}^{b/2} y^i \frac{d^j \psi_s}{dy^j} \, dy.$

Upon evaluating these integrals through integration by parts, the above equation finally becomes

$$\bar{Q}^{(rs)} = 12Pa[\frac{a\phi_r'''(\frac{a}{2}) - 2\phi_r''(\frac{a}{2})}{\epsilon_r^4}][2(2+\nu)\psi_s(\frac{b}{2}) + b\nu\psi_s'(\frac{b}{2})]$$

Similarly, for the cantilever plate:

$$\bar{Q}^{(rs)} = 12Pa[\frac{a\phi_r'''(\frac{a}{2}) - 2\phi_r''(\frac{a}{2})}{\epsilon_r^4}][(2+\nu)\psi_s(b) + b\nu\psi_s'(b)].$$

The shear stress profiles at different cross-sections of a square plate with two parallel clamped edges and two free ones are plotted in figure (4.6) with Poisson's ratio taken as 0.3. Results are obtained using 25 and 49 term series and they coincide within the thickness of the lines except at the clamped edge where relatively large errors - due to the singularity effect - are experienced. However, these edge errors seem to diminish rapidly as the number of terms in the series increases, and the edge shear appears to approach a uniform distribution as expected. On the other hand, as the distance from the clamped edge is increased, the profiles converge towards the well known parabolic distribution expected at a large distance from the edge. At the centre line $(y = 0)$ the deviation from the parabolic distribution is already less than 2%.

A contour representation for the principle stress distributions of the above-mentioned plate, as well as a plate of side ratio 2:1, are shown in figures (4.7) and (4.8). It may be noticed that a stress concentration occurs at the corners for the same reasons argued in section (4.4.1).

Figure (4.9) shows a comparison of the stress distributions obtained using a 63 term series with those obtained using the simple beam theory for a square cantilever plate having a side length of (a) and a value of Poisson's ratio of 0.25. The figure shows large deviations from the beam theory near the clamped edge. At a

distance of (0.25a) this difference drops to only a few percent. The wavy nature of the τ_{xy} curve at the edge reflects the inaccuracy introduced due to the existence of the singular point. It is clear, however, that the shear stress distribution approaches a uniform, rather than a parabolic profile at the clamped edge. Also, the lateral stress σ_x approaches the ideal value $\bar{\sigma}_x$ which is determined by the boundary condition

$$\bar{\sigma}_x - \nu\sigma_y = 0,$$

which is shown by the dotted line on the graph and is obviously far from the zero value assumed by the beam theory. The present comparison is further shown in figure (4.10) which shows that the deviation is almost confined to a region near the clamped edge of a width approximately equal to one third the length of that edge.

For the purpose of comparison, the above problem has also been solved using a finite element discretization, and the results are shown in figure (4.10) superimposed upon the Ritz results. The finite element solution was obtained using 48 first order rectangular elements with a total of 108 degrees of freedom. Since no symmetry exists in the displacement domain, reduction of the degrees of freedom was not possible; this represents an obvious drawback for the displacement method as opposed to the stress function formulation used in this analysis. Due to the nature of the first order rectangular elements, stresses obtained

are *almost* uniform throughout each element with relatively large stress discontinuities at the interface lines. Consequently, the resulting stresses are only reliable at the centres of the elements - provided that the stress variation across the element is approximately linear. Hence, it is not possible to obtain reliable stresses at the plate edges themselves but only half an element's width away from them as shown in the figure. As a result, the finite element solution was not able to match the extremely high stress gradients occurring near the singular points (the plate corners). Agreement between the Ritz and finite element solutions is excellent except at points where the latter - due to the type and size of elements used - is expected to be unable to match the rapid stress variations. This situation is typically indicated at the point (.437a, .917b) where the variation of the stress σ_x is so sharp that the *average* stress obtained by the finite element does not represent the true stress at the centre of the element. The same also happens for σ_y at (.313a, .917b).

A Convergence study based upon the degree of satisfaction of the natural boundary conditions at the clamped edge is shown in figure (4.11). Displacement profiles at the edge as well as at the sections of maximum displacement (relative to the centre line of the plate) are plotted as obtained using 40 and 63 term series with Poisson's ratio taken as 0.25. The same trends observed in section

(4.4.1) for the plate under direct compression are reproduced here. The maximum edge error for the 63 term solution is shown to be less than 5% except in the immediate vicinity of the singular point. The contour representation of the principle stress distributions for the square cantilever treated above is shown in figure (4.12) with Poisson's ratio taken as 0.3 The same technique described in association with figure (4.4) was used for obtaining these contour plots.

4.4.3 Cantilever Plates Under General Gravitational Loads

Although present day aerospace structures may be subject to large gravitational loads during the launch periods, it seems that very little attention has been given to the study of the effect of such forces upon plates. Within the limitations of the linear theory of plates, the effect of a general gravitational load may be obtained by super-position of the effects due to the transverse and inplane components of such a load on the plate. While the effect of a transverse acceleration is relatively simple to analyse as it usually results in a static plate bending problem under a uniform transverse load, the effect of the inplane component is more involved. This latter problem has only been dealt with - to the author's knowledge - by Herrmann [31], Wang and Sussman [32], Frauconneau and Marangoni [33] and by Simons and Leissa [18]; with the main object of studying the effect of such an

acceleration upon the vibration and/or stability of the plate. In all but the last reference, no attempt was made to determine the stress condition that will be set up in the plate due to the acting body force; instead, a linearly varying uniaxial stress was assumed. This assumption implies an acceleration perpendicular to a pair of the plate edges and a complete freedom for the palte to deform in its plane. The first of these assumptions restricts the applicability of the analysis to the said condition, and the second is virtually impossible to achieve in practice. Reference [18], thus, seems to be the only published work which treats the general gravitational loading condition and attempts the solution of the resulting elasticity problem for a practical set of boundary conditions; namely a cantilever plate. In that reference, a four term series solution - which satisfies the equilibrium and compatability conditions throughout the plate, the boundary conditions at the two parallel free edges and the overall equilibrium conditions at the other two edges - was presented.

In this section, the problem treated in the above reference is reexamined using the Ritz formulation presented earlier in this chapter. It will be shown that, since the solution obtained in reference [18] does not consider in any way the natural boundary conditions at the clamped edge, it deviates grossly near that edge. Finite element solutions were also obtained and are shown to

corroborate the results reached by the present analysis.

Figure (4.13) shows the loading condition and coordinate system used for the problem. Since the problem is a linear one, the solution can be obtained by linearly combining the stress resultants due to two fundamental loading conditions; 1) a unit g-acceleration in the y-direction and 2) a unit g-acceleration in the negative x-direction. This separation has the added advantage that the first loading condition results in a symmetric, and the second in an antisymmetric, stress function distribution about the y-axis; consequently reducing the number of equations to be solved for each case by a factor of two. In the following, each of the two loading conditions will be treated separately:

Case 1); a unit g acceleration in the y-direction:

The body-force potential function V defined by equation (4.2) is given by

$$V = \rho g y, \tag{4.25}$$

where ρ is the density of the plate material. By inspection, a function ϕ_o which satisfies the boundary conditions at the three free edges, as well as the overall equilibrium conditions at the clamped edge, is

$$\phi_o = - \rho g\, y^3/6 \ . \tag{4.26}$$

In accordance with the analogy presented in section (4.3) and in view of the symmetry of the problem, the functions ϕ_r are taken to be the set of symmetric clamped-clamped beam functions. Likewise, the functions ψ_s are taken to be

the family of clamped-free *degenerated* beam functions. Substituting *(4.25)* and *(4.26)* into the expression defining $\bar{Q}^{(rs)}$ given by equation *(4.18a)* it becomes

$$\bar{Q}^{(rs)} = \rho g\{-(1-\nu)\int_{-a/2}^{a/2} \frac{\partial}{\partial y}(y\phi_r\psi_s)\,dx - \int_o^b \int_{-a/2}^{a/2} [y(\phi_r''\psi_s + \phi_r\psi_s'') - (1-\nu)\, y\,\phi_r''\psi_s]\,dx dy\}$$

$$= \rho g\{-(1-\nu) I_r^{00}\,[b\psi_s'(b) - \psi_s(b)] + I_r^{00} J_s^{12} - \nu I_r^{02} J_s^{10}\}$$

which finally yields

$$\bar{Q}^{(rs)} = \rho g \nu \left[\frac{2\phi_r'''(a/2)}{a^4 \varepsilon_r^4}\right][b\,\psi_s'(b) - \psi_s(b)].$$

Since the potential function V is of the first order, the coefficients B_{ij} and consequently $\bar{P}^{(rs)}$ are identically equal to zero.

In figure (4.14) the Ritz results are displayed and compared to those of reference [18] and with results obtained using rectangular finite elements for a square plate with Poisson's ratio taken as .25. According to the results of reference [18] $\sigma_x = \tau_{xy} = 0$. However, the present analysis yields considerable lateral and shear stresses particularly near the clamped edge where $\sigma_x = \nu\sigma_y$ due to the boundary condition *(4.11)*. Considerable deviations in the results of reference [18] are also shown in the direct stress σ_y for the plate sections near the clamped edge,

and particularly near the corners where no account for the singularity is reflected in those results. On the other hand, however, excellent agreement between the Ritz and finite element results is achieved. Again here, the deviation in σ_x near the singular point - at the point (.438a, .917b) - is due to the very rapidly changing stress which could not be matched by the relatively coarse finite element mesh.

Figure (4.15) is a convergence study for the problem in the displacement domain. Both 40 and 63 term series were used and displacements - relative to the centre line - are plotted both at the clamped edge and at the sections of maximum relative displacements. Finite element results are also shown indicating very good agreement. Displacements based upon the stress distribution given by reference [18] are also plotted showing very high clamped edge distortions, and hence violating the clamped edge boundary conditions.

The contour representation of the principle stresses as obtained using a 63 term series for a square plate having a value of Poisson's ratio equal to 0.3 is shown in figure (4.16).

Case 2); a unit g acceleration in the negative x direction:

For this case, the body force potential function is given by

$$V = - \rho g x \qquad (4.27)$$

since this function is linear in x, and since no external stresses are applied at the free edges, and in view of the antisymmetry of the problem, it is possible to assume the function ϕ_o in the form

$$\phi_o = \sum_{i=o}^{1} \sum_{j=o}^{2} A_{ij}\, x^{2i+1}\, y^j,$$

which involves six unknown coefficients. One of these coefficients, namely A_{oo}, can be arbitrarily set to zero, while the other five can be determined by the use of the boundary conditions at the free edges. Through this procedure, it can be shown that

$$\phi_o = \rho g \left[\left(\frac{3x}{4} - \frac{x^3}{a^2}\right) y^2 + \frac{x^3}{6}\right], \qquad (4.28)$$

which can also be shown to satisfy the overall equilibrium conditions at the clamped edge $(y = b)$. As with Case 1), the functions ψ_s will be taken as the family of clamped-free degenerated beam functions. In the x- direction, however, the antisymmetric clamped-clamped beam functions will be used for ϕ_r. Substituting from (4.27) and (4.28) into (4.18a) it may be written that

$$\bar{Q}^{(rs)} = \rho g \left((1-\nu) \int_{-a/2}^{a/2} x\phi_r(x)\psi_s'(b)\,dx - \int_{o}^{b} \int_{-a/2}^{a/2} \left\{ (x - \right.\right.$$

$$\left.\left. - \frac{6xy^2}{a^2} - \frac{2x^3}{a^2} + \frac{3x}{2}\right)(\phi_r''\psi_s + \phi_r\psi_s'') - (1-\nu)..\right.$$

$$\cdot[(x - \frac{6xy^2}{a^2}) \phi_r \psi_s'' + (\frac{3x}{2} - \frac{2x^3}{a^2}) \phi_r'' \psi_s -$$

$$- (3y - \frac{12yx^2}{a^2}) \phi_r' \psi_s']\} dxdy),$$

or,

$$\bar{Q}^{(rs)} = \rho g\{(1-\nu) I_r^{10} \cdot \psi_s'(b) - (\frac{3}{2} I_r^{10} - \frac{2}{a^2} I_r^{30}) J_s^{02} +$$

$$+ \nu[I_r^{10} J_s^{02} - \frac{6}{a^2} I_r^{10} J_s^{22} + (\frac{3}{2} I_r^{12} - \frac{2}{a^2} I_r^{32}) J_s^{00}]$$

$$- (1+\nu).(3I_r^{01} J_s^{11} - \frac{12}{a^2} I_r^{21} J_s^{11})\}$$

which, after performing the integrations involved and rearranging, finally yields

$$\bar{Q}^{(rs)} = - \rho g. \frac{2a^4 \phi_r''(a/2)}{\varepsilon_r^4} \{[(\frac{a}{b})^2 - 6\nu]\psi_s'(b) - \frac{12}{b}(2+\nu)\psi_s(b) +$$

$$+24\, b^2 + \frac{\psi_r'''(b) - \psi'''(o)}{\varepsilon_s^4} \}.$$

Here also, since the potential function V is of the first order, $\bar{P}^{(rs)}$ is equal to zero.

In figure (4.17), the stresses σ_x and σ_y obtained using a 63 term series in the Ritz method are plotted and compared to those given by reference [18] as well as finite element solutions. The gross deviation of the results of

reference [18] near the clamped edge - which was noted in Case 1) - is again observed. The good agreement between the Ritz and finite element results is also noticeable except for the regions where the rate of change of the stresses is too high to be matched by the finite element mesh utilized. Here also, the results are for a square plate with Poisson's ratio equal to 0.3.

A convergence study in the displacement domain is shown in figure (4.18). Shown also are the relative displacements associated with the stress distribution suggested in reference [18]. It is noticeable that while the Ritz solutions converge towards zero clamped edge distortions, those of reference [18] seem to have their maximum distortions at the clamped edge; this is to be expected since no consideration was given to satisfying these boundary conditions in the latter solution.

In figure (4.19) contour plots of the principle stresses are displayed for the case of a square plate with Poisson's ratio equal to 0.3.

4.5 Conclusions

Based upon the study conducted in the foregoing sections the following may be concluded:

- The Ritz method as described in Chapter II can be used to advantage for solving the two dimensional elasticity problem, with body forces and mixed boundary

conditions conveniently accommodated. If the stress function formulation is used, the governing differential equation is biharmonic - i.e. the same as that for the plate bending problem. The boundary conditions for the inplane problem, when expressed in terms of the stress function, are also similar to those of the plate in bending. An analogy between the different types of inplane stress and out-of-plane bending boundary conditions has been drawn. With the help of this analogy, the same types of ordinary and modified beam functions used in the previous Chapters for the plate bending problem, can be used for the analogous inplane stress problem. In addition to the fact that these beam functions have proven to be highly accurate in the previous applications, more advantages result from using the same type of functions for the two classes of problems:

Firstly, the same integral coefficients involving multiplications of the beam functions can be used for the inplate stress as well as the out-of-plane bending problems, and thus the algebra required for the solutions is minimized; and secondly, since the study of the plate stability problems (which will be carried out in the next chapter) requires combining the solutions of the inplane stress problem with the out-of-plane vibration problem, it is advantageous to utilize the same class of functions and the same for-

mulation for the solution of both phases of the problem.

Both homogeneous and mixed types of boundary conditions can be equally easy to handle. The assumed functions are required to satisfy only the *essential* (forced) boundary condition of the problem; which in the present case are those concerning specified direct and/or shear stresses at the boundary. The natural boundary conditions, resulting from specified edge displacements, are inherently accounted for in the variational expression being used. As a result, the solutions obtained will converge towards satisfying these natural boundary conditions as more terms are considered in the series as was shown in the numerical results of the preceding section. It has also been shown that the solutions are capable of representing extremely sharp stress variations such as those resulting due to stress concentrations associated with corner singularities. Other methods of solutions such as the Finite Element - or Finite Difference - methods cannot match such high stress gradients if comparable numbers of degrees of freedom are used as was shown in the numerical examples presented in this chapter.

Simple polynomial solutions, such as those obtained by the beam theory or those presented in references [18] and [19] which deal only with equilibrium boundary conditions, are good only at sufficient distances

from the clamped edges. In the regions where the clamped edge effects are predominant, however, these simple solutions may lead to gross deviations since they do not consider the displacement boundary conditions. It was found numerically that for plates having Poisson's ratio (ν) of 0.25, the width of the clamped edge dominant region was roughly equal to $a/4$ where a is the length of the clamped edge. The width of this region increases as ν increases, and it obviously vanishes if ν is equal to zero. The width of this region may thus be considered roughly to be equal to (νa). This value, however, may be reduced if the width of the plate is small with respect to the length of the clamped edge with the parallel edge under stress - type boundary conditions (e.g. a short cantilever).

It has been shown, both numerically and analytically, that singularity exists at the corners between clamped and free edges. The approximate solutions, although unable to yield infinite values at these corners, show very sharp stress gradients in their vicinity and a continuously increasing maximum stress value at the corners. In practice, however, singularity does not exist. This may be due to one or more of the following reasons: 1) Local plastic deformation at the corners. 2) Rounded rather than perfectly

sharp corners. 3) Local deformation of the support itself since it is of finite rigidity. 4) Three dimensional effects (due to stress flow) near the plate edges; since the two-dimensional theory does not apply at distances from the edge which are comparable to the plate thickness.

(a) Normally Restrained Edge

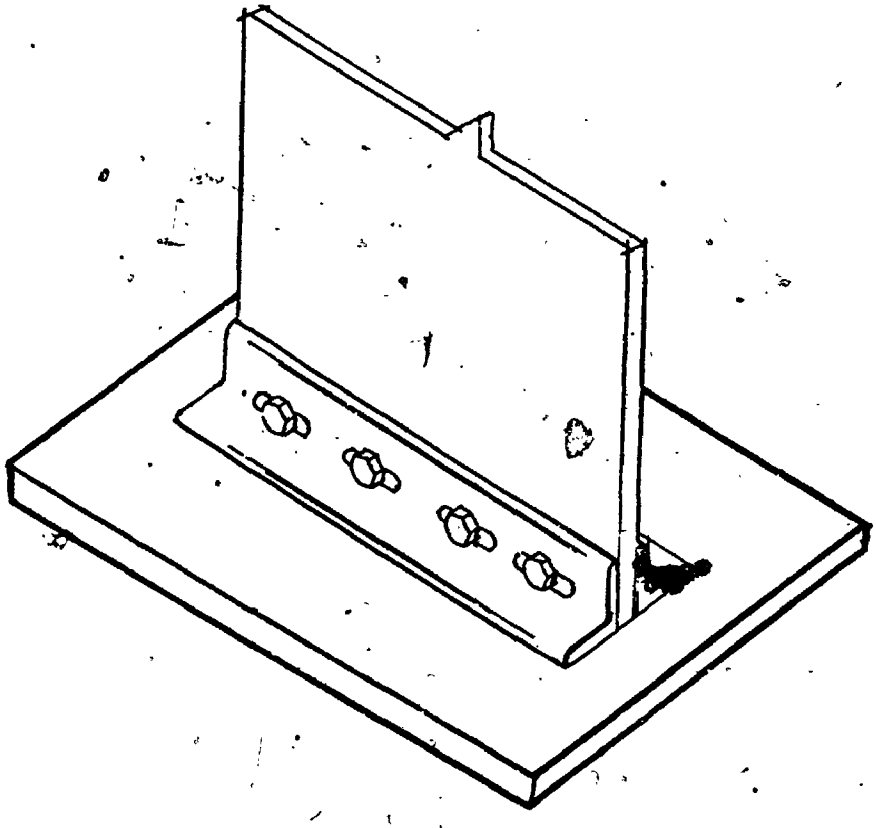

(b) Laterally Restrained Edge

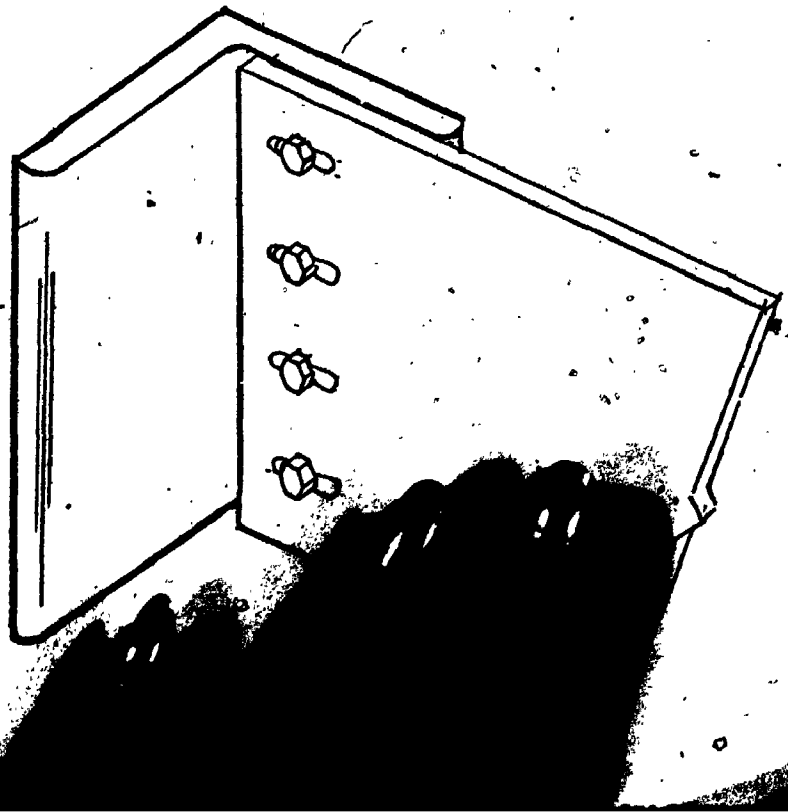

(a) Normally Restrained Edge

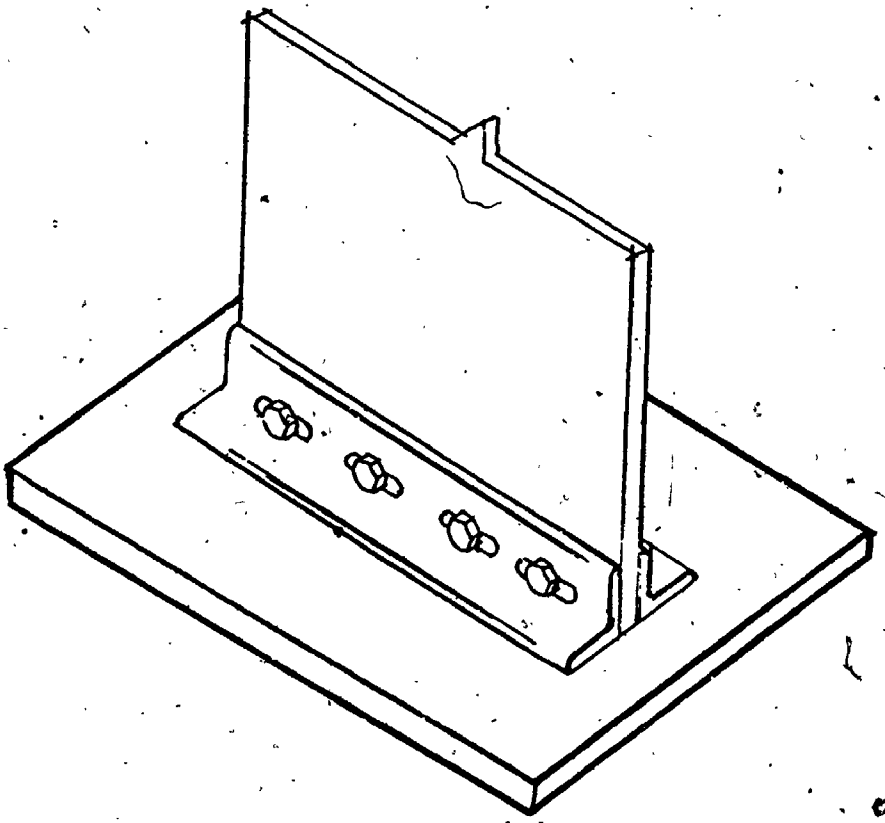

(b) Laterally Restrained Edge

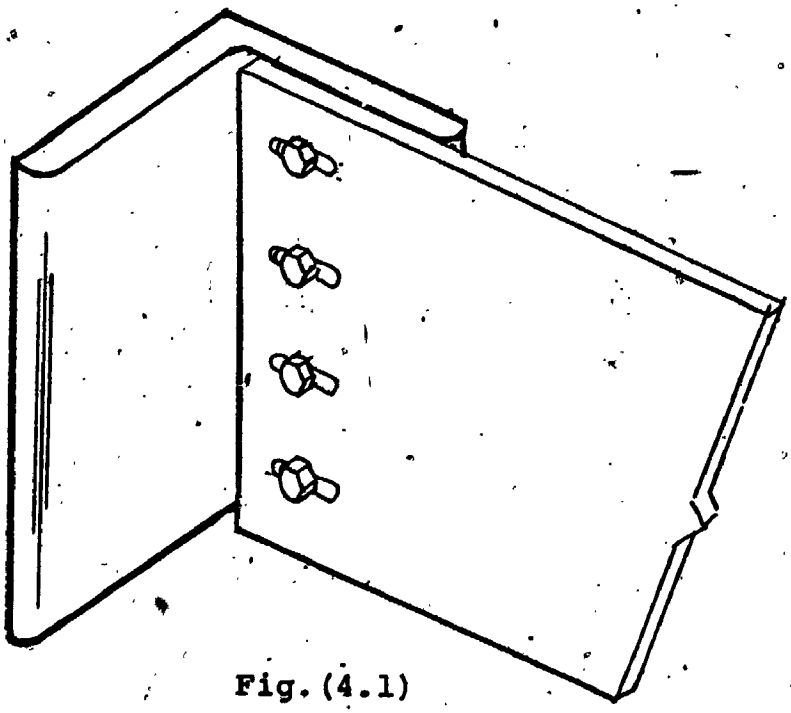

Fig. (4.1)

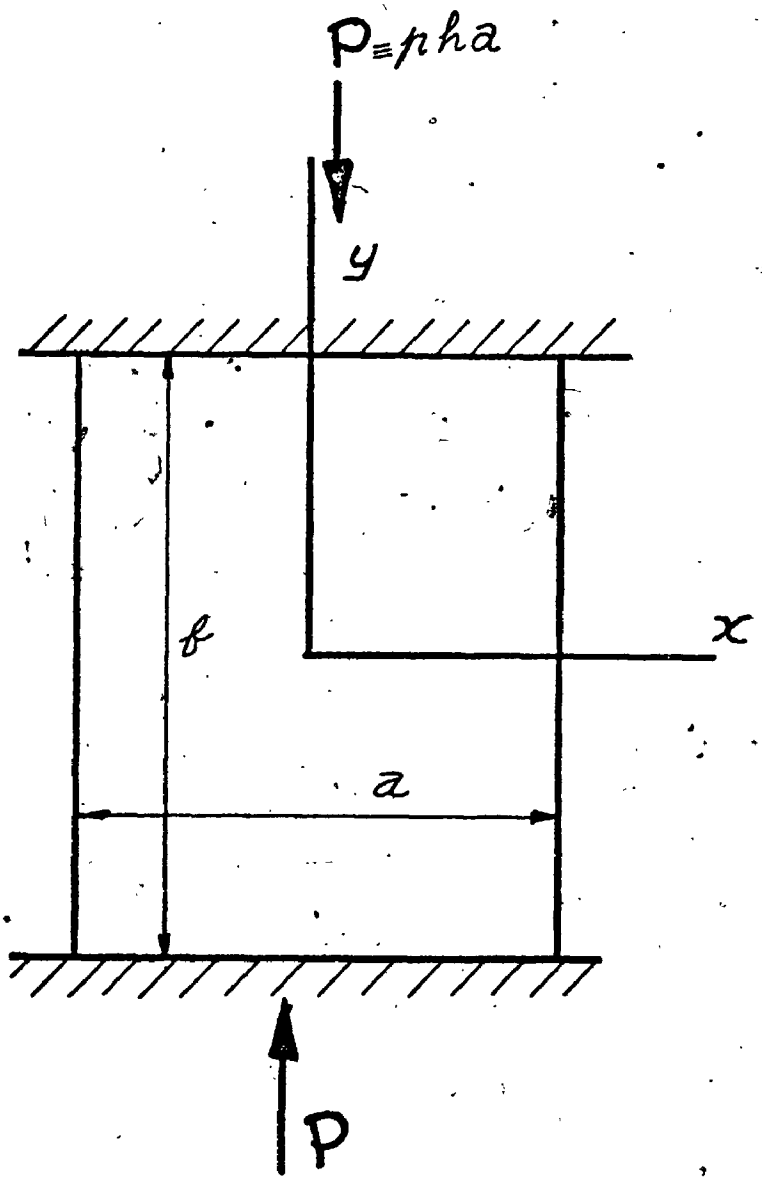

Fig.(4.2)

C-F-C-F Plate Under Direct Compression

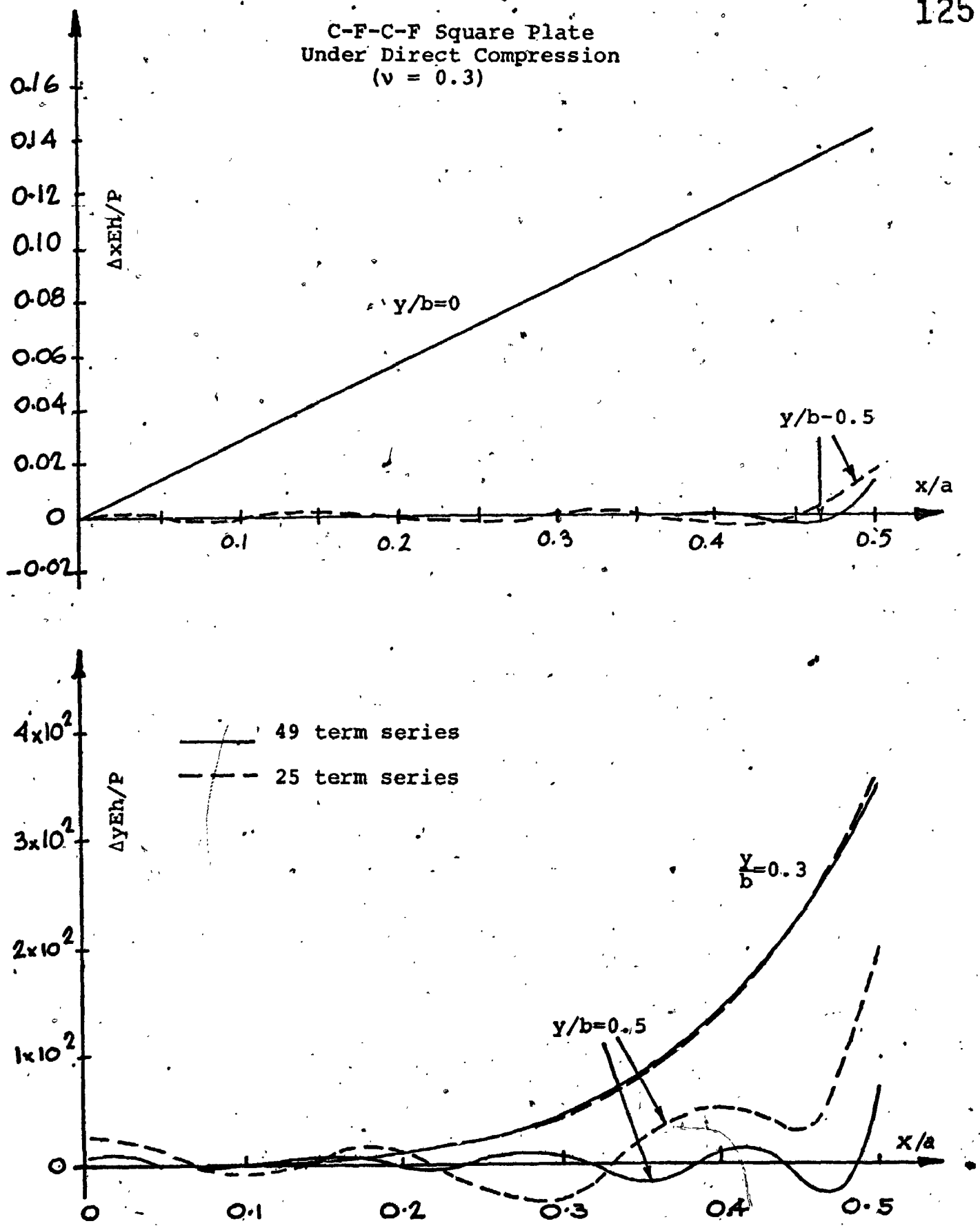
C-F-C-F Square Plate
Under Direct Compression
(ν = 0.3)
0.16
0.14
0.12
0.10
0.08
0.06
0.04
0.02
0
-0.02
ΔxEh/P
y/b=0
y/b-0.5
x/a
0.1
0.2
0.3
0.4
0.5
4x10²
3x10²
2x10²
1x10²
ΔyEh/P
49 term series
25 term series
y/b=0.3
y/b=0.5
x/a
0
0.1
0.2
0.3
0.4
0.5

Fig. (4.3)

FIG. (4.4A)

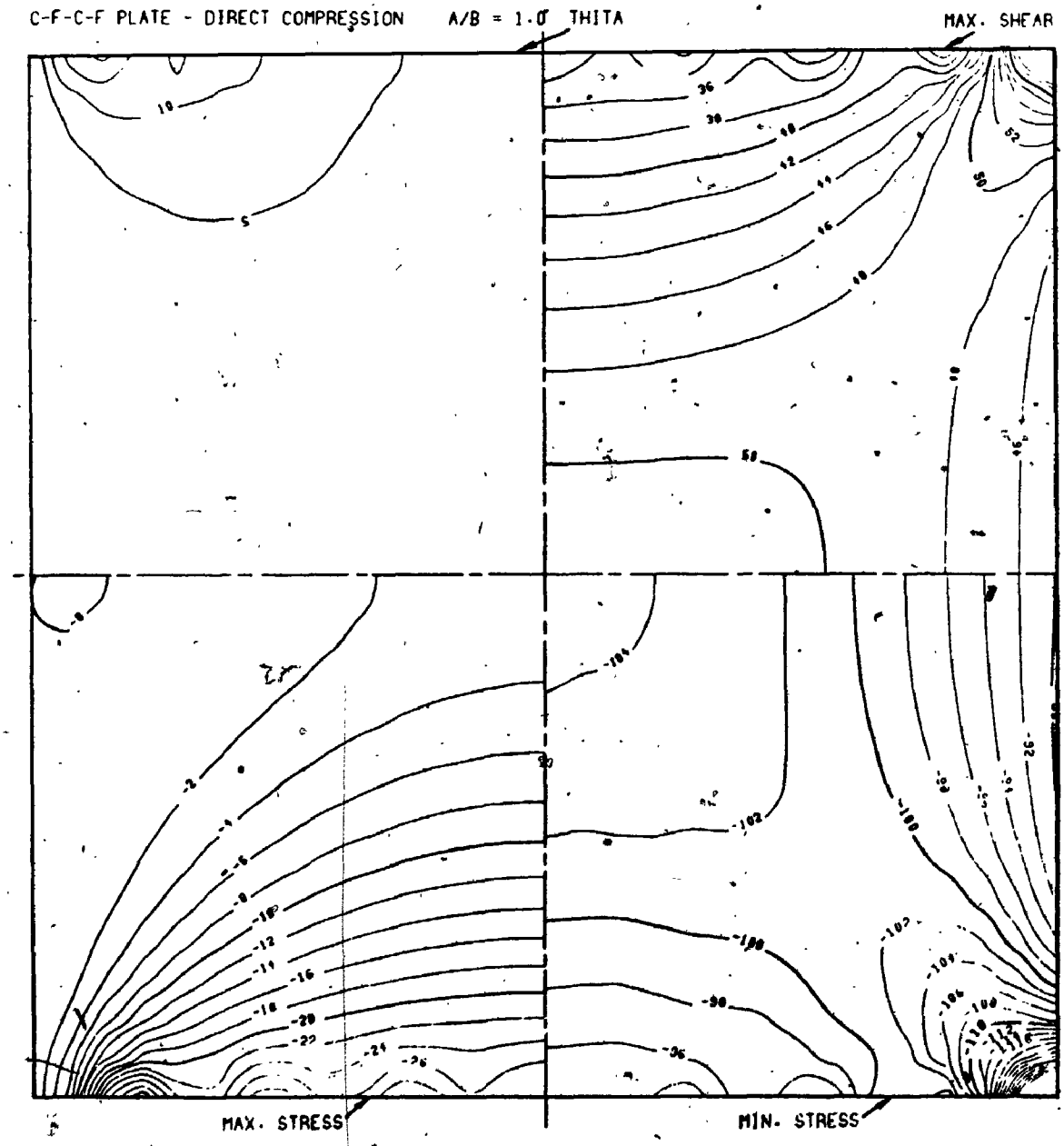
C-F-C-F PLATE - DIRECT COMPRESSION A/B = 1.0 THITA
MAX. SHEAR
MAX. STRESS
MIN. STRESS

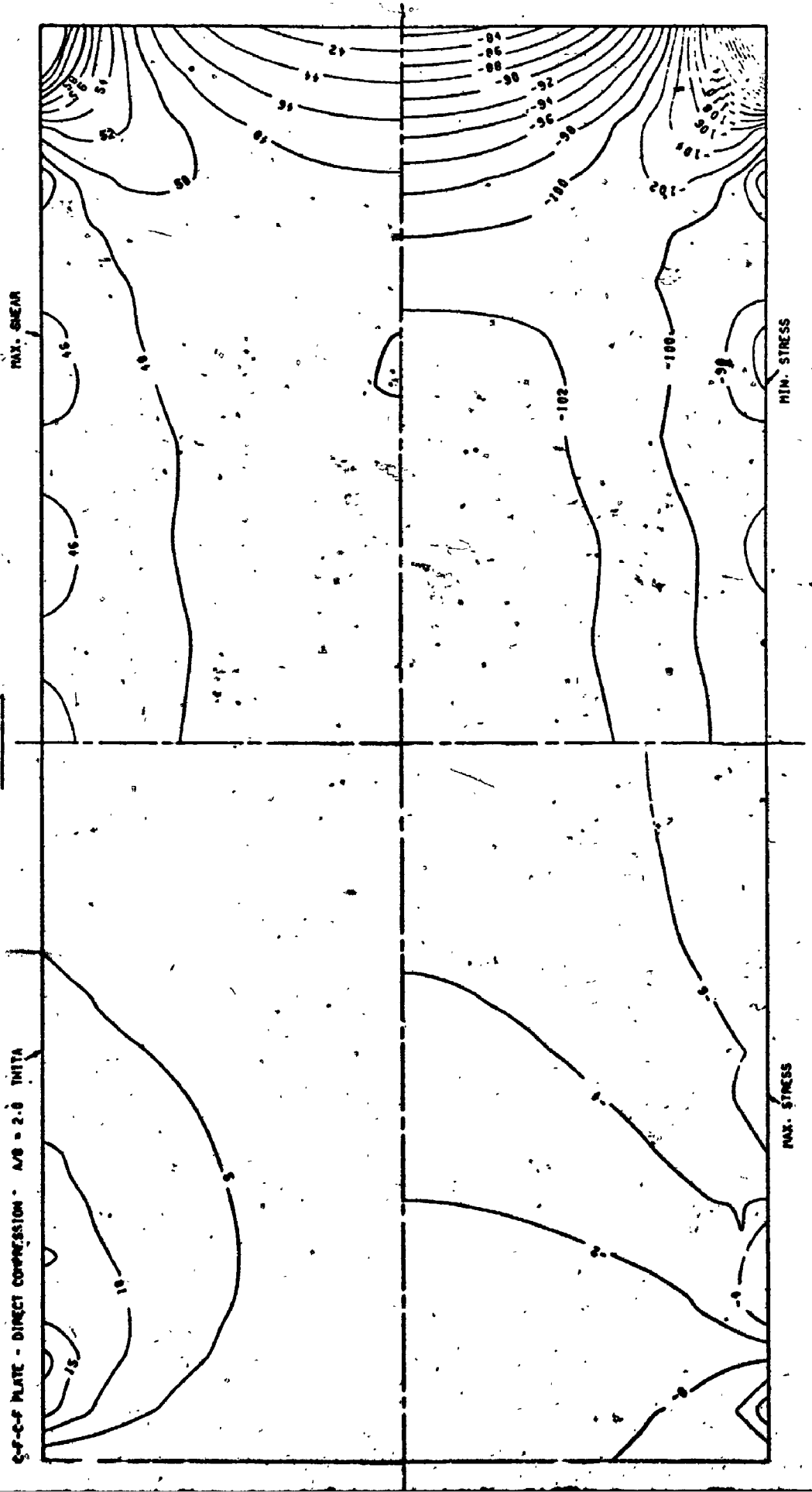
MAX. SHEAR
MIN. STRESS
MAX. STRESS
C-F-C-F PLATE - DIRECT COMPRESSION - A/B = 2.0 THETA

FIG.(4.4B)

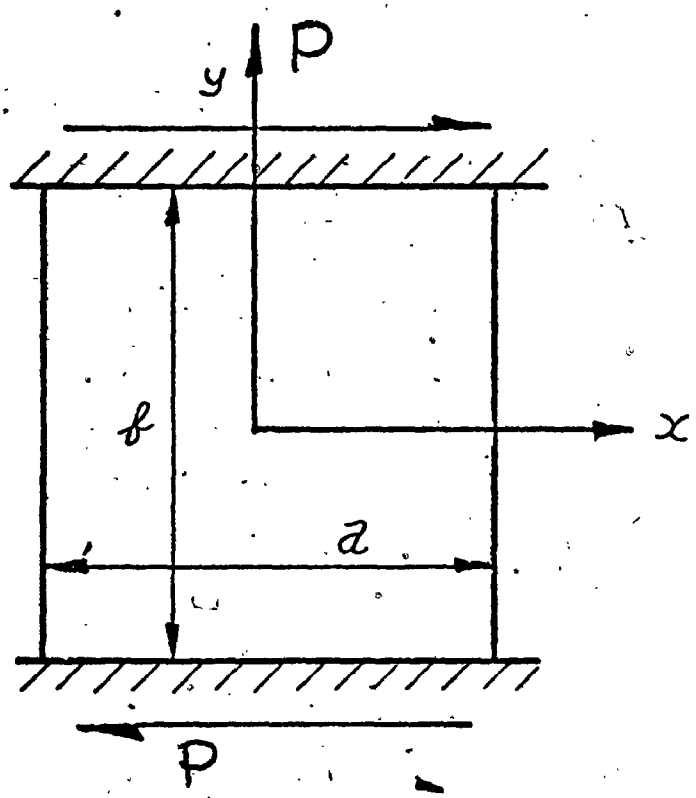

(a) C-F-C-F Plate Under End Shear

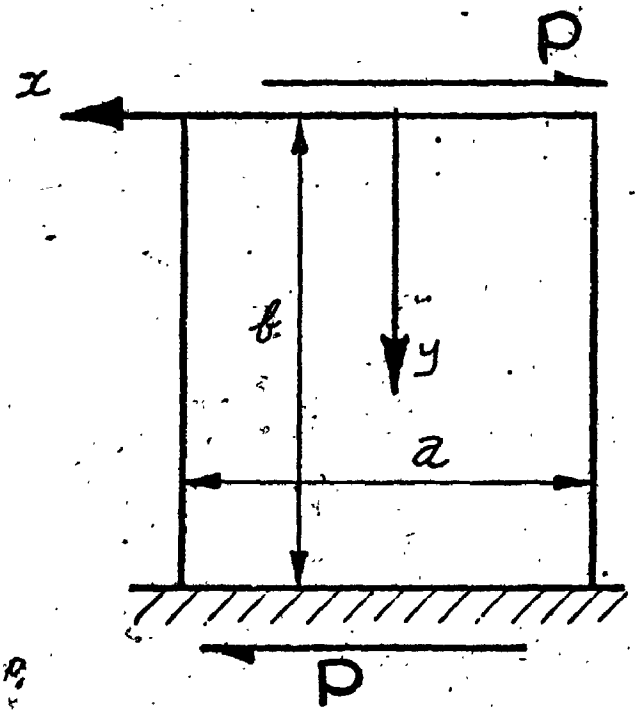

(b) C-F-F-F Plate Under End Shear

Fig. (4.5)

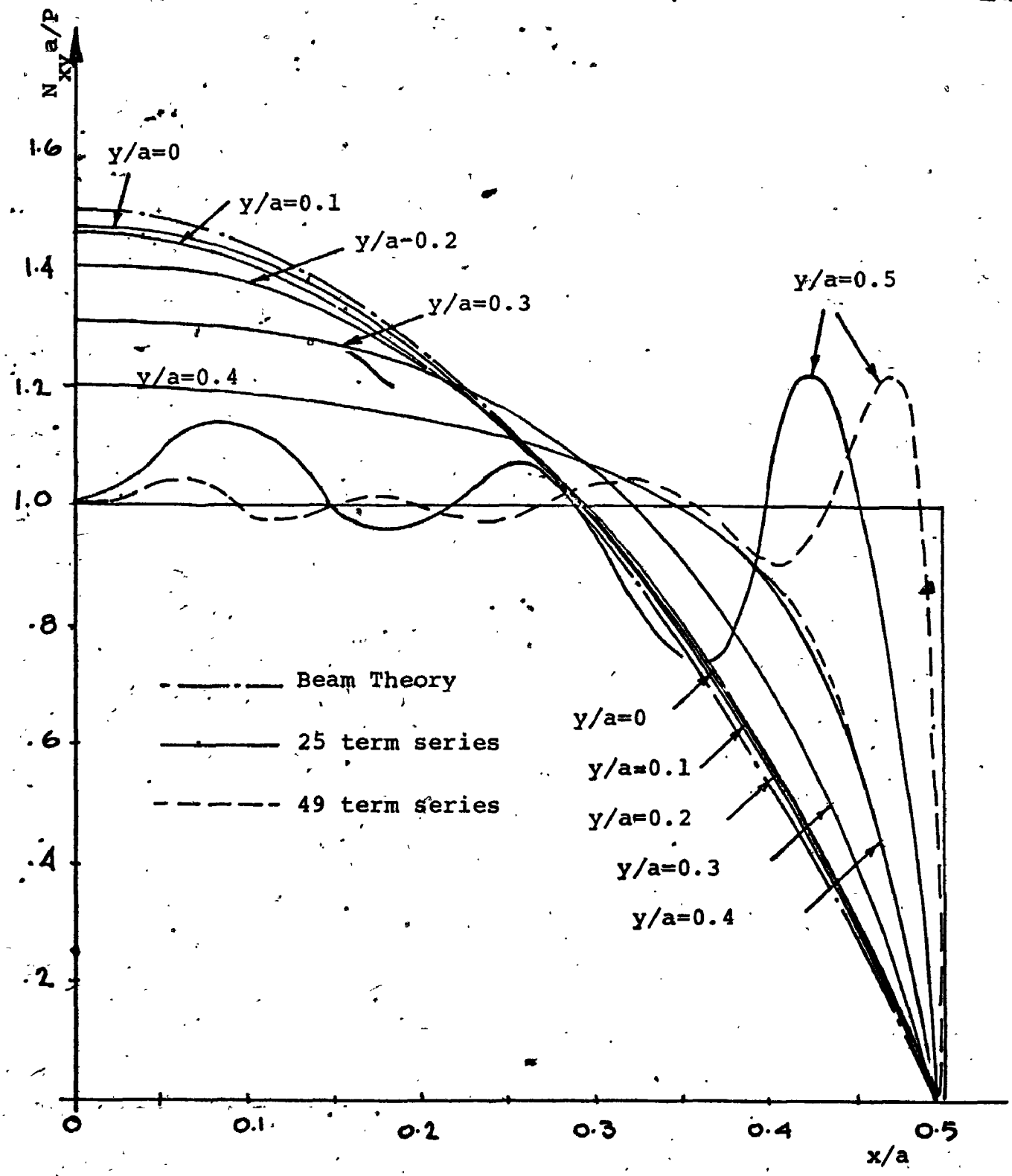

C-F-C-F Square Plate
under end shear (ν = 0.3)

Fig. (4.6)

FIG. (4.7)

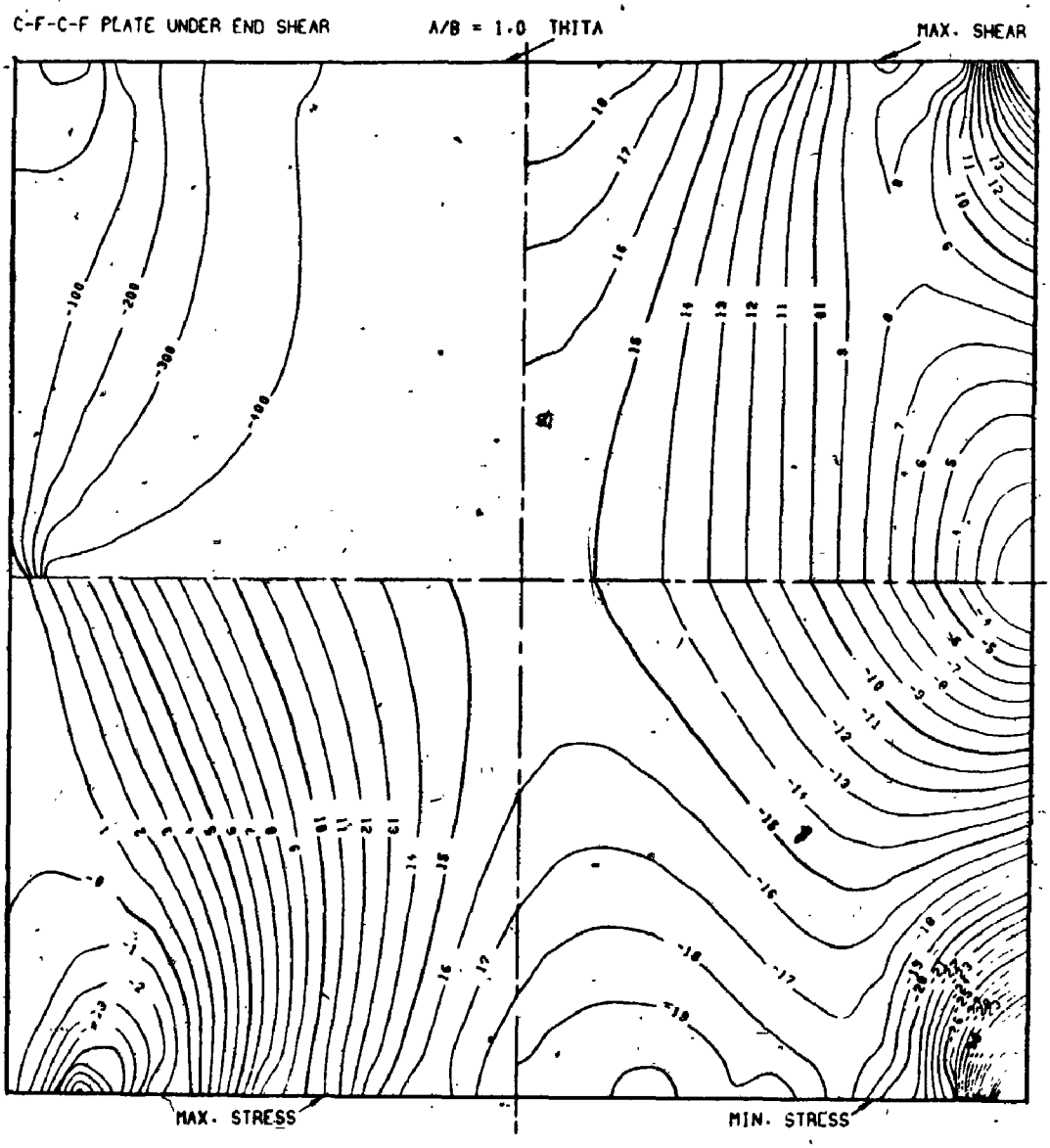
C-F-C-F PLATE UNDER END SHEAR
A/B = 1.0 THITA
MAX. SHEAR
MAX. STRESS
MIN. STRESS

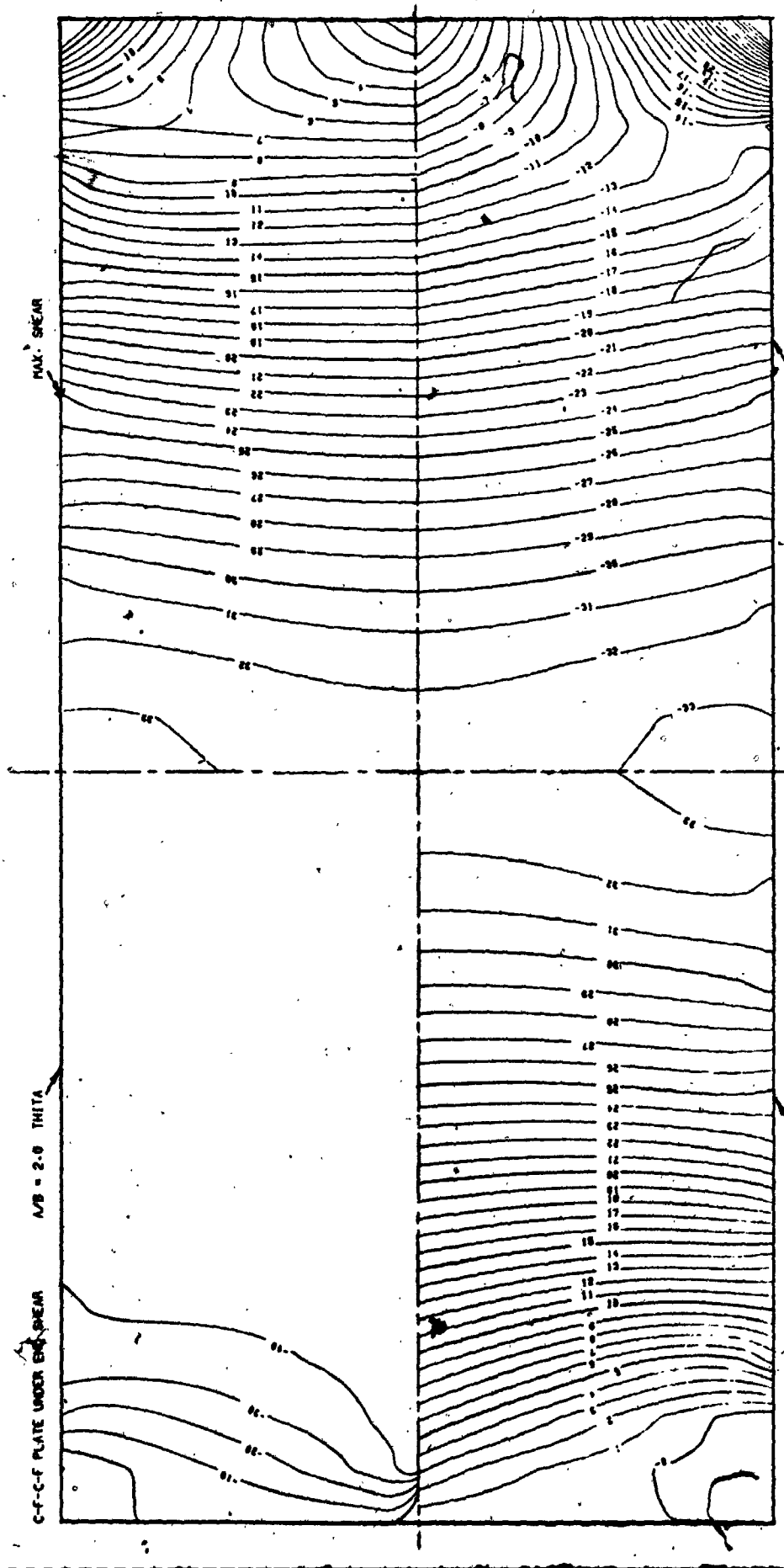
C-F-C-F PLATE UNDER END SHEAR
A/B = 2.0 THITA
MAX. STRESS
MIN. STRESS
MAX. SHEAR

FIG. (4.8)

Fig. (4.9)

Square Cantilevered Plate Under
Parabolic End Shear

($\nu = 0.25$)

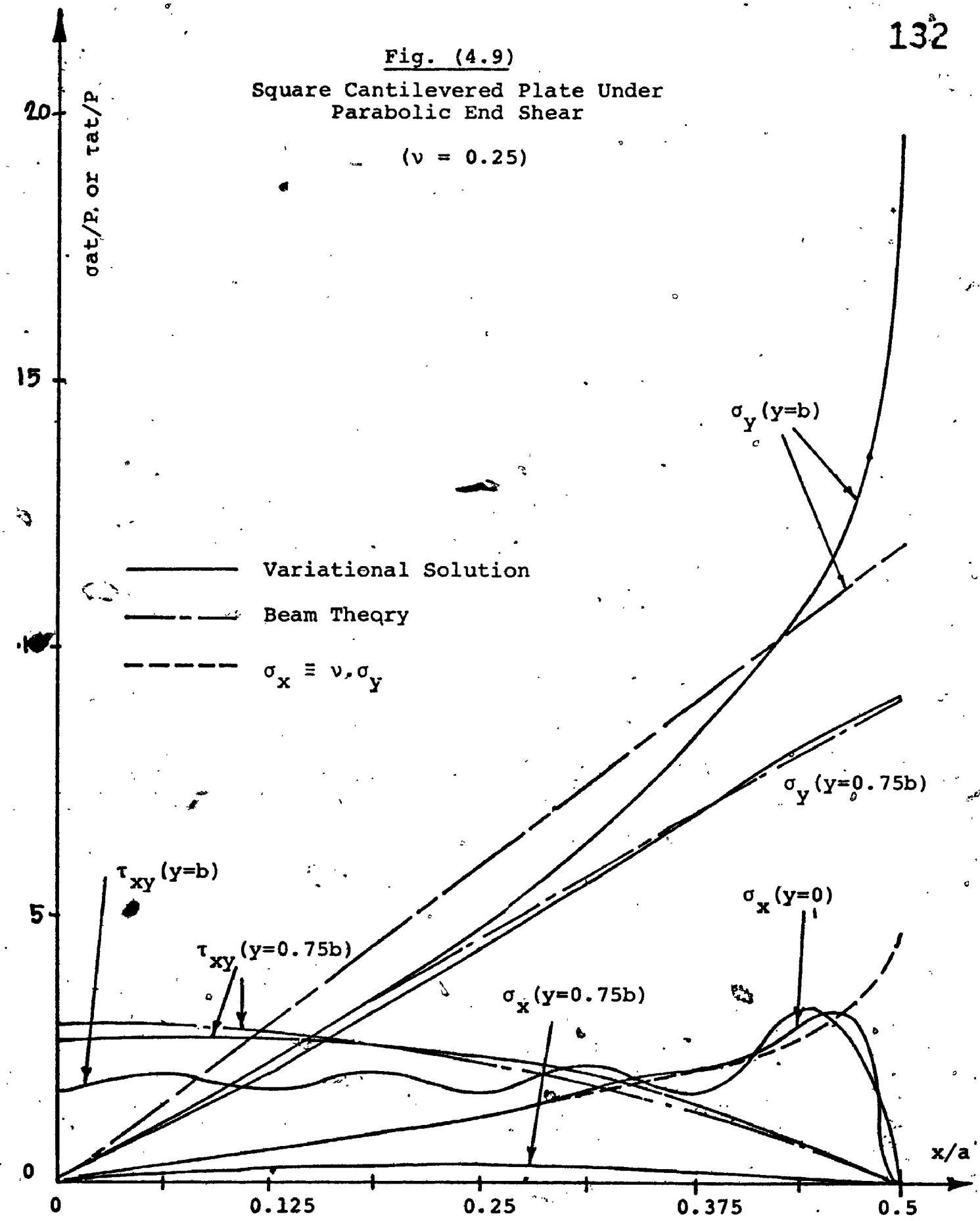

Fig. (4.10)

Square Cantilevered Plate
Under Parabolic End Shear
($\nu = 0.25$)

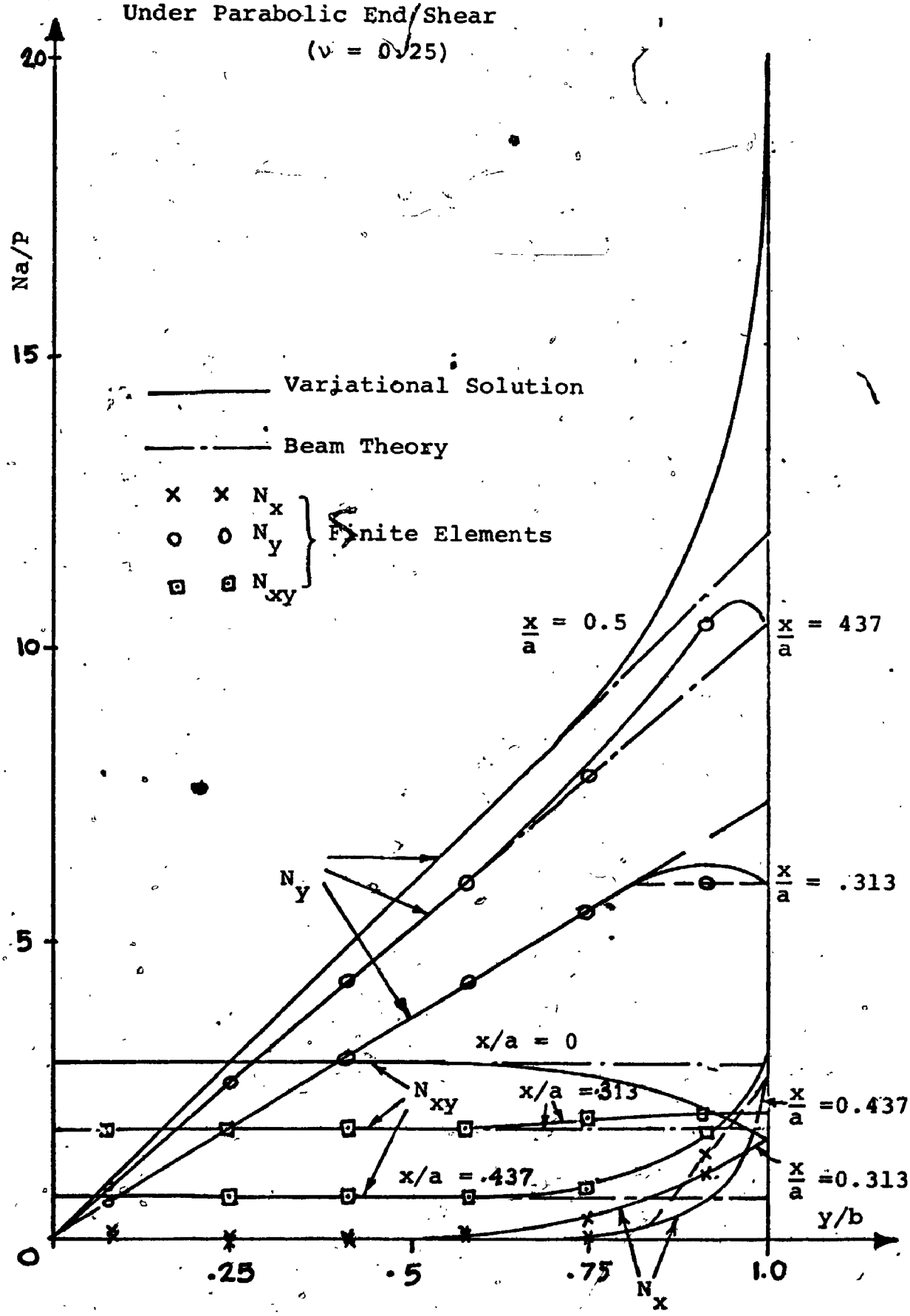

Square Cantilevered Plate
Under Parabolic End Shear
(ν = 0.25)

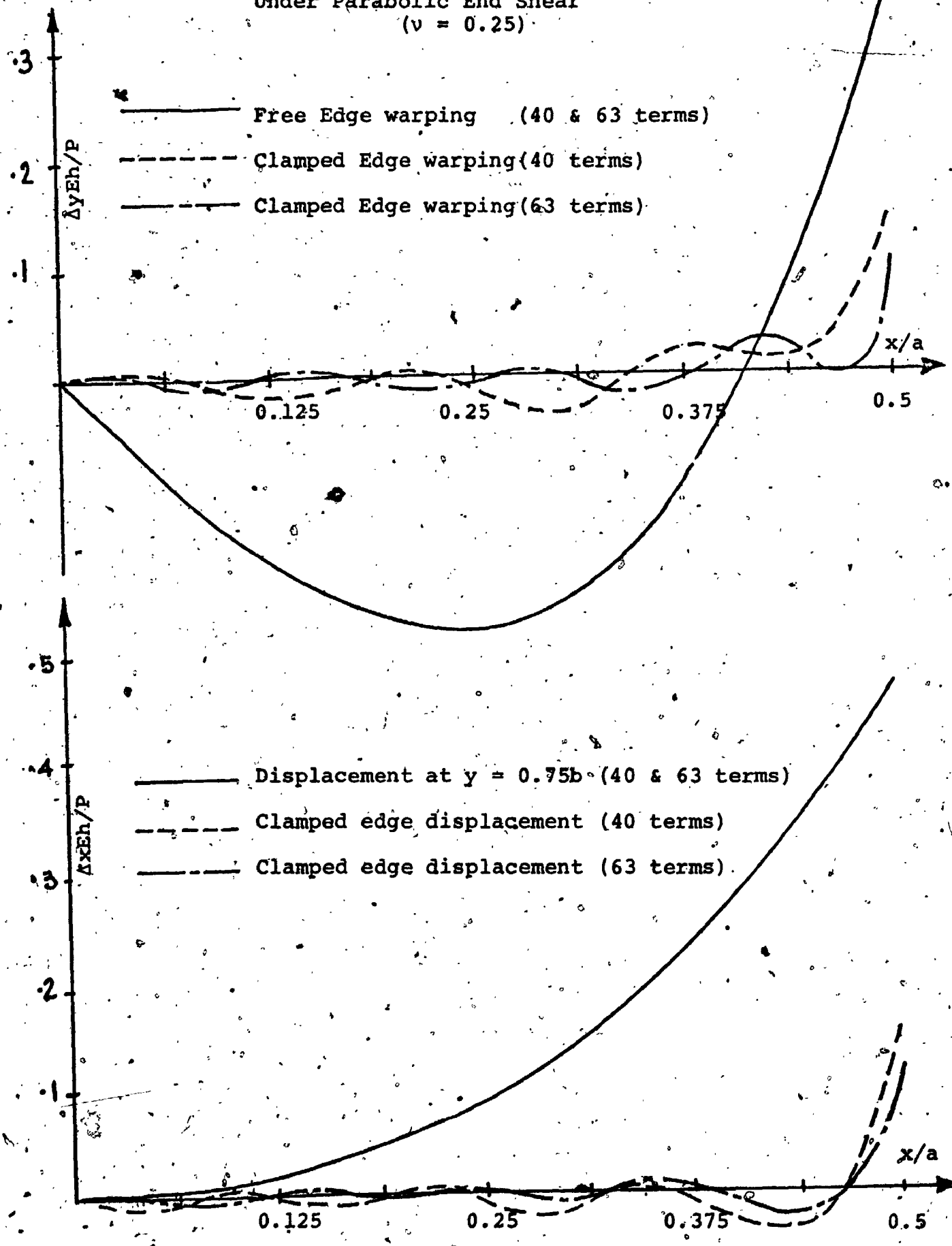

Fig. (4.11)

FIG. (4.12A)

C-F-F-F PLATE - PARABOLIC END SHEAR A/B = 1.0

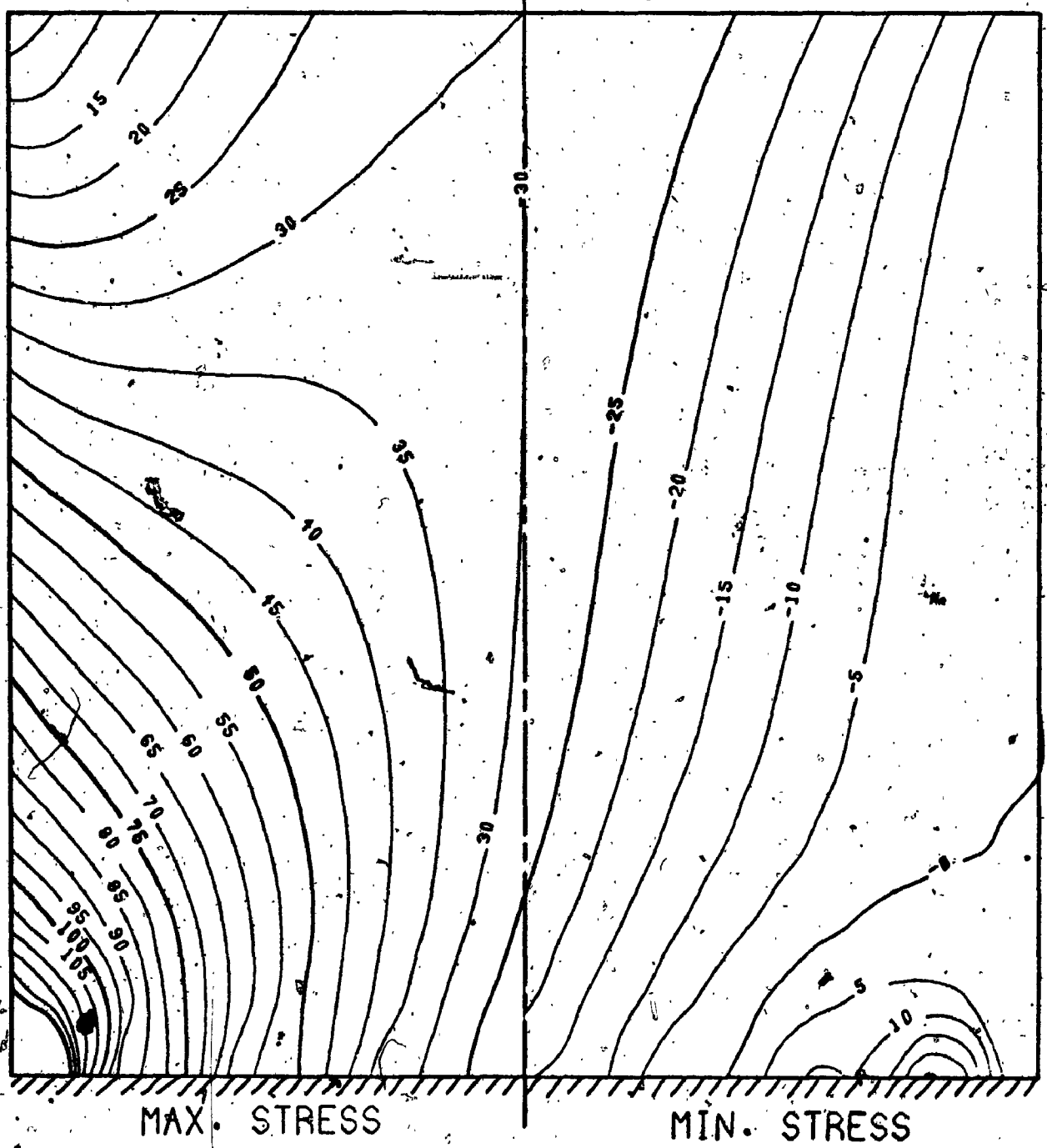

FIG. (4.12B)

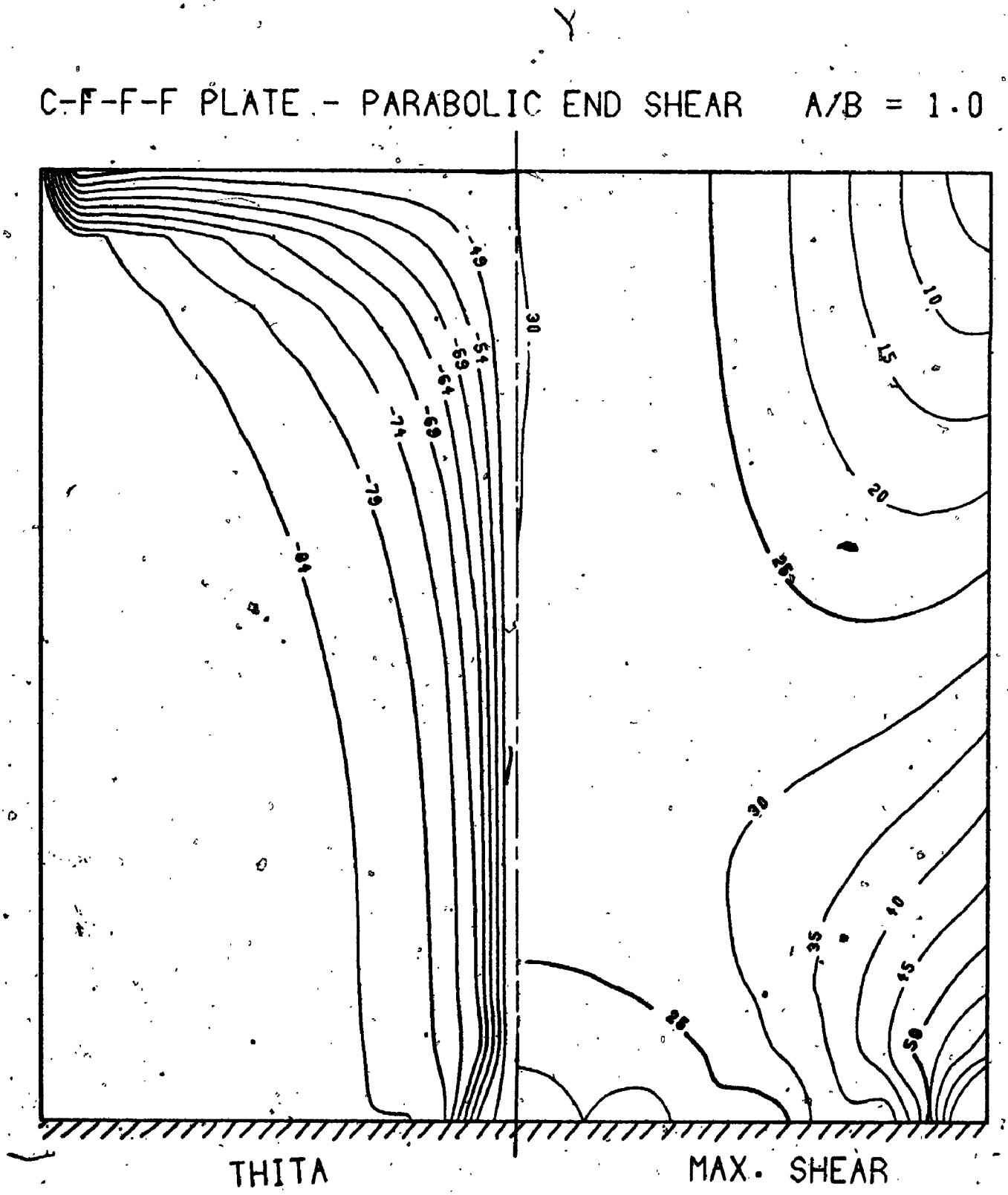

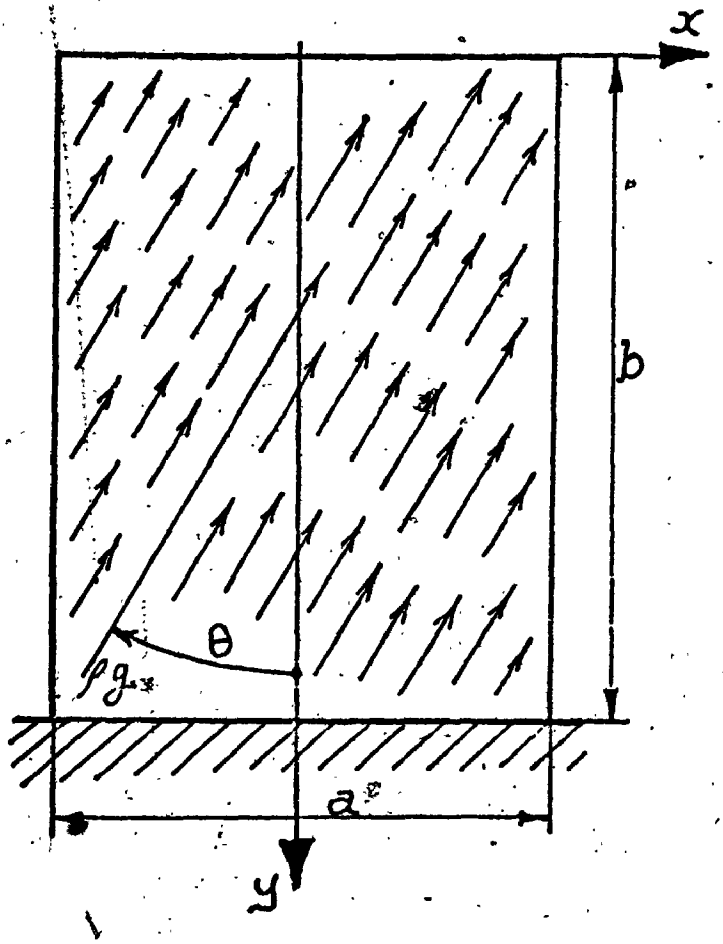

Fig. (4.13)

Cantilevered Plate Under General Inplane Acceleration

Fig. (4.14)

Square Cantilevered Plate Under Direct Acceleration
($\nu = 0.25$)

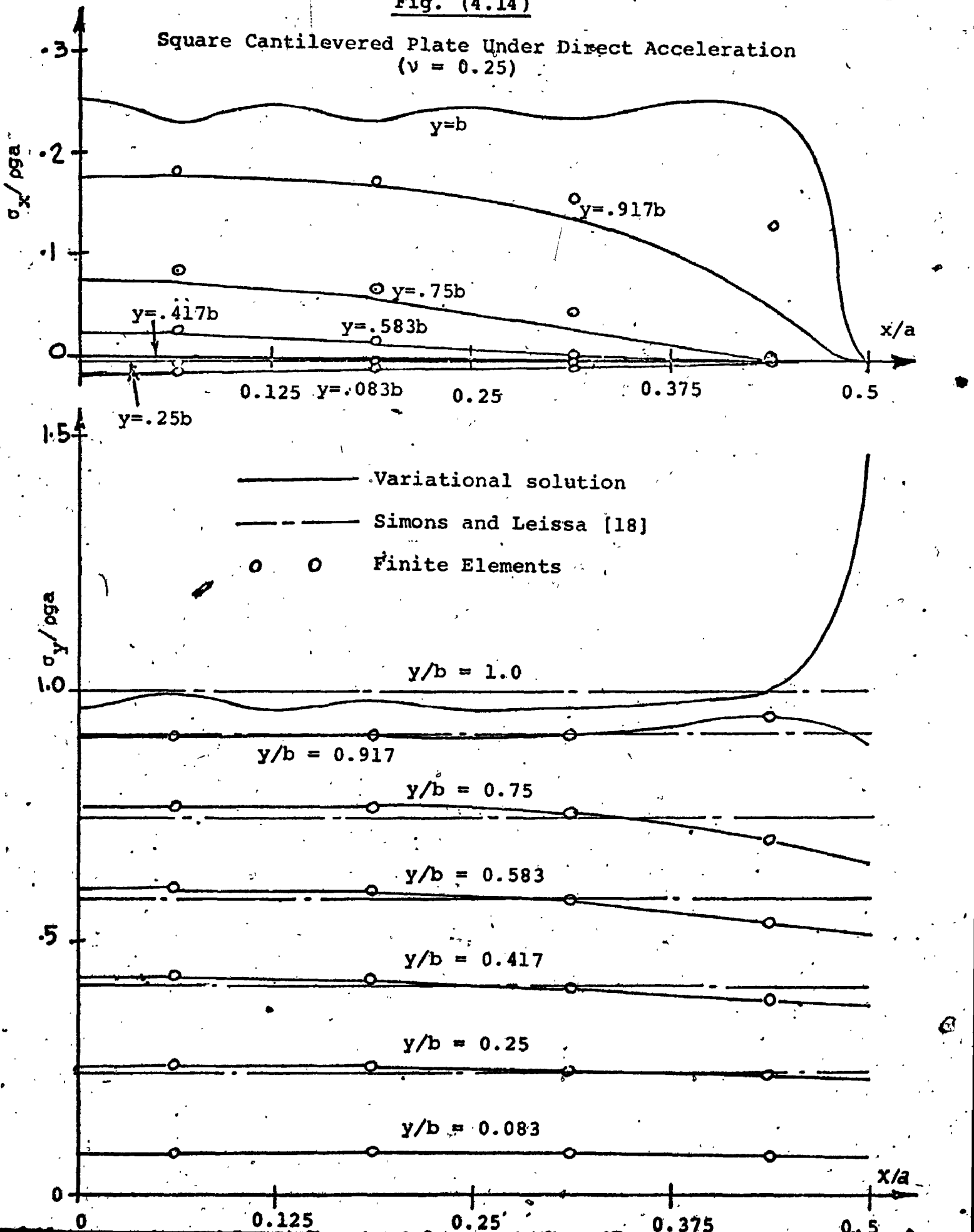

Fig. (4.15)

Square Cantilevered Plate
Under Direct Acceleration

($\nu = 0.25$)

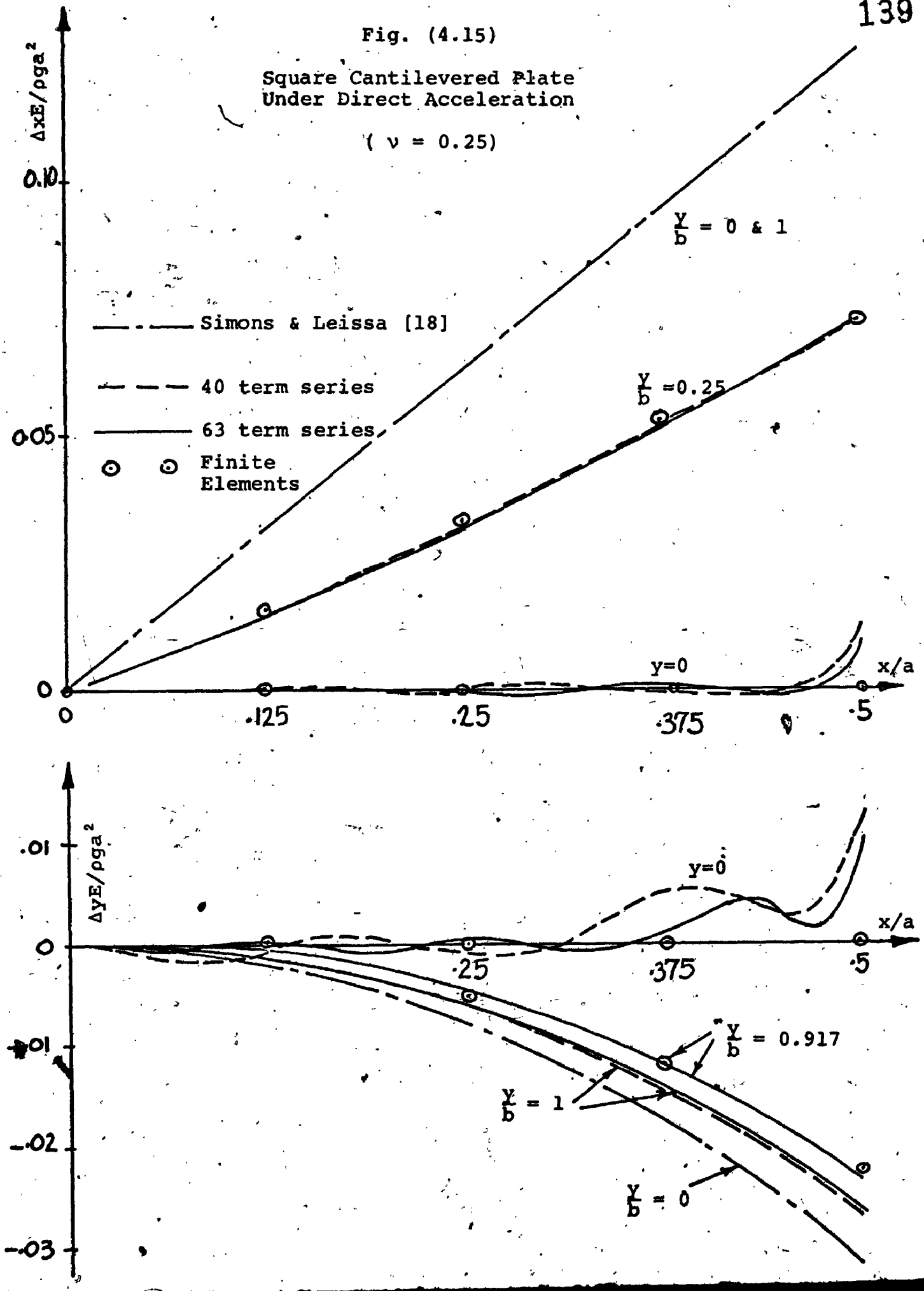

FIG. (4.16A)

C-F-F-F PLATE - DIRECT ACCELERATION A/B = 1.0

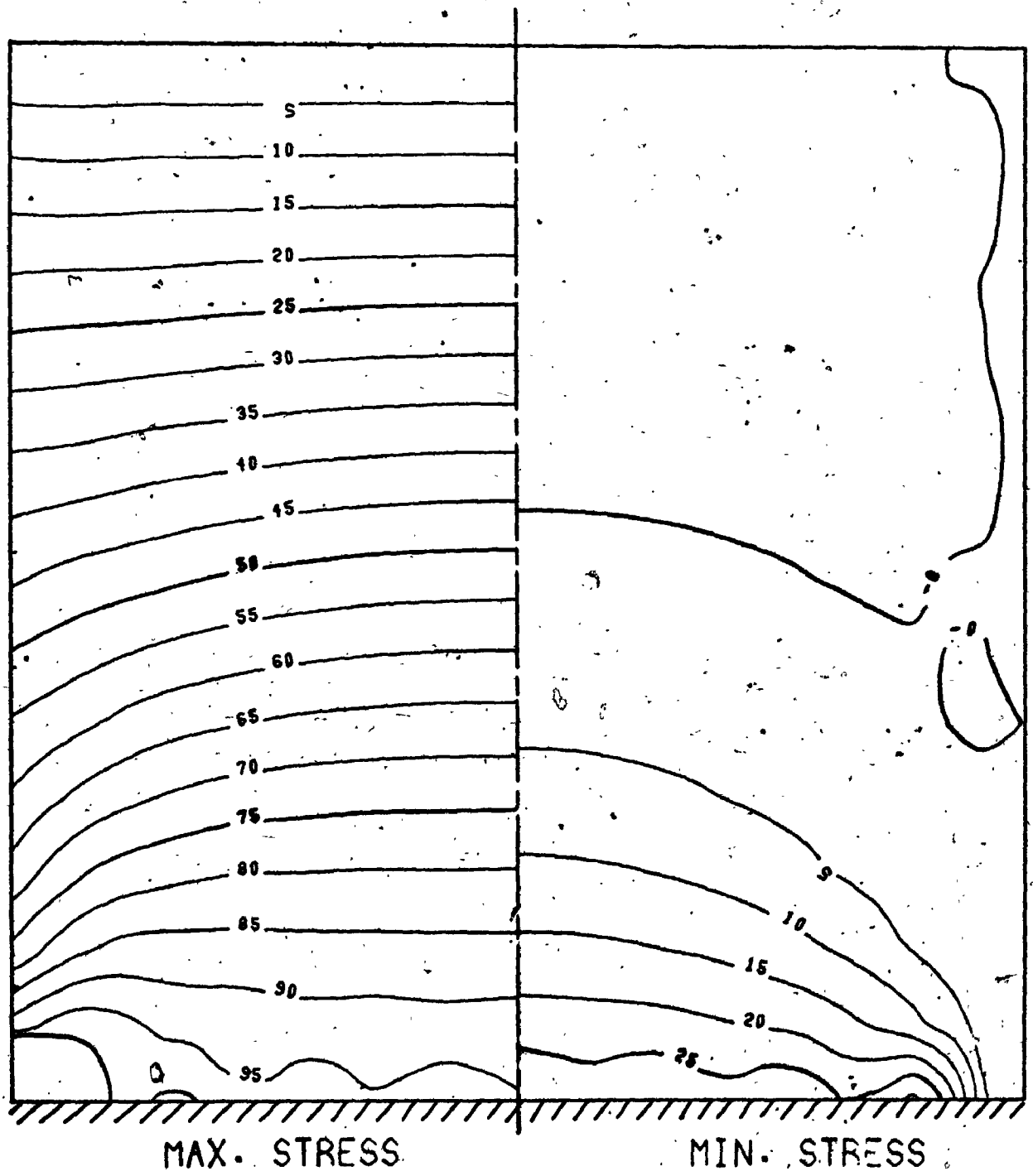

FIG. (4.16B)

C-F-F-F PLATE - DIRECT ACCELERATION A/B = 1.0

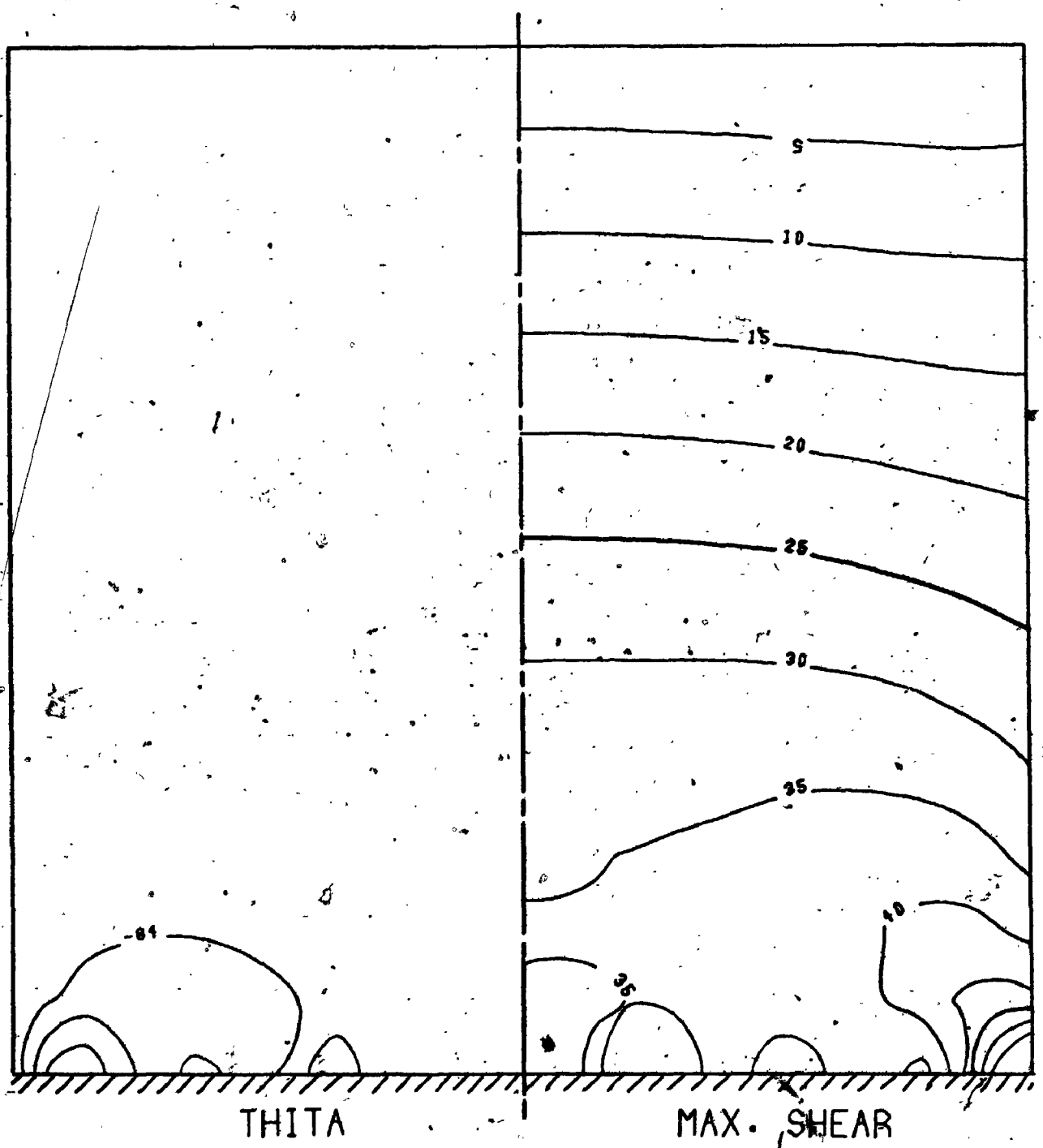

Fig. (4.17)
Square Cantilevered Plate
Under Lateral Acceleration
($\nu = 0.25$)

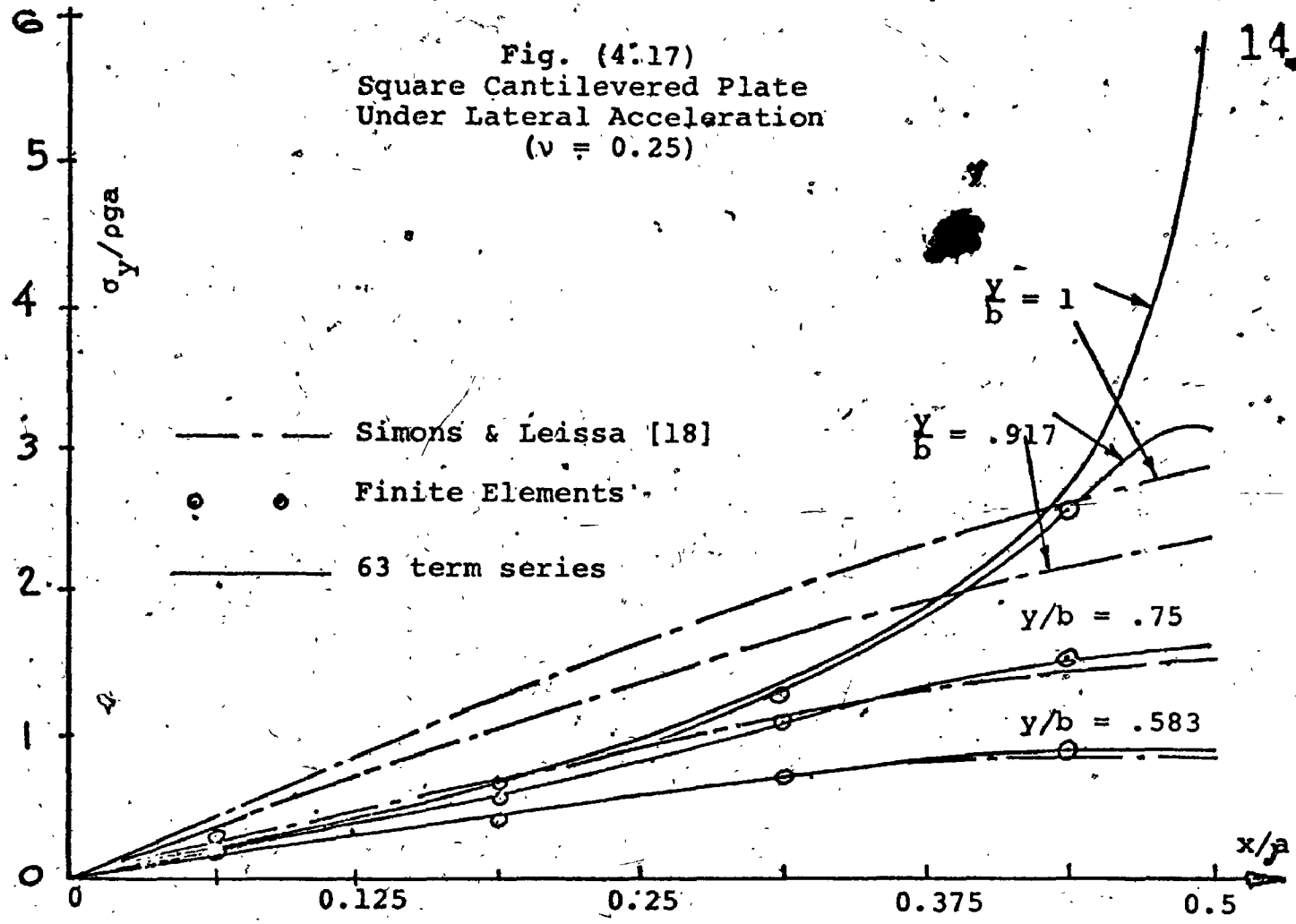

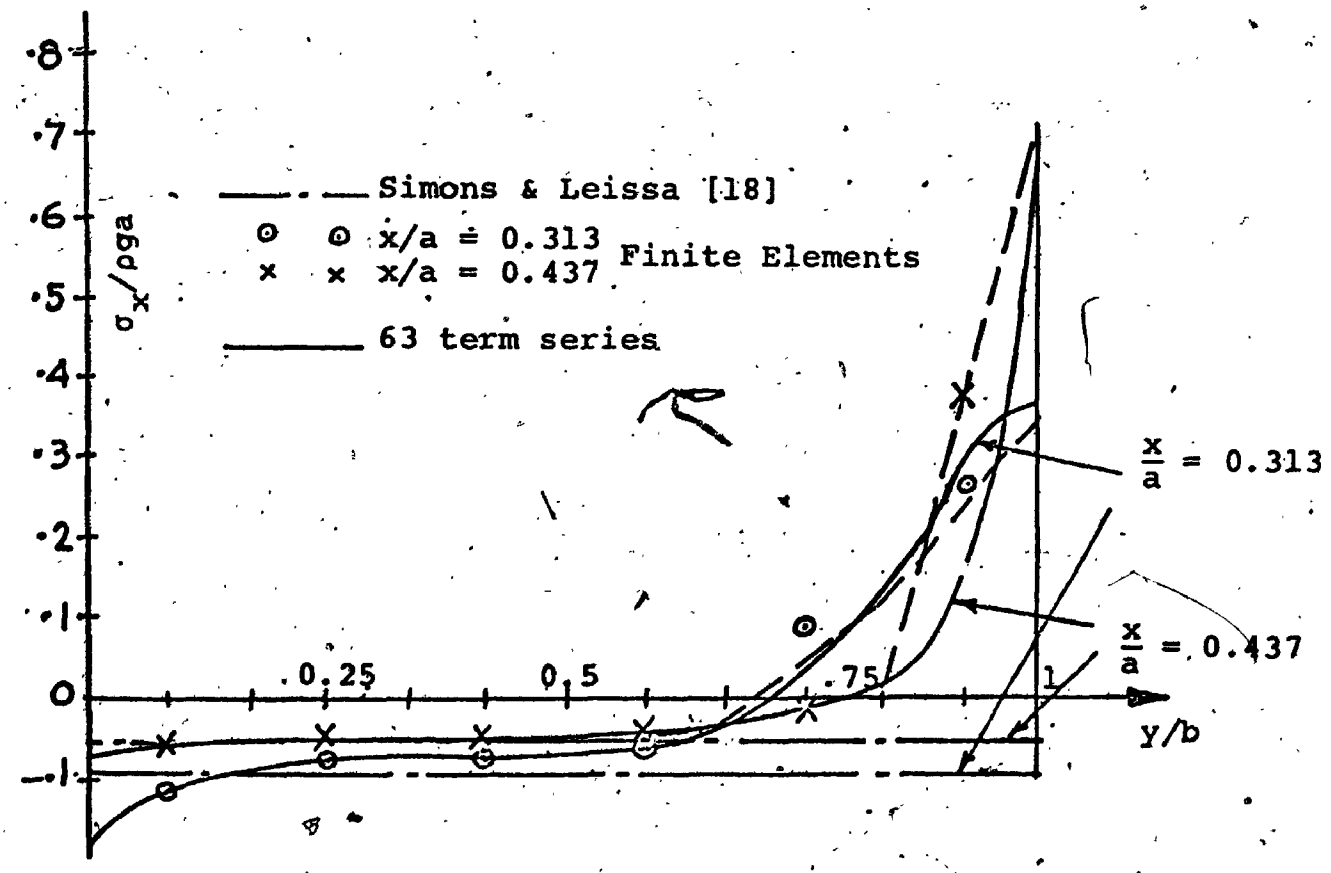

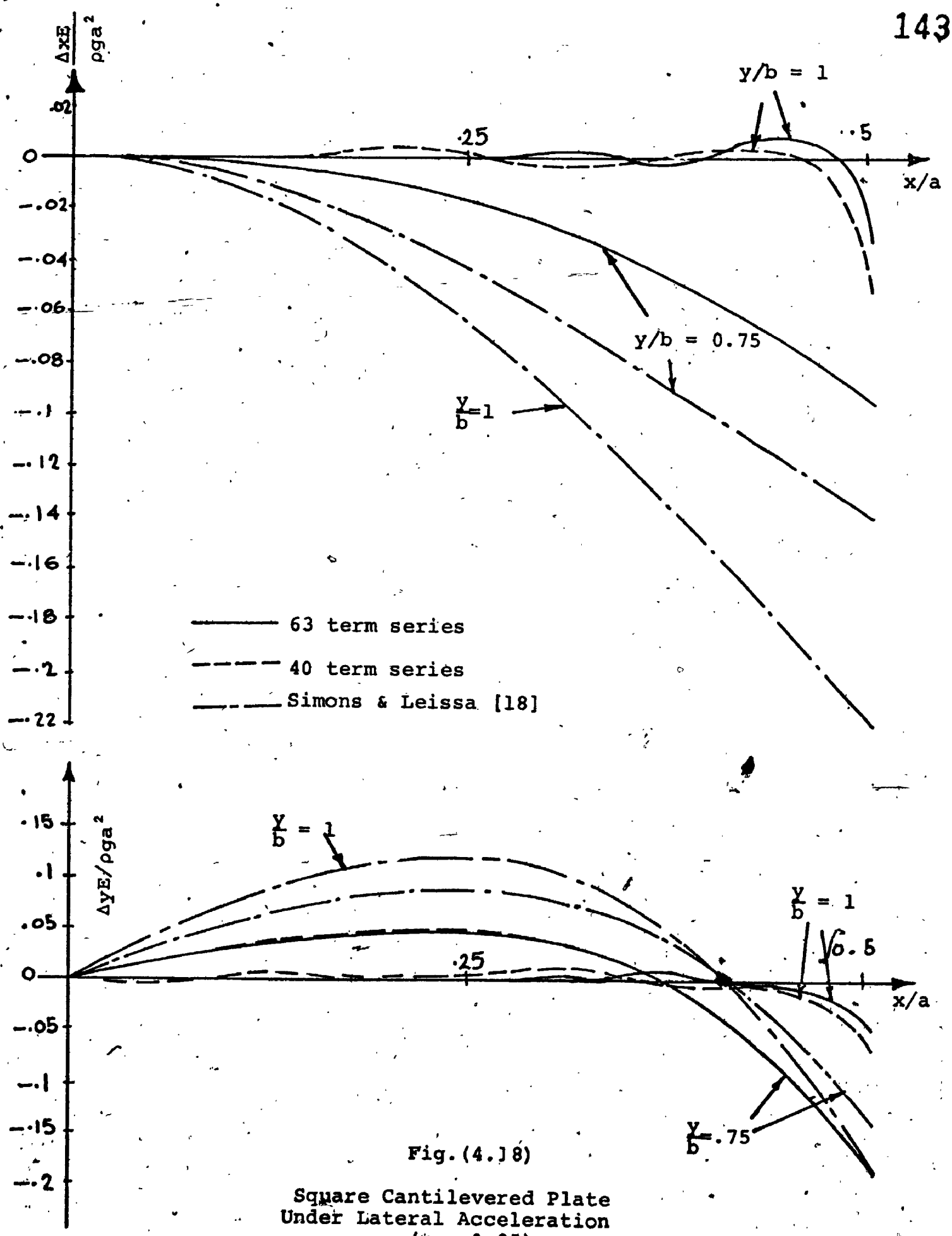

Fig.(4.18)

Square Cantilevered Plate
Under Lateral Acceleration
(ν = 0.25)

FIG. (4.19A)

C-F-F-F PLATE - LATERAL ACCELERATION A/B = 1.0

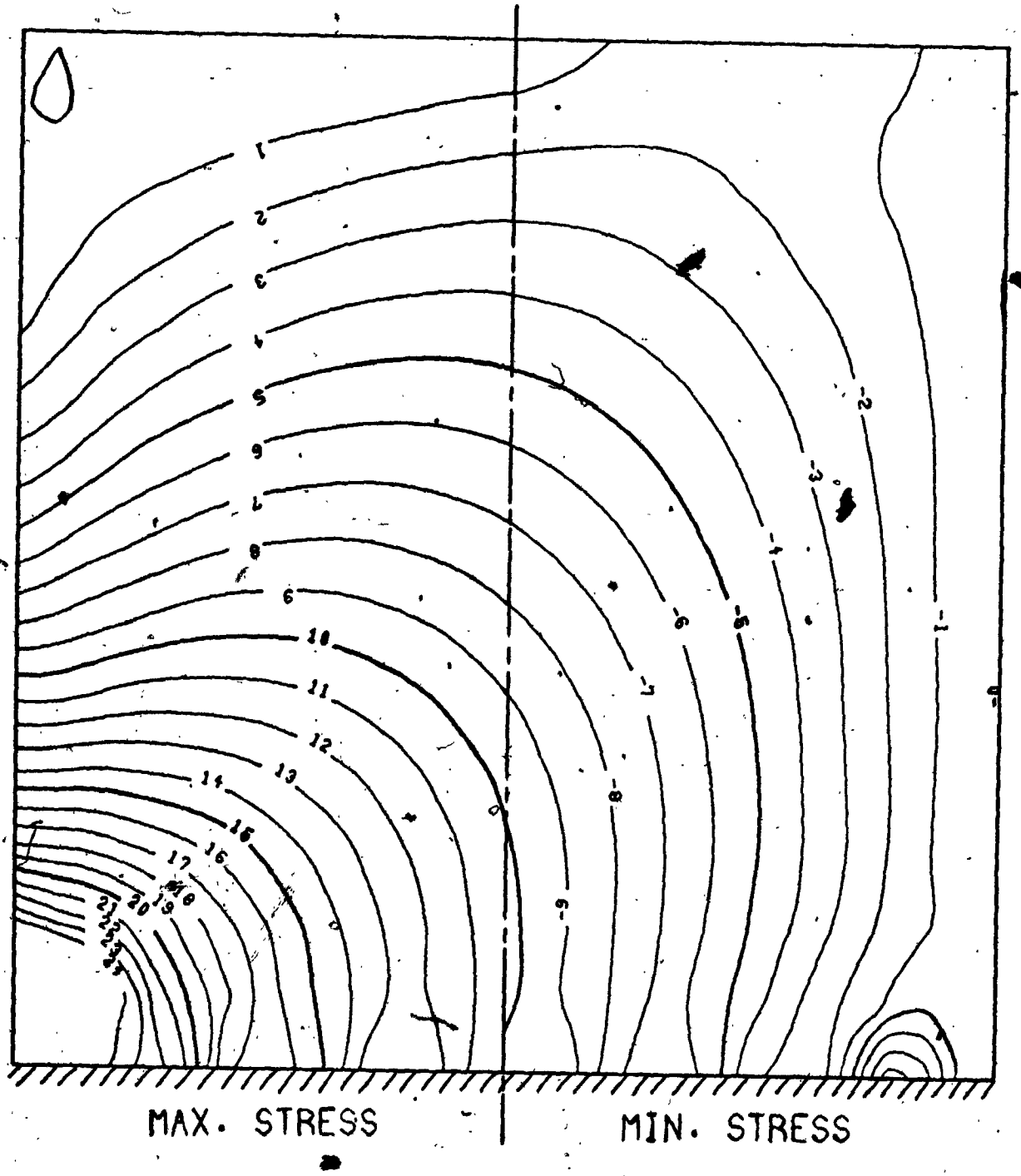

CHART NO. 00

2.00

FIG. (4.19B)

C-F-F-F PLATE - LATERAL ACCELERATION A/B = 1.0

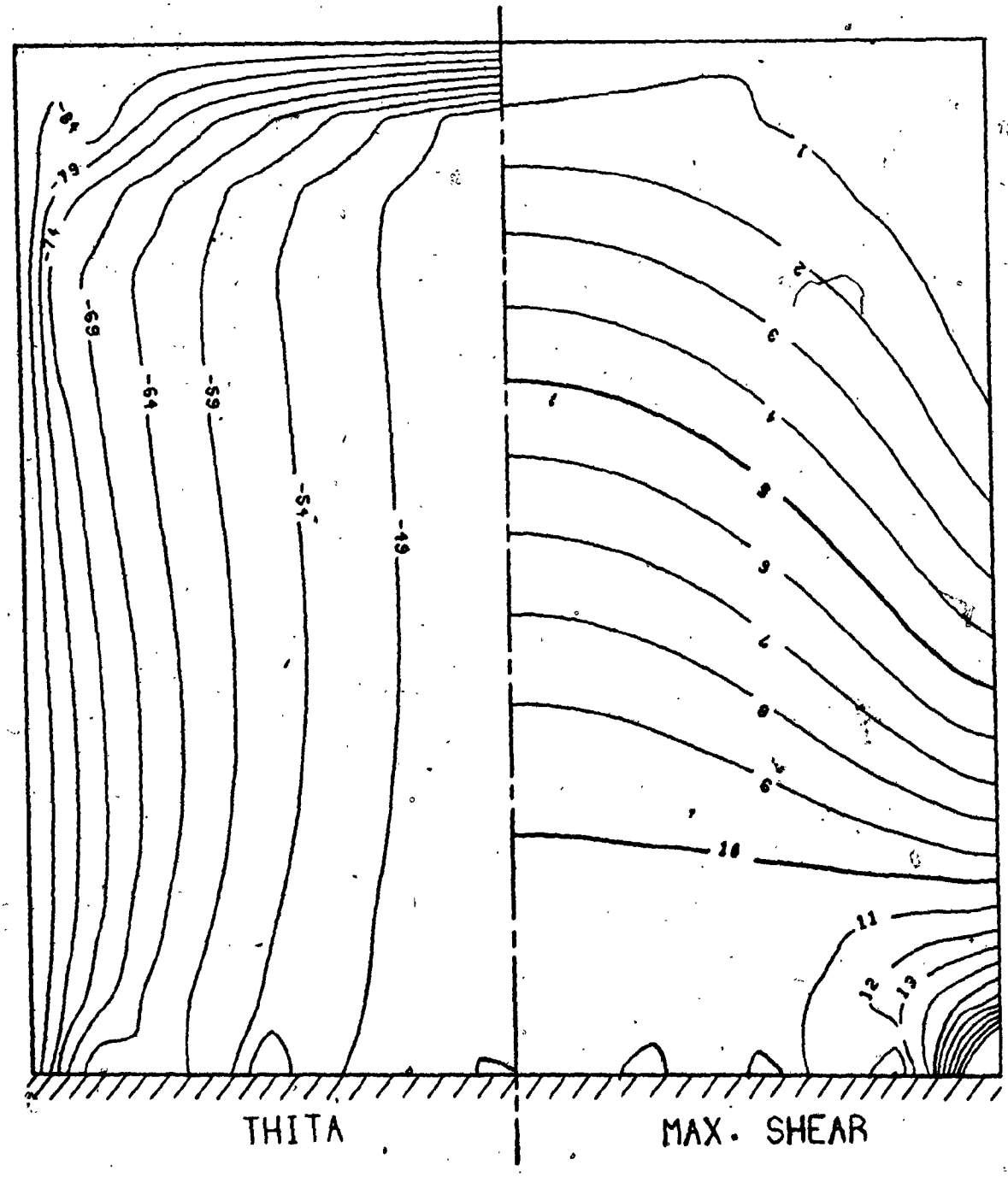

CHAPTER V

THE BUCKLING AND VIBRATION OF PLATES SUBJECT TO INPLANE LOADS

5.1 Statement of the Problem

The buckling and vibration of plates under arbitrary inplane loads has been the subject of a recent research program conducted by the author [1]. Included in [1] is a Ritz formulation which provides an approximate solution for the problem of a rectangular plate having an arbitrary combination of S-S, clamped or free edges, and subject to an arbitrarily specified system of inplane loads defined by a double series of known shape functions weighted by known coefficients. For that solution a displacement series of *ordinary* beam functions was used in order to match all three types of boundary conditions mentioned above.

In this chapter, the work presented in reference [1] is revised in view of the non-completeness of the ordinary beam functions when used for plates involving natural boundary conditions (see Chapters II and III). Here, the series of multiplications of beam functions used in [1] will be replaced by a series of multiplications of ordinary and/or degenerated beam functions according to the set of boundary

conditions imposed. The main effect on the formulation is due to the fact that, unlike the ordinary beam functions, degenerated beam functions are not orthogonal. The basic assumptions and steps of solution presented in [1], however, remain valid.

Moreover, in this work the applied inplane stress fields acting at the middle surface of the undeformed plate, are considered to have the form of those resulting from the plane stress analysis presented in the preceding chapter. Consequently, the inplane forces per unit length - Nx, Ny and N_{xy} - are assumed to take the form

$$Nx = h\frac{\partial^2 \Psi}{\partial y^2} = h\left[\frac{\partial^2 \Phi_o(x,y)}{\partial y^2} + \sum_{k=1}^{p}\sum_{l=1}^{q} \alpha_{kl}\bar{\phi}_k(x)\bar{\psi}_l''(y)\right],$$

$$Ny = h\frac{\partial^2 \Psi}{\partial x^2} = h\left[\frac{\partial^2 \Phi_o(x,y)}{\partial x^2} + \sum_{k=1}^{p}\sum_{l=1}^{q} \alpha_{kl}\bar{\phi}_k''(x)\bar{\psi}_l(y)\right],$$

$$N_{xy} = -h\frac{\partial^2 \Psi}{\partial x \partial y} = -h\left[\frac{\partial^2 \Phi_o(x,y)}{\partial x \partial y} + \sum_{k=1}^{p}\sum_{l=1}^{q} \alpha_{kl}\bar{\phi}_k'(x)\bar{\psi}_l'(y)\right]; \qquad (5.1)$$

where h is the plate thickness, $\bar{\phi}$ and $\bar{\psi}$ are ordinary - or degenerated - beam functions which match the inplane boundary conditions, $\Phi_o \equiv f_o(x) \cdot g_o(y)$ is a function depending upon the loading condition, and α_{kl} are coefficients to be determined from the in-plane stress problem solution as described in Chapter IV. As before, the plate material is assumed to be isotropic, homogeneous, and to obey Hook's

law. The transverse deformations are assumed to take place in accordance with the classical thin plate theory, i.e. lines normal to the originally undeformed middle surface remain straight and normal to the middle surface after deformation, and the stresses in the middle surface are the same before and after deformation.

The solution of the free transverse vibration problem for a plate subject to a given set of inplane loads is performed in two stages; Firstly, the plane elasticity problem must be solved for the given loading case and under the prescribed inplane boundary conditons, yielding the function Φ_o and the coefficients α_{ij} of equations (5.1) using the technique described in Chapter IV. The inplane loading fields thus obtained are then used to solve the free vibration problem. This latter problem is also governed by a fourth-order partial differential equation having variable coefficients and its direct solution is generally not feasible. Consequently, the Ritz method is employed.

5.2 The Ritz Solution

The differential equation representing the equilibrium of a plate, subject to a combination of inplane (membrane) and transverse loads, in the direction perpendicular to the undeformed mid-plane is given by

$$\Delta\Delta(u) - \left[\frac{N_x}{D}\frac{\partial^2 u}{\partial x^2} + \frac{N_y}{D}\frac{\partial^2 u}{\partial y^2} + 2\frac{N_{xy}}{D}\frac{\partial^2 u}{\partial x \partial y}\right] = P(x,y) \quad (5.2)$$

which differs from the biharmonic equation (2.4) by the quantities in the square brackets resulting from the contributions of the membrane loads. With this equation is connected the problem of minimizing the integral

$$\bar{U} = U + \int_D \int [\frac{Nx}{D}(\frac{\partial u}{\partial x})^2 + \frac{Ny}{D}(\frac{\partial u}{\partial y})^2 + 2\frac{N_{xy}}{D}(\frac{\partial u}{\partial x}\cdot\frac{\partial u}{\partial y})]\,dxdy, \tag{5.3}$$

where U is the integral defined by (2.5) in association with the biharmonic equation (2.4).

Following the idea of Ritz and the notations used in Chapter III, the approximate solution is assumed to take the form given by (3.5) and the transverse load by the series (3.5a). The Ritz minimization equations, after interchanging the summation and integration signs, may easily be writen as:

$$\sum_{i=1}^{m}\sum_{j=1}^{n} A_{ij}\{C_{ij}^{(rs)} + \frac{a^3}{b}\int_0^b\int_0^a [\frac{Nx}{D}(\phi_i'\psi_j\cdot\phi_r'\psi_s) + \frac{Ny}{D}(\phi_i\psi_j'\cdot\phi_r\psi_s') + \frac{N_{xy}}{D}(\phi_i'\psi_j\cdot\phi_r\psi_s' + \phi_i\psi_j'\cdot\phi_r'\psi_s')]\,dxdy\} - \bar{P}^{(rs)} = 0, \tag{5.4}$$

where $C_{ij}^{(rs)}$ and $\bar{P}^{(rs)}$ are the coefficients defined in equation (3.7). Substituting for the inplane loads Nx, Ny and N_{xy} from (3.1), and defining the integral coefficients

$$K^{o}_{ir} = a \int_{o}^{a} f_o(x) . \phi_i' . \phi_r' . dx ,$$

$$T^{o}_{js} = b \int_{o}^{b} g_o(y) . \psi_j' . \psi_s' . dy ,$$

$$U^{o}_{ir} = a \int_{o}^{a} f_o''(x) . \phi_i . \phi_r . dx ,$$

$$i,j,r,s,=1,2,\ldots$$

$$V^{o}_{js} = b \int_{o}^{b} g_o''(y) . \psi_j . \psi_s . dy , \qquad (5.5a)$$

$$W^{o}_{ir} = a \int_{o}^{a} f_o'(x) . \phi_i . \phi_r' . dx ,$$

$$Q^{o}_{js} = b \int_{o}^{b} g_o'(y) . \psi_j . \psi_s' . dy ;$$

and

$$K^{k}_{ir} = a \int_{o}^{a} \bar{\phi}_k . \phi_i' . \phi_r' . dx ,$$

$$T^{l}_{js} = b \int_{o}^{b} \bar{\psi}_l . \psi_j' . \psi_s' . dy ,$$

$$U^{k}_{ir} = a \int_{o}^{a} \bar{\phi}_k'' . \phi_i . \phi_r . dx ,$$

$$i,j,r,s,k,l=1,2,\ldots$$

$$V^{l}_{js} = b \int_{o}^{b} \bar{\psi}_l'' . \psi_j . \psi_s . dy , \qquad (5.5b)$$

$$W^{k}_{ir} = a \int_{o}^{a} \bar{\phi}_k' . \phi_i . \phi_r' . dx ,$$

$$Q^{l}_{js} = b \int_{o}^{b} \bar{\psi}_l' . \psi_j . \psi_s' . dy .$$

equation (5.4) can be written in the form

$$\sum_{i=1}^{m}\sum_{j=1}^{n}(C_{ij}^{(rs)} + \bar{C}_{ij}^{(rs)}).A_{ij} = \bar{P}^{(rs)}, \quad (r=1,2,\ldots m, \; s=1,2,\ldots n), \tag{5.6}$$

where

$$\bar{C}_{ij}^{(rs)} = \left(\frac{ha^2}{Db^2}\right)[K_{ir}^{o}.V_{js}^{o} + U_{ir}^{o}.T_{js}^{o} + W_{ir}^{o}.Q_{sj}^{o} + W_{ri}^{o}\,Q_{js}^{o} + \sum_{k=1}^{p}\sum_{l=1}^{q}\alpha_{kl}(K_{ir}^{k}.V_{js}^{l} + U_{ir}^{k}.T_{js}^{l} + W_{ir}^{k}.Q_{sj}^{l} + W_{ri}^{k}.Q_{js}^{l})]. \tag{5.7}$$

Equations (5.6) are a set of m x n linear equations sufficient for the determination of the coefficients A_{ij} in the Ritz solution. In the case of the free vibration problem, it is only necessary to replace the transverse load P by the inertia force parameter $\rho h\omega^2 u/D$ resulting in a standard eigenvalue problem of the order m x n as with the case of the plate free from inplane forces. Thus, in the dynamic case equation (5.6) is replaced by

$$\sum_{i=1}^{m}\sum_{j=1}^{n}[(C_{ij}^{(rs)} + \bar{C}_{ij}^{(rs)}) - \lambda(E_{ir}.I_{js})]\,A_{ij} = 0, \quad (r=1,2,..,m; \; s=1,2,\ldots,n), \tag{5.8}$$

the solution of which yields the approximate eigenvalues and eigenfunctions of the problem.

It can be seen that the above formulation includes three groups of integral coefficients which have to be evaluated before the equations can be set up. The first group comprises those integrals involved in evaluating $C_{ij}^{(rs)}$ and defined by equation *(3.8)*. These integrals depend only upon the out-of-plane boundary conditions imposed upon the plate and have already been discussed in section (3.2.1) in association with plates free from in-plane loads.

The second group of integrals, defined by equation *(5.5b)*, involves the integration of the product of three ordinary and/or degenerated beam functions and their derivatives. These integrals depend upon both the inplane and the out-of-plane boundary conditions of the problem. However, they are independent of the loading condition considered. The evaluation of these integrals is a straightforward generalization of the method of expansion in the form of complex exponentials outlined in section (3.2.1) in association with the integrals of the first group involving the multiplication of two beam functions. Evaluation of the integrals of this group, which are needed in the solution of the examples to follow, is described in detail in Appendix I. Since each of these integral coefficients involves three indices, their evaluation is relatively time consuming. However, since these integrals do not depend upon the loading conditions, they need to be evaluated only once for each set of boundary conditions of interest.

The third group of integrals constitutes those integral coefficients defined by equation *(5.5a)*. These coefficients depend upon the particular loading condition on hand; thus they have to be evaluated separately for each individual problem. The integrals of this group involve the integration of the product of two beam functions and a third function Φ_o or their derivatives. This function Φ_o, as was pointed out in section (4.3), is a low order polynomial for most practical cases. Thus, if the beam functions are represented by complex exponentials as before, integrals of this group can be evaluated easily through several integrations by parts until the polynomial is eliminated through the successive differentiations. The detailed evaluation of the integrals of this class, which are involved in the numerical examples to follow, is presented in Appendix I.

5.3 Numerical Examples

In the following subsections, four numerical examples for the vibrations, and buckling, of plates subject to systems of inplane loads are presented. In addition to demonstrating the applicability of the techniques described earlier, the examples presented are meant to show that simplifying assumptions regarding the actual distribution of the inplane loads may, sometimes, lead to considerable inaccuracies in the buckling and vibration results obtained.

An attempt is also made to provide an insight for the conditions under which the solution of a problem would be insensitive to minor modifications in the pattern of the applied inplane loads.

The inplane load patterns used for these problems had been found in the examples of Chapter IV, and the evaluation of the integral coefficients involved is shown in Appendix I. In each of the examples, the results obtained by the proposed method are compared to those obtained by the simple loading pattern resulting from retaining only the Φ_o term in the assumed loading series - equation *(5.1)* - and with previously published solutions whenever available.

5.3.1 Cantilever Plates Under Inplane Acceleration Loads

This problem has been solved by Simons and Leissa in 1971 [18] using the Ritz methods and a series of multiplications of ordinary beam functions. In [18] the Airy stress function was taken to be a fourth order polynomial which satisfies the compatability equation and the boundary conditions at the two parallel free edges. Only the overall equilibrium conditions were satisfied at the other two edges.

The geometry and the x - y coordinates used for the problem are shown in figure (5.1). The $\bar{x}$ - $\bar{y}$ coordinates shown in the figure correspond to those used in the solution of the inplane stress problem presented in section (4.4.3) and shown in figure (4.12). A simple coordinate

transformation was thus used in Appendix I to transform the inplane stress fields from the $\bar{x}$ - $\bar{y}$ coordinates to the x - y domain prior to performing the integrations involved. As shown in the figure, the edge $y = 0$ is clamped - with respect to both the inplane and out-of-plane motions - while the other three edges are completely free.

Table (5.1) is a convergence study showing the effect of using different numbers of terms in both the inplane load series and the out-of-plane displacement series. It can be seen that, for this particular problem, the frequency parameters are quite insensitive to the slight modifications in the inplane load patterns introduced by changing the number of terms in the load series. It is thus sufficient to use the first term alone (Φ_o) which is a cubic polynomial; further modification being unnecessary. It can also be seen from the table that increasing the number of terms in the displacement series from 24 to 40 makes a difference of less than one half of one percent in the frequency parameter indicating that a good convergence has been already achieved.

Table (5.2) shows a comparison with the results of reference [18] for $\theta = 90°$. It can be seen that the present results are more accurate since they represent a closer upper bound for the exact solution. This improvement is mainly due to the use of the degenerated beam functions rather than the ordinary beam functions employed in reference [18]. Once more the table shows the negligible effect

Table (5.1)

Vibration of a Square Cantilevered Plate Under Gravitational Loads

Convergence of the fundamental frequency parameter with varying numbers of terms in both the inplane and out-of-plane series. Percentage* improvements over shortest series shown in brackets. Poisson's ratio = 0.3.

out-of-plane series (mxn)	inplane series (p x q)	$\rho g=7.5$ $\theta=180°$	$\rho g = 30$ $\theta = o°$
24	0	0.2295 (0.0)	58.799 (0.0)
24	18	0.2368 (0.06)	58.780 (-0.13)
24	35	0.2385 (0.08)	58.775 (-0.20)
40	0	0.2114 (-0.15)	58.753 (-0.38)
40	40	0.2143 (-0.13)	58.745 (-0.45)

*Percentage improvement = $100\,(\lambda^{(pq)}_{mn} - \lambda^{(o)}_{24})/\lambda^{(\text{no load})}_{24}$ %

Table (5.2)

Vibration of a Square Cantilevered Plate Under Lateral Gravitation

Convergence of the frequency parameters and comparison with ordinary beam solutions. $\rho g=15$, $\theta=90°$, m x n = 7 x 7. Poisson's ratio = 0.3

Mode order:	λ_1	λ_2	λ_3	λ_4	λ_5
p x q = 0:	9.9459	64.499	438.496	731.316	974.366
p x q = 40:	9.9443	64.424	438.499	730.820	973.961
Ordinary beams [18]:	10.0806	64.658	442.682	737.123	984.077

of including a large number of terms in the inplane load series; the first term alone being sufficient, and the complete solution of the inplane stress problem becomes unnecessary. A discussion of the conditions under which these conclusions are to be expected will be given in section (5.4)

5.3.2 An Out-of-plane Clamped Plate Loaded in One Direction

The problem of a rectangular plate subject to a uniform uniaxial inplane load has often been considered as a standard example in plate stability analysis. In practice, however, a purely uniaxial state of stress seldom occurs; since the loaded edges usually suffer tangential stresses, at least due to friction with the loading device. A good demonstration for this is the well known barrel shape that an initially cylindrical billet takes after a compression test. This barrel shape, of course, develops due to restraining the Poisson's expansion of the billet because of friction at the jaws. Since the coefficient of dry friction of metal surfaces is usually of the same order as - or greater than - Poisson's ratio, it is reasonable to assume that the loaded edge of a billet - or a plate - behaves as if it were perfectly clamped w.r.t. the plane of loading. This is assumed to be the case for this and the following examples.

In this example, as indicated in figure (5.2), the loaded edges are assumed to be perfectly clamped in both the inplane and out-of-plane directions. The other two edges are assumed to be free in their own plane; however,

displacements and rotations are restrained (i.e. clamped) in the out-of-plane direction. The inplane loading may be assumed to result from either movement of one of the fully clamped edges in the y-direction, or a differential thermal expansion between the plate and the mounting frame. The resulting inplane stress pattern found in section (4.4.1) will be utilized in this example.

Figures (5.3) and (5.4) are plots for the fundamental frequency parameter λ versus the inplane load for a square plate. The results obtained using a uniform uniaxial stress field (achieved by retaining Φ_o only) are also shown and compared with those presented in reference [1] for a clamped square plate under compression. It can be seen that relatively large errors would be obtained if the inplane load is assumed to be uniform. In addition, the buckling load would be *over-estimated* by more than 5%; which is undesirable in practical applications.

The same behaviour is shown in figure (5.5) for a plate of side ratio 2:1. As expected, in this case the deviation is even larger; emphasizing the importance of using a more realistic stress distribution in the solution of the vibration problem. For the third fully symmetric mode, the frequency-load curve is about 78% steeper than that obtained in the case of a uniform uniaxial stress condition.

5.3.3. Clamped-Free-Clamped-Free plates - Direct Load

In this example - figure (4.2) - the two edges para-

llel to the x-axis are considered clamped in both the in-plane and out-of-plane directions, while the other two edges are completely free. As with the previous example, the in-plane loading may be assumed to result from either a differential thermal expansion or a slight movement of the supports in the y-direction. Obviously, the resulting in-plane stress patterns will be the same as in the previous example (section 5.3.2.) since the two plates have the same inplane boundary conditions.

The frequency-load relations obtained for this problem are shown in figures (5.6) and (5.7) for plates of side ratios 1:1 and 2:1. As before, the results obtained using a uniform stress pattern (Φ_o only) are superimposed for comparison. It may be noted that the relative deviations between the results of the two loading conditions for the second and third modes are similar in magnitude and sign to those obtained for the first and second modes of the fully clamped plate of section (5.3.2). The fundamental frequency however, behaves in a rather odd manner; the uniform load results are steeper than those obtained by the modified load pattern resulting from the two-dimensional stress analysis. An attempt to explain this behaviour will be made in section (5.4).

5.3.4 Clamped-Free-Clamped-Free plates - Shearing load.

The boundary conditions of the plates considered here are the same as those for the previous example. The loading, however, is considered to be the result of the relative

movement of one of the supports in the x-direction under the action of a shearing load as shown in figure (4.5). The resulting inplane load patterns were found in section (4.4.2) and will be used here.

This example was first treated in reference [19] using ordinary beam functions in the Ritz method. For the inplane loads, however, a simplified stress pattern was assumed (which corresponds to the first term - Φ_o - of the inplane stress solution of section (4.4.2)).

The frequency-load curves for two plates of side ratios 1:1 and 2:1 are displayed in figures (5.8) and (5.9). Results obtained using the simplified load patterns corresponding to the one term solution (Φ_o), as well as those of reference [19] obtained using the same simplified load patterns but with ordinary beam functions, are also shown in the graphs for comparison. It can be seen that the sole effect of using modified rather than ordinary beam functions, while maintaining the same simplified load patterns, is to slightly lower the natural frequency (about 2%); however, the use of the more rigorous loading patterns results, in some instances, in considerable differences in the natural frequencies predicted. These differences are particularly apparent at the higher load levels and for higher side ratios where the effects of the clamped edges become more dominant. For the plate of side ratio 2:1, differences of about 7% in the buckling loads and 25% in the frequency parameters (relative to the no-load frequency parameter) are indicated.

5.4 Conclusions and Remarks

As a result of the foregoing study, the following conclusions have been reached:

- The problem of the vibrations and buckling of plates subject to general body and/or boundary loads may be conveniently solved by using ordinary and/or degenerated beam functions in the Ritz method. The solution is performed in two steps; first the two-dimensional stress analysis problem is solved in order to determine the stress patterns acting on the middle surface of the plate due to the external loads applied; the plate flexure problem is then solved with the due effect of the inplane loads taken into account in the energy expressions.
- The solution of the inplane problem starts by the choice of a function Φ_o which satisfys the "forced" inplane boundary conditions (those which are directly related to the forces acting along the boundaries, e.g. the free edge boundary conditions) as well as the overall equilibrium conditions of the plate, but not necessarily satisfying the "natural" boundary conditions (e.g. the clamped edge boundary conditions). This function Φ_o, or similar simple functions, have been frequently used [18, 19, 27] to solve directly the plate vibration and/or buckling problem while by-passing the first stage of the solution (i.e. solving the inplane problem). Depending upon the nature of the problem,

varying degrees of accuracy may be obtained through such a simplified solution as was shown in the previous examples.

The adequacy - or inadequacy - of a simplified solution utilizing ϕ_o only as the stress function depends upon many factors; most important are the following

i) The inplane boundary conditions: Since the simplified function ϕ_o does not, generally, satisfy the inplane clamped edge boundary conditions, the accuracy of the simplified solutions deteriorate as a larger portion of the boundary becomes clamped with respect to the inplane motion. This partially explains the fact that the simplified solutions obtained for the cantilever plate of example (1) are much more accurate than those obtained in examples (2) through (4) where two inplane clamped edges are involved. It also explains the fact that larger discrepancies between the simplified and the more rigorous solutions are obtainable for plates of side ratio 2:1 compared to those for a square plate.

ii) The out-of-plane boundary conditions: It is not sufficient to have considerable discrepancies between the actual and the simplified stress patterns to conclude that unacceptable errors would result from the use of such a simplified pattern in solving the vibration problem. The

reason is that the inplane loads in the energy equation for the out-of-plane motion of a plate element are weighted by the *square of the slope* of the element under consideration [see equation (5.3)]. Thus, a large change in the load intensity in a direction where the slope is small contributes a negligible change in the natural frequency of the plate. Since the out-of-plane boundary conditions greatly affect the slopes (at least in the vicinity of the edges where the changes in the inplane load patterns are usually most pronounced), the sensitivity of the dynamic solutions to the accuracy of the load patterns are dependent upon those boundary conditions. This is most clearly shown by comparing the results of examples (2) and (3) where the same loading patterns caused different effects by merely changing the type of boundary conditions at the two unloaded edges. In particular, much less effect is noticeable in the fundamental frequency in example (3) compared to that of example (2); the reason being that much smaller slopes are found in the x-direction in example (3), where there are two parallel free edges, compared to those manifested in the case of example (2) with two parallel clamped edges in the x-direction.

iii) The mode shape: Since the slopes in a certain direction increase rapidly as the number of half waves in that direction - in a given mode of vibration - increases, the mode of vibration becomes an important factor in determining the relative effect of a given deviation in the load pattern used in calculating the frequency of that mode. This explains why larger deviations are noticeable in examples (2) and (3) for the higher modes where more half waves - and hence higher slopes - are manifested in the x-direction in which the forces due to restraining Poisson's contraction have been neglected in the simplified load pattern ($\Phi_o = x^2/2$). Although these forces are relatively small with respect to the stresses in the y-direction, their effect becomes considerable for higher modes since the ratio of the squares of the slopes in the x- and y-directions becomes very large.

In example (2), higher buckling loads are obtained if the simplified load pattern is used. This is explainable since loads due to restraining Poisson's expansion, which have a destabilizing effect, are neglected. On the other hand, however, it was found in example (3) that a lower buckling load is obtained if the simplified load pattern is used. This may be explained, in the light of the previous conclusions, as follows:

a) The simplified load pattern differs from the actual load distribution in three main aspects; firstly, the forces due to restraining Poisson's expansion - which has a destabilizing effect; secondly, the forces due to the singularity at the corners; these forces are accompanied by a reduction in the stresses near the middle of the clamped edges since the overall equilibrium conditions require that the total load at any cross-section remains constant; and thirdly, away from the clamped edges, along a line parallel to the x-axis, the stress σ_y is higher at the centre than it is at the edges of the plate; in the simplified load pattern σ_y is assumed to be uniform.

b) The first and second deviations mentioned above produce negligible effect on the stability of the plate since the associated slopes are negligible for the given boundary conditions in the fundamental mode.

c) Since at any given section parallel to the x-axis the slopes in the y-direction are slightly higher near the free edges than they are near the centre line of the plate, the net effect of the third deviation is a stabilizing action since the reduction in the load near the edges is associated with the higher slopes. Thus, the final result is a higher buckling load than that which

would be predicted if the simplified uniform load pattern were adopted.

For the cantilever plate problem - example (1) - negligible deviations were found due to the use of the approximate load patterns due to the following reasons:

1) Very little deviation between the approximate and rigorous inplane stress patterns were found except for about one quarter of the plate near the clamped edge.

2) In those areas of the plate where the deviation is considerable, the slope of the plate is negligible due to the effect of the clamped edge.

3) Due to the existence of two parallel free edges, the fundamental mode has negligible slope in the x-direction leading to cancellation of the effects of the forces due to restraining Poisson's contraction.

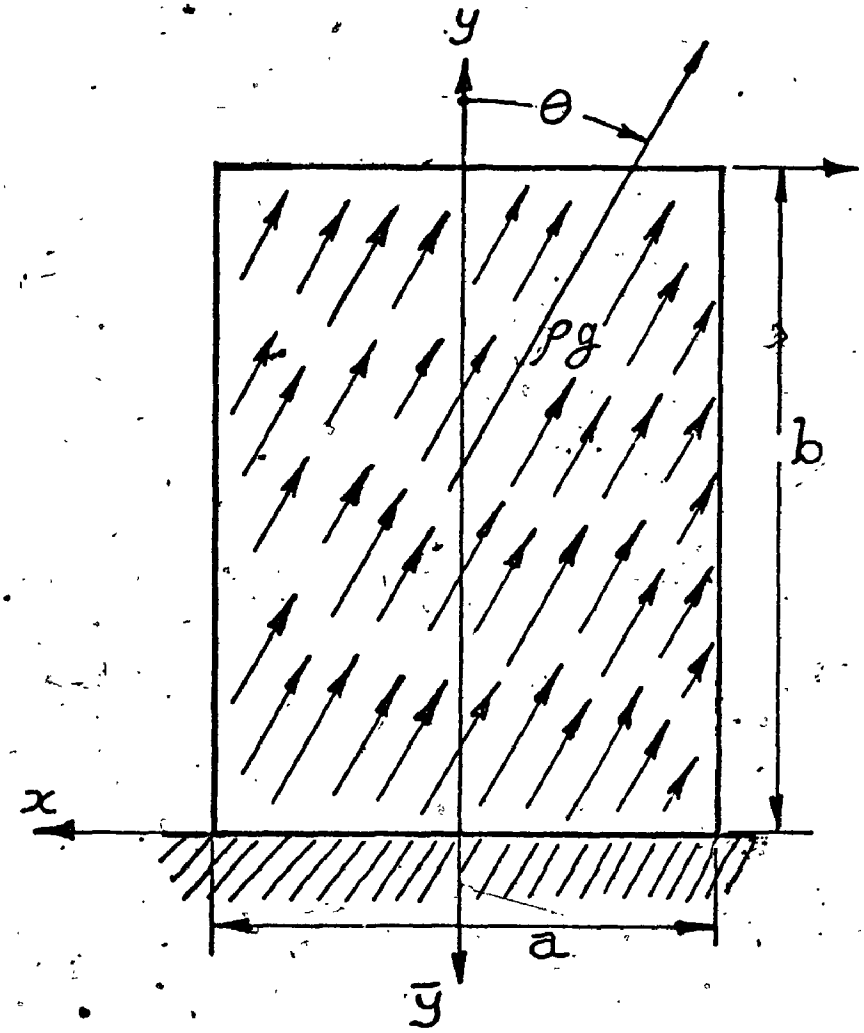

FIG (5·1)

Rectangular Cantilevered Plate – General Gravitational Loads.

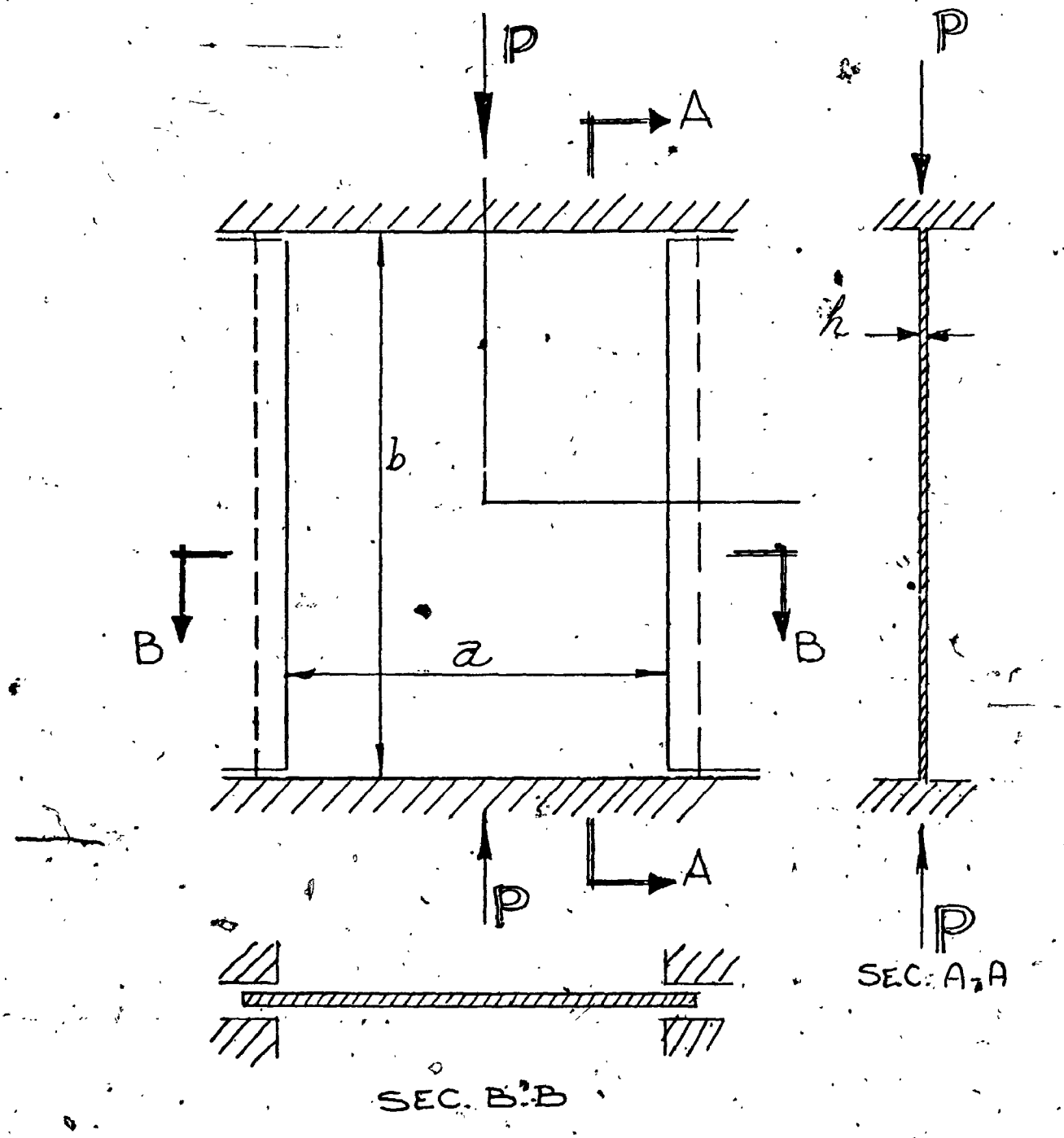

Fig. (5.2)

The Fundamental Frequency Parameter
For a Clamped Square Plate
Under Compressive Inplane Loading

(ν = 0.3)

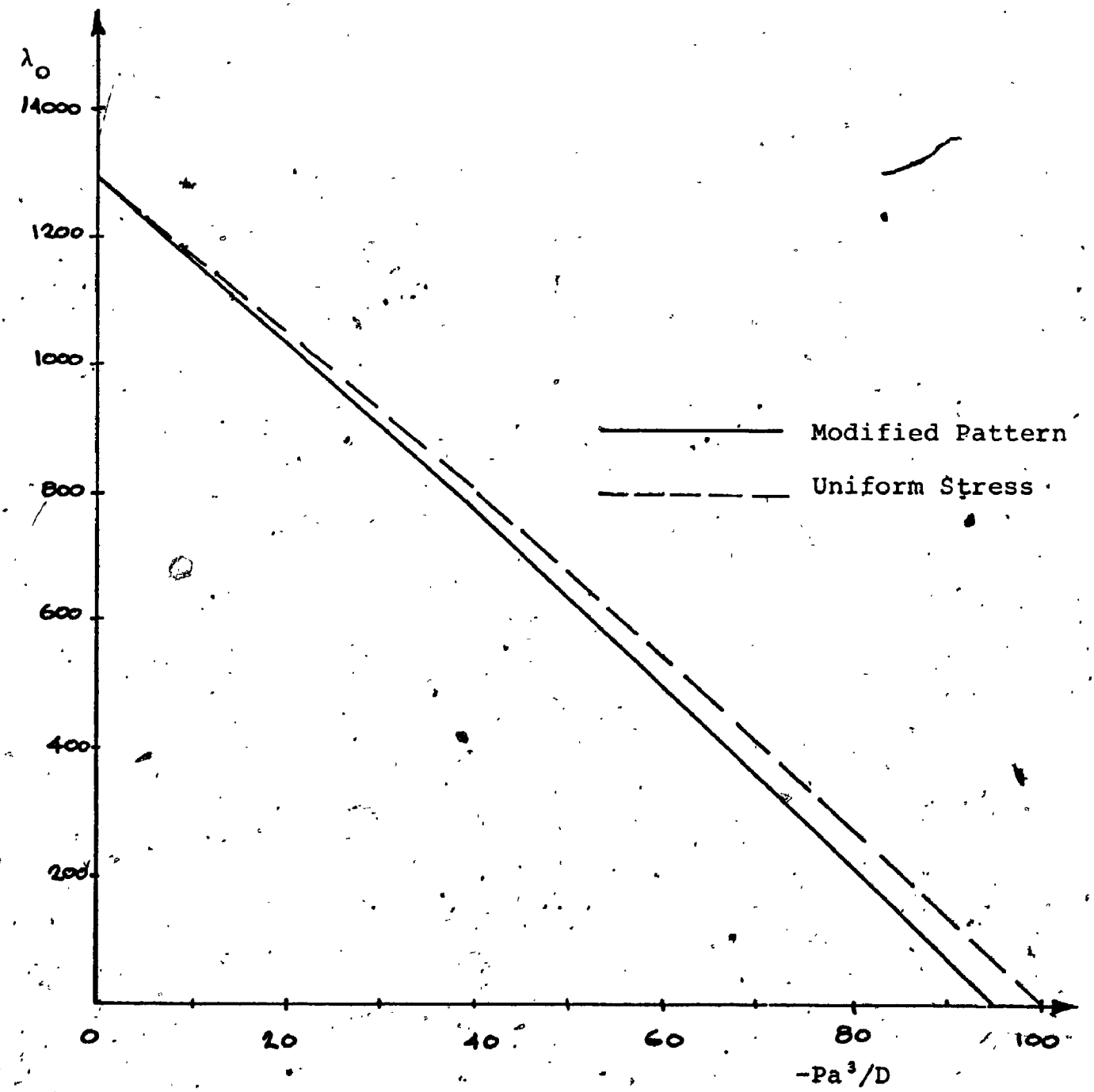

Fig. (5.3)

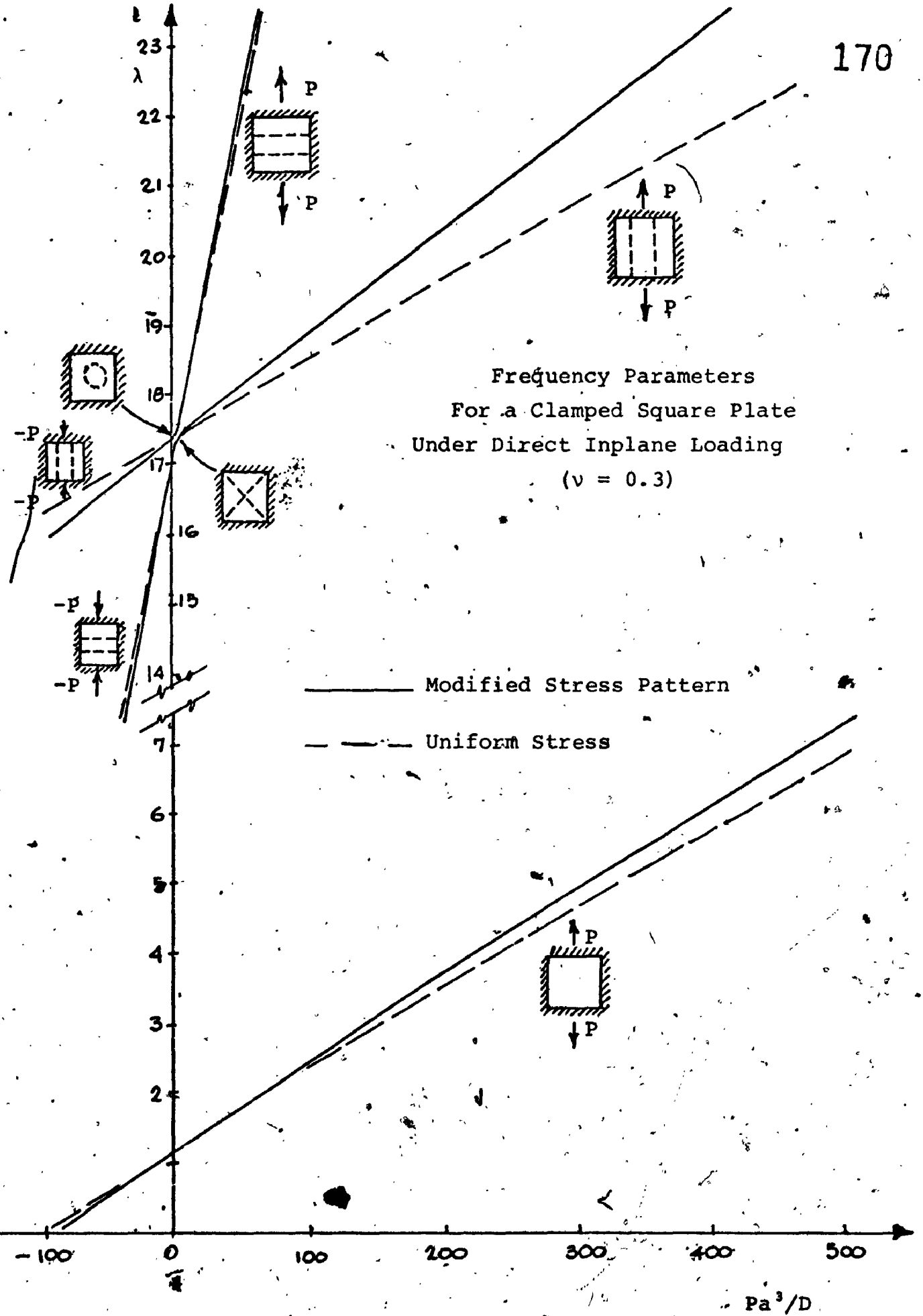
λ
23
22
21
20
19
18
17
16
15
14
7
6
5
4
3
2
P
P
P
P
-P
-P
-P
-P
Frequency Parameters
For a Clamped Square Plate
Under Direct Inplane Loading
(ν = 0.3)
Modified Stress Pattern
Uniform Stress
-100
0
100
200
300
400
500
Pa³/D

Fig. (5.4)

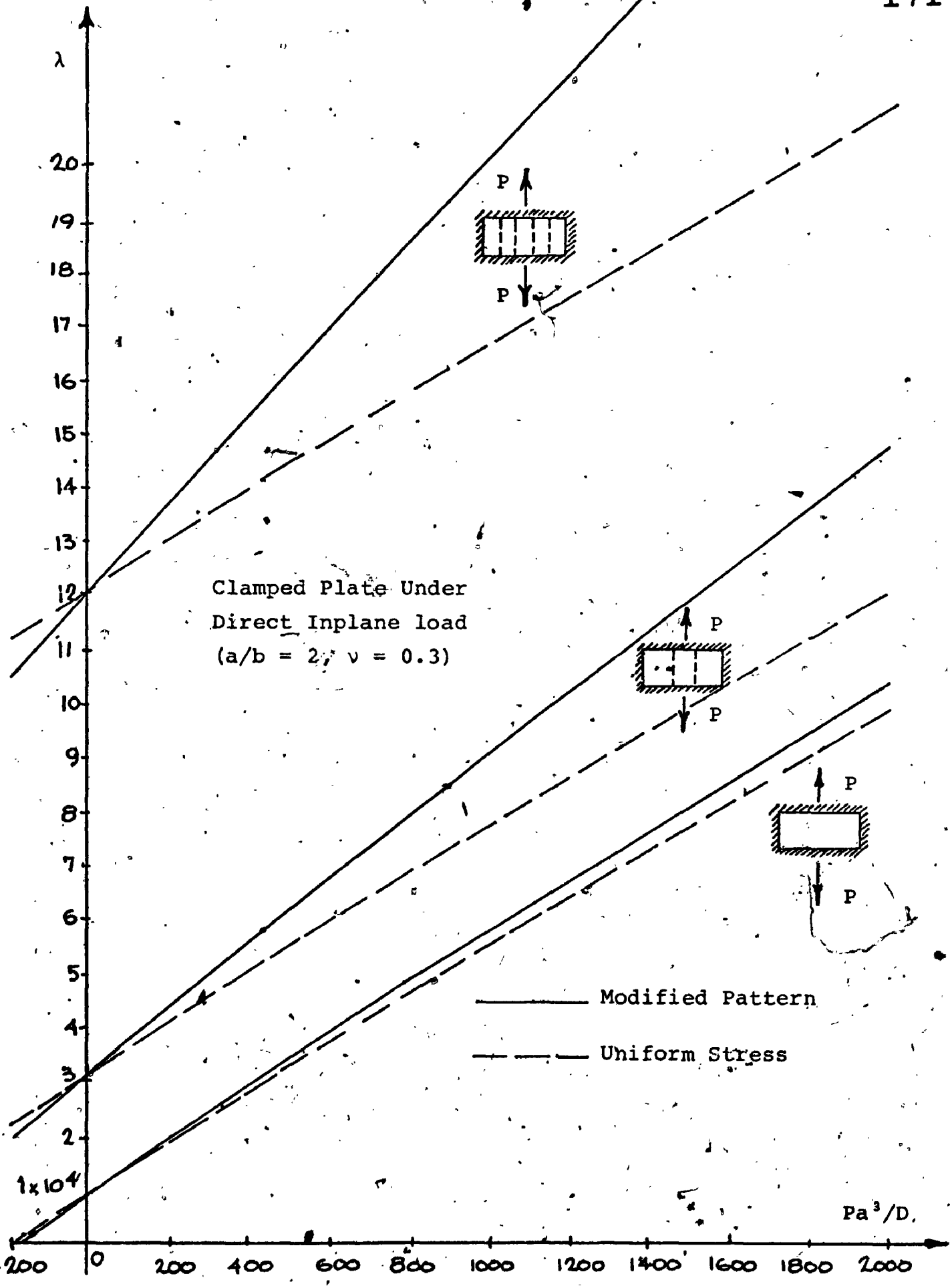
λ
20
19
18
17
16
15
14
13
12
11
10
9
8
7
6
5
4
3
2
1x10⁴
P
P
P
P
P
P
Clamped Plate Under
Direct Inplane load
(a/b = 2, ν = 0.3)
Modified Pattern
Uniform Stress
-200
0
200
400
600
800
1000
1200
1400
1600
1800
2000
Pa³/D

Fig. (5.5)

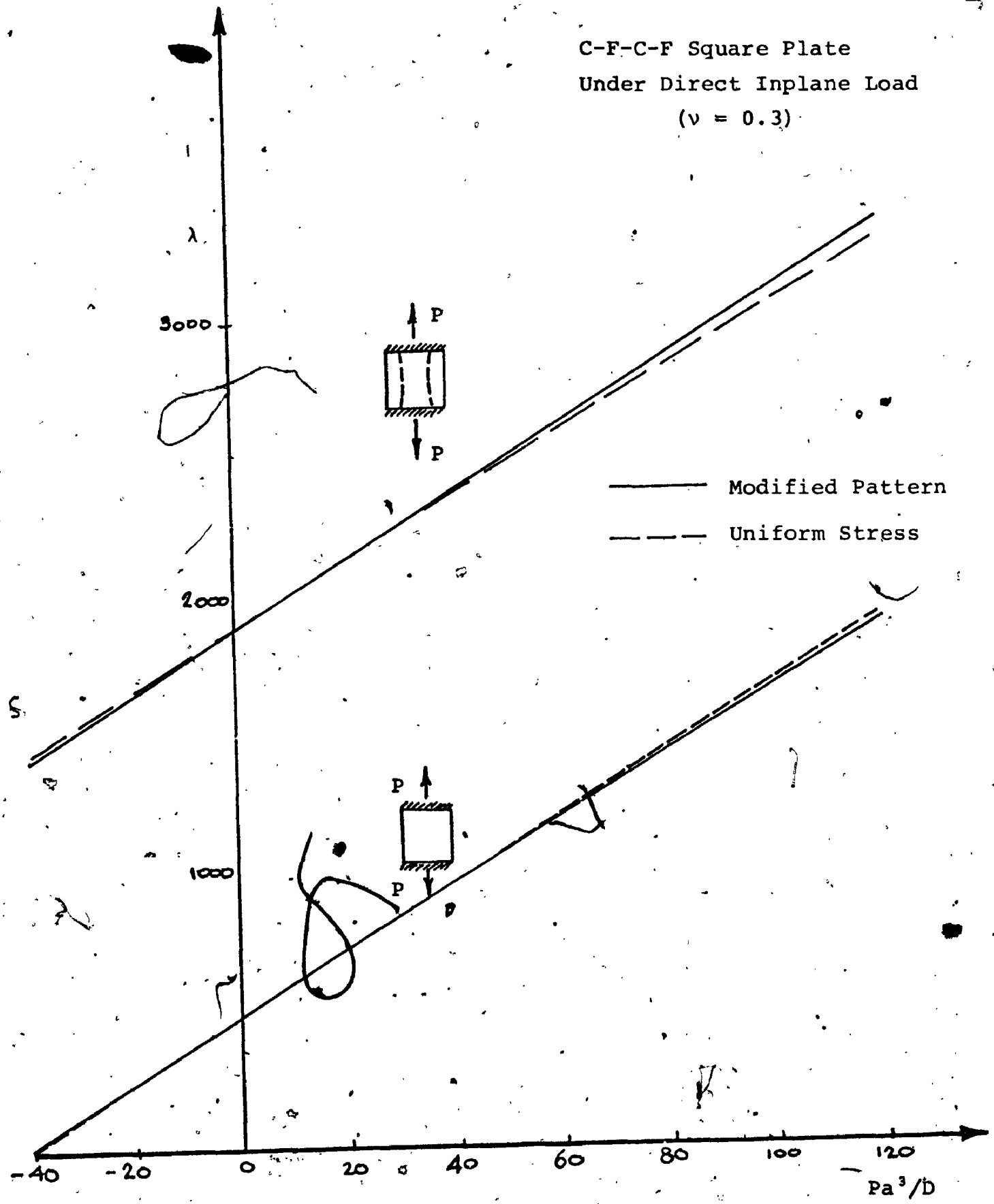
C-F-C-F Square Plate
Under Direct Inplane Load
(ν = 0.3)
λ
3000
2000
1000
P
P
P
P
Modified Pattern
Uniform Stress
-40
-20
0
20
40
60
80
100
120
Pa³/D

Fig. (5.6)

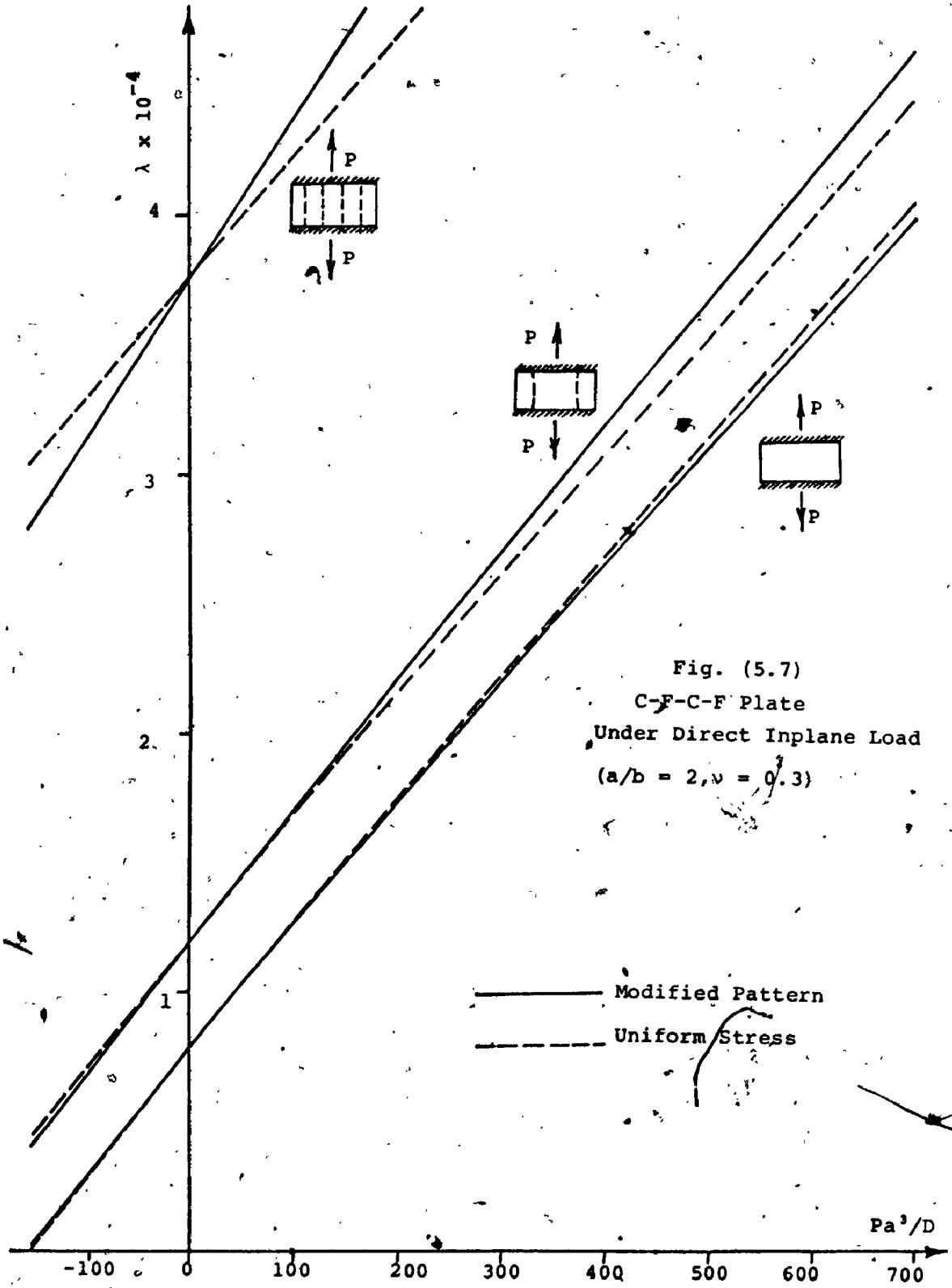

Fig. (5.7)
C-F-C-F Plate
Under Direct Inplane Load
(a/b = 2, ν = 0.3)

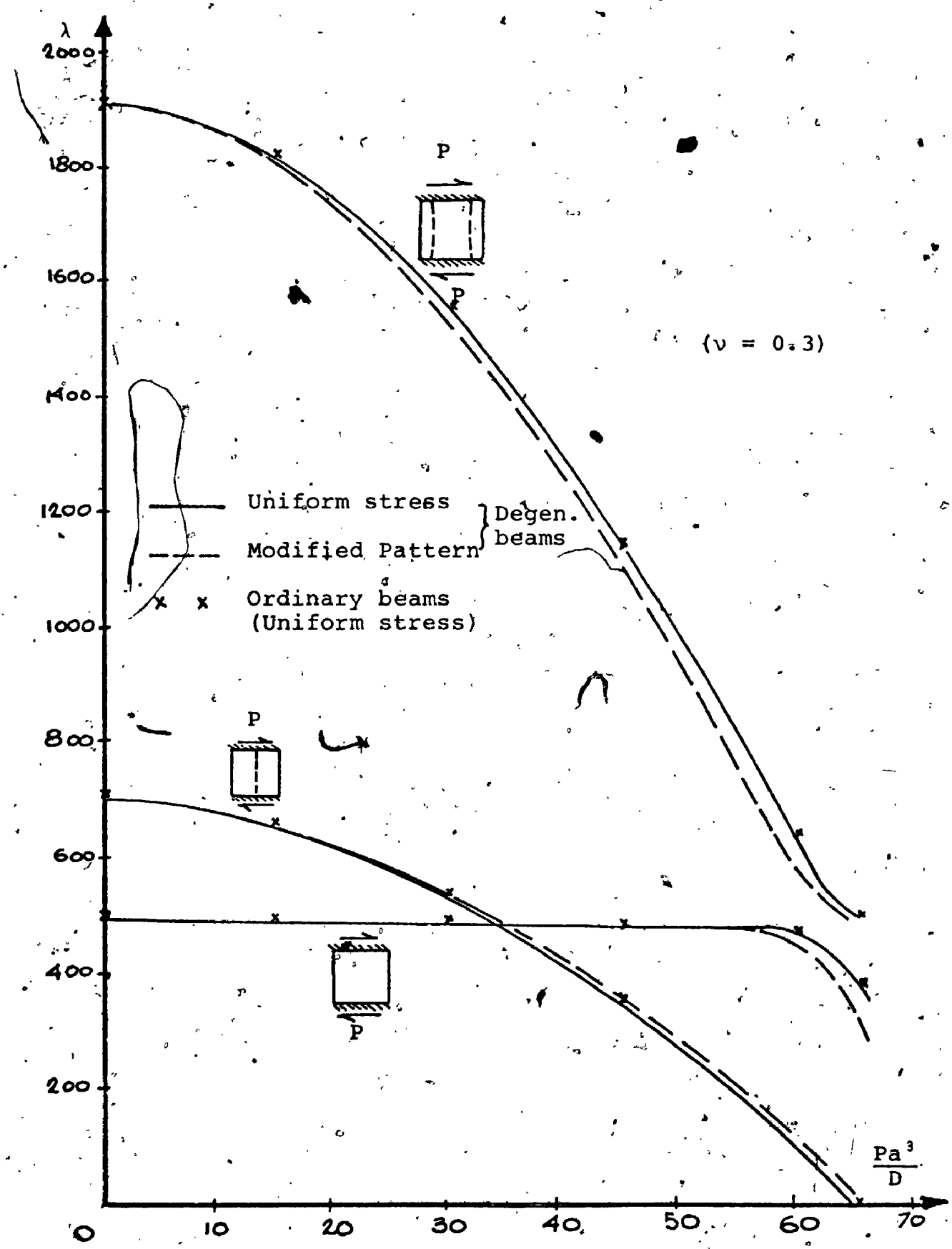

C-F-C-F Square Plate Under Edge Shear

Fig. (5.8)

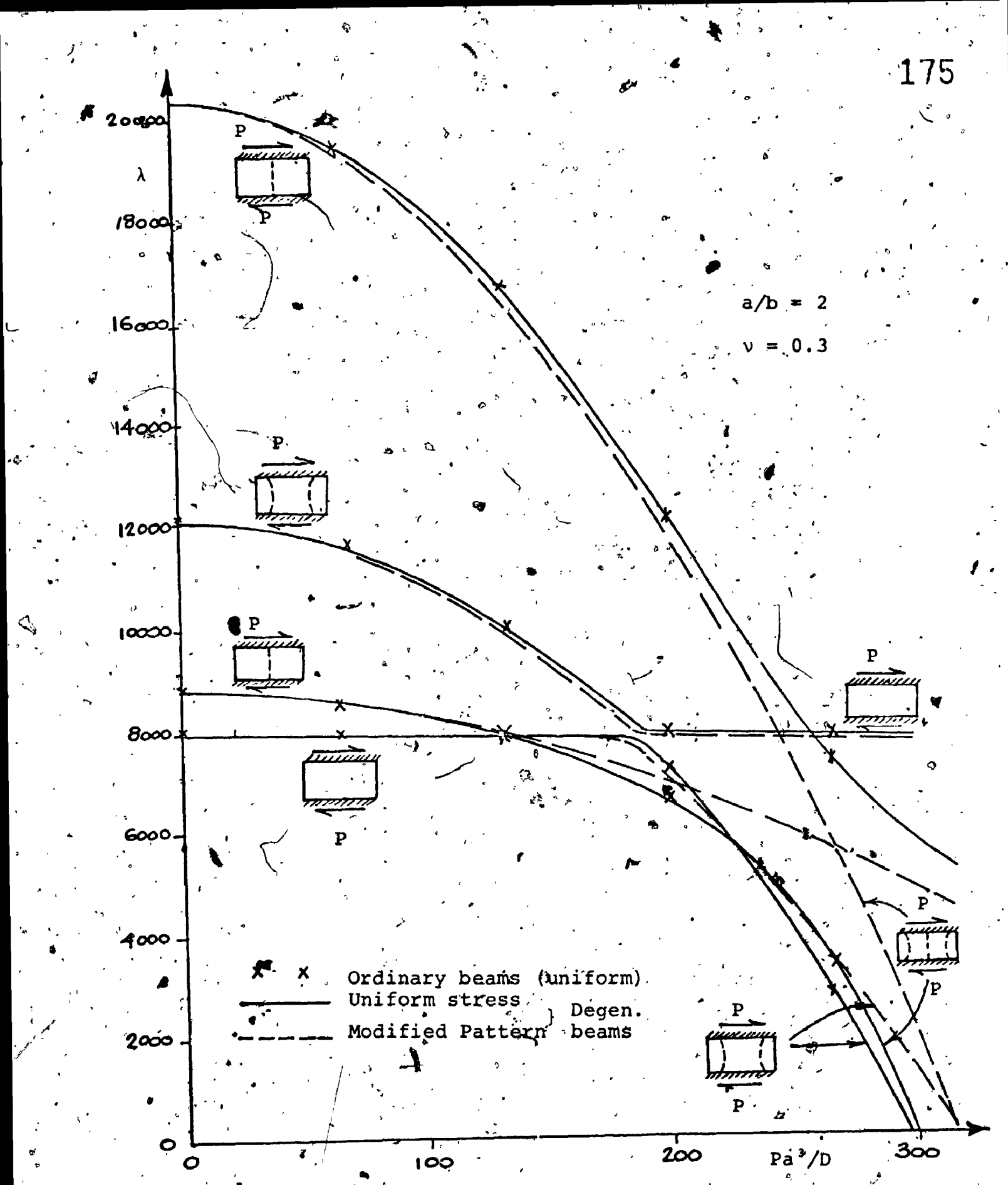

C-F-C-F Plate Under Edge Shear

Fig. (5.9)

36

OF/DE

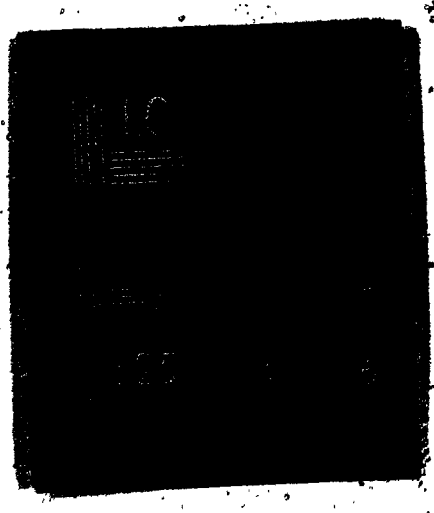

CHAPTER VI

ON THE IDEAL METHOD OF STURCTURAL ANALYSIS - A PRACTICAL POINT OF VIEW

6.1 Introduction

In the previous Chapters, a detailed study for the Ritz variational approach has been presented. Sufficient conditions for a guaranteed minimal trial sequence were stated, and a critical evaluation for the validity of the use of a series of multiplications of beam functions for the solution of plate problems when free edges are involved was presented. As a result of that study, the idea of the "degenerated beam functions" evolved and was proven to be a most satisfactory substitute for "ordinary" beam functions whenever free edges are involved. Moreover, with the degenerated beam functions on hand, it was shown that the same mathematical and numerical formulation can be conveniently applied for the solution of the two - dimensional elasticity problem as well as that of the plate flexure. With a unified approach for the solution of both the inplane and the out-of-plane plate problems, a convenient and accurate solution for the combined problem of the stability and vibrations of plates subject to *arbitrary* inplane edge and body forces became possible.

As a result of the study contained in these chapters, several important conclusions were reached. These conclusions will be summed up in the concluding chapter of this thesis (Chapter XII). Perhaps the most useful conclusion reached, however, is that the Ritz method, in its present development, became a most accurate, simple, and convenient tool for the analysis of problems in solid mechanics in general, and rectangular plates in particular. Unfortunately, the convenient use of the method of Ritz is limited to problems bounded by simple regions and under simple boundary conditions. The majority of practical problems, however, do not fit into this category, and consequently, it is often inevitable that alternate approaches - such as the Finite Element and Finite Difference methods - must be used.

6.2.1 The Qualities of an Ideal Analysis Process

In the search for the ideal analysis process, it is essential to identify the qualities important in such a process. A reasonable definition of an ideal solution process would appear to be one which maximizes the quality of the results and minimizes the *total* effort in obtaining them [15]. The criteria which such a process must satisfy include certain necessary conditions such as reliability and versatility, as well as a *proper balance* of a number of desirable features. These desirable features

were identified in reference [15] as:

1. Simplicity of application in such areas as:
   a) Analytical formulation.
   b) Discretization procedure.
   c) Treatment of complicated configurations.
   d) Treatment of boundaries, interfaces, and discontinuities.
   e) Program development and verification.
2. Expandability to other problem areas.
3. Efficiency in formulation and solution.

While the above list of features seems satisfactorily collective, it does not offer a means for weighting the relative importance of the various features in order to permit comparison of the different approaches on an overall basis. It is therefore felt desirable to re-define the so-called *essential characteristics* and to identify the different phases of the use of the analytical procedure.

From a practical Engineering point of view, the essential features of an ideal analysis process must include:

1. Reliability; which, to an Engineer, means:
   a) a guaranteed convergence to the correct solution of the problem as the solution is refined such that any desired degree of accuracy can be achieved with sufficient refinement of the solution,
   b) preferably, a monotonic and rapid convergence characteristic should be guaranteed in order to provide knowledge as of the sense of the errors

expected (whether the error is on the conservative or the non-conservative sides of the solution is usually of practical importance).

2. Versatility; which means that the method should be applicable to a sufficiently wide, and well defined, class of problems. It is not essential, however, that the same method applicable to a certain class of Engineering problems should be applicable to problems in other unrelated fields of Engineering. Nevertheless, complete versatility may be a desirable feature at least from an academic point of view.

The following two phases can be identified in the use of an analytical procedure:

(i) The development phase; which includes the planning, preparation, and verification of a general purpose computer program based upon the specific analytical approach. This phase is usually performed by highly trained and qualified individuals or teams of Engineers and Scientists.

(ii) The application phase; which includes the day-to-day use of the program developed in the first phase to treat the practical analysis problems encountered. It is desirable that this phase can be performed by ordinary engineering staff with only a basic knowledge of the requirements of the analytical procedure.

The desirable features of an analytical approach pertaining to each of these two phases, and corresponding

to those identified by reference [15], can be classified as follows:

For phase (i):

1. Simplicity of analytical formulation.
2. Simplicity of program development and verification.
3. Expandability to other problem areas.

For phase (ii):

1. Simplicity of the discretization technique (minimum effort required for preparation of the mathematical model).
2. Simplicity of treatment of complicated configurations.
3. Simplicity of treatment of boundaries, interfaces and discontinuities.
4. Efficiency of formulation and solution (minimum cost for obtaining a solution with a given accuracy, or maximum accuracy for a given fixed cost).
5. Ease of use of the method by people other than those who have developed it.

While features corresponding to both of the above two phases are important, those corresponding to the second phase should be weighted much more heavily in an overall comparison. The reason is that, in the long run, the major part of the total expenditure is typically devoted to the day-to-day usage of the program rather than its development.

6.3 An Evaluation for Available Techniques

The classical methods of analysis of continuum mech-

anics may be classified into two groups according to the type of coordinates used for the discretization of the continuum (since attention has to be focused upon only a finite number of the infinite degrees of freedom which a continuum possesses in order to be able to obtain a practical numerical solution). These two groups are:

1. The discrete coordinate methods; examples of which are the Finite Element, Finite Difference, and numerical integration methods.
2. Continuous coordinate methods; such as the Ritz, Galerkin, Lagrangian Multiplier, and the Fourier Series methods.

Due to the nature of the continuous coordinates, the second group of methods cannot be used conveniently for treating complicated configurations or discontinuous boundaries and interfaces. Therefore, these methods typically fail to meet the requirements of "versatility" which is an essential demand for the ideal process defined in the previous section. Consequently, we are left with the discrete coordinate methods which, until very recently, have been the only ones used successfully to treat complicated configurations and/or boundary conditions. In the absence of these complications, however, the continuous coordinate methods are considerably superior from the points of view of efficiency, simplicity, and reliability. A more detailed discussion concerning the relative merits of the Ritz method (as an example for continuous coofdinate

methods) as opposed to the Finite Element method will be given in section (7.1).

Several difficulties usually arise upon the use of ordinary Finite Differences for solving complicated structures (particularly two or three dimensional problems). These difficulties were presented in references [12,13] as:

1. Boundary conditions and discontinuities of the structure cannot be easily accounted for. Fictitious points usually have to be introduced which unduly increase the number of degrees of freedom and causes ambiguities at re-entrant corners.
2. To predict accurately the stresses in a continuum it may be necessary to use a large number of Finite Difference equations. The solution of large systems of Finite Difference equations may become impossible due to round-off errors. This is particularly true if natural boundary conditions are to be applied since they normally lead to ill-conditioning of the stiffness matrices.
3. In general, Finite Difference equations lead to assymetric matrices. This causes the necessity of dealing with the full stiffness matrices rather than the top or bottom halves only as is the case with symmetric stiffness matrices. In addition, some of the efficient solution algorithms, which can only deal with symmetric matrices, cannot be used

with Finite Difference solutions.

4. The results obtained using Finite Differences, in the author's experience, are usually less accurate than those obtained by the use of Finite Elements, not mentioning continuous coordinate methods, for the same number of total degrees of freedom. This will be obvious in several of the numerical examples presented in the following chapters.

In order to overcome some of the above-mentioned difficulties, a Large Finite Element approach was introduced in references [12,13] which combines the Finite Differences with the Finite Element technique. The method was briefly described in section (1.4) and has the major disadvantage of being only applicable to static problems. In addition, no improvement in accuracy over the conventional Finite Difference solutions has been proven.

In addition, recently Noor et. al. [15] suggested the use of a Modified Finite Difference approach with a mixed formulation - see section (1.6). Based upon the list of criteria presented in reference [15] and duplicated in section (6.2) above, it was argued in [15] that the approach promises to offer an ideal analysis process in the years to come. The major points of strength of the suggested approach, however, concern the development phase of the solution (according to the classification presented in section (6.2)) where the simplicity of the mixed formulation makes the

programming and extension to new areas of application particularly simple. The method, on the other hand, loses heavily on the efficiency front due to the large number of unknowns dealt with in the problem. In a plane stress problem, for example, five fundamental unknowns are defined instead of two in Finite Elements and one in conventional Finite Difference solutions. In addition, compared to Finite Elements, it is still considerably more difficult to handle problems involving complicated configurations and/or combinations of different types of structural elements (beams and plates for example). Since the application phase of the use of an analytical method should be weighted more heavily than the development phase - as was argued in section (6.2) - Finite Elements still enjoy an overwhelming popularity in practical Engineering applications.

The major disadvantage of Finite Elements, however, is the considerable effort required for defining the mathematical model because of the large numbers of nodes and finite elements usually involved. In order to acquire sufficient accuracy, a large number of degrees of freedom is normally required. Hence, a number of nodes proportional to these degrees of freedom is to be defined and joined with a large number of finite elements for which properties have to be specified. Consequently, considerable engineering effort is normally spent in the preparation and checking of the huge amounts of data required. While this effort may be justified for an immensely complicated problem, it can

be considered excessive for relatively simple geometric configurations (e.g. rectangular plates with holes and/or partial supports etc.). Other less versatile analytical methods are often resorted to for treatment of such problems in order to avoid the data preparation penalty involved in the use of Finite Elements.

6.4 The Large Element Method - An Optimum Analytical Approach

As a contribution towards the development of an optimum, versatile, analytical system, the concept of a "Large Element" method will be presented in the following chapters. The approach integrates two widely used variational methods; the Finite Element method and the method of Ritz; into one general formulation which literally includes both methods as extreme cases. As a result, the new technique features *all* the advantages of both methods and eliminates most of their shortcomings.

It follows from the discussion presented in the previous section, that for problems having simple configurations, continuous coordinate methods of solution, such as the Ritz method, are most suited. On the other hand, for an immensely complex problem, discrete coordinate methods, and Finite Elements in particular, become optional. The approach proposed in this work is a mixture of continuous and discrete coordinate methods blended together in a variable ratio which can be adjusted for each individual

problem, according to its degree of complexity, in order to obtain a continuously optimal solution for all problems. If for an extreme problem it was felt that a purely continuous, or a purely discrete, coordinate approach would be preferable, the method can still be used to obtain such a solution.

The fact that continuous coordinates are more efficient and easier to use has been recognized upon the introduction of the semi-analytical Finite Element techniques [the Finite Strip and Finite Layer methods which are described in sections (1.2) and (1.3)]. In these methods, continuous coordinates are employed in the direction, or directions, where no geometric, stiffness, or boundary discontinuities occur, while discrete coordinates are used in the direction where it is required due to discontinuities. The Large Element approach, however, is essentially different from those semi-analytical techniques inasmuch as both types of coordinates are completely mixed in both directions in the former while they are still separate in the latter approaches. This mixing provides the extreme flexibility which the Large Element method enjoys, enabling it to become a completely versatile approach; unlike the semi-analytical techniques which can only be used for problems with continuous properties in at least one direction.

In the following chapters, the Large Element approach will be presented and examined. Static and dynamic flexure

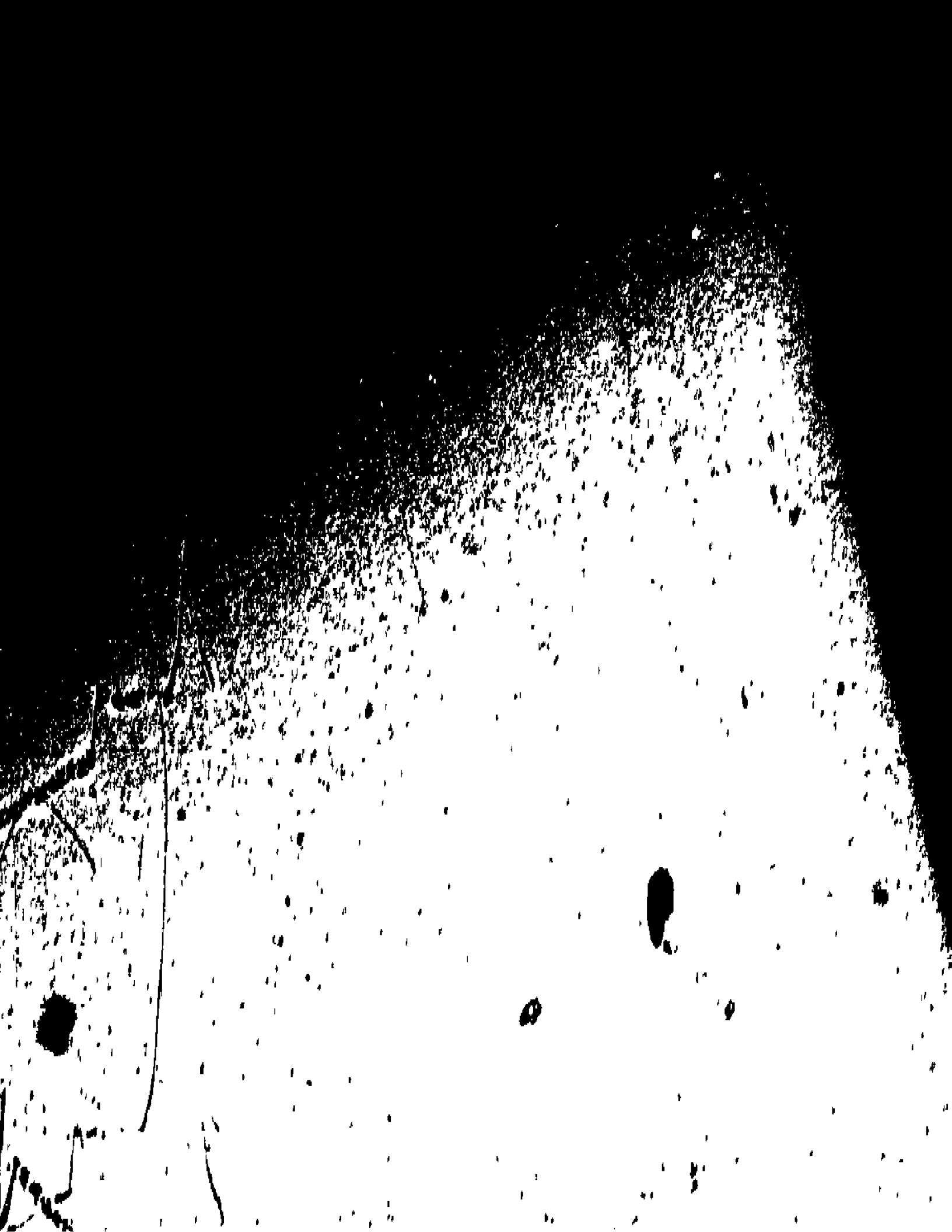

problems, inplane elasticity problems, as well as stability problems, will be presented and discussed. Whenever possible, comparison is made with available solutions and/or solutions obtained by the author using other methods of analysis. In general, only beam and rectangular two dimensional elements are dealt with. The method, however, can be directly expanded to implement other types of elements. Examples for such elements are outlined in Appendix III. and discussed in Chapter XII as suggestions for further work. It is the intention of the author to further develop these elements in the future.

CHAPTER VII

THE LARGE ELEMENT METHOD

7.1 The Large Element Concept - A One Dimensional Element

Perhaps the best way to introduce the concept of the Large Element method is to discuss it in the context of the variational solution of a one dimensional problem, namely, a cantilevered beam flexure (figure 7.1). The variational formulation of this problem starts with a variational expression which, generally, has the form

$$\delta\left[\int_0^l L\,(W,x)\,.\,dx\right] = 0, \qquad (7.1)$$

where W is the beam flexure, x the independent (spatial) coordinate, and L a differential operator. In order to be able to perform the differentiations and integrations involved, an approximate expression defining W as a function of x is assumed such that

$$W = F\,(A_1, A_2, \ldots, A_n; x), \qquad (7.2)$$

where $A_1, A_2, \ldots, A_n$ are independent unknown coefficients yet to be determined. Substituting (7.2) into (7.1) and performing the differentiations and integration, the following results

$$\delta\,[G(A_1, A_2, \ldots, A_n)] = 0.$$

From the fundamental lemma of variational calculus, for the variation to be true the following conditions must be satisfied

$$\frac{\partial G}{\partial A_i} = 0; \quad i = 1, 2, \ldots, n; \qquad (7.3)$$

which is a system of n algebraic equations serving to determine the n unknowns A_i.

7.1.1 The Ritz vs. Finite Element Solutions

As mentioned in Chapter II, Ritz proposed for the expression (7.2) a series of admissible functions $\phi_i(x)$ - see figure (7.1a) - weighted by the coefficients A_i such that

$$W = \sum_{i=1}^{n} A_i \cdot \phi_i(x), \qquad (7.2.a)$$

where the admissible functions $\phi_i(x)$ are continuous together with their derivatives of the first order and satisfy the fundamental (slope-deflection) boundary conditions of the problem as well as the completeness conditions discussed in Chapter II.

On the other hand, for a Finite Element solution, the continuum is virtually "cut" into a finite number of "elements" which are joined together at certain "nodal points" at which continuity of fundamental quantities (deflections and slopes) is to be maintained - see figure

(7.1b). In order to achieve this continuity, two fundamental variables (degrees of freedom) are assigned to each node; denoted as W_i and $\theta_i \equiv \frac{\partial W_i}{\partial x}$. No more variables are assigned elsewhere and the deflections at any point within an element are assumed to be a simple function of the degrees of freedom at the two adjacent nodes as well as the local spatial coordinate x_i or $\eta_i \equiv (\frac{x_i}{l_i})$, such that

$$W(x_i) = f\,(W_{i-1},\ \theta_{i-1},\ W_i,\ \theta_i,\ x_i). \qquad (7.4)$$

Hence, the overall deflected shape can be determined as a function of the global coordinate x as well as the assumed set of degrees of freedom W_i and θ_i such that:

$$W(x) = F(W_1, W_2, \ldots, W_n;\ \theta_1, \theta_2, \ldots, \theta_n;\ x), \qquad (7.2.b)$$

which is similar in form to equation (7.2).

One of the common convenient ways for the choice of the function f in equation (7.4), which leads to separation of the unknown quantities, is to express it as the sum of four shape functions having the form shown in figure (7.2a) each of them weighted by one of the unknown degrees of freedom. Thus equation (7.4) becomes:

$$W(\eta_i) = W_{i-1} \cdot \Phi_{i-1}(\eta_i) + \theta_{i-1} \cdot \Psi_{i-1}(\eta_i) +$$

$$+ W_i \cdot \Phi_i(\eta_i) + \theta_i \cdot \Psi_i(\eta_i). \qquad (7.4a)$$

It can be seen from figure (7.2a), that the functions Φ_i

have unit deflections and zero slopes at the i^{th} nodes and zero slopes and deflections at the other node . Likewise, the functions Ψ_i have unit slopes and zero deflections at the i^{th} node and zero slopes and deflections at the other nodes. An example for the functions Φ_i and Ψ_i are the simple cubic expressions (Hermitian polynomials of the first order) shown in figure (7.2a). With the adoption of equation *(7.4a)*, equation *(7.2b)* may now be written as

$$W(x) = \sum_{i=1}^{n} W_i \cdot \Phi_i(\eta_{i,i+1}) + \theta_i \cdot \Psi_i(\eta_{i,i+1}), \quad (7.2c)$$

where

$$fu.(\eta_{i,i+1}) \equiv fu.(\eta_i) + fu.(\eta_{i+1}) .$$

This equation is similar in form to *(7.2a)* and is represented in figure (7.2b). Thus, generally speaking, the Finite Element method may be looked upon as a particular case of the method of Ritz. However, due to the particular nature of the functions Φ_i and Ψ_i shown in figures (7.2a & b), the following advantages are realized in the case of the Finite Element approach:

1. While different sets of functions have to be used for every particular combination of *end conditions* in the case of the conventional Ritz method; in Finite Elements no such difficulty exists. The artificial (slope/deflection)boundary conditions are simply handled by eliminating, or restraining, the unwanted degrees of freedom with a corresponding

reduction in the number of unknowns in the problem. As with any variational solution, no particular attention needs to be paid to the natural boundary conditions since they are automatically accounted for in the variational expression.

2. Due to the localized nature of the displacement functions Φ_i and Ψ_i, and due to the element-oriented procedure of building up the stiffness - and mass - matrices in the case of the Finite Element approach, it is particularly simple to deal with geometric, stiffness and/or boundary *discontinuities*. Existence of such discontinuities renders the use of the conventional Ritz method very difficult and frequently impractical.

On the other hand, due to the very nature of the functions used in the Finite Element method, the following disadvantages are noticeable as compared to the method of Ritz:

1. While each of the assumed functions in a Ritz solution normally covers variations over the whole structure, each of the functions used in a Finite Element representation covers only a small portion of the continuum [and hence no more than four functions are non-zeros at any point - see figure (7.2b)]. Consequently, for the same total number of unknowns, it is expected that the Ritz displacement functions will normally provide higher flexibility to the structure than would the equivalent finite element

displacement functions. In other words, while the distribution of the degrees of freedom along the spatial coordinates is predetermined by the distribution of the nodes in a finite element solution; in the Ritz method, the distribution of the total degrees of freedom along the spatial coordinates is free and solely governed by the energy optimization criterion applied to the solution. As a result of this added flexibility which the displacement function of the Ritz method enjoys, it is a common practice that Ritz solutions are usually *more accurate* that those obtained by Finite Elements using the same number of unknowns. While this effect can be partially alleviated by particularly distributing the nodes to provide more degrees of freedom at points where sharp variations are expected (e.g. near load or constraint application points), this alleviation is only achieved on the account of more modelling effort and better guessing as of the best required distribution. In addition, this procedure becomes less feasible if more than one set of loading and/or boundary conditions is to be tackled using the same structural model and if more than one mode of vibration is of interest.

2. While the displacement functions used in the Finite Element approach ensure continuity of the fundamental quantities (slopes and deflections) at the nodes,

continuity of higher order quantities (e.g. bending moments) is not provided. Conversely, the displacement functions used in the conventional Ritz method usually yield continuous stresses and are most frequently continuously differentiable. Once more this results in better solutions being obtained by the use of the Ritz method. Moreover, the discontinuous higher derivatives usually result in stepped stress diagrams and offer difficulty in representing high stress gradients.

3. Since, in Finite Elements, the structure has to be physically subdivided into a large number of elements, a considerable effort is usually spent in *preparing data* providing the necessary information concerning the position of the nodal points as well as information about each of the connecting finite elements. No comparable effort expenditure is necessary for a Ritz solution since only the basic data about the continuum have to be provided with no additional "artificial" subdividing lines.

4. The question of *convergence* is more easily dealt with in the case of the Ritz method. The Ritz advantage in this respect is twofold: Firstly, from a users point of view, all it takes to examine the convergence of a Ritz solution is to successively increase the value of the parameter indicating the number of terms to be used in the series solution.

With Finite Elements, however, for each convergence step a new nodal pattern has to be defined with the associated data prepared. The amount of data preparation involved could become prohibitive, and in many practical cases limits the number of convergence steps that can be considered. In order to obtain consistent results, each convergence step should include all the nodal points used in the previous step. Consequently, the number of nodes in convergence sequences must take the form n, $2n$, $4n$, ...; which may quickly push the size of the problem beyond the economically feasible limits. Unlike Finite Elements, convergence sequences used for the Ritz solutions can take the form of any increasing sequence with no particular conditions. Secondly, from the mathematical point of view, since the displacement series in a Finite Element solution does not generally include the displacement functions used in the previous convergence step, monotonic improvement of the solutions obtainable cannot always be ensured. With the Ritz method, on the other hand, since each new solution series physically includes the previous ones, a monotonically improving solution is guaranteed. However, if certain conditions are satisfied by the displacement functions, and if the number of terms in the successive solutions follow the sequence n, $2n$, ...; monotonic con-

vergence may also be achieved by a Finite Element solution.

From the above comparison, it can be argued that the Ritz method is *generally* more accurate, easier to use, and it is easier to assess its accuracy; while the Finite Element method is more versatile and deals with the boundary conditions in a simpler manner. Indeed, subdividing the structure into finite elements serves a dual purpose: *Firstly*, to provide a means for discretizing the structure so that an approximate solution could be obtained and improved through the use of finer divisions; and *secondly*, to provide a means for handling geometrical, structural and/or boundary discontinuities whenever they exist. While the second objective is well justified since it provides the method with its great versatility, and since it is quite reasonable to subdivide the structure into its natural elements wherever there are physical discontinuities; the first objective - i.e. convergence - does not seem to be best achieved through further "cutting" of the structure into smaller elements as it leads to all the disadvantages discussed earlier.

7.1.2 The Large Element Approach

The proposed Large Element method is basically a blend of the Finite Element and the Ritz methods into an optimum combination which offers the advantages of the two methods and practically eliminates all their short-

comings. In this blend, the character of each of the two constituents is preserved and, should it be desirable, a pure Ritz or a pure Finite Element solution may be obtained for a problem. For an optimum solution, the structure is subdivided into the minimum possible number of simple elements free from discontinuities. Refinement of the solution - or convergence - is achieved within each element by virtue of the Ritz procedure.

To form this blend, the Ritz displacement series *(7.2a)* is superimposed upon the Finite Element displacement function *(7.4a)* to form the Large Element displacement series as:

$$W(\eta_i) = W_{i-1} \cdot \Phi_{i-1}(\eta_i) + \theta_{i-1} \cdot \Psi_{i-1}(\eta_i) + W_i \cdot \Phi_i(\eta_i) + \theta_i \cdot \Psi_i(\eta_i) + \sum_{j=1}^{m} A_j \phi_j(\eta_i) \quad (7.5)$$

Further, in order to ensure continuity of slopes and deflections at the boundary, the functions $\phi_j(\eta_i)$ are kept local within the large element by requiring them to have zero slopes and deflections at both ends $(\eta_i = 0,1)$. In other words, functions ϕ_j are assumed to be a set of admissible functions for a clamped-clamped beam; one example of such a set is the well known family of clamped-clamped beam vibration modes. With this choice, the duties of the different types of displacement functions are separated; the finite element-type functions are used to provide the degrees of freedom (as well as the constraints) at the

nodes, while the Ritz-type functions provide the flexibility within the large element itself.

A simple example for the application of the Large Element method is shown in figure (7.3). Studying the vibrations of the stepped cantilevered beam shown, requires a minimum of two elements due to the discontinuity caused by the step. With two degrees of freedom assigned at each node, the total number of degrees of freedom at the nodes is only four. Since this number of degrees of freedom is usually not sufficient to represent the behaviour of the beam with reasonable accuracy, more degrees of freedom have to be assigned for a practical solution. In Finite Elements, a *piece-wise* convergence is sought by further subdividing each of the two large elements into smaller ones. In Large Elements, however, this added freedom is achieved by assigning $n1$ and $n2$ Ritz-type degrees of freedom within large elements I and II respectively [figure (7.3)]. Further convergence is achieved *term-wise* through increasing the numbers of terms $n1$ and $n2$ in the Ritz-type series assigned to the large elements.

After the desired numbers of degrees of freedom are assigned to each large element, the matrix relations (stiffness and mass matrices) for each element are constructed using the conventional Ritz method as will be shown in the following sub-section. The next step is to assemble the individual large element stiffness and mass matrices into the global stiffness and mass matrices

- using the appropriate coordinate transformations if necessary - in the same manner as is done in the standard Finite Element technique.

7.1.3 Derivation of the Stiffness and Mass Matrices for a Large Beam Bending Element

The differential equation governing the transverse vibration of a prismatic beam element is given by

$$EI \cdot \frac{\partial^4 w}{\partial x^4} = - \mu \frac{\partial^2 w}{\partial t^2}, \qquad (7.6)$$

where E, I and μ are the modulus of elasticity cross sectional area moment of inertia, and mass per unit length of the beam element respectively. Associated with this differential equation is the variational expression:

$$\delta \left[EI \left(\frac{d^2 W}{dx^2} \right)^2 - \mu \omega^2 W^2 \right] = 0, \qquad (7.7)$$

in which harmonic motion ($w = W e^{i\omega t}$) is assumed. Assuming the displacement W to take the form of equation (7.5), and re-writing it as:

$$W(\eta_i) = \sum_{j=1}^{m+4} A_j \cdot \phi_j(\eta_i), \qquad (7.8)$$

where

$$A_{m+1} = W_{i-1}, \quad \phi_{m+1} = \Phi_{i-1}(\eta_i),$$

$$A_{m+2} = \theta_{i-1} \cdot a_i, \quad \phi_{m+2} = \Psi_{i-1}(\eta_i)/a_i,$$

$$A_{m+3} = W_i, \qquad \phi_{m+3} = \Phi_i(\eta_i), \tag{7.8a}$$

$$A_{m+4} = \theta_i \, a_i, \qquad \phi_{m+4} = \Psi_i(\eta_i)/a_i;$$

in which a_i is the length of the element on hand. The functions ϕ_1 through ϕ_m are the first m clamped-clamped beam function while the functions Φ and Ψ are as defined in figure (7.2b). Substituting *(7.8)* into *(7.7)* and following the Ritz procedure as described before, the resulting matrix equation takes the form

$$([K^i]_{(m+4)x(m+4)} - \omega^2 [M^i]_{(m+4)x(m+4)}).\{A\}_{(m+4)} = 0. \tag{7.9}$$

In Finite Element terminology, $[K^i]$ and $[M^i]$ represent the well known *stiffness* and *mass matrices* for the i^{th} large beam element in pure flexure. The coefficients of these matrices are given by

$$K^i_{\alpha,\beta} = E_i I_i \, F_{\alpha,\beta}/a_i^3 \tag{7.10}$$

$$M^i_{\alpha,\beta} = \mu_i \, B_{\alpha,\beta} \, a_i \, ;$$

where

$$B_{\alpha,\beta} = \int_0^1 \phi_\alpha(\eta_i) \, \phi_\beta(\eta_i) \, d\eta_i, \tag{7.11}$$

and $$F_{\alpha,\beta} = \int_0^1 \phi_\alpha''(\eta_i) \, \phi_\beta''(\eta_i) \, d\eta_i.$$

The integral coefficients $B_{\alpha,\beta}$ and $F_{\alpha,\beta}$ are computed in a manner similar to that described in section (3.2.1) and

Appendix I, and their numerical values are given in Appendix II.

7.2 The Large Two-Dimensional Element

So far, only one dimensional problems have been discussed. Extension to two-dimensional problems, however, is straight forward. For simplicity, since the object of this work is only to introduce the concept of the Large Elements and demonstrate its advantages, only rectangular plate elements will be dealt with in detail in this and the following chapters. The basic steps for the development of several other large elements will be discussed in Appendix III, however, no attempt will be made in order to examine their behaviour. Moreover, although the discussion will be limited here to plate bending problems, it will be shown later that the same analysis applies to the solution of the two-dimensional elasticity problem.

The main step is the derivation of the Large Element Characteristic (stiffness and mass) Matrices using the Ritz method as has been demonstrated in the case of the beam element. Since each element can be looked upon as a simple flat rectangular plate, the variational expressions and Ritz solution procedure explained in Chapters II and III may be directly applied for the derivation of the element characteristic matrices. Here, however, the more general case of an *orthotropic* plate element will be considered. For such a plate, the governing variational

expression takes the form:

$$\delta\{\int_0^b\int_0^a [D_x(\frac{\partial^2 W}{\partial x^2})^2 + D_y(\frac{\partial^2 W}{\partial y^2})^2 + 2D_{xy}(\frac{\partial^2 W}{\partial x^2}\cdot\frac{\partial^2 W}{\partial y^2}) + 4D_k(\frac{\partial^2 W}{\partial x \partial y})^2 - \rho h\omega^2 (W)^2]\,dx\,dy\} = 0; \qquad (7.12)$$

where

$$D_x = \frac{Exh^3}{12(1-\nu_x\nu_y)} \quad D_y = \frac{Eyh^3}{12(1-\nu_x\nu_y)},$$

$$D_k = \frac{Gh^3}{12}, \text{ and } \quad D_{xy} = D_x\nu_y + 2D_k;$$

which are the elastic constants for the orthotropic plate element.

The next and the most important step in the solution is the choice of the displacement series. In light of the discussions of the previous section concerning the beam elements, the obvious choice is a double series composed of a multiplication of two series of the type given by equations (7.5) and (7.8). It is thus assumed that

$$W(\eta_i, \xi_j) = \sum_{k=1}^{m+4}\sum_{l=1}^{n+4} A_{kl}\cdot\phi_k(\eta_i)\cdot\phi_l(\xi_j); \qquad (7.13)$$

where η_i & ξ_j are the non-dimensional local spatial coordinates for the element; A_{kl} equals A_k x A_l; and the quantities A_k, A_l, ϕ_k, and ϕ_l are the same as defined in equation (7.8a).

With the displacement series on hand, the element characteristic matrices can easily be constructed as was

shown in the case of the beam element. Substituting the displacement function (7.13) into the variational expression (7.12), minimizing through differentiation with respect to each of the unknown coefficients A_{rs}, interchanging the differentiation and integration signs, and rearranging; the following set of equations results:

$$\sum_{k=1}^{m+4}\sum_{l=1}^{n+4} A_{kl}\left[Dx\cdot\frac{b_j}{a_i^3}\cdot F_{k,r}\cdot B_{l,s} + Dy\cdot\frac{a_i}{b_j^3}\cdot B_{k,r}\cdot F_{l,s} + \right.$$

$$+ Dxy\cdot\frac{1}{a_i b_j}\cdot(C_{k,r}\cdot C_{s,l} + C_{r,k}\cdot C_{l,s}) + 4Dk\cdot\frac{1}{a_i b_j}\cdot$$

$$\left.\cdot E_{k,r}\cdot E_{l,s} - \rho_{i,j} h_{i,j}\omega^2\cdot a_i b_j\cdot B_{k,r}\cdot B_{l,s}\right] = 0$$

$$(r=1,2,\ldots,m+4;\ s=1,2,\ldots,n+4)$$

The above equations can be written in the well known matrix notation:

$$\underset{(m+4)(n+4)\times(m+4)(n+4)}{([K^{i,j}]} - \omega^2\underset{(m+4)(n+4)\times(m+4)(n+4)}{[M^{i,j}]})\cdot\underset{(m+4)(n+4)}{\{A\}} = \underset{(m+4)(n+4)}{0}, \qquad (7.14)$$

where $[K^{i,j}]$ and $[M^{i,j}]$ are the stiffness and mass matrices of the $(i,j)^{th}$ element. The coefficients of these matrices are given by:

$$\overline{K^{i,j}_{kl,rs}} = Dx\cdot\frac{b_j}{a_i^3}\cdot F_{k,r}\cdot B_{l,s} + Dy\cdot\frac{a_i}{b_j^3}\cdot B_{k,r}\cdot F_{l,s} +$$

$$\frac{D_{xy}}{a_i b_j} \cdot (C_{k,r} \cdot C_{s,l} + C_{r,k} \cdot C_{l,s}) + \frac{4D_k}{a_i b_j} \cdot E_{k,r} \cdot E_{l,s} \,,$$

and

$$M^{i,j}_{kl,rs} = \rho_{ij} h_{ij} a_i b_j \cdot B_{k,r} \cdot B_{l,s} \,; \qquad (7.15)$$

where

$$C_{k,r} = \int_0^1 \phi_k(\eta_i) \cdot \phi_r''(\eta_i) \cdot d\eta_i \,,$$

$$E_{k,r} = \int_0^1 \phi_k'(\eta_i) \cdot \phi_r'(\eta_i) \cdot d\eta_i \,, \qquad (7.16)$$

and $B_{k,r}$, $F_{k,r}$ are the same as defined in equation *(7.11)*. Numerical values for the integral coefficients *B*, *C*, *E*, and *F* are tabulated in Appendix II .

7.3 Distribution of Degrees of Freedom in a Two-Dimensional Bending Element

Since the assumed displacement series *(7.13)* results from the multiplication of two series of the type given by equation *(7.5)*, and since each of the series *(7.5)* is the result of the superposition of two types of functions (the Ritz-type - or local - functions and the Finite Element - type - or nodal - functions); the resulting double series *(7.13)* includes three types of functions:

i) $m \times n$ Ritz-type (or local) functions; resulting from the multiplications of $\phi_l(\eta_i)$ through $\phi_m(\eta_i)$ with $\phi_l(\xi_j)$ through $\phi_n(\xi_j)$. These functions represent the local degrees of freedom within the rectangular

element since they possess zero slopes and deflections along the boundaries - see figures (7.4a) through (7.4d).

ii) Sixteen Finite Element-type (or nodal) functions; resulting from the multiplications of $\phi_{m+1}(\eta_i)$ through $\phi_{m+4}(\eta_i)$ with $\phi_{n+1}(\xi_j)$ through $\phi_{n+4}(\xi_j)$. These functions compose the displacement function for the well known four degrees of freedom per node conforming Finite Element rectangle [34,35,9]. The four degrees of freedom resulting at each corner (node) are; pure translation, rotation about each of the two edges, and pure twist - see figures (7.4e) through (7.4h).

iii) $4X(m+n)$ hybrid (or edge) functions; resulting from the cross products of the Ritz - and Finite Element - type functions. These cross products provide m (or n) translational and m (or n) rotational degrees of freedom for each of the two edges parallel to the η-(or ξ-) direction - see figures (7.4i) through (7.4l).

Hence, it can be seen that the assumed displacement series (7.13) provides for all the necessary rotational and translational degrees of freedom within the large element, at its four corner nodes, as well as along the element edges (or nodal lines). Figure (7.5) represents a typical element $[i,j]$ surrounded by eight other elements.

The distribution of the degrees of freedom within and around the element is also schematically represented. As with Finite Elements, in order to ensure continuity of slopes and deflections between adjacent elements, the same corner (nodal) degrees of freedom have to be assigned to all elements having a common corner. To do so, the corner degrees of freedom are to be defined as "nodal" properties rather than element properties. Likewise, the edge degrees of freedom are to be common between any two adjacent elements; thus, they should be defined as "edge properties" rather than "element properties". The "local" degrees of freedom, however, are element properties and are to be defined as such.

It is thus seen that, not only element nodes are of special importance as with Finite Elements, but also are the element edges; continuity of slopes and deflections is ensured all along the boundary, and loading can be applied at the nodes, along the edges, or distributed over the entire element. Likewise, application of the boundary conditions, or constraints in general, is achieved through suppressing the appropriate degrees of freedom not only at the nodes, but also along the edges. From a practical point of view, hence, it is necessary not only to number the nodes sequentially, but also to number the connecting edges; since degrees of freedom and constraints are to be assigned for both sets during the solution procedure.

It is worth mentioning that if the two parameters m and n were both set to zero, only the sixteen Finite Element-type corner nodes will remain, and the Large Element will be identical to the four degrees of freedom per node conforming Finite Element Rectangle first used in 1965 by Butlin [35], which in turn is one of the most accurate plate bending Finite Elements, as will be shown in the numerical examples of the following Chapters. It is thus seen that the Large Element approach literally includes a Finite Element solution, and any advantages that may be claimed for the Finite Elements can be realized, if not exceeded, by the Large Element method.

7.4 The Static Load Vector

While it is necessary in Finite Elements to approximate the applied static loads by an equivalent set of concentrated loads acting at the nodal points; in Large Elements, this procedure is no longer necessary nor sufficiently accurate in the general case. Three general types of loads will be discussed here; a distributed load, a concentrated load, and a line load. The case of a distributed load, being the more general case, will be treated first. The latter two cases will then be treated as simplified special cases.

The governing variational expression for the deflection of a large plate element under a load $p(x,y)$ - similar to expression *(7.12)* given for the dynamic case - may be

written as:

$$\delta\{\int_0^b\int_0^a [D_x(\frac{\partial^2 W}{\partial x^2})^2 + D_y(\frac{\partial^2 W}{\partial y^2}) + 2D_{xy}(\frac{\partial^2 W}{\partial x^2} \cdot \frac{\partial^2 W}{\partial y^2}) +$$

$$+4D_k(\frac{\partial^2 W}{\partial x \partial y})^2 - p(x,y) \cdot W]\, dx \cdot dy\} = 0 \qquad (7.17)$$

where D_x, D_y, D_{xy} and D_k are as defined before. Substitution of the assumed displacement series (7.13) into this expression, minimizing with respect to the unknown coefficients A_{rs} and rearranging as before, the following matrix relation results:

$$\underset{(m+4)(n+4)\,x\,(m+4)(n+4)}{[K^{i,j}]} \cdot \underset{(m+4)(n+4)}{\{A\}} = \underset{(m+4)(n+4)}{\{P\}}, \qquad (7.18)$$

where $[K^{i,j}]$ is the element stiffness matrix defined before, and $\{P\}$ is the loading vector given by;

$$P_{rs} = \int_0^b\int_0^a p(x,y) \cdot \phi_r(\eta_i) \cdot \phi_s(\xi_j) \cdot dx.dy. \qquad (7.19)$$

In the most general case, these coefficients P_{rs} can be evaluated by numerical integration. However, considerable simplification of the computations is possible if the load $p(x,y)$ were defined in the form of a series similar to that assumed for the displacement W; i.e.

$$p(x,y) = \sum_{k=1}^{m+4}\sum_{l=1}^{n+4} \alpha_{kl} \cdot \phi_k(\eta_i) \cdot \phi_l(\xi_j), \qquad (7.20)$$

where α_{kl} are known coefficients and ϕ_k and ϕ_l are as defined by equation (7.8a). Substituting (7.20) into (7.19),

the load vector can now be written as

$$P_{rs} = \sum_{k=1}^{m+4} \sum_{l=1}^{n+4} \alpha_{kl} \cdot a_i b_j \cdot B_{k,r} \cdot B_{l,s} \quad , \quad (7.21)$$

with the integral coefficients $B_{k,r}$ and $B_{l,s}$ as defined before. While the use of equation *(7.21)* eliminates the necessity of performing any extra integration, the real effort involved lies in the determination of the coefficients α_{kl} corresponding to a given load distribution. In the most general case, up to sixteen coefficients α_{kl} ($k = m+1$ through $m+4$, and $l = n+1$ through $n+4$) can be directly determined by inspection of the value of the loading function $p(x,y)$ and its derivatives at the element corners through making use of the special properties of the functions ϕ_k and ϕ_l. For example:

$$\alpha_{m+1,\ n+1} = p(o,o) \quad ,$$

$$\alpha_{m+4,\ n+4} = \frac{\partial^2 p(a_i, b_j)}{\partial x \cdot \partial y} \cdot a_i \cdot b_j \quad ,$$

$$\alpha_{m+3,\ n+2} = \frac{\partial p(a_i, o)}{\partial y} \cdot b_j \quad \ldots \quad \text{etc.}$$

Once these sixteen coefficients are determined, the coefficients corresponding to the "edge degrees of freedom" described earlier can then be easily determined using the ordinary Fourier approach. For example, the coefficients α_{kl}, with $k = 1$ through m and $l = n+1$, representing the translational degrees of freedom along the edge $y = 0$,

can be determined from:

$$\alpha_{k,n+1} = \int_0^{a_i} \phi_k(\eta_i) \cdot [p(x,o) - \sum_{r=m+1}^{m+4} \alpha_{r,n+1} \cdot \phi_r(\eta_i)] \cdot d\eta_i$$

With the coefficients corresponding to the corner and edge degrees of freedom determined as above, the balance of the load coefficients (corresponding to the local degrees of freedom of the element) can be determined through making use of the orthogonality properties of the Ritz-type functions, such that:

$$\alpha_{k,l} = \int_0^{b_j} \int_0^{a_i} \phi_k(\eta_i) \cdot \phi_l(\xi_j) \cdot [p(x,y) - \sum_{r=1}^{m+4} \sum_{s=n+1}^{n+4} \alpha_{r,s} \cdot \phi_r(\eta_i) \cdot \phi_s(\xi_j) - \sum_{r=m+1}^{m+4} \sum_{s=1}^{n} \alpha_{r,s} \cdot \phi_r(\eta_i) \cdot \phi_s(\xi_j)] \, d\eta_i \cdot d\xi_j \; ; \; k=1,\ldots,m; \; l=1,\ldots,n.$$

The evaluation of the above expressions, although requiring numerical integration in the general case, is considerably less difficult than the direct evaluation of equation (7.19). The real value of expression (7.21), however, is in the special case where the load $p(x,y)$ is - or may be adequately approximated by - a multiplication of two general cubic polynomials. In such a case the sixteen loading coefficients corresponding to the corner degrees of freedom - which can be obtained directly by inspection

without integration as mentioned above - will suffice for describing the load.

In the case of a concentrated load $\bar{P}$ acting at a given point (x_o, y_o), equation (7.19) then yields:

$$P_{rs} = \bar{P} \cdot \phi_r\left(\frac{x_o}{a_i}\right) \cdot \phi_s\left(\frac{y_o}{b_j}\right) \quad (7.22)$$

which serves directly for the determination of the load vector. Further, if the load $\bar{P}$ is acting at one of the plate corners, all the coefficients of the load vector P_{rs} become zeros except for the term corresponding to that corner displacement. For example, if the load $\bar{P}$ is acting at the corner (a_i, o), the coefficient $P_{(m+3),(n+1)}$ will be equal to $\bar{P}$ while all other terms will vanish.

Finally, in the case where $p(x,y)$ is defined only along a line, the general equation (7.19) may be used for the most general case. If the loaded line happened to be straight and parallel to one of the element coordinate axes, e.g. $x = x_o$, the load may then be expressed as

$$p(y) = \sum_{l=1}^{n+4} \alpha_l \cdot \phi_l(\xi_j) \cdot$$

The loading vector will then become

$$P_{rs} = \phi_r\left(\frac{x_o}{a_i}\right) \cdot b_i \cdot \sum_{l=1}^{n+4} \alpha_l \cdot B_{l,s} \quad (7.23)$$

If, moreover, the loading is along a nodal line, e.g. $x_1 = a_i$, equation (7.23) becomes:

$$P_{rs} = b_i \cdot \sum_{l=1}^{n+4} \alpha_l \cdot B_{l,s}, \quad (r = m+3)$$

$$= 0, \quad (r \neq m+3)$$

and similarly for the other nodal lines (element edges).

7.5 The Large Strip method - A Semi-Analytical Large Element Approach

For problems in which variations in geometry, stiffness, and boundary conditions are restricted to only one dimension, the Finite Strip method [8] was proposed as a semi-analytical Finite Element approach leading to considerable improvement over conventional Finite Elements. In the Finite Strip method, as described in section (1.2), a series of ordinary beam functions is assumed in the direction where no discontinuities occur (along the strip) and Finite Element-type polynomials (the same as Equation [7.4a]) are considered across each strip. The method is of particular interest if the two parallel edges, perpendicular to the direction where no variations are permitted, are simply supported. In such a case, the assumed series becomes uncoupled and the problem becomes essentially unidimensional. In that case, the Finite Strip method becomes equivalent in concept to the axi-symmetric shell Finite Elements where decoupled sine waves are assumed along the circumference of the shell.

An equivalent improvement can be achieved with the

Large Element method in the case of uni-dimensional variations leading to what can be called the *Large Strip Method*. In this method, a series of ordinary or modified beam functions is assumed in the direction where no variations are permitted, and a series similar to that used for the large beam element (7.5) is assumed in the other direction. It is thus assumed that:

$$w^i(\eta_i, \xi) = \sum_{j=1}^{m+4} \sum_{k=1}^{n} A_{jk}\, \phi_j(\eta_i) \cdot \psi_k(\xi) \; ; \qquad (7.24)$$

where $\phi_j(\eta_i)$ is the same as defined by (7.8) in conjunction with the Large Beam Element, and $\psi_k(\xi)$ are ordinary or degenerated beam functions as defined in Chapter II. The type of beam functions $\psi_m(\xi)$ is chosen to match the boundary conditions along the edges $\xi = 0, 1$ [see figure (7.6)] in the same manner as described in conjunction with the Ritz method in Chapters II and III. If one (or both) of the edges is free, degenerated - rather than ordinary - beam functions are used. In the case of two parallel clamped edges, no modification to the Large Element is necessary since the functions assumed for the Large Element already include a series of Clamped-Clamped beam functions and the Large Element and Large Strip become identical.

The derivation of the stiffness and mass matrices follows very closely that shown for the Large Element leading to the matrix relation:

$$\left([K^i]_{(m+4)\ (n)\ x\ (m+4)\ (n)} - \omega^2\ [M^i]_{(m+4)\ (n)\ x\ (m+4)\ (n)} \right) \cdot \{A\}_{(m+4)\ .\ (n)} = 0 \quad (7.25)$$

where $[K^i]$ and $[M^i]$ are the stiffness and mass matrices of the $(i)^{th}$ strip. The coefficients of these matrices are given by:

$$K^i_{jk,rs} = D_x \cdot \frac{b}{a_i^3} \cdot F_{j,r} \cdot I_{k,s} + D_y \cdot \frac{a_i}{b^3} \cdot B_{j,r} \cdot S_{k,s} +$$

$$\frac{D_{xy}}{a_i b} \cdot (C_{j,r} \cdot R_{s,k} + C_{r,j} \cdot R_{k,s}) + \frac{4D_k}{a_i b} \cdot E_{j,r} \cdot J_{k,s}$$

and $$M^i_{jk,rs} = \rho h a_i b \cdot B_{j,r} \cdot I_{k,s} \quad ; \quad (7.28)$$

where the integral coefficients B, F and C, E are the same as defined by (7.11) and (7.16) respectively in association with the Large Element; and the coefficients I, J, R, and S are the same as defined by equation (3.8) in relation with the Ritz solution.

If simply-supported and/or sliding edges are involved in the x-direction, the following two advantages will be realized for the Large Strip method over and above those discussed in relation with the Large Element method:

Firstly: The simply-supported (or sliding) edge natural boundary condition of zero bending moment (or shear force) will be exactly satisfied by the beam functions; in the case of the Large or Finite Element methods, the natural boundary conditions are satisfied approx-

imately during the Ritz minimization procedure.

Secondly: If *both* edges are simply supported and/or sliding, separation of variables will be feasible, and the order of the matrices to be solved at any one time will be considerably reduced, leading to substantial savings in both the computer storage requirements and solution time.

Compared with the Finite Strip method, the Large Strip method offers all the advantages that the Large Element method offers over the Finite Elements.

RITZ METHOD:

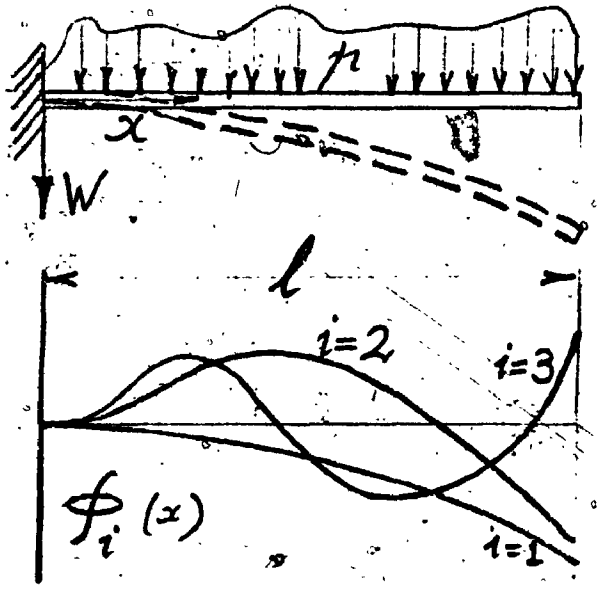

(a)

FINITE ELEMENTS:

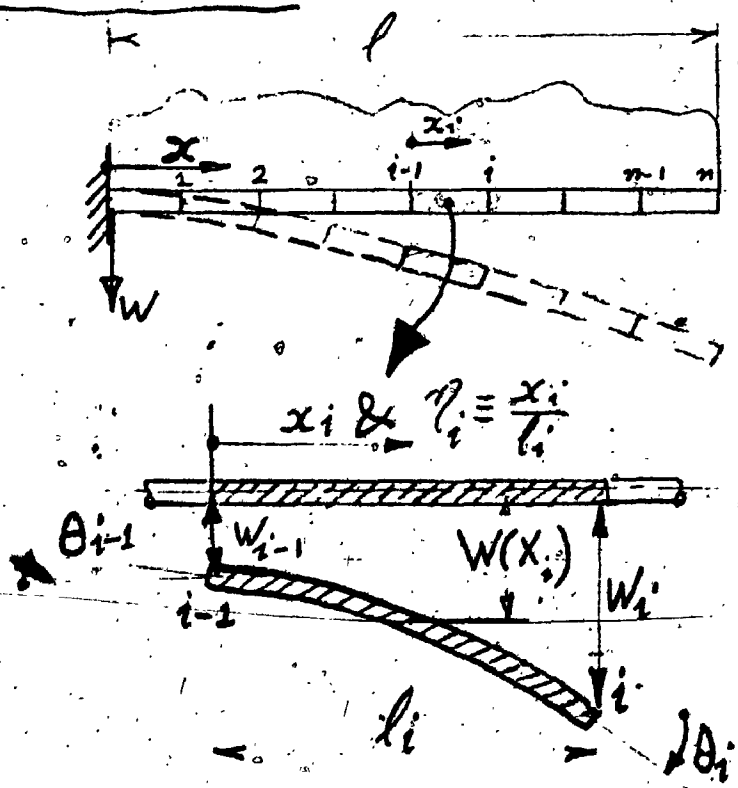

(b)

FIG. (7-1)

RITZ AND FINITE ELEMENT SOLUTIONS FOR A CANTILEVERED BEAM UNDER AN ARBITRARY LOAD

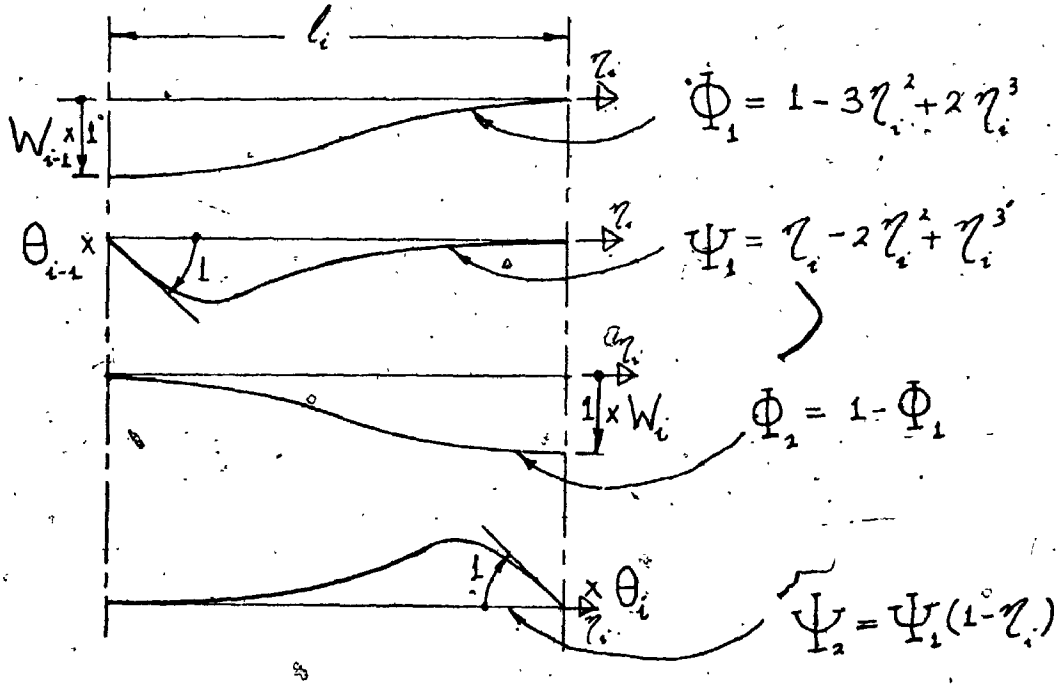

FIG. (7-2a)

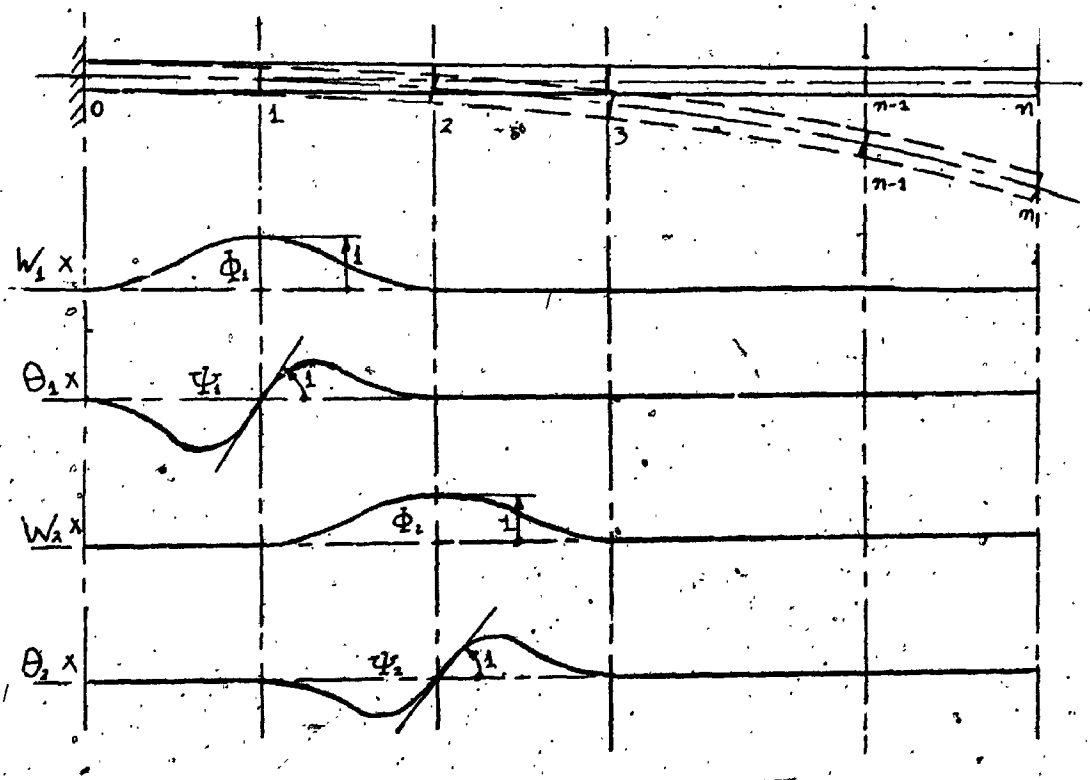

FIG (7-2b)

DISPLACEMENT FUNCTIONS FOR FINITE BEAM ELEMENTS

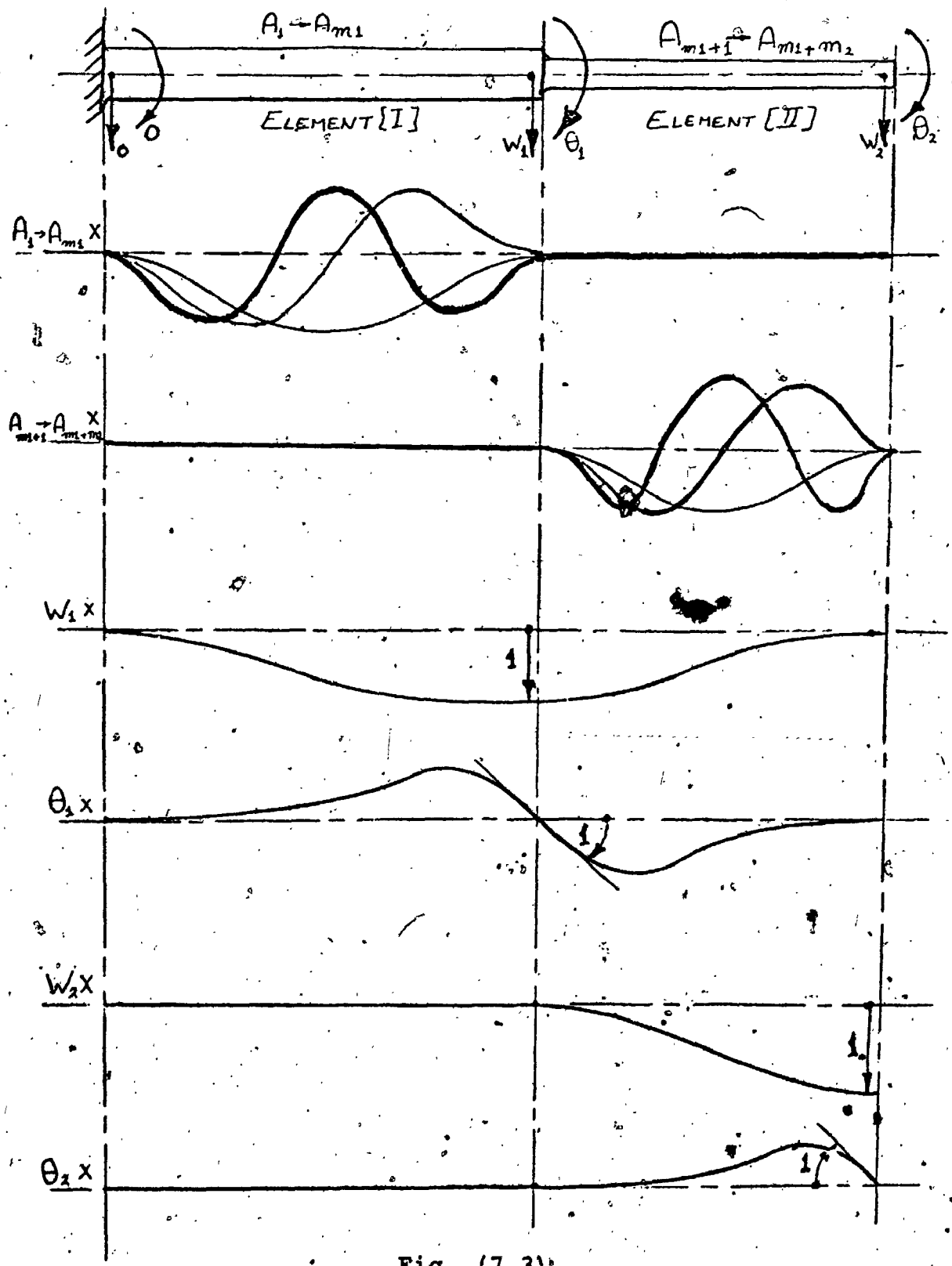

Fig. (7.3)
Large Element Displacement Functions for a Stepped Cantilevered Beam Problem

Fig. (7.4)

Typical Shape Functions for the Large Rectangular Plate Elements

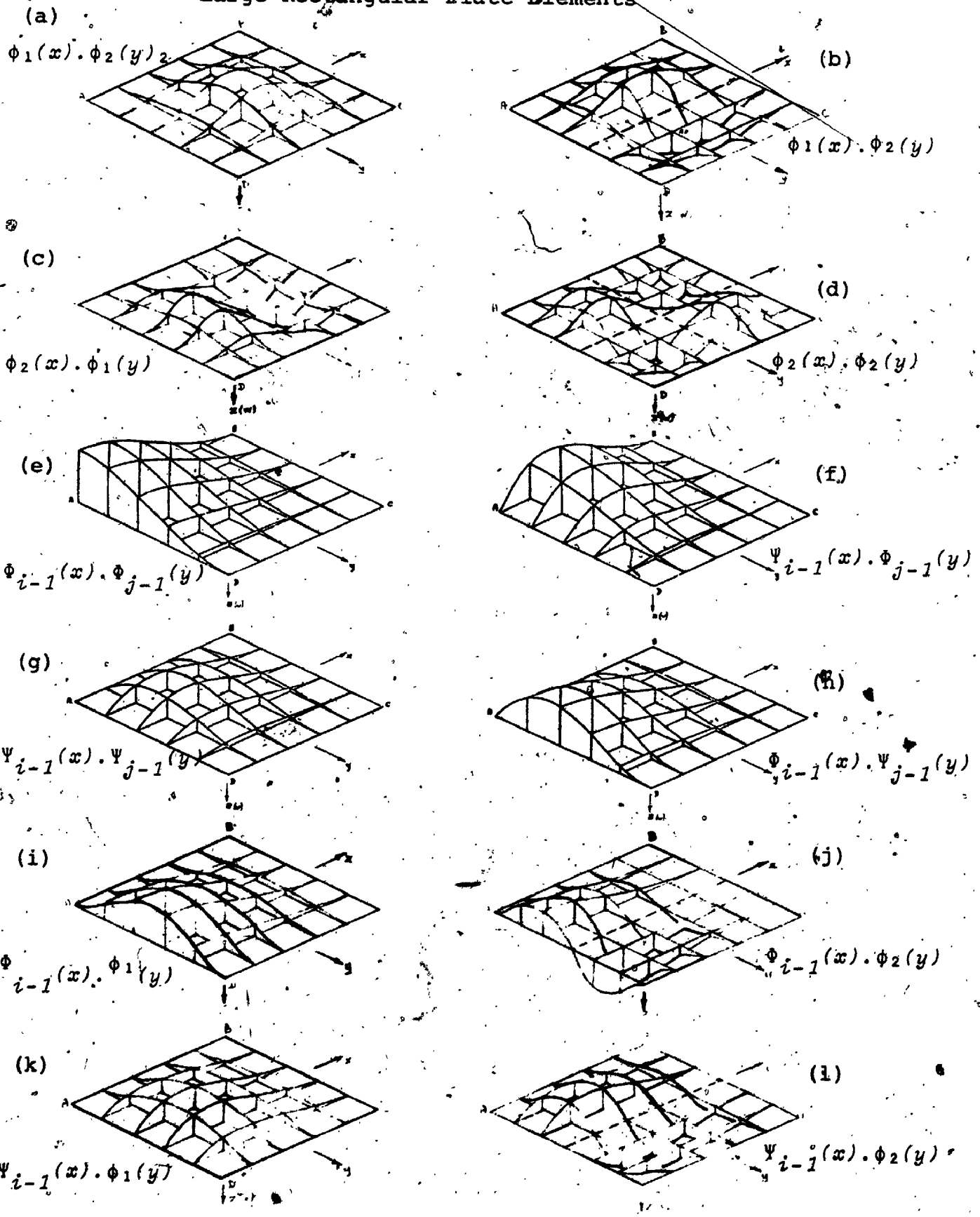

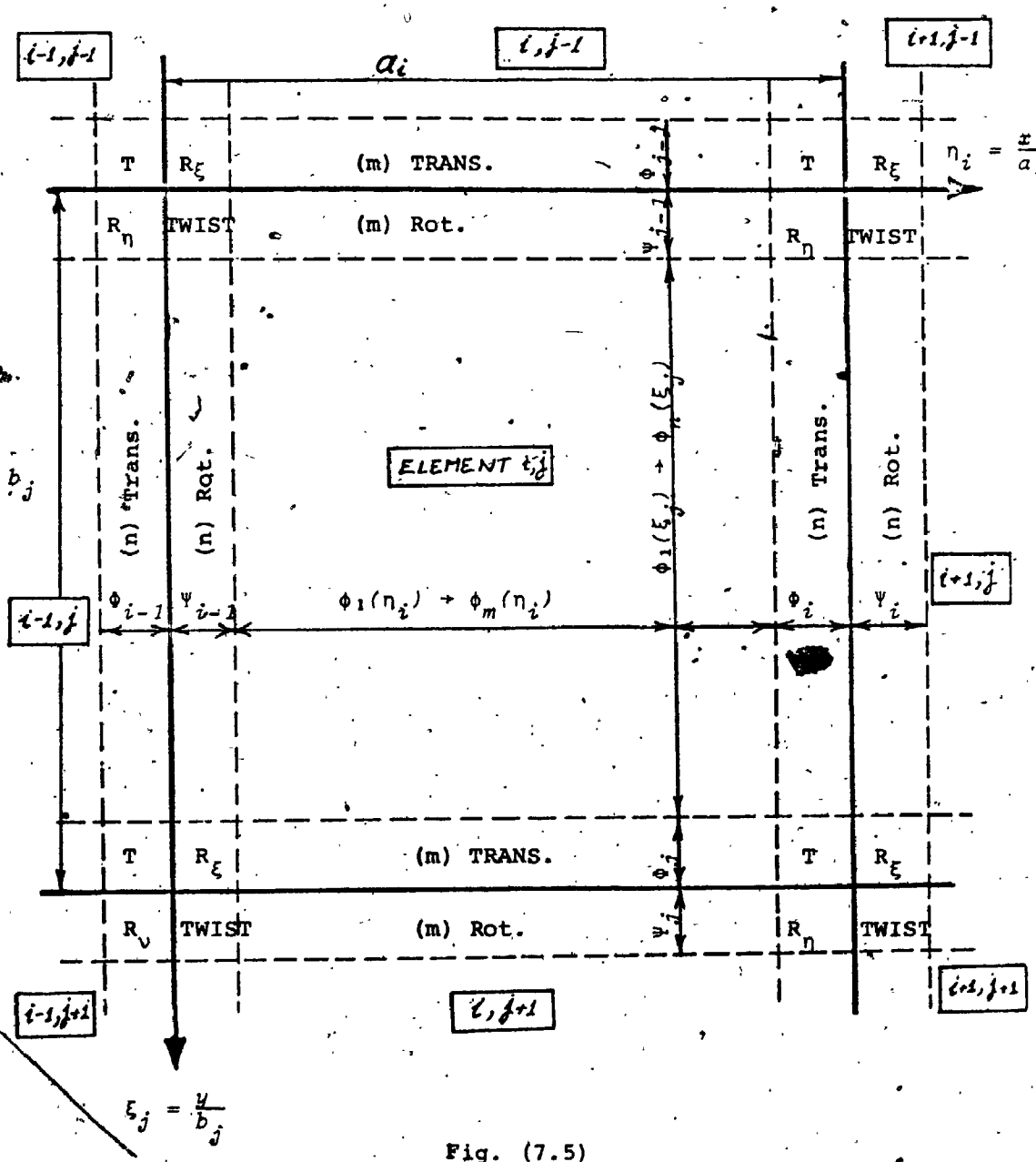

Fig. (7.5)

Distribution of degrees of freedom in Large Rectangular Plate Elements

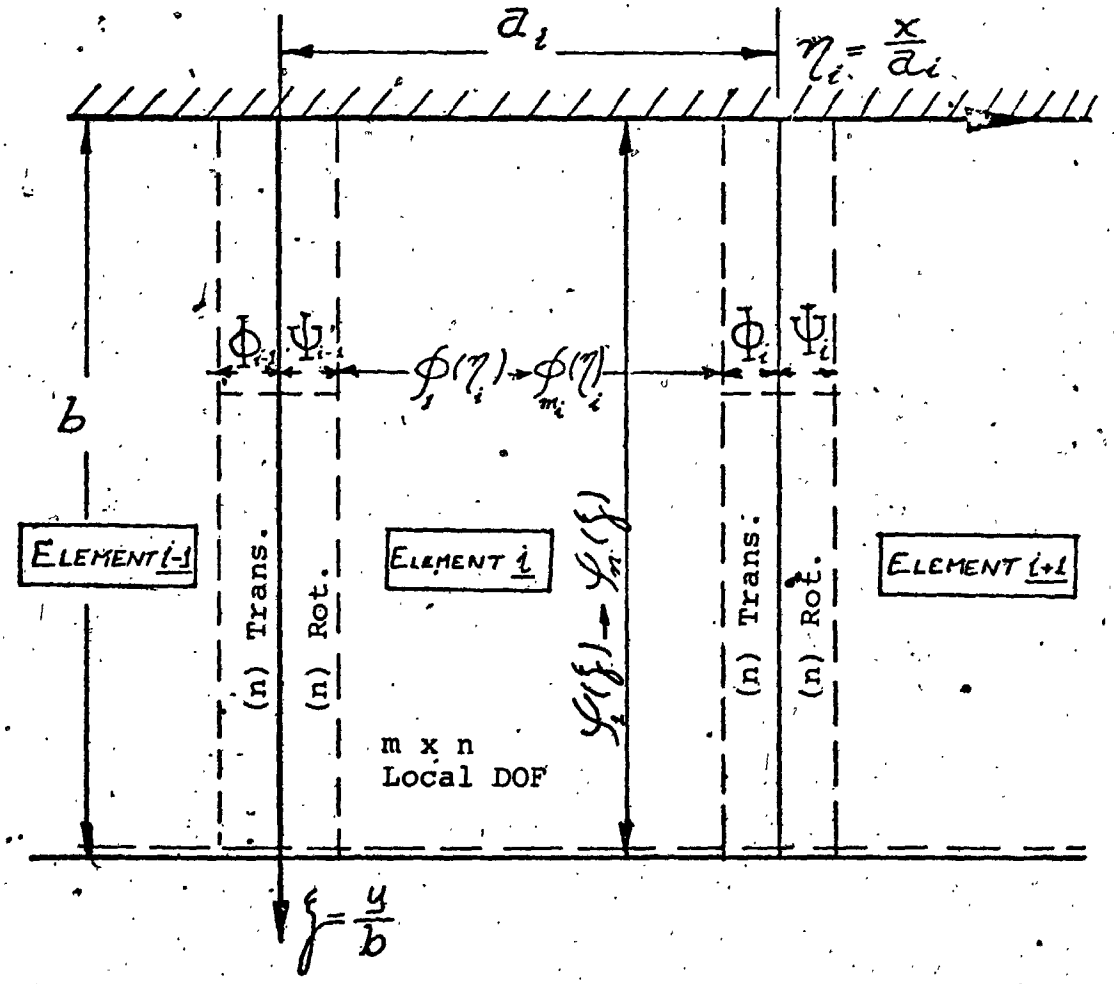

Fig. (7.6)

Distribution of Degrees of Freedom in Large Plate Strips

CHAPTER VIII

TEST PROBLEMS

8.1 Introduction

In the following, the Large Element and Large Strip methods developed in the previous chapter are evaluated for application to both static and dynamic problems. The methods are thus used to solve simple numerical examples for which the exact solutions are known. These examples are also used as a basis for comparing the accuracy obtainable by the proposed methods with that of conventional approaches such as the Finite Element, Finite Difference and the Ritz methods.

Two sets of examples will be treated here; the first is a set of *static* standard test problems which are traditionally used to asses the accuracy of the different types of Finite Elements. Another simple static problem is also used for comparison with Finite Differences. The second set of problems; however, are vibration problems which have been adopted previously in order to assess the accuracy of the Ritz solutions of Chapters II and III.

In addition to evaluating the accuracy of the Large Element and Large Strip solutions, the present test problems are meant to demonstrate the general procedure of

applying the methods to different types of problems. Moreover, the first set of test problems will be used to demonstrate that the four degrees of freedom per node Finite Element rectangle, which has been used as a basis for the Large Element rectangle presented here, is amongst the most accurate known Finite Elements.

8.2 Static Problems

Four simple static plate problems will be treated in this section. These problems are:

1. A simply-supported plate under a uniform load,
2. A simply-supported plate under a central concentrated load.
3. A clamped plate under a central concentrated load.
4. A plate having two parallel edges clamped and two simply supported under a load sinusoidally varying across the simply supported span and uniformly distributed in the other direction.

In all cases, the plates are assumed to be thin, flat, homogeneous and square. Except for the last problem, the above are standard test problems which have frequently been used to assess the accuracy of the different Finite Elements. References [9], [34] and [36] contain extensive comparative results based upon the first three problems. These results are reproduced here and compared with those obtained using the same numbers of degrees of freedom in the Large Element method. The same problems are also solved

with the Large Elements being used as ordinary Finite Elements, showing clearly the relative merits of the Large Element approach. These merits may be even more appreciated upon recalling that the Finite Element obtained in that case is amongst the best available.

For the solution of a typical problem using Large Elements, the following data have to specified:

1. The geometry definition; this is achieved through supplying an identification number and the coordinates of each nodal point, as well as an identification number and the connectivity for each nodal line (edge).
2. The element connectivity; this is defined through specifying the nodes and the nodal lines (edges) to which each element is connected.
3. The element properties; which includes the specification of both the stiffness and mass properties for each large element.
4. The number of degrees of freedom; this is determined by the choice of the parameters m and n defining the number of terms in the displacement series assumed for each element.
5. The definition of constraints; this specifies the basic boundary conditions for the problem. In most cases, it is sufficient to specify the identification numbers for the constrained edges as well as the type of constraint; whether it is translational, rotational

or both. The corresponding degrees of freedom at the two nodes defining the specified edge (the terminal nodes) are automatically constrained. It is possible, however, to apply additional constraints at the nodal points; a procedure which is only needed in certain particular situations, as will be shown in the numerical examples of the following chapters.

6. Specification of the load vector; this is only necessary in the case of a static problem. For the two important special cases of a concentrated load at a node or a uniform load on an element, it is only necessary to specify the magnitude of the load and the identification number of the node - or the element - to which the load is applied. In the more general cases, however, the techniques described in section (7.4) are to be used to specify the loading vector directly depending upon the particular loading case.

The six items mentioned above will, thus, have to be specified for each of the examples treated in this and the following chapters in order to completely define the problem. It is worth mentioning here that, except for item number 4, the above items of data are required for any conventional Finite Element solution. In the case of Finite Elements, however, considerably larger numbers of elements and nodes are to be specified in order to achieve a degree of accuracy comparable to that obtainable with a few large elements.

8.2.1 The Large and Finite Element Models

Figure (8.1) shows the Large Element model representing problems number (1) and (2). Due to symmetry, one large element is used to represent only one quarter of the plate. Identification (ID) numbers are assigned to the four corners (nodes) and four edges (nodal lines) independently, however, constraints defining the boundary conditions are specified only at the latter. If rotations are constrained along an edge, both the rotations about this edge and the twisting degrees of freedom are automatically restrained at the two terminal nodes. Likewise, if displacements are constrained along an edge, both translations and rotations about an axis perpendicular to that edge, are constrained automatically at the nodal points defining the edge. It can thus be seen from figure (8.1) that only one degree of freedom will remain unconstrained at each of the four element corners; namely twist at node 1, rotation about the x-axis at 2, rotation about the y-axis at 3, and pure translation at node number 4. The total number of degrees of freedom as a function of the parameter m will then be equal to $(m+2)^2$.

A Large Element model representing example (3) is shown in figure (8.2). Again, only a quarter of the fully clamped plate under investigation is represented and one large element is employed. The symmetry and boundary conditions of the problem are specified through the edge constraints table shown in the figure. These edge constraints

imply also that all the corner degrees of freedom at the four nodes, except for pure translation at node number 4, are to be eliminated. The total degrees of freedom may thus be expressed as $(m+1)^2$

As mentioned before, the Large Elements can be used as ordinary Finite Elements by setting the parameters m and n to zero.. This is shown in figure (8.3) for the case of the square simply-supported plates of examples (1) and (2).. In this model, two elements are used along each half side of the plate, yielding a total of 4 elements and 9 nodes. There is no need in this case for assigning ID numbers to the element edges (nodal lines) since no degrees of freedom are assigned along these edges in the case of $m = n = 0$ (finite elements). Since no degrees of freedom are assigned to the element edges, the constraints have to be applied directly to the nodes as indicated by the table shown in figure (8.3). With the constraints shown in the figure, the remaining number of degrees of freedom is 16 which is equivalent to that obtained by setting $m = 2$ in the Large Element model shown in figure (8.1). Indeed, a general relation between the parameter m and the equivalent number of finite elements N along a side of the large element may be given as

$$N = (m/2) + 1. \qquad (8.1)$$

Obviously, a new Finite Element model has to be constructed for each individual value of N, and of course the constraints table is to be redefined. This procedure

becomes particularly tedious for large values of N.

In a similar way, a Finite element model for the clamped plate of example (3) is constructed in figure (8.4) for the value of $N = 3$ (i.e. three elements along a half side). As expected, all four degrees of freedom are constrained along the clamped edges. Using equation (8.1), the case $N = 3$ corresponds to a large element having $m = 2\ (N-1) = 4$, which in turn corresponds to a total number of degrees of freedom equal to $(m+1)^2$ or 25. This number can be arrived at directly from the total numbers of nodes and constraints shown in the figure.

In addition to the models presented above, a loading vector for each type of loads is to be defined. The plates of examples (2) and (3) are loaded with a unit force at the centre. As was mentioned in section (7.4), this loading condition yields a simple case where all the terms in the loading vector except one vanish. This term corresponds to the corner of the element that coincides with the centre of the plate. In element coordinates, this corner corresponds to $\eta = 1$, $\xi = 1$. Hence the coefficient of the loading vector $P\ (m+3,\ m+3)$ will be equal to unity for elements number I in figures (8.1) and (8.2); element number IV in figure (8.3); and element number IX in figure (8.4).

On the other hand, the plate of example (1) is loaded with a uniformly distributed load (p). This load may be expressed in the form of expression (6.20) such that

$\alpha_{kl} = p$; for $k = (m+1)$ or $(m+3)$; and $l = (n+1)$ or $(n+3)$

$\alpha_{kl} = o$; for $k \neq (m+1)$ or $(m+3)$; and/or $l \neq (n+1)$ or $(n+3)$

Equation (7.21) then becomes:

$$P_{rs} = p \cdot \left(\frac{a}{2}\right)^2 \cdot (B_{m+1,r} + B_{m+3,r}) \cdot (B_{n+1,s} + B_{n+3,s}), \quad (8.2)$$

which serves for the determination of the loading vector.

So far, Large and Finite Element models for examples (1) through (3) have been treated. For Example (4), however, a semi-analytical Large Element (Large Strip) model will be presented, since a comparison is to be made with a semi-analytical Finite Difference solution in which a half sine wave is assumed across the simply-supported span. The model is shown in figure (8.5) together with the constraints applied at the edges. In the case of the Large Strip model, it is only necessary to specify the nodal lines and the elements connecting between them as shown in the figure. It is obvious from the model and the constraints shown that the total degrees of freedom is equal to $(m+1)$. In a manner similar to that used for the derivation of the load vector in the Large Element method - section (7.4) - it can be shown that

$$P_{rs} = p_o \cdot \frac{a^2}{2} \cdot (B_{m+1,r} + B_{m+3,r}) \cdot I_{1,s}, \quad (8.3)$$

where I is the same as defined by equation (3.8). Since two edges $Y = 0, a$ are simply-supported, the integral coefficient $I_{1,s}$ is equal to 0.5 if s equals 1, and zero

otherwise, which justifies the choice of n (the number of terms in the x-direction) as unity.

8.2.2 Numerical Results and Comparison

Deflection and stress results for each of the above examples were computed using different numbers of terms in the Ritz-type series in the Large Element and Large Strip solutions, different numbers of elements in the Finite Element solutions, and different mesh sizes in the Finite Difference method.

Figures (8.6) and (8.7) show the central displacements for the plates of examples (2) and (3) as obtained using large elements, the finite Element option of the large elements, finite differences [37], an equivalent beam lattice by Hrennikoff [38], and six other types of compatible and incompatible finite element solutions compiled by references [34] and [9]. The comparison of the results is based upon the number of subdivisions along the half side of the plate for all finite element solutions. The large element solutions are chosen to have the same number of degrees of freedom as the corresponding four degrees of freedom per node finite element solutions.

Another set of finite element comparison results for the displacements of example (2) was reported in reference [36]. These results are reproduced in figure (8.8) with the large elements' and its finite element version's results superimposed upon those of reference [36]. A com-

parison of the stresses in the plates of examples (1) and (3), as obtained using the large and finite element models presented in the previous sub-section with those published in reference [36] using five different types of finite elements, is shown in figures (8.9) and (8.10) respectively.

It is obvious from the results displayed in figures (8.6) through (8.10) that in general better accuracy is obtainable by the use of large elements both for displacements and stresses. In addition, it can be seen that the finite element version of the large element presented in this work is amongst the most accurate plate bending finite elements available.

In addition to the greater accuracy obtainable by the use of large elements, an obvious advantage is the better continuity of stresses achievable. This is clearly demonstrated in figure (8.11) where the stresses across the centre lines of the plates of examples (1), (2) and (3), obtained using both large elements and incompatible triangular finite elements [9], are shown. The ability of large elements to represent sharp stress variations is also obvious from the figure.

It is worth noting in figure (8.6) that two different sets of results are shown for the four degrees of freedom per node rectangular element. The first set is reproduced from reference [34] while the second set has been generated using the model shown in figure (8.3). Although the details of the model used in reference [34]

were not published, it is believed that the reason for the discrepancy is that the corners of the plate were considered clamped in reference [34], while in the present analysis twisting has been permitted at the plate corners. This belief was verified by constraining the twisting degree of freedom at the corner of the plate shown in figure (8.3), in which case the results published in reference [34] were reproduced. It is believed, however, that restraining the corner twist is not justified, since the exact solution of the problem contains a finite value for the twisting moment at the simply-supported plate corners, and hence the model used by reference [34] is over-restrained.

The central displacements for the plate of example (4) as obtained using the large strip model shown in figure (8.5), as well as a semi-analytical finite difference solution, are shown in table (8.1). In the finite difference solution, a sine wave was assumed in the direction perpendicular to the simple-supports, and a one dimensional finite difference mesh assumed in the other direction. It can be seen that the percentage errors obtained in the case of finite differences are almost two orders of magnitude larger than those obtained using *the same number of degrees of freedom* with the large element method.

8.3 Dynamic Problems

In this section, the accuracy and convergence of the large element and large strip methods, when used to

Table (8.1)

Statically Loaded SS-C-SS-F Square Plates

Convergence of central deflections and comparison with Finite Difference solutions. Percentage errors based upon exact solution $W_{max} D/Pa^2 = .024654$

Large Strip		Finite Difference	
DOF = 3	DOF = 5	DOF = 5	DOF = 20
0.37%	0.07%	6.17%	0.53%

Table (8.2)

Vibration of a SS-F-SS-F Square Plate

Percentage deviations from exact solutions. Maximum displacement normalized to unity in all cases (exact solutions given in brackets). Poisson's ratio = 0.3.

Method of Solution:	Large Strip			Large Element	Ritz
Degrees of Freedom:	5	7	9	42	7
eigenvalue [92.762755]	0.002	0.0002	0.0001	0.002	0.0000
Edge Rise ($W_{max} - W_{min}$) [0.13559]	---	0.004	0.002	0.019	0.0001
Maximum M_B [1.76208]	---	0.14	0.10	-0.50	-0.003
Max. edge M_B^* [zero]	---	3.5	1.6	4.5	-0.005

* % error related to exact maximum M_B

solve vibration problems, are demonstrated. Two examples for the transverse vibrations of square homogeneous plates, which have been used previously to assess the accuracy of the Ritz solutions, will be examined here. The problems will be treated using different numbers of degrees of freedom in both the Large Strip and Large Element methods and the results compared to the exact solutions and the solutions obtained previously by the Ritz method. The two examples which will be dealt with here are:

1. A square plate having two parallel edges simply supported and the other two free undergoing free vibration .
2. A square plate with two parallel edges simply supported, a third edge clamped, and the fourth edge free undergoing free vibration .

A large strip model for the first example is shown in figure (8.12). The model comprises one strip which represents one half of the plate with symmetry conditions applied along the centre line. The number of terms across the width of the strip (m) can be arbitrarily changed, with the total degrees of freedom changing as $(m+3)$. Due to the existence of two parallel simply-supported edges, the modes of vibration corresponding to different numbers of half waves (n) in the Y-direction are separable. It is therefore feasible to consider only one value at a time, and the value $n = 1$ was used here to obtain the fundamental mode.

In addition to the Large Strip model, figure (8.13) shows a Large Element model in which one element is used to represent one quarter of the plate making use of the symmetry conditions. Both symmetry and anti-symmetry can be applied along the centre lines of the plate. However, for the fundamental mode, symmetry conditions were applied as shown in the figure. The relation between the parameters m and n and the total degrees of freedom (TDF) can be written as

$$TDF = (m+3), \quad (n+2),$$

which, for $m = n = 4$, gives a total of 42 degrees of freedom.

The percentage errors in the results obtained using the above mentioned models as well as those previously obtained using degenerated beam functions in the Ritz method - see table (3.1) - are displayed in table (8.2) for comparison. It can be seen from the table, that rapid convergence is achieved when the number of terms (m) is increased in the Large Strip solution. It can also be seen that for the same number of terms in the x-direction $(m = 4)$, better results are obtained using the Large Strip rather than the Large Element method. This is due to the fact that while an exact function is used in the y-direction in the Large Strip method, an approximate series is used in both directions in the case of the Large Element solution; thus introducing more errors. In addition, the fact that separation of

variables is impossible in the case of Large Elements - as compared to the Large Strip method - yields a much larger number of total degrees of freedom to be dealt with for the determination of any one mode of vibration.

A comparison between the percentage errors in the Large Strip and the Ritz solutions indicates that considerably more accurate results are obtained from the latter. Two possible reasons for this are:

Firstly: Due to their physical significance, beam functions may better resemble the vibration modes of plates with free edges.

Secondly: The beam functions used in the Ritz solutions exactly satisfy the symmetry conditions at the plate centre line, while the Large Strip solutions satisfy exactly the zero slope condition and only approximate the natural boundary condition of zero shear force.

For example (2), two different large strip models were used, these are shown in figure (8.14). Again, due to the existence of two parallel simply-supported edges, separation of variables is feasible and only one term in the y-direction at a time is sufficient. Thus for the lowest mode n was taken as a unity in both models. It is clear from the models and the applied constraints that the total number of degrees of freedom for the one strip model can be given by: $TDF = m + 2$. Likewise, for the

two strip model, this total is: $TDF = m_1 + m_2 + 4$.

In figure (8.15), a Large Element model for the same problem is shown. Only one half of the plate needs to be modeled with symmetry conditions applied along the centre line in order to obtain the lowest mode. For the purpose of comparison, a two element model is used as shown in the figure. Although theoretically not required, the number of rotational and/or translational degrees of freedom along an edge parallel to the y-axis was taken, in this example as well as the examples to come, to be equal to the parameter "n" representing the number of terms in the y-direction in the double series of internal (local) element degrees of freedom. Consequently, the parameter "n" was taken to be the same for all elements lying in one column parallel to the y-axis. Likewise, all elements in a row parallel to the x-axis were assigned the same value for the parameter "m". As a result, the total number of degrees of freedom in the model shown by figure (8.15) may be expressed as $TDF = (m_1 + m_2 + 4) \times (n + 2)$.

A comparison of the fundamental eigenvalue results obtained using the above-mentioned large element and large strip models with exact solutions and solutions obtained using degenerated beam functions in the Ritz method is shown in table (8.3) The two strip model includes two large strips each having the same number of degrees of freedom as the corresponding one strip model. Consequently,

Table (8.3)

Vibration of a SS-C-SS-F Square Plate

Convergence and comparison of fundamental eigenvalues. Percentage errors based upon exact solutions [λ = 160.96804]. Poisson's ratio = 0.3.

Large Strip		Large Element	Ritz
DOF = 6	DOF = 12	DOF = 50	DOF = 9
0.017	0.0025	0.038	0.0018

improvement of the solution through the use of two large strips instead of one is expected in the same sense in which piece-wise convergence occurs with the Finite Strip method. It is also expected, however, that if the same total number of degrees of freedom (12) were used in a one large strip model instead of a two strip model, a further improvement would occur. As with example (1), it is shown that the large element model yields less accurate results than those obtained by the large strip models for the same reasons stated therein. Again, the Ritz results are still more accurate than those obtained by both the large element and large strip models.

8.4 Conclusions and Remarks

The following may be concluded from the results of the test problems presented in this chapter:

- The use of Large Elements or Large Strips provides the possibility of achieving convergence through three different mechanisms:
  a. A piece-wise convergence in which the parameters m and n are set to zero and the number of elements is gradually increased. In this case the Large Element becomes equivalent to a four degrees of freedom per node Finite Element - figures (8.3), (8,4) and (8.13).
  b. A term-wise convergence in which the parameters m and n are gradually increased while keeping the

number of elements in the model constant - figures (8.1), (8.2), (8.12) and (8.14).

c. A hybrid convergence; where both the parameters m, n and the number of elements are increased - figures (8.14) and (8.15).

Compared to other methods of solution of comparable versatility - e.g. Finite Elements, Finite Differences, Hrennikoff's beam lattice ... etc. - better accuracy is generally obtained through the use of Large Elements in *any* of its convergence mechanisms.

For the same total degrees of freedom, the term-wise convergence is consistently more efficient than an equivalent piece-wise or Hybrid convergence. This is to be expected in view of the discussion presented in section (7.1). With the obvious advantages of the considerably reduced modelling and data preparation effort, and that it is not necessary to construct a new model for each convergence step, it becomes clear that the term-wise convergence is superior in all respects.

With this conclusion in mind, the choice of the Large Element model to be used for a given problem is greatly simplified. The structure is simply subdivided into the smallest number of elements which sufficiently approximate the geometry of the problem. The parameters m and n for each of the elements

are then chosen in accordance with the accuracy required and the expected stress gradients within the particular element. It is worth mentioning here that while the side ratio of a finite element has to be kept as close as possible to a unity, there is no such limitation on the choice of the large elements, since different flexibilities can be assigned in the longer and shorter directions of the element. Convergence may then be studied easily, using the same model, by simply changing the parameters m and n for some or all of the elements of the model.

When modelling a simply-supported corner (the corner between two simply-supported edges) using either Large Elements or a four degrees of freedom per node Finite Element, the corner should not be treated as a clamped ~~corner~~ and the twisting degrees of freedom should not be restrained, otherwise an overly restrained model will result - see figure (8.6).

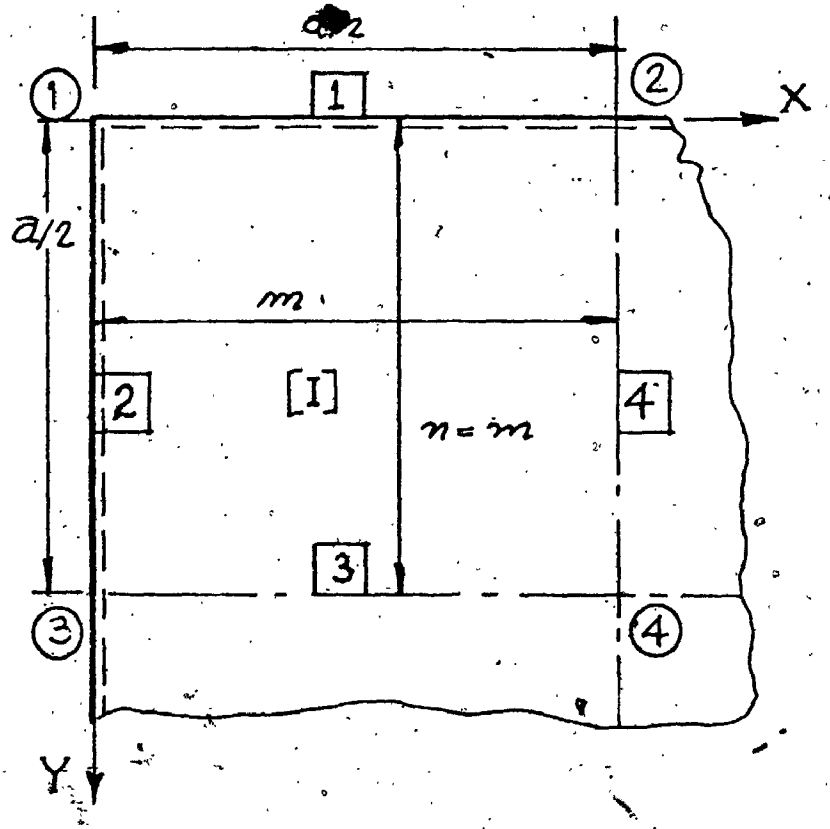

Stiffness:

$\nu = 0.3$

$D_x = D_y = D$

(Isotropic)

Constraints

Edge No.	Type of Constraint
1	d*
2	d
3	r*
4	r

Fig. (8.1)

* d = displacement, r = rotation

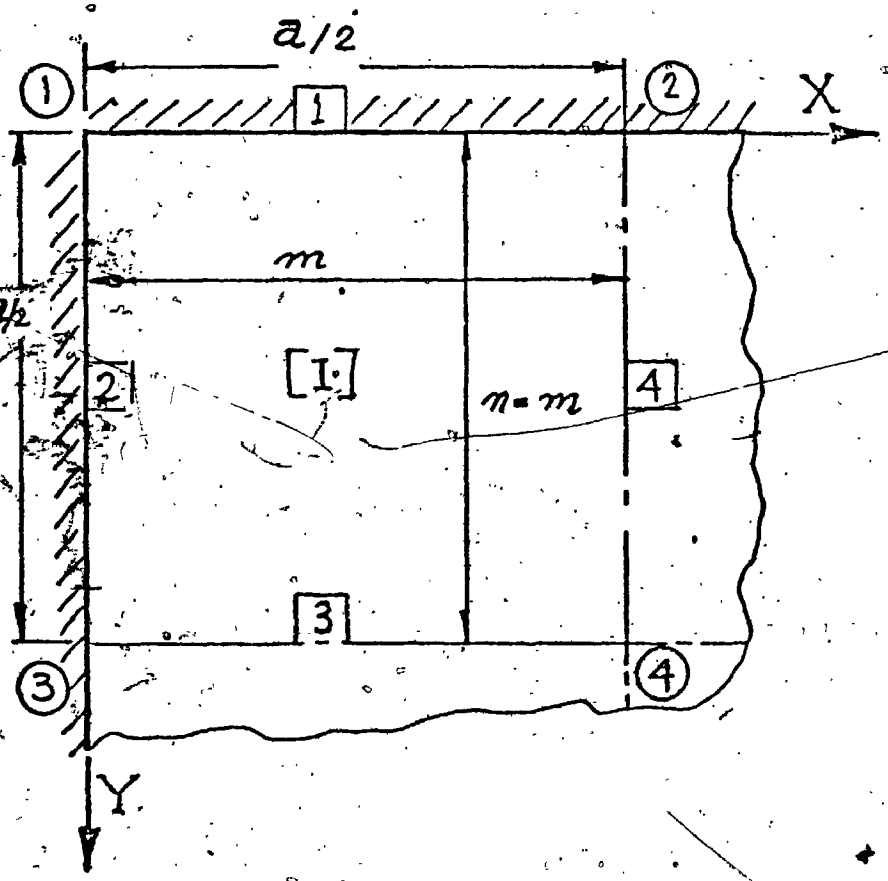

Stiffness

$\nu = 0.3$

$D_x = D_y = D$

(Isotropic)

Constraints

Edge No.	Type of Constraint
1	d^*, r^*
2	d, r
3	r
4	r

Fig. (8.2)

* d = displacement, r = rotation

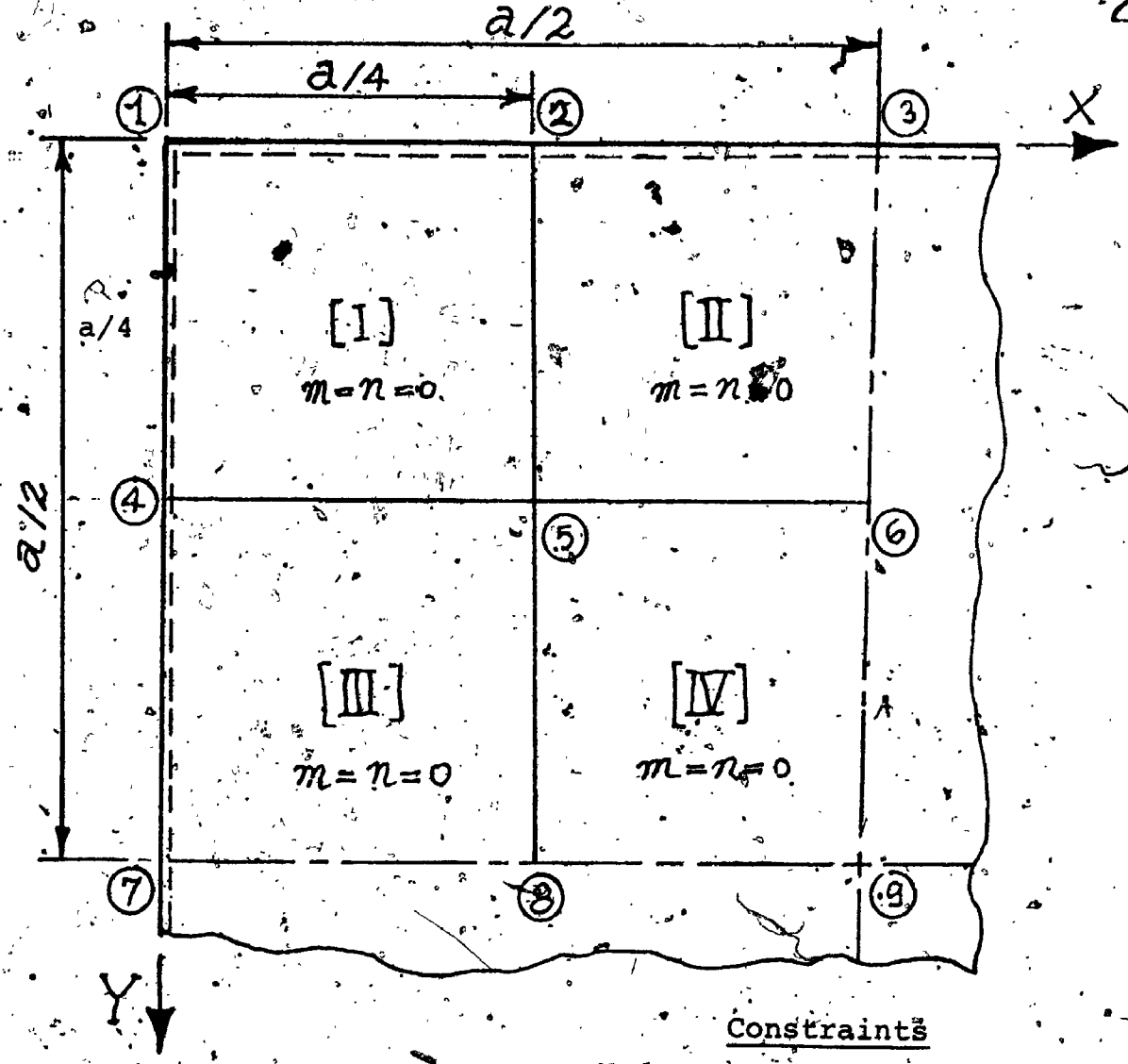

Stiffness

$\nu = .3$

$D_x = D_y = D$

(Isotropic)

Constraints

Node No.	Type of Constraint
1	d, rx, ry
2	d, ry
3	d, ry, t
4	d, rx
6	ry, t
7	d, rx, t
8	rx, t
9	rx, ry, t

Note: d ≡ displacement, rx ≡ rotation about x-axis
ry ≡ rotation about y-axis, t ≡ twist $(\partial^2 w/\partial x \partial y)$

Fig. (8.3)

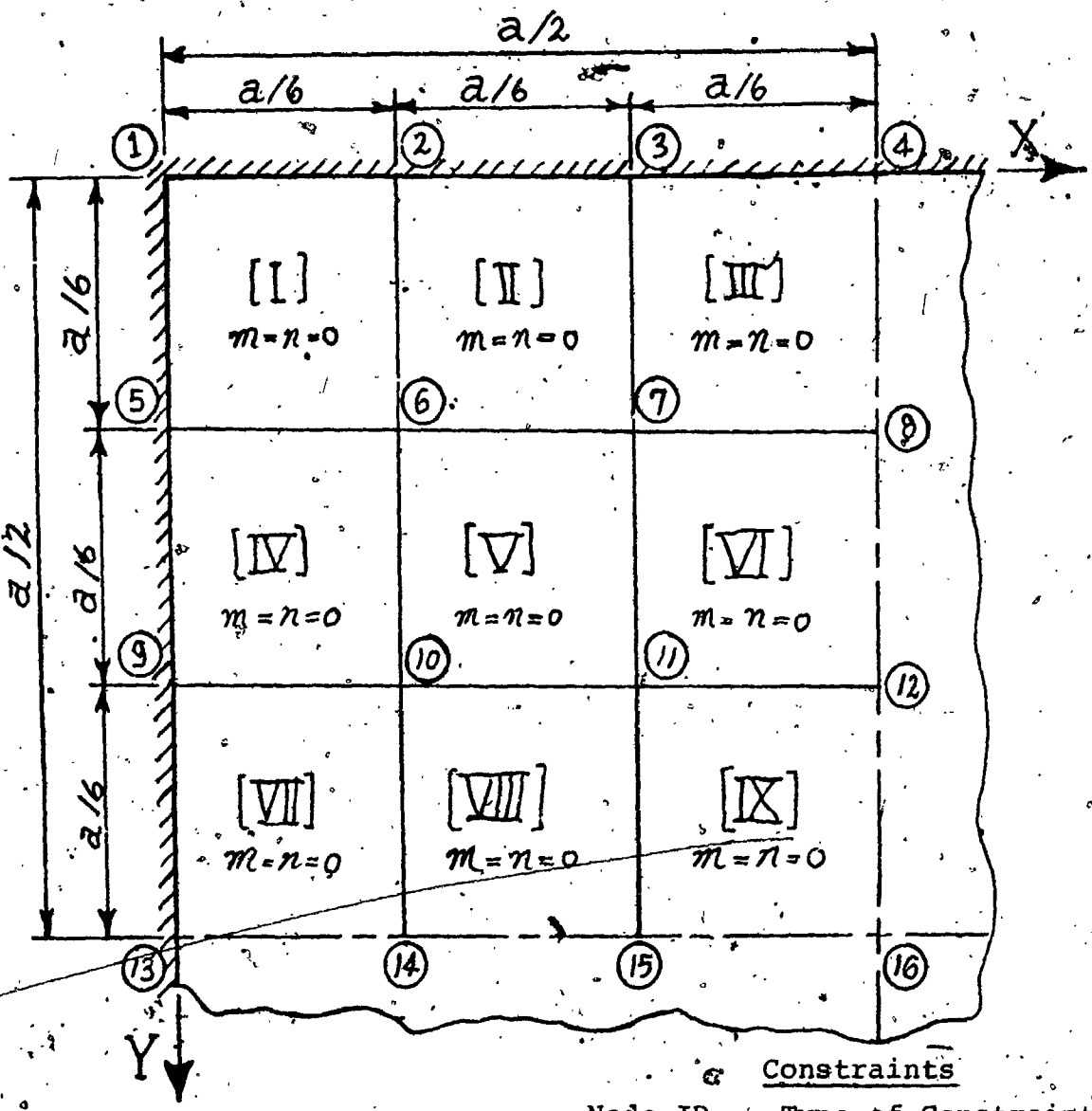

Stiffness

$\nu = .3$

$D_x = D_y = D$

(isotropic)

Constraints

Node ID	Type of Constraint
1	d, rx, ry, t
2	d, rx, ry, t
3	d, rx, ry, t
4	d, rx, ry, t
5	d, rx, ry, t
8	ry, t
9	d, rx, ry, t
12	ry, t
13	d, rx, ry, t
14	rx, t
15	rx, t
16	rx, ry, t

Note: d≡ displacement, rx ≡ rotation about x-axis, ry≡ rotation about y-axis; t ≡ twist $(\partial^2 w/\partial x \partial y)$

Fig. (8.4)

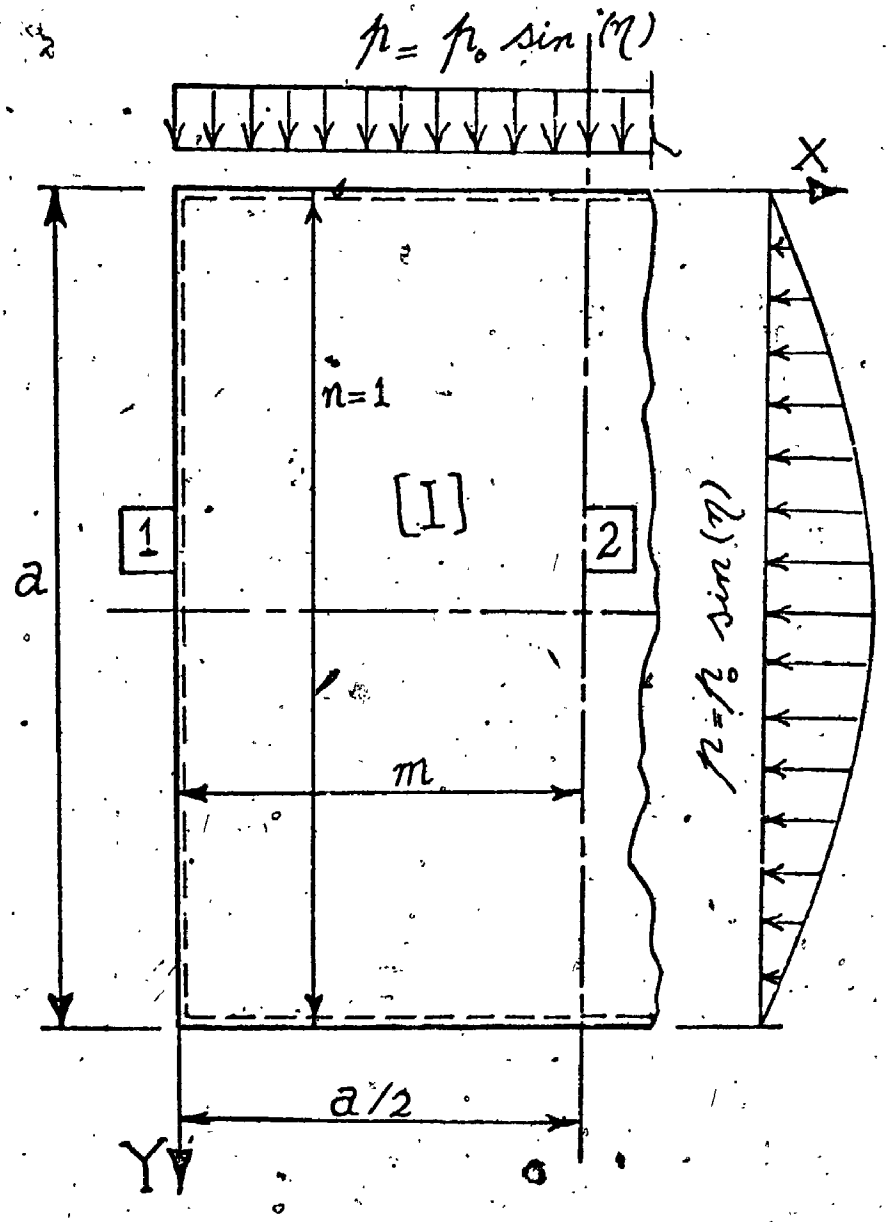

Stiffness

$\nu = 0.3$

$D_x = D_y = D$

(Isotropic)

Constraints

Edge No.	Type of Constraint
1	d^*, r^*
2	r

Fig. (8.5)

---

* d = displacement, r = rotation

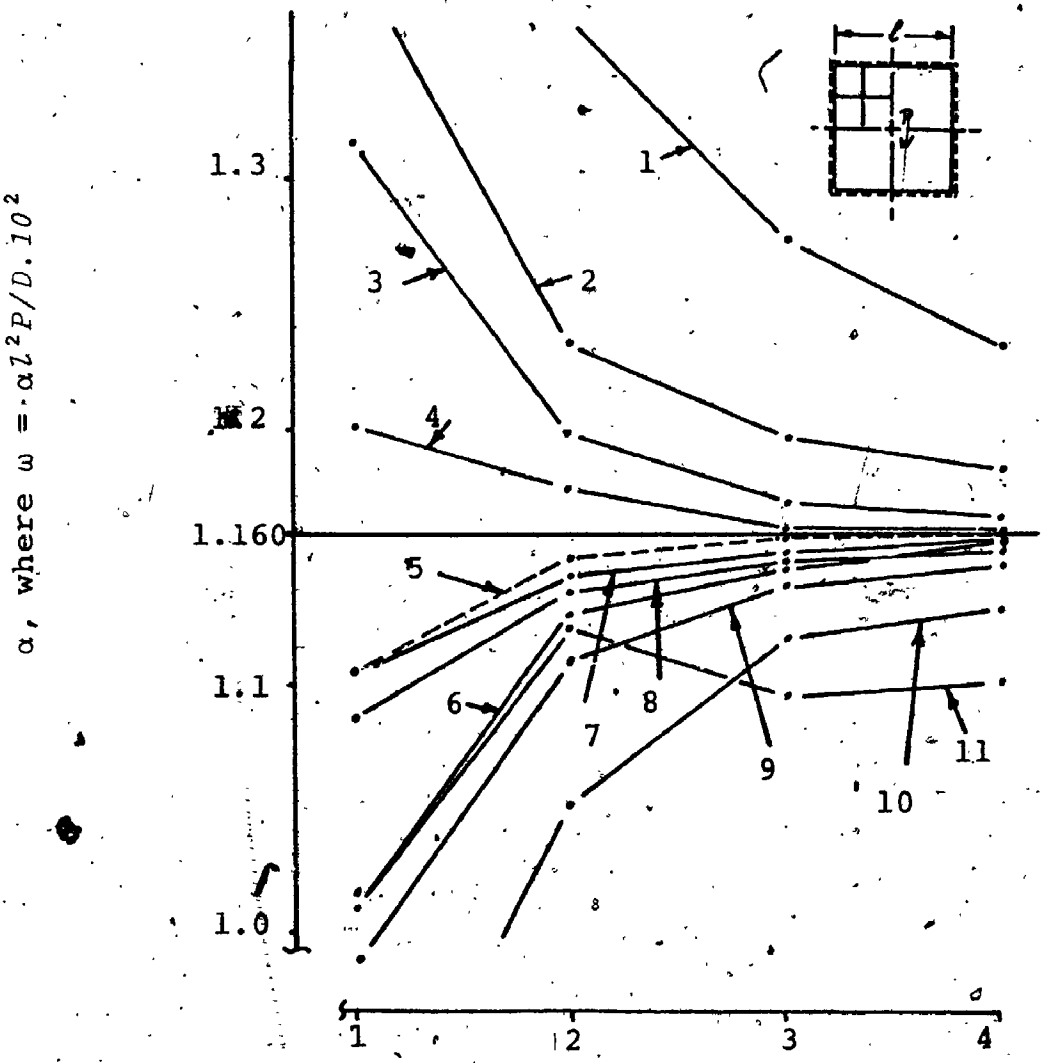

1. Finite Difference
2. Lindberg - incompatible rectangle
3. Incompatible triangle [9]
4. Hrennikoff - Beam lattice
5. Large Element
6. 16 DOF rectangle - ref. [34]
7. 16 DOF rectangle-generated
8. Vebeke [9]
9. Clough rectangle [9]
10. Compatible triangle [9]
11. 12 DOF rectangle - ref. [34]

Central Displacement of a Square S.S. Plate Under Central Load

Fig. (8.6)

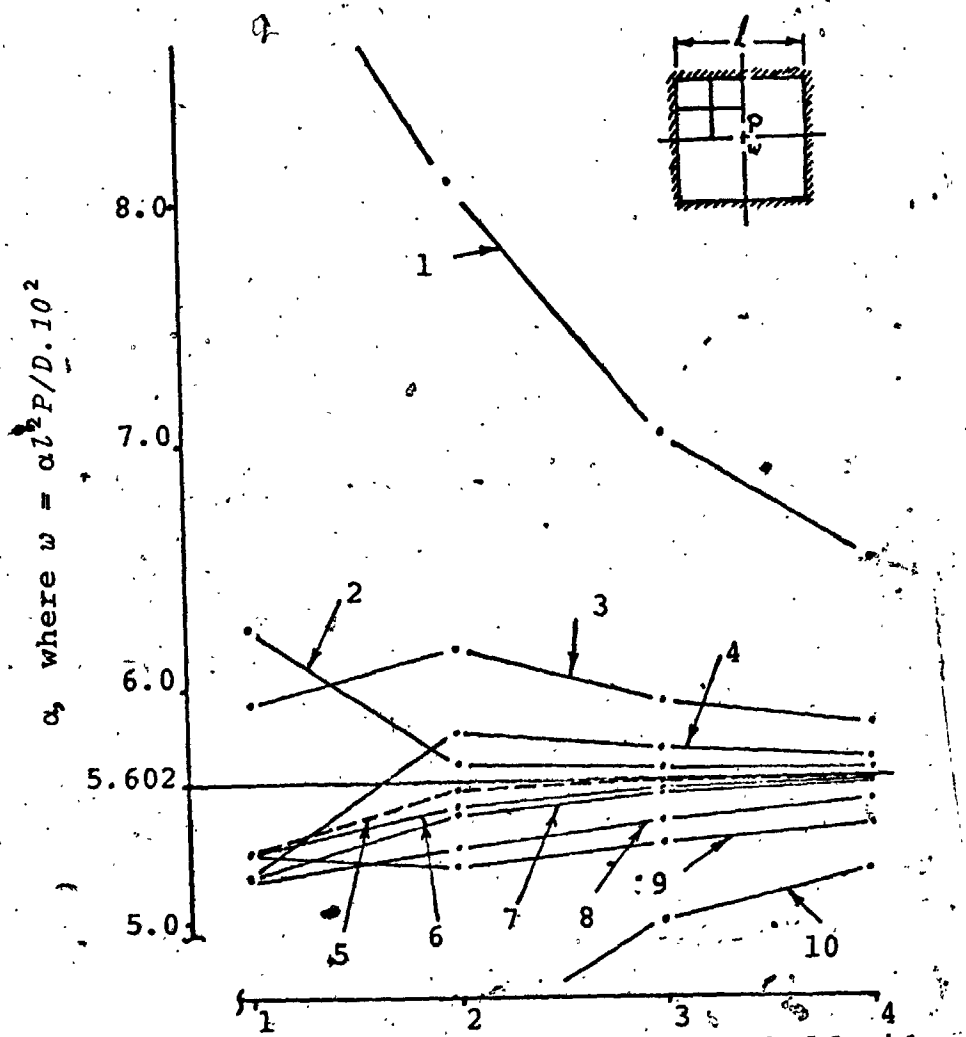

1. Finite Difference
2. Hrennikoff - beam lattice
3. Lindberg - Incompatible rectangle
4. Incompatible triagle [9]
5. Large Element
6. 16 DOF rectangle
7. Vebeke [9]
8. Clough Rectangle [9]
9. 12 DOF rectangle [34]
10. Compatible triangle [9]

Central Displacement of a Square Clamped Plate
■ Under Central Point Load

Fig. (8.7)

Fig. (8.8)

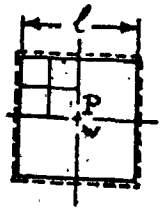

Central displacement of square S.S. plate under central load

Fig. (8.9)

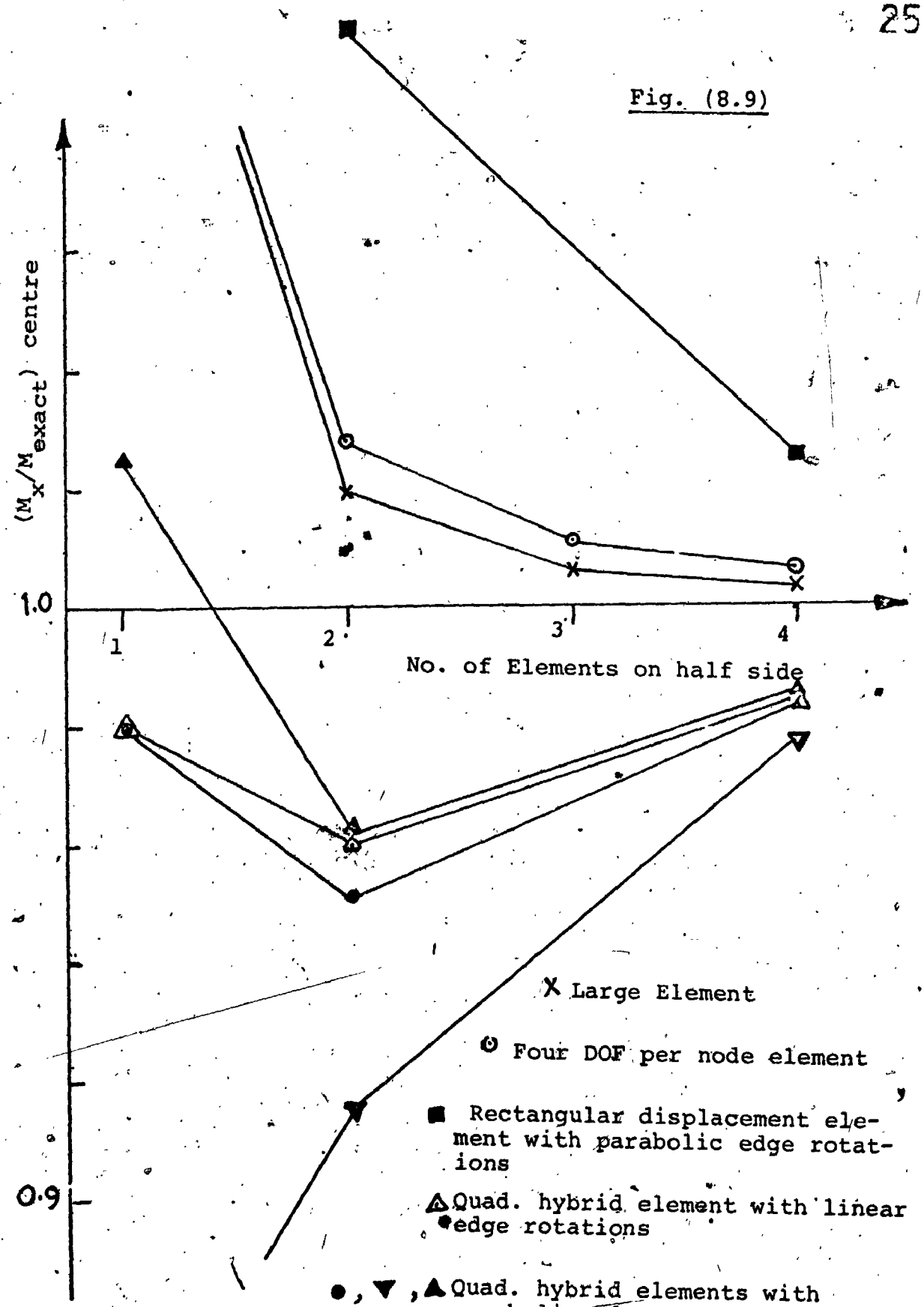

Uniformly loaded Simply-Supported Plate-Max. Stress

Fig. (8.10)

Centrally-loaded Clamped Plate
-edge stresses

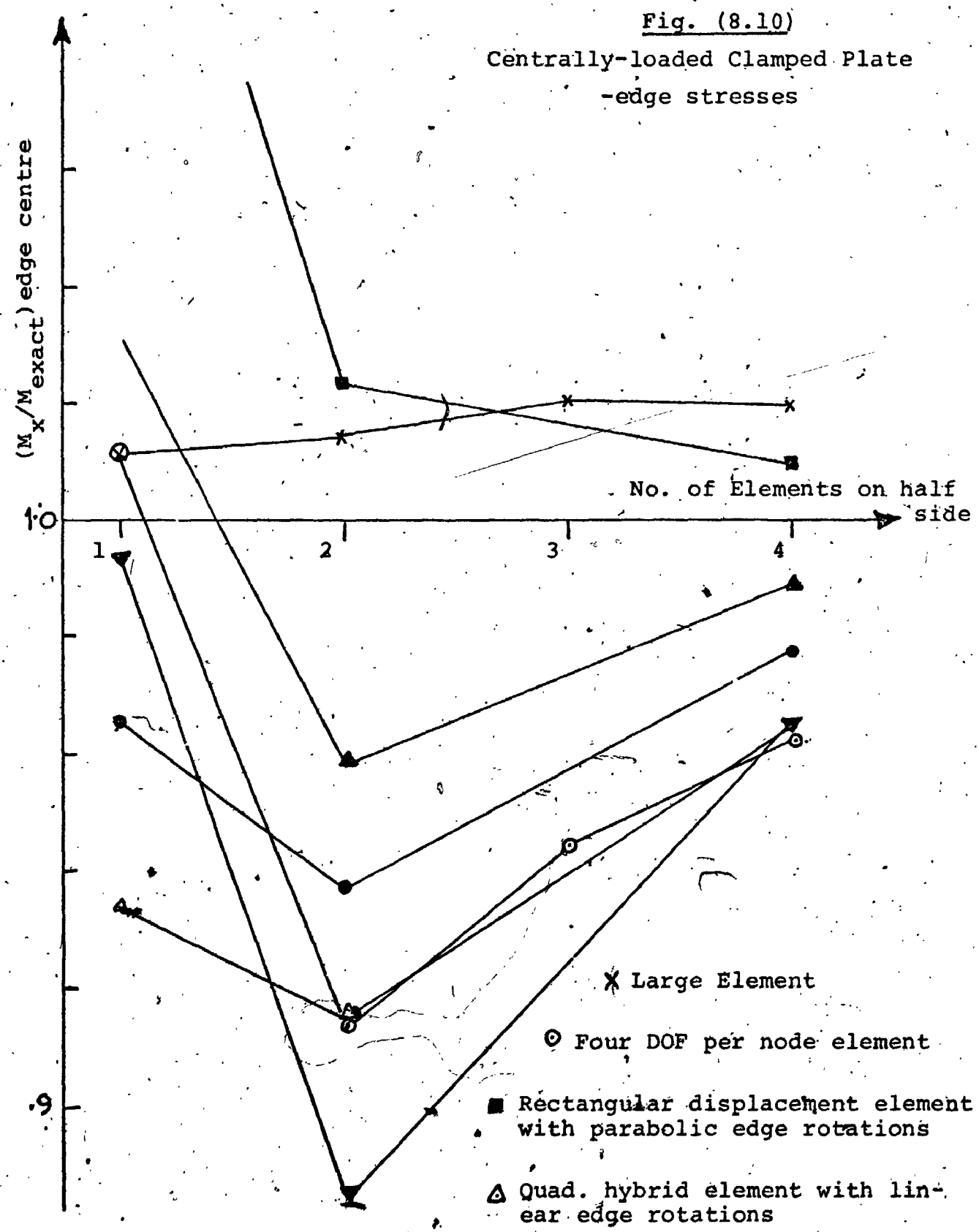

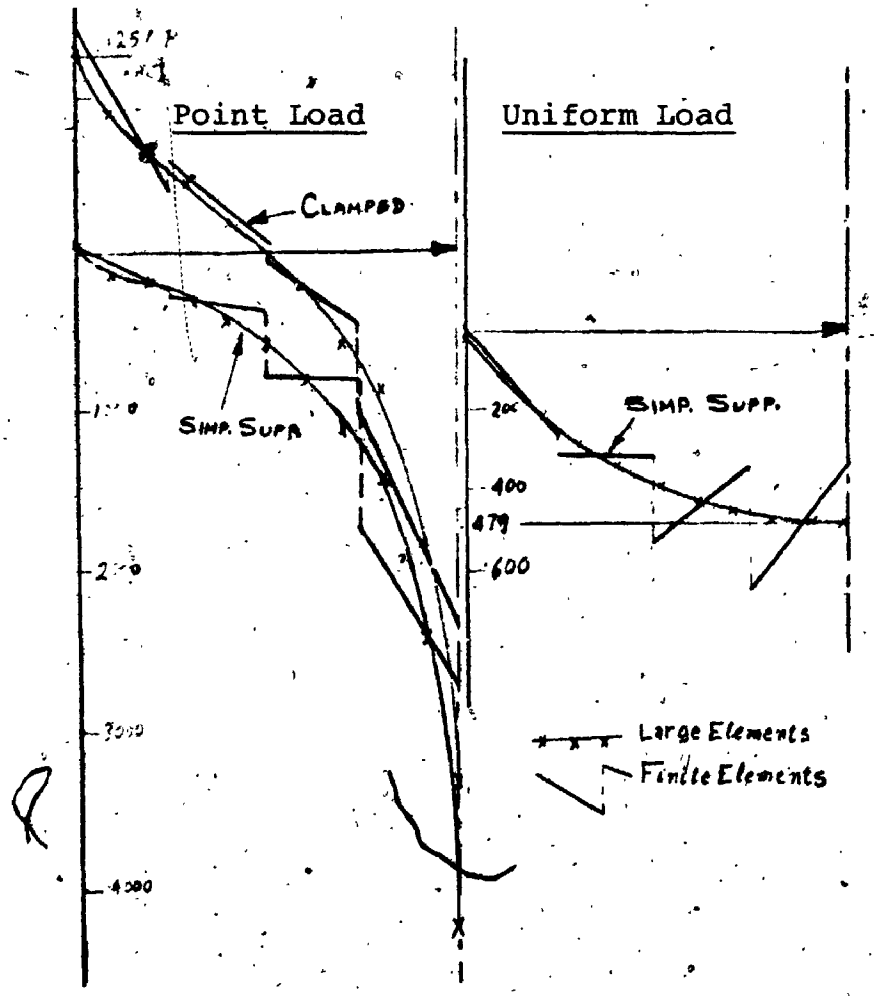

Fig. (8.11)

Bending Moments Across the Centre-Lines of Statically-Loaded Square Plates

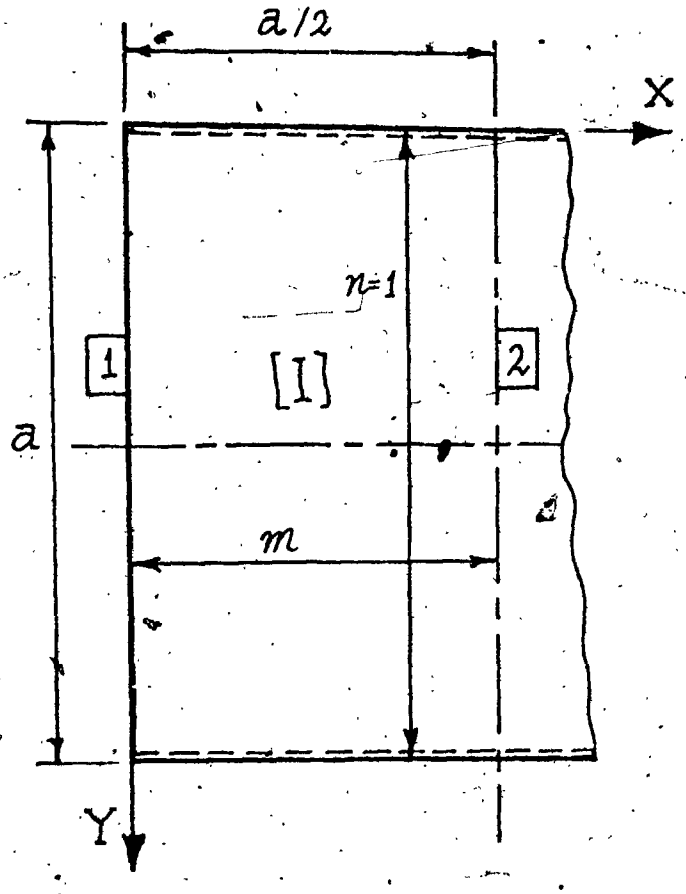

Stiffness:

$\nu = .3$

$D_x = D_y = D$

(Isotropic)

Constraints

Edge No.	Type of Constraint
2	rotation

Total Degrees of Freedom = (m+3)

Figure (8.12)

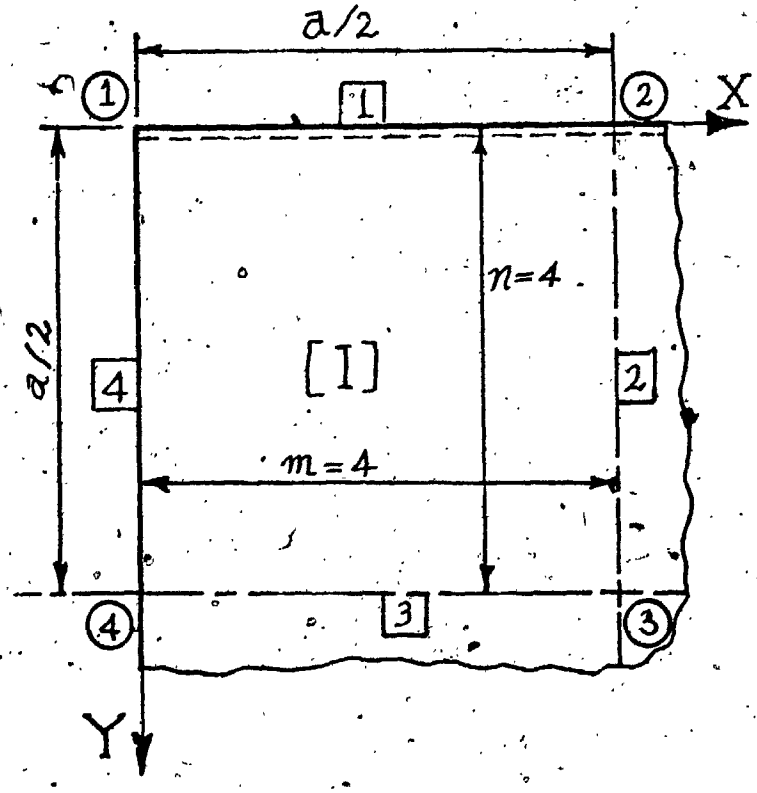

Stiffness

$\nu = .3$

$D_x = D_y = D$

Constraints

Edge	Type of Constraint
1	displacement
2	rotation
3	rotation

Total Degrees of Freedom = 42

Figure (8.13)

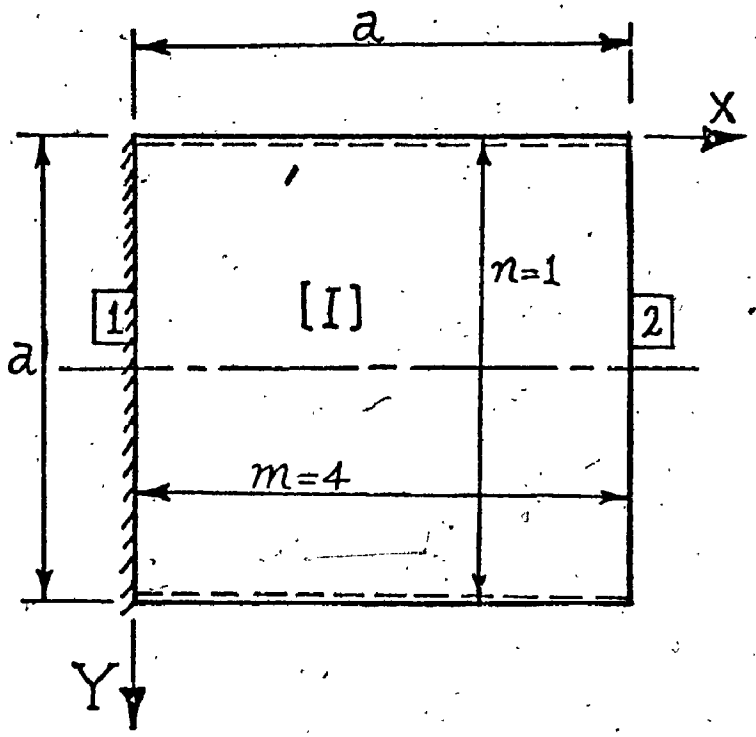

Stiffness

$\nu = 0.3$

$D_x = D_y = D$

(Isotropic)

Constraints

Edge No.	Type of Constraint
1	disp. & rot.

Total DOF = 6

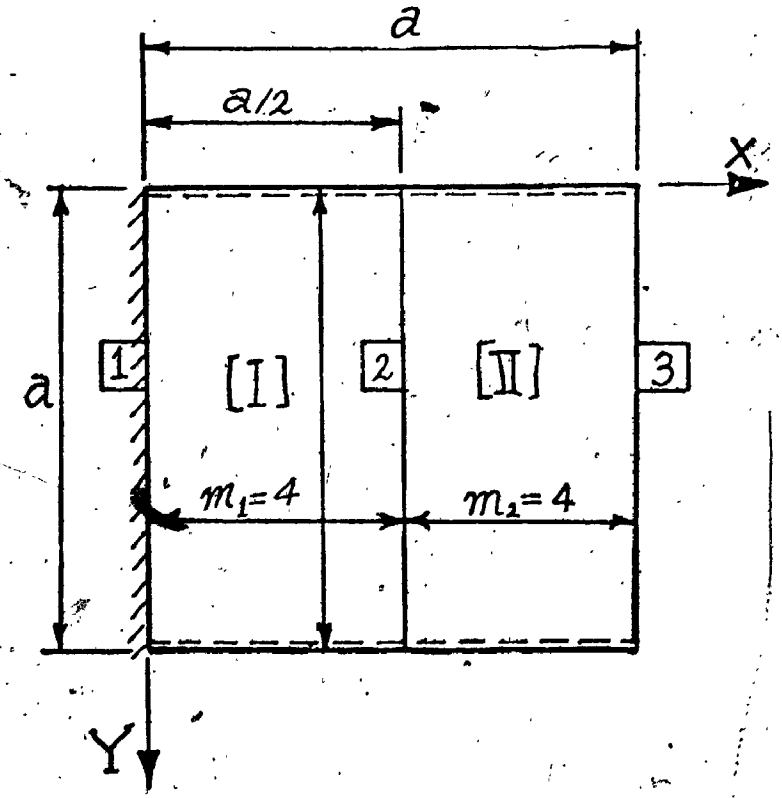

Stiffness

$\nu = 0.3$

$D_x = D_y = D$

Isotropic)

Constraints

Edge No.	Type of Constraint
1	disp. & rot.

Total DOF = 12

Fig. (8.14)

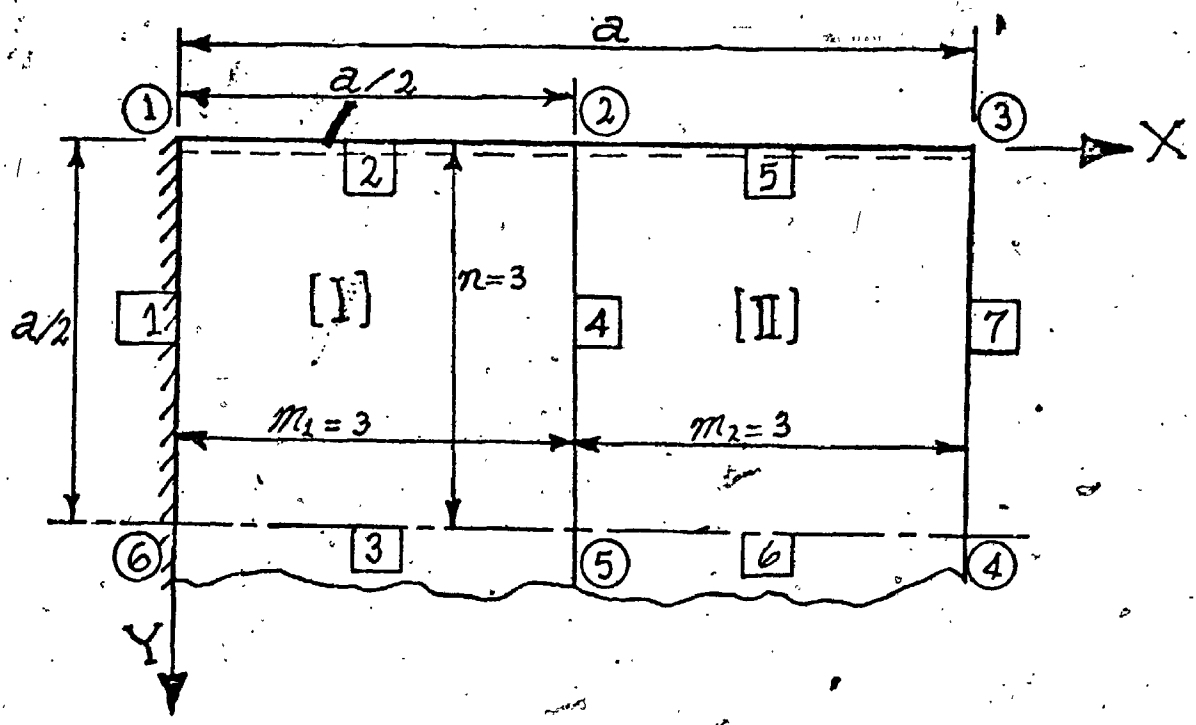

Stiffness

$\nu = .3$

$D_x = D_y = D$

(Isotropic)

Constraints

Edge No.	Type of Constraint
1	disp. & rotat.
2	disp.
3	rotat.
5	disp.
6	rotat.

Total degrees of freedom: TDF = 50

Fig. (8.15)

CHAPTER IX

VIBRATION AND BUCKLING PROBLEMS

9.1 Introduction

In the previous chapter, the accuracy of the results obtainable through the Large Element approach, for both static and dynamic problems, has been established. For that purpose, the method was applied to several simple problems for which exact solutions are available for comparison. In this and the following chapters, however, a large number of essentially more complicated problems will be tackled in order to demonstrate the wide class of problems to which the method could be advantageously applied. Since, in general, no exact solutions are known for such problems, an indication for the accuracy of the results is provided in each case through comparison with other available approximate solutions and/or examining the rate of convergence of the results by using different numbers of terms in the series (term-wise convergence).

The vibration problems to be discussed embrace four rectangular plates with either geometric (holes) or support discontinuities, two continuous isotropic and orthotropic plates, and a closed thin walled box. An example for the

buckling of a short "I" column under the action of uniform compressive loads is also considered. In addition to the non-dimensional frequency or buckling parameters for each of these problems, the normalized eigenfunctions (or mode shapes) are also presented in the form of computer-generated contour plots.

9.2 Plates with Discontinuous and Point Supports

Two examples of rectangular plates will be treated in this section:

i) A plate with four point supports at its corners.

ii) A plate clamped along two symmetrically-located segments of its edges and simply-supported along the balance of its boundary.

The geometry of, and the Large Element model used for, the first example are shown in figure (9.1). Due to symmetry (or anti-symmetry) only one quarter of the plate needs to be analysed. The set of constraints shown in the figure are for the fully symmetric modes. For anti-symmetric modes - of course - the translations rather than the rotations are to be restrained at edges number 3 and 4. It is worth noting that while normally constraints need only to be explicitly specified at the element edges (nodal lines) with the constraints at the nodal points (corners of elements) applied automatically through knowledge of the constraints at the adjacent edge (e.g. if one of the ad-

jacent edges is clamped the corner point will also be clamped); in this example, additional constraints are applied directly to the nodal points. Obviously, this is due to the existence of the point supports, which indicates that displacements are restrained only at the corners while the adjacent edges are left free. This is reflected in the model presented in figure (9.1) by the "*Additional Constraints*" table which specifies that the translation at corner number "2" is restrained.

Frequency parameters obtained using the above model are shown in table (9.1) for a square plate. A 24-term series solution by Reed [39] is presented for comparison with the doubly-symmetric modal frequency parameters shown in the table. Since the second of these modes exists also for the fully free plate, a comparison is made with the results of reference [40] obtained for the free plate. In addition, comparison is also made with Finite Difference results obtained by Cox and Boxer [41] using a mesh size $\Delta a = \Delta b = a/6$ for the doubly-symmetric modes. Differences of the order of 10% between the present results and those of reference [41] are shown. Judging by the rates of convergence of the results of reference [41], it is felt that most of these discrepancies are due to the Finite Difference solution.

In figure (9.2), the geometry and the Large Element model for the rectangular plate of example "2" are shown.

Table (9.1)

Vibrations of a Square Plate Point Supported at its Corners

Comparison of the frequency parameter $(\omega a^2\sqrt{\rho h/D})$ for doubly-symmetric modes. Percentage deviations based upon 48 DOF Large Element solutions. Poisson's ratio = 0.3.

Mode No.	Large Elements DOF = 48	Finite Difference 6 x 6 mesh [41]	24 term series [39]	Free Plate solution [40]
1	7.111 (0.0%)	7.050 (-0.8%)	7.12 (0.1%)	---
2	19.596 (0.0%)	17.566 (-10.6%)	19.60 (0.002%)	19.596 (0.0%)
3	44.370 (0.0%)	40.264 (-9.2%)	44.40 (0.007%)	---

Table (9.2)

Vibration of a Square Simply-Supported Plate Clamped Along Two Symmetrically Located Segments

Convergence and comparison of the frequency parameter $(\omega a^2\sqrt{\rho h/D})$ for the doubly-symmetric modes.

Mode No.	Large Elements			Ref. [42]	Ref. [43]
	DOF=54	DOF=64	DOF=65		
1	27.747	27.719	27.710	27.1*	27.31*
2	99.546	--	--	--	--
3	122.830	--	--	--	--

* These values are expected to be too low since the clamped edge conditions are only approximately satisfied.

Thanks to symmetry, two Large Elements are sufficient to represent one quarter of the plate. The problem has been solved previously by Ota and Hamada [42] and by Kurata and Odamura [43], using a simply supported plate solution with moments applied along the edges and adjusted to approximate the zero slope condition along the clamped segments. Since these solutions only approximate the clamped edge boundary conditions, the results obtained are expected to err on the flexible side. This is shown in table (9.2) where the results presented in references [41] and [43] for the fundamental frequency of a square plate, with $\ell = a/3$, are compared to those obtained using the Large Element method. Different numbers of terms are used in the Large Element solutions in order to examine the rate of convergence of the results and hence provide a feel for the accuracy obtained. It is expected that the Large Element solutions are accurate to better than 0.2%, and hence the frequencies obtained in references [42] and [43] are one to two per cent too low. The frequency parameters corresponding to the second and third doubly-symmetric modes are also shown in the table.

The mode shapes for the lowest two doubly-symmetric modes of the square plate are shown in figure (9.3). For each large element, the values of the normalized displacements are calculated at each of the corners of an 11 x 11 grid. Contours representing points of equal displacements are then plotted on a Calcomp graph plotter using linear

interpolation between the mesh points. A smoothing function is applied upon joining the interpolated points to provide the continuous contour lines shown. Finally, the contours obtained for the different elements are assembled together and photographically reduced to the size shown.

9.3 Plates with Square Holes

Despite its practical importance, very little information is available in the literature about the vibration of plates with square holes. In a recent paper by Paramasivam and Sridhar Rao [44], the Finite Difference method was first applied to this class of problems overcoming the problem of the re-entrant corners. A few months earlier, in September 1972, a new variational technique for the solution of problems involving minor modifications to simple regions was presented by Chi, Dame, and Basdekas [14], which is outlined in section (1.5). In their paper they presented an example of a simply-supported plate with a square hole. The problem, however, does not seem to be clearly stated in the paper and the solutions do not seem to show the dependence upon Poisson's ratio. Therefore, no comparison could be made with the results of reference [14].

Figure (9.4) represents the Large Element models used for simply-supported and clamped plates with square holes. Three large elements are needed in each case in

order to model one quarter of the plate with symmetry and/or anti-symmetry conditions applied at the centre lines. Two sets of results corresponding to values of Poisson's ratio of zero and 0.3 were generated and are shown in table (9.3). Finite Difference results from reference [44] are quoted for comparison. Note that only the solutions for the case of $(\nu = 0)$ were obtained in reference [44], since this results in a considerable simplification of the expressions for the boundary conditions at the edges of the opening and the re-entrant corners which were taken advantage of in deriving the expressions for the finite difference operators presented therein. No such restriction exists in the case of Large Elements, and a difference of about 15% is obtained in the fundamental frequency parameter due to a change of Poisson's ratio from zero to 0.3; thus indicating the importance of considering its true value in the approximate solution.

A comparison of the results of reference [44] with those obtained from the Large Element models shows differences of about 5% and 17% for the simply-supported and clamped plates respectively. The results published in the reference are based upon an 8 x 8 finite difference grid. In a typical case presented in the same reference, however, improvements of 4.5% and 16% over the 8 x 8 grid solutions were realized when a 16 x 16 grid was used. It may be concluded, hence, that the 5% and 16% differences shown in table (9.3) are predominantly due to the Finite Difference

Table (9.3)

Vibrations of Plates with Square Holes

Convergence of doubly-symmetric frequency parameters ($\omega^2\sqrt{\rho h/D}$) and comparison with Finite Difference results [44].

Plate Type	Method	Large Elements				Finite Differences
	Poisson's ratio	0.3	0.3	0.0	0.0	0.0
Simply Supported	DOF =	15	53	15	55	(8x8) mesh
	$\omega_1 a^2\sqrt{\rho h/D}$	23.56	23.48	26.81	26.73	25.45
	$\omega_2 a^2\sqrt{\rho h/D}$	78.13	74.27	85.89	82.17	---
clamped	DOF =	40	65	40	85	(8x8) mesh
	$\omega_1 a^2\sqrt{\rho h/D}$	65.40	65.38	68.51	68.49	57.98
	$\omega_2 a^2\sqrt{\rho h/D}$	103.83	103.44	114.24	113.84	---

discretization errors. This conclusion is also supported by the convergence of the Large Element solutions shown in the table.

Computer contour plots for the lowest two doubly-symmetric vibration modes of each case are shown in figures (9.5) and (9.6) for the simply-supported and clamped plates respectively. The plots are for Poisson's ratio of 0.3, and are produced in the manner described earlier in section (9.2).

9.4 The vibration of Continuous Plate Structures

Numerous examples for continuous plate structures are encountered in civil engineering applications. Examples of such structures are bridge decks and building floor slabs. Two simple examples which have been previously solved by other authors [45, 46] are treated here. The two examples presented in this section are:

i) A two-panel continuous *orthotropic* plate clamped along one longitudinal edge and simply-supported at the balance of the boundary.

ii) A four-panel continuous isotropic plate simply-supported along the longitudinal edges and one of the end sides, and clamped along the other end.

For an orthotropic plate, four stiffness coefficients are to be specified. Arbitrarily these coefficients are chosen to be D_x, D_y, D_k, and ν_y. If D_y is equal to D_x,

and D_k is not specified, the plate is considered to be isotropic and D_k is taken as $D_x \cdot (1-\nu_y)/2$. The numerical values for the orthotropic plate stiffness coefficients for the plate of example (i) are shown in figure (9.7) together with the large element model used for the determination of the symmetric modes. In the case of the anti-symmetric modes, however, the line of anti-symmetry represents a simply-supported edge leading to a plate with two parallel simply-supported edges. In this case, the use of a large strip approach is advantageous since it leads to separation of variables with a corresponding considerable reduction in computer time and storage requirements. The Large Strip model used for this case is shown in figure (9.8).

The natural frequencies obtained using different numbers of terms in the series for both the symmetric and anti-symmetric cases are shown in table (9.4). For comparison, results published in reference [45] obtained using the finite strip method are also quoted in the table. The number of degrees of freedom used in reference [45], was not published but is estimated to be at least 60 for both the symmetric and anti-symmetric cases. Figures (9.9a) through (9.9d) are contour plots representing the lowest four mode shapes of the plate.

The model used for example (ii) is composed of four large strips and is shown in figure (9.10). A comparison

Table (9.4)

Vibrations of an Orthotropic Two-panel Continuous Plate

Convergence of frequency parameters ($\omega a^2\sqrt{\rho h/D_y}$) and comparison with Finite Strip results [45]. $D_x=3D_y$; $D_k = 0.74\ D_y$; $\nu_{xy}=0.26$.

Mode Type	Symmetric			Anti-Symmetric		
Method of solution	Large Elements		Finite Strips	Large Strips		Finite Strips
DOF	25	35	60*	5	7	60*
Mode No.						
1	37.370	37.366	37.36	30.380	30.277	30.25
2	69.829	69.821	--	65.261	65.256	--
3	96.738	96.717	--	120.076	119.96	--

* number of degrees of freedom is estimated.

Table (9.5)

Vibrations of a four-panel continuous plate

Comparison of frequency parameters ($\omega a^2\sqrt{\rho h/D}$) with exact [46] and Finite Strip solutions [45]. %deviations from exact are given in brackets.

Mode No.	Large Strips DOF = 20	Finite Strips DOF = 26*	Exact Solution
1	20.014 (0.02%)	(0.5%)†	20.01 (0.0%)
2	22.063 (0.01%)	(2.0%)†	22.06 (0.0%)

* number of degrees of freedom is estimated

† % quoted in the text of reference [45]

of the lowest two natural frequencies with those obtained using the same number of degrees of freedom in the finite strip method [45] is shown in table (9.5). Earlier results of reference [46] are also quoted in the table for comparison. As expected, more accurate results are obtained with large strips than with finite strips for the [illegible]. The mode shapes corresponding to the lowest two eigenvalues are shown in the form of contour plots in figure (9.11).

9.5 Vibrations of Box-type Structures

A comprehensive study for the possible analytical approaches for the study of the vibrations of box structures has been given by Dickinson [47] and by Dickinson and Warburton [48]. Finite element solutions for the problem were also presented by Kendall and Warburton [49] and by Popplewell [50] in 1971. An important application of box-type structures is the study of the response of houses and - with some modifications - car body vibration analysis. In order to assess the accuracy and demonstrate the applicability of the large element method when used for the study of this type of structure, a box identical to that used in references [47], [49], and [50] is analyzed. The dimensions of the closed box to be studied are 9.6 in. x 12 in. x 14.4 in. x 0.125 in., and the material is steel of $E = 30. \times 10^6$ p.s.i. and $\rho = 0.284$ lb. per cu. in. The same assumptions employed in the three references are adopted here.

These assumptions - in addition to those generally applied in this work - are:

i) The internal acoustic back pressure can be neglected.

ii) The inplane flexibility of the box faces is negligible compared to its out-of-plane flexibility. Consequently, corner deflections are not allowed.

iii) The box common edges are free to rotate such that adjacent plate edges remain at right angles.

While, generally speaking, a box is a three-dimensional structure with the elements representing the different faces lying in different planes (thus requiring coordinate transformations to be applied between the element local coordinate system and the global system of the structure); coordinate transformations can be avoided by developing the box faces into a planar form as shown in figure (9.12). Certain "additional constraint" relationships have to be applied in this case in order to ensure matching the degrees of freedom along the common edges as shown in the figure. It is to be noticed that symmetry conditions about three planes are utilized in order to allow the analysis of only one eighth of the box using three large elements. The table of constraints shown in the figure corresponds to the fully symmetric condition. In all, eight combinations of symmetry conditions can be conceived, but only two were studied in this work.

While the first two of the "additional constraints" listed in figure (9.12) are obvious (due to continuity of

slopes), the third condition is not. The necessity of this condition can be proven as follows:

The first constraint condition may be written as

$$\left.\frac{\partial W}{\partial X}\right|\Big|_{\text{edge No. 2}} = -\left.\frac{\partial W}{\partial Y}\right|\Big|_{\text{edge No. 8}}$$

Since this condition is applicable identically along the common edge, it also implies that

$$\left.\frac{\partial}{\partial Y}\left(\frac{\partial W}{\partial X}\right)\right|\Big|_{\text{edge No. 2}} = -\left.\frac{\partial}{\partial Y}\left(\frac{\partial W}{\partial Y}\right)\right|\Big|_{\text{edge No. 8}}$$

Since this condition is applicable along the common edge, including the corner point (No. 3), it follows that

$$\left.\frac{\partial^2 W}{\partial Y \partial X}\right|\Big|_{\text{at point 3}} = -\left.\frac{\partial^2 W}{\partial X \partial Y}\right|\Big|_{\text{at point 3}}$$

which can only be satisfied if condition (3) of figure (9.12) is satisfied.

Table (9.6) shows a comparison of some of the frequencies of the box under consideration as computed using the large element method with those of references [47], [49], and [50]. The percentage differences shown in the table are based upon the results obtained by Dickinson in reference [47]. Those results were shown to converge monotonically from the flexible side, and hence are expected to compose lower bounds for the true frequencies. Since all of the other results are higher bounds, the per-

Table (9.6)

Vibrations of a Closed Box.

Comparison of natural frequencies (Hz) with 3-degrees of freedom per node [49] and 4-degrees of freedom per node [50] Finite Element solutions, and with series solutions (lower bounds) of reference [47]. % deviations are based upon the series solution of [47]. Box dimensions are 9.6" x 12" x 14.4" x 0.125". $E = 30 \times 10^6$ psi; and $\rho = 0.284$ lb/cu.in.

Mode No.	Symmetry† in x, y, z directions		3-DOF Finite Elements [49] total DOF ≥ 30	4-DOF Finite Elements [50] 6 DOF	4-DOF Finite Elements [50] 36 DOF	Large Elements 36 DOF	Series Solution [47]
1	S,S,S	Hz		183.2	179.7	179.48	179.35
		%	2.8	2.1	0.20	.07	0.0
4	S,S,S	Hz		277.3	272.9	272.49	272.32
		%	2.4	2.0	0.21	.06	0.0
6	S,S,S	Hz		342.8	334.0	333.44	333.25
		%	2.7	2.9	0.23	0.06	0.0
9	A,S,A	Hz		480.3	439.0	437.14	436.68
		%	4.4	9.9	.53	.11	0.0
14	A,S,A	Hz		693.8	580.8	577.06	576.51
		%	4.3	20.2	.74	0.10	0.0

† S = Symmetric; A = Anti-symmetric.

centage differences shown in the table are conservative estimates for the true errors contained in the different types of solution. It can be noted that, in general, the errors corresponding to the three-parameter finite element solutions are an order of magnitude larger than those of the four parameter elements. Indeed, those of the four parameter finite elements are, in turn, an order of magnitude larger than those corresponding to the large element solutions. Noticing that the percentage differences between the large element solutions and the series solutions of reference [47] are of the same order as the expected accuracy of the series solutions themselves, the comparison of the relative accuracy of the different solutions favours the large element approach even more. It is important to note that the comparison is based upon comparable numbers of total degrees of freedom.

9.6 The Buckling of Short Thin-walled Columns

To the author's knowledge, no data is available in the literature about the stability of thin-walled columns for which the height to width ratio is not very large. Buckling loads were established independent of this ratio, assuming it to be "sufficiently large". In addition, the assumption of a very long column led to the solutions being independent of the column end conditions, and hence allowed separation of variables, assuming the displacements to vary

4 6

OF/DE

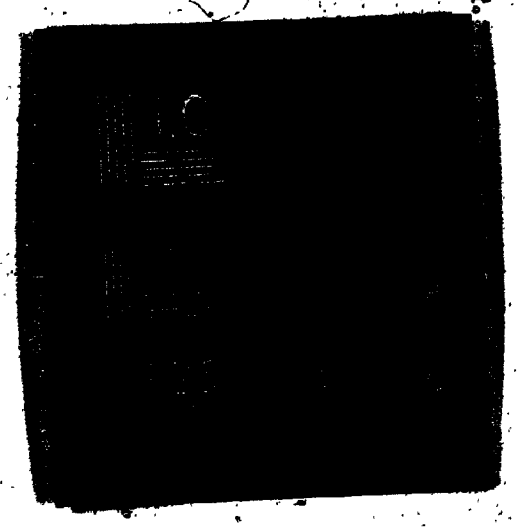

sinusoidally in the longitudinal direction. In the absence of such an assumption, i.e. if the column height to width ratio is not large enough, the buckling loads become a function of that ratio and, more important still, dependent upon the boundary conditions at the column ends. The study of the stability of such a short column will be the subject of this section.

The contribution of the inplane loads acting in the mid-surface of a plate element, undergoing an out-of-plane displacement, to the strain energy of the plate element, may be written as:

$$d(\Delta E) = N_x \left(\frac{\partial W}{\partial x}\right)^2 + N_y \left(\frac{\partial W}{\partial y}\right)^2 + 2N_{xy} \cdot \frac{\partial W}{\partial x} \cdot \frac{\partial W}{\partial y} .$$

Consequently, the total energy contribution to a large element's strain energy may be obtained by integrating this quantity over the area of the large element, yielding:

$$\Delta E = \int_0^b \int_0^a \left[N_x \left(\frac{\partial W}{\partial x}\right)^2 + N_y \left(\frac{\partial W}{\partial y}\right)^2 + 2N_{xy} \cdot \frac{\partial W}{\partial x} \cdot \frac{\partial W}{\partial y}\right] dx \cdot dy . \quad (9.1)$$

Upon applying the Ritz variational procedure as described in section (7.2) in association with the vibration of a plate element, the following matrix equation finally arises:

$$\left([K^{i,j}] + [KD^{i,j}] - \omega^2 [M^{i,j}]\right) \cdot \{A\} = 0. \quad (9.2)$$

In this equation, the additional matrix $[KD^{i,j}]$ is the well known element "differential stiffness matrix" arising from the added energy contribution ΔE defined in equation (9.1)

above. Apart from this matrix, equation (9.8) is identical to equation (7.14), which represents the vibration of a plate element free from inplane loads. It can be easily verified that the differential stiffness matrix may be given by:

$$KD^{i,j}_{kl,rs} = \int_0^b \int_0^a \{N_x \cdot (\phi_k' \cdot \phi_l)(\phi_r' \cdot \phi_s) + N_y \cdot (\phi_k \cdot \phi_l')(\phi_r \cdot \phi_s') + N_{xy}[(\phi_k' \cdot \phi_l)(\phi_r \cdot \phi_s') + (\phi_k \cdot \phi_l')(\phi_r' \cdot \phi_l)]\} \, dx \cdot dy. \qquad (9.3)$$

In the most general case, the above integral can be evaluated numerically if the stress fields N_x, N_y and N_{xy} are defined over the plate area. An alternate procedure is to expand the stress fields in the form of a double series in terms of the same functions $\phi(x)$ and $\phi(y)$ and/or their derivatives, and to proceed in the same way as was done in the case of the simple plates of Chapter V. In this section, in order to simplify the integration, the investigation will be limited to the special case of a uniform uniaxial compressive stress $(-\bar{\sigma}y.h_{ij})$ acting on each plate element, where h_{ij} is the thickness of the element (i,j). Equation (9.3) then simplifies to

$$KD^{i,j}_{kl,rs} = -\bar{\sigma}y \, h_{ij} \int_0^b \int_0^a [(\phi_k \cdot \phi_r)(\phi_l' \cdot \phi_s')] \, dx \cdot dy,$$

$$= -\bar{\sigma}y \cdot (h_{ij} \, a_i/b_j) \cdot B_{k,r} \cdot E_{l,s}, \qquad (9.4).$$

where the integral coefficients $B_{k,r}$ and $E_{l,s}$ are the same

as defined by equations *(7.11)* and *(7.16)* respectively, and are tabulated in Appendix II .

With the matrix $[KD^{i,j}]$ on hand, equation *(9.2)* can then be used to investigate both the vibration and the buckling of the structure. If only buckling is of interest, the frequency ω is set to zero, and hence the mass matrix may be dropped. Equation *(9.2)* can then be written as:

$$([K^{i,j}] - \bar{\sigma}y\ [\overline{KD}^{i,j}]) \cdot \{A\} = 0 \qquad (9.5)$$

where the coefficients of $[\overline{KD}^{i,j}]$ are given by

$$\overline{KD}\ {}^{i,j}_{k\ell,rs} = (h_{ij} \cdot a_i/b_j) \cdot B_{k,r} \cdot E_{\ell,s} \cdot \qquad (9.6)$$

Equation *(9.5)* is of the standard eigenvalue form, the solution of which yields the eigenvalues $\bar{\sigma}y$ - or the critical stresses - and the buckling modes as its eigenfunctions.

Figure (9.13a) shows the *I*-column under consideration. Both ends of the column are bolted to heavy gusset plates which are considered rigid. The edges thus are considered clamped with respect to the out-of-plane motion. It is assumed, however, that the lateral motion of the edges is *not* restrained while the vertical motion (warping) is completely hindered by the rigid gussets. As a result, a state of uniform uniaxial stress(σy) is admissible in both the web and the flanges. In order to reduce the number of parameters to be varied, a typical standard *I*-column cross-

section is considered for which $b = a/2$, and $t_f = 1.5\ t_w$ as shown in figure (9.13b).

Use is made of the existence of three planes of symmetry in order to permit analysing only one-eighth of the structure using two large elements. From considerations of the geometry of the section, the buckling mode will - in general - take the form shown in figure (9.13b) irrespective of the column height or cross-section dimensions. Consequently, only symmetry about the X-X axis and anti-symmetry about the Y-Y axis were considered, while both symmetry and anti-symmetry conditions about the horizontal centroidal plane were taken into account. Element [II] - see figure (9.13a) - is taken to possess only half the bending stiffness of the web (D_w), as well as half its thickness (t_w) which means that it is carrying only half the compressive force in the web $(\sigma y \times t_w)$.

The table accompanying figure (9.13) shows the non-dimensional buckling loads obtained for columns of different height to width ratios (H/a). The results are compared with those obtained by treating the web as a fully clamped plate. The figure corresponding to (H/a) equals infinity is that published in the literature [51] for long columns. It can be seen that assuming the web to be completely clamped overestimates the buckling loads by more than 12%. Even larger errors (however, on the conservative side) are obtained if the results for a long column were used for a column of an (H/a) ratio equal to, or less than, two.

Contour lines representing the buckling modes for the three columns considered are shown in figures (9.14) through (9.18). Both the lowest symmetrical and anti-symmetrical modes are shown for the columns of height ratios 2 and 3 since the corresponding buckling loads are very close.

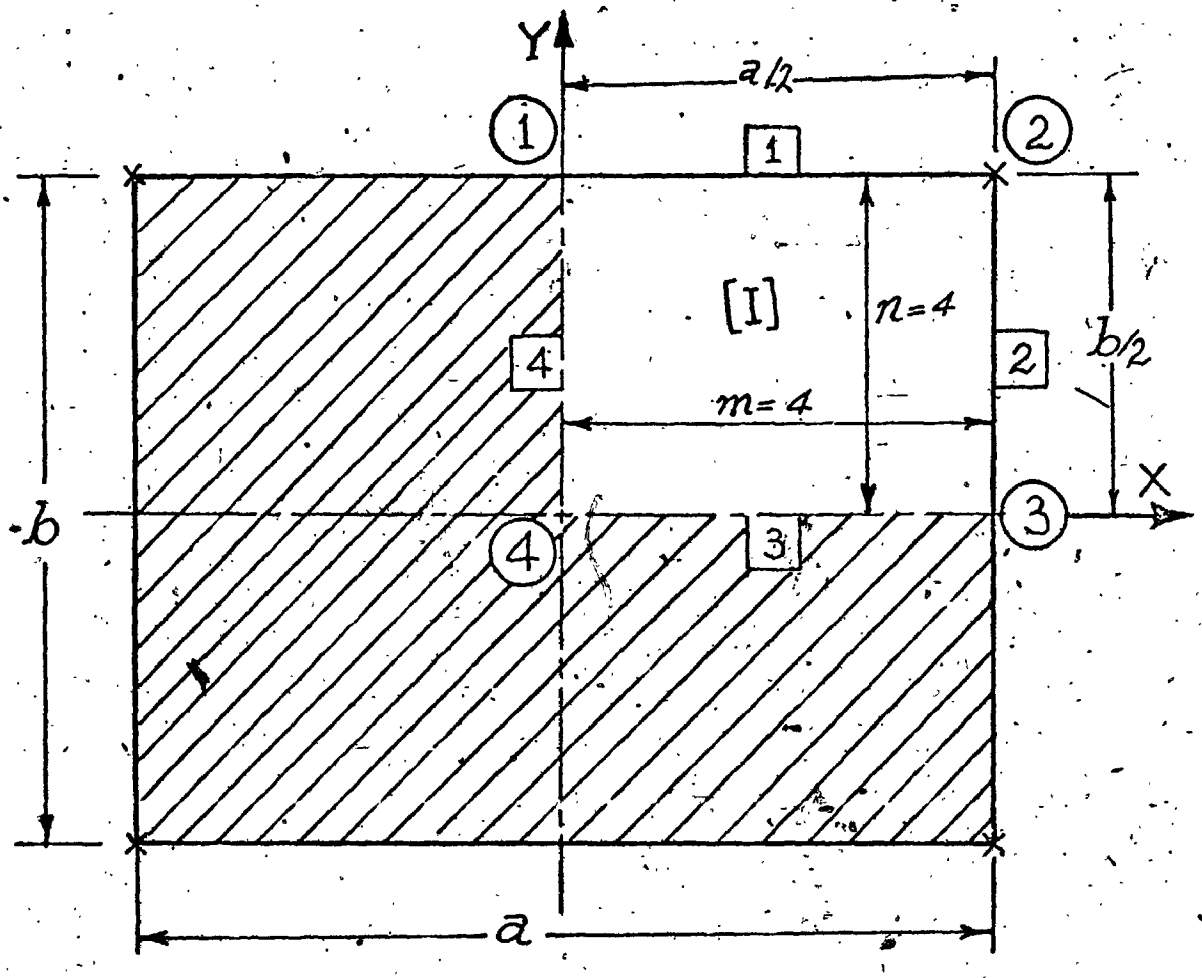

Stiffness

$\nu = 0.3$

$D_x = D_y = D$

(Isotropic)

Constraints

Edge No.	Type of Constraints
3	rotat.
4	rotat.

Additional Constraints

node No.	Type of constraint
2	Trans.

Total DOF = 48

Fig. (9.1)

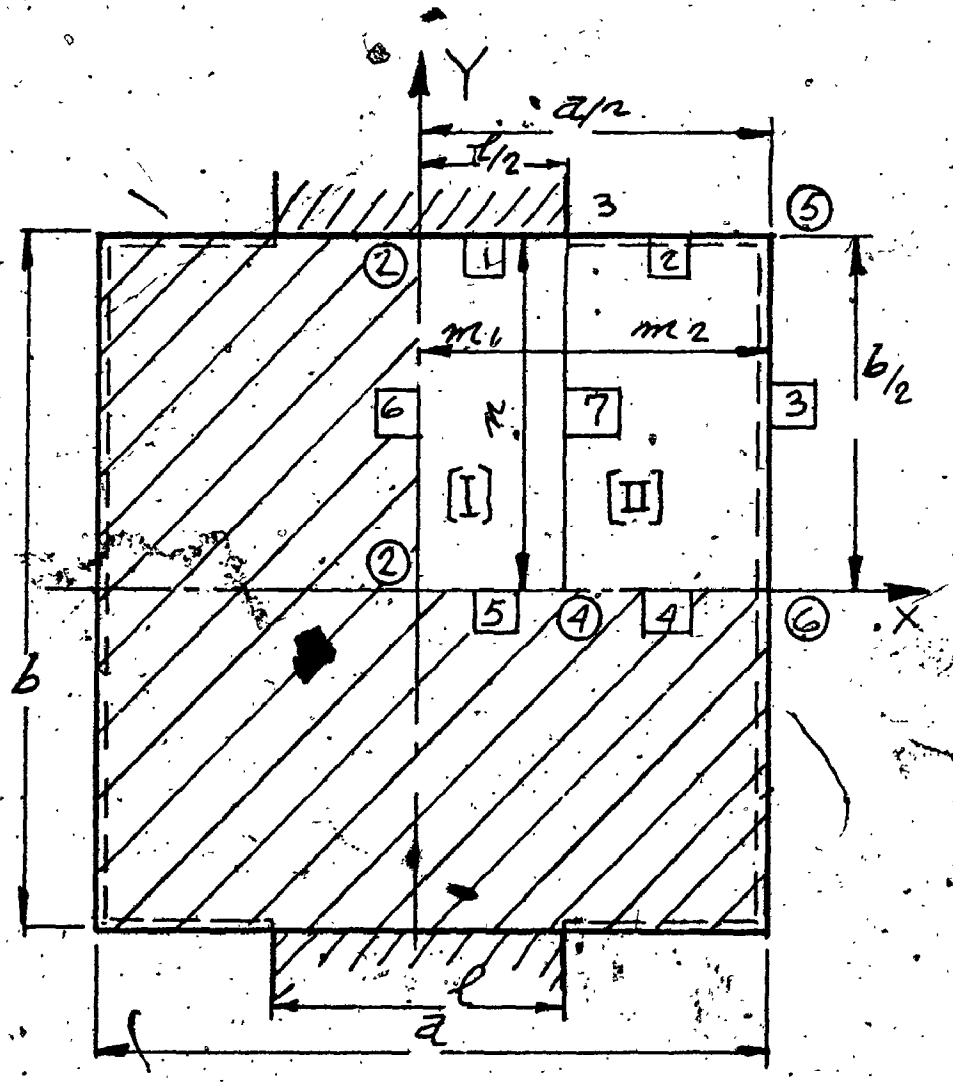

Stiffness

$\nu = 0.3$

$D_x = D_y = D$

(Isotropic)

Constraints

Edge No.	Type of Constraints
1	r, t
2	t
3	t
4	r
5	r
6	r

Fig. (9.2)

FIG. (9.3)

PLATE CLAMPED AT TWO SEGMENTS

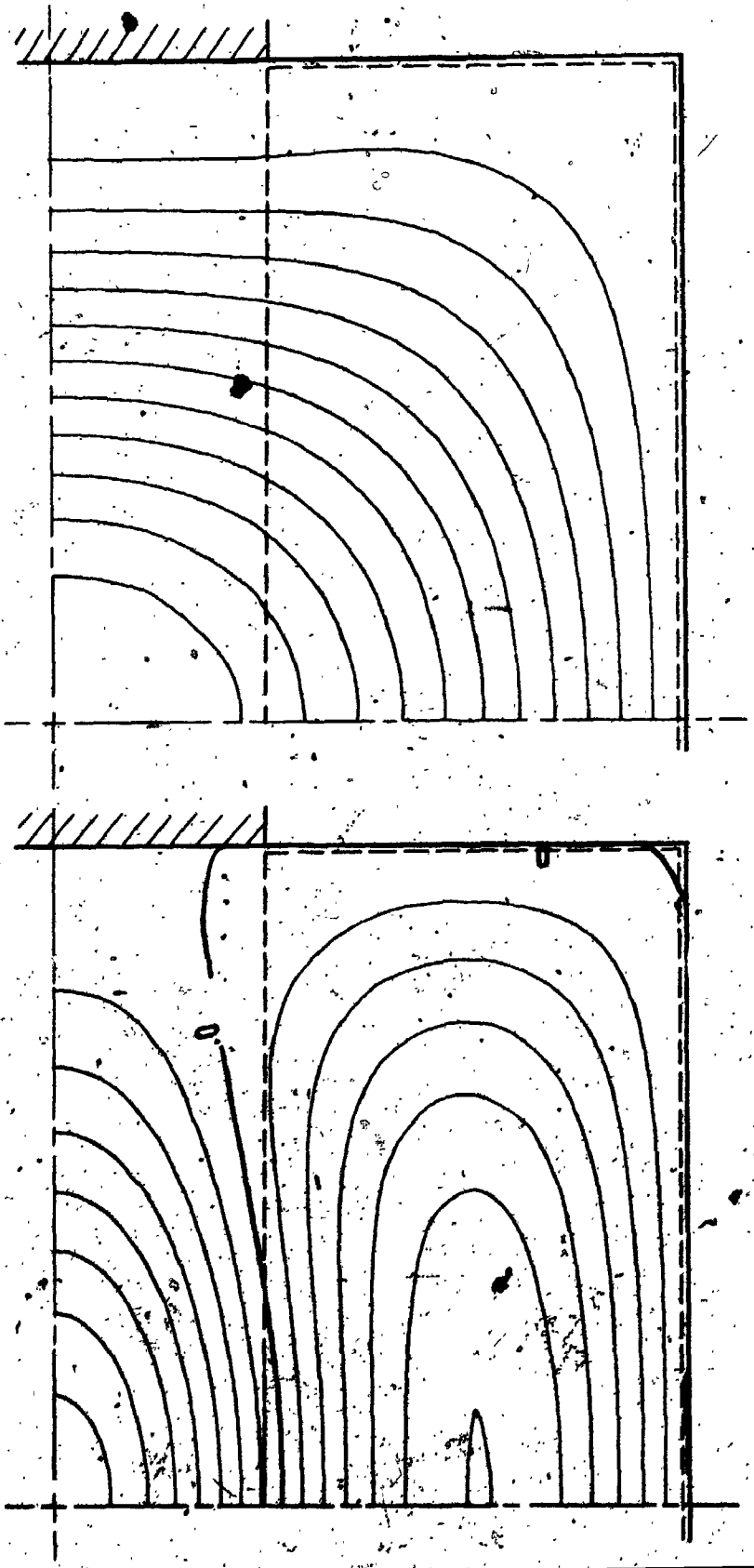

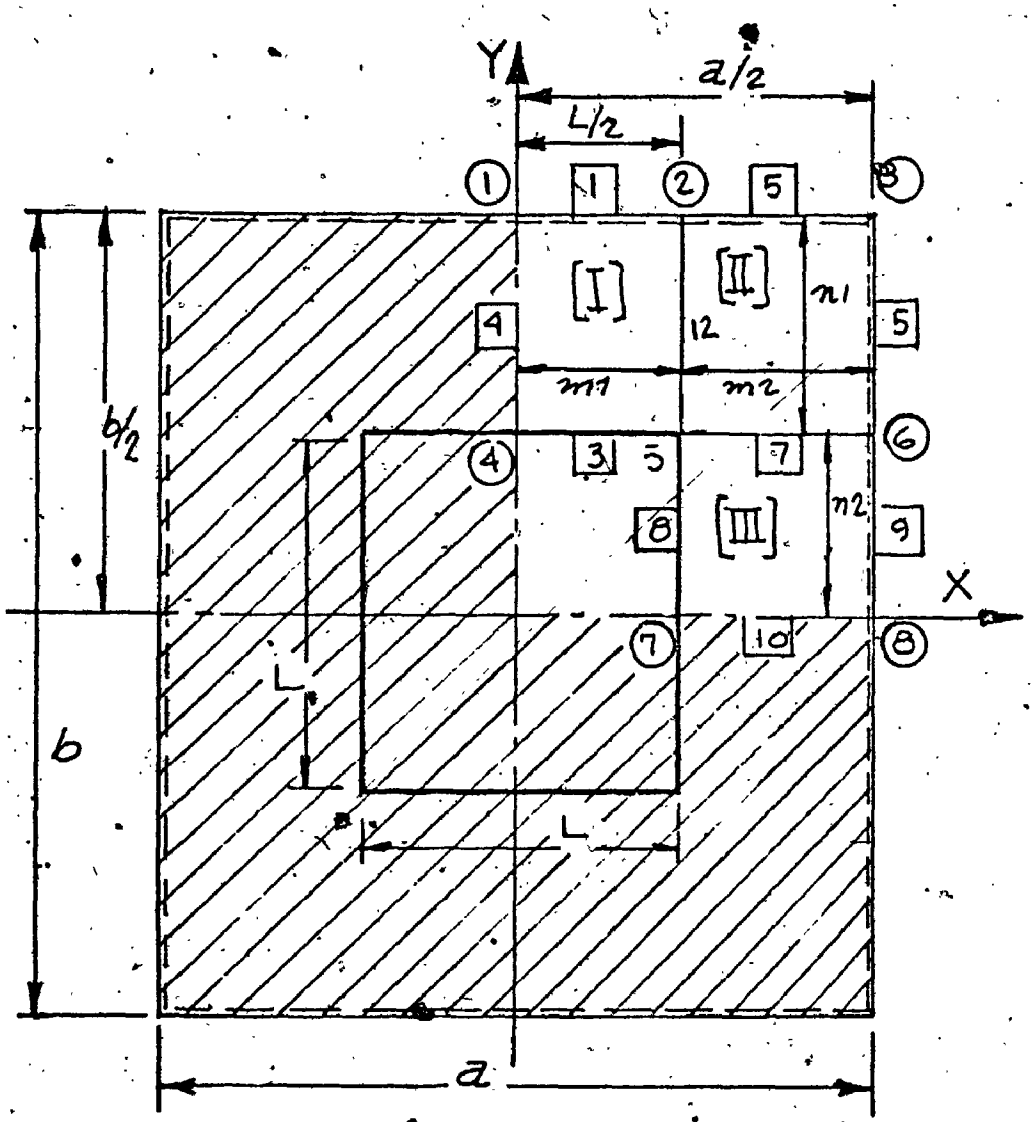

Stiffness

$\nu = 0$ and 0.3

$D_x = D_y = D$

(Isotropic)

Constraints

Edge No.	Type of Constraint
1	t^*
4	r^*
5	t
6	t
9	t
10	r

Fig. (9.4a)

---

* t = translation, r = rotation.

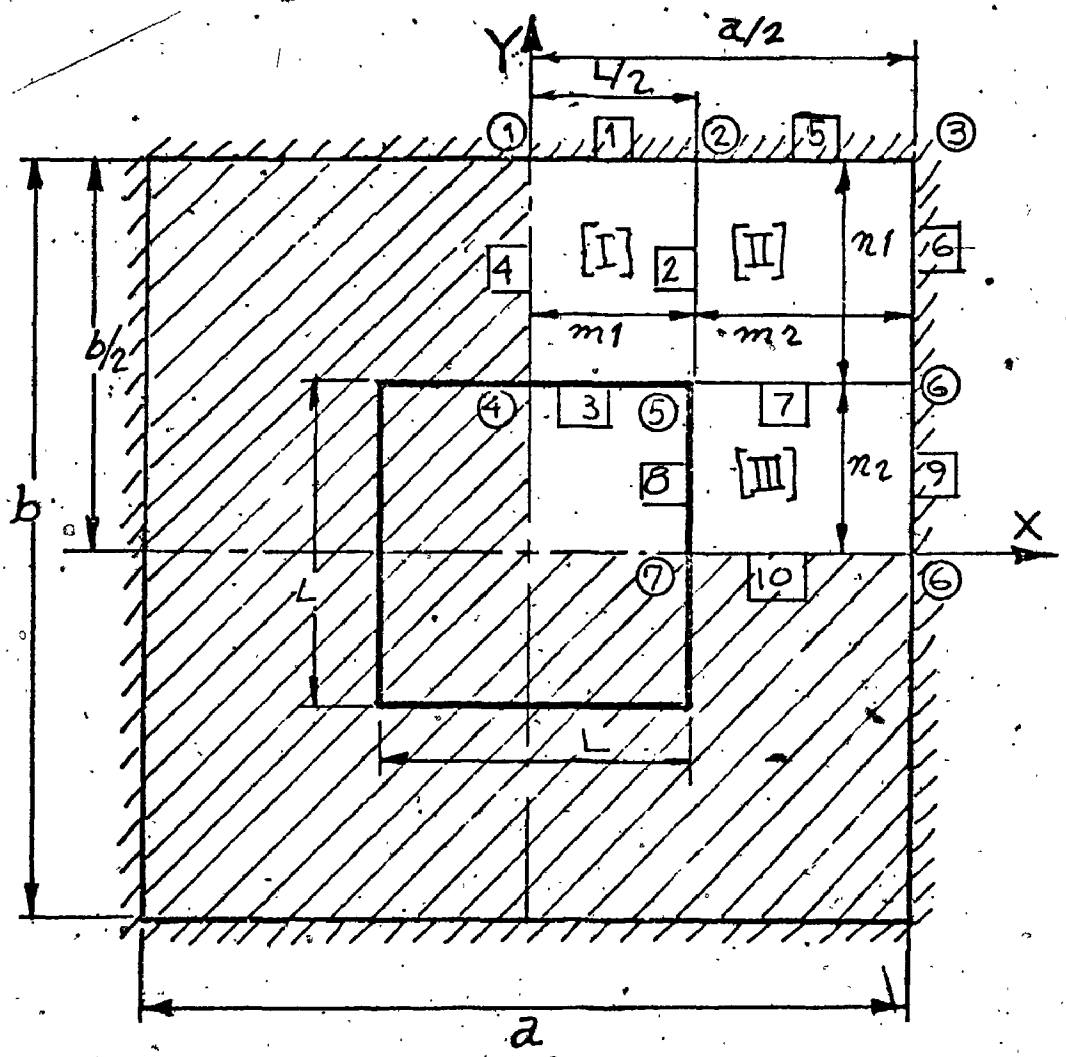

Stiffness

$\nu = 0$ and 0.3

$D_x = D_y = D$

(Isotropic)

Constraints

Edge No.	Type of Constraint
1	t^*, r^*
4	r
5	t, r
6	t, r
9	t, r
10	r

Fig. (9.4b)

* t = translation, r = rotation

FIG (9.5)

SIMP. SUPP. PLATE WITH SQUARE HOLE

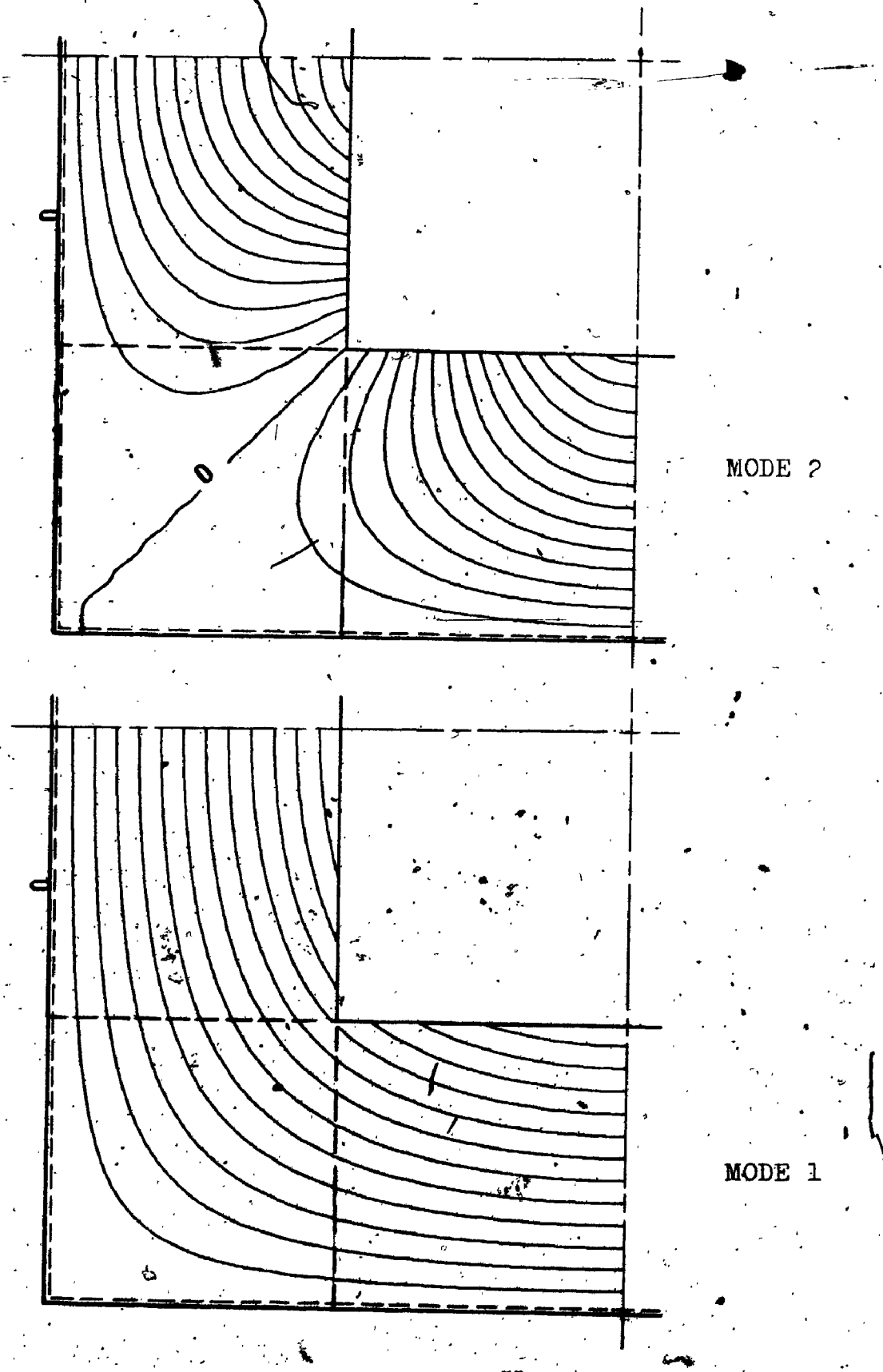

FIG. (9.6)

CLAMPED PLATE WITH A SQUARE HOLE

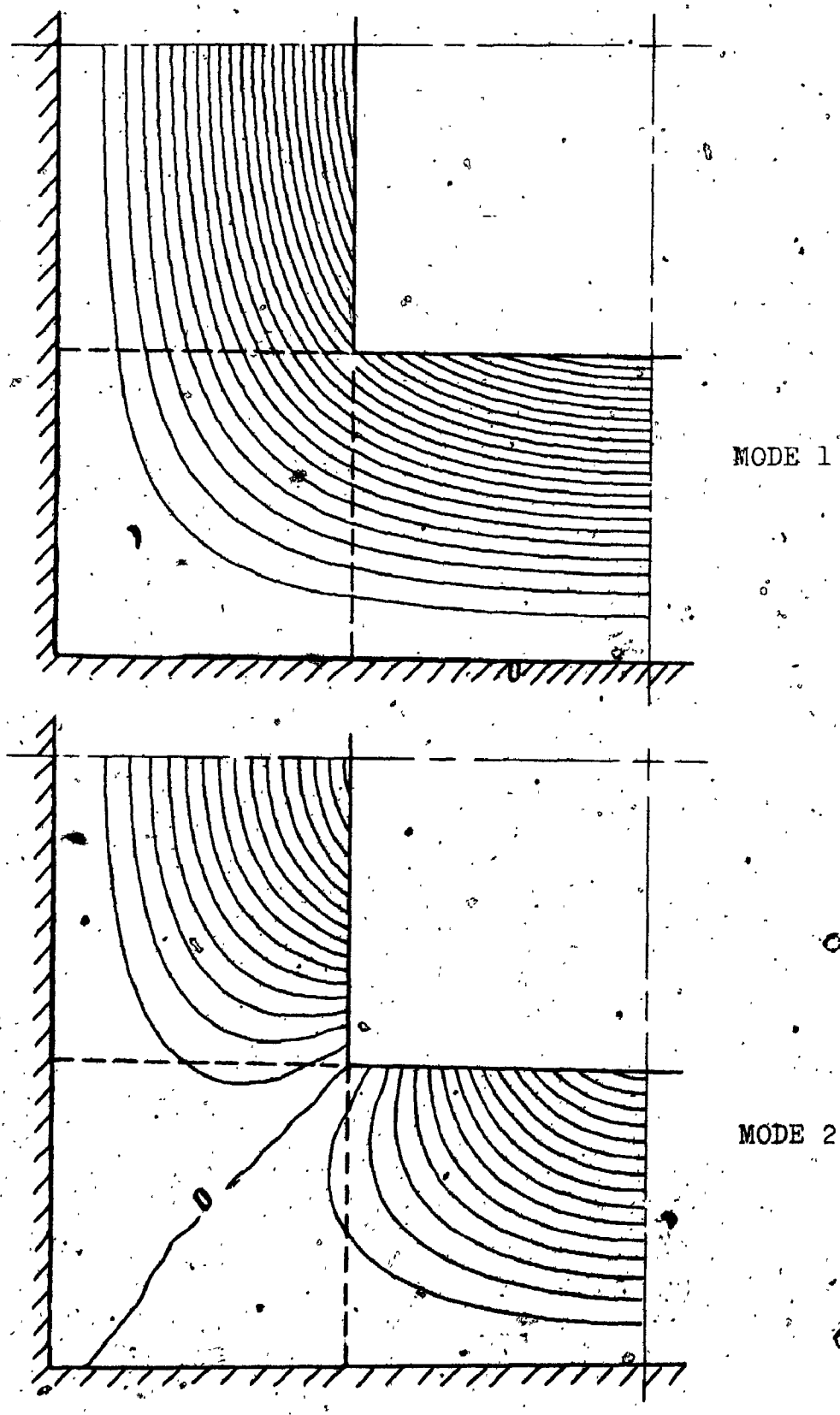

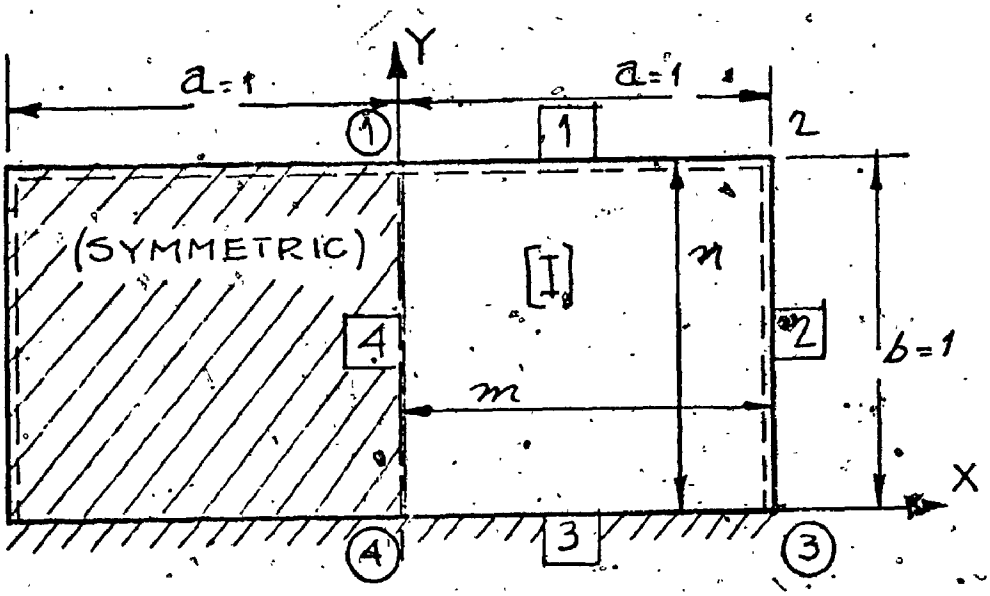

Stiffness

$D_x = 3$
$D_y = 1$
$D_k = 0.74$
$\nu_x = 0.26$

Constraints

Edge. No.	Type of Constraint
1	t
2	t
3	r, t
4	r, t

Fig. (9.7)

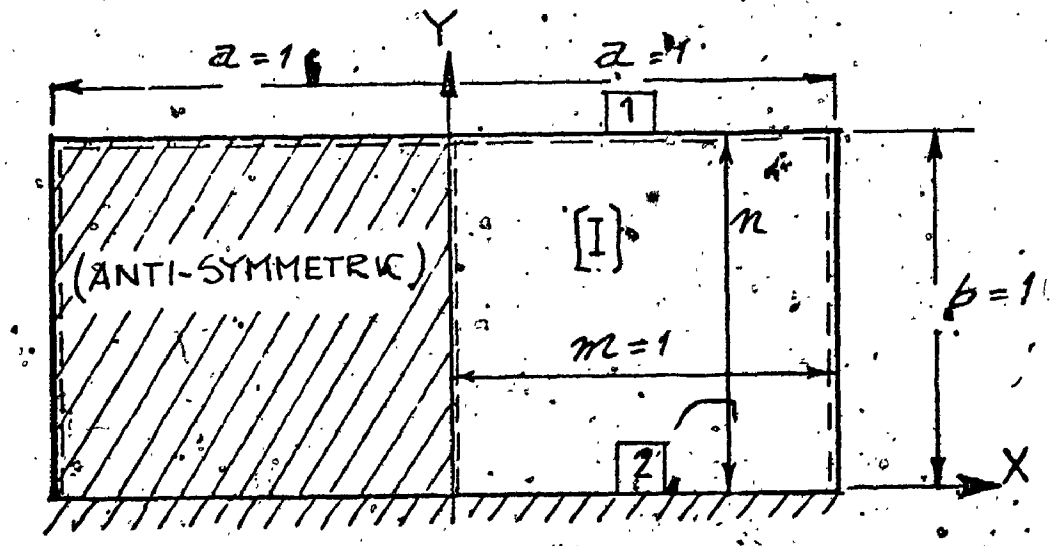

Stiffness

$D_x = 3$
$D_y = 1$
$D_k = 0.74$
$\nu_x = 0.26$

Constraints

Edge No.	Type of Constraint
1	t
2	r, t

Fig. (9.8)

FIG. (9.9A)

TWO PANEL ORTHOTROPIC PLATE — MODE SHAPE No. 1

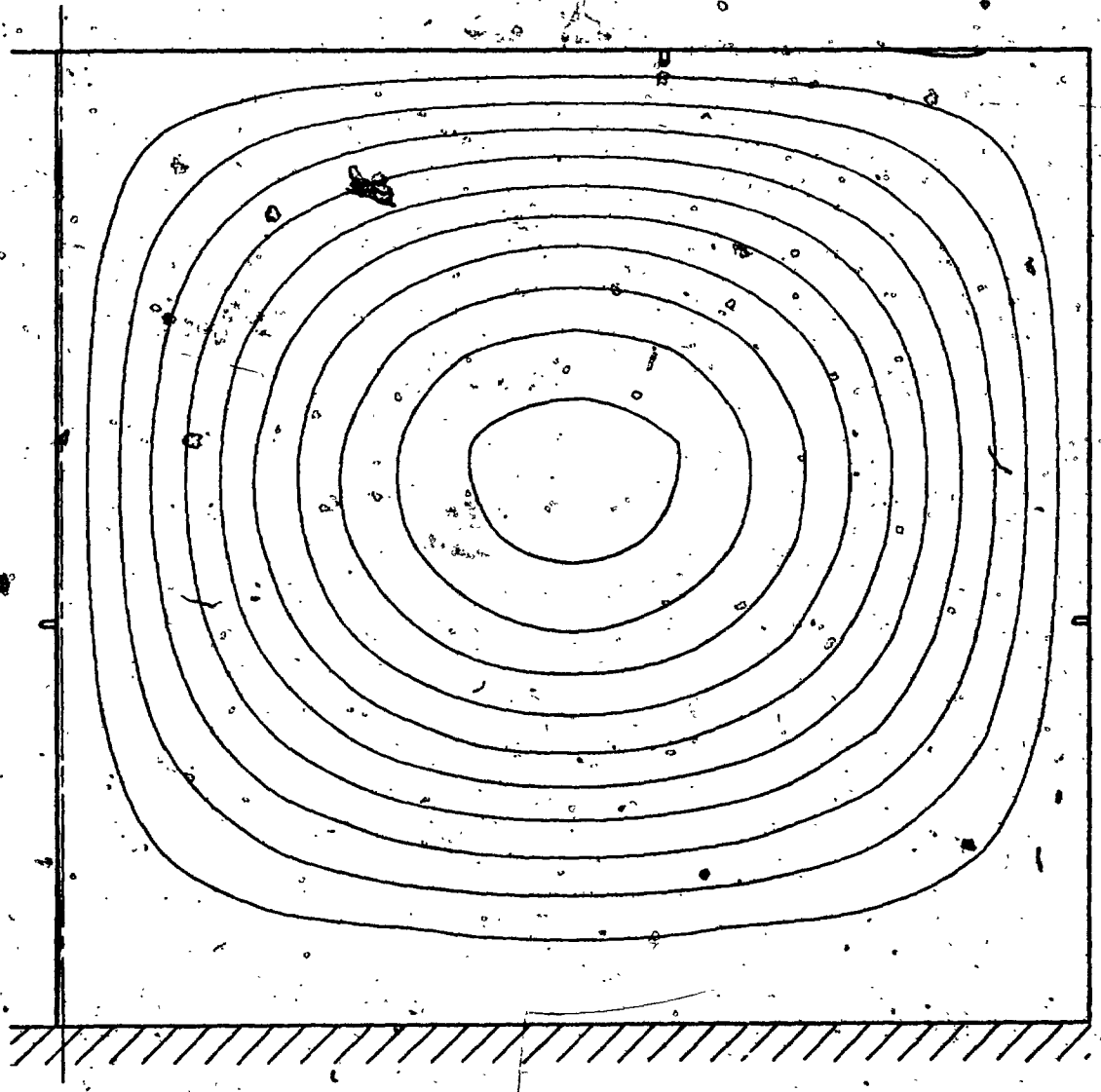

ASYMMETRIC

FIG. (9.9B)

TWO PANEL ORTHOTROPIC PLATE

MODE SHAPE No. 2

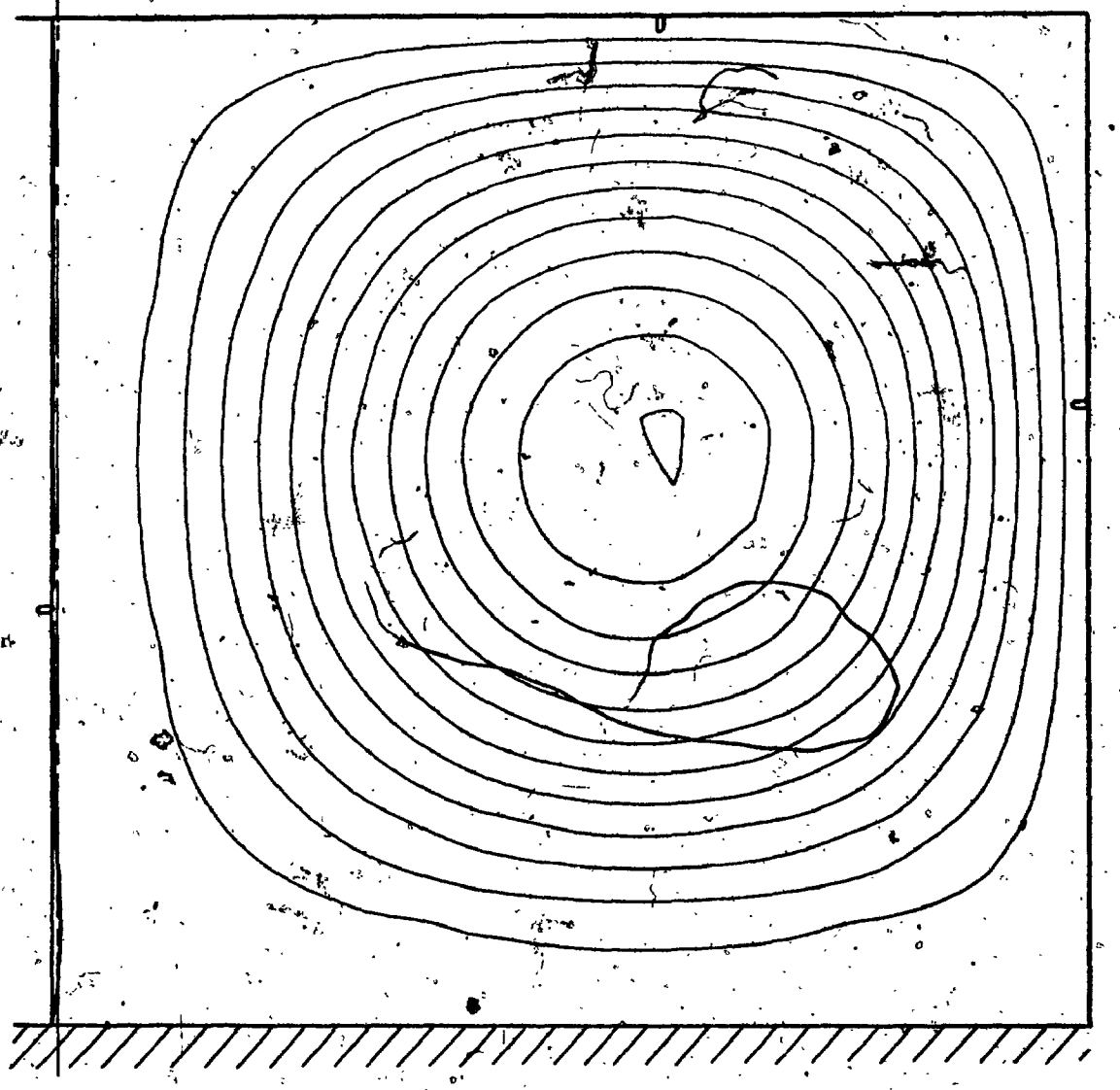

FIG. (9.9C)

TWO PANEL ORTHOTROPIC PLATE

MODE SHAPE No. 3

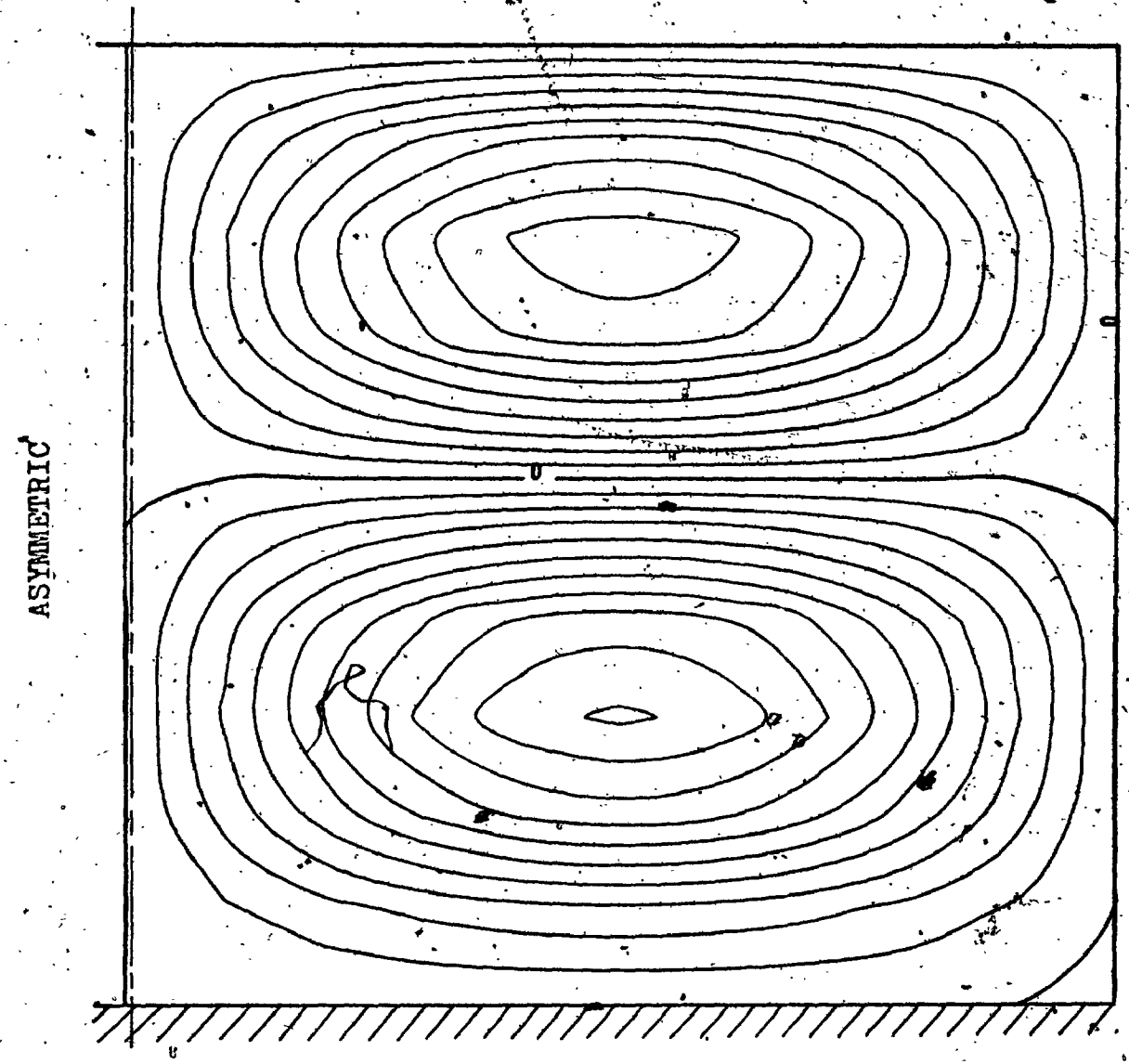

FIG. (9.9D)

TWO PANEL ORTHOTROPIC PLATE

MODE SHAPE No. 4

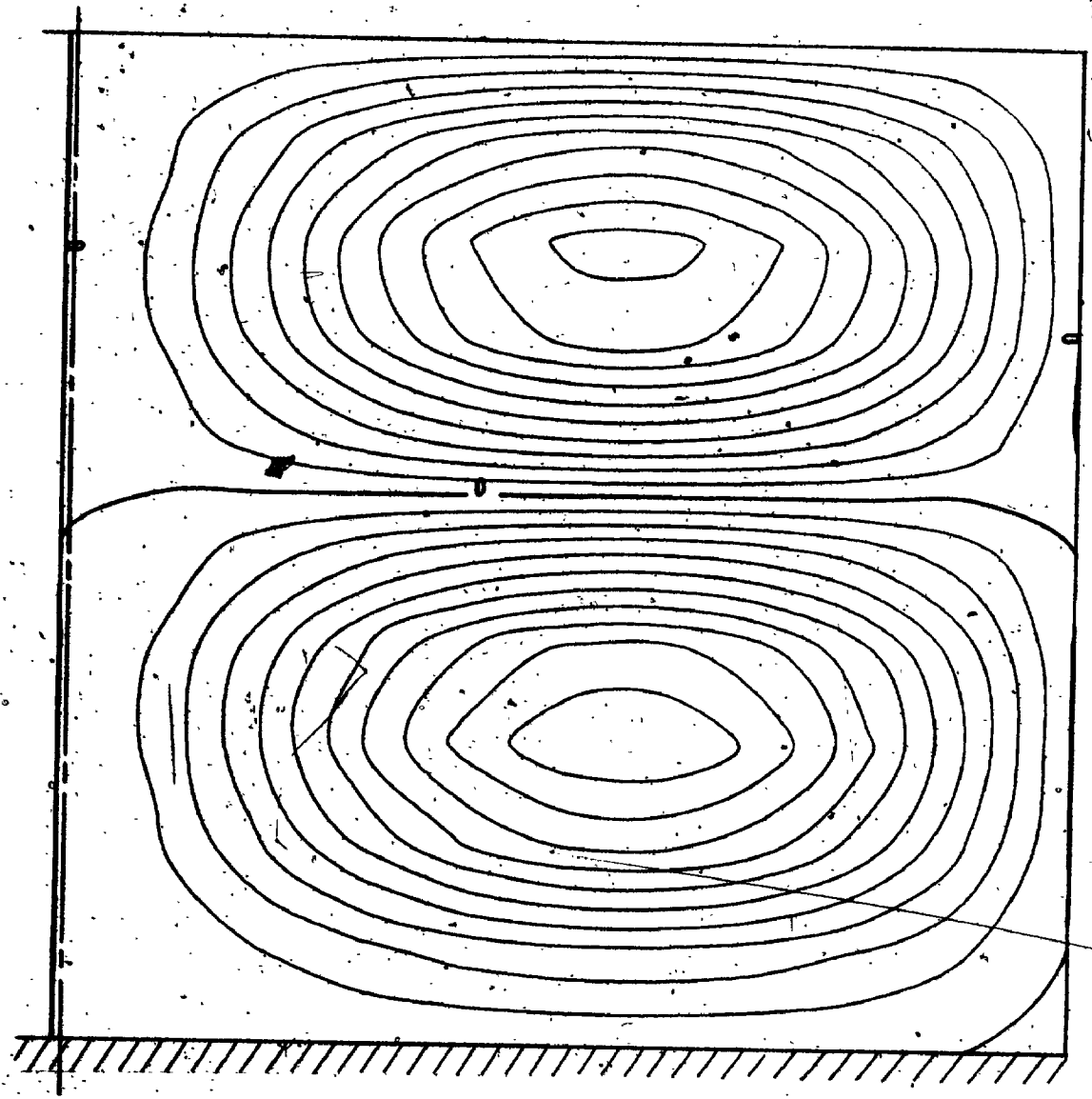

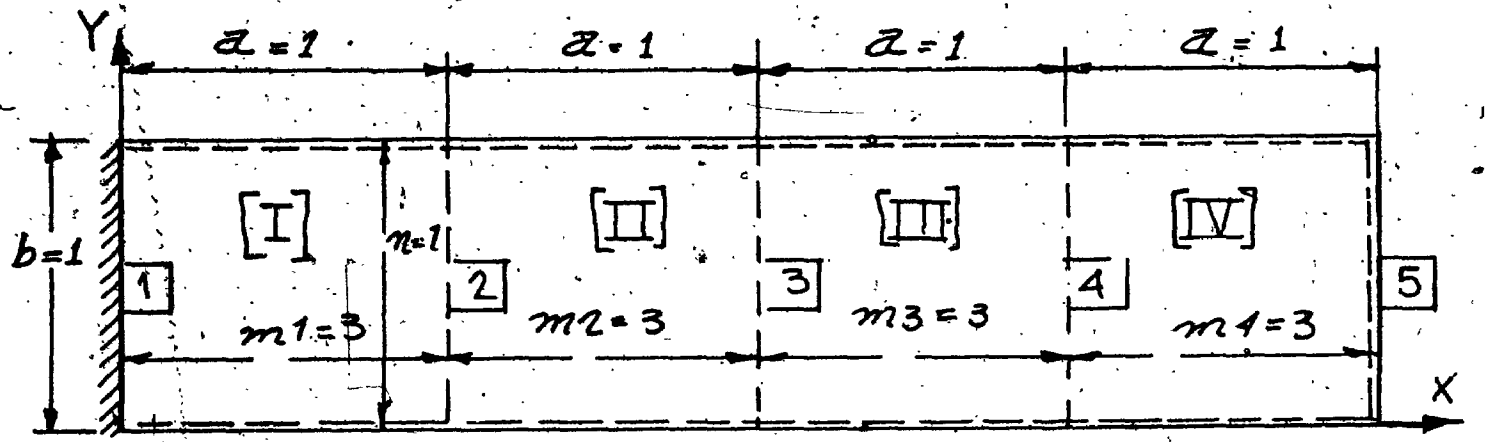

Stiffness

$\nu_x = \nu_y = 0.3$

$D_x = D_y = 1$

(Isotropic)

Constraints

Edge No.	Type of Constraint
1	t, r
2	t
3	t
4	t
5	t

Fig. (9.10)

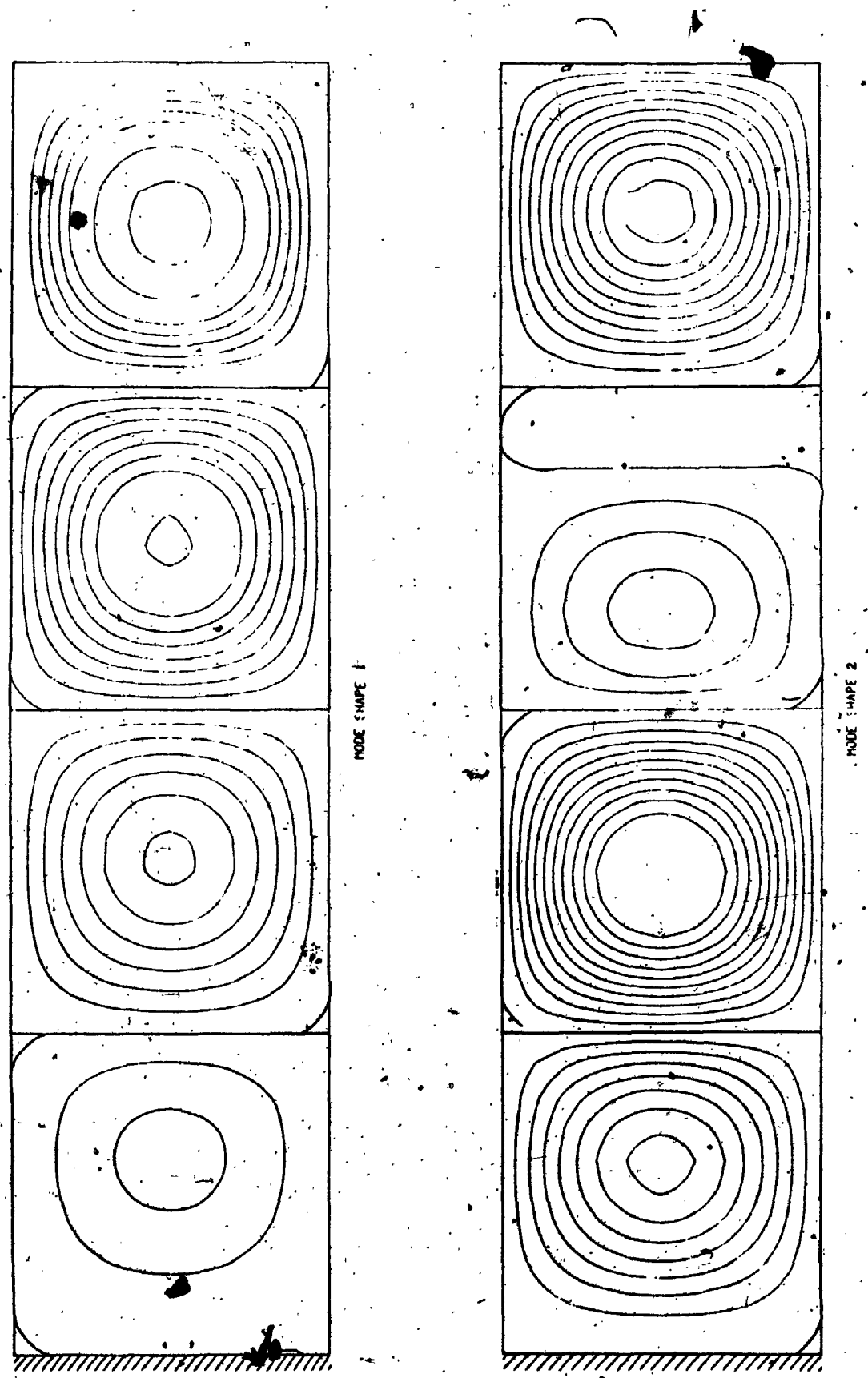

FIG. (9-11)
FOUR PANEL CONTINUOUS PLATE

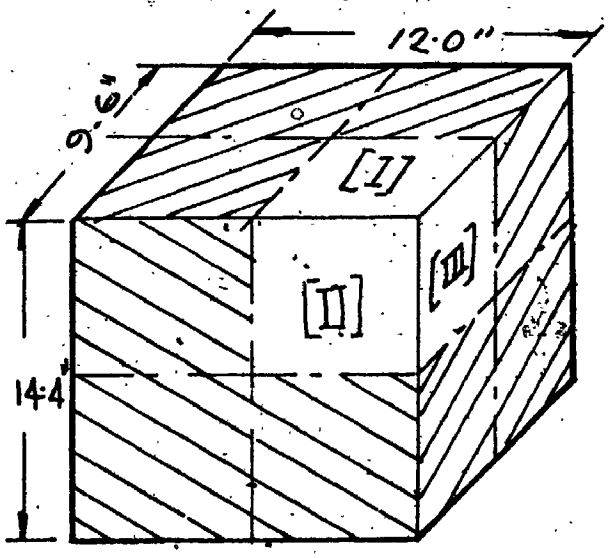

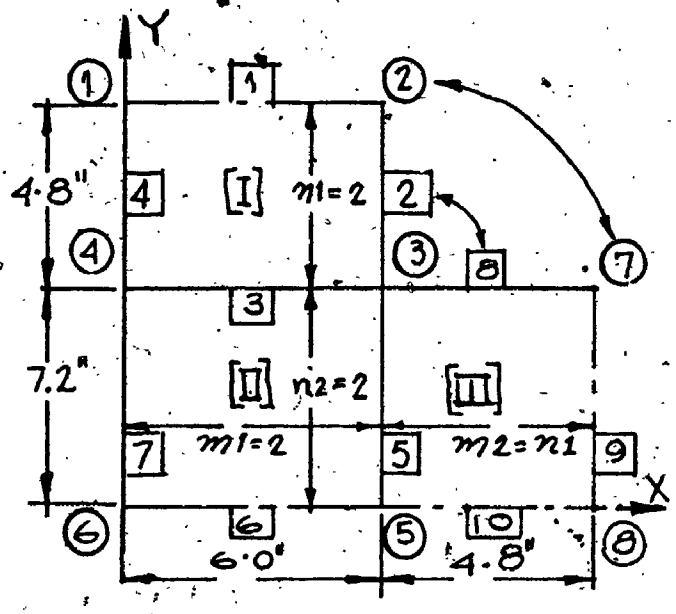

Stiffness

$\nu_x = \nu_y = 0.3$

$D_x = D_y = 30 \times 10^6 \times (0.115)^3/12$

(Isotropic)

Additional Constraints

(1) rot. at edge No. 2 $(\partial W/\partial X)$ = -rot. at edge No. 8 $(\partial W/\partial Y)$

(2) rot. at corner No. 2 $(\partial W/\partial X)$ = -rot. at corner No. 7 $(\partial W/\partial Y)$

(3) twisting at corner No. 3 $(\partial^2 W/\partial X \partial Y) = 0$

Constraints

Edge No.	Type of Constraint
1	r*
2	t*
3	t
4	r
5	t
6	r
7	r
8	t
9	r
10	r

Fig. (9.12)

---

* t = translation, r = rotation

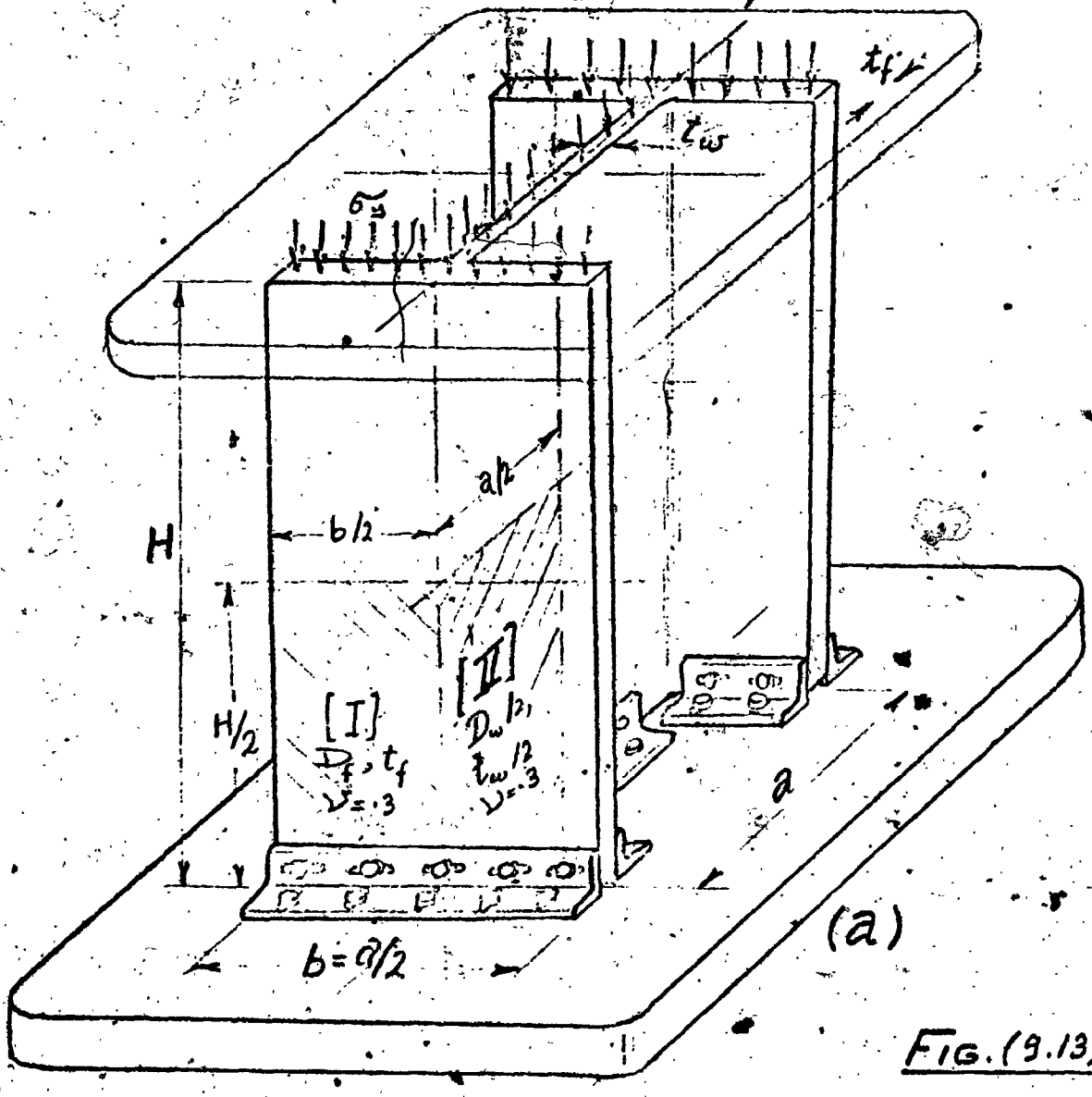

FIG. (9.13).

$$K = \sigma_{crit} \cdot t_w \cdot a^2 / D_w$$

H/a	I-Section		Clamped Plate
	Symm.	Antti-Sym.	
1	88.93	—	99.6
2	70.77	69.56	78.2
3	65.36	65.25	73.5
∞	61.2	61.2	68.8

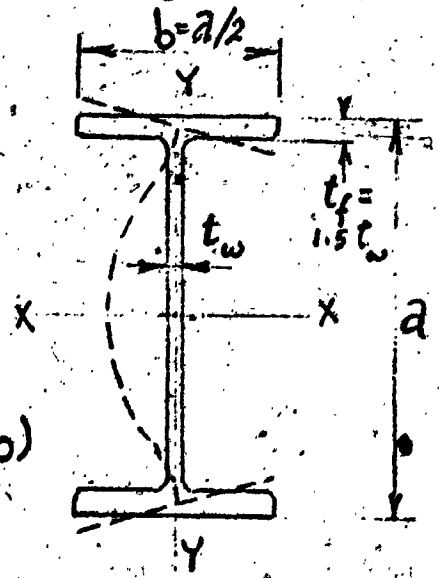

FIG. (9.14)

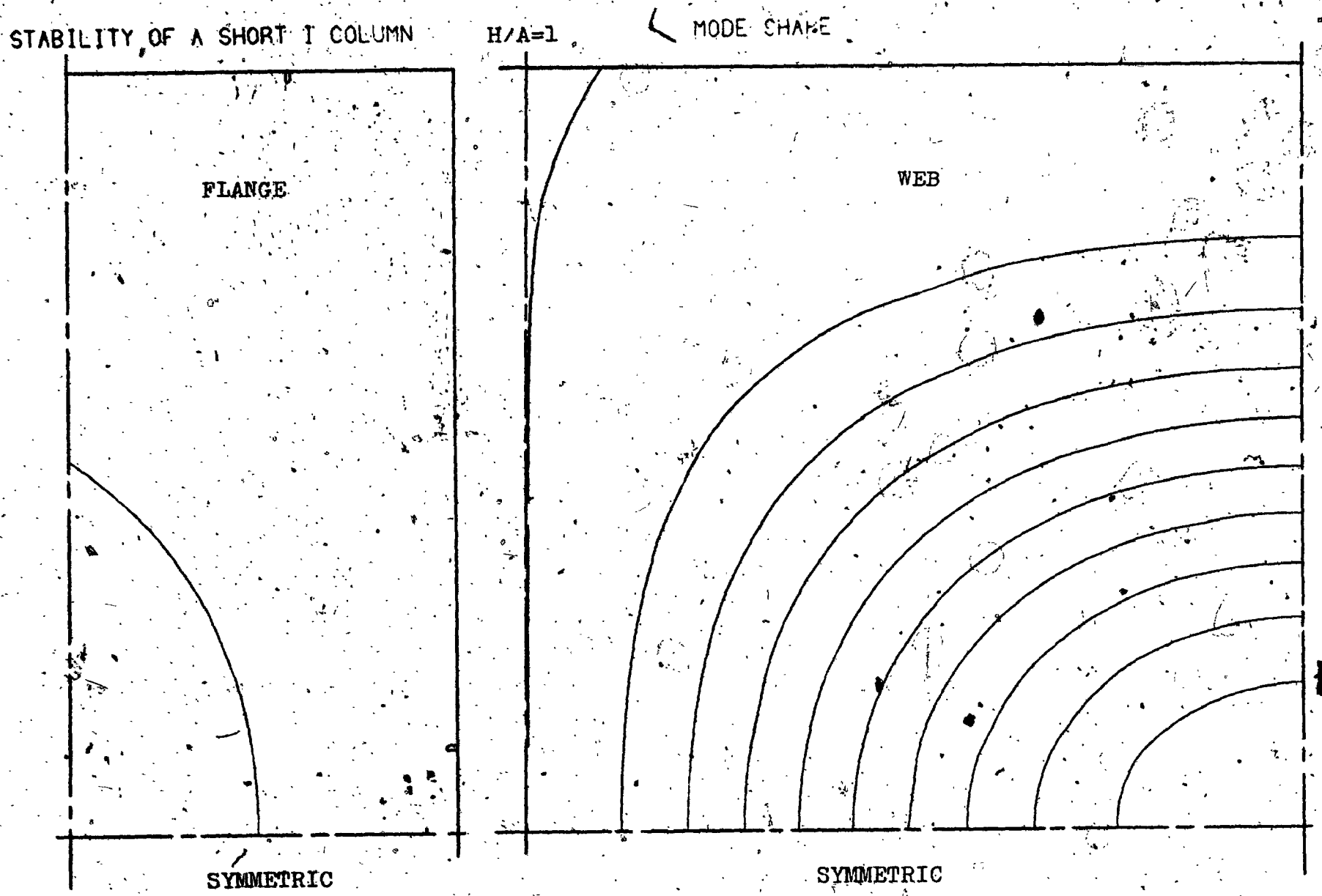
STABILITY OF A SHORT I COLUMN
H/A=1
MODE SHAPE
FLANGE
WEB
SYMMETRIC
SYMMETRIC

FIG. (9.15)

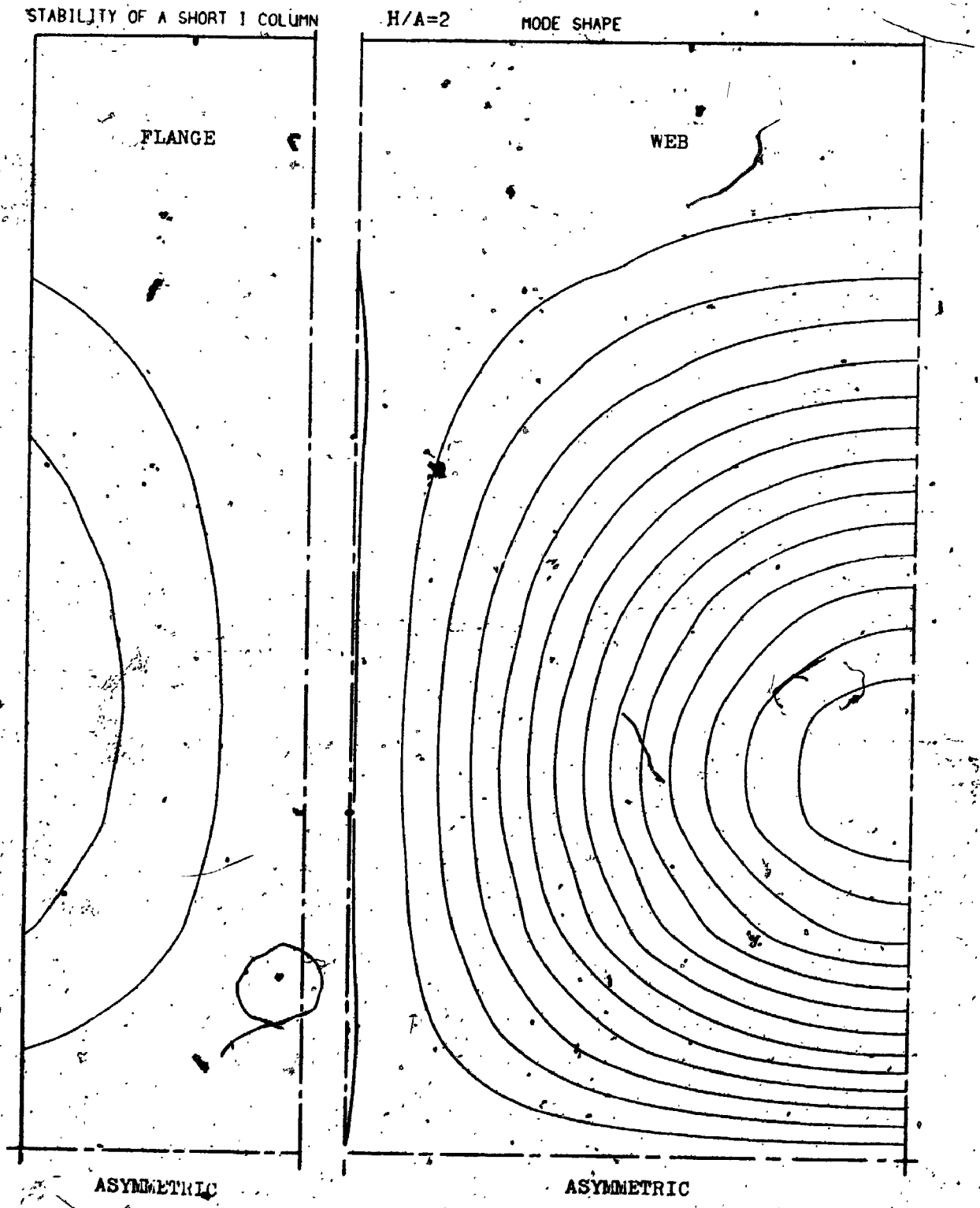
STABILITY OF A SHORT I COLUMN
H/A=2
MODE SHAPE
FLANGE
WEB
ASYMMETRIC
ASYMMETRIC

FIG. (9.16)

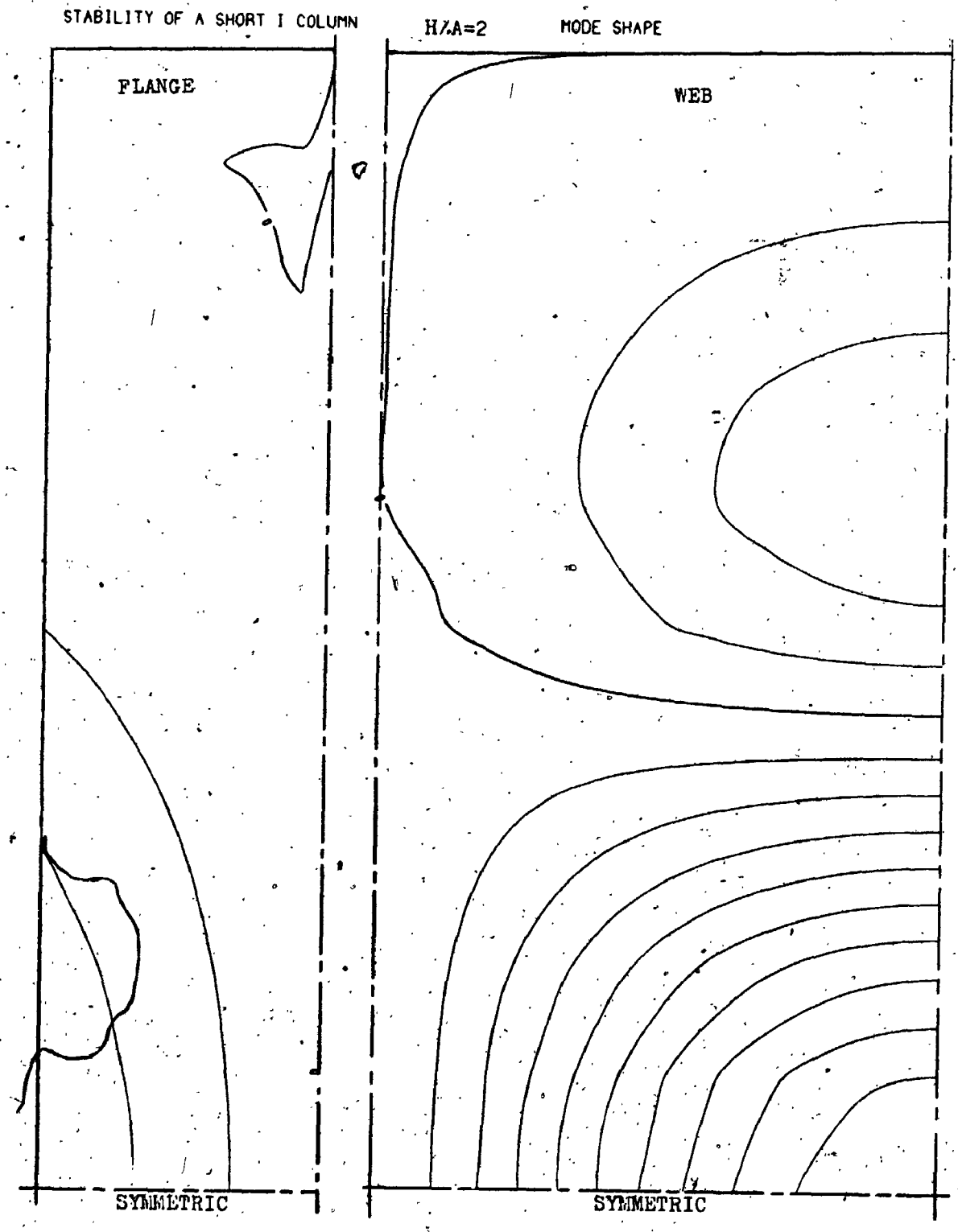
STABILITY OF A SHORT I COLUMN
H/A=2
MODE SHAPE
FLANGE
WEB
SYMMETRIC
SYMMETRIC

FIG. (9.17)

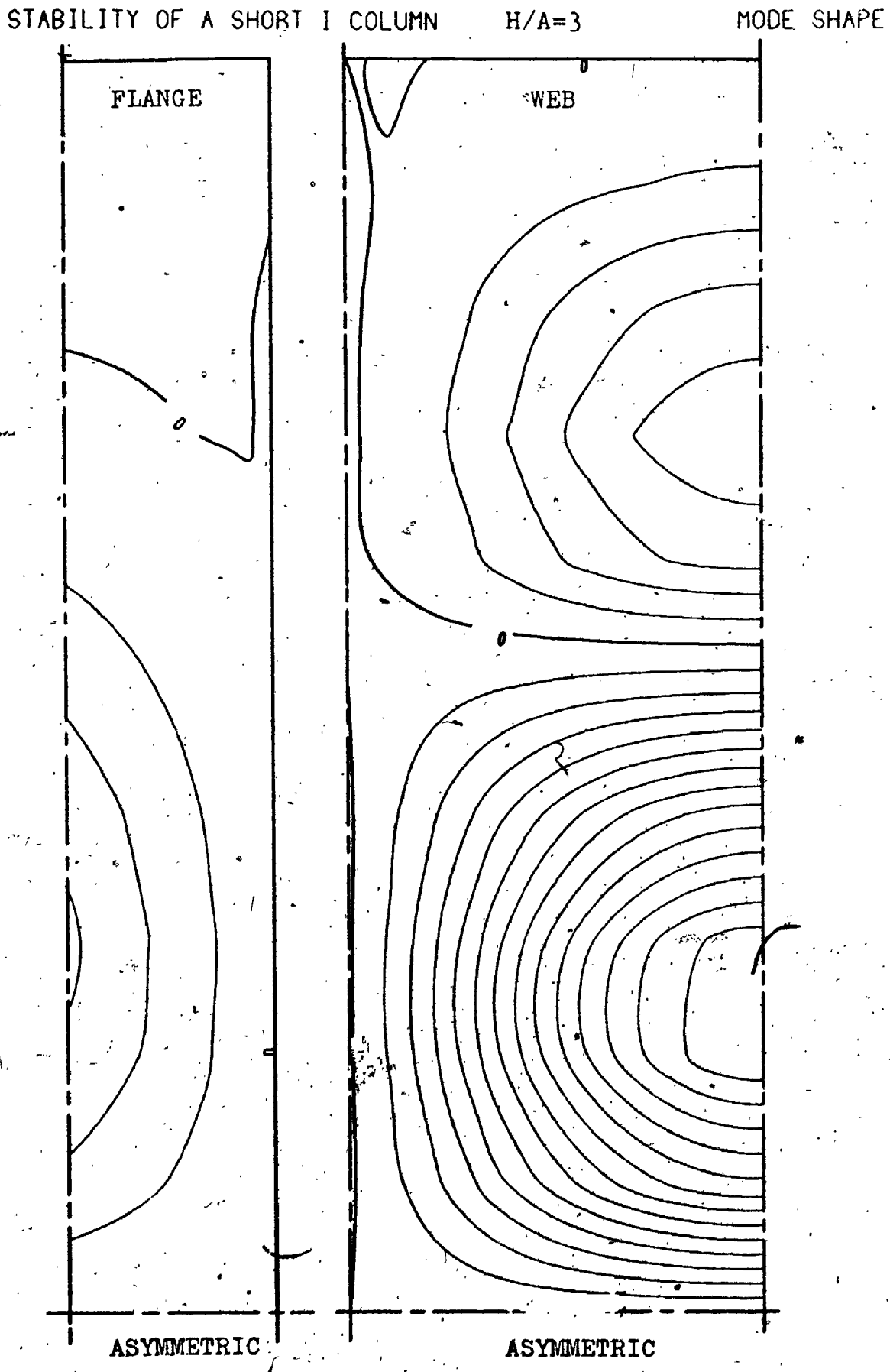
STABILITY OF A SHORT I COLUMN H/A=3 MODE SHAPE
FLANGE
WEB
0
0
0
ASYMMETRIC
ASYMMETRIC

FIG. (9.18)

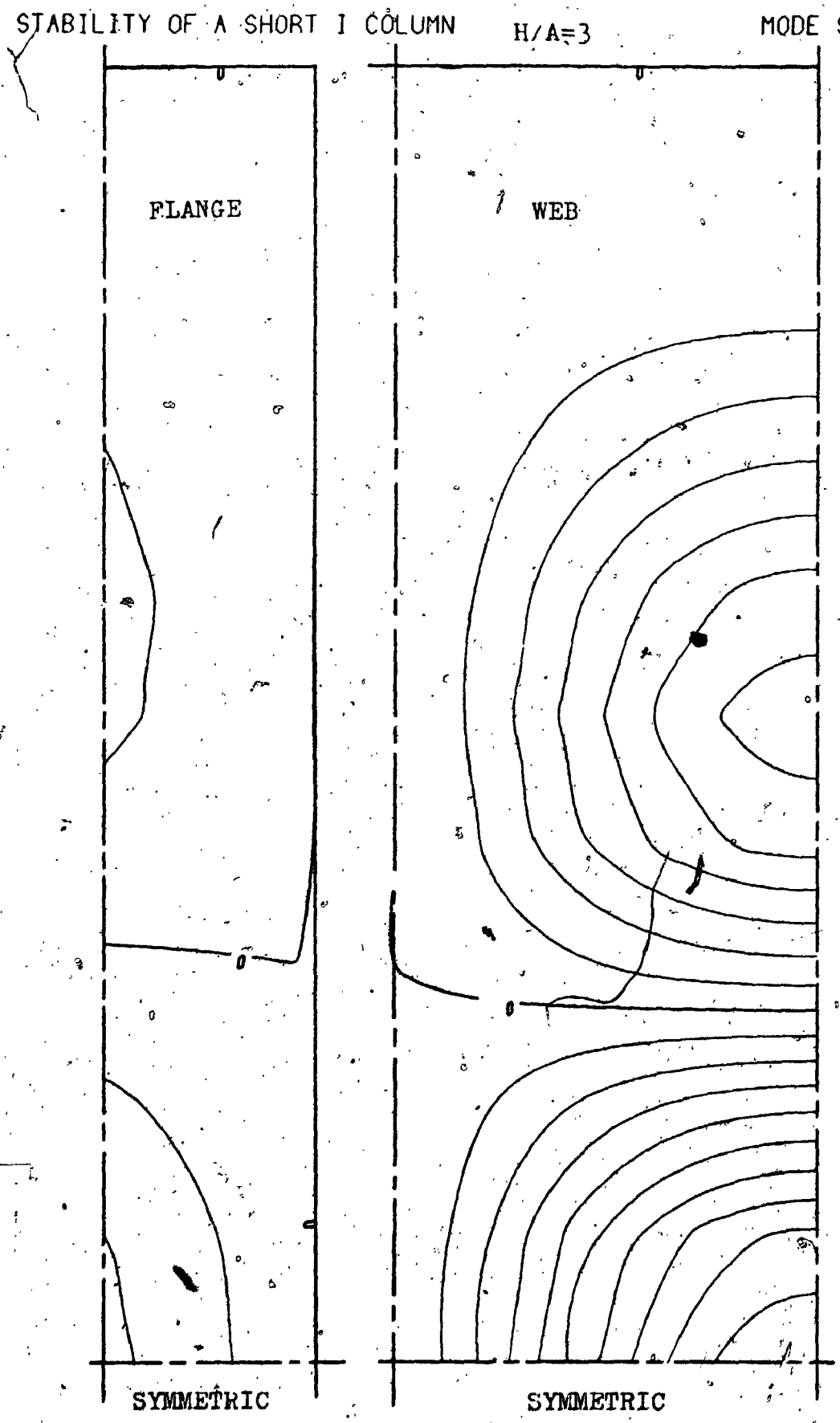
STABILITY OF A SHORT I COLUMN
H/A=3
MODE SHAPE
FLANGE
WEB
SYMMETRIC
SYMMETRIC

CHAPTER X

STATIC PROBLEMS -

The Stiffness of Slabs Connecting Shear Walls

10.1 Introduction

In the preceding chapters, the Large Element method was developed and applied to a large variety of problems which are mainly of academic interest. In this chapter, the method will be used to treat an important practical Civil Engineering problem. That is the evaluation of the bending stiffness of slabs connecting shear walls in tall cross-wall buildings. The purpose of this investigation is to provide a useful design tool for the evaluation of the interaction bending stiffness of the slabs for use in conjunction with one of the existing methods for calculating the horizontal stiffness or vertical load redistribution in shear-wall systems.

To the author's knowledge, this subject has only been investigated by Qadeer and Smith [52] in 1969 where they used Finite Differences to solve the problem and presented graphical results for one of the most common shear wall structural configurations. It was the intended scope of this chapter to firstly examine the accuracy of the Large

Element method through comparing its results with those published in reference [52] for certain typical examples, and then to use the Large Elements to extend the solutions to other types of configurations for shear-wall structures. However, after a few typical cases were examined, it became obvious that the stiffness parameters published in [52] were between 20 and 30% too low (depending upon the geometry of the slabs). It became inevitable then that the author take the following line of action; firstly, to establish the credibility of the obtained Large Element results through alternate approaches; secondly, to examine closely the method of solution used in reference [52] looking for a reason for the discrepancies found; thirdly, to generate a practically complete set of data to serve as a replacement for those of reference [52] in order to be used as a convenient design tool; and finally, to generate similar design data for use with other common shear wall building configurations. Furthermore, it was found, based upon obvious considerations, that an alternative choice of the non-dimensional geometry parameters can yield to a considerable simplification of the problem since the stiffness of the slabs will depend mainly upon that parameter and changes only slightly - within the range of practical interest - with the rest of the parameters. It became possible, therefore, to devise a simple design formula which defines the slab effective width as a function of a single geometry parameter. Unfortunately, this was

not possible in the case of some other shear wall geometric configurations.

10.2 The Double-row Cross-wall Structure

This is the basic shear wall structure configuration which has been analysed by Qadeer and Smith in their above-mentioned paper [52]. The idealized structure of a multi-story building with regularly spaced pairs of shear walls is shown in figure (10.1). A plane and a cross section for this idealized structure are shown in figure (10.2). Horizontal external forces acting along the length of such a building are usually not a problem in design, but when they act across the width of the building the interaction between the walls and the floor slabs, or connecting beams, becomes considerably more difficult to analyze.

Methods of analysis are presently available for determining the lateral behaviour of a pair of shear walls connected by beams [53]. These methods could be applied to cases in which slabs are the interconnecting elements, provided that the stiffness of the slabs against the parallel rotation of pairs of in-line walls is known, or equivalent beams can be devised to provide the same rotational resistance as the actual slabs. Figure (10.3) shows the deformed configuration of the structure under horizontal loading. It can be seen that the deformation of the slabs are due to *parallel* rotations of the pairs of walls connected to the slabs. Other

cases in which the wall-slab interaction takes essentially the same form (as far as the individual slabs are concerned) are pointed out in reference [52].

The following assumptions have been introduced in reference [52] and will be implemented here:

a. Since the pairs of walls are equally spaced, it is assumed sufficient to analyze only one typical bay, e.g. ABCD, in figure (10.2a) with the slab symmetrical and continuous across its boundaries AB and DC. The discussion in reference [52] concerning the special case of the end bays will be assumed valid and no further consideration will be given to such bays.

b. The inplane stiffness of the walls is considered very high compared to the bending stiffness of the slab. Also, warping of the wall sections as the wall bends is neglected. Consequently, the wall cross-sections at their intersection with the slabs remain plane after deformation of the system takes place (which is consistent with the classical beam theory). It is suggested however, since local deformations are likely to occur at the corners between the walls and the slab, to use Michel's correction [54] which calls for extending the span length (L) in figure (10.2a) by an amount equal to the thickness of the slab in order to account for such deformations. This effect, however, will not be considered in the analysis and will be left to the individual designers, who may wish to

use the present results, as to whether they would like to take it into account or not.

In addition to the above assumptions, symmetry about the line M - N and anti-symmetry about H - J permits the analysis of only one quarter of the bay of concern. Hence the region AHEM was analyzed using three large elements. The Large Element model used for the analysis is shown in figure (10.4) together with the set of constraints applied. In order to ensure that the line of anti-symmetry (H-E) remains straight and horizontal, translations along edge No. 9 were constrained. Translations at the corners H and E (nodes No. 7 & 8) are then set equal to unity resulting in an overall translation of the whole edge H - E while remaining straight and horizontal. Since the degrees of freedom corresponding to the translations at nodes number 7 and 8 are prespecified as unity, the corresponding rows and columns in the stiffness matrix are partitioned out as follows:

$$\left[\begin{array}{c|c} K_{11} & K_{12} \\ \hline K_{21} & K_{22} \end{array}\right] \left\{\begin{array}{c} A_1 \\ \hline A_2 \end{array}\right\} = \left\{\begin{array}{c} O \\ \hline P \end{array}\right\}, \qquad (10.1)$$

in which A_2 represents the known displacements while A_1 represents the unknown degrees of freedom, and P are the unknown forces of constraint (reactions) applied at the points of prescribed displacements. After partitioning, this equation is re-written as

$$[K_{11}]\ \{A_1\} = -\ [K_{12}]\ \{A_2\}, \qquad (10.2a)$$

and $[K_{21}]\{A_1\} + [K_{22}]\{A_2\} = \{P\}$. (10.2b)

The R.H.S. of equation (10.2a) is known; hence the equation can be solved for the unknown displacements $\{A_1\}$, thus allowing the determination of the deflected shape. The second equation (10.2b) can then be used directly to compute the reaction forces $\{P\}$ after the displacement vector $\{A_1\}$ has been determined from (10.2a). As soon as the reaction vector $\{P\}$ is determined, the bending moment (M) acting at the shear wall centre is determined by multiplying the sum of the reactions (ΣP) by the distance $(L + W)/2$. The non-dimensional slab stiffness (K), as defined in reference [52], can then be written as:

$$K \equiv \frac{M}{D\theta} = \left(\frac{L+W}{2}\right)^2 \cdot \frac{\Sigma P}{D\delta} , \qquad (10.3)$$

which has been shown to be a function of the geometry parameters Y, L, W, and C.

Since most of the restraint force due to the shear wall occurs near its leading edge (node number 6), the effect of the width of the shear wall (W) upon the reaction force ΣP is expected to be small provided that the ratio (Y/W) is not too large (<4) - which is usually the case in practice. In order to make use of this fact, it is necessary to define another stiffness parameter (K') which does not depend upon the parameter W. This is done by focusing only upon the rotation (θ') and bending moment (M') as seen from the leading edge of the shear wall - see figure (10.4). The stiffness (K') is then defined as:

$$K' = \frac{M'}{D\theta'} = \left(\frac{L}{2}\right)^2 \cdot \frac{\Sigma P}{D\delta} , \qquad (10.4)$$

which depends upon W only through the reaction force ΣP, which in turn varies very slowly with (W), as will be shown in the numerical results.

It follows from the same reasoning that since the overhang (C) is even further away from the leading edge of the shear wall, its effect upon the stiffness of the slab is minimal. Based upon the results presented in reference [52] and upon several extreme cases examined by the author, in no case was the effect of the overhang (C) more than 2 or 3 percent of the slab stiffness. In the majority of cases, this effect was even smaller than a percent. As a result, the basic geometry parameters are expected to be (L) and (Y).

Another important parameter of interest is the ratio (Y_e/Y), where (Y_e) is the width of an equivalent beam having the same depth and elastic modulus, and providing the same rotational stiffness as the original slab. It has been shown in [52] that this parameter can be represented by:

$$\frac{Y_e}{Y} = \frac{K\, L^2/(L + W)^2}{6(1-\nu^2)(Y/L)} , \qquad (10.5)$$

which, making use of equations (10.3) and (10.4), can be rewritten as:

$$\frac{Y_e}{Y} = \frac{K'}{6(1-\nu^2)(Y/L)} . \qquad (10.6)$$

It is obvious from equation (10.6) that the ratio $(\frac{Y_e}{Y})$ depends upon the parameter (W) only inasmuch as (K') does.

A comparison of the results obtained using Large Elements with those of reference [52] (Finite Differences) for four typical examples is presented in table (10.1). The percentage differences (as percentages from the

TABLE (10.1)

Ex. No.	$\frac{Y}{X}$	$\frac{L}{X}$	$\frac{C}{X}$	K = M/Dθ		
				Large El.	Ref. [52]	Finite El.
1	.5	.75	0	3.75	3.05 [-19%]	---
2	.5	.5	0	8.38	6.6 [-21%]	8.25 [-1.4%]
3	.25	.25	0	23.75	18.6 [-22%]	---
4	.495	.162	1/16	69.74	49 [-30%] 41* [-41.5%]	---

*This value was given in the text of the paper [52] and does not coincide with the value read off the graph presented in the same paper (which is 49).

higher values) between the two sets of results are shown in brackets. A paradox has been encountered in example number (4) of the table above, which was originally used in reference [52] as an example showing how the graphical results presented therein should be used. The value of K was quoted as "41" while the value which could be read off the graph is about "49". It is felt that this is either due to some error in the plotting or the reproduction of the graphs, or that the value "41" is the result of a

solution using a mesh size larger than that used to produce the results shown on the graph. The possibility of a printing error is minimized because the same figure "41" was repeated four times throughout the example. It is felt, however, that the value "49" is more likely to be the correct one.

It can be seen from the above table that the Finite Difference results presented in reference [52] are at least 20 to 30% lower than those computed by the author using the Large Element method. Since from previous use of the Large Elements in similar problems (e.g. plates with partial supports etc.) the results are usually over-estimated by no more than a percent, it is expected that most of the difference reported in the table is due to the inaccuracy of the Finite Difference solutions presented in [52]. A discussion of the possible sources of error, and their expected magnitudes, in the solutions of reference [52] will be presented in the next section.

In order to positively support the credibility of the Large Element solutions shown in table (10.1), and since no results are available in the literature concerning this particular problem, a Finite Element solution was devised in order to provide the required confidence in the present results. The Finite Element model used for the test analysis is shown in figure (10.5), which corresponds to the geometry parameters of example No. (2) in table (10.1). For reliability a well tested, commercially avail-

able, Finite Element program (NASTRAN) was used for the solution. A non-conforming quadrilateral bending element was employed, which is known to "generally" converge from the weak side (i.e. under-estimates the stiffness) as shown in reference [11]. The non-dimensional stiffness parameter obtained in this case is also shown in table (10.1) for comparison. Since this value is expected to be a lower bound, while the Large Element solutions are guaranteed to be an upper bound for the stiffness, the difference between the two results (1.4%) represents the sum of the errors resulting from both solutions. It is estimated, therefore, that the Large Element solutions are higher than the exact values by less than a percent. Reaching this conclusion, it remains to investigate the possible sources of inaccuracy in the Finite Difference results of reference [52]. This will be the subject of the following section.

10.3 Sources of Inaccuracy in the Results of Reference [52].

As mentioned before, Qadeer and Smith in reference [52] have used a Finite Difference approach in order to determine the equivalent stiffness of the slabs of the type shown in the previous section. In addition, they published the results of an experimental investigation conducted using an Asbestos cement slab and a pair of heavy steel plate columns. Figure (10.6) is reproduced from reference [52]

showing the details of the clamps used for supporting the slab (a,b), and a comparison between the theoretical and experimental results obtained (c). In the following, a discussion concerning the possible sources of inaccuracy in both the theoretical and experimental results of the above reference is presented.

The discretization error in any Finite Difference solution (ε_d) is known to be proportional to the square of the mesh size, i.e.:

$$\varepsilon_d \alpha (1/n)^2 \qquad (10.7)$$

where n represents the number of divisions along a typical length of the structure. In addition to this error, another error due to the existence of the discontinuous support conditions has been introduced in this particular problem. This error (ε_s) will be shown here to be proportional to the mesh size; or

$$\varepsilon_s \alpha \left(\frac{1}{n_c}\right), \qquad (10.8)$$

where n_c is the number of divisions along the cantilevered portion of the slab-wall centre line - i.e. along the edge EF in figure (10.7). The figure represents a typical Finite Difference mesh of the type used in reference [52] (it was mentioned in the reference that an 18 x 18 mesh was generally used to cover the whole of the bay ABCD - i.e. 9 divisions along the edge EM as shown in the figure). Along

the wall width (W) the boundary conditions of zero deflection and slope were applied. Hence, the displacements W_5 through W_9 were all set to zeros, and the slopes $\frac{\partial W}{\partial Y}$ were also set to zeros at these points. Along the edges EF and MG, the slope $\frac{\partial W}{\partial y}$ and the shear force Q_y were supressed. Since the governing differential equation for the plate deflection is of the fourth order, two boundary conditions along each edge suffice for the solution, and no additional boundary conditions are admissible. As a result, the condition that the slope $(\frac{\partial W}{\partial x})$ at point No. 5 must be zero (due to continuity of slope between the supported and the cantilevered portions) cannot be *explicitly* applied. It can be seen, however, that as the number of divisions n increases, points 5 and 6 - at which the displacement W is equal to zero - become closer and the slope $\frac{\partial W}{\partial x}$ at point 5 approaches zero in the limit.

In order to quantitatively investigate the effect of this error, the limiting case in which the width of the slab *(Y/2)* becomes very small in comparison with its length *(L + 2W + 2C)* will be solved here. In this case, the slab may be represented by a beam as shown in figure (10.8) whose stiffness (E.I) equals to (D.Y). The beam is divided into 9 equal divisions each of a length equal to A. In addition, four ficticious points are defined, two at each end, in order to accommodate the free boundary conditions. The governing differential equation for this beam may be

written as:

$$\frac{d^4W}{dx^4} = (\Sigma P/D.Y) \Big|\Big|_{\text{at point 10}}$$

which, in a difference form, may be written as:

$$W_{i+2} - 4\,W_{i+1} + 6\,W_i - 4\,W_{i-1} + W_{i-2} = 2\frac{\Sigma P\Delta^2}{D.Y.} \Big|\Big|_{i=10}$$

Applying this equation at points 1, 7, 8, 9 and 10, the following results:

$$\overset{o}{W}_3 - 4\,\overset{o}{W}_2 + 6\,W_1 - 4\,W_o + W_{-1} = 0, \qquad (a)$$

$$W_9 - 4\,W_8 + 6\,W_7 - 4\,\overset{o}{W}_6 + \overset{o}{W}_5 = 0, \qquad (b)$$

$$W_{10} - 4\,W_9 + 6\,W_8 - 4\,W_7 + \overset{o}{W}_6 = 0, \qquad (c)$$

$$W_{11} - 4\,W_{10} + 6\,W_9 - 4\,W_8 + W_7 = 0, \qquad (d)$$

$$W_{12} - 4\,W_{11} + 6\,W_{10} - 4\,W_9 + W_8 = 2\Sigma P\Delta^3/DY\,. \qquad (e)$$

In addition, four other equations can be written by applying the free-end boundary conditions at the two end points 1 and 10:

$$\frac{d^2W}{dx^2} = \frac{d^3W}{dx^3} = 0 \Big|_{N=1,10}; \text{ or:}$$

$$W_o - 2\,W_1 + \overset{o}{W}_2 = 0, \qquad (f)$$

$$W_3 - 2W_2 + 2W_0 - W_{-1} = 0 \qquad (g)$$

$$W_{11} - 2W_{10} + W_9 = 0 \quad \text{and} \qquad (h)$$

$$W_{12} - 2W_{11} + 2W_9 - W_8 = 0 \qquad (i)$$

Solving the above 9 equations for W_{-1}, W_0, W_1, W_7, W_8, W_9, W_{11}, W_{12} and ΣP, the following results:

$W_{-1}=W_0=W_1=0$, $W_7=2/15$, $W_8=11/30$, $W_9=10/15$, $W_{11}=20/15$,

$W_{12}=51/30$, and $\frac{\Sigma P \Delta^3}{DY} = \frac{1}{30}$.

Consequently, the non-dimensional stiffness "K" can be given by:

$$K = \left(\frac{L+W}{2}\right)^2 * \frac{\Sigma P}{D\delta} = 36\Delta^2 * \frac{Y}{30\Delta^3},$$

$$\text{or} \quad K = 1.2\,\frac{Y}{\Delta} = 9.6\left(\frac{Y}{L}\right). \qquad (10.9)$$

The exact solution for this example is straightforward;

$$K = \left(\frac{L+W}{2}\right)^2 * \frac{\Sigma P}{D[\Sigma P*(L/2)^3/3DY]}$$

$$= 13.5\left(\frac{Y}{L}\right). \qquad (10.10)$$

Hence, it can be seen that the results of the Finite Difference solution presented above is about 28.9% lower than the exact value.

If, however, the condition of zero slope is explicitly applied at point No. 6 - in which case an additional fictitious point has to be conceived at the same location as

point 5; say 5' - the following equation is added:

$$W_7 - W_{5'} = 0, \qquad (j)$$

and equation (b) above is replaced by

$$W_5 - 4W_8 + 6W_7 - 4W_6 + W_{5'} = 0. \qquad (b')$$

In this case it can be easily shown that:

$$\frac{\Sigma P \Delta^3}{DY} = \frac{1}{22},$$

and $$K = \left(\frac{L+W}{2}\right)^2 * \frac{\Sigma P}{D\delta} = 36\Delta^2 * \frac{Y}{22\Delta^3} = 13.09\left(\frac{Y}{L}\right), \qquad (10.11)$$

which is only 3.1% lower than the exact answer and 25.8% higher than the answer given by equation *(10.9)*. It can thus be seen that the error in equation *(10.9)* is composed of two parts; the discretization error ε_d which is equal to 3.1%, and an additional error ε_s which is due to the representation of the support condition and is equal to 25.8%. While the introduction of the additional ficticious point 5' does not seem to complicate the solution for the one dimensional case just described, its extension to the two dimensional case is not obvious due to the dual value of the displacement resulting at point 5. More important in this context is that no such provision has been used in reference [52], and hence the error ε_s does exist in the solutions presented therein (it was stated in [52] that the theoretical results presented represent a slab pinned at the nodal points along the wall).

In addition to the above example, a direct estimate for the magnitude of the error ε_s can be established analytically as follows:

Considering the two beams shown in figure (10.9) the tip displacement due to a load P can be given by;

$$\delta_1 = \frac{Pl^3}{3EI} , \quad \delta_2 = \frac{Pl^3}{3EI} \left[1 + \frac{\Delta}{l}\right] ,$$

where δ_1 represents the tip displacement for the cantilever, and δ_2 represents the displacement of the beam pinned along the two points M and N as shown in the figure. Since the second of these two cases corresponds to the Finite Difference representation for the clamped beam as shown in figure (10.8), it can be seen that the error ε_s is of the order $(\frac{\Delta}{l})$. Assuming that $n1$ represents the number of Finite Difference cells along the cantilevered portion $(L/2)$, it can be concluded that

$$\varepsilon_s \alpha \left(\frac{1}{n1+1}\right) = \left(\frac{100}{n1+1}\right) \%. \qquad (10.12)$$

In the example shown in figure (10.8) $n1$ is equal to (4) and equation (10.12) gives $\varepsilon_s = 20\%$. (Comparison of this value with the 25.8% found in the numerical example indicates that equation (10.12) underestimates the true error).

So far, the existence, the order, and the magnitude of the error ε_s have been established for the case of a one-dimensional problem. In the two dimensional problem,

the order of the error is expected to remain the same (i.e. $\varepsilon_d \alpha\ 1/n^4$), but the magnitude of the error will be somewhat reduced since the effect of the clamped boundary becomes less dominant with the increase of the slab width (Y). In order to establish the magnitude of this error in the two-dimensional case, the Large Element model shown in figure (10.10) was devised to simulate the boundary conditions used in the Finite Difference solutions - and hence establish the error ε_s. The model was used to solve both examples No. 1 and 2 shown in table (10.1). In addition, these two examples were also solved using only three point supports along the wall intersection. The results are shown in table (10.2) compared with those obtained using a completely clamped edge and with those published in reference [52] obtained using Finite Differences.

TABLE (10.2)

Comparison of the Stiffness Parameter K as Obtained Using Different Approaches

Ex. No.	Y/X	L/X	C/X	Large Elements			Finite Differences
				Clamped along wall	Four point supp.	Three point supp.	[52]
1	.5	.75	0	3.75 (0.0%)	3.5 (-7%)	3.38 (-10%)	3.05 (-19%)
2	.5	.5	0	8.38 (0.0%)	7.3 (-13%)	6.92 (-17%)	6.6 (-21%)

*Percentage errors based upon the Large Element solution with slab clamped along the wall.

It can be seen from the table that a considerable portion of the errors included in the Finite Difference solutions is due to the error component ε_s. Also, comparing magnitudes of the errors obtained by using three and four support points in the first example, it can be seen that the errors are proportional to $\frac{1}{n1+1}$ ($n1$ for the four point support condition is 9 and for the three point support condition is 6) which is the same result reached using the simple one-dimensional example mentioned earlier. The same conclusion can be reached from the second example also.

In the above discussion, it has been speculated that a considerable error is introduced in the Finite Difference solutions of reference [52] due to the existence of the discontinuous boundary support. Another indication for the possibility of obtaining such large errors in those results (20 to 30%) is offered by the convergence study presented in reference [52] and shown earlier in figure (10.6). The figure shows differences of the order of 15 to 20% between the results obtained using a 12 x 12 mesh and those obtained using a 24 x 24 mesh. Since it was shown that the error included in these Finite Difference solutions is of the order of the mesh size (rather than the square of the mesh size as is usually the case in Finite Difference solutions), an extrapolated solution based upon the two sets of results shown in the figure and the assumption that the errors are proportional to the mesh size would lie

another 15 to 20% above the 24 x 24 mesh solutions as shown by the chain line in figure (10.6). Since the bulk of the results presented in reference [52] are based upon an 18 x 18 mesh size, they should lie mid-way between the 12 x 12 and the 24 x 24 mesh solutions. As a result, errors of the order of 20 to 30% in the Finite Difference results shown in table (10.1) are quite consistent with those expected based upon the convergence study presented in figure (10.6).

So far, the question of the accuracy of the theoretical results presented in reference [52] has been discussed. Unfortunately, an equivalent discussion regarding the experimental results published in the same reference - and shown in part by figure (10.6) - is not feasible. The reason is that firstly; insufficient information was published in the reference concerning the details of the experimental procedure, the dimensions of the model, and the physical properties of the materials used, and secondly; no experimental results on this subject were generated by the present author nor are available in the literature to permit meaningful comparison with those of reference [52]. In this respect, however, the following comments are believed to be valid:

- Due to the great difference in stiffness between the slab material (Asbestos Cement) and the wall material (hard steel), considerable local plastic deformations are expected to occur in the slab near the leading

edge of the wall where both the bending and shear stresses are "theoretically" infinite (based upon the *elasticity* theory). Such deformations are expected to cause the experimental solutions to be considerably lower than the theoretical ones. The mere fact that a certain amount of local deformation is likely to happen in reality does not justify accepting such errors to occur in the experimental model since the amount of such a deformation depends upon the strength of the slab and the wall materials, the relative thicknesses of the slab and the wall, the details of the corner juction, as well as the level of the stresses existing in the building, in addition to all the parameters taken into account in the results presented in the reference. It is felt therefore that a *separate* account for these local deformations should be considered - depending upon the above parameters - and they should not be mixed with the overall stiffness of the slab which depends upon a separate sub-set of those parameters.

Two types of slab-wall connections were used in the experimental results of reference [52] - Fig. (10.6 a,b) - "the first held the slab along the whole section of the wall, and was intended to represent the actual conditions in a shear wall; the second *pinned* the slab to the walls only at the ends and middle of

the length of the wall to represent the nodal deformations assumed for the theoretical analysis. In fact, the difference in the measured stiffness was insignificant ...". The above statement - made in reference [52] - contradicts the theoretical investigations presented earlier in this section which showed that significant differences occur between the two types of fixity mentioned above. Differences between 10 and 25% were shown to occur depending upon the width of the slab and the distance between the pin supports (Δ) as compared to the actual free span between the walls (L). The only justification for this contradiction is that some source(s) of experimental inaccuracy (e.g. local deformations of the slab ... etc.) have caused significant errors which have over-shadowed the above-mentioned effect.

10.4 Design Data for the Double-row Cross-Wall Structure

As a result of the above discussion, it is felt desirable to present a new set of data for the equivalent stiffness of the slabs connecting shear walls in the double-row cross-wall structure discussed in the previous sections. As mentioned before, the effect of the over-hanging portion of the slab (c) is very small throughout the range of practical interest. Therefore, the only independent parameters which will be considered are $(\frac{Y}{L})$ and $(\frac{W}{L})$. The

stiffness parameters $(\frac{Y_e}{Y})$ and (K') are plotted in figure (10.11) as functions of the abscissa $(\frac{Y}{L})$ and the parameter $(\frac{W}{L})$ for a spectrum covering almost all the region of practical interest. The range covered was arbitrarily defined by:

$$0. \leq \frac{Y}{L} \leq 6, \quad \frac{1}{3} \leq \frac{W}{L} \leq 3, \quad 0 \leq \frac{Y}{W} \leq 4. \qquad (10.13)$$

It can be seen from figure (10.11) that, as expected, the stiffness changes widely with (Y/L) but very slowly with the parameter (W/L) throughout the range specified above. Consequently, for most practical purposes, the only parameter that counts is the ratio of the span width (Y) to the free length of the slab (L). It is interesting to note that for a very narrow span $(Y/L \to 0)$ the effective width may become somewhat larger than the full span width (i.e. $Y_e/Y>1$) due to the fact that the anticlastic curvature of the slab will be restrained. As expected, the maximum value for (Y_e/Y) approaches $1/(1-\nu^2)$ - or 1.04 - due to the above reason.

Should it be of interest to designers, an approximate expression for the effective width ratio (Y_e/Y) as a function of the parameter (Y/L) only has been obtained by fitting an exponential curve to the average values of the bundle of curves shown in figure (10.11). This formula may be written as:

$$\frac{Y_e}{Y} = 0.15 + 0.89\, e^{-.57(\frac{Y}{L})} \qquad (10.14)$$

which fits the curves of figure (10.11) to better than 5%, and is applicable throughout the range defined by the inequalities *(10.13)* stated earlier.

Apart from its simplicity, the importance of formula *(10.14)* lies in the fact that it is far more versatile than the initial curves from which it was found [i.e. figure (10.11)]. Since formula *(10.14)* depends only upon the width-to-span ratio of the slab, and is independent of the width of the shear walls, it becomes equally applicable to symmetric as well as asymmetric shear wall arrangements - figure (10.12) types (1), (2) and (3). Moreover, since the effective width is independent (within reasonable design accuracy) of both the width of the wall and the amount of overhanging slab, it may be concluded that what happens within the free span does not depend upon what happens at the far ends of the walls. Consequently, the same formula may be used for buildings including more than two raws of shear walls such as the three row construction shown in figure (10.12) type (4).

10.5 The Four-Wall Rotationally Symmetric Structure

Another less commonly used type of shear-wall construction is composed of four-walls partially surrounding the floor slabs as shown in figure (10.13a). Upon attempting to evaluate the lateral stiffness of the structure, the same problem concerning the equivalent stiffness of

the floor slabs arises. Adopting the same approach used with the double-row structure described in section (10.2) as well as reference [52], the problem is reduced to that of evaluating the resistance of the slab to the enforced deformations imposed by the rotation of the wall sections. These enforced deformations are schematically shown in figure (10.13b). Once more, the assumption that the wall plane cross-sections remain plane and perpendicular to the wall centre lines after deformations is used. In addition, if the heights of the four wall-centres after deformations remain the same, the two differential deformations Δ_1 and Δ_2 shown in figure (10.13b) may be related to the angle of rotation θ by the following relationships:

$$\Delta_1 = (L + W) \cdot \theta \,, \qquad (10.15a)$$

and

$$\Delta_2 = (W/2) \cdot \theta = \left(\frac{X-L}{X+L}\right) \cdot \frac{\Delta_1}{2} \qquad (10.15b)$$

The Large Element model used for this problem is also shown in figure (10.13). Due to the existence of the rotational (polar) symmetry condition, it became possible to model only one half of the structure. The boundary conditions along the line of symmetry (the $x_1 - x_2$ axis) are rather involved compared to the case of a direct symmetry, or anti-symmetry, condition. In the present case, the displacements along the centre line are anti-symmetric about the centre (node No. 5). The normal slopes $\partial W/\partial y$ along this centre line, however, are symmetric about the

centre point. In order to satisfy these conditions most conveniently, four elements were used; two at each side of the centre point. Also, two coordinate systems x_1-y_1 and x_2-y_2 were used in order to represent the two sides of the model with the appropriate coordinate transformation applied along the common edge (edge No. 6). Additional constraints had to be used to serve a dual purpose; firstly, to define the enforced deformations applied to the slab, and secondly to match the degrees of freedom along the symmetry line on both sides of the centre point according to the symmetry conditions stated above.

The two stiffness parameters K' and Y_e/Y defined by equations *(10.4)* and *(10.6)* were computed for different values of the geometry parameters L/X and Y/X. These results are plotted in figure (10.14) for three different values of Y/X and for L/X varying between 0.4 and 0.8. The application of the stiffness parameters K' and Y_e/Y to this problem is based upon assuming that the lateral behaviour of the structure may be represented by that of a pair of co-planar shear walls each having the same dimensions and stiffness as any of the two lateral walls of width W, connected by a row of fictitious beams each having a length L and a bending stiffness K'. Alternatively, the connecting beams may be assumed to have a length L, a width Y_e, and a height equal to the slab depth.

It is important to note that the axes of symmetry (X and Y) for a structure of this type are not principle

axes. Hence, coupled torsional and bending motion may arise due to a lateral excitation, and an estimate for the torsional stiffness of the structure may become essential. No effort, however, will be made here to study the coupling effects nor the torsional stiffness of the structure since this is outside the scope of the present investigation.

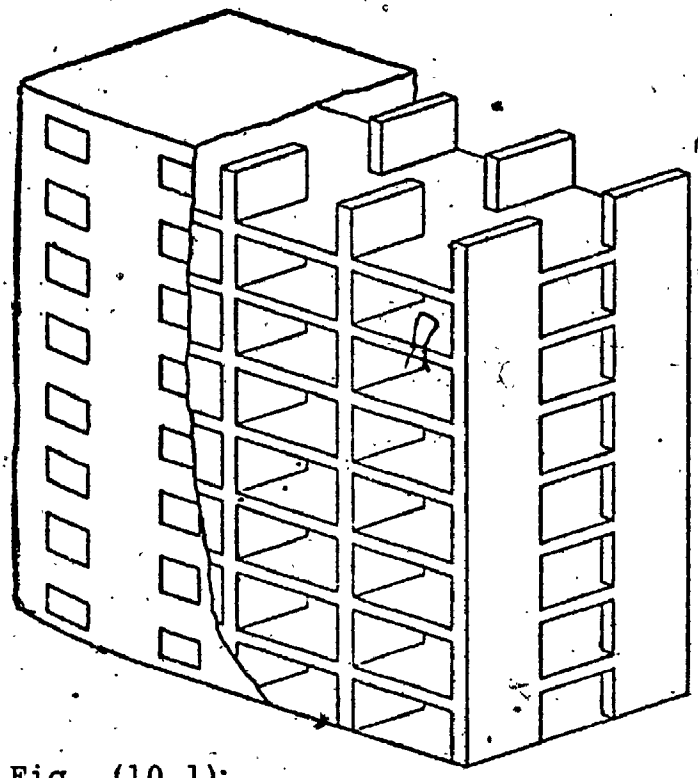

Fig. (10.1):
Idealized slab and cross-wall building

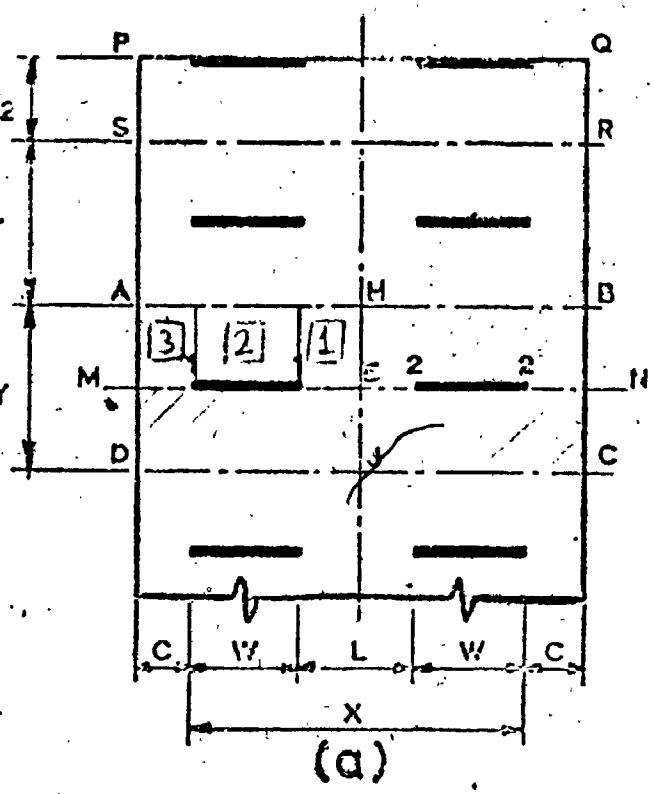

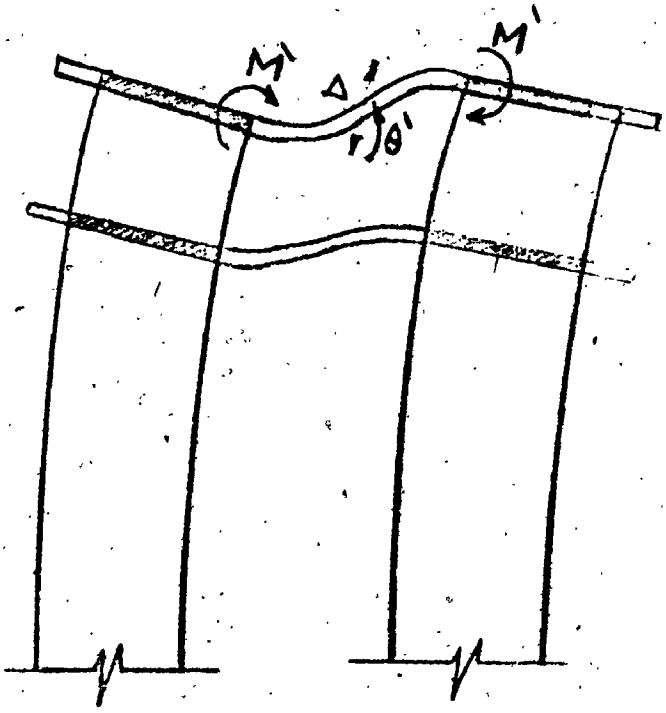

Fig. (10.3): Deformation Mechanism

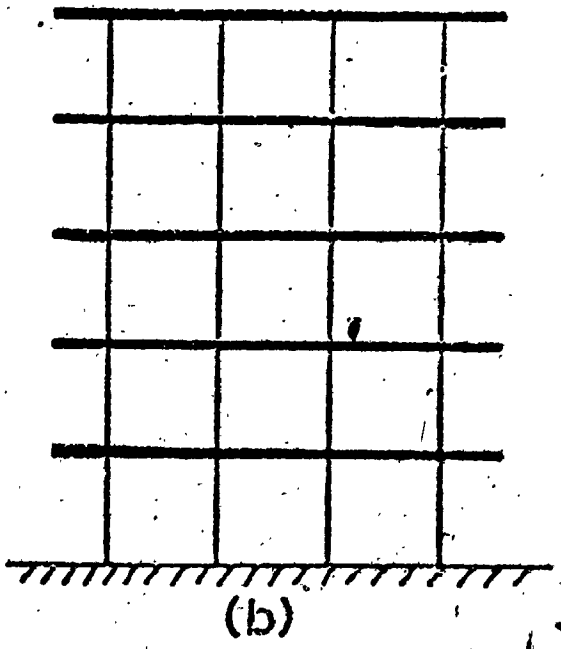

Slab and cross-wall structure; (a) plan; and (b) elevation
Fig. (10.2)

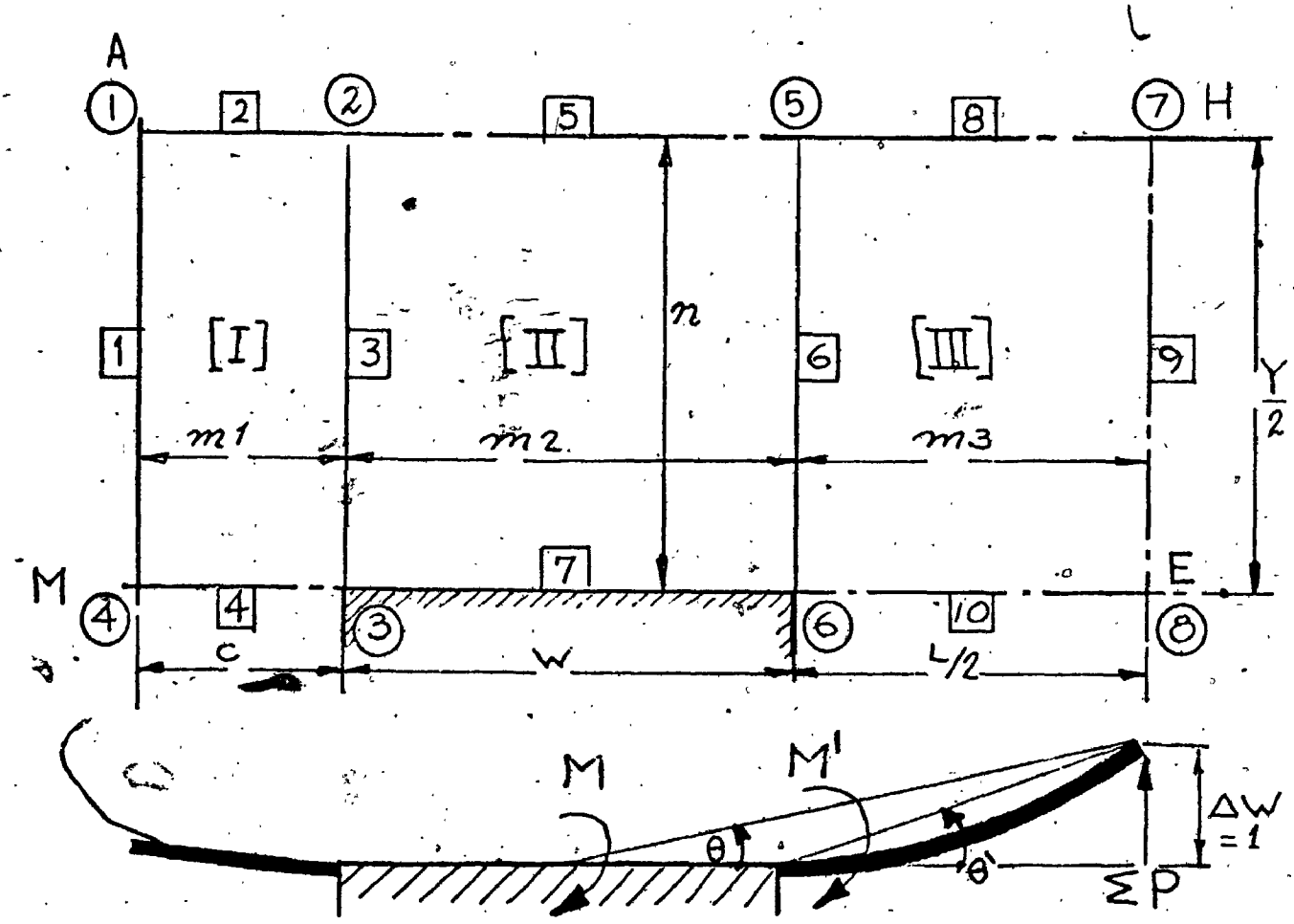

Stiffness

$\nu = 0.19$

$D_x = D_y = D$

(Isotropic)

Additional Constraints

Node No.	Constraint relationship
7	$t = 1$
8	$t = 1$

Constraints

Edge. No.	Type of Constraints
2	r
4	r
5	r
7	t, r
8	r
9	t
10	r

Fig. (10.4)

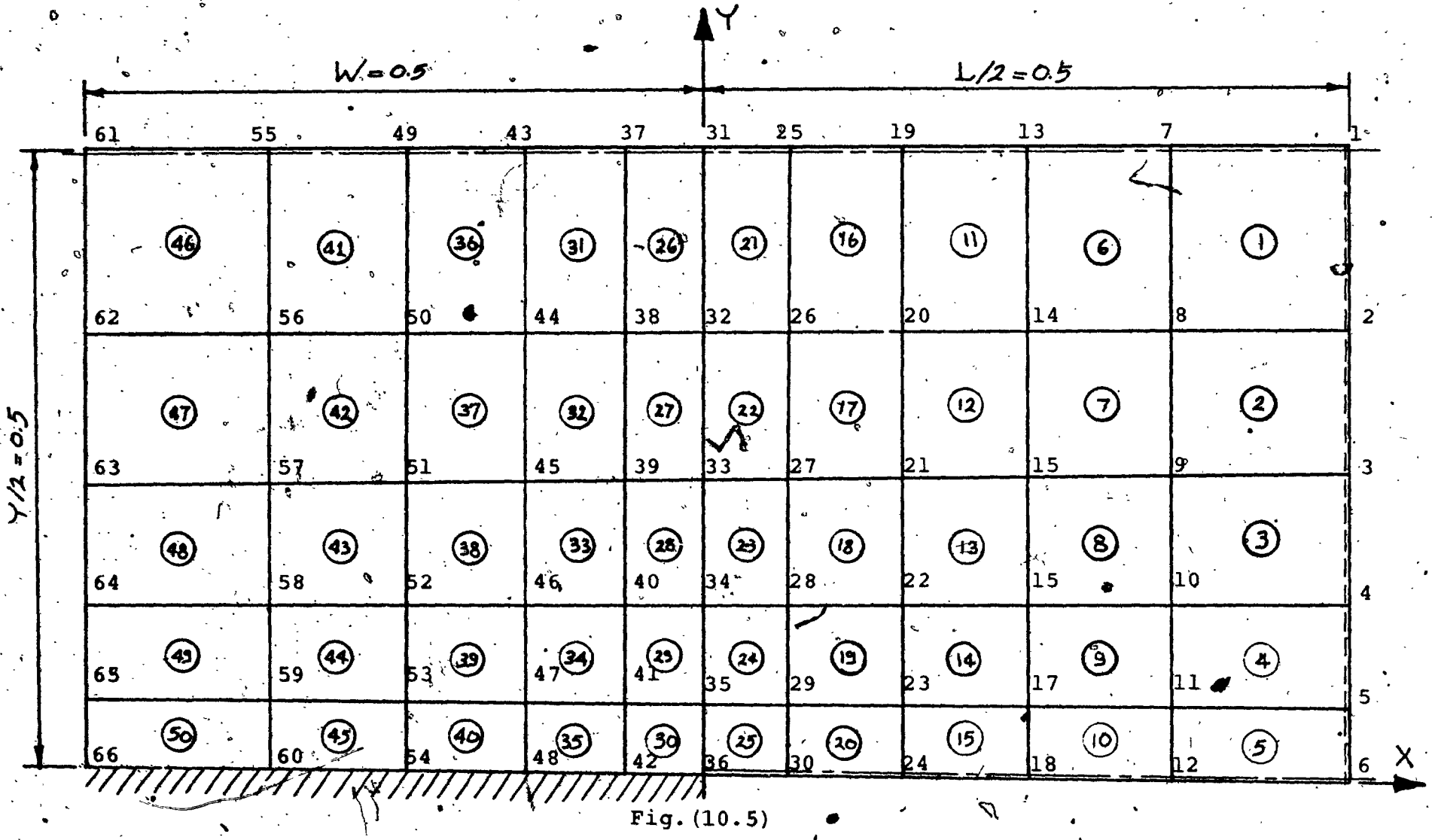

Fig. (10.5)

The NASTRAN Finite Element Mesh Used for Example No. 2.

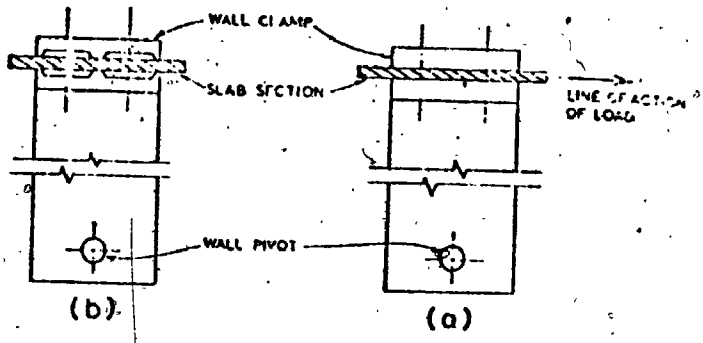

Details of clamps used for supporting slab

Fig. (10. 6a)

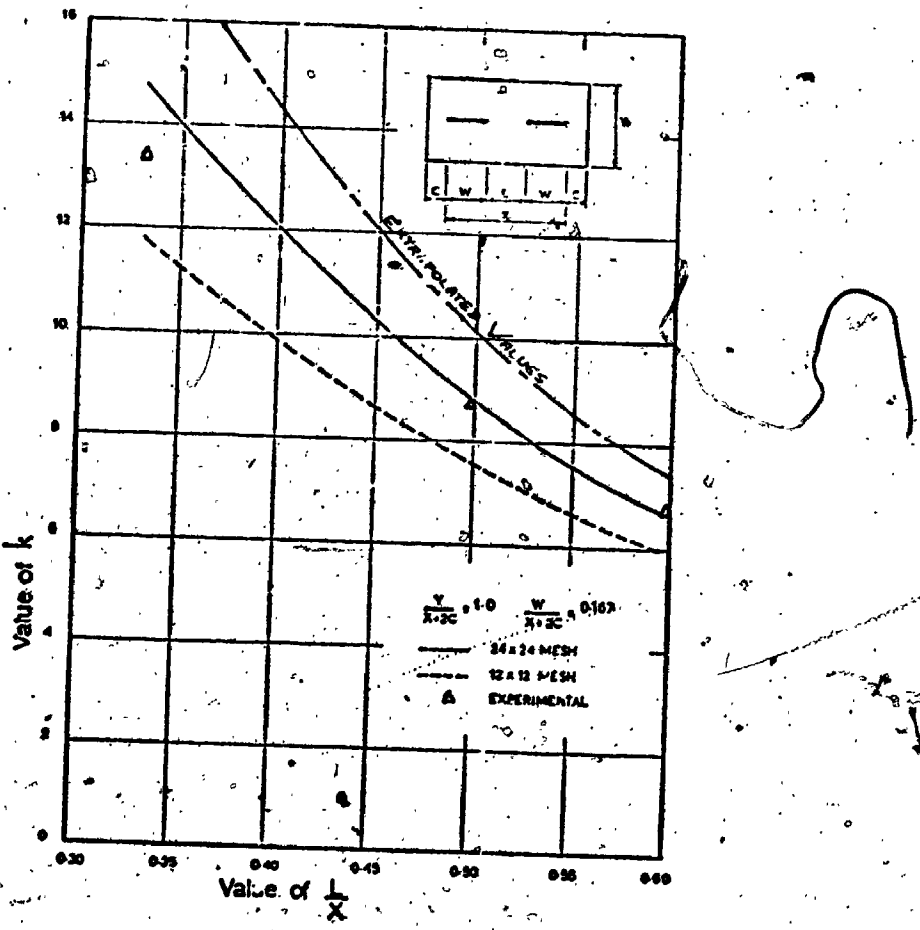

—Value of slab stiffness number k as a function of L/X for $Y/(X+2C) = 1$ and $W/(X+2C) = 0.167$, and comparison with experiments

Fig. (10. 6 b)

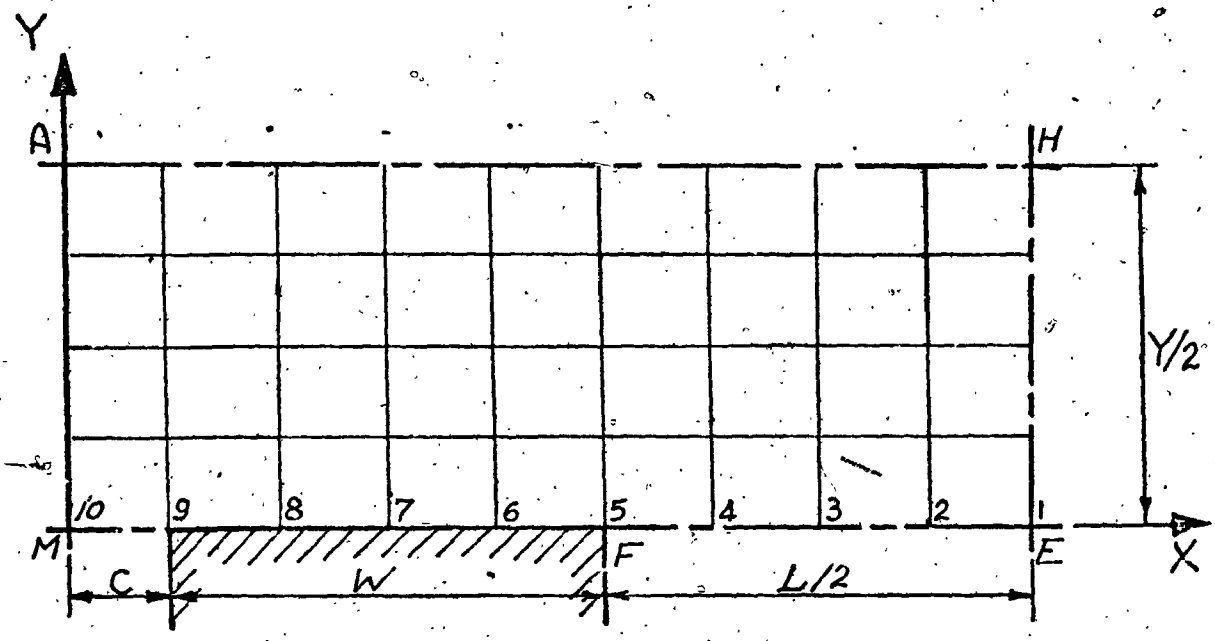

Fig. (10.7)

A Typical F.D. mesh for analysis of the quadrant A-H-E-M.

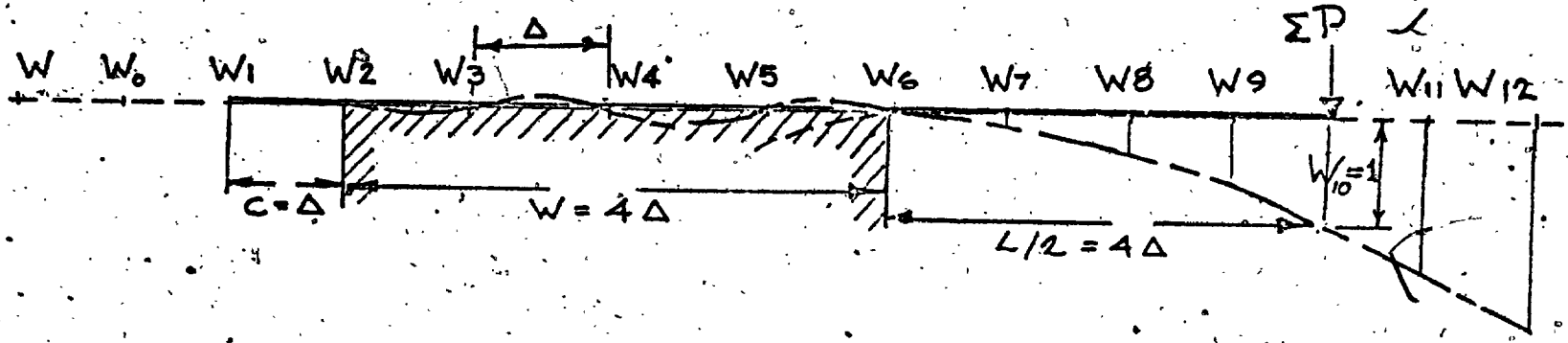

Fig. (10.8)

A one-dimensional F.D. mesh for analysis of the limiting case $Y \ll L - \Delta = L/8$.

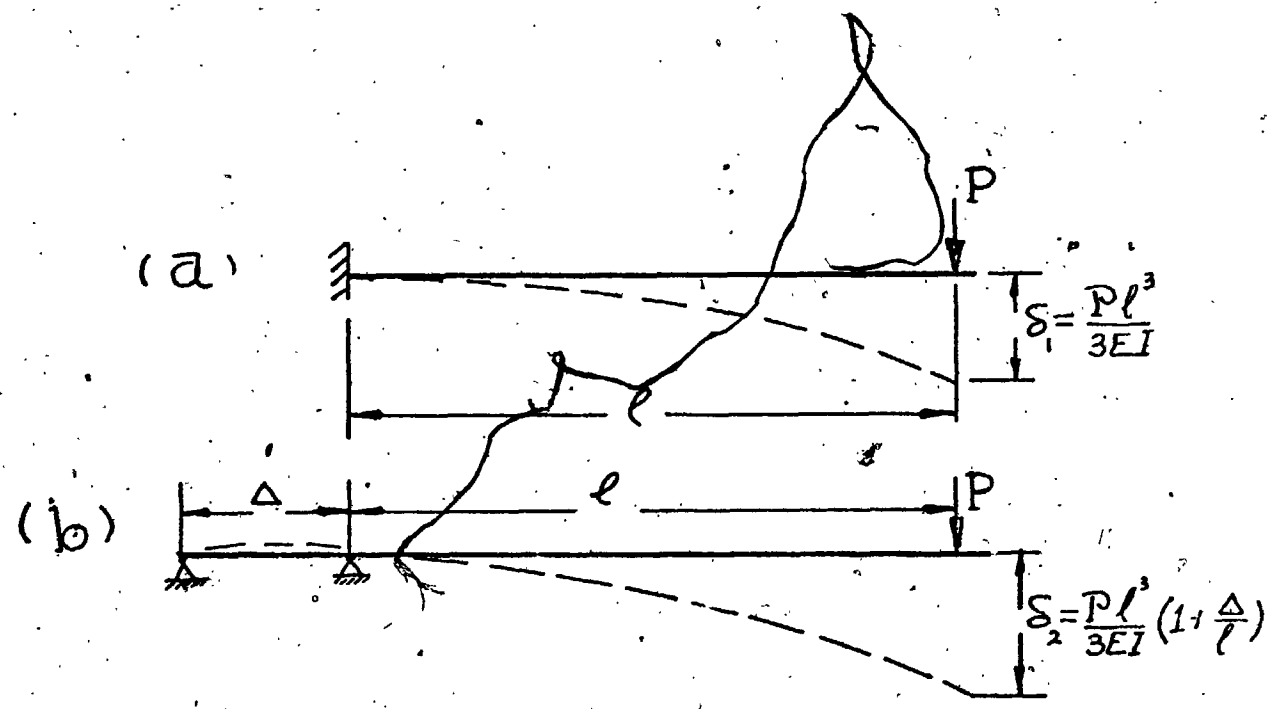

FIG (10.9)

Stiffness of a cantilevered beam as opposed to a beam pinned at two close points.

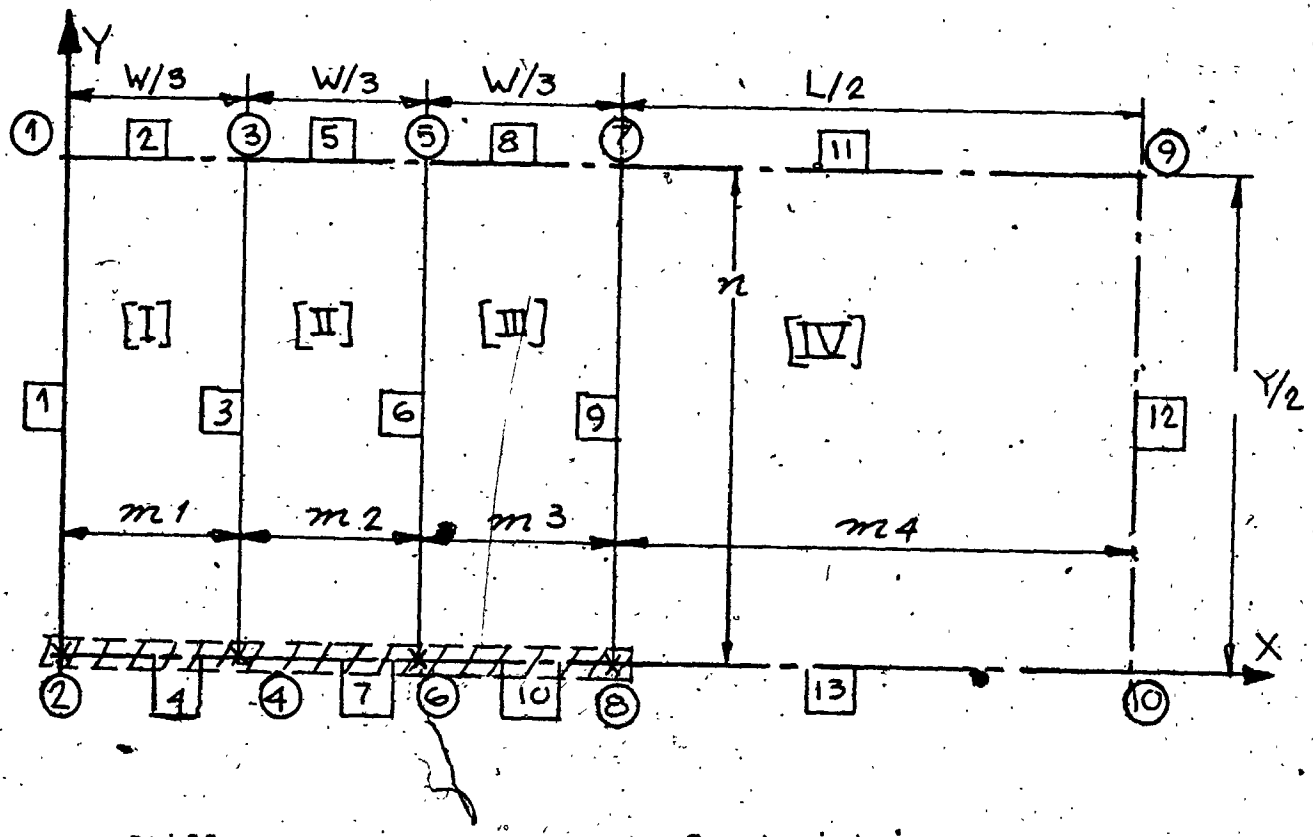

Stiffness

$\nu = 0.19$

$D_x = D_y = D$

(Isotropic)

Additional Constraints

Node No.	Constraint relationship
2	$t = 0$
4	$t = 0$
6	$t = 0$
8	$t = 0$
9	$t = 1$
10	$t = 1$

Constraints

Edge No.	Type of Constraint
2	r
4	r
5	r
7	r
8	r
10	r
11	r
12	t
13	r

Fig. (10.10).

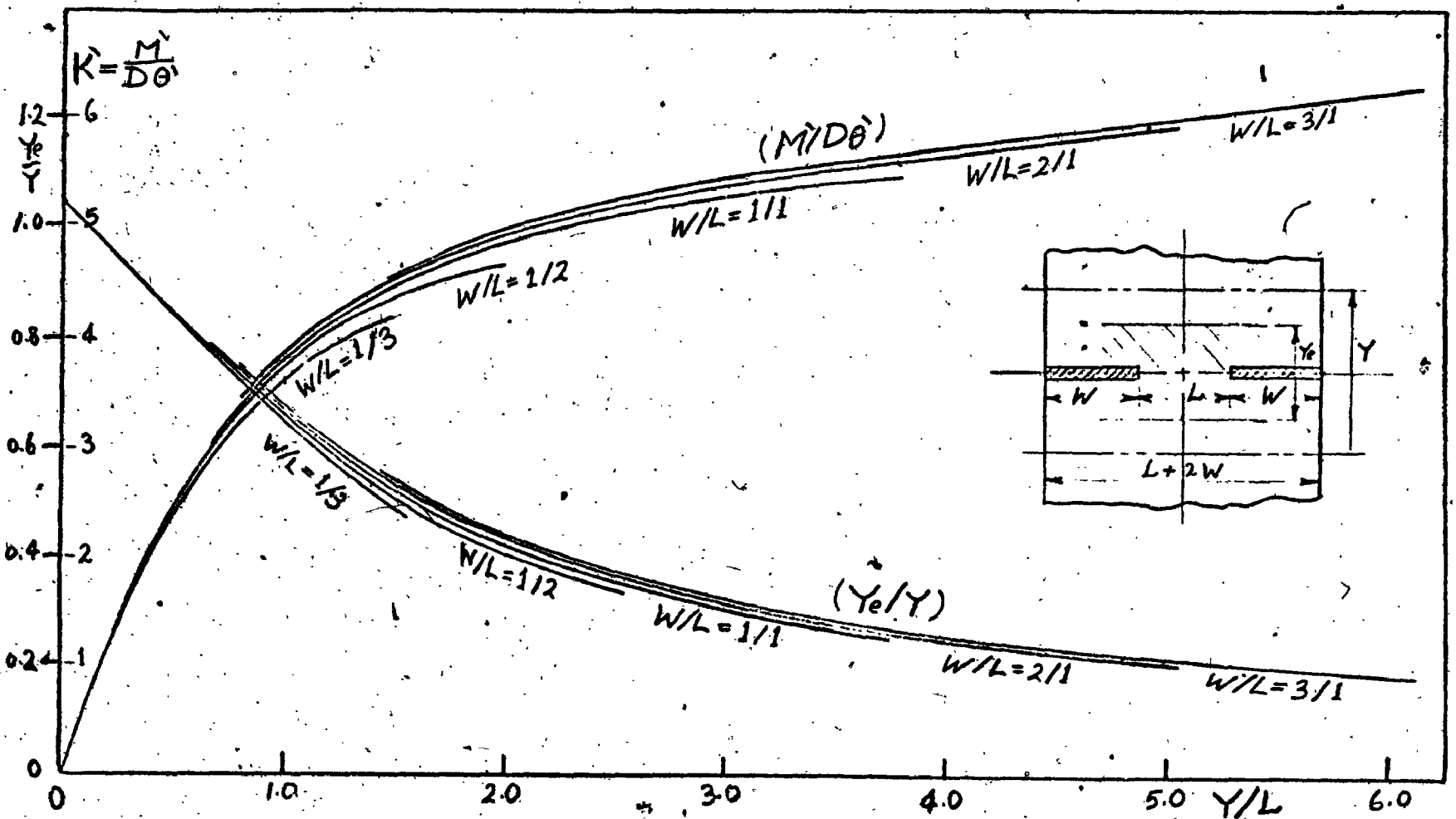
K̂ = M̂ / Dθ̂
Ye/Y
1.2
1.0
0.8
0.6
0.4
0.2
0
6
5
4
3
2
1
(M̂/Dθ̂)
W/L=3/1
W/L=2/1
W/L=1/1
W/L=1/2
W/L=1/3
(Ye/Y)
W/L=1/3
W/L=1/2
W/L=1/1
W/L=2/1
W/L=3/1
Ye
Y
W
L
W
L+2W
0
1.0
2.0
3.0
4.0
5.0
Y/L
6.0

FIG. (10-11)

Fig. (10.12)

Type (1)

Two raws, symmetric, no overhangs.

$$\frac{Y_e}{Y} = f_n\left(\frac{Y}{L}\right)$$

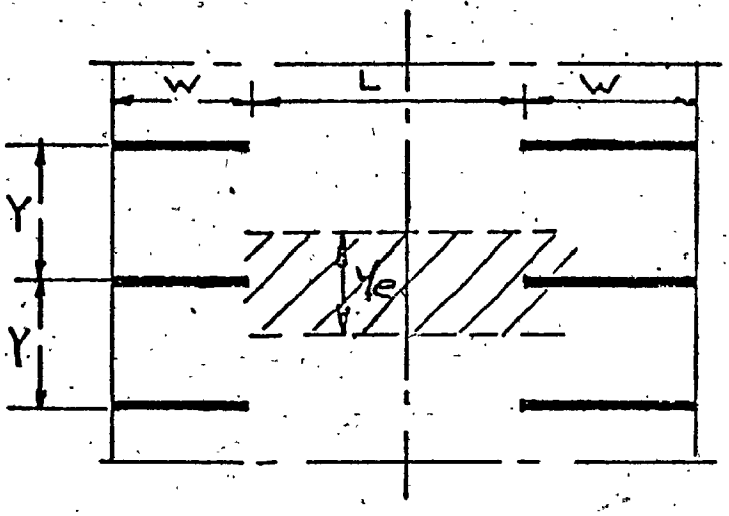

Type (2)

Two raws, symmetric, with overhangs.

$$\frac{Y_e}{Y} = f_n\left(\frac{Y}{L}\right)$$

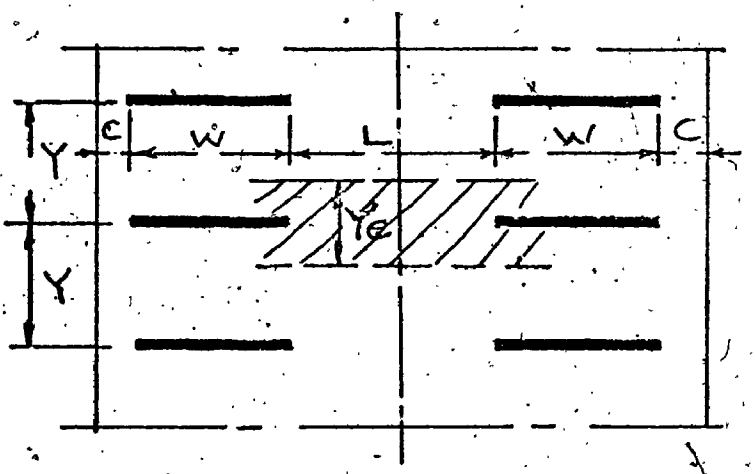

Type (3)

Two raws, asymmetric, with one.overhang.

$$\frac{Y_e}{Y} = f_n\left(\frac{Y}{L}\right)$$

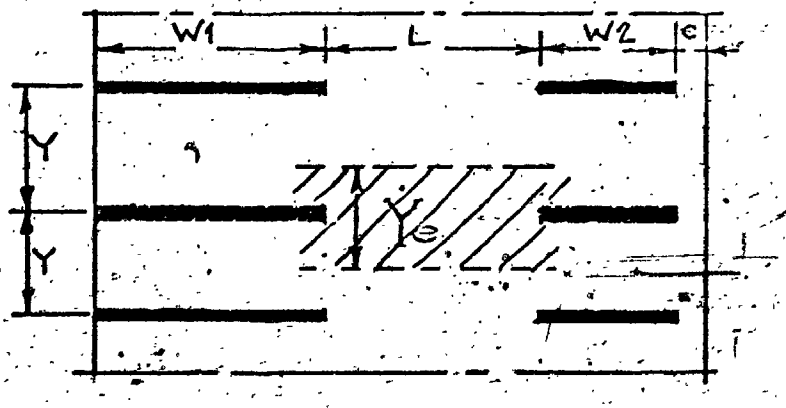

Type (4)

More than two raws, asymmetric with over-hangs.

$$\frac{Y_{e_1}}{Y} = f_n\left(\frac{Y}{L_1}\right)$$

$$\frac{Y_{e_2}}{Y} = f_n\left(\frac{Y}{L_2}\right)$$

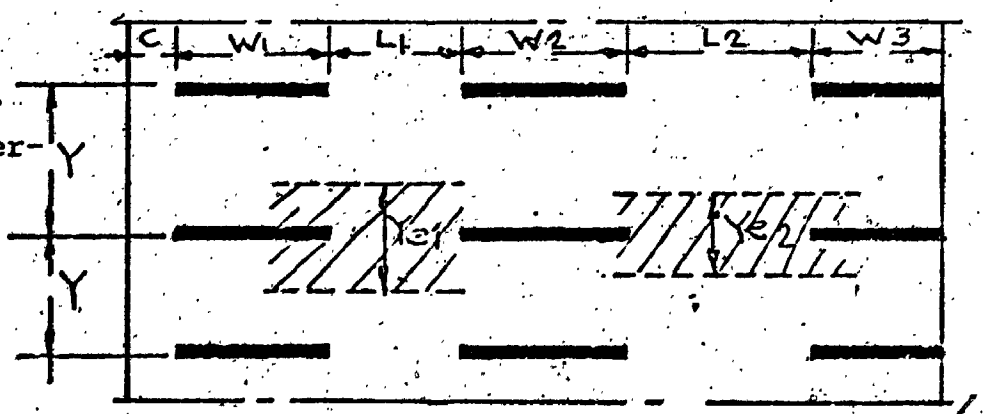

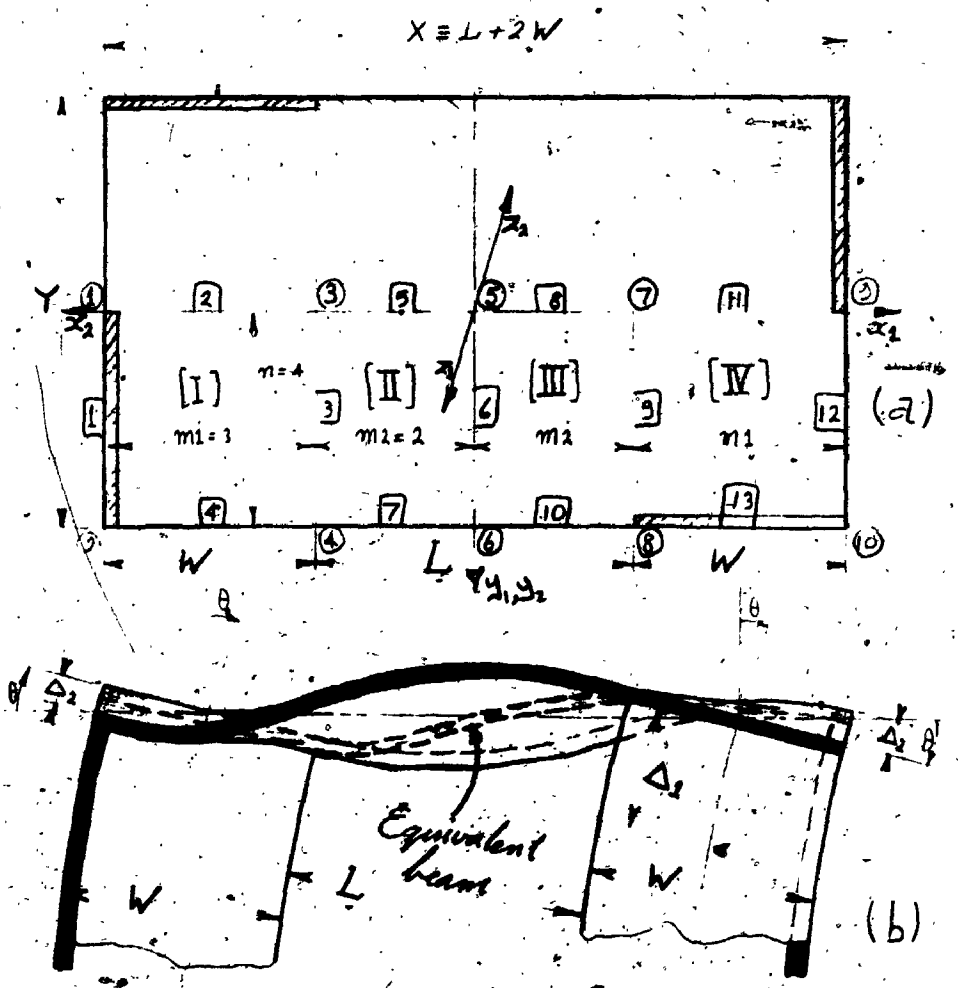

Stiffness:

$D_x = D_y = D$

$\nu = 0.19$

Constraints:

Edge No.	Type of Constraint
1	Trans. & Rot.
13	Trans. & Rot.

Additional Constraints:

- Trans. at node 1 = Trans. at node 2 = Trans. at node 9 = $.5\Delta_1 + \Delta_2$
- Trans. at node 3 = Trans. at node 7
- Trans. at node 8 = Trans. at node 10 = $.5\Delta_1$
- Trans. at node 5 = 0
- X-Rot. at node 9 = Y-Rot. at node 9 = 0
- X-Rot. at node 3 = X-Rot. at node 7
- Y-Rot. at node 3 = -Y Rot. at node 7
- Twist at node 3 = -Twist at node 7
- Twist at node 5 = 0
- Trans. at edge 2 = Trans. at edge 11
- Trans. at edge 5 = Trans. at edge 8
- Rot. at edge 2 = -Rot. at edge 11
- Rot. at edge 5 = -Rot. at edge 8

FIG. (10.13)

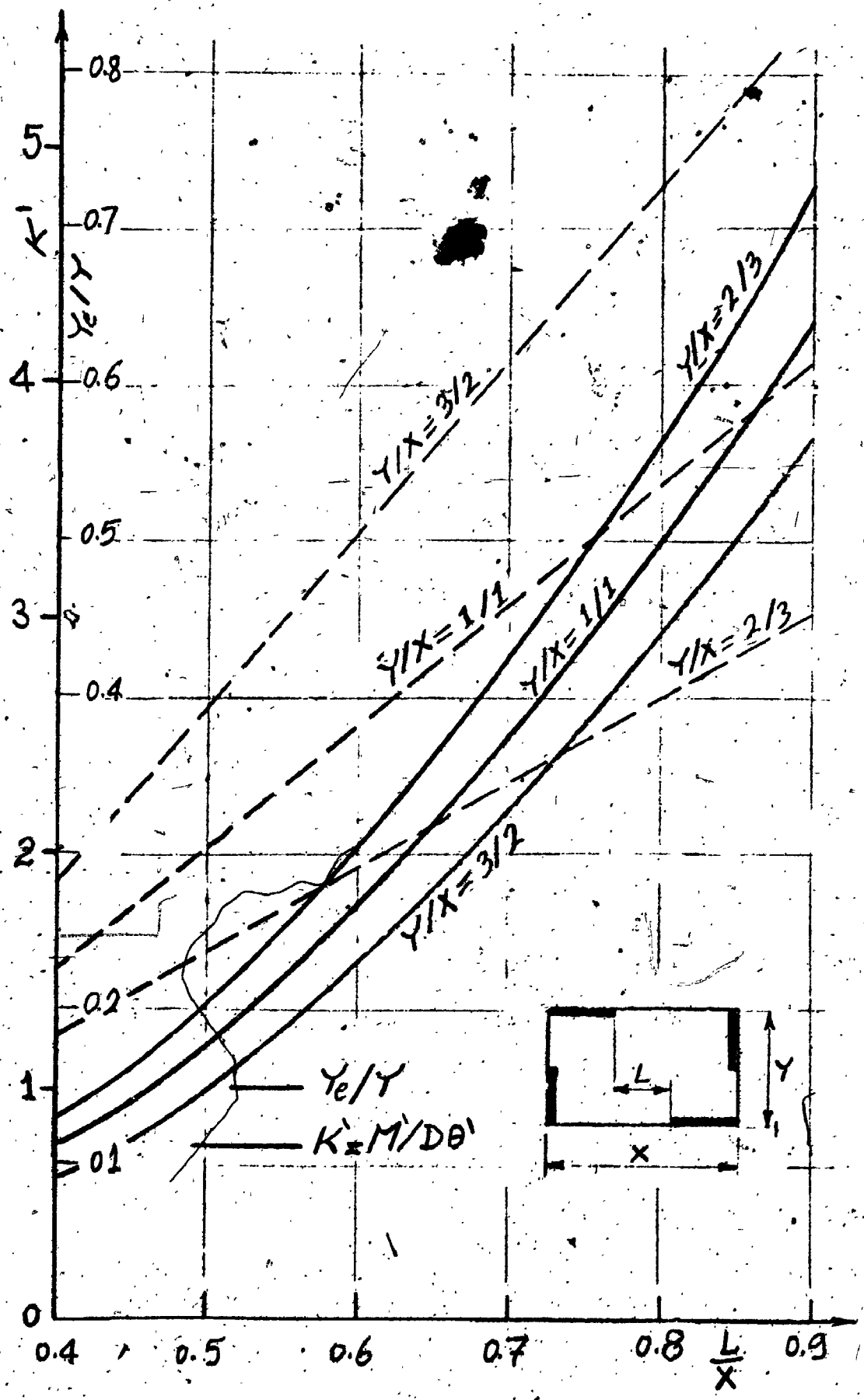

Fig. (10.14)

Design Data for the Four-Wall Rotationally-Symmetric Structure

CHAPTER XI

THE LARGE INPLANE STRESS ELEMENT

11.1 Introduction

In Chapter IV, the variational approach (Ritz method) was used to treat the two dimensional elasticity problem for a rectangular isotropic plate having any combination of simple boundary conditions. It was shown that the equations and the boundary conditions are directly analogous to those of the static plate bending problem. As a result, it was shown that the same assumed series of functions and even the same computer program (with minor modifications) can be used for both the plate bending problem and the inplane elasticity problem. Extending this idea, it was found desirable to use the same approach in order to obtain the inplane elasticity element analogous to the large plate bending element derived in Chapter VII.

As with the plate bending element, an orthotropic material will be assumed. A potential function-type formulation will be used and the same displacement series employed for the plate bending element will be assumed for the potential function. Characteristic matrices directly analogous to those of the bending element will then

be derived. The modifications which had to be introduced into the computer program in order to be able to handle the inplane stress problem will also be pointed out.

In order to test and demonstrate the use of the Large Inplane Stress Element, several examples have been solved and compared, whenever possible, with already available theoretical and/or experimental results. The following four examples will be considered:

i) A narrow deep girder of a rectangular cross-section, fixed at both ends and uniformly loaded along its top edge.

ii) Uniformly loaded deep I-girder.

iii) Rectangular plate with a square hole under uniform edge traction.

iv) Tip loaded short T-cantilever.

11.2 Derivation of the Characteristic Matrices

As with the plate bending element, the first step is to define the governing variational expression for the problem. In the present problem, this may be achieved by writing the strain energy expression for the element and requiring it to be stationary:

$$\delta(U)=\delta\{\frac{1}{2} \cdot t \int_0^b \int_0^a (\sigma_x \cdot \varepsilon_x + \sigma_y \cdot \varepsilon_y + \tau_{xy} \cdot \varepsilon_{xy}) \cdot dx \cdot dy\} = 0, \quad (11.1)$$

where (U) represents the strain energy of the large element; σ_x, σ_y and τ_{xy} the components of the plane stress; and

ε_x, ε_y and ε_{xy} are the inplane strain components. For an orthotropic elastic material under plane stress conditions the following stress-strain relationships may be written:

$$\varepsilon_x = \frac{1}{E_x}(\sigma_x - \nu_y \cdot \sigma_y),$$

$$\varepsilon_y = \frac{1}{E_y}(\sigma_y - \nu_x \cdot \sigma_x), \quad \text{and} \qquad (11.2)$$

$$\varepsilon_{xy} = \tau_{xy} / G,$$

where E_x, E_y, ν_y, ν_x and G are the elasticity constants for the orthotropic material, and are related by the relation

$$E_x \cdot \nu_x = E_y \cdot \nu_y . \qquad (11.3)$$

Also defining a force potential function $\bar{\Psi}$ such that

$$N_x = \frac{\partial^2 \bar{\Psi}}{\partial y^2}, \quad N_y = \frac{\partial^2 \bar{\Psi}}{\partial x^2}, \quad N_{xy} = -\frac{\partial^2 \bar{\Psi}}{\partial x . \partial y},$$

$$\text{or:} \quad \sigma_x = \frac{1}{t} \cdot \frac{\partial^2 \bar{\Psi}}{\partial y^2}, \quad \sigma_y = \frac{1}{t} \cdot \frac{\partial^2 \bar{\Psi}}{\partial x^2}, \quad \tau_{xy} = -\frac{1}{t} \cdot \frac{\partial^2 \bar{\Psi}}{\partial x . \partial y} . \qquad (11.4)$$

Here, a "force" potential and not "stress" function was defined since, at an interface between two elements, continuity of *forces* rather than *stresses* is to be preserved, as will be shown in the examples of section (11.3).

Making use of *(11.2)* through *(11.4)*, equation *(11.1)* becomes:

$$\{1/2 \int_0^b \int_0^a [\bar{D}_x \left(\frac{\partial^2 \bar{\Psi}}{\partial x^2}\right)^2 + \bar{D}_y \left(\frac{\partial^2 \bar{\Psi}}{\partial y^2}\right)^2 + 2 \cdot \bar{D}_{xy} \left(\frac{\partial^2 \bar{\Psi}}{\partial x^2} \cdot \frac{\partial^2 \bar{\Psi}}{\partial y^2}\right)$$

$$+ 4 \bar{D}_k \left(\frac{\partial^2 \bar{\Psi}}{\partial x \cdot \partial y}\right)^2] . dx . dy\} = 0, \qquad (11.5)$$

where;

$$\bar{D}_x = \frac{1}{t . E_x} , \quad \bar{D}_y = \frac{1}{t . E_y} ,$$

$$\bar{D}_k = \frac{1}{4tG} , \quad \text{and} \quad \bar{D}_{xy} = - \frac{\nu_y}{t . E_x} . \qquad (11.5a)$$

Equation *(11.5)* is identical in form to equation *(7.12)*, which is the variational expression stated for the plate flexure problem, except for the absence of the inertia term which is peculiar to dynamic problems.

Proceeding by assuming the potential function $(\bar{\Psi})$ to take the form of a double series identical to that used for the displacement (W) in the flexure problem - equation *(7.13)* - it becomes:

$$\bar{\Psi}(\eta_i, \xi_j) = \sum_{k=1}^{m+4} \sum_{l=1}^{n+4} A_{kl} \cdot \phi_k(\eta_i) \cdot \phi_l(\xi_j) ; \qquad (11.6)$$

where η_i, ξ_j, A_{kl}, ϕ_k and ϕ_l have the same meaning as in equation *(7.13)*.

Proceeding in the same manner as described in section (7.2) in connection with the plate bending element, the following matrix equation is finally reached:

$$[\bar{K}^{i,j}]_{(m+4)(n+4) \times (m+4)(n+4)} \cdot \{A\}_{(m+4)(n+4)} = 0, \qquad (11.7)$$

where $[\bar{K}^{i,j}]$ is the characteristic matrix for the two-dimensional inplane stress element. The coefficients of this matrix are given by:

$$\bar{K}^{i,j}_{kl,rs} = \bar{D}_x \cdot \frac{b_j}{a_i^3} \cdot F_{k,r} \cdot B_{l,s} + \bar{D}_y \cdot \frac{a_i}{b_j^3} \cdot B_{k,r} \cdot F_{l,s}$$

$$+ \frac{\bar{D}_{xy}}{a_i \cdot b_j} \cdot (C_{k,r} \cdot C_{s,l} + C_{r,k} \cdot C_{l,s}) + \frac{4\bar{D}_k}{a_i \cdot b_j} \cdot E_{k,r} \cdot E_{l,s} \,, \qquad (11.8)$$

which, as expected, is identical to equation (7.15) with $(\bar{D})$ replacing (D) throughout, and includes the same integral coefficients defined therein.

The above formulation is for an element free from body forces. Body forces, however, can easily be accommodated in the formulation in the same manner as shown in Chapter IV for single isotropic plate problems using modified beam functions. With the resulting characteristic equation (11.7) being homogeneous, the only source of loading is through the prescribed boundary conditions. In the case of the modified beam functions solution presented in Chapter IV, an additional function (ϕ_o) - usually a polynomial - had to be provided in order to represent the boundary loading conditions. Here, however, the assumed series (11.6) already includes degrees of freedom associated with the element edges and corner points. It is these boundary degrees of freedom that make it possible to match

any set of prescribed boundary loading and constraint conditions using series *(11.6)* only. This will be described in the following:

In general, any inplane boundary condition may be specified as a combination of any two of the following basic conditions;

1. Prescribed normal loading $p(s)$, or

$$\frac{\partial^2 \bar{\psi}}{\partial s^2}\Big|_\Gamma = p(s). \qquad (11.9)$$

2. Prescribed shear force $q(s)$, or

$$-\frac{\partial^2 \bar{\psi}}{\partial n \cdot \partial s}\Big|_\Gamma = q(s). \qquad (11.10)$$

3. Prescribed normal displacements $U_n(s)$, or;

$$u_n\Big|_\Gamma = U_n(s) \qquad (11.11)$$

4. Prescribed tangential displacements $U_s(s)$, or;

$$u_s\Big|_\Gamma = U_s(s). \qquad (11.12)$$

Where, in the above expressions, n and s are the normal and tangential coordinates at any point along the boundary Γ; also U_n and U_s are the normal and tangential components of the boundary displacement. In the following sub-sections, each of the above basic conditions will be dealt with separately.

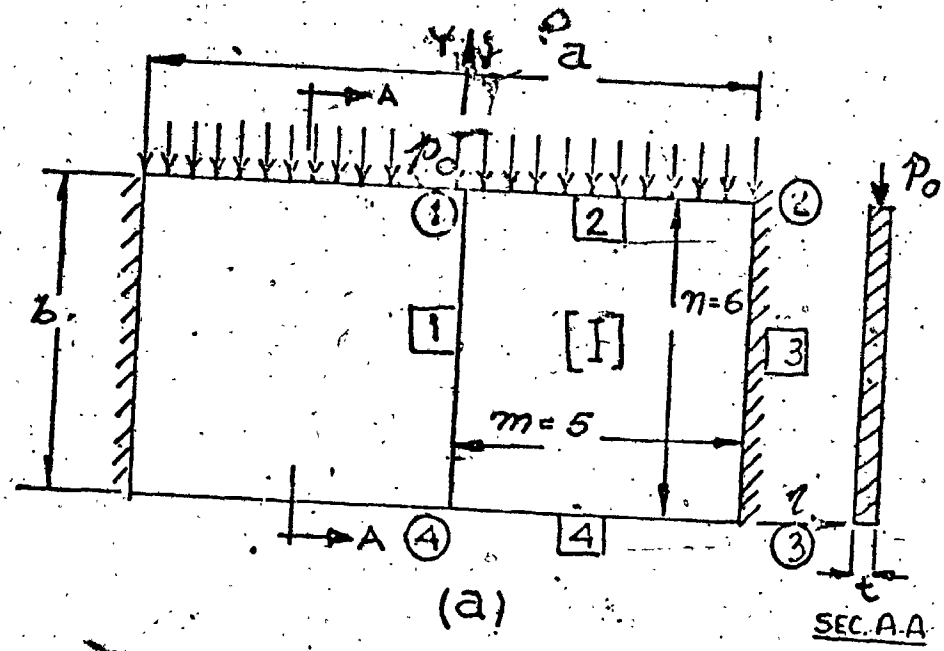

(a)

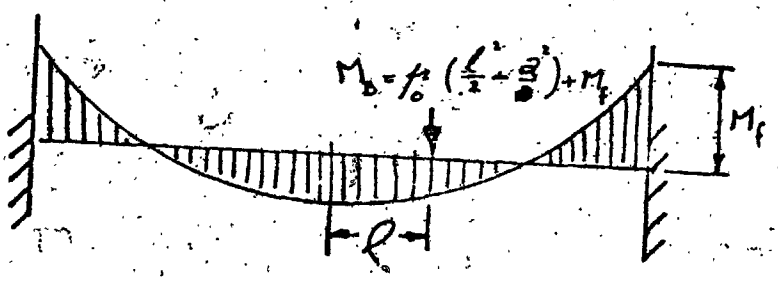

(b)

Stiffness

$\nu = 1/6$

$\bar{D}_x = \bar{D}_y = 1/tE = 1$

(Isotropic)

Constraints

Edge No.	Type of Constraint
1	r
2	t , r
4	t, r

Additional Constraints

- Trans. at Node (1) = $p_o a^2/8$
- Rot. about (ξ) at Node (2) = $- p_o a/2$
- Trans at Node (3) = Trans. at Node (4) $\neq 0$

Fig. (11.1)

$$A_{m+1,n+1} = -M_B(0),$$

$$A_{m+1n+2} = \frac{-1}{b_j} d[M_B(0)]/d\xi_j$$

$$A_{m+1,n+3} = -M_B(1), \quad \text{and} \tag{11.15}$$

$$A_{m+1,n+4} = \frac{-1}{b_j} d[M_B(1)]/d\xi_j .$$

The coefficients $A_{m+1,l}$, for l equals 1 through n, can then be evaluated by making use of the orthogonality property of the beam functions $\phi_l(\xi_j)$. These are given by:

$$A_{m+1,l} = \int_0^1 -\bar{M}_B(\xi_j) \cdot \phi_l(\xi_j) \cdot d\xi_j \quad (l=1,2,\ldots,n); \tag{11.16}$$

where

$$\bar{M}_B(\xi_j) = M_B(\xi_j) + \sum_{l=n+1}^{n+4} A_{m+1,l} \cdot \phi_l(\xi_j) . \tag{11.16a}$$

The same general procedure described above can be used for the case where any other edge is loaded with prescribed normal forces.

In many practical problems, however, the load $p(s)$ is concentrated at a point, uniformly distributed, or linearly varying over the edge of an element. In such cases, the bending moment (M_B) becomes a cubic function and can be completely represented by the last four terms of the assumed series (i.e. the Hermitian functions) only, thus eliminating the need for evaluating the integrals involved in equation (11.16). Equation (11.15) will thus suffice

for defining the boundary condition (11.9).

11.2.2 The Prescribed Shear Load Boundary Condition

The direct integration of equation (11.10) with respect to (s) yields:

$$\frac{\partial \Psi}{\partial n}\Big|_{\Gamma} = -\int_{a}^{s} q(z) \cdot dz + C_3, \qquad (11.17)$$

where the constant of integration C_3 is an arbitrary constant which may be chosen to be zero. The integral appearing in the right hand side represents the cumulative (total) inplane shear force at any point. Only the terms in the series expression for Ψ-equation (11.6) - which represent the rotational degrees of freedom along the portion of the boundary of interest will contribute to the left hand side of equation (11.17). Considering the case where the edge $(\eta = 0)$ of the element (i,j) is loaded with the shear load $q(\xi_j)$, which results in the cumulative shearing force $Q_x(\xi_j)$, the boundary condition (11.17) may be written as:

$$\sum_{l=1}^{n+4} A_{m+2,l} \cdot \phi_l(\xi_j) = -Q_x(\xi_j) \qquad (11.18)$$

The coefficients $A_{m+2,l}$ may be determined from equation (11.18) in the same manner described in the previous subsection using the relations:

$$A_{m+2,n+1} = -Q_x(0),$$

$$A_{m+2,n+2} = -\frac{a}{b_j}\, d[Q_x(0)]/d\xi_j,$$

$$A_{m+2,n+3} = - Q_x(1),$$

$$A_{m+2,n+4} = - \frac{1}{b_j} \cdot d[Q_x(1)]/d\xi_j \cdot , \quad \text{and}$$

$$A_{m+2,l} = - \int_0^1 \bar{Q}_x(\xi_j) \cdot \phi_l(\xi_j) \cdot d\xi_j \quad (l=1,2,\ldots,n);$$

where

$$\bar{Q}_x(\xi_j) = Q_x(\xi_j) + \sum_{l=n+1}^{n+4} A_{m+2,l} \cdot \phi_l(\xi_j). \qquad (11.19)$$

If the shear load $q(s)$ is uniform, linear, or parabolic over the edge of an element, the cumulative force $Q(s)$ will be of the third degree - or less - and can be represented by a combination of the four Hermitian functions only. In such a case, no integration will be needed in order to represent this boundary condition.

11.2.3 The Prescribed Normal Displacements Boundary Condition

Differentiating equation (11.11) with respect to (s) gives:

$$\frac{\partial u_n}{\partial s}\Big|_\Gamma = (\varepsilon_{xy} - \frac{\partial u_s}{\partial n})\Big|_\Gamma = U_n'(s),$$

where ε_{xy} is the shear strain. Differentiating once more this becomes:

$$(\frac{\partial \varepsilon_{xy}}{\partial s} - \frac{\partial \varepsilon_s}{\partial n})\Big|_\Gamma = U_n''(s),$$

in which $(\frac{\partial u_s}{\partial s})$ was replaced by the tangential strain ε_s. Substituting from equation (11.2) then (11.4) and (11.5a)

the above relation can be written as:

$$\left[(\bar{D}_{ns} + 4\bar{D}_k) \frac{\partial^3 \bar{\Psi}}{\partial n . \partial s^2} + \bar{D}_s \frac{\partial^3 \bar{\Psi}}{\partial n^3} \right] \Big|_{\Gamma} = - U_n''(s) \quad (11.20)$$

For a zero right hand side of this equation - i.e. if $U_n(s)$ is a linear expression - the above equation becomes a natural boundary condition for the variational expression *(11.5)*. Consequently, no particular action would be necessary to account for this boundary condition. However, for the general case where $U_n''(s)$ is non-zero, an additional term has to be added to equation *(11.5)* to account for the work done due to the distortion of the edge. This added term can be directly obtained by comparing equation *(11.20)* with the natural boundary conditions of the general biharmonic equation *(2.10)*. Hence, after comparison with the variational expression *(2.5)*, the following line integral (I_1) has to be added inside the variational expression *(11.5)*:

$$I_1 = - \int_{\Gamma} U_n''(s) \, . \, \bar{\Psi} \, . \, ds \, .$$

With this expression taken into account, the matrix equation *(11.7)* becomes:

$$\underset{(m+4)\,(n+4)}{[\bar{K}^{i,j}]} \; \underset{(n+4)}{\{A\}} = \underset{(m+4)}{\{\bar{P}^{i,j}\}} \quad (11.21)$$

where

$$\bar{P}^{i,j}_{k,l} = \int_{\Gamma} U_n''(s) \, . \, \phi_k(\eta_i) \, . \, \phi_l(\xi_j) \, . \, ds \, . \quad (11.22)$$

Since this line integral is defined along the corresponding

edge - or edges - of the boundary, only the terms corresponding to the "translational" degrees of freedom along these edges will be non-zeros. For example, if (Γ) represents the edge ($\eta_j=0$), the integral (11.22) becomes:

$$\bar{P}^{i,j}_{m+1,l} = b_j \int_0^1 U_n''(\xi_j) \cdot \phi_l(\xi_j) \cdot d\xi_j \,,$$

$$\bar{P}^{i,j}_{k,l} = 0 \qquad \text{for } (k \neq m+1) \cdot \quad (11.23)$$

Similar expressions for $\{\bar{P}\}$ can be obtained for any of the other edges of the large element. In most applications, however, the constrained edge remains straight, and the right hand vector $\{\bar{P}\}$ vanishes.

11.2.4 The prescribed Tangential Displacements Boundary Condition

Starting with equation (11.12) and differentiating w.r.t.(s) yields:

$$\frac{\partial u_s}{\partial s}\Big|_\Gamma = \varepsilon_s\Big|_\Gamma = U_s'(s). \qquad (11.24)$$

Substituting from equation (11.2) then (11.4) and (11.5a), this becomes:

$$-\left(D_s \cdot \frac{\partial^2 \bar{\Psi}}{\partial n^2} + D_{ns} \cdot \frac{\partial^2 \Psi}{\partial s^2}\right)\Big|_\Gamma = U_s'(s) \qquad (11.25)$$

If $U_s(s)$ is a constant, i.e. a zero tangential strain condition, equation (11.25) becomes a natural boundary condition for the variational expression (11.5). In such a case, it is not necessary to take any action in order to satisfy

such conditions beforehand as was shown in Chapters II and III. If the right hand side of equation (11.25) is non-zero, however, an account for the work done due to the resulting edge tangential strain has to be taken into account in equation (11.5). To do so, the following line integral (I_2) is to be added inside the variational expression (11.5):

$$I_2 = \int_\Gamma U_s'(s) \cdot \frac{\partial \Psi}{\partial n} \cdot ds \ .$$

With this added term, the matrix equation (11.7) becomes:

$$[\bar{K}^{i,j}] \cdot \{A\} = \{\bar{\bar{P}}^{i,j}\}, \qquad (11.26)$$

where

$$\bar{\bar{P}}^{i,j}_{k,l} = - \int_\Gamma U_s'(s) \cdot \frac{\partial}{\partial n}[\phi_k(\eta_i) \cdot \phi_l(\xi_j)] \cdot ds \ . \qquad (11.27)$$

Only the terms corresponding to the "rotational" degrees of freedom along the portion of the boundary (Γ) of interest will contribute non-zero values to the loading vector $\{\bar{\bar{P}}^{i,j}\}$. For example, if (Γ) represents the edge ($\xi_j=1$), the above vector becomes:

$$\bar{\bar{P}}^{i,j}_{k,n+4} = - a_i \int_0^1 U_s'(\eta_i) \cdot \phi_k(\eta_i) \cdot d\eta_i \ ,$$

$$\bar{\bar{P}}^{i,j}_{k,l} = 0 \qquad \text{for } (l \neq n+4). \qquad (11.28)$$

Similar expressions can be obtained if (Γ) is along any other edge of the large element. In most practical applications, however, the tangential stress along the edge is zero and

the vector $\{\bar{P}\}$ is zero.

11.3 Application to Practical Examples

In order to apply the formulations derived in the previous section to practical examples, certain modifications had to be introduced into the computer program initially written to handle flexure problems using large elements. The following are the major modifications introduced:

- Replace the stiffness parameters D_x, D_y, D_{xy} and D_k by the parameters $\bar{D}_x$, $\bar{D}_y$, $\bar{D}_{xy}$ and $\bar{D}_k$ defined by equation *(11.5a)*.
- The boundary conditions of types (1) and (2) - i.e. prescribed edge inplane loads - were handled in the same manner as the prescribed displacements in flexure problems which were discussed in section (11.2). A simple routine to compute the coefficients $(A_{k,l})$ along the boundary as defined by equations *(11.13)* through *(11.19)*, and introduce their values as "additional constraints", was written and modified individually for each problem.
- Boundary conditions of types (3) and (4) - i.e. prescribed edge inplane displacements - require the calculation of the load vectors $\{\bar{P}\}$ or $\{\bar{P}\}$. The same procedure described in section (7.4) for defining the static load vector $\{P\}$ was used directly to handle the

vectors $\{\bar{P}\}$ and $\{\overline{\bar{P}}\}$ defined by equations *(11.22)* through *(11.28)*.

The data reduction routine used initially to compute, and prepare plots for, the displacements and bending moments in the flexure problem had to be modified in order to output the inplane stresses σ_x, σ_y, and τ_{xy} as defined by equation *(12.4)* - instead. In addition, the principal stresses σ_{max}, σ_{min} and τ_{max}, as well as the Isoclinics (lines defining the direction of the principle stress-θ) as defined by equations *(4.13)*, were computed and plotted in the form of contour maps.

After the above-mentioned modifications were introduced, the program was used to solve several examples of practical and/or academic interest. A brief description for these examples as well as the results obtained, is given in the following sub-sections. Whenever possible, comparisons with available results are made.

11.3.1 Uniformly Loaded Deep Girder of a Narrow Rectangular Section

This problem may be idealized as a plane elasticity problem with mixed boundary conditions. The geometry of the problem is shown in figure (11.1a). The girder has clamped ends and is uniformly loaded along its top edge. Values of the length/depth ratio *(a/b)* of 1,2 and 3 will be considered. This problem has been previously treated in references [55]

and [15] using ordinary and modified Finite Differences respectively. The girder is assumed to be thin and isotropic, and Poisson's ratio taken as (1/6).

Making use of the symmetry, one large element is used to model half the girder as shown in figure (11.1a). The boundary conditions along the clamped edge (edge 3) are natural and no constraints need to be specified there. Along the line of symmetry (edge 1) the boundary conditions are zero normal displacements and zero shearing force. The first of these is natural and does not need any particular action, while the second requires that the "rotational" degrees of freedom be constrained along the edge according to equation *(11.17)*. The shearing force is equal to zero along the top and bottom edges, leading to constraining the "rotational" degrees of freedom along these two edges as well. Due to the loads applied, the normal inplane load along the top edge (edge 2) is equal to p_b. Accordingly, the determination of the corresponding constraints involves the second integral of the load - or the bending moment diagram - along that edge, which is shown in figure (11.1b). The value of the fixed end moment at node No. 2 (M_f) is statically indeterminate. In order to get rid of this undetermined value, the constant of integration C_1 shown in equation *(11.13)* is set equal to $(-M_f)$ causing $(\bar{\psi})$ to be equal to zero at node No. 2. Due to symmetry, however, the constant C_2 must be set to zero. Since the bending moment

distribution is parabolic, it can be completely represented by the Hermitian functions - through making use of equations *(11.15)* - which represent the degrees of freedom at nodes No. 1 and 2. Thus, the "translational" degrees of freedom along the top edge should also be restrained.

Since the normal load along the bottom edge is zero, equation *(11.13)* indicates that $(\bar{V})$ should be equal to $(C_1 + C_2 s)$. Again, due to symmetry, the constant (C_2) must be set to zero. The constant (C_1), however, cannot be arbitrarily fixed. This is due to the fact that the free portions of the boundary are not simply-connected and that only three integration constants can be arbitrarily specified in any one problem. Therefore, the translational degrees of freedom at nodes (3) and (4) are taken to be equal, and their common value is left as an unknown degree of freedom to be determined during the energy minimization process.

The results obtained for the square *(a=b)* are compared to those of references [55] and [15] in figure (11.2). The ratio of the tangential stress to the normal stress along the top chord of the girder (edge 2) is plotted in the figure as obtained using a 49-term series. For comparison, the results of reference [55] obtained using a 12 x 12 Finite Difference mesh (about 100 equations to represent half the plate) and an Airy stress function formulation are superimposed upon the Large Element results. In addition, results obtained using Modified Finite Differences and a mixed formulation [15] on a 7 x 7 mesh (a total of about 160 equations)

are shown on the graph. Three sets of results were reproduced from reference [15] that correspond to boundary approximations of the order of $(1/n)$, $(1/n^2)$ and $(1/n^3)$ and show continuous improvement near the corners. As was shown in Chapter IV, the corner between a clamped and a free edge represents a singular point. Consequently, the exact solution for the problem includes infinite stresses at the corners. Since the Large Element solution yields a higher corner stress (compared with the other two solutions), this indicates that it is more capable of representing sharp stress variations and consequently yields "better" results than the other two solutions.

Contour plots representing the distribution of the principle stresses in the girder, as well as the Isoclinic lines, were generated using the same procedure described in section (4.4.1). These plots are reproduced in figures (11.3) through (11.5) for girders having depth to length ratios of 1:1, 1:2 and 1:3 respectively.

The bending stresses (σ_x) along the line of symmetry of the girder are shown in figure (11.6) for three depth/length ratios. It can be seen that although the stress distributions quickly approach the linear law corresponding to the beam theory, the actual values of the stress are still considerably different.

11.3.2 Uniformly-loaded Deep I-Girder

This example is an extension of the previous problem

into a more complicated three-dimensional structure. The uniformly-loaded deep girder of this example is a metal beam (steel) of an I-type cross-section as shown in figure (11.7a). As with the first example, the beam is built-in at both ends, uniformly loaded along its top, and free at its bottom. To the author's knowledge, no published results concerning this problem are available.

Two planes of symmetry can be recognized in this problem: the (η-ξ) and the (ξ-μ) planes. As a result, three large elements can be used in order to represent one quarter of the structure as shown in figure (11.7). Since the thicknesses of these elements are small with respect to their linear dimensions, it is evident that their bending stiffnesses (which are proportional to t^3/l^3) can be neglected in comparison with their in-plane stiffnesses (which are proportional to t/l). In other words, the bending stiffness of the flanges about their own neutral axes can be neglected in comparison with the bending stiffness of the whole girder. As a result, only the inplane deformations of the three large elements need to be taken into account in the analysis; and hence the element derived in section (11.2) can be used directly. The material properties and dimensions of the cross-section assumed are also shown in figure (11.7).

Since the potential function ($\bar{\Psi}$) is a scalar, each of the elements can be treated individually - without the need to coordinate transformations - provided that continuity

conditions are applied in order to ensure compatibility between the elements. This is demonstrated in figure (11.7b) where the structure is developed into its three elements and then the "additional constraints" table is used to match the common degrees of freedom. Due to symmetry about the (ξ-η) plane, the boundary conditions at edges No. (2), (6) and (10) are zero shear and zero normal displacements. The second of these conditions is natural, while the first has to be enforced by constraining the "rotational" degrees of freedom along these edges. Since edges No. (3), (7) and (11) are completely fixed, the resulting boundary conditions there are all natural and no constraints need be applied. On the other hand, the two external edges - edges No. (1) and (12) - are completely free. Consequently, both translational and rotational degrees of freedom have to be constrained.

Along the common edges (4) and (5), as well as (8) and (9), both the shearing forces and the tangential displacements have to be continuous between the web and the flange elements. For continuity of the shearing forces, the rotational degrees of freedom have to be matched between edges (4) and (5) and between (8) and (9). Continuity of the tangential displacements, however, is a natural condition. Similarly, degrees of freedom corresponding to rotations about the common edges and twisting are to be matched between nodes number (1) and (8); (2) and (7); (3) and (10); and (4) and (9). In addition, since the normal

loading on the top and bottom edges of the web (element No. I) is identical to that in the case of the rectangular girder of section (11.3.1), the same "additional constraints" listed in figure (11.1) as well as the related discussions are applicable to edges No. (5) and (8) of the present example.

As with the previous example, the problem was solved for three depth-to-length ratios; namely b:a equals 1:1, 1:2 and 1:3. The results are shown in figures (11.8) through (11.13) in the form of contour plots for the principle forces (the principle stresses multiplied by the thickness of the element) as well as the Isoclinic lines for each of the three elements.

11.3.3 Rectangular Plate With a Square Hole Under Edge Traction

The interior planning of buildings to admit light and ensure easy communications involves introducing discontinuities in the structure. Study of the stress distributions due to sudden changes in the cross-sections of walls caused by windows and doorways has therefore become a classical problem in the subject of two-dimensional elasticity. The conformal transformations approach has been widely used for determining the stress distributions around holes of different shapes in infinitely large plates. If the size of the hole is comparable with the size of the plate itself, however, the resulting boundary-value problem becomes co-

siderably more difficult due to the fact that the boundary is not simply-connected. Consequently, experimental techniques were often used to investigate problems of this type. The effect of piercing a wall with a square opening was investigated in reference [56] using the Photo-Elasticity method. The experimental model used in reference [56] has the overall dimensions shown in figure (11.14). In order to avoid excessive stresses which would cause failure of the experimental model, the corners of the hole were rounded off to a definite radius.

In order to investigate the problem using the Large Element method, a mathematical model made up of three large inplane stress elements - as shown in figure (11.14) - was devised. Thanks to symmetry, only one quarter of the plate had to be modelled. Since the corners of the hole are considered sharp, they represent singular points. Despite this singularity, a fairly accurate solution can still be obtained at a small distance away from the singular point as was shown in several previous examples and as will be shown here through comparison with the experimental results of reference [56].

Since all the external plate edges, as well as the edges of the hole, are either free or subject to a *uniform* normal loading, both "translations" and "rotations" are to be restrained at edges No. (2), (3), (5), (6), (8) and (9). The symmetry conditions along edges No. (1) and (10) require that "Rotations" be constrained there. As expected,

the bending moment diagram resulting from the uniform load (p_o) is parabolic. As with the previous two examples, the constants of integration in equation (11.13) can be arbitrarily selected in order to simplify the boundary conditions. "Additional constraints" are then used to specify the degrees of freedom at nodes number (1), (2) and (3) according to equation (11.16). In order to ensure a zero shear force along the side defined by nodes number (1), (4) and (7), the "rotations" normal to the edge at these three nodes are to be made equal. Also, as in example (1), since the free boundary is not simply-connected, the uniform value of $\bar{F}$ along the interior boundary, defined by nodes number (6), (5) and (8), cannot be arbitrarily fixed as zero. Therefore, the "displacements" at nodes number (5), (6) and (8) are to be made equal to a common unknown value which is to be determined during the energy minimization procedure.

Contour plots for the principle stresses due to an overall tensile load of 44 lbs. acting on a plate 0.186 in. thick are shown in figure (11.15a) through (11.15c). The Isoclinics are plotted in figure (11.15d). In order to avoid discontinuities in the contour lines at the inter-element boundaries, the values of the tangential stresses along these boundaries (edges number 4 and 7) as computed from the two mating elements, were averaged prior to the computation of the principle stresses. Since the "displacements" and "normal slopes" are always continuous between the elements, the shear and normal inplane forces are

also continuous.

A comparison of the stresses obtained from the Large Element model described above with those measured on the Photo-Elastic model and published in reference [56] is shown in figure (11.16). Stresses along the vertical and horizontal centre-lines, the vertical plate edges, and the horizontal hole edges are plotted and compared. It can be seen that the theoretical and experimental results are in a good general agreement. Considerable local deviations, however, tend to occur in two particular areas. The first is near the corners of the hole; which is due to two obvious reasons: firstly, the difference in geometry, since the experimental model has its hole corners rounded into finite radii in order to avoid excessive stress concentrations; and secondly, the existance of the singular points in the theoretical solution at the sharp corners, which the approximate solution fails to duplicate accurately. The second area where local deviations occur is near the loaded plate edges. Although the experimentally measured stresses published in reference [56] and duplicated in figure (11.16) *purposely* do not extend the stress curves up to the loaded edges, it is obvious from these general trends that they tend towards considerably lower stress levels near the centres of the edges and higher values near the corners. This deviation is believed to be solely due to experimental inaccuracies, since it is known that it is extremely difficult to experimentally simulate a uniformly

loaded edge. Due to the existence of the hole, the central portions of the plate edges become less stiff than the extreme portions, and hence more of the applied load is transmitted to the extreme portions while less load is transmitted to the central portions. Even without the hole, it was shown in the example of section (4.4) that during a tensile or a compressive loading test more load is transmitted to the plate corners - where singularity exists - and less load is carried by the middle portions of the edges. On the other hand, the theoretical solution yields "exact" normal stresses along the plate edges since this is one of the imposed boundary conditions in the inplane stress elements used. It is interesting to note that the computed and measured values of the compressive bending stress acting at the centres of the horizontal edges of the hole are identical up to the full accuracy of the published experimental value (335 psi).

The Isoclinic lines experimentally obtained by the use of Photo-elasticity [56] are reproduced in figure (11.17). It can be seen that they are generally similar to those shown in figure (11.15d) resulting from the Large Element analysis. Once more, deviations occur near the corners of the hole for the reasons discussed above. In addition, some deviations occur near the inter-element boundaries due to the discontinuity of the tangential stresses (which were averaged up as previously mentioned).

It is worth noting here that the solution of this problem does not depend upon Poisson's ratio, which is ex-

pected for a problem under homogeneous boundary conditions and which does not include natural boundary conditions (the natural boundary conditions introduced along the lines of symmetry can be shown to be independent of Poisson's ratio since Poisson's ratio is multiplied by the normal slope which is zero along these lines).

11.3.4 Tip-loaded Short T-Cantilever

In this example, the problem of determining the stress distribution in a short cantilever partially loaded along its top edge is considered. The beam is assumed to have a T-type cross-section and carries a load of ($2P$) distributed along a short length (ℓ) near its tip. A common example for this beam is the crane girder carrying cantilever. In order to economize in the use of material, the bottom free corner of the cantilever is often cut away as shown in figure (11.13). A suggestion for a reasonable cut-off position will be made as a result of this investigation.

Since the loading is discontinuous, the resulting bending moment diagram has a sudden discontinuity in curvature as shown in figure (11.18). In order to match the value of the potential function Ψ along the top edge with this bending moment distribution, one of two approaches may be taken. In the first, the bending moment distribution may be treated as a continuous function and equations (11.14) through (11.16) used directly in order to provide a generalized Fourier series approximation for the moment distribution. In this

case, the resulting stress distribution will be continuous throughout the beam web, however, the representation of the boundary conditions will be only approximate. In the second approach, the sudden change in loading is treated as a discontinuity, and hence the web is divided into two elements interconnected along the line of load discontinuity. Matching the function $\bar{F}$ with the bending moments along each of the two elements then becomes a simple task and requires only the use of equation (11.15). In this manner, the boundary conditions will be exactly satisfied along the top edge, however, discontinuity in tangential stresses may occur along the inter-element boundary. Nevertheless, the second approach is more convenient for the user and more reliable since it exactly satisfies the boundary conditions. Therefore, the second approach will be used here.

Making use of symmetry, the beam is idealized by four large elements as shown in figure (11.18). The constraint conditions defining the boundary conditions along the free portions of the boundary are shown in the "constraints" table in figure (11.18). The "additional constraints" table provides the conditions necessary for defining the loading condition, as well as matching the shearing force between the web and the flange elements. It is to be noticed that the load $(2P)$, in this problem represents the *total load* applied along the length "c", and hence its intensity is $(2P/c)$.

Figure (11.19) shows the distribution of the normal

stresses along the clamped edge as obtained from the large element solution for three length to depth ratios. Shown also are the stress distributions obtained by applying the classical beam theory for each case. It can be seen that, due to stress concentrations, considerably higher stresses result from the large element analysis near the corners where free and clamped edges intersect - a condition which leads to singularity as was shown in section (4.4.1). In general, however, the difference between the stresses obtained by the large elements and those calculated using thin beam theory is not too great at this section of the beam.

Contour plots representing the distribution of the principal forces in both the flange and the web of the beam are shown in figures (11.20) through (11.31) for beams having length-to-depth ratios of 1:1, 2:3, and 3:2. The Isoclinic lines are also shown for each case. In order to ensure continuity of the contour lines as they cross the inter-element boundaries, the tangential stresses along these boundaries as computed from each of the two mating elements are averaged before the principal forces and isoclinics are computed.

It can be seen from the contour plots, that the lines of maximum shear (which represents the failure criterion in ductile materials) near the free corner of the web are approximately parallel and inclined at about 45° for all three length-to-depth ratios. In addition, the stress distribution along the free edge ($\eta=a$) shown in figure (11.32)

indicates that the bottom half of the flange near its free edge contributes very little to the load carrying capacity of the beam (the hatched tail area represents only about 10% of the total area under the stress curve). It is therefore suggested that the free corner of the web can be cut-off along a line inclined at 45° and starting at the point $(a, b/2)$ as shown by the dotted lines in figures (11.20) through (11.32). It is believed that cutting off this corner will produce negligible effect upon the stress distribution elsewhere in the structure except in the immediate vicinity of the cut-off line where the stresses are already low (about 20% of maximum).

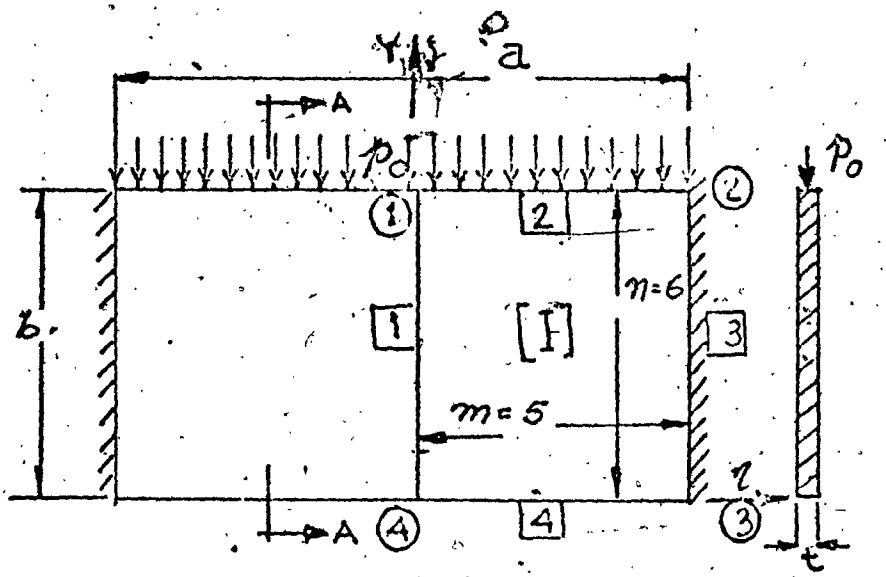

(a)

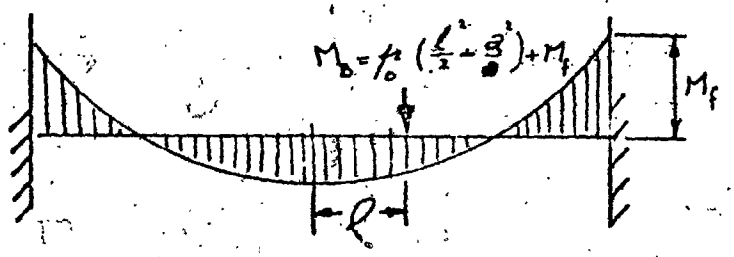

(b)

Stiffness

$\nu = 1/6$

$\bar{D}_x = \bar{D}_y = 1/tE = 1$

(Isotropic)

Constraints

Edge No.	Type of Constraint
1	r
2	t , r
4	t, r

Additional Constraints

- Trans. at Node (1) = $p_o a^2/8$
- Rot. about (ξ) at Node (2) = $- p_o a/2$
- Trans at Node (3) = Trans. at Node (4) $\neq 0$

Fig. (11.1)

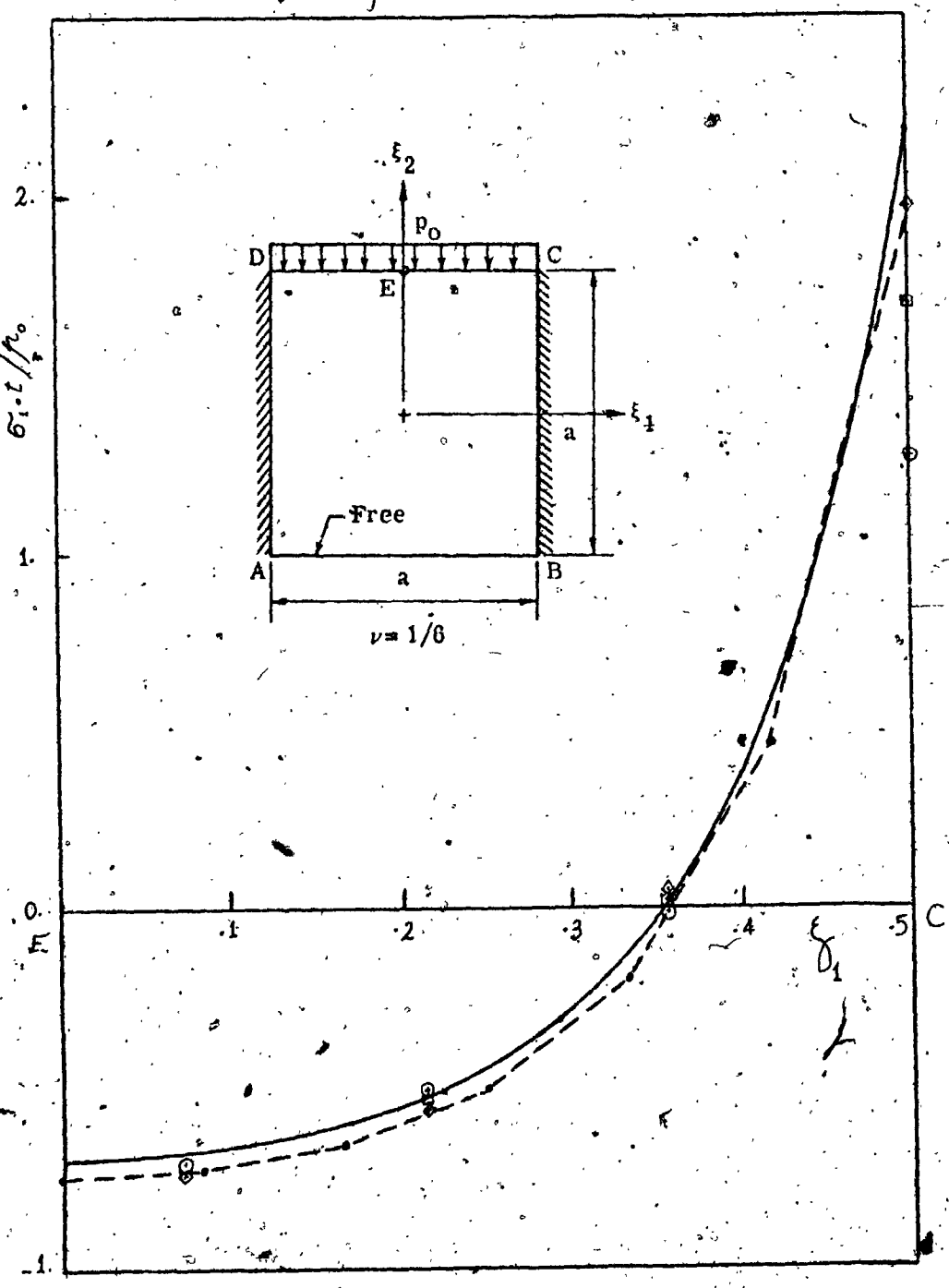

——— Large Elements (49 Equations)

– – – – – Ordinary F.D. ($\approx$ 100 Equations)-ref.[55]

⊙ ⊡ ◇ Modified F.D. - boundary approximations of order (l), (l^2), and (l^3) -($\approx$ 160 equations) ref.[15]

Fig.(11.2)
Distribution of Normal Stress, σ_1, in a Uniformly-Loaded Deep Girder

FIG. (11.3A)

UNIFORMLY LOADED DEEP GIRDER

A/B=1

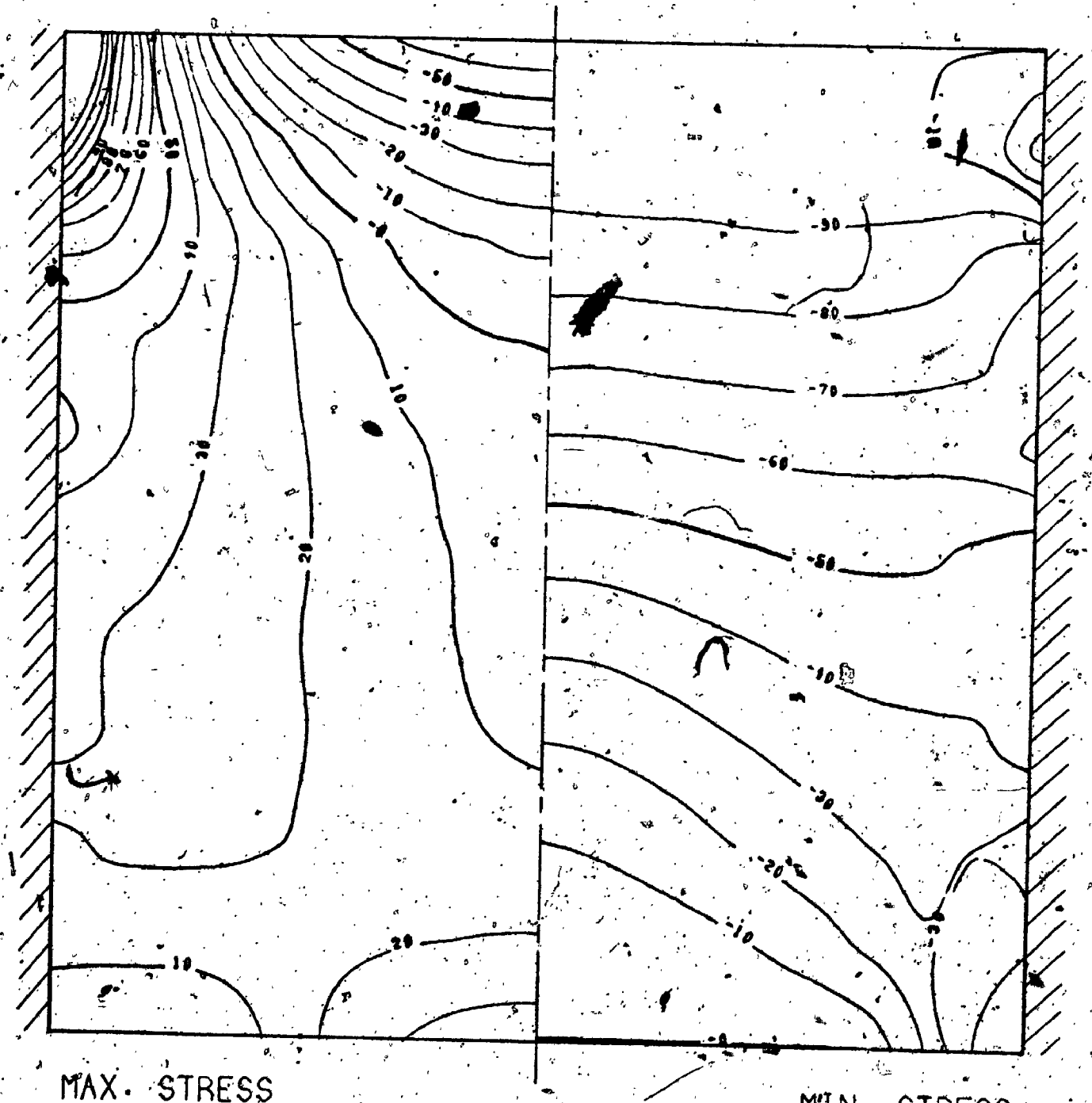

MAX. STRESS

MIN. STRESS

FIG. (11.3B)

UNIFORMLY LOADED DEEP GIRDER A/B=1.

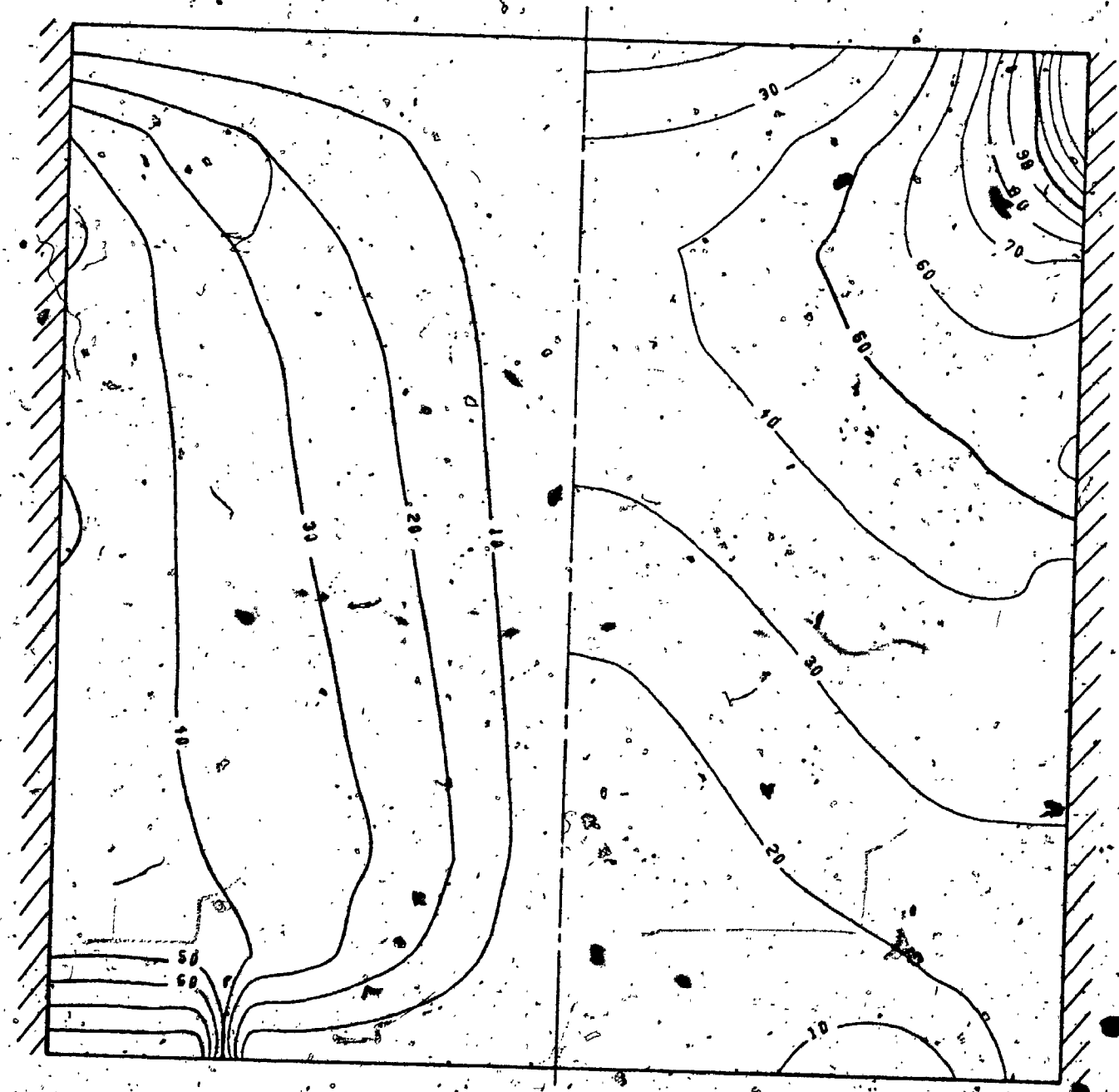

THITA

MAX. SHEAR

CHART NO. C

RECORDING CHARTS GRAPHIC CONTROLS CANADA LTD.

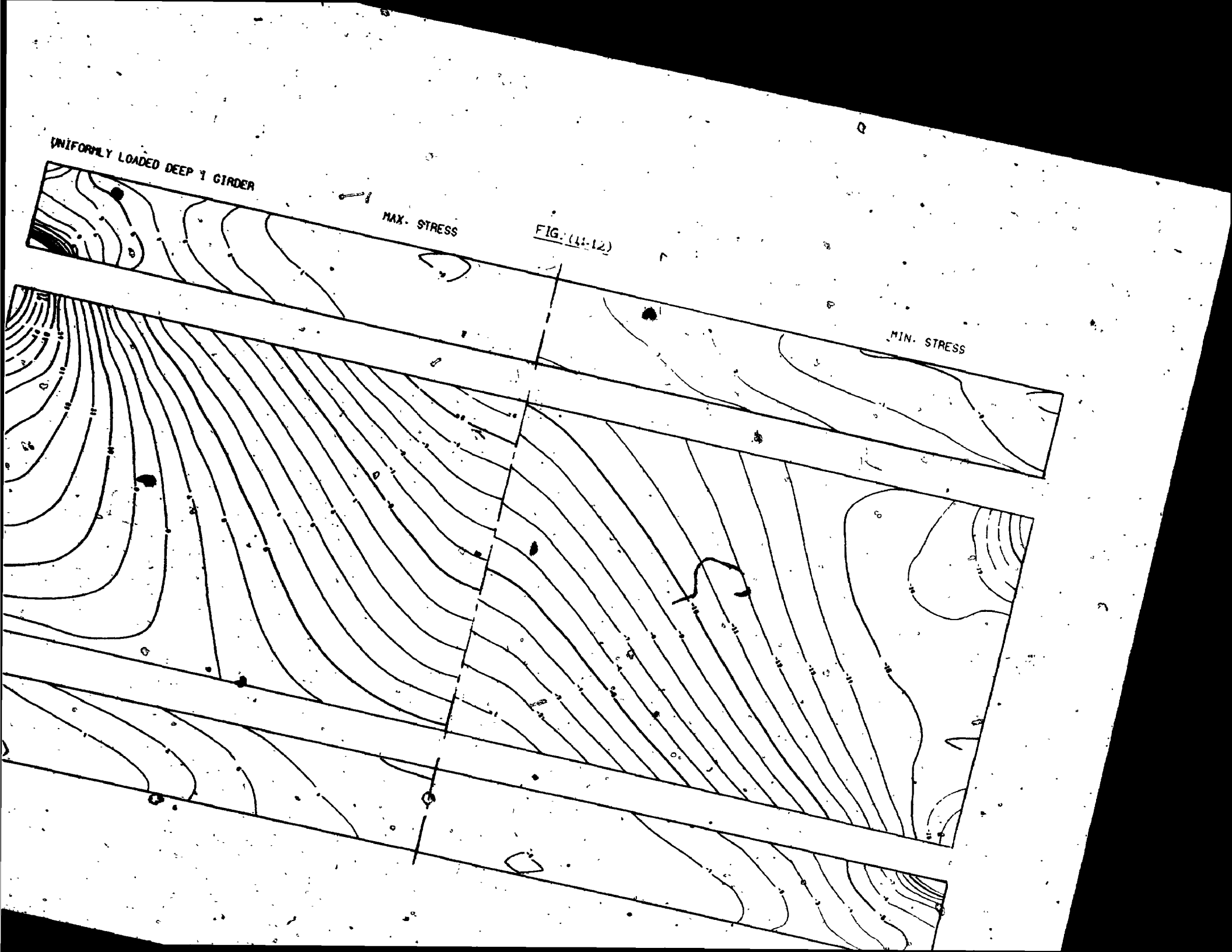

FIG. (11-12)

FIG. (11.3A)

UNIFORMLY LOADED DEEP GIRDER A/B=1

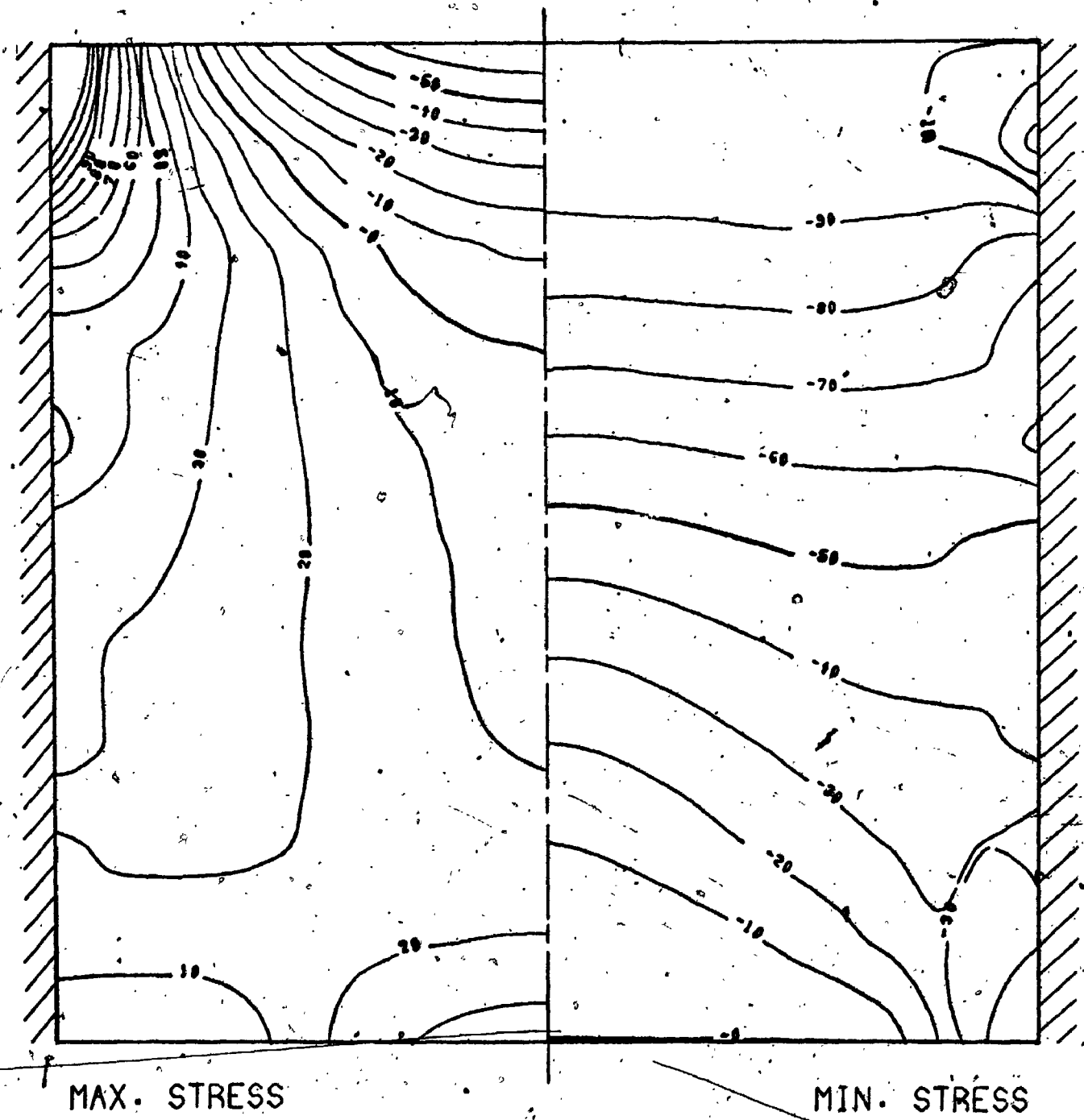

FIG. (11.3B)

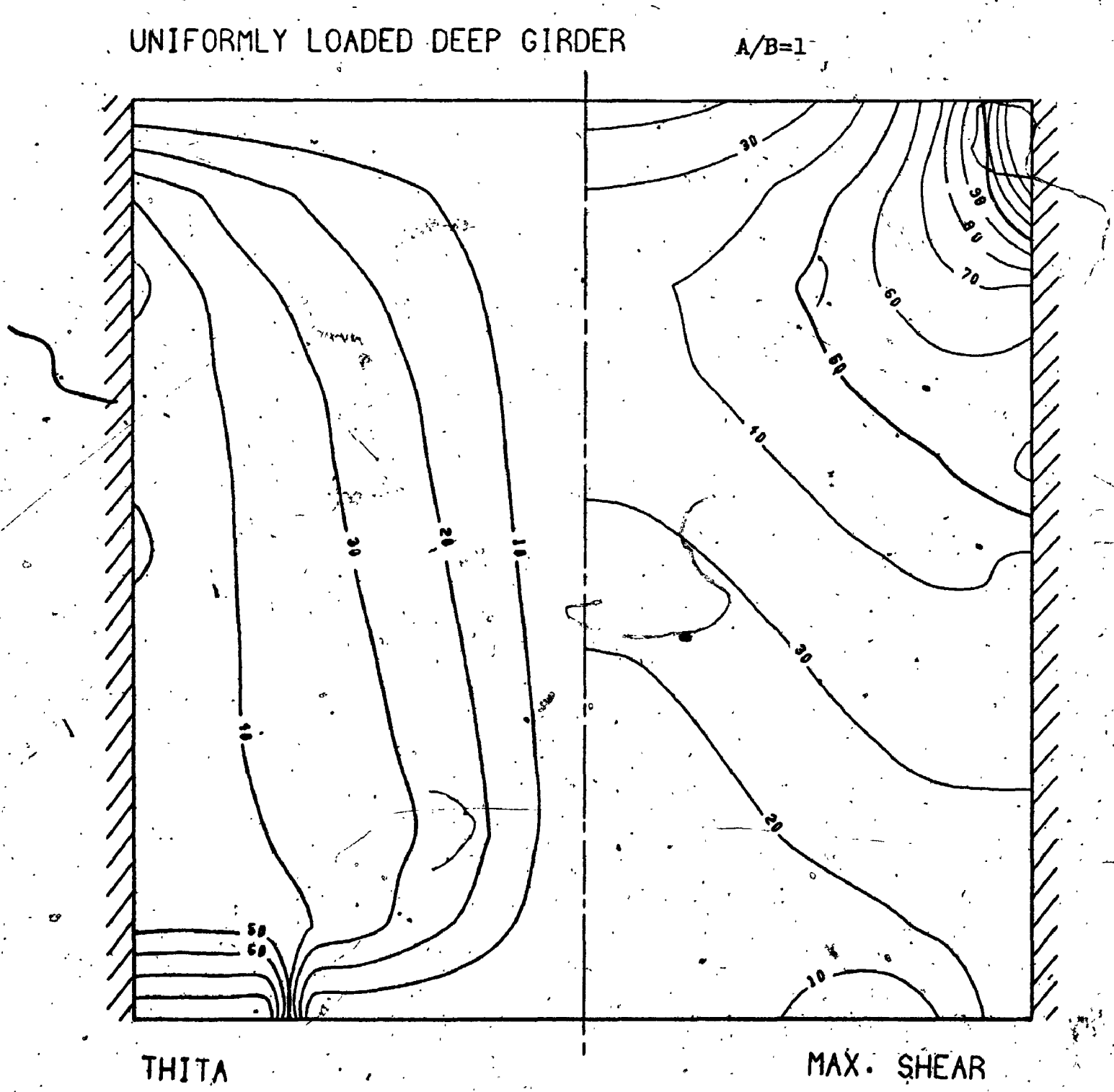

FIG. (11.4A)

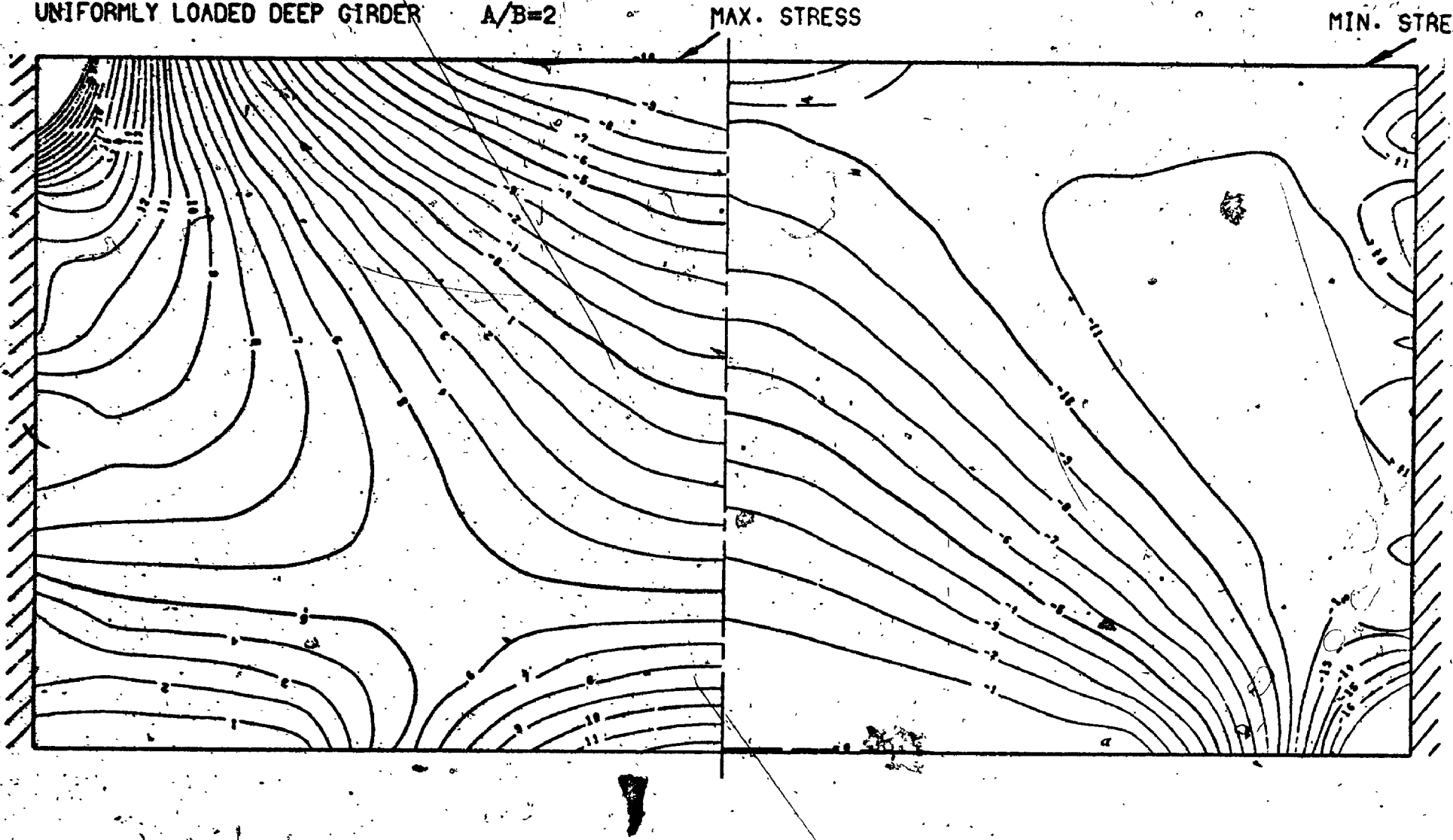

FIG. (11.4B)

UNIFORMLY LOADED DEEP GIRDER A/B=2 MAX. SHEAR

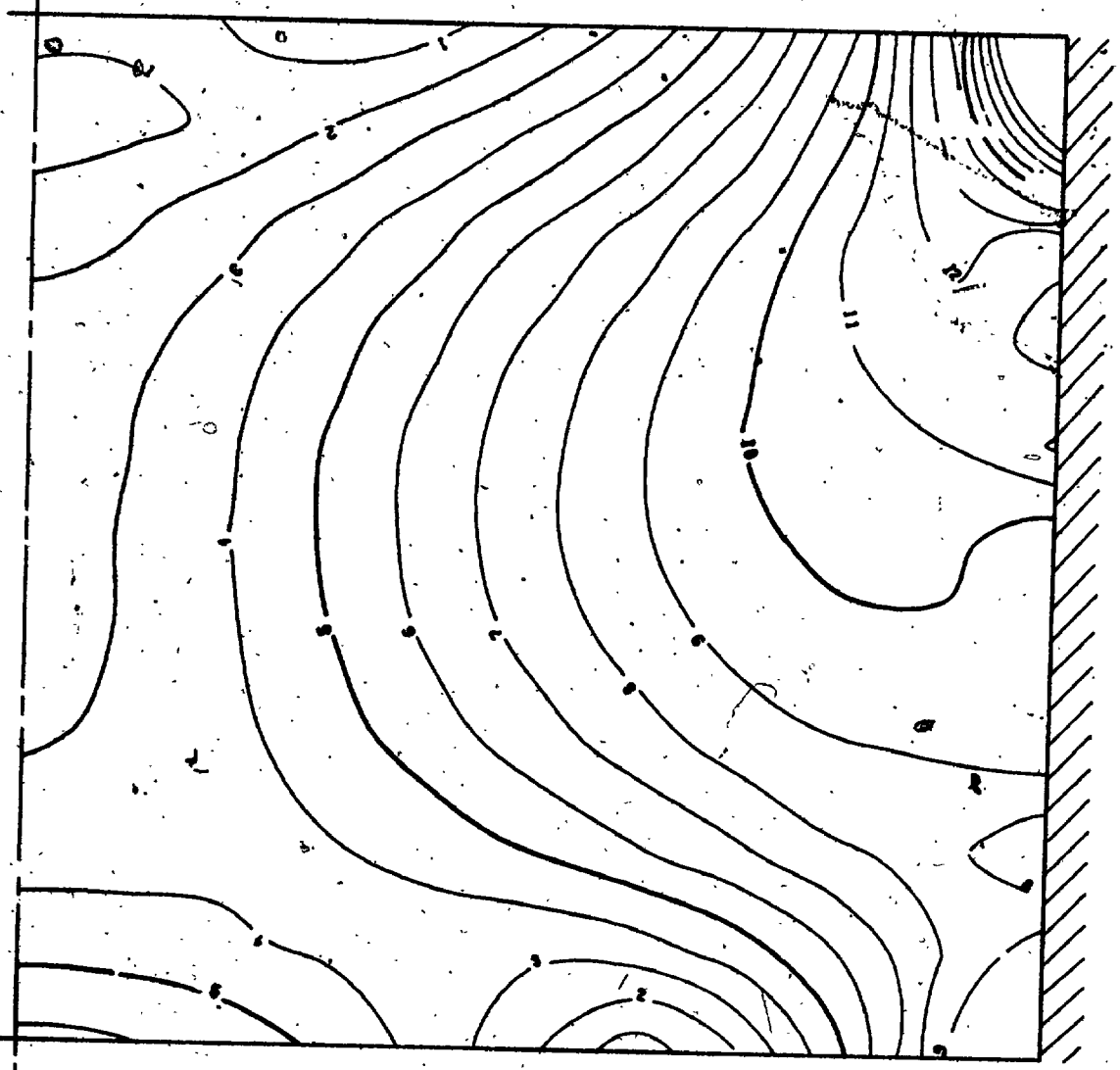

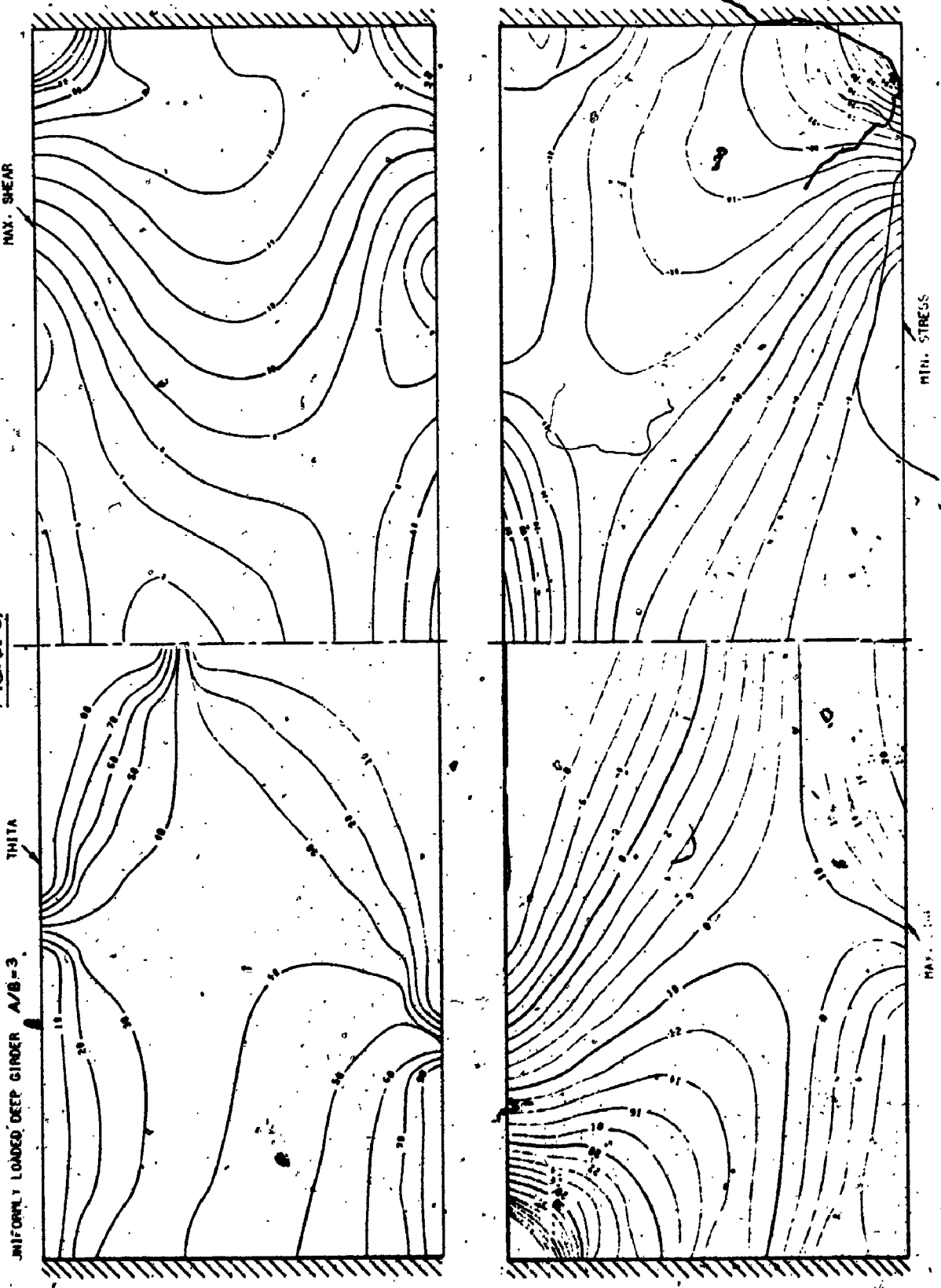
MAX. SHEAR
MIN. STRESS
THITA
MAX.
UNIFORMLY LOADED DEEP GIRDER A/B=3

FIG. (11-5)

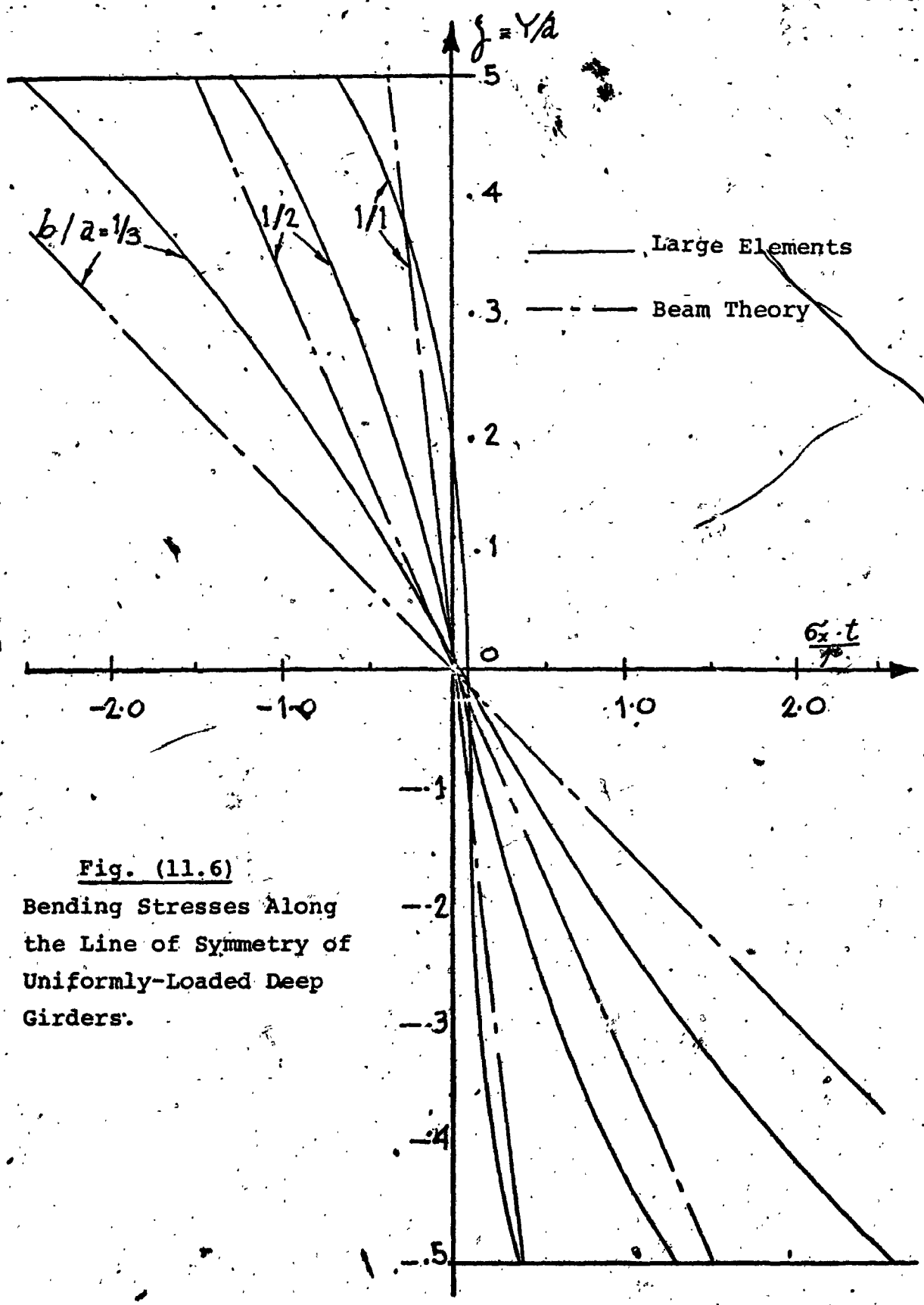

Fig. (11.6)
Bending Stresses Along the Line of Symmetry of Uniformly-Loaded Deep Girders.

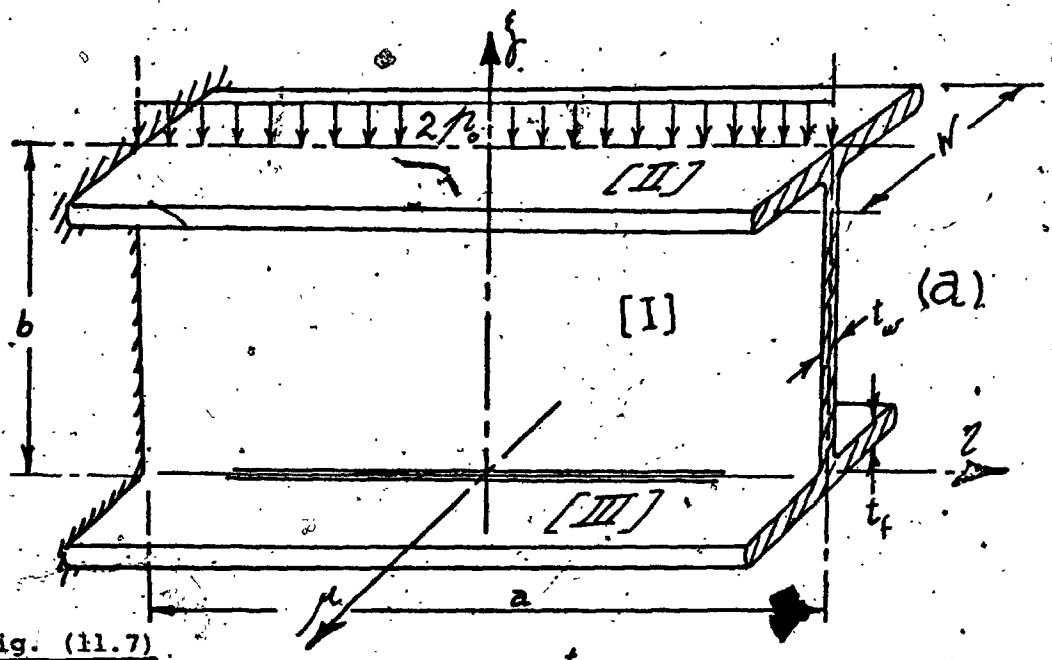

Fig. (11.7)

Stiffness

$\bar{E}_x = \bar{E}_y = E=1,\ \nu = 0.3$

(Isotropic)

$t_f = 1.5 * t_w = 3,\ W = b/2$

Constraints

Edge No.	Type of Constraint
1	t, r
2	r
5	t
6	r
8	t
10	r
12	t, r

Additional Constraints

- Rot. at edge (4) = Rot. at edge (5).
- Rot. at edge (8) = Rot. at edge (9).
- Rot. about (η) at Node (1) = Rot. about (η) at Node (8)
- Rot. about (η) at Node (2) = Rot. about (η) at Node (7).
- Rot. about (η) at Node (3) = Rot. about (η) at Node (10).
- Rot. about (η) at Node (4) = Rot. about (η) at Node (9).
- Twist at Node (2) = Twist at Node (7).
- Twist at Node (3) = Twist at Node (10).
- The three "Additional Constraints" of fig. (11.1) to be applied.

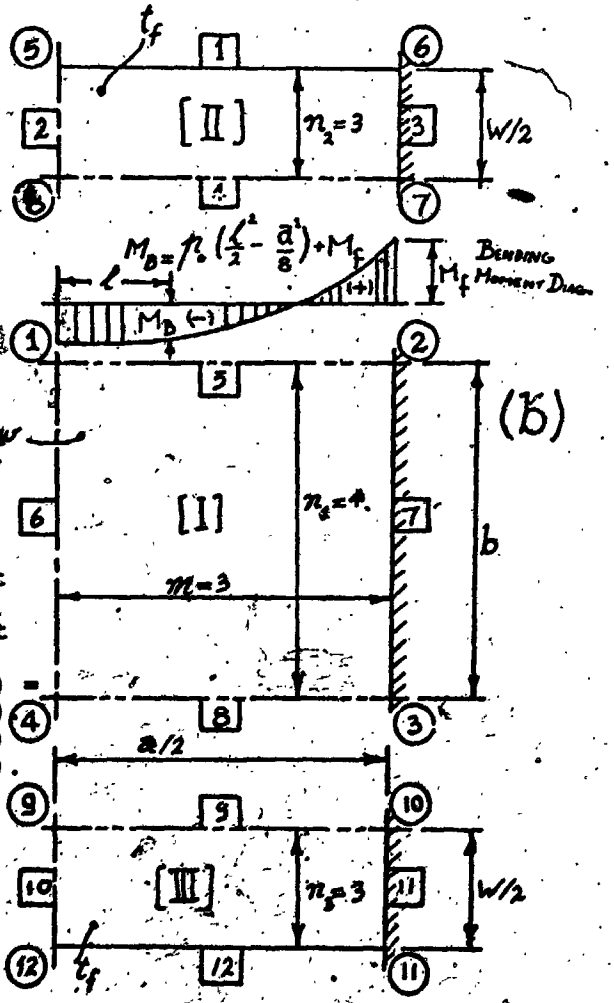

FIG. (T1.8)

UNIFORMLY LOADED DEEP I GIRDER A/B=1

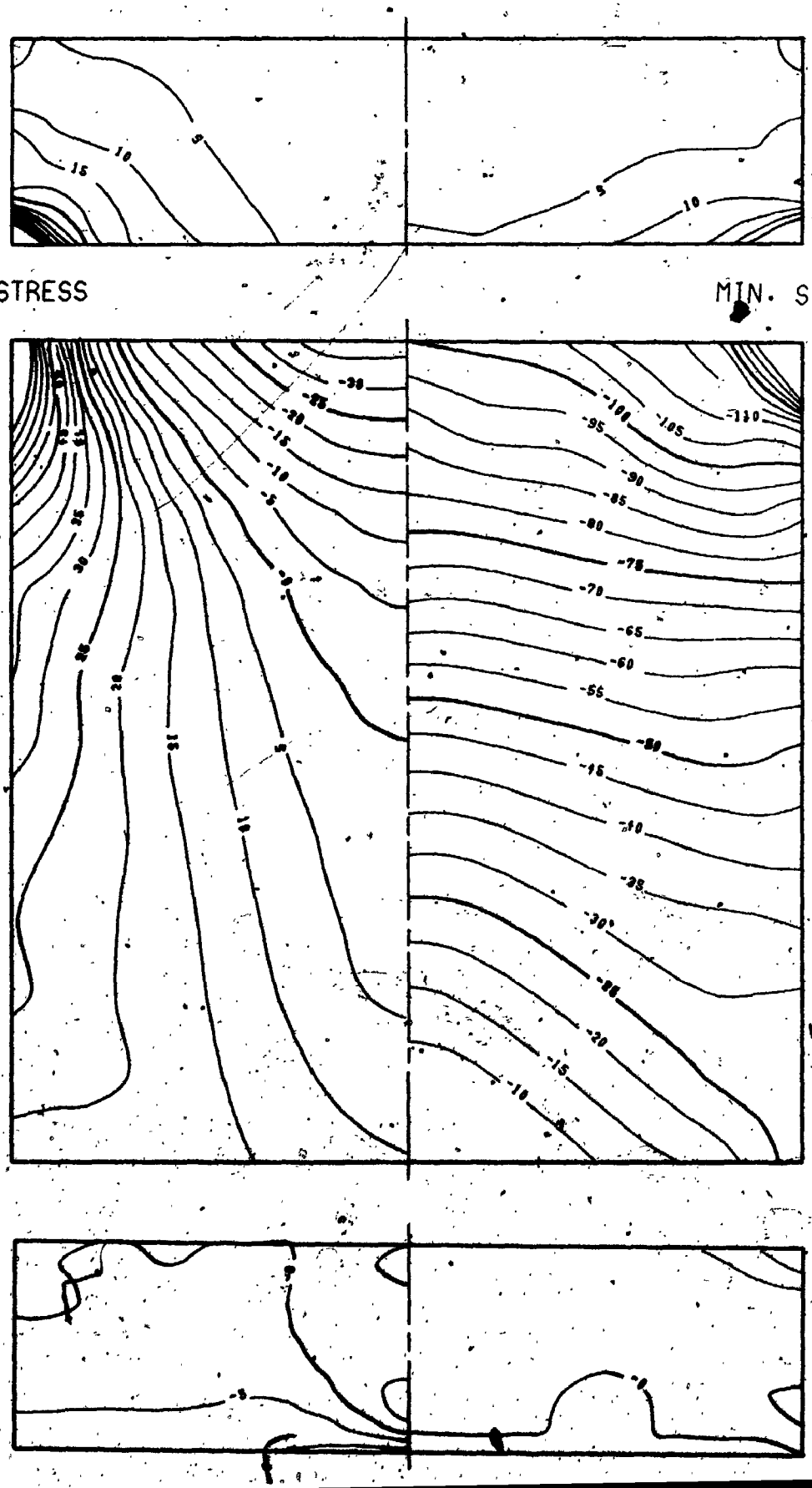

FIG. (11.9)

A/B=1

THITA UNIFORMLY LOADED DEEP I GIRDER MAX. SHEAR

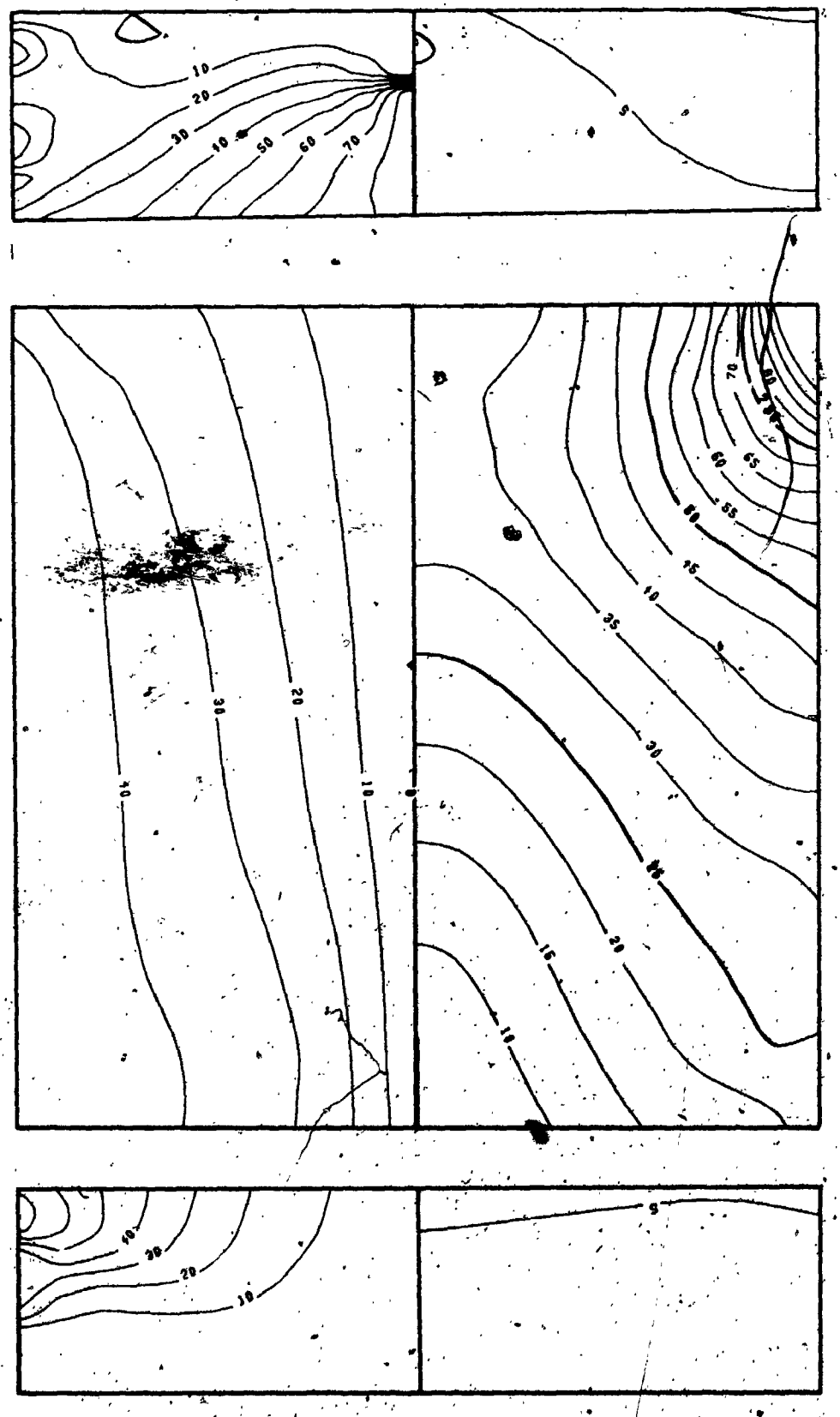

FIG. (11.10)

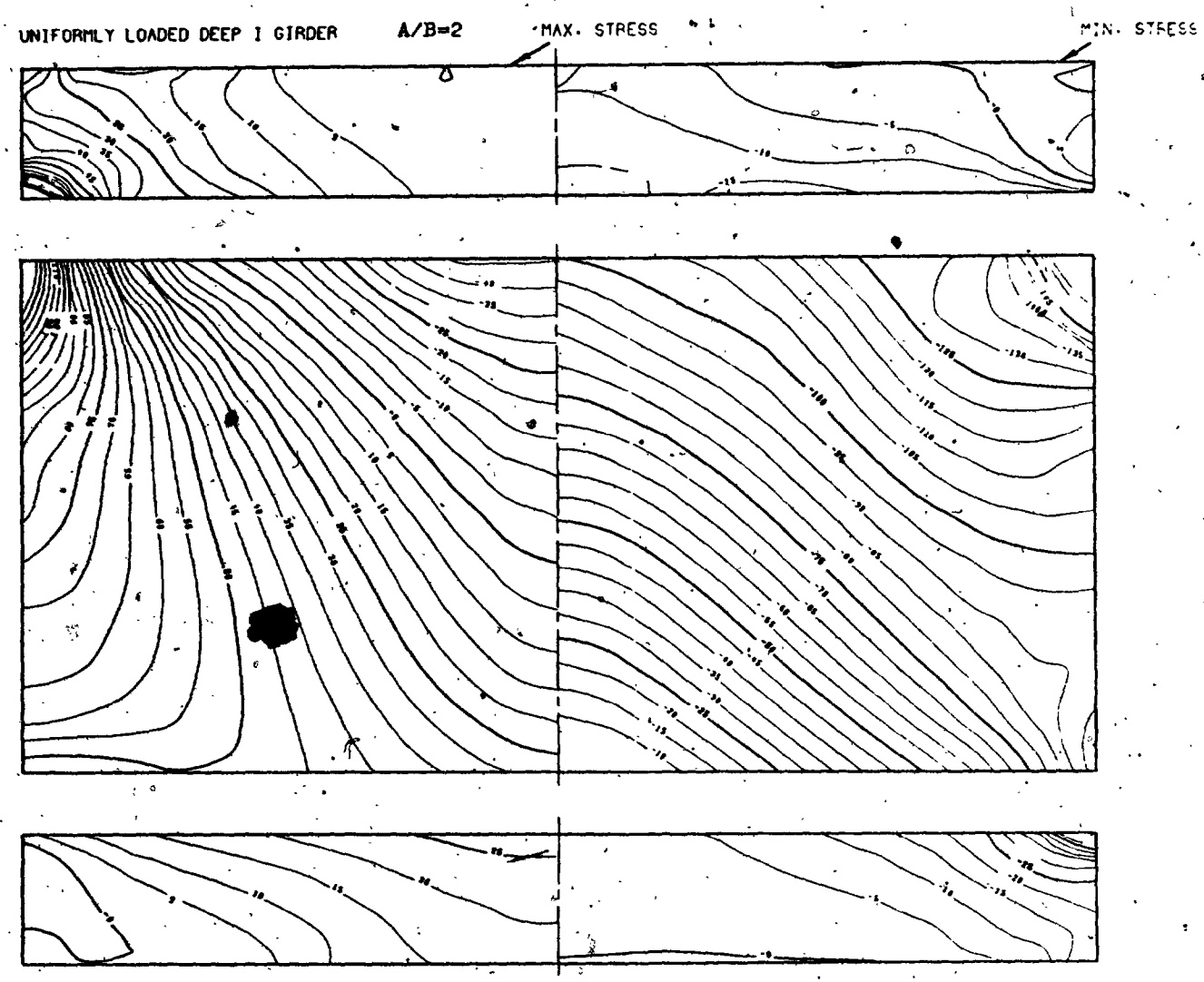

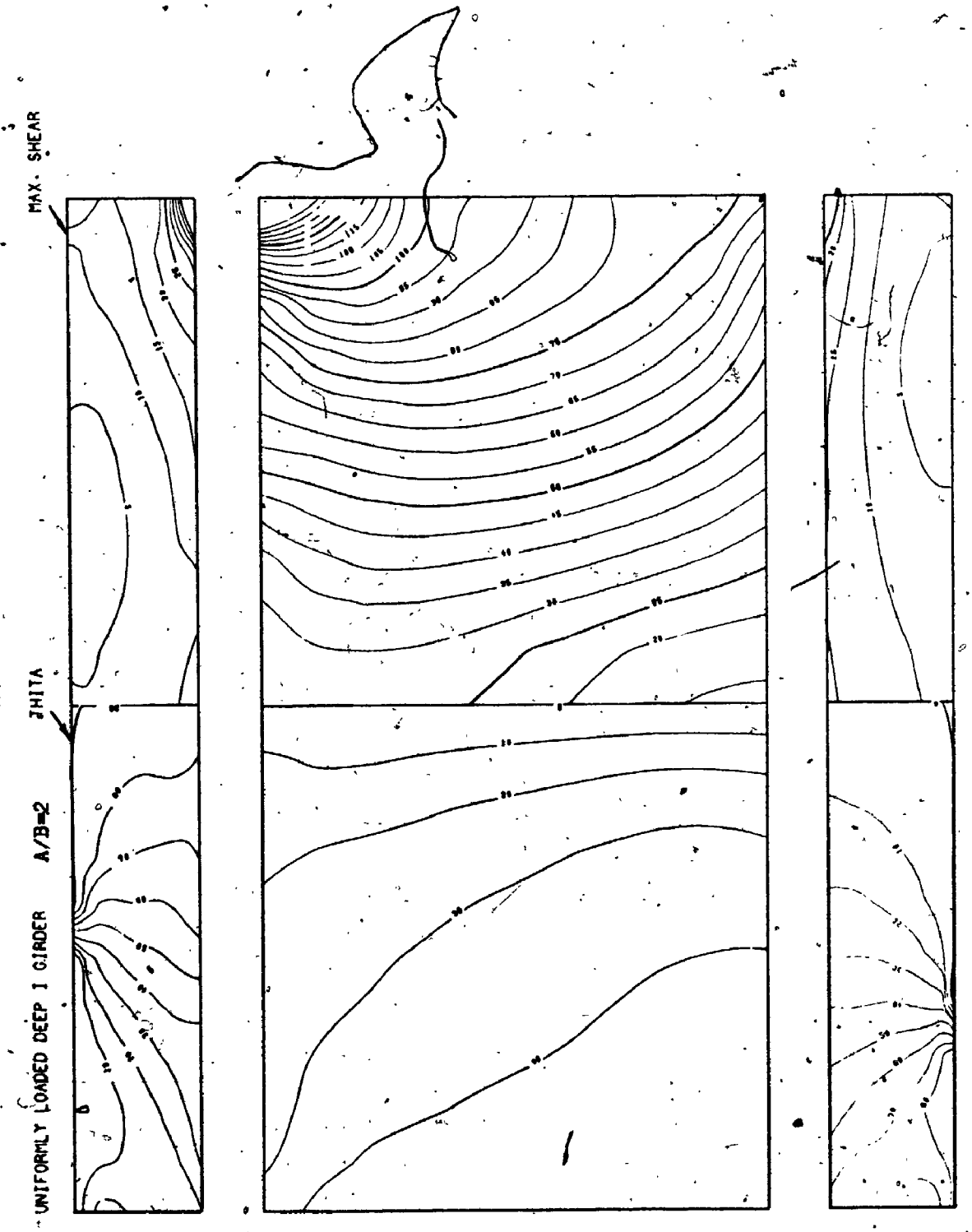

FIG. (11.11)

UNIFORMLY LOADED DEEP 1 GIRDER

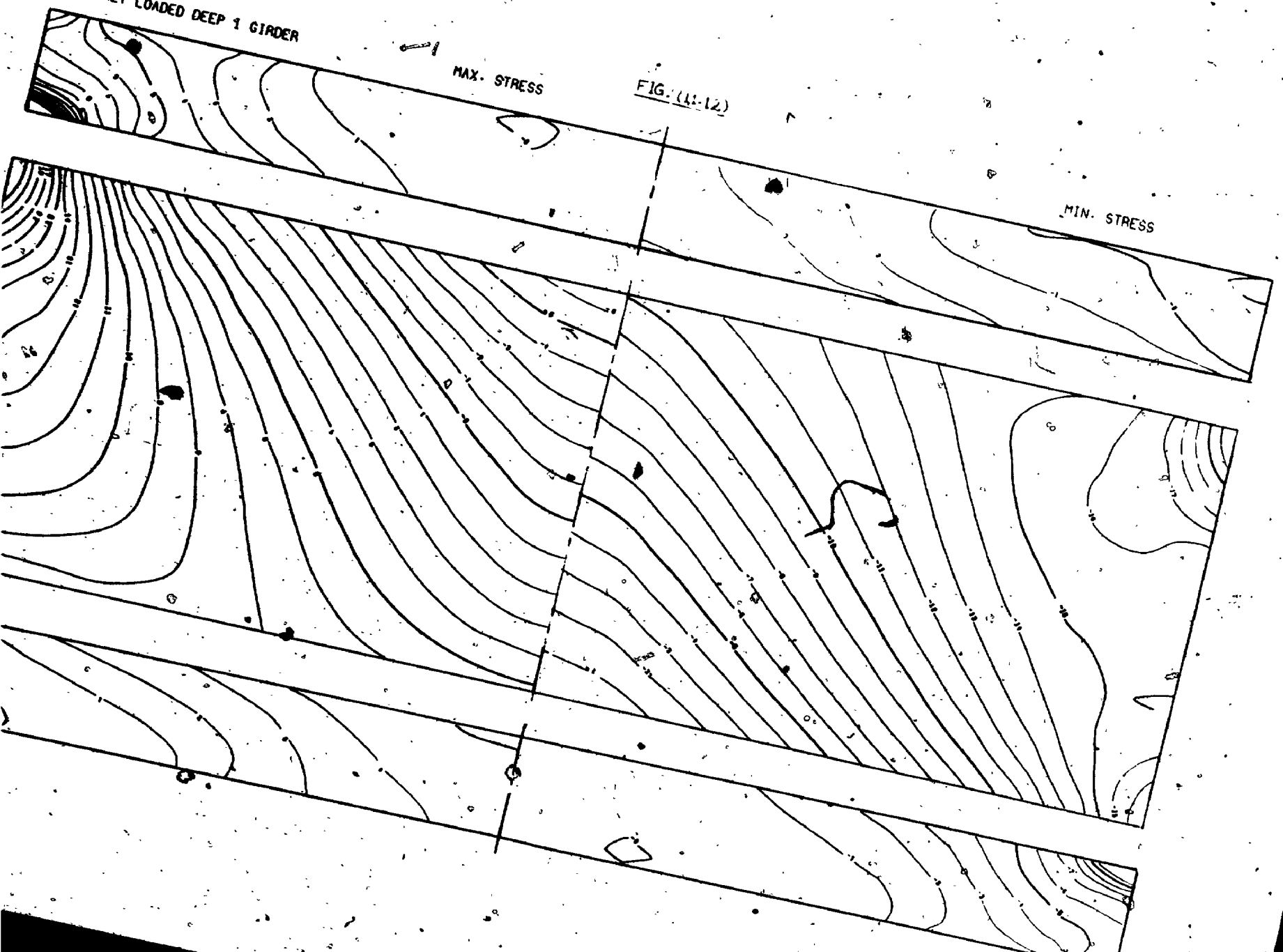

FIG. (4.12)

UNIFORMLY LOADED DEEP I GIRDER

FIG. (11-12)

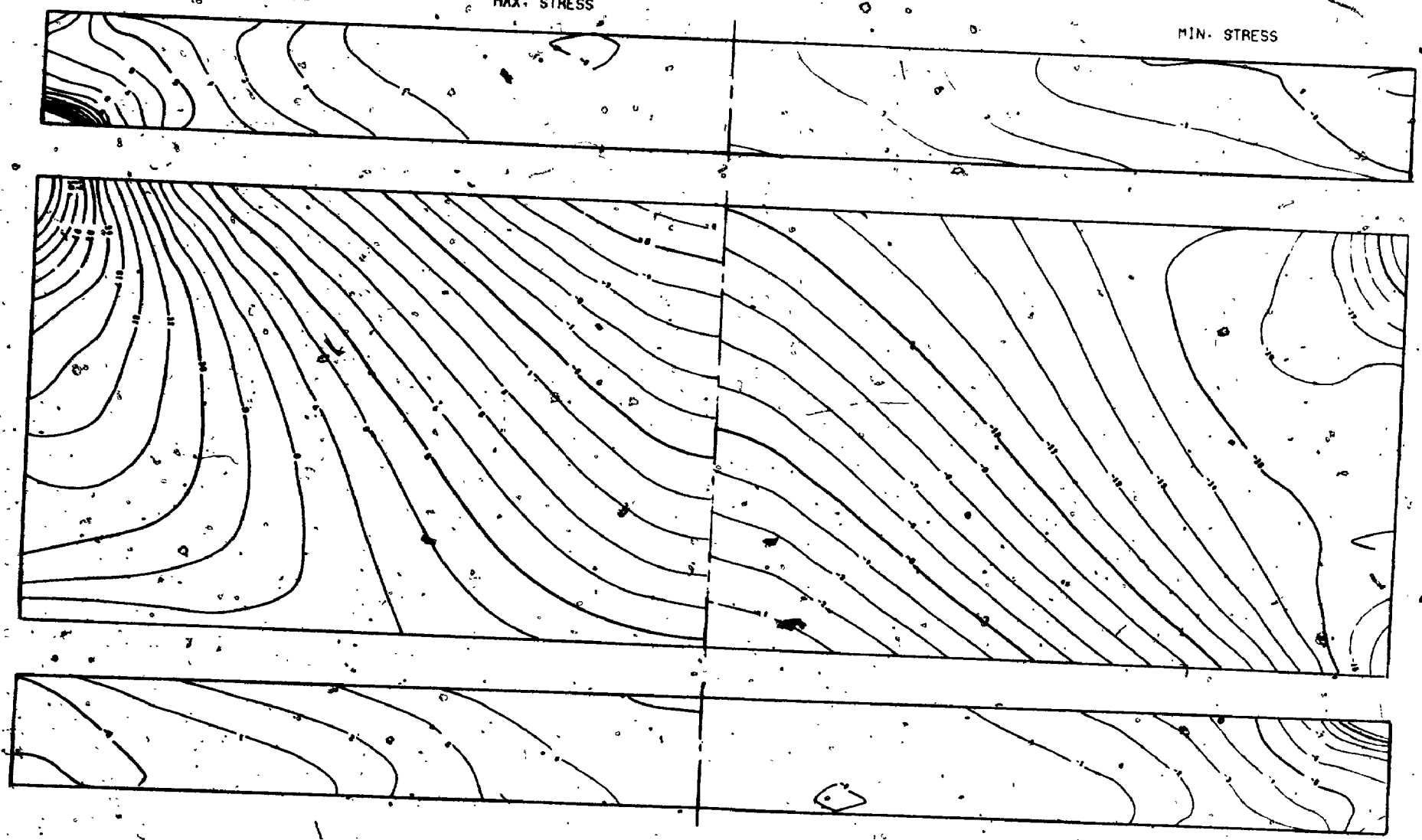

FIG. (11.13)

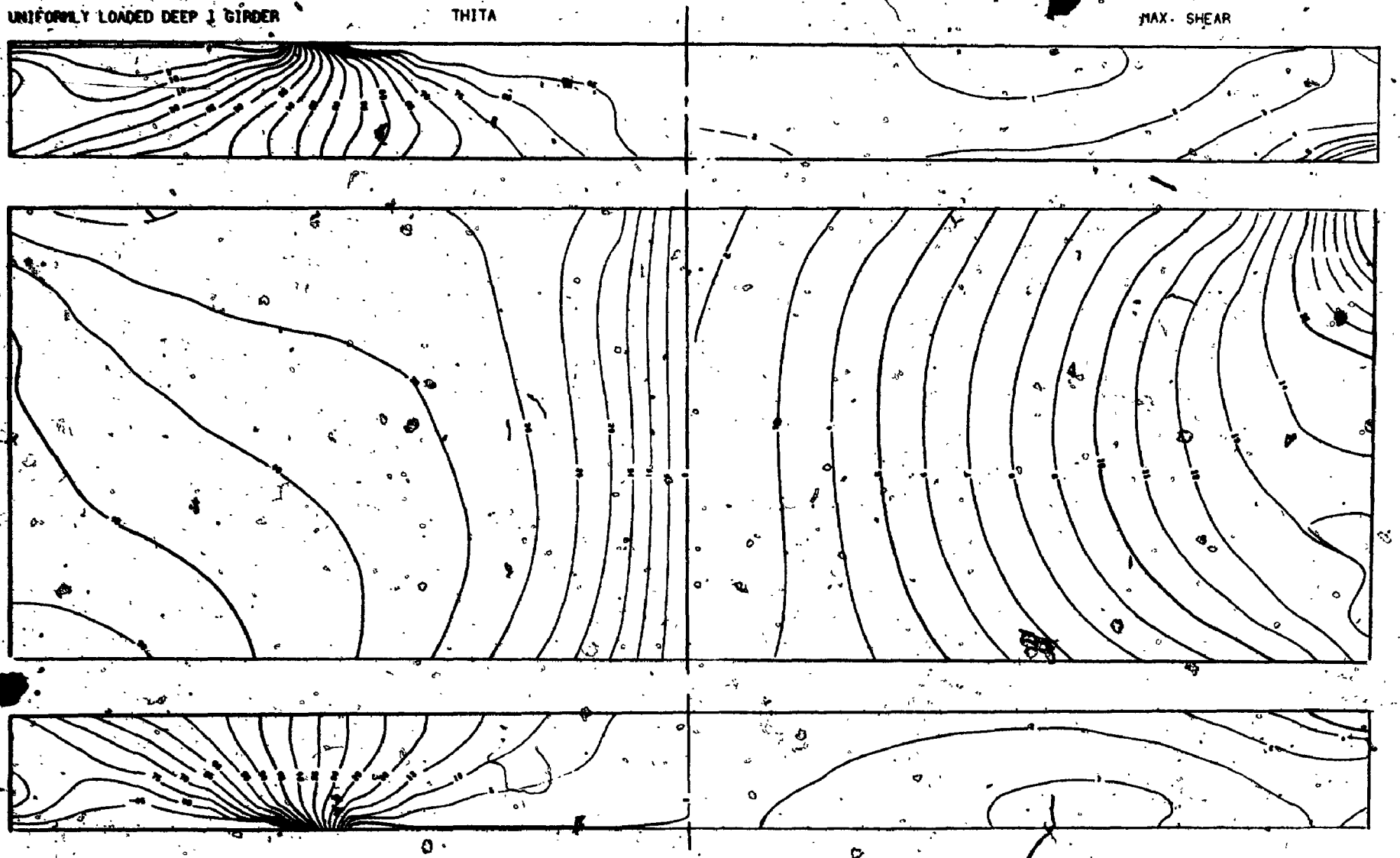

Stiffness

$\nu = 0.3$

$E_x = E_y = E = 1$ (Isotropic)

$t = 0.186"$

Constraints

Edge No.	Type of Constraints
1	r
2	t, r
3	t, r
5	t, r
6	t, r
8	t, r
9	t, r
10	r

Additional Constraints

- Trans. at Node (2) = $-p_o(a^2-c^2)/8$
- Trans. at Node (3) = $-p_o a^2/8$
- Trans. at Node (5) = Trans. at Node (6) = Trans. at Node (8) = 0
- Rot. about (ξ) at Node (2) = $-p_o c/2$
- Rot. about (ξ) at Node (1) = Rot. about (ξ) at Node (4) = Rot. about (ξ) at Node (7) = $-p_o a/2$.

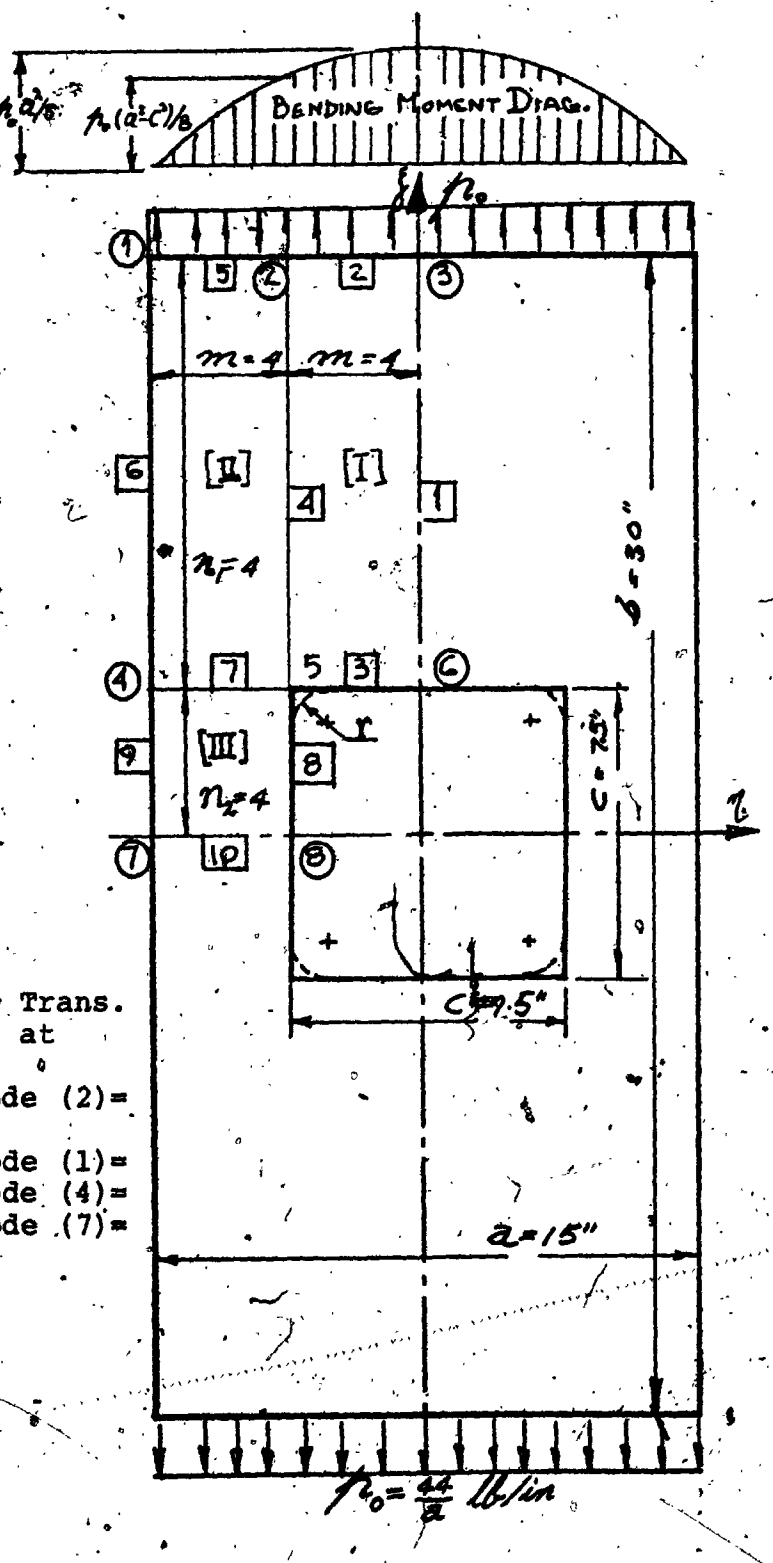

Fig. (11.14)

FIG. (11-15A)

RECTANGULAR PLATE WITH A SQUARE HOLE MAX. STRESS

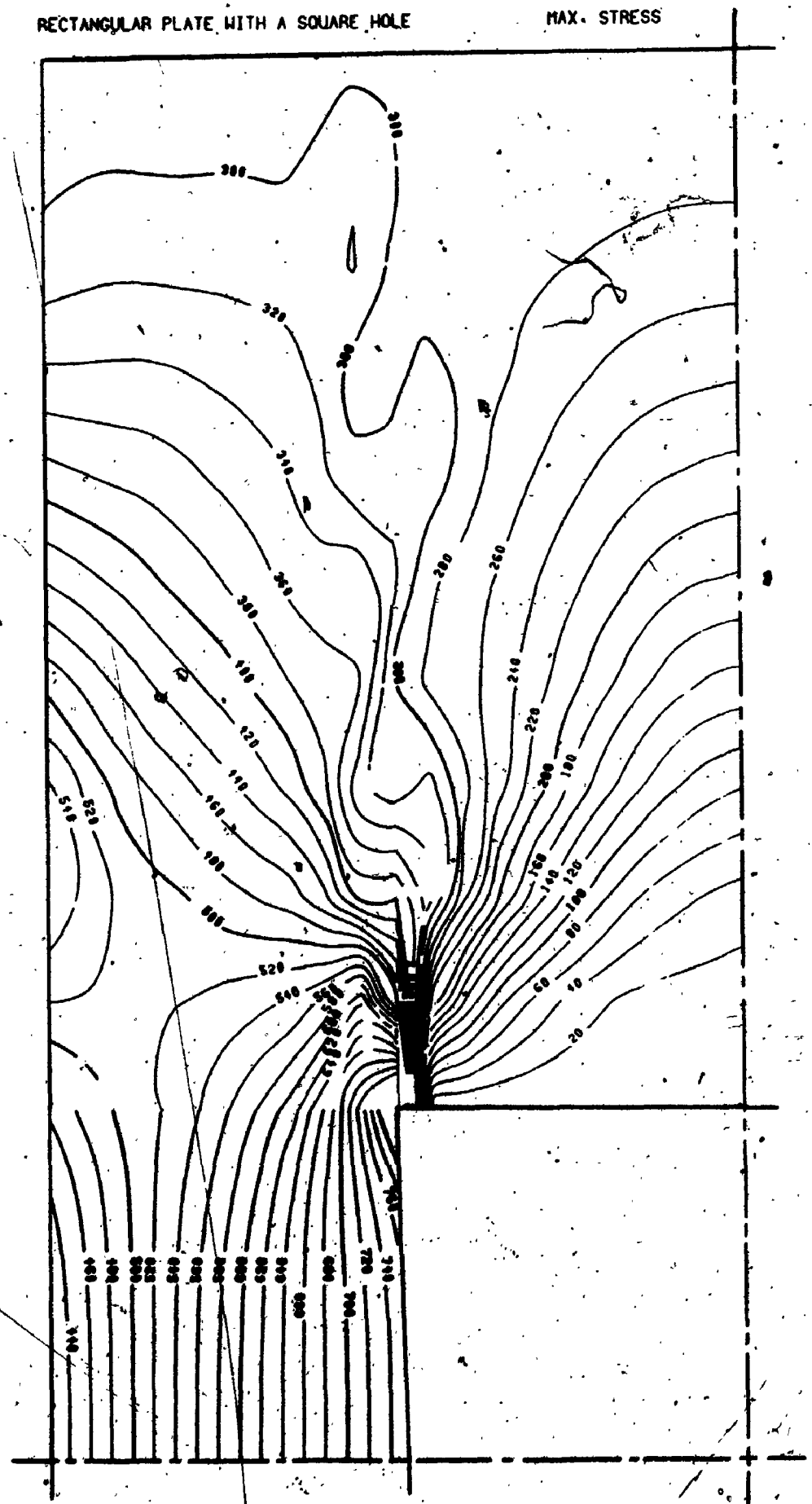

FIG. (11.15B)

RECTANGULAR PLATE WITH A SQUARE HOLE MIN. STRESS

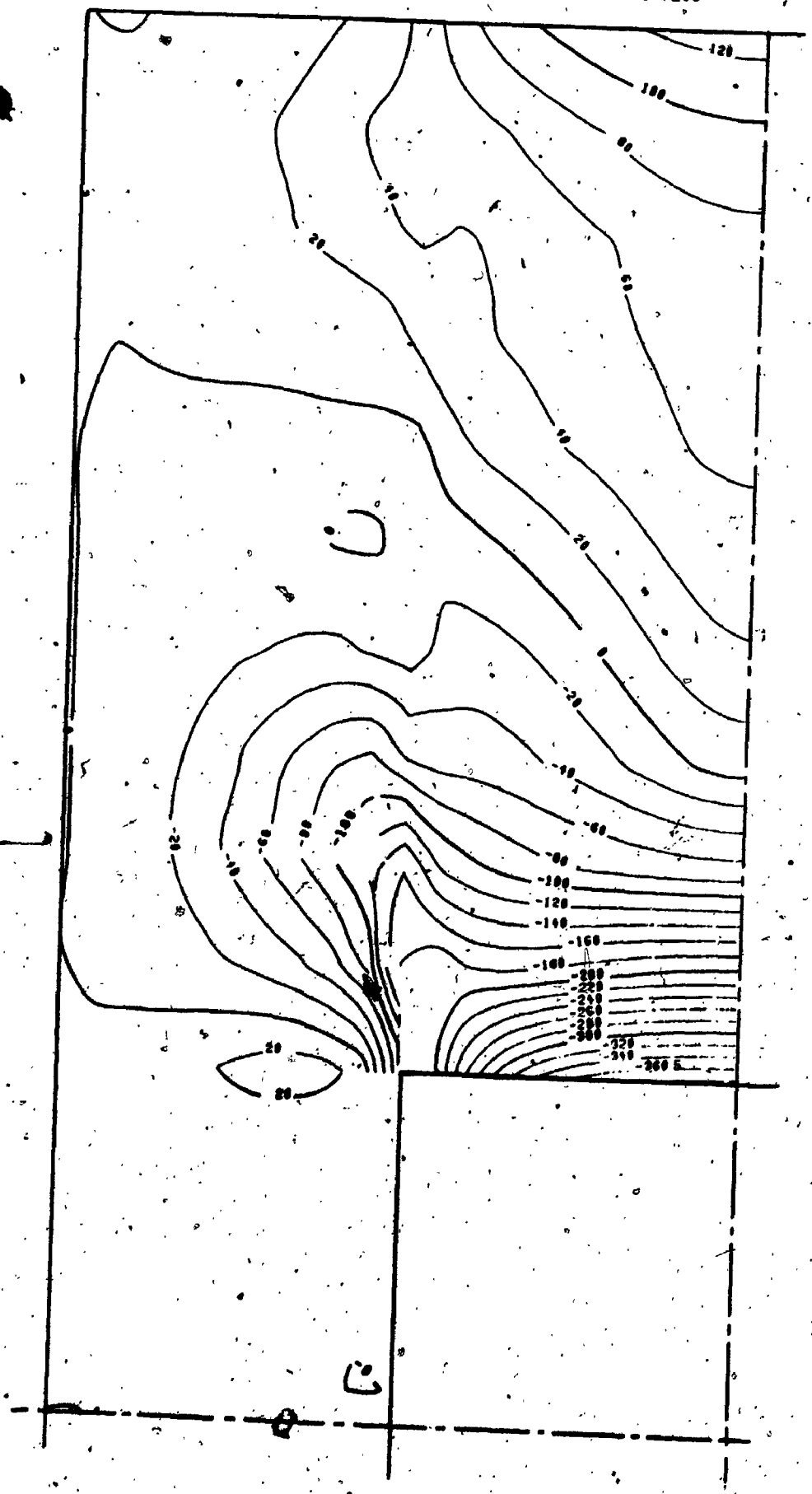

FIG. (11-15C)

RECTANGULAR PLATE WITH A SQUARE HOLE MAX. SHEAR

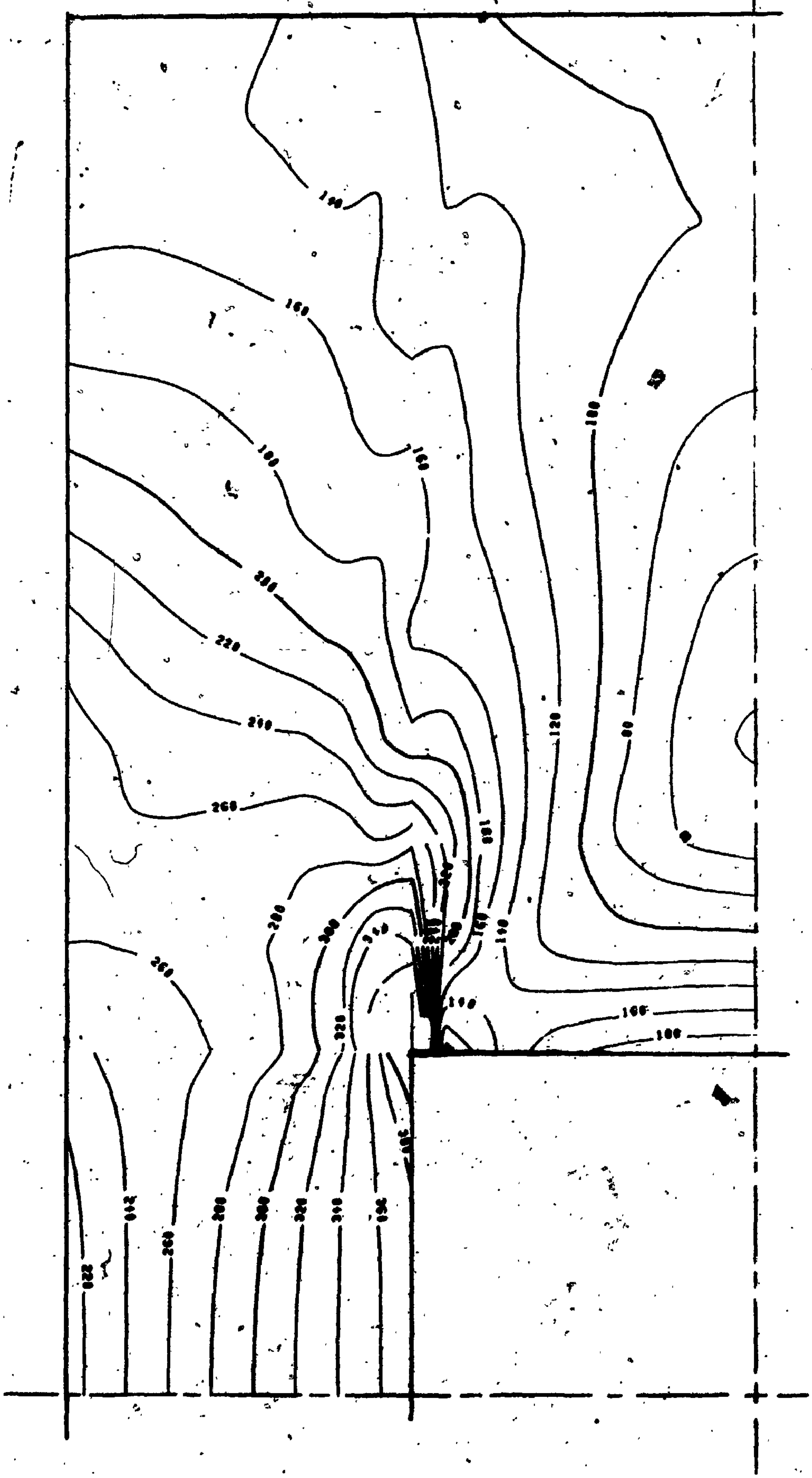

FIG. (11-15D)

RECTANGULAR PLATE WITH A SQUARE HOLE

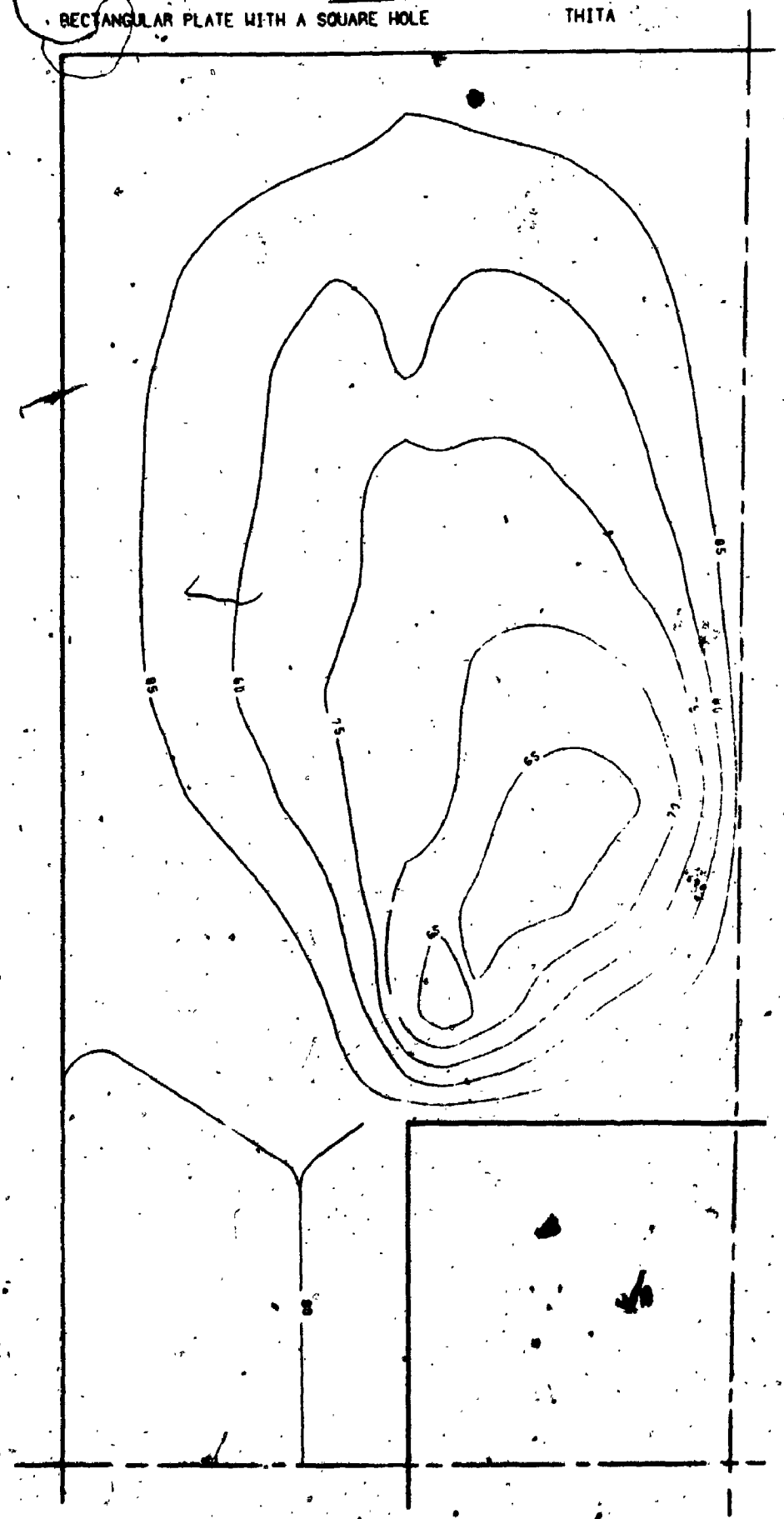

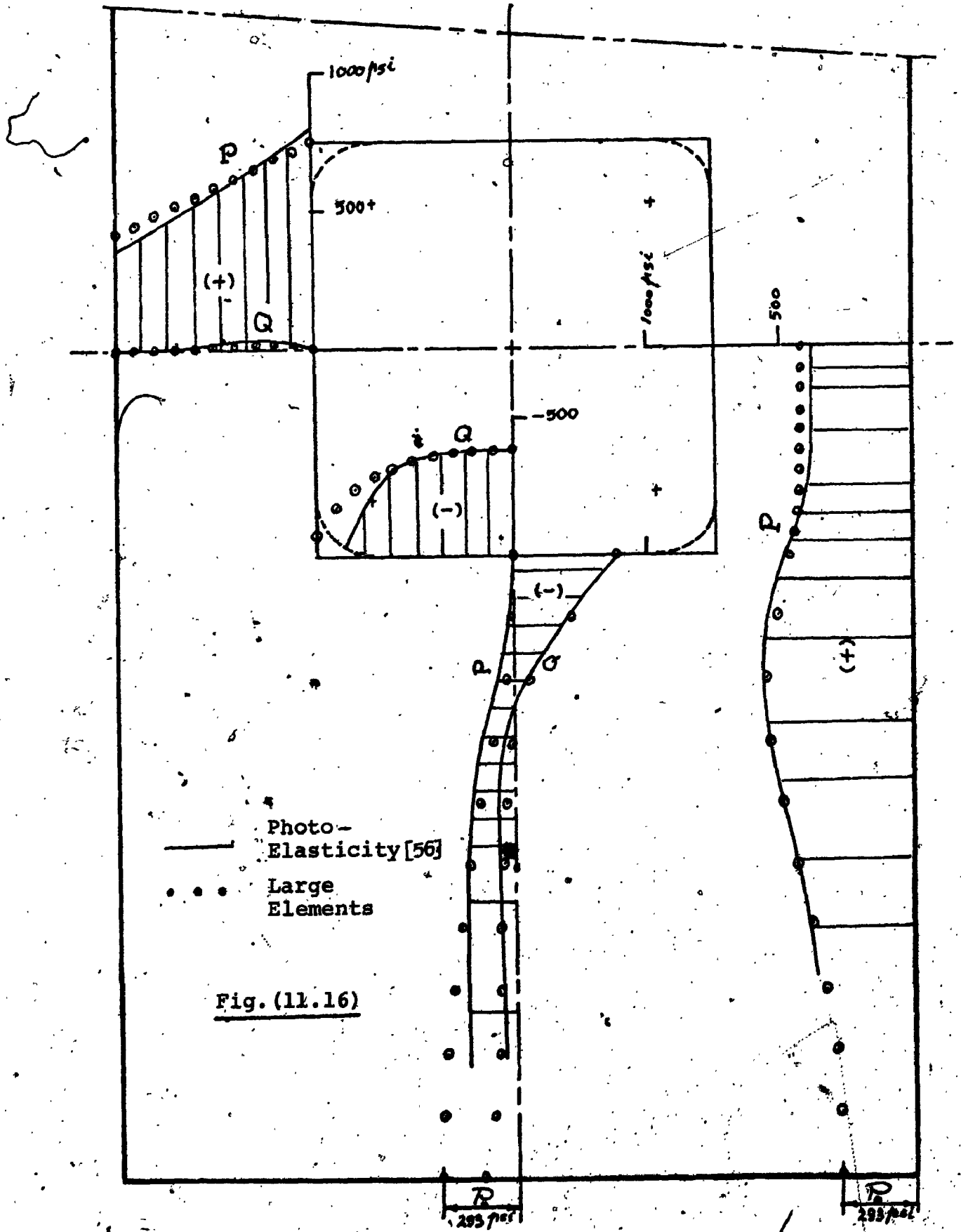

Fig. (11.16)

Rectangular Plate with a Square Hole under Edge Traction

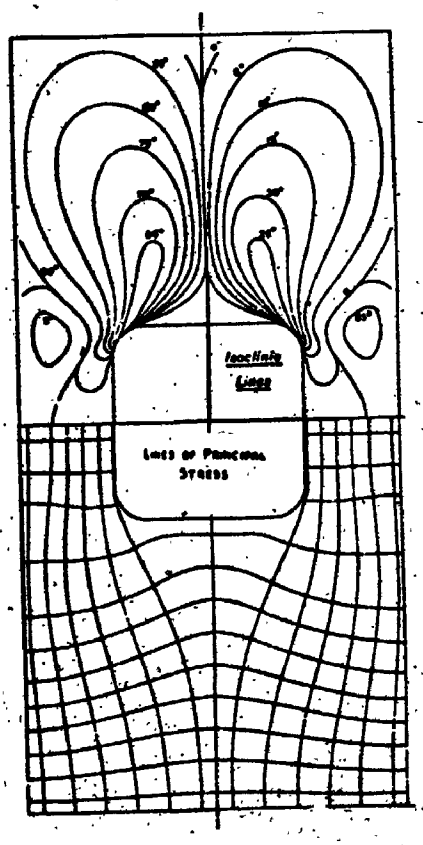

Isoclinics and lines of principal stress in a wall with a square opening in it.— Ref [56]

Fig.(11.17)

Stiffness

$E_x = E_y = E = 1$,

$\nu = 0.3$,

$G = \frac{E}{2(1+\nu)}$

$t_f = t_w = 2$, $W = b/2$, $C = a/4$.

Constaints

Edge No.	Type of Constraint
1	t, r
2	t, r
5	t, r
8	t
9	t
12	t, r
13	t, r
14	t, r

Additional Constraints

- Rot. at edge (6) = Rot. at edge (8)
- Rot. at edge(7) = Rot. at edge (9)
- Rot. about (η) at Node (4) = Rot. about (η) at Node (7)
- Rot. about (η) at Node (5) = Rot. about (η) at Node (8).
- Twist at Node (4) = Twist at Node (7).
- Twist at Node (5)=Twist at Node (8).
- Trans.at Node (7) = $-P(a-c/2)$
- Trans.at Node (8) = $-P.c/2$.
- Rot.about (ξ) at Node (7) = P
- Rot.about (ξ) at Node (8) = P

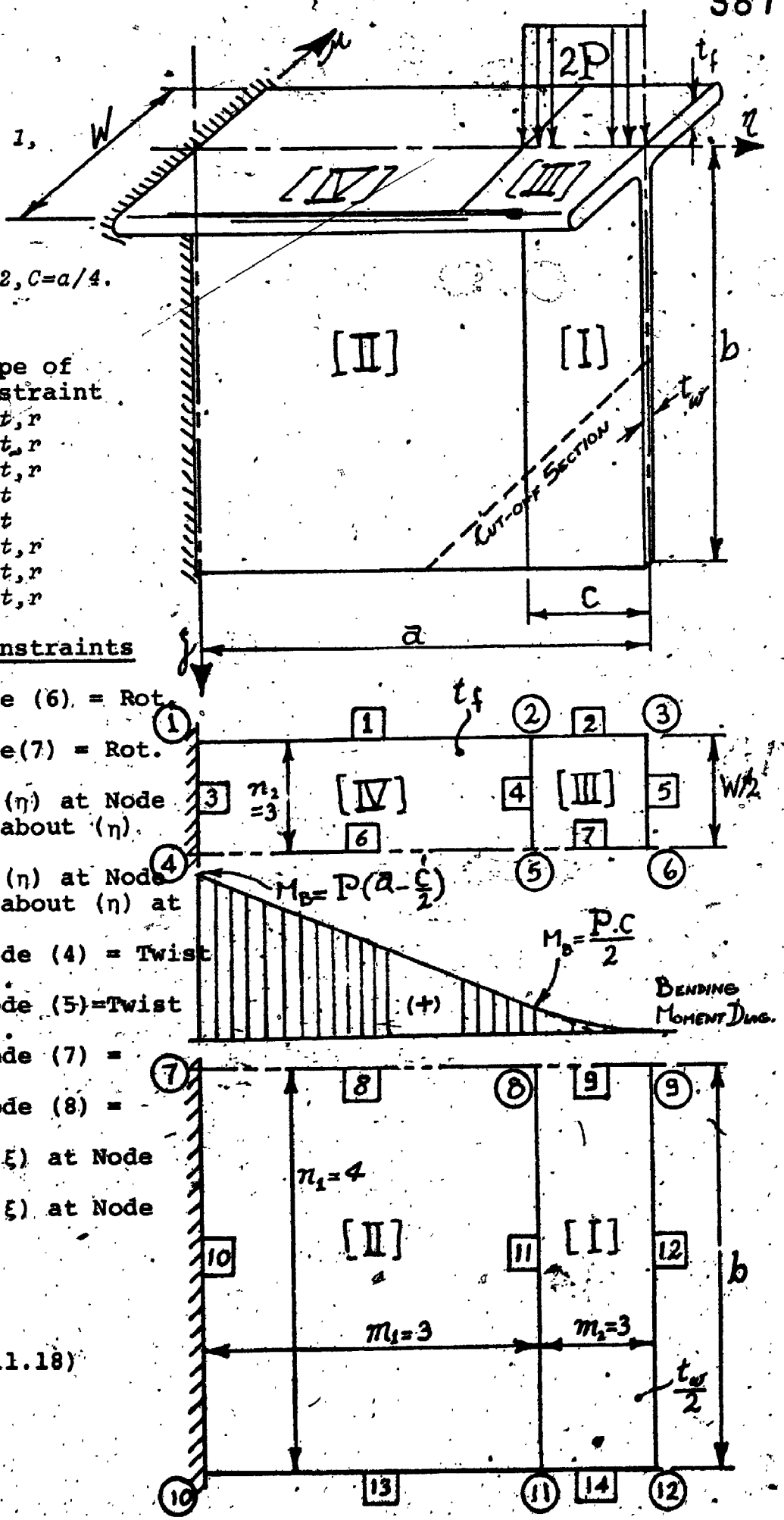

Fig. (11.18)

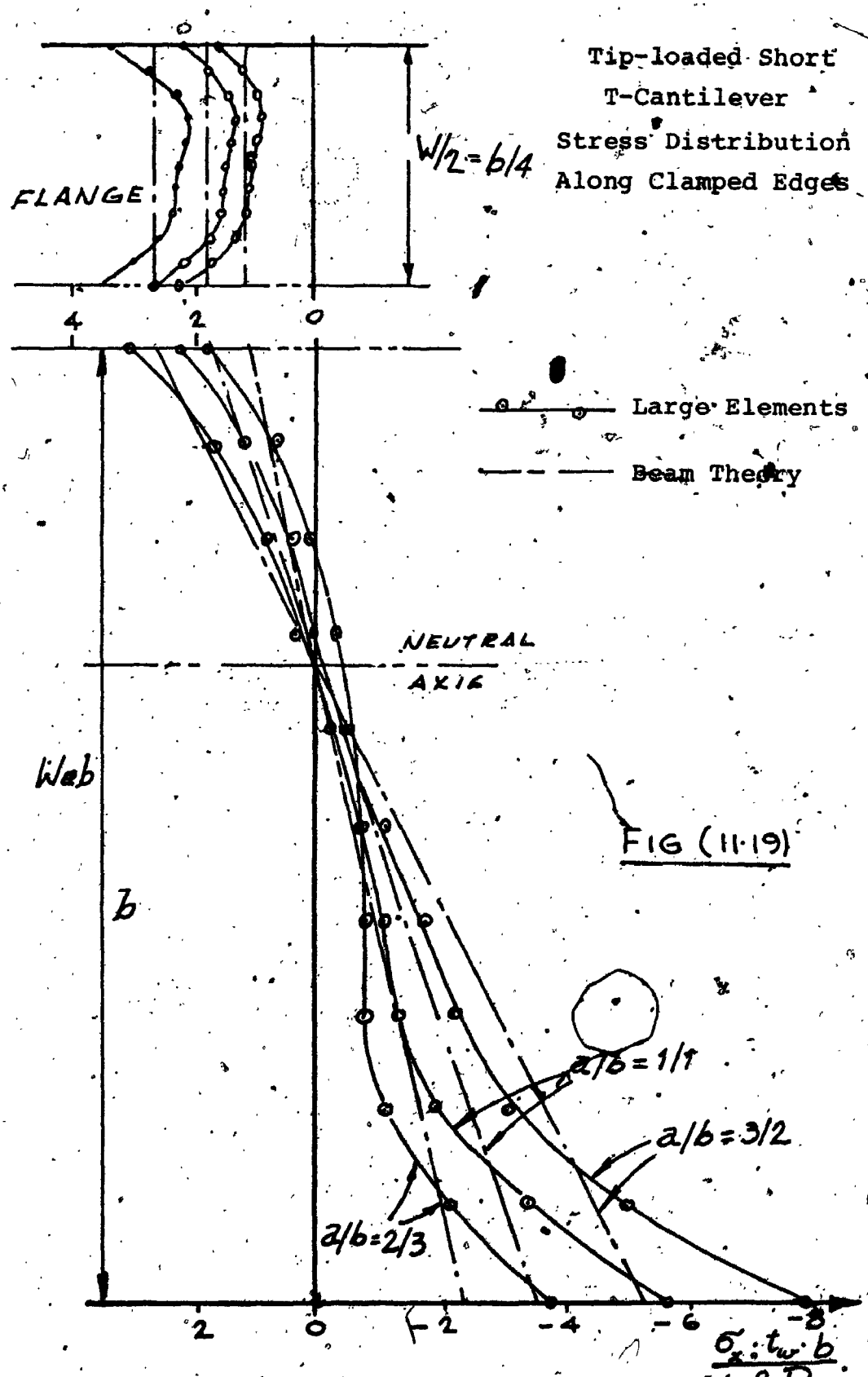
Tip-loaded Short
T-Cantilever
Stress Distribution
Along Clamped Edges
FLANGE
W/2 = b/4
4
2
0
Large Elements
Beam Theory
NEUTRAL
AXIS
Web
b
a/b = 1/1
a/b = 3/2
a/b = 2/3
2
0
-2
-4
-6
-8
σx : tw · b
2P

FIG (11.19)

FIG. (11.20)

TIP LOADED SHORT T CANTILEVER A/B=1 MAX. STRESS

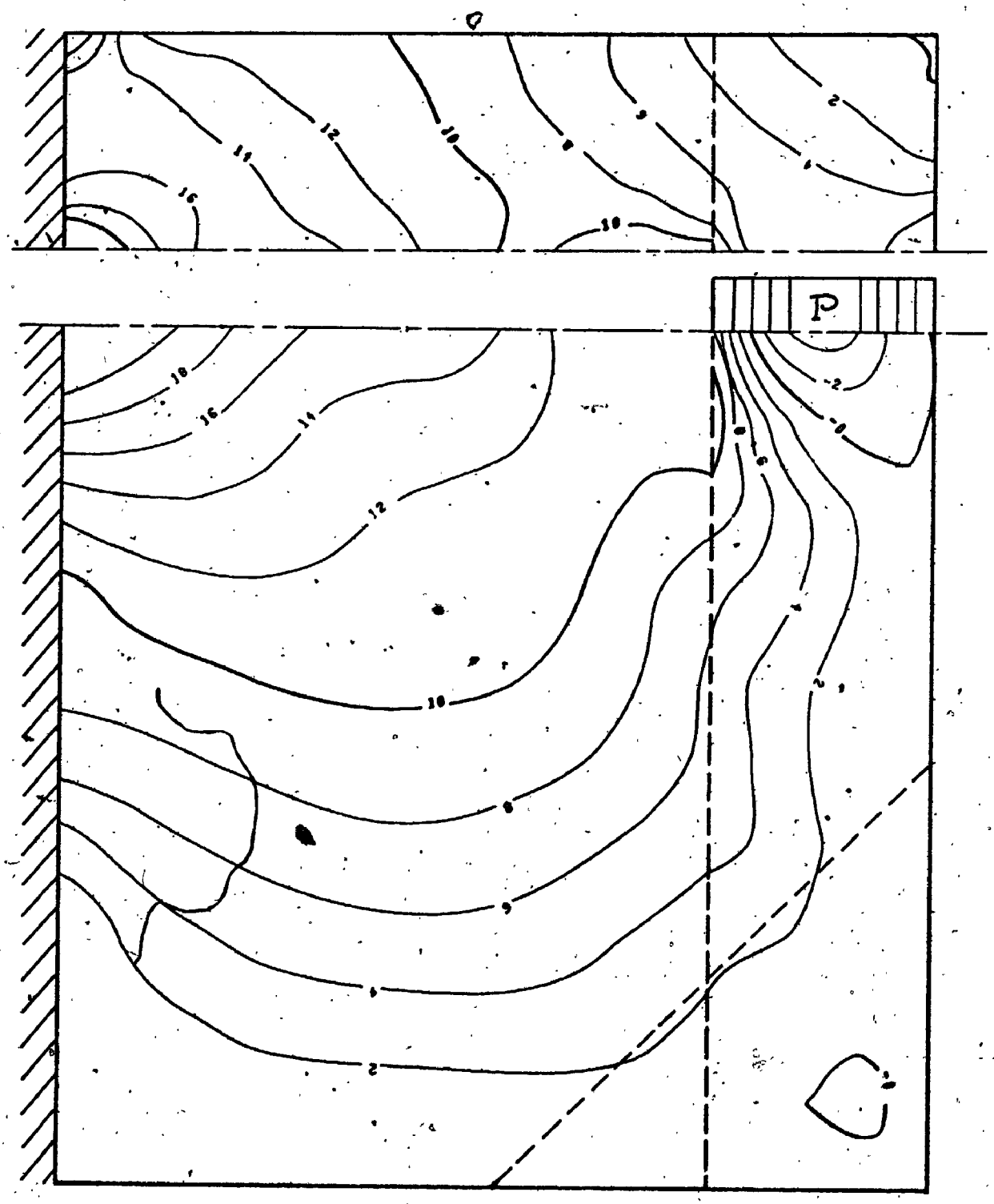

FIG. (11.21)

TIP LOADED SHORT T CANTILEVER A/B=1 MIN. STRESS

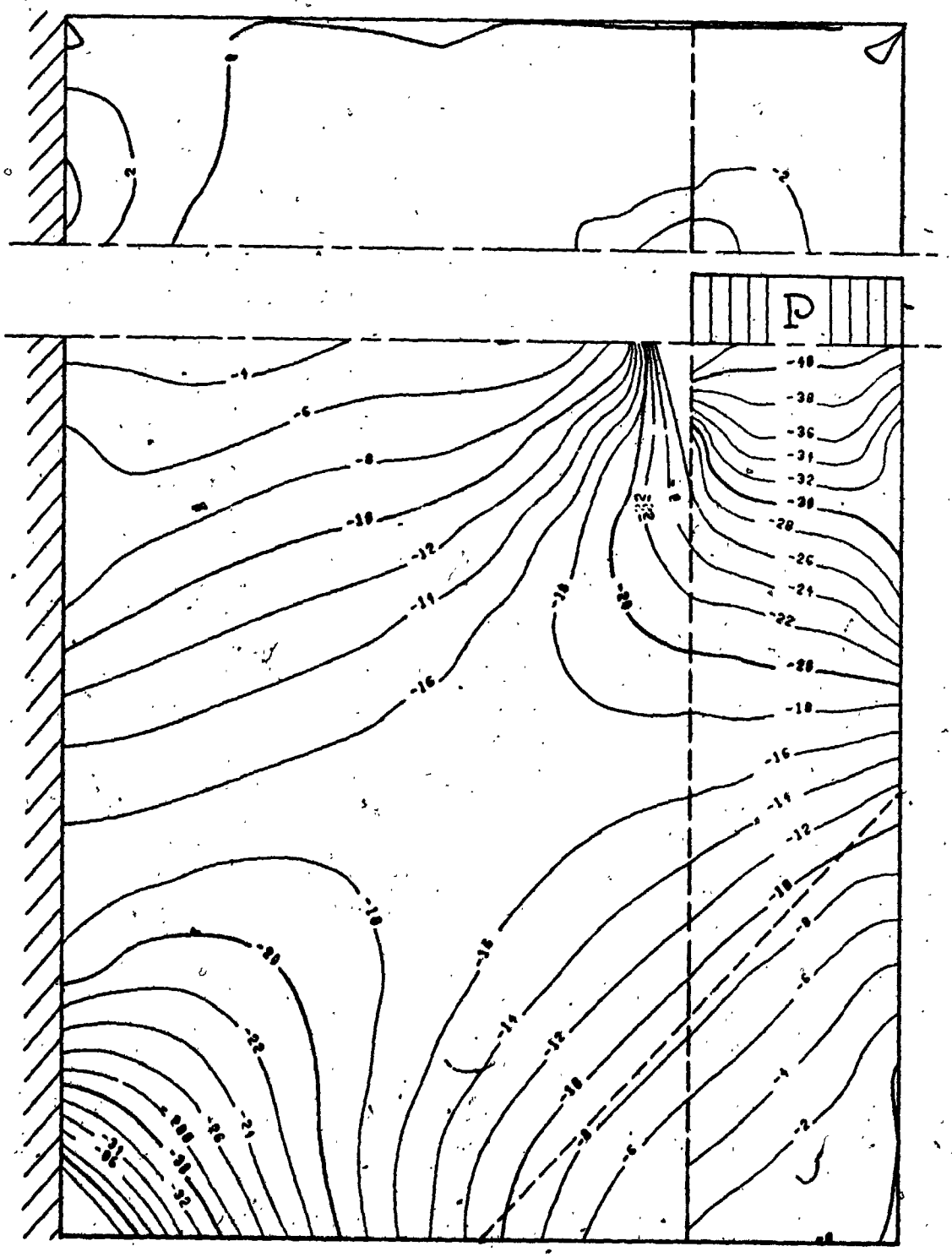

FIG. (11.22)

TIP LOADED SHORT T CANTILEVER A/B=1 MAX. SHEAR

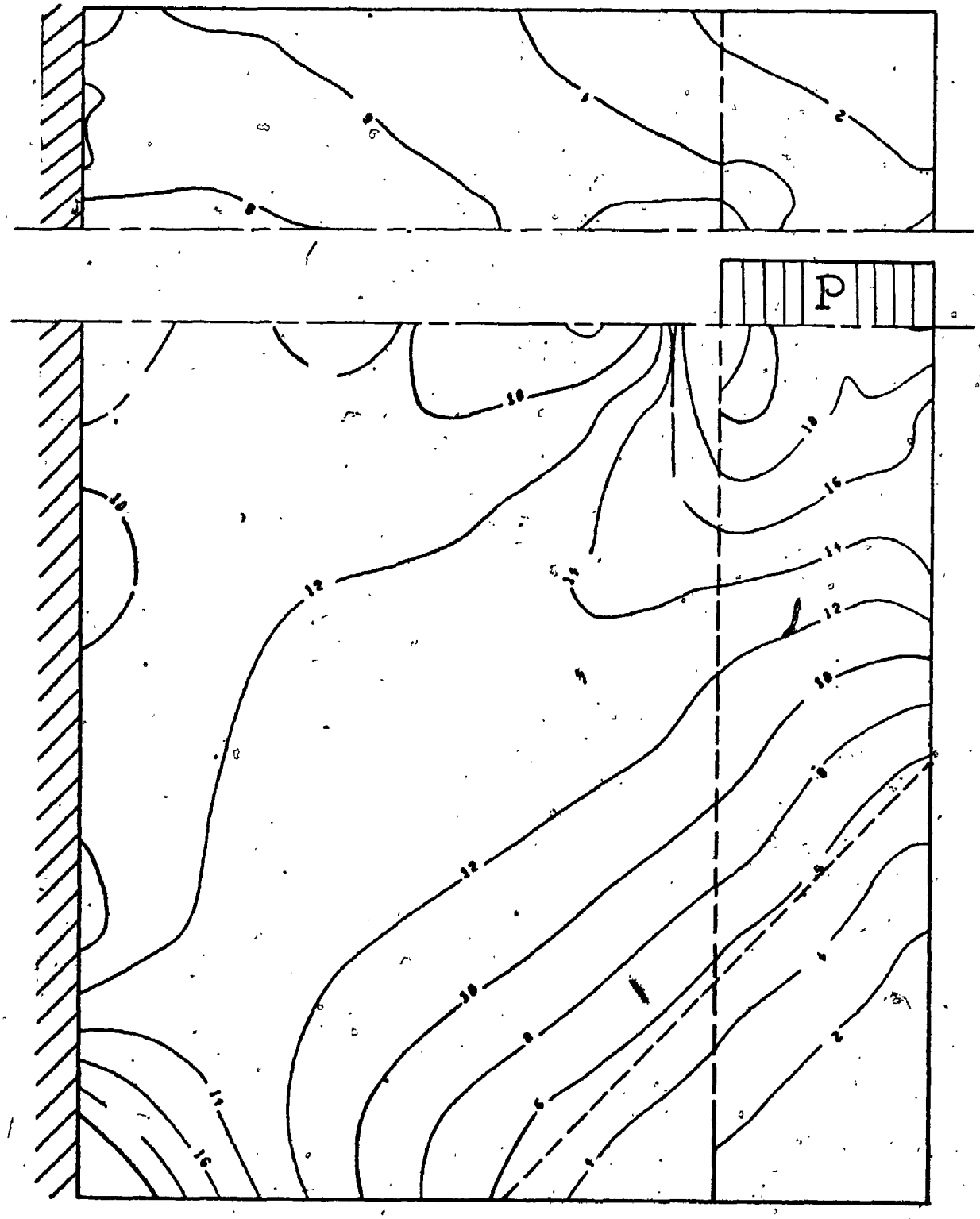

FIG. (11.23)

TIP LOADED SHORT T CANTILEVER A/B=1 THITA

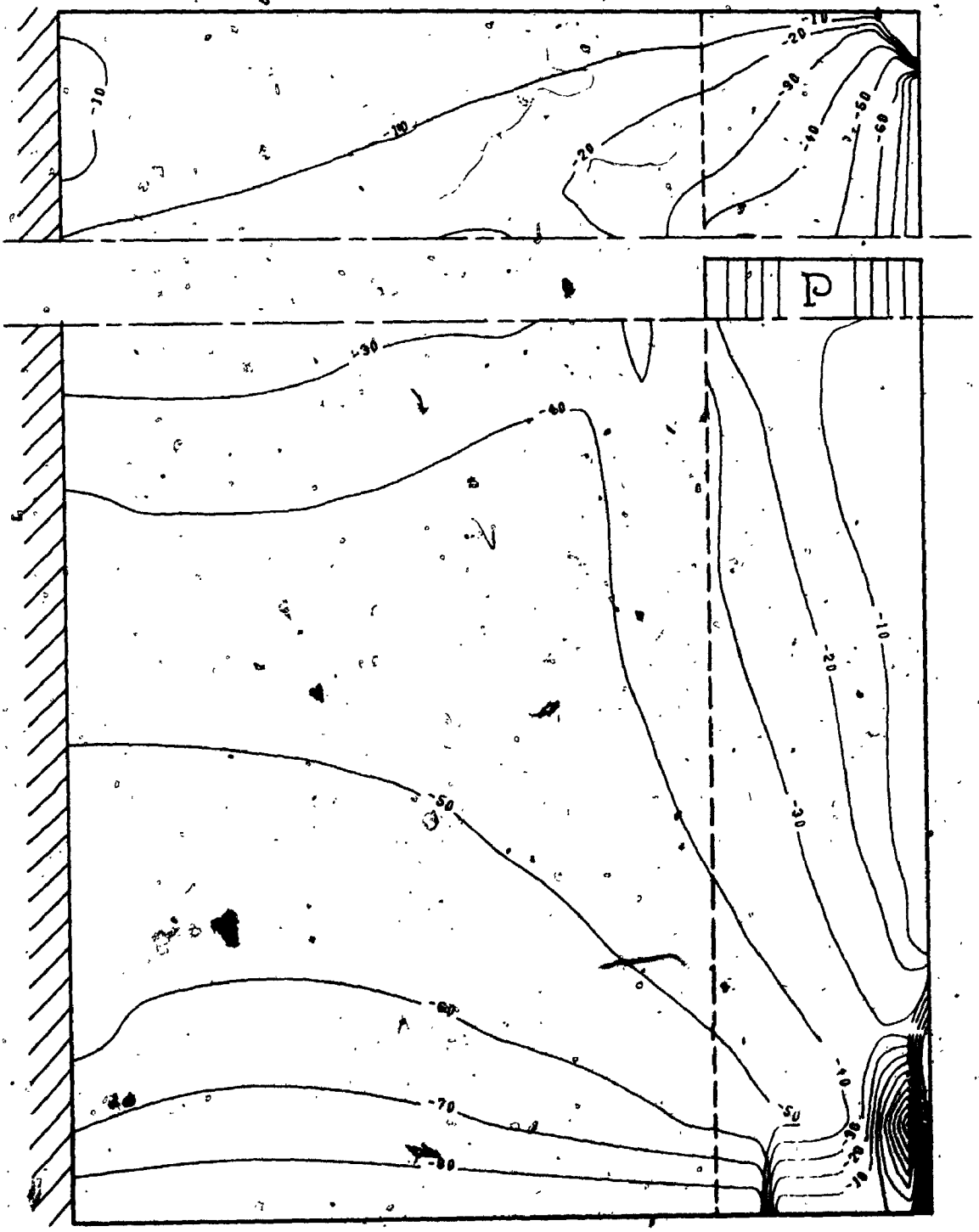

CHAR

TIP LOADED SHORT T CANTILEVER A/B=3/2 MAX. STRESS

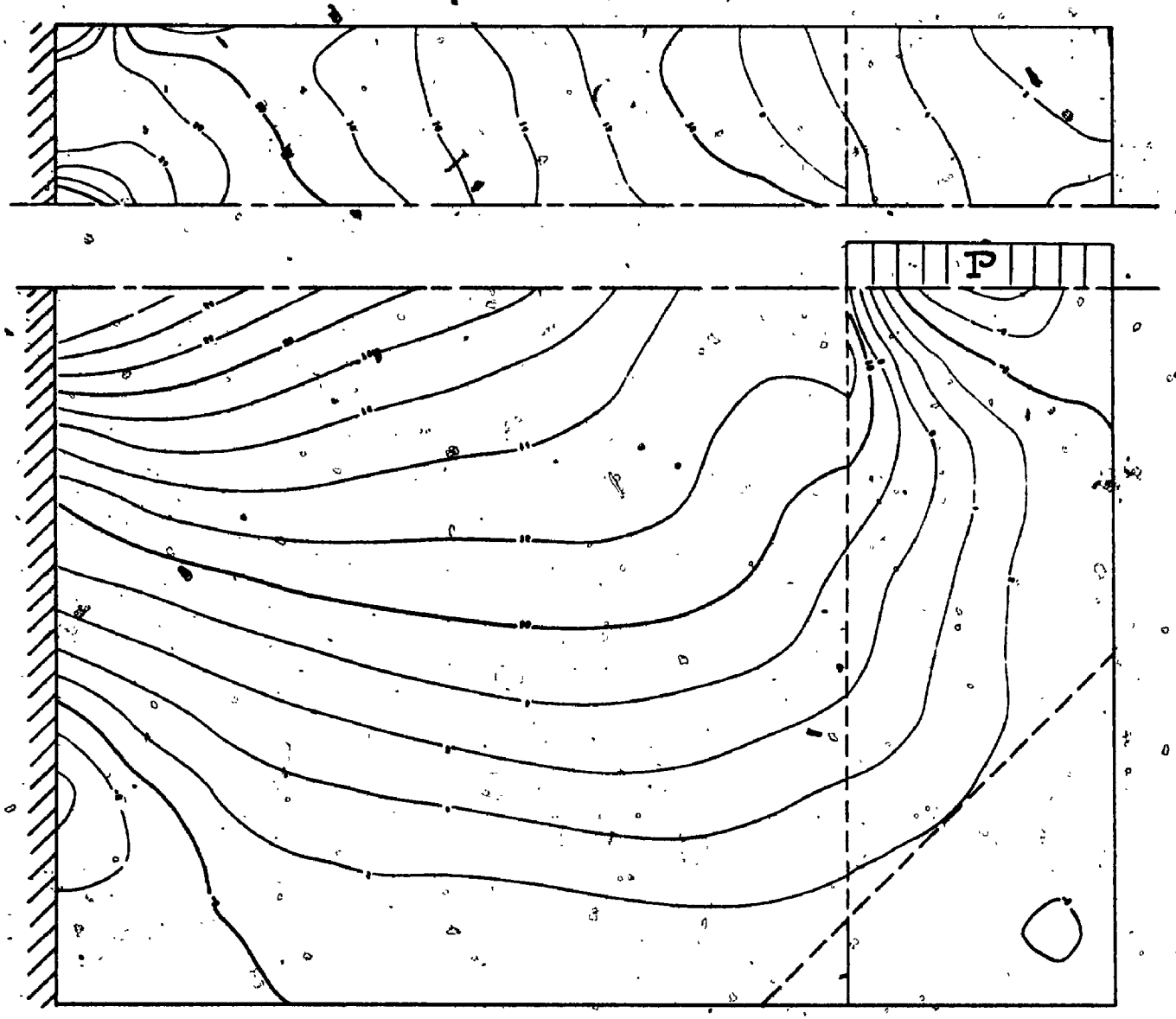

FIG. (11.24)

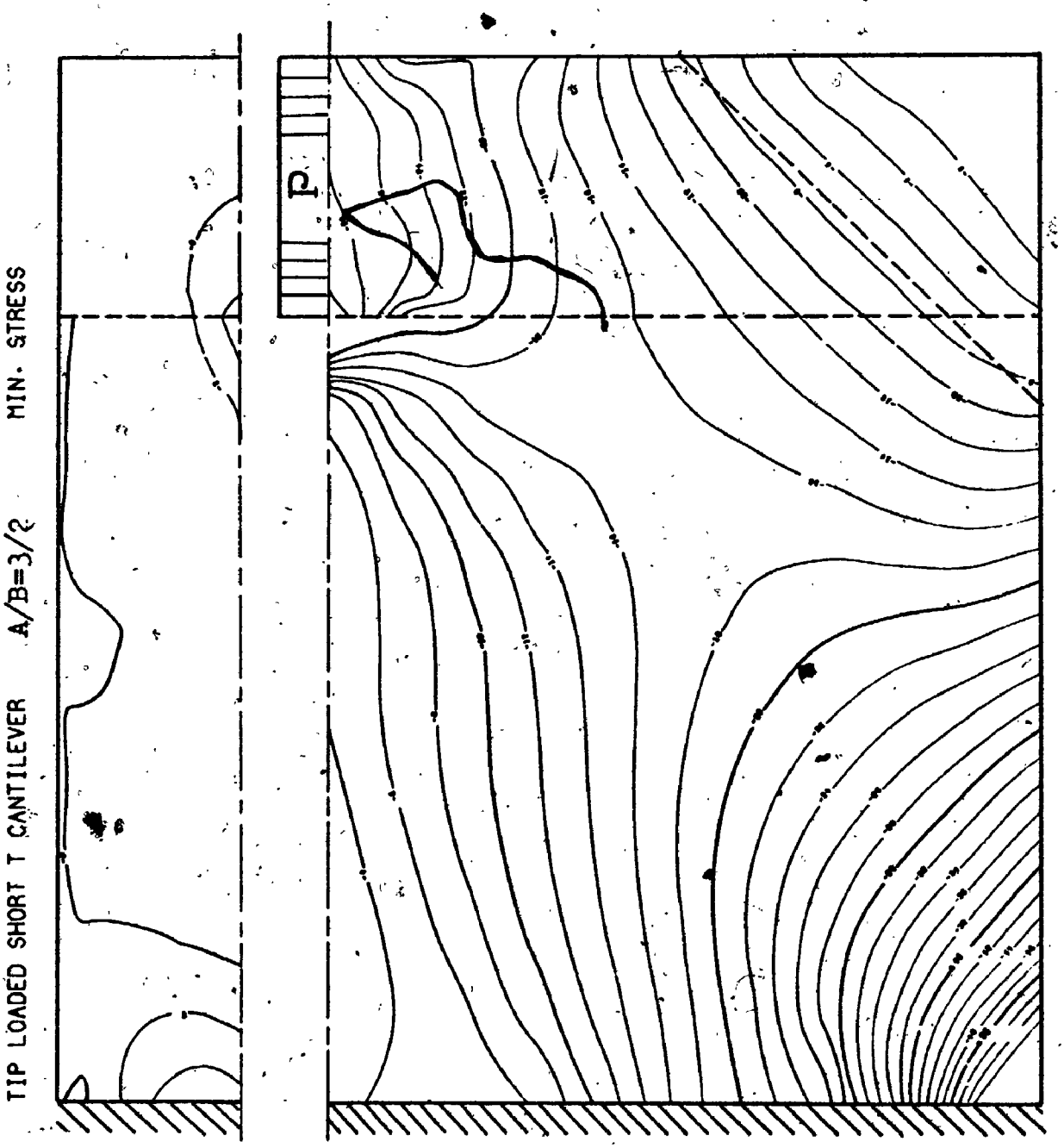

FIG. (11.25)

TIP LOADED SHORT T CANTILEVER A/B=3/2 MAX. SHEAR

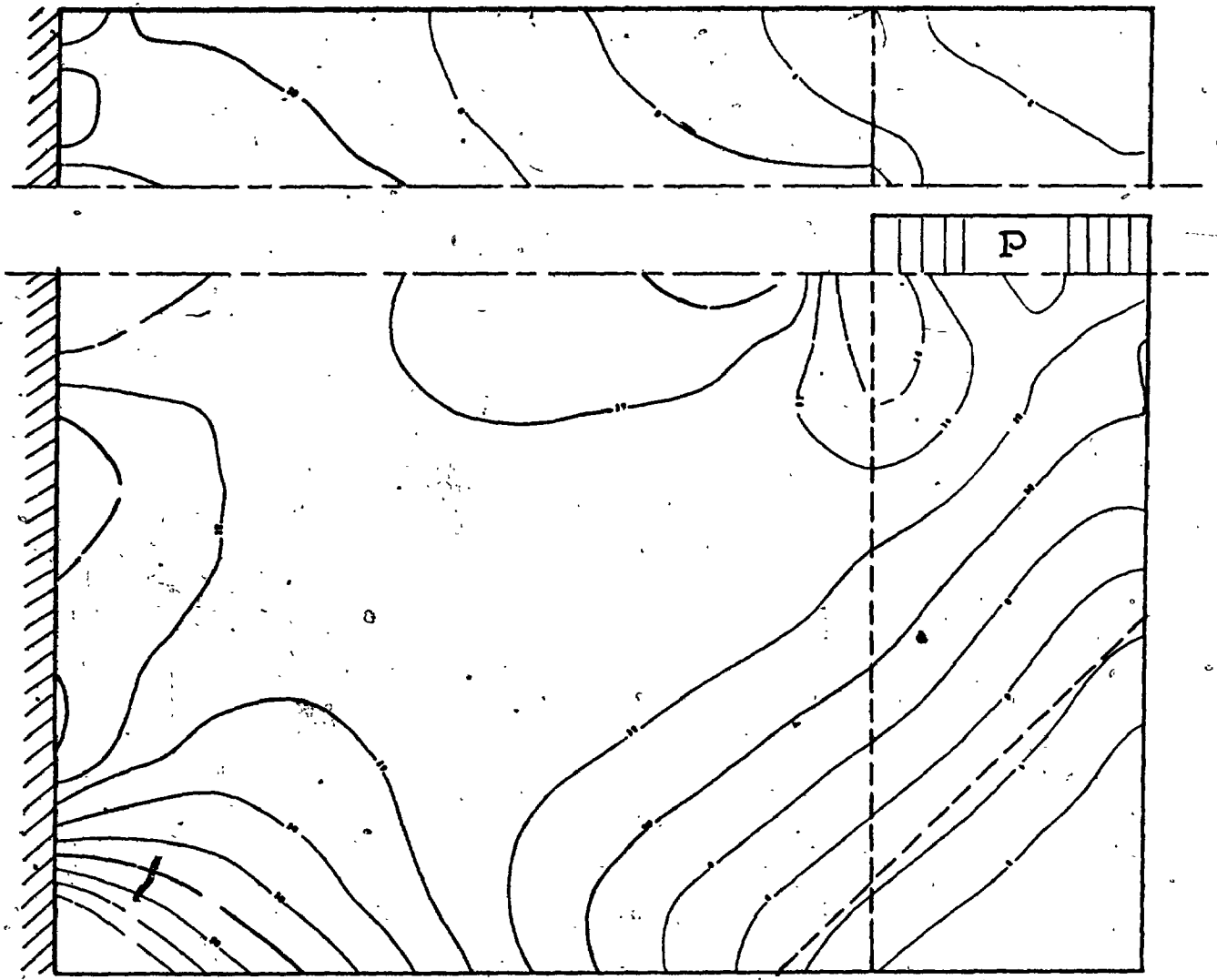

FIG. (11.26)

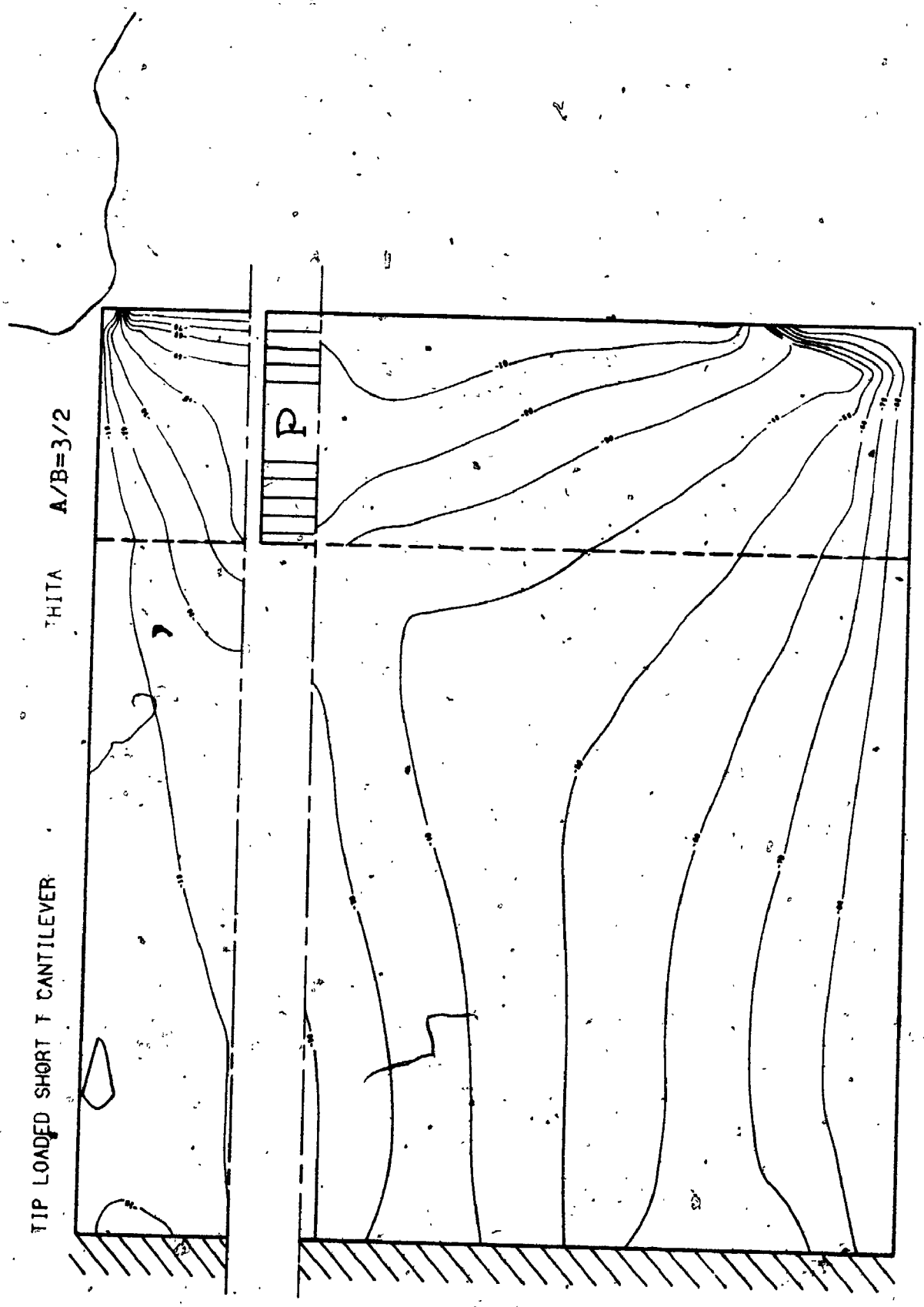

FIG. (11.27)

FIG. (11.28)

TIP LOADED SHORT T CANTILEVER A/B=2/3 MAX. STRESS

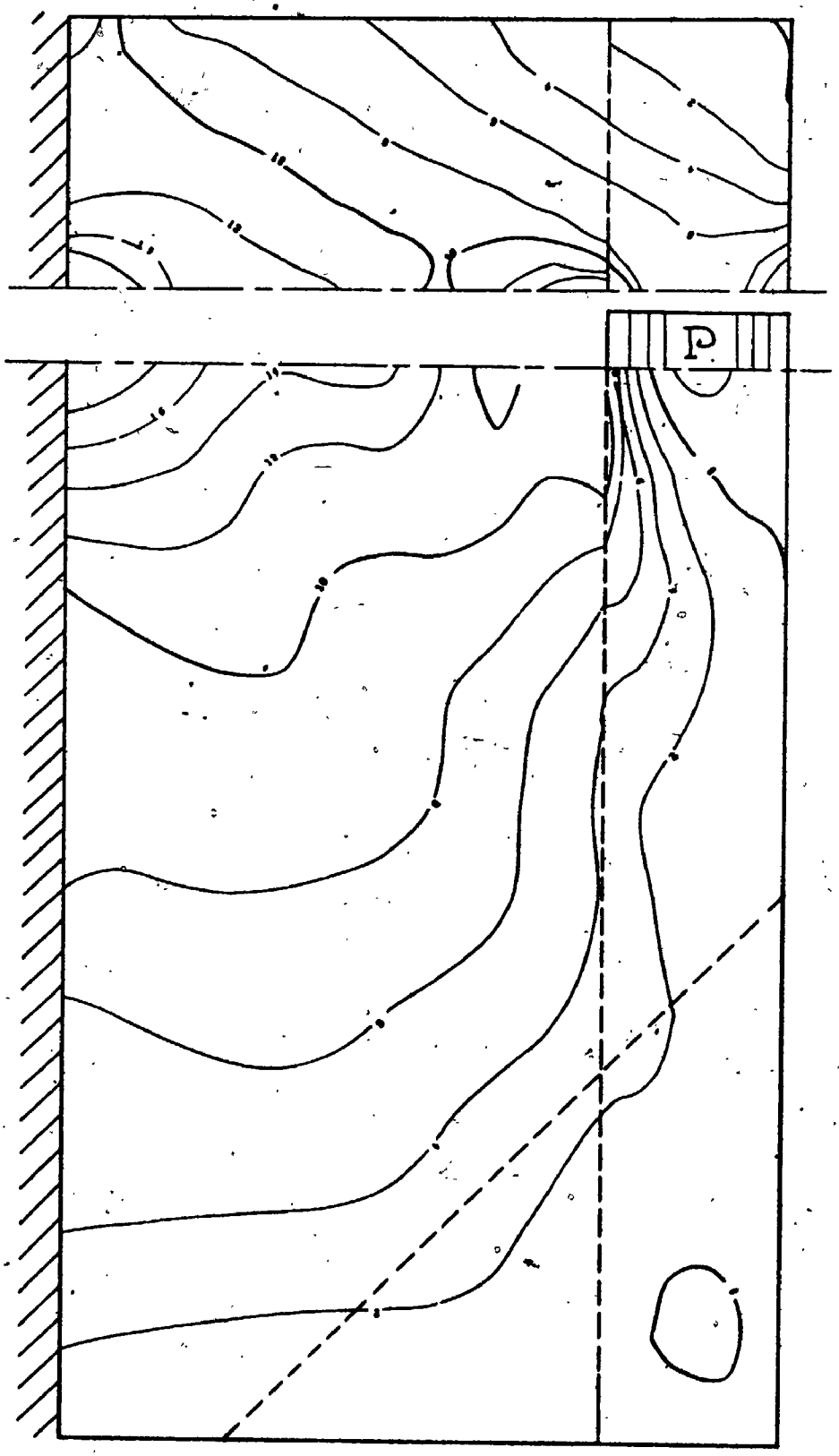

FIG. (11.29)

TIP LOADED SHORT T CANTILEVER A/B=2/3 MIN. STRESS

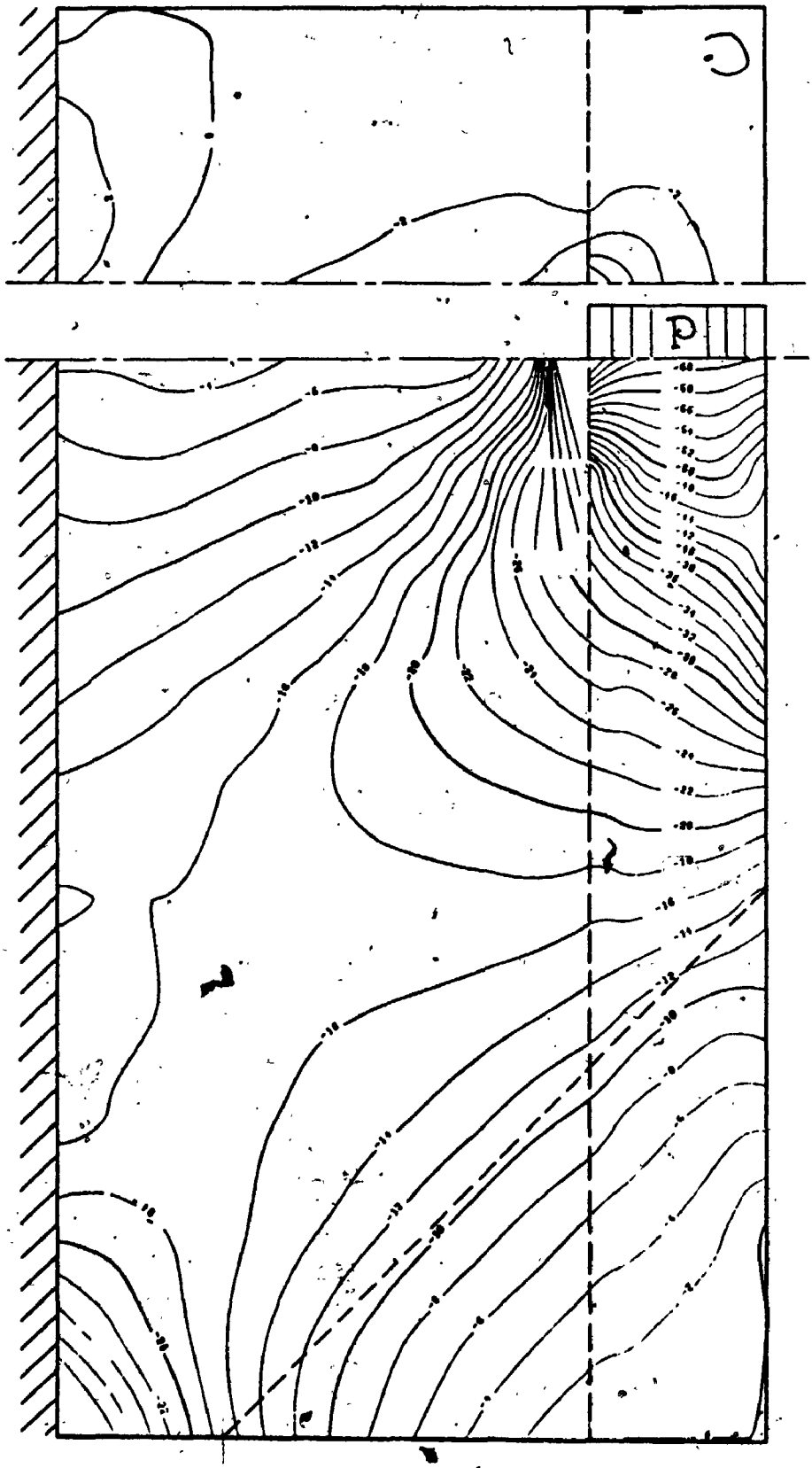

FIG. (11.30)

TIP LOADED SHORT T CANTILEVER A/B=2/3 MAX. SHEAR

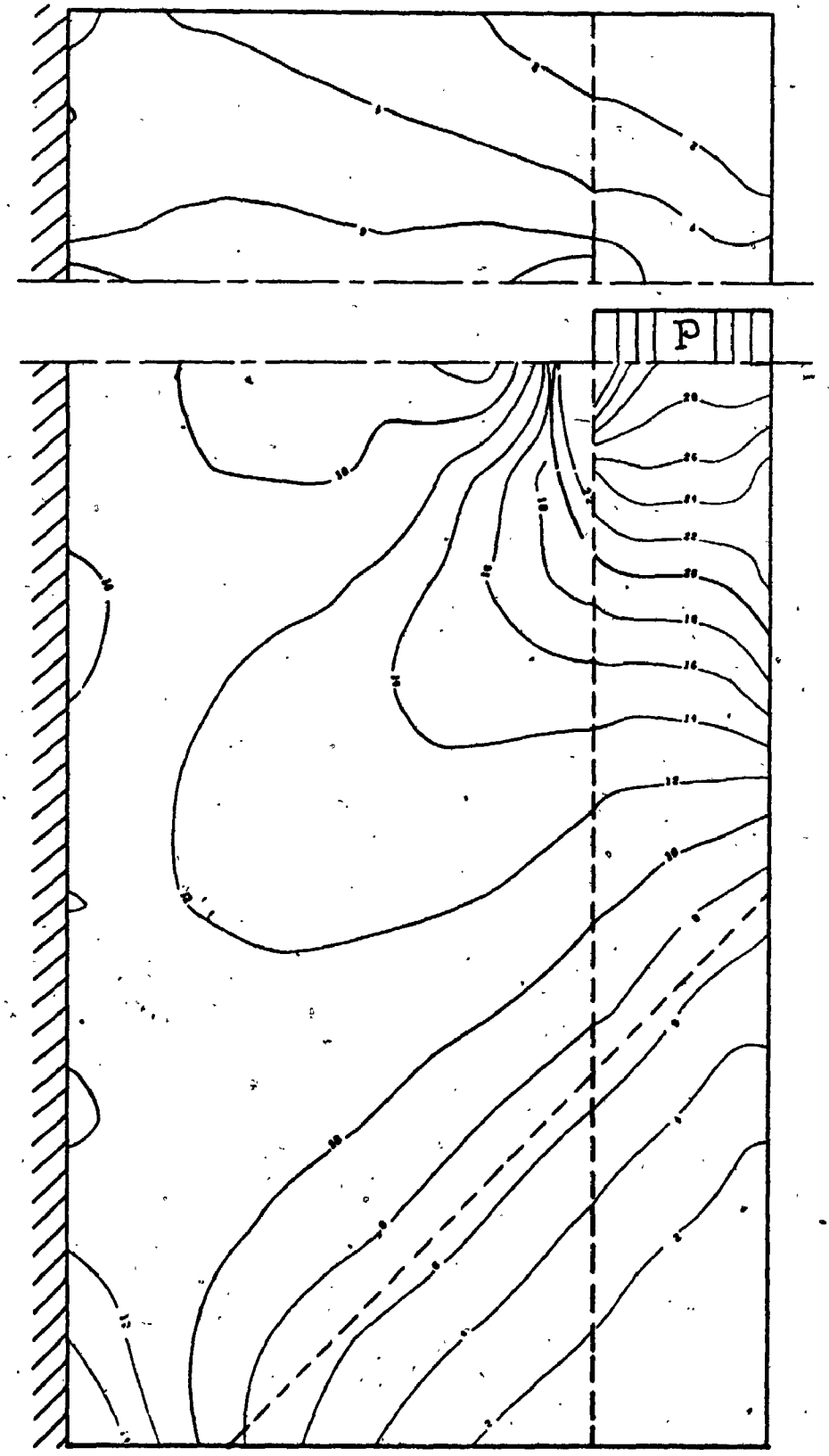

FIG. (11.31)

TIP LOADED SHORT T CANTILEVER A/B≒2/3 THITA

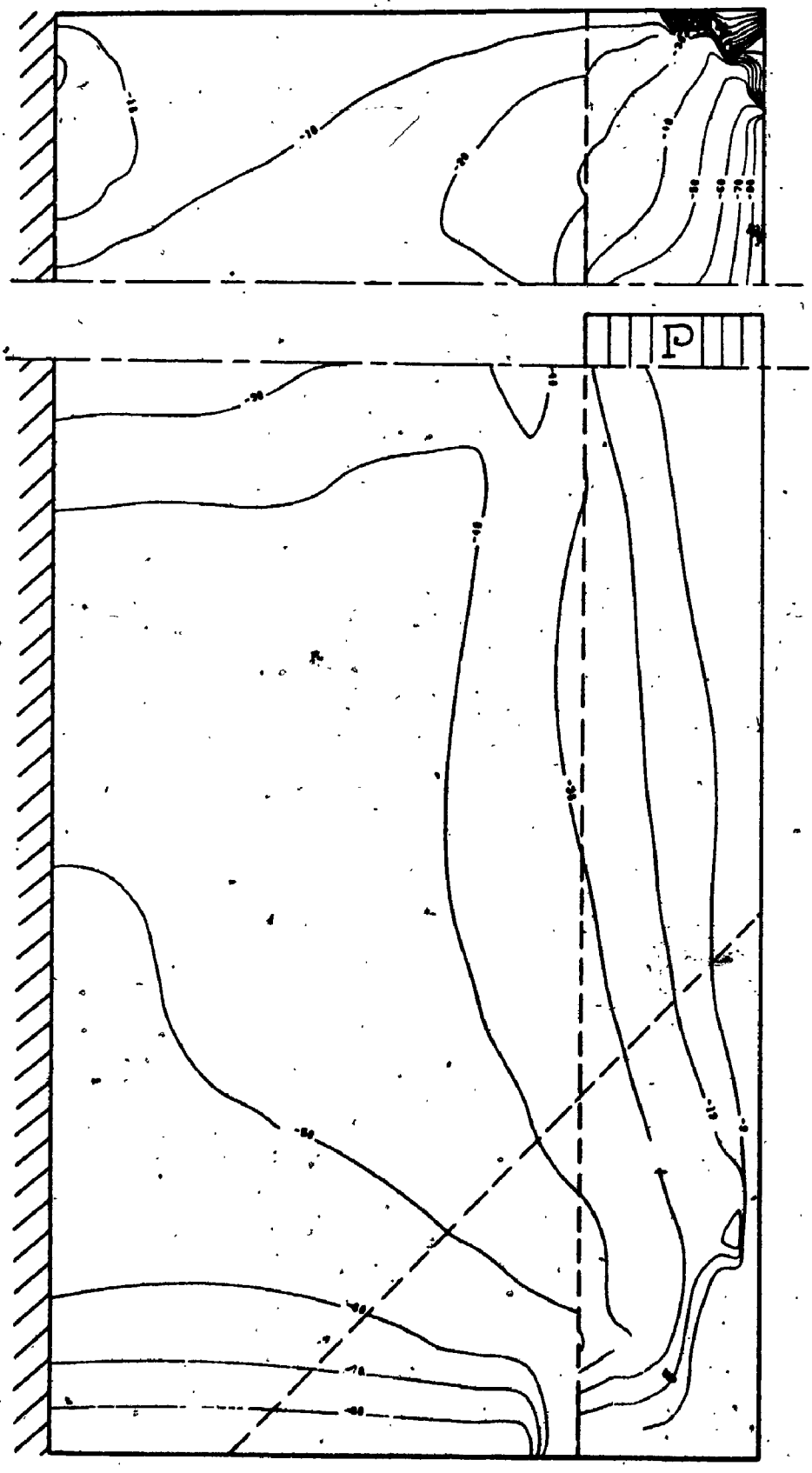

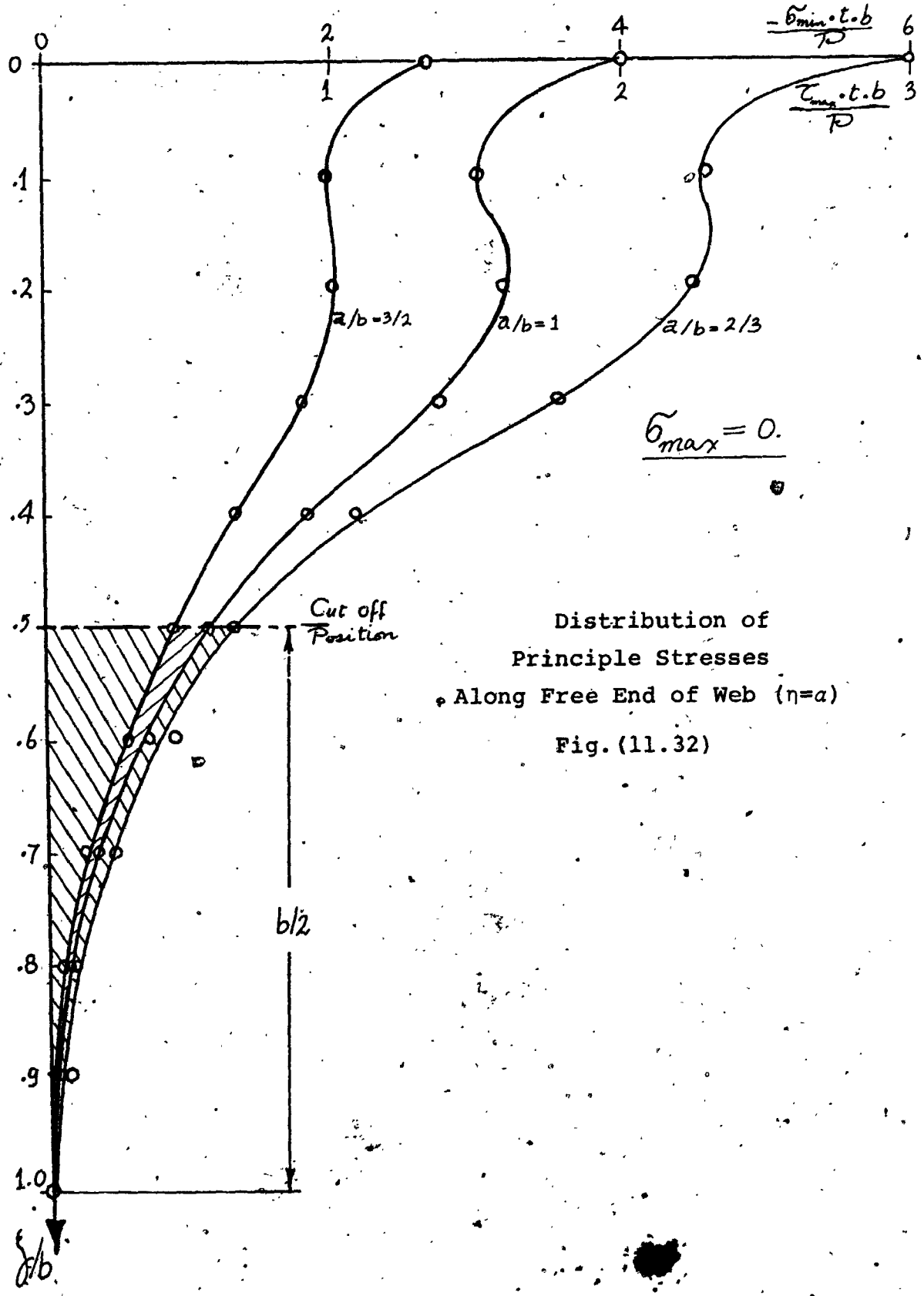

Distribution of Principle Stresses Along Free End of Web ($\eta = a$)

Fig. (11.32)

CHAPTER XII

CONCLUSIONS AND SUGGESTIONS FOR FURTHER WORK

12.1 General Conclusions

During the course of this study, a number of interesting conclusions have been drawn. In general, these conclusions have been presented and discussed previously in the appropriate sections. However, the more important of these conclusions will be reiterated in this Chapter.

- As a result of the study of the requirements of the Ritz method and the investigation of the suitability of the beam functions for use in the Ritz method in the case where natural boundary conditions are involved, the following observations were made:

  1. Pre-satisfaction of the natural boundary conditions by the individual members of an assumed series is not necessary. The Ritz solution will automatically converge towards satisfying both the differential equation and the natural boundary conditions along the portions of the perimeter which are not subject to any of the "forced" (e.g. slope/deflection in the case of a flexure problem) boundary conditions. It is sufficient in this respect that the assumed functions provide the

possibility of satisfying these natural boundary conditions through some linear combination of them. This was referred to by Kantorovich [6] as the completeness condition at the boundary. Pre-satisfaction of the free boundary conditions, however, is a desirable condition if such functions could be obtained.

2. It has been the common notion that since the free-free beam functions satisfy the free beam boundary conditions, which are somewhat similar to the plate free edge boundary conditions, this should expedite convergence towards satisfying the plate boundary conditions. This, however, does not seem to be the case. The very fact that these functions satisfy the free beam boundary conditions makes them incomplete at the boundaries in the sense mentioned above. The result expected, hence, is slow convergence and incorrect stress predictions.

3. A most satisfactory solution for the problem was the development of the "degenerated beam functions". The idea was to relax the unnecessary beam end conditions imposed upon the beam functions through the particular choice of the parameters (λ and ε) involved in them. This was best achieved by *floating* the values of the λ's, i.e. replacing

their numerical values by unknown coefficients to be determined subsequently during the Ritz minimization procedure. Since the beam functions depend linearly upon the λ's, floating their values results in *degenerating* each of the ordinary beam functions into its two basic constituent functions. For example, a family of Free-Free beam functions *degenerates* into two families of circular and hyperbolic functions.

The above conclusions were substantiated through the numerical solution of a number of test problems. Study of the results of these examples revealed the following:

1. Highly accurate solutions and very good convergence characteristics are obtainable through the use of a relatively small number of terms (five to nine terms in each direction) in a family of degenerated beam functions. Although these functions are intentionally chosen so that the individual members do not satisfy any end conditions at the free edges, the series converges rapidly towards satisfying the natural boundary conditions at these edges. Conversely, ordinary beam functions yield considerably less accurate eigenvalues and mode shapes when used in a problem involving free boundaries, even if a large number of terms is

used in the solution. Moreover, while inaccuracies in the frequencies and displacements obtained decrease with increasing the number of terms and may be - therefore - somewhat tolerable, the errors in the stresses obtained are certainly not acceptable. Generally, the errors in the stresses near the free edges, obtained using ordinary beam functions, increase as the number of terms in the series increases.

2. It is striking that in a degenerated beam function solution, the largest errors in the stresses predicted generally occur at the clamped edges (if they exist) where the boundary conditions are presatisfied, rather than at the free edges. This can be explained since a virtual force (or moment) near a clamped edge does negligible work; while a virtual force near a free edge, where the slopes and displacements are usually at their peak, contributes considerably to the energy of the system. A minimum energy criterion will, thus, tend to render more attention to stresses near the free edges compared to those at a clamped edge. It is hence, conceivable that, contrary to that which is commonly believed, problems under natural boundary conditions are better behaved and easier to solve approximately than those involving forced boundary conditions (e.g. the Derichlet problem), where inaccurate

stresses may result at the clamped edges.

3. Since *sufficient*, rather than *necessary*, conditions for the convergence of a sequence of functions are normally conceived through the techniques of functional analysis, it becomes very difficult to present a full analytical proof for the inadequacy of the ordinary beam functions. Therefore, the fact that beam functions are incomplete in the sense defined in section (2.3) in addition to the results of the numerical examples of Chapter III, is considered sufficiently strong evidence that ordinary beam functions lead to inaccurate eigenvalues and displacements as well as incorrect stresses, at least for the classes of problems investigated here.

Based upon the study presented in Chapter IV, it was shown that the Ritz method can be used to advantage for solving the two dimensional elasticity problem in rectangular regions. Body forces and mixed boundary conditions can be conveniently accommodated in the analysis. The following remarks pertain to the results of this study:

1. When a stress function type formulation is used in the two-dimensional elasticity problem, the governing differential equation is biharmonic - i.e., the same as that for a plate bending problem. An analogy has been drawn between the differ-

ent types of inplane stress and out-of-plane bending boundary conditions showing a very strong similarity and a one-to-one correspondence.

2. Due to the above-mentioned similarity, it was possible to use the same formulations and the same types of ordinary and degenerated beam functions used in the plate bending problem for the solution of the analogous inplane stress problem. In addition to the fact that beam functions proved to be highly accurate in plate bending problems, the use of the same functions in the inplane problem made it possible to use the same integral coefficients already evaluated for the use with the former problem. This proved particularly useful in the study of the plate stability problem since the same functions and the same formulation can be used for the two phases of the problem (i.e.,the inplane and out-of-plane phases).

3. As with the plate bending problem, the assumed functions are required to satisfy only the *essential* (forced) boundary conditions of the problem(which in this case are those concerning specified boundary forces). The natural boundary conditions resulting from restraining the edge displacements will be satisfied automatically during the minimization procedure when sufficient terms are considered in the assumed series.

4. The variational stress function formulation presented here was shown to be capable of representing sharp stress gradients such as those resulting from corner singularities. It was shown that for the same number of degrees of freedom, other methods of solution - such as Finite Elements and Finite Differences - cannot match such a high stress gradient as that which can be represented by the present approach.

5. Simple polynomial solutions for the inplane elasticity problem, such as those presented in references [1] and [18], which do not satisfy the compatibility conditions near the clamped edges, are good only at a sufficient distance from such edges. Gross errors, however, may result from such solutions in the regions where the clamped edge effects are predominant. It has been argued that the width of such a region is approximately equal to $(\nu \cdot a)$ where (ν) is Poisson's ratio, and (a) is the length of the clamped edge. This width, however, may be reduced for a very narrow plate where it might be affected by the region of influence of the close-by parallel edge.

The problem of the buckling and vibration of plates subject to general body and/or boundary loads may be conveniently solved using ordinary and/or degenerated beam functions in the Ritz method. The solution is

performed in two phases; first the two-dimensional stress analysis problem is solved in order to determine the stress distribution in the plane of the plate due to the external loads applied; the plate flexure problem is then solved with the due effect of the inplane loads taken into account in the strain energy expression used. An overly-simplified inplane stress distribution has usually been used to solve directly the plate stability problems [1, 18, 19] while by-passing the first phase of the solution. Depending upon the nature of the problem, varying degrees of accuracy maybe obtained through such a simplified solution. The major factors affecting the accuracy of a stability solution utilizing an assumed stress distribution satisfying only the equilibrium conditions of the problem have been identified. These factors were successfully used to predict the behaviour of the solutions in a variety of examples which are presented in Chapter V. These major factors are:

1. Since the simplified stress distributions assumed usually do not satisfy the compatibility boundary conditions at the clamped edges, the accuracy of these assumed stress expressions deteriorates as a larger portion of the boundary is considered clamped (with respect to the inplane motion). As mentioned before, the range of influence of a

clamped edge increases as the length of such an edge is increased.

2. The inplane loads in the energy equation for the out-of-plane motion of a plate element are weighted by the square of the slope of the element under consideration. Thus, a large change in the inplane load intensity in a direction where the slope is small may contribute a negligible change to the eigenvalues of the problem (frequencies or critical loads). Conversely, a moderate error in the inplane loads assumed in a direction where the slopes are large can contribute significant errors to the eigenvalues. Since the out-of-plane boundary conditions greatly affect the slopes (at least in the vicinity of the plate edges, where the errors in the assumed load patterns are usually most pronounced), the sensitivity of the dynamic solutions to the accuracy of the assumed load patterns are largely dependent upon those boundary conditions. In particular, out-of-plane simply-supported edges cause large relative errors since they result in the maximum slopes occurring at the edges where the maximum errors in the inplane stresses normally occur.

3. In a normalized mode shape, it is known that the slopes in a certain direction increase as the number of half waves in that direction increases.

Consequently, the mode of vibration - or buckling - is an important factor in estimating the relative effect of a particular deviation in the assumed inplane load pattern. Hence, for a given problem, the same assumed set of stresses produces different relative errors in the eigenvalues associated with the different mode shapes which, generally, increase as the order of the mode increases. In some examples it was found that the errors even have different senses in the different modes.

The ideal analysis process was defined as one which maximizes the quality of the results and minimizes the total effort in obtaining them. Reliability (guaranteed convergence - preferably monotonic - to the correct solution) and versatility (applicability to a sufficiently wide - and well defined - class of problems) are essential features for an ideal process. Two phases were identified in the course of the use of an analytical process; the *development phase*, which includes the planning, preparation, and verification of a general purpose computer program incorporating the analytical approach; and the *application phase*, which represents the day-to-day use of the program to solve practical Engineering problems. Simplicity of the analytical formulation and the ability to be extended to other problem areas are features desirable

during the development phase. The following were identified as features desirable during the application phase of an analytical process. It was considered that these features are more important than those corresponding to the development phase since the major expenditure is usually devoted to the day-to-day usage of the program rather than its development. These features are:

1. Simplicity of the discretization technique in order to minimize the effort required for the preparation of the mathematical model.
2. Simplicity of the treatment of complicated configurations.
3. Simplicity of treatment of boundaries, interfaces, and discontinuities.
4. Ease of use of the method by people other than those who have developed it.
5. Efficiency of formulation and solution.

In an effort to evaluate the existing methods of analysis, they were classified into two categories according to the nature of the generalized coordinates employed. These categories are; discrete coordinate methods (such as Finite Difference, Finite Element, and numerical integration methods), and continuous coordinate methods (such as Ritz, Galerkin, Lagrangian multipliers, and Fourier series methods). A comparison between a typical disqrete coordinate

method (Finite Elements) and a typical continuous coordinate method (Ritz) in the light of the criterion for an ideal analytical process mentioned above revealed the following:

1. While different sets of assumed coordinates (functions) have to be used for different *boundary conditions* in the case of a continuous coordinate method, in Finite Elements (discrete coordinate methods) no such difficulty exists. The boundary conditions are simply handled by restraining the unwanted degrees of freedom at the boundary coordinates; usually with a corresponding reduction in the number of unknowns in the problem.
2. Due to the localized nature of discrete coordinates, and due to the element-oriented procedure of building the stiffness - and mass - matrices in the case of the Finite Element approach, it is particularly simple to deal with geometric, stiffness, and boundary *discontinuities*. Existence of such discontinuities renders the use of continuous coordinate methods very difficult and often impractical; thus violating the essential *versatility* requirement.
3. Due to the local nature of the discrete coordinates, and due to the fact that the spatial distribution of the degrees of freedom is fixed and pre-determined by the choice of the location of the control

points (nodes) in a discrete coordinate solution; continuous coordinates normally provide higher flexibility to the structure than do an equivalent number of discrete coordinates. Since the accuracy of the solution is a function of the flexibility provided to the structure, while the cost is a function of the number of coordinates used; discrete coordinate methods are usually *less efficient* than continuous coordinate approaches.

4. Discrete coordinate solutions ensure continuity of the fundamental quantities (at least at the control points) but not their derivatives (e.g. stresses). Continuous coordinate methods, however, normally provide continuity of the unknowns as well as their higher derivatives. This results in better quality solutions being obtainable through the use of continuous coordinate methods as compared to discrete coordinate approaches. In addition, these discontinuities offer difficulty in representing high stress gradients.

5. Since in Finite Elements the structure has to be physically subdivided into a large number of elements, considerable effort is usually spent in the *preparation of the data required for the mathematical model*. Data providing information regarding the location of the control points as well as information about each of the connecting finite

elements have to be prepared and checked. No comparable effort expenditure is necessary for a Ritz solution since only the basic data about the continuum have to be provided with no additional "artificial" subdividing lines.

6. Questions of *convergence and reliability* are more easily dealt with in the case of continuous coordinate methods, both from the mathematical and practical application points of view. In particular, in the case of discrete coordinate methods the number of nodes in a convergence sequence must take the form n, $2n$, $4n$,..., so that each step includes all the nodes used in the previous ones. In a continuous coordinate method, however, any increasing sequence can be used to examine the convergence of a solution. Moreover, monotonic convergence is not always granted with Finite Elements except if certain restrictive continuity conditions are met by the element displacement functions. Continuous coordinate methods, of variational origin, guarantee monotonic convergence.

It can be concluded from the above comparison that neither of the two categories of methods meets the requirements of an ideal process as stated earlier. In particular, continuous coordinate methods fail to provide sufficient generality and versatility; and hence are applicable only for relatively simple problem

elements have to be prepared and checked. No comparable effort expenditure is necessary for a Ritz solution since only the basic data about the continuum have to be provided with no additional "artificial" subdividing lines.

6. Questions of *convergence and reliability* are more easily dealt with in the case of continuous coordinate methods, both from the mathematical and practical application points of view. In particular, in the case of discrete coordinate methods the number of nodes in a convergence sequence must take the form n, $2n$, $4n$,..., so that each step includes all the nodes used in the previous ones. In a continuous coordinate method, however, any increasing sequence can be used to examine the convergence of a solution. Moreover, monotonic convergence is not always granted with Finite Elements except if certain restrictive continuity conditions are met by the element displacement functions. Continuous coordinate methods, of variational origin, guarantee monotonic convergence.

It can be concluded from the above comparison that neither of the two categories of methods meets the requirements of an ideal process as stated earlier. In particular, continuous coordinate methods fail to provide sufficient generality and versatility; and hence are applicable only for relatively simple problem

configurations. On the other hand, discrete coordinate methods fall short on questions of simplicity, efficiency, and reliability, as compared with continuous coordinate methods. These added modelling difficulties and efficiency drop, however, may become justifiable for immensely complicated problems. It was felt, therefore, that an approach incorporating both discrete and continuous coordinate systems would promise a potential of providing an optimum analytical approach; hence the Large Element method was proposed.

The Large Element approach is basically a blend of the Finite Element and Ritz methods into an optimum combination which offers the advantages of the two methods and *practically* eliminates all their shortcomings. In this blend, the character of each of the two constituents is preserved, and - should it be desirable - a pure Ritz or a pure Finite Element solution may be obtained for a problem. For an optimum solution, the structure is to be subdivided into the minimum possible number of simple elements free from discontinuities. Refinement of the solution - or convergence - is achieved within each element by virtue of the Ritz procedure.

Compared with Finite Elements, the Large Element approach has the following two *disadvantages:*

1. Due to the fact that Large Elements combine both the Ritz and Finite Element methods, a somewhat larger programming and development effort is required for its practical implementation. This is not a serious disadvantage, however, since the development effort is involved only once and therefore does not appreciably offset the effort saved during modeling the structure; a process which is to be carried out during the day-to-day application of the method. In addition, the development of higher order Finite Elements is usually as complicated, and sometimes more difficult, than the development of a large element.
2. While any type of conforming finite elements, theoretically, can be used as a basis for the derivation of a large element, non-conforming finite elements cannot be generalized into large elements. Again, this is not a serious disadvantage since it is sufficient to develop one type of large element for each different application (triangular and rectangular plate bending and inplane elements, beam elements, three dimensional elements ... etc.). With the stiffness of the large elements being continuously adjustable it is not necessary to have many alternative elements for the same type of application.

As a result of a number of test problems in which

Large Element and Large Strip solutions were compared to those obtained by other available approaches, the following conclusions were drawn:

1. The use of Large Elements or Large Strips provides possibility of achieving convergence through three different mechanisms:
   i) A piece-wise convergence; which is similar to that obtained in a discrete coordinate method (e.g. Finite Elements).
   ii) A term-wise convergence; in which the number of elements is kept constant while the number of continuous coordinates in each element is gradually increased.
   iii) A hybrid convergence; where both the number of elements and the number of continuous coordinates in each element are increased simultaneously.
2. Compared to other methods of solution of comparable versatility (i.e., discrete coordinate methods) such as Finite Elements, Finite Differences, and Hrennikoff's beam lattice ... etc., better accuracy is generally obtainable through the use of Large Elements in *any* of its convergence mechanisms.
3. For the same total number of degrees of freedom, the term-wise convergence is consistently more efficient than an equivalent piece-wise or hybrid convergence. With the obvious advantages of the

considerably reduced modelling effort and the lack of necessity of constructing a new model for each convergence step, it is clear that the use of term-wise convergence is optimal.

4. With this result in mind, the choice of the model to be used for a given problem is greatly simplified. The structure is simply subdivided into the smallest number of elements which sufficiently approximate the geometry of the problem. The number of the continuous coordinates in each element is then chosen according to the degrees of accuracy required and to the expected stress gradients.
5. It is useful to notice that while the side ratio of a finite element should be kept as close to unity as possible, there is no such limitation on the choice of the large elements since different flexibilities can be assigned to the different directions of the element.

As a result of the application of the Large Element approach to a number of problems of practical interest, the following conclusions were reached:

1. In the study of the initial buckling loads of short I-columns having built-in edges, assuming the web of the column to be a fully clamped plate results in an overestimation of the column carrying capacity of up to 12%. Even larger errors on the conservative side, however, would be committed

if the results for long columns were adopted in the case of a column having a height to width ratio (H/a) of two or less.

2. The design data presented by Qadeer and Smith in reference [52] regarding the equivalent stiffness of slabs connecting shear walls are about 20 to 30% underestimated. The results of reference [52] were computed using a Finite Difference discretization for an idealized portion of the slab. Due to the existence of a discontinuity in the boundary conditions along one of the edges of that idealized portion, it was shown that an error approximately proportional to the mesh size of the Finite Difference network is introduced, in addition to the normal discretization errors which are of the order of the squared mesh size. It was therefore felt desirable to repeat the work of reference [52] and present a new set of design data for the equivalent stiffness of slabs connecting shear walls.

3. A simple exponential formula - equation *(10.14)* - relating the relative effective width of a slab to the ratio between the width of the slab and its unsupported length, in a double row shear wall structure, was presented. The formula is believed to approximate the behaviour of the slabs to better than 5% throughout the range of interest as defined

by the relationships *(10.14)*. The effect of variations in the length of the overhanging portion of the slab - denoted by "C" in figure (10.2) - and the width of the shear walls was shown to be of a secondary order. As a result, it was argued that the approximate formula *(10.14)* is applicable to structures including more than two rows of shear walls and/or asymmetric shear wall arrangements of the types shown in figure (10.2), even though it was obtained based upon the solution of a symmetric double-row shear wall structure.

4. The problem of the stress distribution in a tip-loaded short T- cantilever was considered. This type of construction is frequently used for crane girder carrying cantilevers. As a result of the stress distributions obtained, it was suggested that the free corner of the cantilever web can be safely cut-off without any appreciable effect upon the maximum stress in the beam. The cut-off line was suggested to start at the middle of the depth of the web at the free end of the cantilever and to make an angle of 45° with the beam axis.

12.2 Suggestions For Further Work

The work presented in this thesis is by no means

pretended to be complete. Several avenues remain to be explored in order to make a fuller use of the results achieved in this research work. In the following, a number of areas for possible future development will be identified. It is the intention of the author to attempt as many of these fields as may be possible in the near future:

(i) While the discussions and applications of the degenerated beam functions presented in Chapters II through V are devoted to isotropic rectangular plates, their extension to a number of other areas is straightforward. Examples for these areas are orthotropic plates, skewed and sectorial plates, and cylindrical shells. The extension to orthotropic plates, for instance, requires only the replacement of the potential energy expression *(2.5)* by the appropriate expression for an orthotropic plate *(7.12)*. The matrix equations obtained are also very similar and involve the same integral coefficients as the isotropic case but multiplied by different material stiffness constants. The extension to skewed plate problems, on the other hand, requires also the evaluation of new integral coefficients. This can easily be done using the integration technique described in Appendix I. Extension of the analysis to sectorial plates, however, requires the use of polar coordinates and involves somewhat more complicated integrals which may

have to be evaluated separately for each individual problem.

(ii) To the author's knowledge, the only experimental results available for the problem of the vibrations of inplane loaded plates are those due to Lurie [57]. He examined the vibrations of a simply-supported plate and another having two clamped edges and the other two simply-supported, under an inplane uniaxial compression. Lurie found disagreement between his experimental results and the theoretical predictions, apparently due to small initial curvatures in the plates tested. It is therefore suggested that an experimental study be carried out investigating the problems presented in Chapter V. Of particular importance is the problem concerning plates having two parallel clamped edges and two free ones under an end inplane shearing force. This problem is particularly interesting due to the ease by which the prescribed loading condition can be experimentally simulated. In addition, it is believed that the effect of slight initial imperfections on this problem is less significant and may be further reduced by examining the effect of both positive and negative shear loads on the same plate.

(iii) In the work presented so far regarding the Large Element and Large Strip methods, only one dimensional

and rectangular two dimensional elements were dealt with. The same approach, however, can be extended to incorporate a number of other useful elements, examples for which are the following groups:

1. Tapered beam and rectangular plate bending elements.
2. Sectorial large plate and large strip elements.
3. Rectangular and triangular inplane displacement-type elements.
4. Three-dimensional rectangular and triangular prismatic elements.
5. Axi-symmetric triangular and rectangular solid ring elements.
6. Cylindrical, conical, and spherical axi-symmetric shell elements.
7. Triangular plate bending elements.

The same type of displacement functions presented in Chapter VII can be used for the elements of the first two groups above. The appropriate energy expressions and/or appropriate coordinate transformations will have to be used. The derivation of the stiffness matrices, however, follows the same procedure used in Chapter VII.

Suggestions for displacement functions suitable for use with elements belonging to groups number (3) through (5) are presented and discussed in Appendix III. They involve basically a combination of lin-

ear first order polynomials and trigonometric functions. The displacement functions used with these problems are essentially less complicated than those used for bending problems due to the fact that the governing differential equations are of the second rather than the fourth order; hence continuity of the slopes is not required.

The elements of group number (6), while requiring continuity of both displacements and slopes, are essentially one-dimensional elements; since Fourier series can be utilized in the circumferential direction. All three components of displacement, however, have to be considered, and one of the available shell theories needs to be applied.

Derivation of a triangular plate bending element is probably the most involved. It is essential to start with corner degrees of freedom which correspond to a compatible Finite Element. Examples for such elements are the Clough triangle and the triangular element described by Zienkiewicz [9] utilizing singular shape functions. In addition to these corner degrees of freedom, functions providing the internal (local) degrees of freedom to the elements have to be defined. For this, a mutually complete set of functions satisfying the conditions of zero slopes and deflections along the boundary is to be used. Finally, an additional set of displacement functions,

providing the necessary "edge" degrees of freedom, is to be added. An example for a set of displacement functions which can be used for this purpose is given in Appendix III.

(iv) In order to be able to make practical use of the Large Element method, a general purpose computer program utilizing a library of Large Elements - as well as ordinary Finite Elements - is to be developed. Since the development of a powerful program of that nature is a major undertaking, it may be advantageous to make use of the already available NASTRAN (NAsa STRuctural ANalysis) Finite Element program for this purpose. NASTRAN [11] features the possibility of using a "General Element", which connects an arbitrary number of nodal points and contains an arbitrary number of degrees of freedom. The stiffness and mass matrices for such elements can be directly input to the program in terms of the global coordinate system. The degrees of freedom associated with the "continuous" coordinates in the Large Elements can be defined as "scalar points" or as additional dummy nodes defined inside, or along the edges of the Large Elements. The task of developing a general purpose program for Large Elements can thus be reduced to that of the preparation of pre- and post-processors for the NASTRAN program in order to prepare the stiffness matrices as "direct input" matrices, and to use

the computed "displacement" parameters for the calculation of the displacements and stresses within the Large Elements themselves.

(v) The Large Element approach is readily extensible to applications in other areas of Applied Mechanics. In particular, extension to field problems (e.g. heat flow and fluid flow problems) can be easily achieved using the same approaches utilized for the extension of the Finite Element method to this class of problems. An extensive and useful discussion for this latter subject was given by Zienkiewvicz [9] in his well known reference.

(vi) In section (10.3) several queries were raised regarding the validity of the experimental results presented in reference [52] concerning the stiffness of slabs connecting shear walls. It is therefore suggested that an experimental program should be carried out in order to corroborate the theoretical investigations presented in Chapter X. It is believed that a high strength material (e.g. steel) of sufficiently small thickness should be used to represent the slab (instead of the Asbestos cement sheets used in reference [52])in order to avoid excessive local deformations at the corners of the slab-wall joints. Also, sufficiently small lateral displacements should be applied in order to minimize the chance of inducing

plastic deformations at such corners, and to ensure that the assumptions of the small-deflections theory are still reasonably valid.

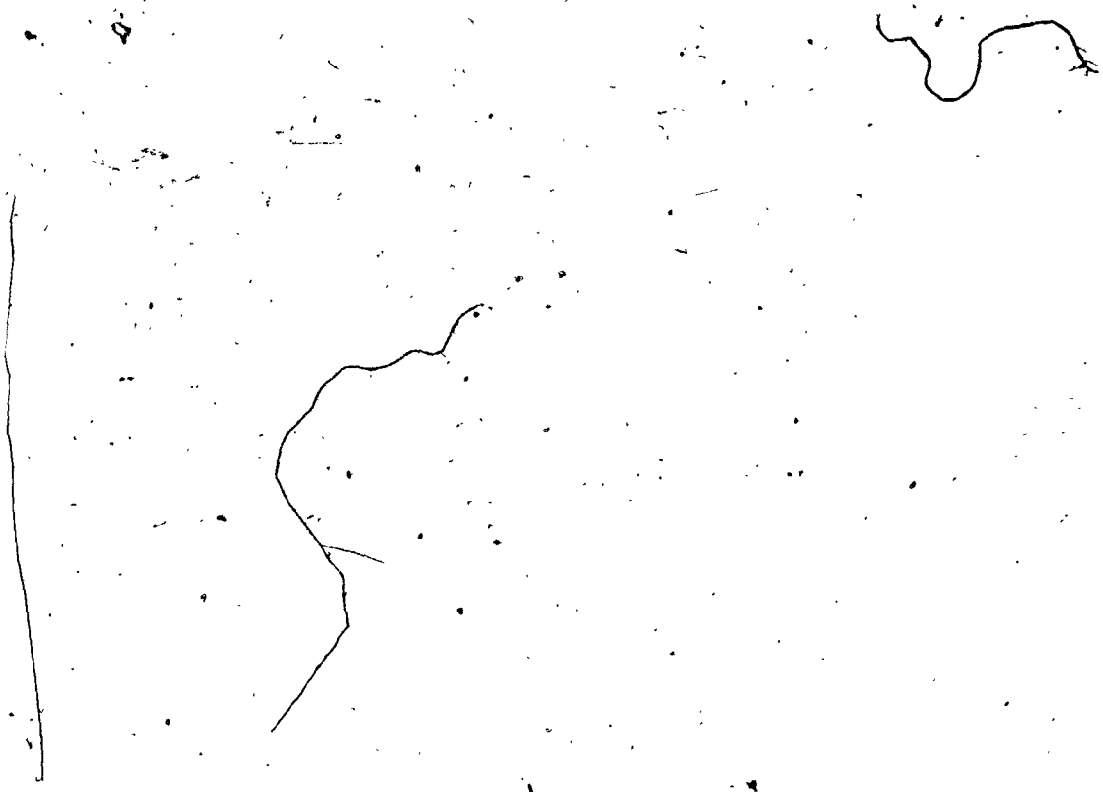

BIBLIOGRAPHY

1. Bassily, S.F., *Buckling and Vibration of Plates Subject to Inplane Loads*, Master's thesis, The University of Western Ontario, 1973.

2. Trubert, M., and Nash, W.A., *Effect of Membrane Forces on Lateral Vibrations of Rectangular Plates*, Developments in Mechanics, Vol. 1, ed. by J.E. Lay and L.E.Molvern, Plenum Press, New York, 1961, pp. 39-46.

3. Bassily, S.F. and Dickinson, S.M., *Vibration of Plates Subject to Arbitrary In-plane Loads - A Perturbation Approach*, Trans. ASME, J. of Appl. Mech., Vol. 40, Series E, No. 4, 1973, pp. 1023-28.

4. Bassily, S.F. and Dickinson, S.M., *A Multi-parameter Perturbation Approach for the Vibration of Plates Subject to Arbitrary, Independent, In-plane Loads* , Accepted for Publication in Trans. of ASME, J. of Appl. Mech.

5. Bassily, S.F., and Dickinson, S.M., *Comment on the Free Vibration of Generally Orthotropic Plates*, J.A.S.A., Vol. 52, No. 3, (part 2), 1972, pp. 1050-53.

6. Kantorovich, L.V. and Krylov, V.I., *Approximate Methods of Higher Analysis* , Interscience (1958).

7. Keer, A.D., *An Extension of the Kantorovich Method For the Solution of Eigenvalue Problems* , Int. J. Solids Structures, Vol. 5, Pergamon Press, 1969, pp. 559-572.

8. Cheung, Y.K., *Finite Strip Method-Analysis of Elastic Slabs* , Proc. ASCE, December 1968, pp. 1356-78.

9. Zienkiewicz, O.C., *The Finite Element Method in Engineering Science* , McGraw Hill Book Co., London England, 1971.

10. Cheung, Y.K. and Chokrabarti, S., *"Analysis of Simply Supported Thick, Layered Plates"*, J. of Eng. Mech. Div., Proc. ASCE, EM3, 1971, pp. 1039-44.

11. Richard, H. MacNeal (Editor), *The NASTRAN Theoretical Manual*, NASA SP-221 (01), April 1972.

12. Ghali, A. and Bathe, K.J., *Analysis of Plates Subject to In-plane Forces Using Large Finite Elements*, IABSE Publications, 30-I-1970, pp. 61-72.

13. Ghali, A, and Bathe K.J., *Analysis of Plates in Bending Using Large Finite Elements*, IABSE Publications, 30-II-1970.

14. Dame, M.,Chi, R., and Basdekas, N.L., *A New Variational Method for Solving Static and Dynamic Responses of Structures of High Complexity*, Conference on Variational Methods in Engineering. Southampton Univ., Sept. 1972 pp. 1051-63.

15. Noor, A.D., Stephens, W. B., and Fulton, R.E., *An Improved Numerical Process for Solution of Solid Mechanics Problems*, NASA-Langley Research Center, Hampton, Virginia, pp. 1-49.

16. Ritz, W., *Theorie der Transversalschwingungen*, einer Quadratischen Platte mit freien Randern. Ann. Physik, Bd. 28, 1909, pp. 737-786.

17. Young, D., *Vibration of Rectangular Plates by the Ritz Method*, J. Appl. Mech., Vol. 17, No. 4, Dec. 1950, pp. 448-53.

18. Simons, D.A., and Leissa, A.W., *Vibrations of Rectangular Cantilever Plates Subject to In-Plane Acceleration Loads*, J. Sound Vib., Vol. 17, No. 3, 1971, pp. 407-22.

19. Bassily, S.F., and Dickinson, S.M., *Buckling and Lateral Vibration of Rectangular Plates Subject to In-plane Loads - A Ritz Approach*, J. Sound and Vib., Vol. 24, No. 2, 1972, pp. 219-39.

20. Bazley, N.W., Fox, D.W., and Stadter, J.T., *Upper and Lower Bounds for the Frequenceis of Rectangular Free Plates*, Tech. Memo TG-707, Appl. Physics Lab., The Johns Hopkins Univ., Aug. 1965.

21. Bazley, N.W., Fox, D.W., and Stadter, J.T., *Upper and Lower Bounds for Frequencies of Rectangular Cantilever Plates*, Tech. Memo. TG-705, Appl. Physics Lab., The Johns Hopkins Univ., July 1965.

22. Barton, M.V., *Vibration of Rectangular and Skew Cantilever Plates*, J. Appl. Mech., Vol. 18, No. 1, June 1951, pp. 129-34.

23. Sigillito, V.G., *Improved Upper Bounds for Frequencies of Rectangular Free and Cantilever Plates*, Eng. Memo. EM-4012, Appl. Phys. Lab., The Johns Hopkins Univ., Dec. 1965.

24. Forsyth, E.M., and Warburton, G.B., *Transient Vibration of Rectangular Plates*, J. Mech. Eng. Sci., Vol. 2, No. 4, Dec. 1960, pp. 325-330.

25. Lemke, A., *Experimentelle Untersuchungen zur W. Ritzschen Theorie der Transversalschwingungen Quadratischer Platten*, Ann. Physik, Bd. 4, ser. 86, 1928, pp. 717-50.

26. Pavlik, B., *Beitrag zur Theoretischen und Experimentellen Untersuchung der Biegungs-schwingungen bei rechteckigen Platten mit freien Randern*, Ann. Physik, 1936, pp. 532-42.

27. Bulson, P.S., *The Stability of Flat Plates*, Chatto and Windus, London, 1970.

28. Leissa, A.W., *Vibration of Plates*, NASA SP-160, 1969.

29. L'Heureux, G., *Study of the Anticlastic Curvature in Beams and Plates in Free-Free Bending Vibration*, Laboratory of Vibrations and Elasticity, Faculty of Science, Univ. of Laval, Report No. ve.2, Jan. 1973, (In French).

30. Timoshenko, S.P., *The Approximate Solution of Two-Dimensional Problems in Elasticity*, Phil. Mag., Vol. 47, 1924, pp. 1095-1104.

31. Herrmann, G., *The Influence of Initial Stress on the Dynamic Behaviour of Elastic and Viscoelastic Plates*, Publ. Int. Assoc. Bridge Struct. Engng., Vol. 16, 1956, p. 275.

32. Wang, T.M. and Sussman, J.M., *Elastic Stability of a Simply Supported Plate Under Linearly Variable Compressive Stresses*, AIAA, Jl, 5, 1967, pp. 1362-64.

33. Fauconneau, G., and Marangoni, R.D., *Natural Frequencies and Elastic Stability of a Simply-Supported Rectangular Plate Under Linearly Varying Compressive Loads*, Int. J. Solids Structures, Vol. 7, 1971, pp. 473-493.

34. Butlin, G.A. and Leckie, F.A., *A Study of Finite Elements Applied to Plate Flexure*, Symposium of Numerical Methods for Vibration Problems, July 12-15, 1966.

35. Butlin, G.A., *On the Finite Element Technique in Plate Bending Analysis - A Derivation of Basic Stiffness Matrix*, Technical Report, Cambridge Univ., Engineering Laboratory, April 1965.

36. Cook, R.D., *Some Elements for Analysis of Plate Bending*, J. Eng. Mech. Div., Proc. ASCE., December, 1972, pp. 1453-70.

37. Ang, A.H.S. and Newmark, N.H., *A Numerical Procedure for the Analysis of Continuous Plates*, 2nd Conference on Electronic Computation, ASCE, 1960.

38. Hrennikoff, A.P., *Solution of Problems of Elasticity by the Framework Method*, Trans. ASME, J. Appl. Mech., Vol. 8, 1941.

39. Reed, R.E., Jr., *Comparison of Methods in Calculating Frequencies of Corner-Supported Rectangular Plates*, NASA TN D-3030, 1965.

40. Iguchi, S., *Die Eigenschwingungen und Klangfiguren der vierseitig freien rechteckigen Platte*, Inge.-Arch., Bd. 21, ser. 303, Heft 5-6, 1953, pp. 304-22.

41. Cox, H.L. and Boxer, J., *Vibration of Rectangular Plates Point-Supported at the Corners*, Aeron. Quart., Vol. 11, No. 1, Feb. 1960, pp. 41-50.

42. Ota, T., and Hamada, M., *Fundamental Frequencies of Simply Supported but Partially Clamped Square Plates*, Bull. JSME, Vol. 6, No. 23, Aug. 1963, pp. 397-403.

43. Kurata, M. and Okamura, H., *Natural Vibrations of Partially Clamped Plates*, J. Eng. Mech. Div., Proc. Am. Soc. Civil Eng., June 1963, pp. 169-186.

44. Paramasivam, P., Sridhar, Rao, and Jawalker, K., *Free Vibrations of Square Plates with Stiffened Square Openings*, Int. J. Eng. Sci., Pergamon Press, Vol. 15, 1973, pp. 117-22.

45. Cheung, Y.K., and Cheung, M.S., *Flexural Vibrations of Rectangular and Other Polygonal Plates*, Research Report, Dept. of Civil Eng., Univ. of Calgary, July 1970.

46. Veletsos, A.S. and Newmark, M., *Determination of Natural Frequencies of Continuous Plates Hinged Along Two Opposite Edges*, Trans. ASME, J. Appl. Mech., Vol. 23, 1956, pp. 97-102.

47. Dickinson, S.M., *Flexural Vibration of Rectangular Plate Systems*, Doctoral Thesis, Mechanical Engineering Department, Nottingham Univ., England 1966.

48. Dickinson, S.M., and Warburton, G.B., *Vibration of Box-Type Structures*, J. Mech. Eng. Sci., Vol. 9, No. 4, 1967, pp. 325-35.

49. Henshell, R.D. and Warburton, G.B., *Finite Element Techniques Applied to the Vibration of Plate Systems*, Symposium on the Numerical Methods for Vibration Problems, Univ. of Southampton, 1966.

50. Popplewell, N., *The Vibration of a Box-Type Structure - Natural Frequencies and Normal Modes*, J. Sound Vib., Vol. 14, No. 3, 1971, pp. 357-65.

51. Bulson, P.S., *The Stability of Flat Plates*, Chalto and Windus 1970, pp. 305-307.

52. Qadeer, A., and Stafford-Smith, B., *The Bending Stiffness of Slabs Connecting Shear Walls*, ACI Journal, June 1969, pp. 464-73.

53. Coull, A. and Chaudhury, J.R., *Stresses and Deflections in Coupled Shear Walls*, ACI Journal Proc., Vol. 64, No. 2, Feb. 1967, pp. 65-72.

54. Michael, D., *The Effect of Local Wall Deformation on the Elastic Interaction of Cross Walls Coupled by Beams*, Tall Buildings, Pergamon Press Limited, London, 1967, pp. 253-70.

55. Ambartsuvmian, S.A., *Theory of Anisotropic Plates - Strength, Stability and Vibration*, Nauka, Moscow, 1967, (In Russian).

56. Coker, E.G. and Filon, L.N.G., *A Treatise on Photo-Elasticity*, Cambridge, The University Press, 1957.

57. Lurie, H., *Lateral Vibrations as Related to Structural Stability*, J. Appl. Mech., Vol. 19, No. 2, June 1952, pp. 195-204.

APPENDIX I

EVALUATION OF INTEGRALS INVOLVING BEAM FUNCTIONS

The solutions of rectangular plate problems using ordinary or degenerated beam functions in the Ritz method, presented in Chapters III through V, require the evaluation of certain integrals involving beam functions and/or their derivatives of the first and second order. In particular, three classes of such integrals were defined and used for the solution of the numerical examples presented in those three chapters. The procedure and expressions used for the evaluation of each of these groups of integrals will be presented in this Appendix.

In general, in order to simplify the algebra involved and systemize the evaluation of the integrals with a maximum degree of reliability, each beam function (ordinary or degenerated) or its derivative is expressed as the sum of up to four complex exponentials such that:

$$F_n(\xi) = \sum_{i=1}^{4} \alpha_{i,n} \cdot e^{(\beta_i \gamma_n \xi)} \qquad (I.1)$$

where $\beta_1 = 1$, $\beta_2 = -1$, $\beta_3 = j$ and $\beta_4 = -j$ (where $j=\sqrt{-1}$) and the α's and γ's are complex coefficients depending upon the type of the beam function and its order (n). The non-

The series for v can also be expanded in an analogous form. The functions enclosed in the first pair of square brackets represent the corner degrees of freedom, those in the second pair of brackets are edge degrees of freedom, and those in the last pair of brackets are the local degrees of freedom corresponding to the u variable. The above series thus includes sufficient degrees of freedom for the rectangular inplane stress element on hand. Figure (III.1) also shows a diagramatic representation for the distribution of these degrees of freedom over the area of the large element, as well as the definition of the element coordinates η_i, ξ_i. It is worth mentioning that the functions corresponding to the corner degrees of freedom are the same as those for the known "first order Finite Element rectangle".

2. A Triangular Inplane Stress Element

Suitable displacement functions for a displacement-type inplane stress triangular element compatible with the rectangular element presented in the previous section will be given here. The same requirements presented for the rectangular inplane element functions are applicable to the triangular inplane element. Figure (III.2) graphically shows the three groups of displacement functions required.

One convenient means for providing functions of the types shown in the figure will be presented here. The idea is to make use of the set of modes of a rectangular (or a

1. The Ordinary SS-SS Beam Function

$$\gamma_n = \frac{n+1}{2}\pi; \qquad n = 0, 1, 2, \ldots .$$

$$\alpha_{1,n} = \alpha_{2,n} = 0,$$

$$\alpha_{3,n} = \alpha_{4,n} = \sqrt{2}\ ; \quad \text{for } n=0,2,4,\ldots$$

$$\alpha_{3,n} = -j\sqrt{2}\ ; \ \alpha_{4,n} = j\sqrt{2}; \quad \text{for } n=1,3,5,\ldots$$

The coefficients α' and α" can be easily obtained through simple differentiation as:

$$\alpha'_{i,n} = \alpha_{i,n} \cdot \beta_i \cdot \gamma_n , \quad \text{and}$$
$$\alpha''_{i,n} = \alpha'_{i,n} \cdot \beta_i \cdot \gamma_n . \qquad (I.2)$$

Equations *(I.2)* above are general and apply to *all* types of beam functions.

2. The Ordinary C-C Beam Function

$$F_n(\xi) = \cosh\gamma_n\xi + \lambda_n \cos\gamma_n\xi \ ; \ \text{for } n = 2,4,6,\ldots ;$$

$$F_n(\xi) = \sinh\gamma_n\xi - \lambda_n \sin\gamma_n\xi \ ; \ \text{for } n = 3,5,7,\ldots ;$$

where the values of γ_n are obtained as roots of:

$$\tan(\gamma_n) + (-1)^n \tanh(\gamma_n) = 0,$$

and $\lambda_n = \sinh(\gamma_n)/\sin(\gamma_n)$.

Hence, $\alpha_{1,n} = 0.5$,

$$\alpha_{2,n} = (-1)^n \cdot 0.5,$$

$$\alpha_{3,n} = \alpha_{4,n} = \lambda_n/2, \qquad n = 2,4,6,\ldots;$$

$$\alpha_{3,n} = -\alpha_{4,n} = -j\lambda_n/2 \qquad n = 3,5,7,\ldots .$$

3. The Degenerated F-F Beam Function

As described in Chapter II, the degenerated F-F functions are either $1, \xi$, a trigonometric function (sine or cosine), or a hyperbolic function (sinh or cosh) depending on its order. In order to be able to handle all these types of functions as one series, it was found convenient to use both positive and negative values of the integer n. The negative values were assigned to the trigonometric functions, the integers 0, and 1 for the linear functions (1 and ξ), and the positive integers greater than 1 for the hyperbolic functions. Also, as before, even integers were assigned to even (symmetric) functions and odd integers to odd (anti-symmetric) functions. In order to avoid having a gap at n equals (-1), the (sine) functions were started at $(n=-1)$ instead of $(n=-3)$. This distribution is represented by the nomogram shown in figure (I.1). These functions may thus be represented as:

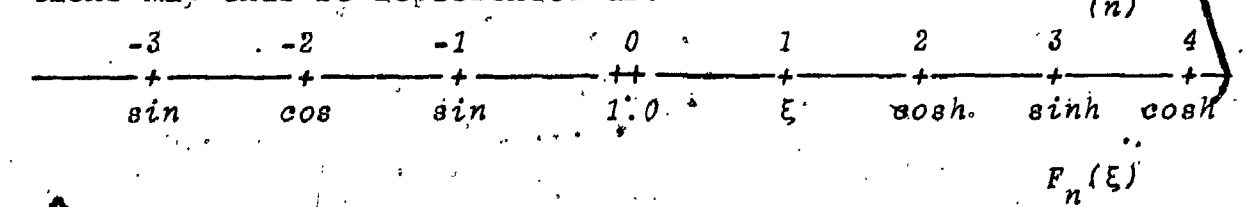

Fig. (I.1)

$$F_0(\xi) = 1.0 = \cosh(0) ;$$

$$F_1(\xi) = \xi = \lim_{\gamma_1 \to 0} \left[\frac{\sinh \gamma_1}{\gamma_1}\right]$$

$$F_n(\xi) = \cosh(\gamma_n \xi) \; ; \quad n = 2,4,6,\ldots;$$

$$F_n(\xi) = \sinh(\gamma_n \xi) \; ; \quad n = 3,5,7,\ldots;$$

$$F_n(\xi) = \cos(\gamma_{-n} \xi); \quad -n = -2, -4, -6, \ldots;$$

$$F_n(\xi) = \sin(\gamma_{2-n} \xi); \quad 2-n = -1, -3, -5, \ldots;$$

where γ_n (for $n \geq 2$) is the same as defined for the C-C beam functions, and ξ varies between -1 and 1. The value of γ_o was set equal to zero, and that of γ_1 to a very small number (0.0001). Special attention must be given to the value of γ_1 since too small a value may lead to numerical problems when the function is differentiated or multiplied by another of the same type. At the same time a relatively large value of γ_1 may lead to loss of accuracy due to misrepresentation of the function. In all cases, it is advisable to check the resulting integrals by alternate means when F_1 is involved.

Hence, for $n \geq 0$:

$$\alpha_{1,n} = 0.5,$$

$$\alpha_{2,n} = (-1)^n \times 0.5,$$

$$\alpha_{3,n} = \alpha_{4,n} = 0;$$

and, for $n<0$:

$$\alpha_{1,n} = \alpha_{2,n} = 0,$$

$$\alpha_{3,n} = \sqrt{(-1)^n} \times (-1)^n \times 0.5,$$

$$\alpha_{4,n} = \sqrt{(-1)^n} \times 0.5.$$

4. The Degenerated C-F Beam Function

As given by equation (2.19), the degenerated C-F beam functions may be represented by:

$$F_n(\xi) = e^{\gamma_n \xi} - \cos(\gamma_n \xi) - \sin(\gamma_n \xi);$$

$$n = \pm 1, \pm 2, \pm \ldots;$$

where γ_n are the *positive and negative* solutions of the equation:

$$\cosh \gamma_n \cdot \cos \gamma_n = -1;$$

and ξ varies between 0 and 1.

Hence;

$$\alpha_{1,n} = 1,$$

$$\alpha_{2,n} = 0,$$

$$\alpha_{3,n} = (j-1)/2, \text{ and}$$

$$\alpha_{4,n} = -(j+1)/2 .$$

5. The Degenerated F-C Beam Function

This set of functions is physically the same as the C-F functions presented above. However, in order to eliminate the necessity of having to apply coordinate transformations during the integration procedure, the coordinate transformation will be applied here in obtaining the F-C functions from the C-F functions. After representation in the form of exponential functions, the C-F degenerated beam functions may be written as: $F_n(\xi) = e^{\gamma_n \xi} + (\frac{j-1}{2}) e^{j\gamma_n \xi} - (\frac{j+1}{2}) e^{-j\gamma_n \xi}$. The (F-C) function may be obtained through replacing ξ by $(1-\xi)$ in the above expression yielding:

$$F_n(1-\xi) = (e^{\gamma_n}) e^{-\gamma_n \xi} - (\frac{j+1}{2} e^{-j\gamma_n \xi}) e^{j\gamma_n \xi} +$$

$$(\frac{j-1}{2} e^{j\gamma_n}) e^{-j\gamma_n \xi} .$$

Thus, the coefficients $\alpha_{i,n}$ for the $(F-C)^0$ functions may be written as:

$$\alpha_{1,n} = 0,$$

$$\alpha_{2,n} = e^{\gamma_n},$$

$$\alpha_{3,n} = -(\frac{j+1}{2}) e^{-j\gamma_n}, \text{ and}$$

$$\alpha_{4,n} = (\frac{j-1}{2}) e^{j\gamma_n} .$$

The Evaluation of Integrals Involving Two Beam Functions

Integrals involving the multiplication of two beam

functions and/or their derivatives of the first and second order were needed in all the classes of problems treated in Chapters III through V. These integrals result from the energy expression of the plates with or without inplane loads, as well as the inplane strain energy expression. The integrals required in the case of a rectangular isotropic (or orthotropic) plate are given by equation *(3.8)*. With the help of the expressions presented above for the various beam functions and their derivatives, any of these integrals may be expressed in the form:

$$I_{mn} = \int_a^1 \sum_{i=1}^{4} \sum_{j=1}^{4} \alpha_{i,m} \cdot \alpha_{j,n} \cdot e^{(\beta_i \gamma_m + \beta_j \gamma_n)\xi} \cdot d\xi \ ,$$

which can be easily integrated yielding:

$$I_{mn} = \sum_{i=1}^{4} \sum_{j=1}^{4} \frac{\alpha_{i,m} \cdot \alpha_{j,n}}{\beta_i \gamma_m + \beta_j \gamma_n} \left[e^{\beta_i \gamma_m + \beta_j \gamma_n} - e^{(\beta_i \gamma + \beta_j \gamma_n)a} \right] \quad (I.2)$$

where *(a)* is either *(0)* or *(-1)* depending upon the type of beam functions. Substituting the appropriate values of the α's, β's and γ's into the above expressions, any of the integrals *(3.8)* may be easily evaluated. Of course, complex arithmetic has to be used in programming the above integrals for computation. This was conveniently performed on the CDC-6400 computer in a simple FORTRAN routine which calls upon the appropriate sets of coefficients (α's, and γ's) from a library containing the coefficients for the different types of functions which was prepared previously.

The resulting tables of integral coefficients were then printed and punched out on cards (or may be stored on a magnetic tape) for repeated use in the Ritz programs. A useful check for examining the correctness of the integrals is to ensure that the imaginary part of (I_{mn}) is always zero (within the limits of the rounding-off errors). This is useful to ensure that the coefficients α, β, and γ correspond to functions F_m and F_n which are real. Another useful check is to ensure that the integral resulting from the multiplication of an odd with an even function must be zero. After examining the soundness of the program, the above facts may be used to increase the efficiency of the program through skipping the unnecessary operations. This is usually not necessary since the integrals need only be evaluated once and they usually require only a few seconds of computer time. Another useful tool for increasing the efficiency of the program is to skip the summation step if either $\alpha_{i,m}$ or $\alpha_{j,n}$ is zero.

The Evaluation of integrals Involving Three Beam Functions

Integrals involving the multiplication of three ordinary and/or degenerated beam functions were needed for the solution of the class of problems presented in Chapter V. They result from the contribution of the inplane loads in the strain energy due to the flexural deformation of a plate if both the inplane loads and the displacement func-

tions were expressed in terms of series of beam functions. The different integrals required in the case of a rectangular isotropic (or orthotropic) plate are given by equations (5.5b). Extending the approach used with integrals involving two beam functions, any of these integrals may be expressed as:

$$I_{m,n,r} = \int_a^1 \sum_{i=1}^{4} \sum_{j=1}^{4} \sum_{k=1}^{4} \alpha_{i,m} \cdot \alpha_{j,n} \cdot \alpha_{k,r} \cdot e^{(\beta_i \gamma_m + \beta_j \gamma_n + \beta_k \gamma_r)\xi} \cdot d\xi,$$

which after performing the integration yields:

$$I_{m,n,r} = \sum_{i=1}^{4} \sum_{j=1}^{4} \sum_{k=1}^{4} \frac{\alpha_{i,m} \cdot \alpha_{j,n} \cdot \alpha_{k,r}}{\beta_i \cdot \gamma_m + \beta_j \gamma_n + \beta_k \gamma_r} \left[e^{\beta_i \gamma_m + \beta_j \gamma_n + \beta_k \gamma_r} - e^{(\beta_i \gamma_m + \beta_j \gamma_n + \beta_k \gamma_r)a} \right] \quad (I.3)$$

where (a) is either (0) or (-1) as before. Substituting the appropriate values for the α's, β's, and γ's into the above expression and performing the complex arithmetic involved results in any of the sets of integrals (5.5b) which may be required. All the comments discussed in connection with the integrals of two beam functions are applicable to this case. It is worth noting however, that the computer time used for the evaluation of a set of integrals involving three beam functions is usually two orders of magnitude larger than that required for the evaluation of one involving only two beam functions. This time, however, is still within a few minutes. Therefore, the measures for improving the efficiency discussed earlier may be more appropriate to apply in this case than with the integrals of two beam functions.

The Evaluation of Integrals Involving Beam Functions as Well as Power Series

The need for evaluating integrals involving the multiplications of power series and beam functions arose in two different situations through the course of this work. The first situation was due to the contribution of the inplane loads in the strain energy of the flexure of a plate when the inplane load representation involved a power series while the displacement function of the plate was represented in terms of a series of beam functions. The second situation arose when both beam functions and cubic power series were used together as the displacement functions for large plate and beam elements. In the first situation, the integrals resulting - which are defined by equations *(5.5a)* - involved the multiplication of a power series by two beam functions or derivatives thereof. In the second situation, the integrals resulting - defined by equations *(7.11)* and *(7.16)* - involved the multiplication of a cubic power series and one beam function. Since the second situation may be considered as a special case of the first, the evaluation of the following integral will be discussed as the most general case:

$$I^{r}_{mn} = \int_{a}^{1} \xi^{r} \cdot F_m(\xi) \cdot F_n(\xi) \cdot d\xi \ .$$

Expressing the beam functions in the form of expression *(I.1)*, this becomes:

$$I^r_{mn} = \int_{\alpha}^{1} \xi^r \sum_{i=1}^{4} \sum_{j=1}^{4} A_{i,m} \cdot A_{j,n} \cdot e^{(\beta_i \gamma_m + \beta_j \gamma_n)\xi} \cdot d\xi \ ,$$

which can be integrated by successive reduction yielding:

$$I^r_{mn} = \sum_{i=1}^{4} \sum_{j=1}^{4} A_{i,m} \cdot A_{j,n} \cdot \{ \frac{e^b}{b} [1 - \frac{r}{b} + \frac{r(r-1)}{b^2} - \ldots +$$

$$+ (-1) \frac{r!}{b^r}] - \frac{e^{ab}}{b} [a^r - \frac{r a^{r-1}}{b} + \frac{r(r-1) a^{r-2}}{b^2} \ldots +$$

$$+ (-1)^r \frac{r!}{b^r}] \} \ ; \qquad (I.4)$$

where $b = \beta_i \gamma_m + \beta_j \gamma_n$, and a is either 0 or -1. With the help of this expression, the integral of the multiplication of a polynomial and two beam functions or derivatives thereof can be easily evaluated. Expression *(I.4)* can be easily modified for the case where a polynomial is multiplied by any number of beam functions (e.g. one or three), should it be desirable.

APPENDIX II

Integrals Involved in the Stiffness and Mass Matrices of the Large Rectangular Element

$$B_{i,j}=\int_0^1 \phi_i \phi_j \, d\eta$$

$$E_{i,j}=\int_0^1 \phi_i' \, \phi_j' \, d\eta$$

$$C_{i,j}=\int_0^1 \phi_i \phi_j'' \, d\eta$$

$$F_{i,j}=\int_0^1 \phi_i'' \phi_j'' \, d\eta$$

APPENDIX III

SUGGESTED DISPLACEMENT FUNCTIONS FOR SOME LARGE ELEMENTS

In addition to the three large elements derived in Chapters VII and XI, guidelines for the derivation of five other large elements will be presented here. These five elements are:

1. A rectangular inplane stress element-displacement formulation.
2. A triangular inplane stress element-displacement formulation.
3. A triangular plate bending element.
4. A three-dimensional rectangular prism.
5. A three-dimensional triangular prism.

As mentioned in Chapter VII, the major step in the derivation of the characteristic matrices for a particular element is the choice of a suitable displacement function, or series of functions. Once this is accomplished, the derivation of the element stiffness and mass matrices follows standard routes. In the general case, the well known Finite Element procedure [9], described in sections (1.2) and (1.3) in association with the Finite Strip and Finite layer methods can be used. The more straightforward Ritz

procedure - described in Chapter II and employed in section (7.2) for the derivation of the large rectangular plate bending element - can be beneficially applied if the strain energy expressions are readily known. In the Finite Element practice, it is usually concluded that evaluation of the integrals involved in the derivation of the stiffness and mass matrices is most conveniently performed using one of the known numerical integration techniques. Only in the case of rectangular elements (and some simple triangular elements) is closed form integration of the expressions involved normally feasible. Consequently, simplicity of the expressions to be used in the displacement functions is not an essential condition.

In the following, examples for displacement functions suitable for use with each of the elements mentioned above will be presented. In general, it is not claimed that the sets of functions presented here are the most suitable or most convenient ones to use; they are merely examples presented in order to show that derivation of such elements is a feasible task. The accuracy and efficiency of these elements remain to be examined.

1. A Rectangular Inplane Stress Element

Unlike the inplane stress rectangular element presented in Chapter XI, a displacement-type element will be discussed here. The fundamental variables in this formulation are the

components of the inplane displacements u and v.

The expression for the principle of stationarity of the strain energy for a plate (12.1) may be rewritten in a form which contains derivatives of u and v no higher than first order; thus the assumed displacement functions for u and v need only be continuous and have finite first order derivatives with a finite number of discontinuities. Continuity of slopes is therefore not required, and only boundary conditions concerning the fundamental variables themselves need be satisfied. With this in mind, and by virtue of analogy with the plate bending element, three groups of displacement functions have to be provided:

a. Functions providing the corner freedoms. Only the variables u and v themselves need be defined but not their derivatives.

b. Functions providing the flexibilities within the element itself, or local degrees of freedom. These functions must have zero values at the edges.

c. Functions providing flexibilities for the element edges. For each edge, a mutually complete set of functions providing the possibility of approximating any arbitrary displacement pattern the edge may take while displacements along other edges are suppressed.

A displacement function for each of u and v may be obtained by the multiplication of two series of the type shown in figure (III-1). This may be written as:

$$u(\eta_i, \xi_j) = \sum_{k=1}^{m+2} \sum_{l=1}^{n+2} A_{kl} \cdot \phi_k(\eta_i) \cdot \phi_l(\xi_j) \quad , \qquad (III.1)$$

$$v(\eta_i, \xi_j) = \sum_{k=1}^{m+2} \sum_{l=1}^{n+2} B_{kl} \cdot \phi_k(\eta_i) \cdot \phi_l(\xi_j) \quad , \qquad (III.2)$$

where

$$A_{m+1,n+1} = u_{i-1,j-1}, \quad B_{m+1,n+1} = v_{i-1,j-1}, \quad \phi_{m+1} = \Phi_1(\eta_i);$$

$$A_{m+2,n+1} = u_{i,j-1}, \quad B_{m+2,n+1} = v_{i,j-1}, \quad \phi_{m+2} = \Phi_2(\eta_i);$$

$$A_{m+1,n+2} = u_{i-1,j}, \quad B_{m+1,n+2} = v_{i-1,j}, \quad \phi_{n+1} = \Phi_1(\xi_j);$$

$$A_{m+2,n+2} = u_{i,j}, \quad B_{m+2,n+2} = v_{i,j}, \quad \phi_{n+2} = \Phi_2(\xi_j);$$

and ϕ_1 through ϕ_m (or ϕ_n) are the first m (or n) simply-supported beam functions - i.e. sine waves - and Φ_1, Φ_2 are as defined in figure (III.1). Thus equation (III.1) may be re-written in the expanded form:

$$u(\eta_i, \xi_j) = [u_{i-1,j-1} \Phi_1(\eta_i) \cdot \Phi_1(\xi_j) + u_{i,j-1} \Phi_2(\eta_i) \cdot \Phi_1(\xi_j)$$

$$+ u_{i-1,j} \cdot \Phi_1(\eta_i) \cdot \Phi_2(\xi_j) + u_{i,j} \cdot \Phi_2(\eta_i) \cdot \Phi_2(\xi_j)] + [\Phi_1(\eta_i)$$

$$\cdot \sum_{l=1}^{n} A_{m+1,l} \cdot \sin(l\pi\xi_j) + \Phi_2(\eta_i) \cdot \sum_{l=1}^{n} A_{m+2,l} \cdot \sin(l\pi\xi_j) +$$

$$\Phi_1(\xi_j) \cdot \sum_{k=1}^{m} A_{k,n+1} \cdot \sin(k\pi\eta_i) + \Phi_2(\xi_j) \cdot \sum_{k=1}^{m} A_{k,n+2} \cdot \sin(k\pi\eta_i)] +$$

$$[\sum_{k=1}^{m} \sum_{l=1}^{n} A_{kl} \cdot \sin(k\pi\eta_i) \cdot \sin(l\pi\xi_j)] \ .$$

The series for v can also be expanded in an analogous form. The functions enclosed in the first pair of square brackets represent the corner degrees of freedom, those in the second pair of brackets are edge degrees of freedom, and those in the last pair of brackets are the local degrees of freedom corresponding to the u variable. The above series thus includes sufficient degrees of freedom for the rectangular inplane stress element on hand. Figure (III.1) also shows a diagramatic representation for the distribution of these degrees of freedom over the area of the large element, as well as the definition of the element coordinates η, ζ. It is worth mentioning that the functions corresponding to the corner degrees of freedom are the same as those for the known "first order Finite Element rectangle".

2. A Triangular Inplane Stress Element

Suitable displacement functions for a displacement-type inplane stress triangular element compatible with the rectangular element presented in the previous section will be given here. The same requirements presented for the rectangular inplane element functions are applicable to the triangular inplane element. Figure (III.2) graphically shows the three groups of displacement functions required.

One convenient means for providing functions of the types shown in the figure will be presented here. The idea is to make use of the set of modes of a rectangular (or a

skewed) plate with simply-supported or sliding edges, which have two nodal lines along the diagonals of the plate. In order to do that, three sets of skewed coordinate systems (η_k, ξ_k) are defined. Each of these coordinate systems has its origin at one of the three vertices of the triangular element (k), its η_k axis along a line which bisects the opposite edge, and its ξ_k axis parallel to that same edge. The unit vectors along η_i and ξ_i are normalized so that the three vertices of the triangle $(k,k+1,k+2)$ would have the coordinates $(0,0)$, $(1,1)$ and $(1,-1)$ respectively as shown in figure (III.3).

The displacement functions required for each of the displacement components u and v may be obtained as the sum of three sets of functions. Each of these functions is composed of the difference of two Fourier expansions in one of the three skewed coordinate systems (η_k, ξ_k) in addition to a simple linear function such that:

$$u = \sum_{k=1}^{3} \{u_k(1-\eta_k) + \sum_{i=0}^{mk} \sum_{j=i+1}^{mk+1} A_{i,j,k}[\phi_i(\eta_k)\cdot\phi_j(\xi_k) - \phi_j(\eta_k)\cdot\phi_i(\xi_k)] + \sum_{i=0}^{nk} \sum_{j=i+1}^{nk+1} B_{i,j,k}[\psi_i(\eta_k)\cdot\psi_j(\xi_k) - \psi_j(\eta_k)\cdot\psi_i(\xi_k)]\} \; ; \quad (0<\eta_k<1; \; -\eta_k<\xi_k<\eta_k) \; ; \quad (III.3)$$

in which:

$$\phi_0(z) = z, \; \phi_l(z) = \sin(l\pi z), \; l = 1, 2, \ldots$$

and $\psi_o(z) = 1,\ \psi_l(z) = \cos\left(\frac{2l-1}{2}\pi z\right),\quad l=1,2,\ldots;$

and (u_k) is the displacement component at the vertex (k). A similar expression is assumed for the other displacement component (v).

In order to appreciate the relationship between this series and the functions represented in figure (III.2), it may be rewritten in the expanded form:

$$u = \sum_{k=1}^{3}\Big([u_k.(1-\eta_k)]+\Big[\sum_{j=1}^{mk+1} A_{o,j,k}\{\eta_k \sin(j\pi\xi_k) - \xi \sin(j\pi\eta_k)\}+\sum_{j=1}^{nk+1} B_{o,j,k}\{\cos\left(\frac{2j-1}{2}\pi\xi_k\right)-\cos\left(\frac{2j-1}{2}\pi\eta_k\right)\}\Big]$$

$$+\Big[\sum_{i=1}^{mk}\sum_{j=i+1}^{mk+1} A_{i,j,k}\{\sin(i\pi\eta_k).\sin(j\pi\xi_k) - \sin(j\pi\eta_k).\sin(i\pi\xi_k)\}+\sum_{i=1}^{nk}\sum_{j=i+1}^{nk+1} B_{i,j,k}.\{\cos\left(\frac{2i-1}{2}\pi\xi_k\right).\cos\left(\frac{2j-1}{2}\pi\xi_k\right)$$

$$-\cos\left(\frac{2j-1}{2}\pi\eta_k\right).\cos\left(\frac{2i-1}{2}\pi\xi_k\right)\}\Big].$$

The functions in the first square brackets represent the corner degrees of freedom. Those within the second pair of square brackets represent anti-symmetric and symmetric edge degrees of freedom (compatible with those of the rectangular element presented earlier). Finally, the series within the last pair of square brackets represent the local degrees of freedom for the triangular element. It can be easily seen that the functions corresponding to the corner degrees of freedom are the same as those ordinarily used in the Finite Element known as the "Constant Strain Triangle".

3. A Triangular Plate Bending Element

Since the energy expression for a plate bending problem (7.12) includes second order derivatives of the displacement *(w)*, *continuity of the normal slopes* along the edges of a Large Element has to be guaranteed. Consequently, the Large Element has to be based upon a *compatible* Finite Element. Either the "Clough" triangle or the element presented by Zienkewvicz [9] using singular shape functions can be used for this purpose. In both cases the mid-edge nodes should be constrained, resulting in normal slopes linearly varying from one corner to the other along any of the element's edges. Thus a basic compatible element with three degrees of freedom (one displacement and two slopes) at each node is provided. The derivation of the explicit displacement expressions will not be given here, and can be found elsewhere in the literature [9,11]. The displacement function for this basic Finite Element - which corresponds to the *corner degrees of freedom* - will be referred to here as Φ_o.

In addition to the function Φ_o, functions providing arbitrary edge freedoms for both displacements and normal slopes have to be defined. As with the rectangular element presented in section (7.2), the functions providing the displacement degrees of freedom along a certain edge should have: (i) zero normal slopes all around the perimeter; (ii) zero displacements along all other edges; and (iii) displacements varying according to one of the clamped-

clamped beam functions along that particular edge. Similar conditions apply to the functions corresponding to the normal slope degrees of freedom along an edge.

One possible way for providing functions which satisfy these conditions is to use the three sets of Cartesian coordinates shown in figure (III.4). One coordinate system is defined for each edge with the x-axis running along the edge and the origin at its mid-point. Each function is enclosed within a parabolic segment which lies completely inside the triangle. The functions taper off at the parabolic boundary where they have zero slopes and deflections. Outside the parabolic regions the functions are zeros. This set of functions can be represented by:

$$\phi^k_{ij}(x_k,y_k) = \phi_i\left[\left(\frac{x_k}{a_k}\right)\left(\frac{b_k}{b_k-y_k}\right)^{1/2}\right] H_j\left(\frac{y_k}{b_k}\right)\left(\frac{a^2_k}{a^2_k-x^2}\right)\Bigg] \quad ;$$

$$(i=1,2,\ldots,n;\ j=1,2;\ k=1,2,3) \quad ; \quad (III.4)$$

where $H_1(z) = (1+2z)(1-z)^2$, for $0<z<1$,

$= 0$, for $z>1$;

$H_2(z) = z(1-z)^2$ for $0<z<1$,

$= 0$, for $z>1$;

which are Hermitian functions of the first order (the same as those used with the rectangular element); and $\phi_i(z)$ are clamped-clamped beam functions (also the same as with the rectangular element).

One more set of functions is required. These are to provide for the *local degrees of freedom* within the tri-

angular element. This has to be a mutually complete set with its members possessing zero slopes and deflections along the perimeter. Figure (III.5) shows the skewed co-ordinate system (η,ξ) used to define this set of functions. The axes are along two of the edges of the triangle, and the unit vectors along them are normalized such that the coordinates of the three vertices of the triangle become $(0,0)$, $(0,1)$, and $(1,0)$. This set of functions (Ψ^k_{ij}) is composed of three subsets. Each of these subsets is made up by the multiplication of two Clamped-Clamped beam functions parallel to two of the edges of the triangle. Hence, the following subsets are defined:

$$\Psi^1_{ij} = \phi_i\left(\frac{\eta}{1-\xi}\right) \cdot \phi_j\left(\frac{\xi}{1-\eta}\right),$$

$$\Psi^2_{ij} = \phi_i\left(\frac{\xi}{1-\eta}\right) \cdot \phi_j\left(\frac{\eta}{\eta+\xi}\right),$$

$$\Psi^3_{ij} = \phi_i\left(\frac{\eta}{\eta+\xi}\right) \cdot \phi_j\left(\frac{\eta}{1-\xi}\right); \quad (0<\xi<1, 0<\eta<1-\eta); \quad (III.5)$$

where $\phi_k(z)$ are the beam functions.

With the three sets of functions as described above, the displacement function for the large triangular bending element can now be written as:

$$W = \phi_o + \sum_{k=1}^{3} \sum_{i=1}^{m} \left[\sum_{j=1}^{2} A^k_{ij} \cdot \phi^k_{ij} + \sum_{\mu=1}^{n} B_{ijk} \cdot \Psi^k_{ij} \right]; \quad (III.6)$$

where (ϕ^k_{ij}) and (Ψ^k_{ij}) are as defined by (III.4) and (III.5) respectively, and ϕ_o is the basic displacement function for any compatible Finite Element triangle as mentioned before.

4. A Three-Dimensional Rectangular Prism

The rectangular prism three-dimensional (3-D) element can be obtained through a straight-forward extension of the Rectangular inplane stress displacement-type element presented earlier in this Appendix. For a three dimensional element, all three displacement components u, v, and w are treated as fundamental variables. The expression for the principle of stationarity of the strain energy contains no derivatives higher than the first order in u, v and w; hence continuity of the fundamental variables, but not their derivatives, is required. Analogous to the functions used for the rectangular inplane elements - equations *(III.1)* and *(III.2)* - and referring to the coordinate system defined in figure (III.6), the following displacement functions can be conveniently used with the 3-D element:

$$u(\eta_i,\xi_j,\lambda_k)=\sum_{r=1}^{m+2}\sum_{s=1}^{n+2}\sum_{t=1}^{p+2} A_{rst}\cdot\phi_r(\eta_i)\cdot\phi_s(\xi_j)\cdot\phi_t(\lambda_k), \quad (III.7)$$

$$v(\eta_i,\xi_j,\lambda_k)=\sum_{r=1}^{m+2}\sum_{s=1}^{n+2}\sum_{t=1}^{p+2} B_{rst}\cdot\phi_r(\eta_i)\cdot\phi_s(\xi_j)\cdot\phi_t(\lambda_k), \quad (III.8)$$

$$w(\eta_i,\xi_j,\lambda_k)=\sum_{r=1}^{m+2}\sum_{s=1}^{n+2}\sum_{t=1}^{p+2} C_{rst}\cdot\phi_r(\eta_i)\cdot\phi_s(\xi_j)\cdot\phi_t(\lambda_k); \quad (III.9)$$

where

$$A_{m+1,n+1,p+1}=u_{i-1,j-1,k-1}, \quad B_{m+1,n+1,p+1}=v_{i-1,j-1,k-1},$$

$$C_{m+1,n+1,p+1}=w_{i-1,j-1,k-1};$$

$A_{m+2,n+1,p+1} = u_{i,j-1,k-1}$, $B_{m+2,n+1,p+1} = v_{i,j-1,k-1}$,

$C_{m+2,n+1,p+1} = w_{i,j-1,k-1}$;

$A_{m+1,n+2,p+1} = u_{i-1,j,k-1}$; ... etc. ;

and

$$\phi_{m+1} = \phi_1(\eta_i), \quad \phi_{n+1} = \phi_1(\xi_j), \quad \phi_{p+1} = \phi_1(\lambda_k) \quad ;$$

$$\phi_{m+2} = \phi_2(\eta_i), \quad \phi_{n+2} = \phi_2(\xi_j), \quad \phi_{p+2} = \phi_2(\lambda_k) \quad ;$$

and ϕ_1 through ϕ_m (ϕ_n, or ϕ_p) are the first m (n or p) simply-supported beam functions - i.e. sine waves - and ϕ_1, ϕ_2 are as defined in figure (III.1).

Extending the analogy with the rectangular inplane element, the above sets of degrees of freedom may be classified into the following four subsets:

i) Functions providing the corner degrees of freedom u, v, and w at the eight corners of the solid element. These functions correspond to those of the basic first order solid Fihite Element.

ii) Functions providing the flexibilities within the element itself, or *local* degrees of freedom. These functions have zero values at the exterior boundary of the solid.

iii) Functions providing the flexibilities for the straight edges of the solid. These degrees of freedom enable the edges to take arbitrary shapes while the corner freedoms are suppressed.

iv) Functions providing the flexibilities within the plane faces bounding the element. They allow arbitrary displacements on any - or all - of the bounding surfaces while the corners and edges are restrained. These degrees of freedom correspond to double Fourier series within each of the boundary plane surfaces multiplied by linear functions in the direction perpendicular to those surfaces.

An interesting special case of this element results when (p) is set to zero in equations *(III.7)* through *(III.9)*, and $C_{rs1} = C_{rs2}$ in *(III.9)* for a thin element (the dimension along the λ_k axis is small relative to the other two dimensions). In this case, a combined thin plate inplane and bending element results. These assumptions correspond to linearly varying inplane strains, a zero normal strain, and constant shear strains across the depth of the element. This element takes into account the effect of the shear deformations on the distortions of the plate. The assumption that the normal strains - rather than the normal stresses - are zeros across the depth of the element can be corrected through a proper modification in the strain energy expression. The total number of degrees of freedom for this element is $5(m+2)(n+2)$. If an equivalent element were made up through combining the displacement functions for the bending element presented in Chapter VII and the inplane element presented earlier in this Appendix, the total degrees of freedom resulting would be $[3(m+3)(n+2)+2(m+n)+12]$.

This number is less than that of the reduced 3-D element for $(m+n)\geq 2$. This is the price paid because the assumptions that the lines originally normal to the middle plane remain normal after deformation, and the bending and membrane actions of the plate are independent, introduced by the thin plate small deflections theory, were not respected. The reduced 3-D element, therefore, may be used equally well for both small and large deflection problems. In addition, since the stresses in the 3-D element require only single, rather than double, differentiations of the independent variables, the resulting bending stresses are expected to be more accurate than those obtained from the bending element for the same degree of accuracy in displacements. The question of the relative efficiency of the two types of elements, therefore, remains unresolved pending an actual comparison of the solutions obtainable for a test problem and upon the parameter $(m+n)$.

5. A Three-Dimensional Triangular Prism

Similar to the 3-D rectangular prism, the triangular prism can be obtained by a straight-forward extension of the triangular inplane element presented earlier. Referring to the coordinate systems defined in figure (III.7), suitable displacement functions can be obtained through multiplying equation *(III.3)* by a series of functions $\phi_t(\lambda)$ similar to that used in the (λ_k) direction of the rectangular

prism elements such that:

$$u = \sum_{t=1}^{p+2} \sum_{k=1}^{3} \{u_{k,t}(1-\eta_k) + \sum_{i=0}^{mk} \sum_{j=i+1}^{mk+1} A_{i,j,k,t}[\phi_i(\eta_k).\phi_j(\xi_k) - \phi_j(\eta_k).\phi_i(\xi_k)] + \sum_{t=0}^{nk} \sum_{j=i+1}^{nk+1} B_{i,j,k,t}[\psi_i(\eta_k).\psi_j(\eta_k) - \psi_j(\eta_k).\psi_i(\xi_k)]\}.\phi_t(\lambda); \quad (0<\eta_k\leq 1;\ -\eta_k<\xi_k<\eta_k) \quad (III.11)$$

in which $\phi_i(\eta_k)$, $\phi_j(\eta_k)$, $\phi_i(\xi_k)$, $\phi_j(\xi_k)$ and ψ are the same as defined in association with *(III.3)*; $\phi_t(\lambda)$ is the same as in *(III.8)* through *(III.10)*. $u_{k,p+1}$ and $u_{k,p+2}$ are the u displacement components at the corners of the prism, while $u_{k,t}$ (for $t=1$ through p), $A_{i,j,k,t}$ and $B_{i,j,k,t}$ are generalized displacement coordinates. Expressions similar to *(III.11)* are to be assumed for the displacement components v and w.

The displacement functions defined by equation *(III.11)* above may be classified into the same four subsets of degrees of freedom identified for the 3-D rectangular prism. It is worth noting that the degrees of freedom at the corners, along the straight edges, and on the *rectangular* faces of both the triangular and rectangular prisms presented here are identical. Hence, the two types of 3-D elements are compatible and may be used together. It is worth mentioning also that a reduced 3-D element similar to that discussed in the previous section may be obtained and used as an alternative combined inplane and bending triangular plate element.

6 6

OF/DE

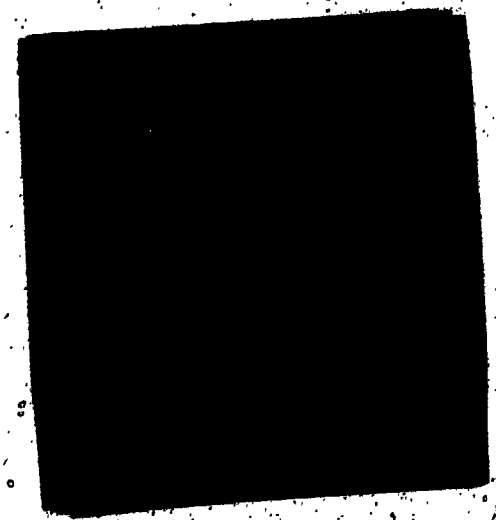

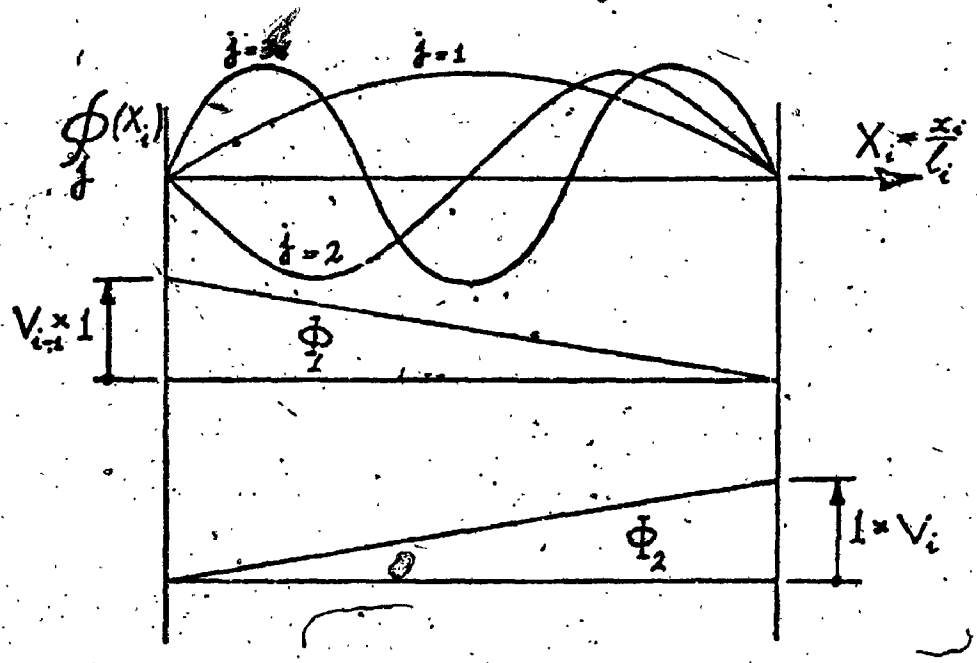

$$V(X_i) = V_{i-1} \cdot \Phi_1(X_i) + V_i \cdot \Phi_2(X_i) + \sum_{j=1}^{n} \phi_j(X_i)$$

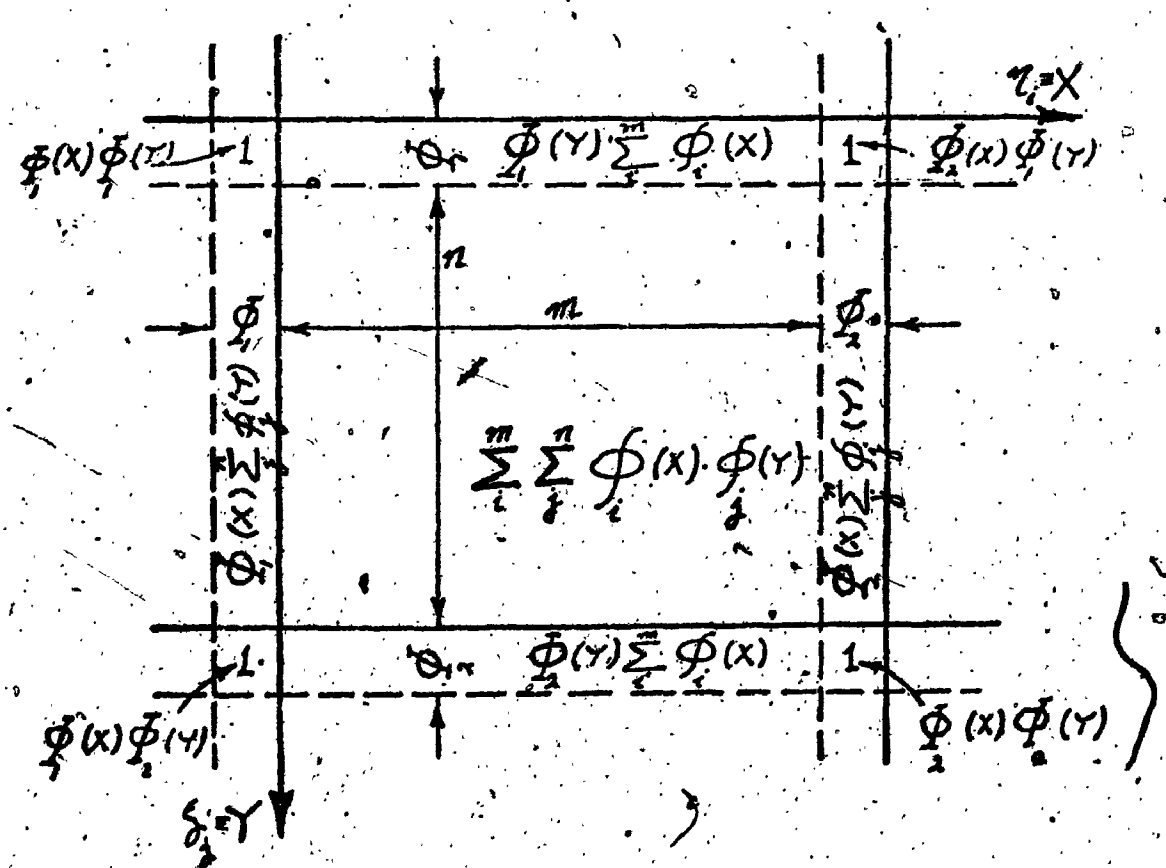

Distribution of degrees of freedom in a Rectangular Plane-stress Large Element.

Fig. (III-2)

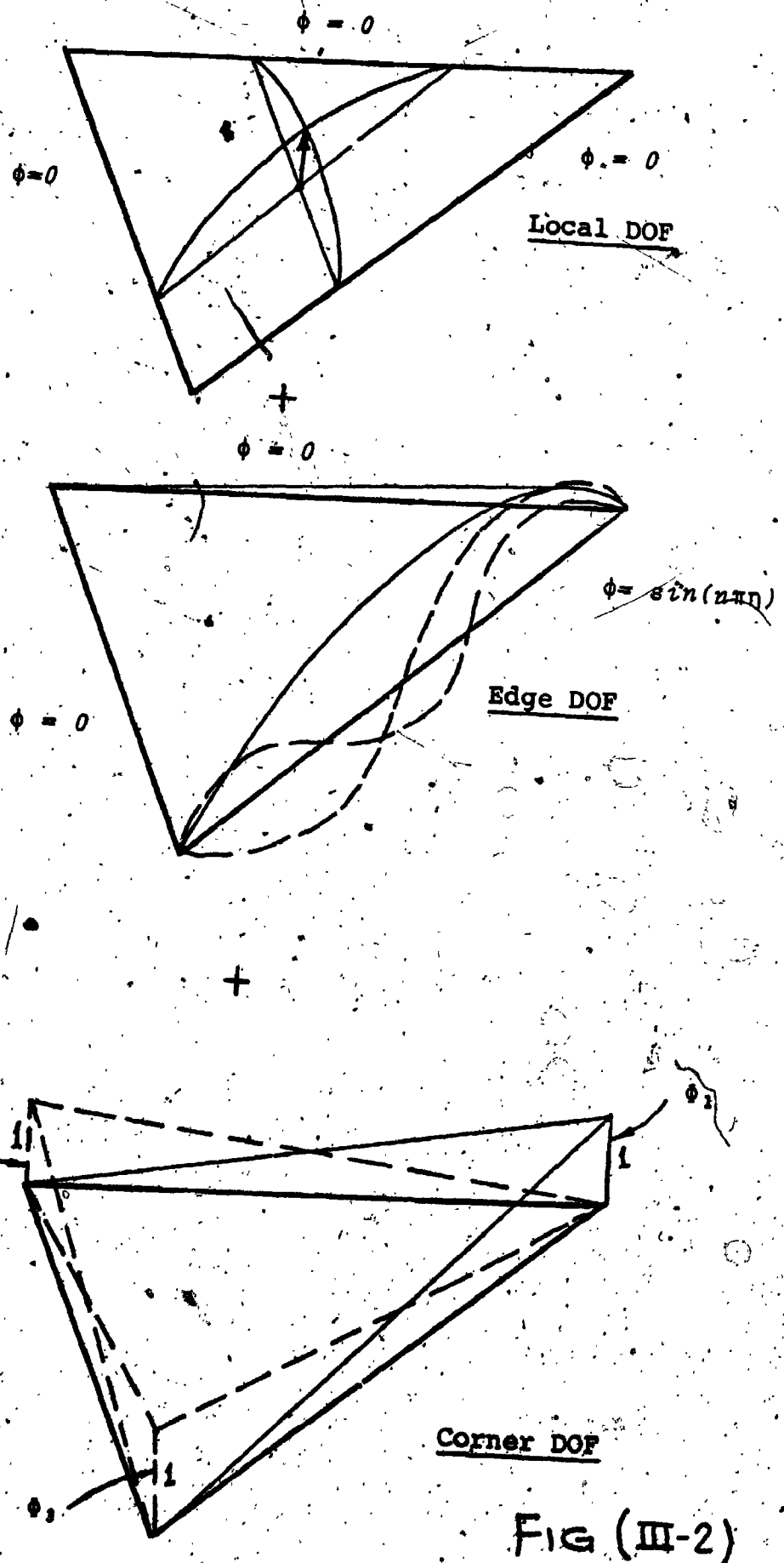

FIG (III-2)

Typical Shape Functions For a Large Triangular Inplane

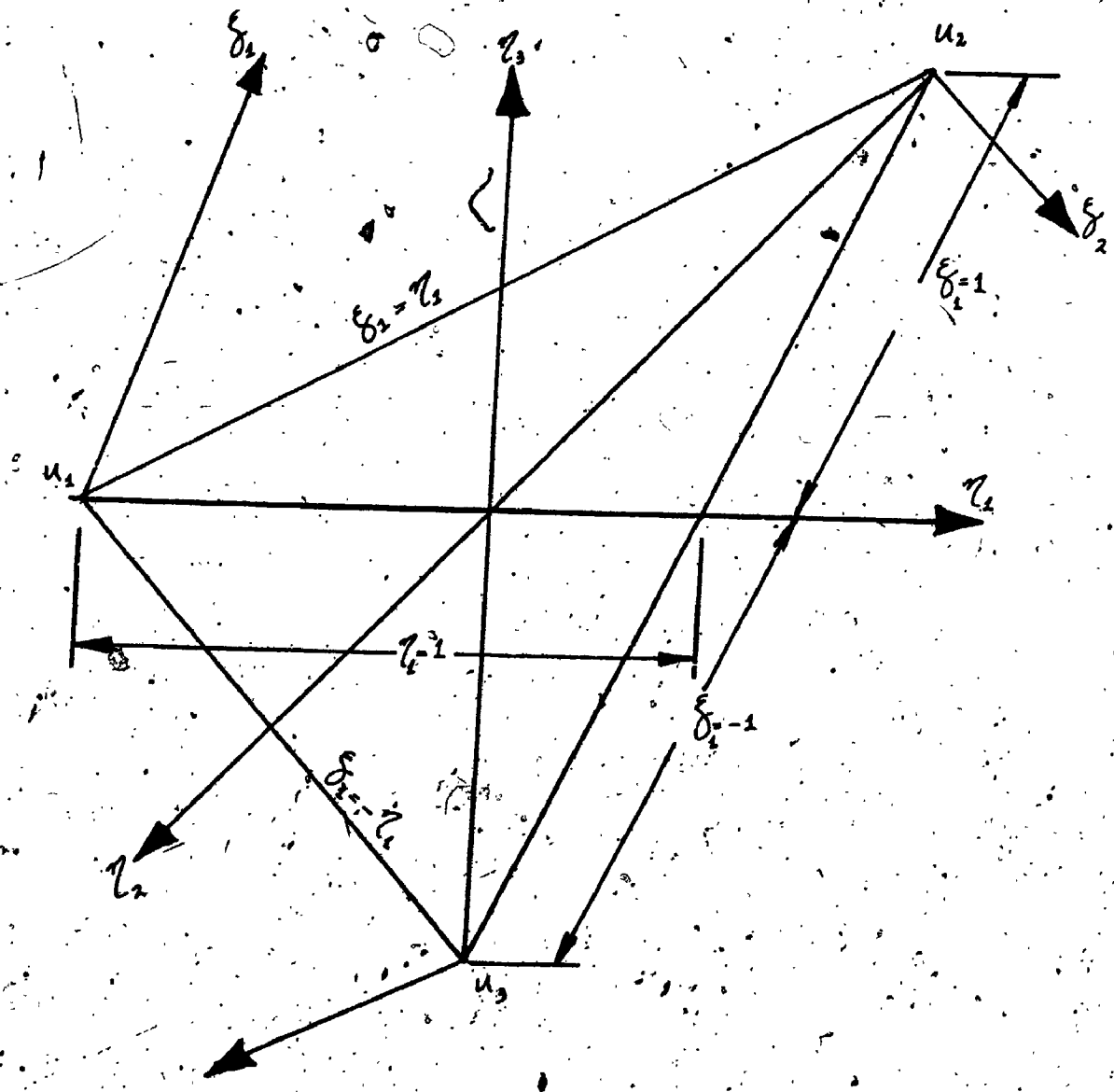

Fig. (III.3)
Coordinate Systems for a Large
Triangular Inplane Stress Element

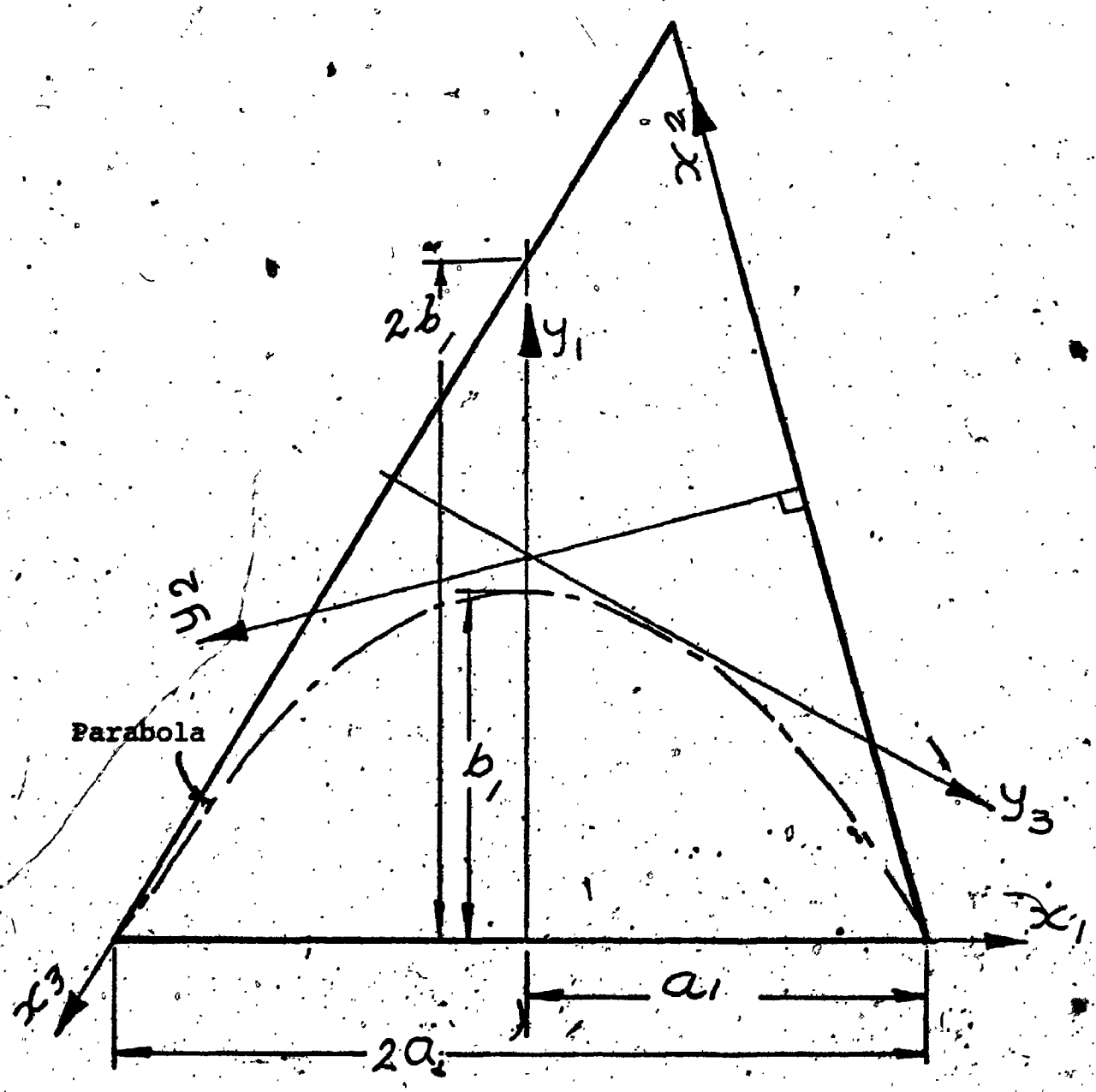

Fig. (III.4)

Coordinate Systems for the Large Triangular Plate Bending Element - Edge DOF

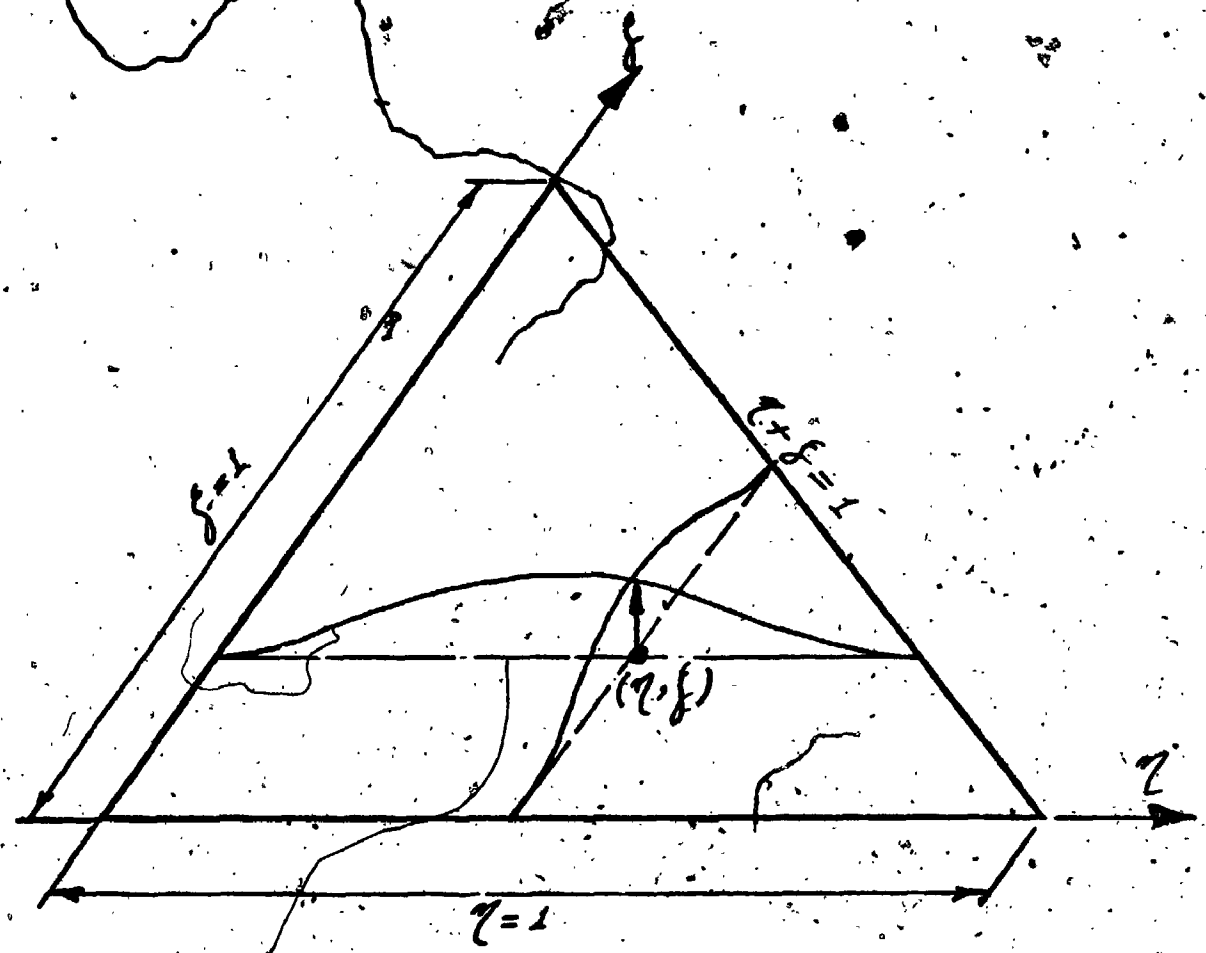

Fig. (III.5)

Coordinate System for the Large Triangular Plate Bending Element - Local DOF

Fig. (III.6)

Coordinate System and Degrees of Freedom for a 3-D Lame Rectangular Prism Element

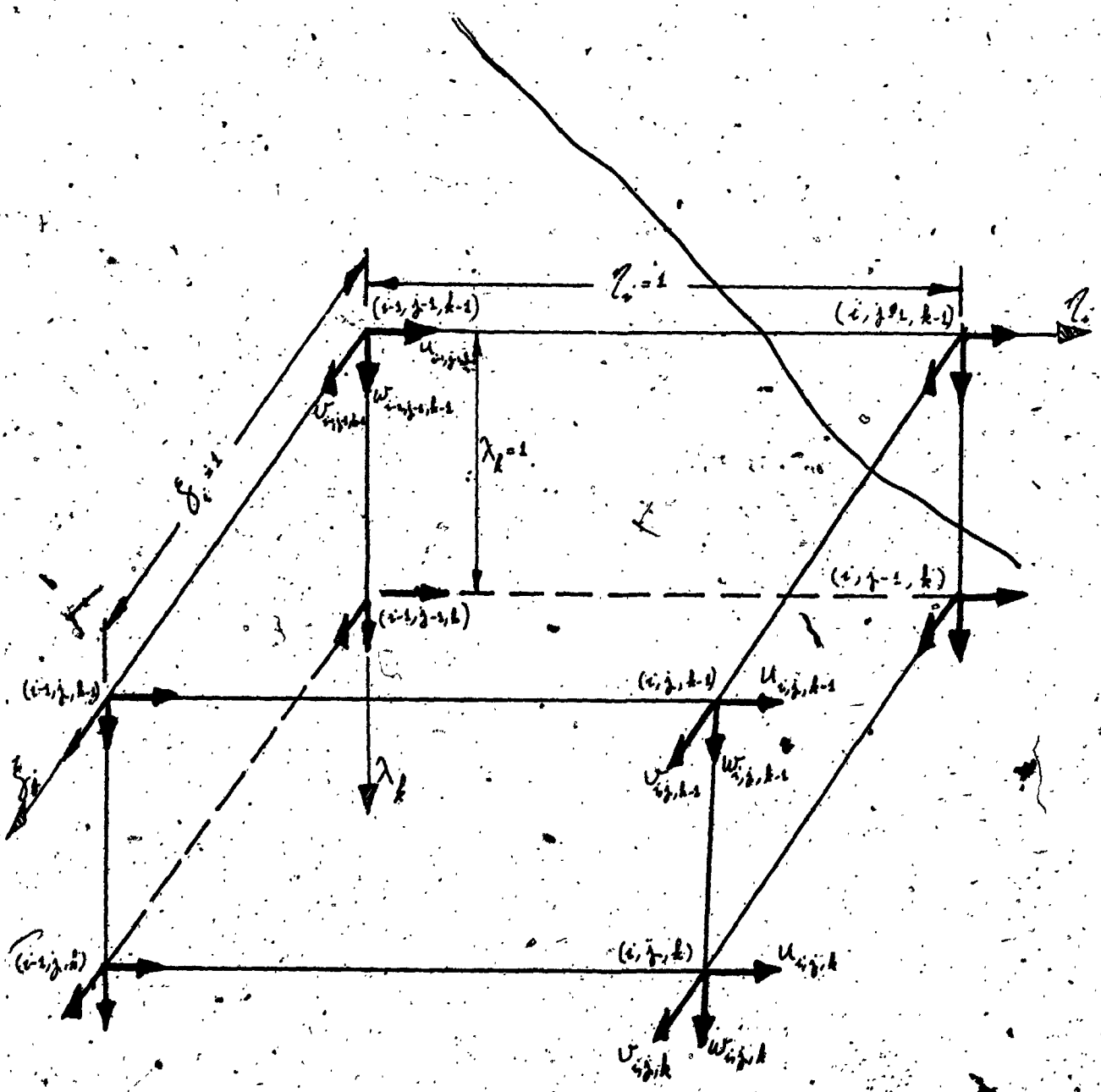

Fig.(III.7)
Coordinate Systems and Degrees of Freedom
for a 3-D Large Triangular Prism Element